การจำลองการกำจัดความชื้นในโรงงานด้วยเครื่องลดความชื้นแบบรังผึ้งหมุนชนิดต่างๆ

นางสาว อรจิรา รุ่งอรุณแสงชัย

SIMULATION OF REMOVAL OF HUMIDITY IN A FACTORY USING VARIOUS ROTARY HONEYCOMB DEHUMIDIFIERS

Miss Ornjira Rungarunsangchai

Thesis Title	Simulation of Removal of Humidity in a Factory Using Various Rotary Honeycomb Dehumidifiers
By	Miss Ornjira Rungarunsangchai
Field of Study	Chemical Engineering
Thesis Advisor	Professor Wiwut Tanthapanichakoon, Ph.D.

Accepted by the Faculty of Engineering, Chulalongkorn University in Partial Fulfillment of the Requirements for the Master's Degree

………………………………………… Dean of Faculty of Engineering

(Professor Somsak Panyakeow, Dr.Eng)

THESIS COMMITTEE

………………………………………….. Chairman

(Associate Professor Chirakarn Muangnapoh, Dr.Ing.)

………………………………………….. Thesis Advisor

(Professor Wiwut Tanthapanichakoon, Ph.D.)

………………………………………….. Member

(Associate Professor Tawatchai Charinpanitkul, D.Eng.)

………………………………………….. Member

(Somprasong Srichai, Ph.D.)

อรจิรา รุ่งอรุณแสงชัย : การจำลองการกำจัดความชื้นในโรงงานด้วยเครื่องลดความชื้นแบบรังผึ้งหมุนชนิด ต่างๆ (SIMULATION OF REMOVAL OF HUMIDITY IN A FACTORY USING VARIOUS ROTARY HONEYCOMB DEHUMIDIFIERS) อ. ที่ปรึกษา : ศ.ดร.วิวัฒน์ ตัณฑะพานิชกุล, 320 หน้า. ISBN 974—03—0255—6.

ในวิทยานิพนธ์นี้ แบบจำลองคณิตศาสตร์ที่พัฒนาขึ้นสำหรับเครื่องลดความชื้นของอากาศด้วยการดูดกลืนแบบ รังผึ้งหมุนที่เคลือบด้วยลิเทียมคลอไรด์ ซึ่งประกอบด้วยกลุ่มสมการอนุพันธ์ธรรมดาได้ถูกดัดแปลงและขยายให้ ครอบคลุมกรณีเครื่องลดความชื้นอากาศด้วยการดูดซับบนซิลิกาเจลและซีโอไลท์-13X สมการของ Dubinin-Astakhov ถูกใช้ในการสร้างเส้นสมดุลที่อุณหภูมิคงที่ของการดูดซับไอน้ำบนทั้งซิลิกาเจลและซีโอไลท์-13X ที่เคลือบบนแผ่น เซรามิค ความน่าเชื่อถือของแบบจำลองได้รับการพิสูจน์โดยการเปรียบเทียบกับข้อมูลการทดลองอย่างละเอียดของ A. Kodama และคณะ (1993,1994) แบบจำลองนี้ได้รับการแสดงให้เห็นว่า สามารถทำนายได้อย่างถูกต้องแม่นยำทั้ง สมรรถนะการลดความชื้นและปรากฏการณ์ระดับท้องถิ่นของการถ่ายเทความร้อนและมวลพร้อมกันในรังผึ้งเครื่องลด ความชื้น จากการเปรียบเทียบการกระจายของอุณหภูมิและความชื้นของอากาศภายในเครื่องลดความชื้นแบบหมุน พบว่า ให้ผลสอดคล้องอย่างดีกับผลการทดลองข้างต้น

จากนั้น ได้ทำการศึกษาถึงตัวแปรที่อาจมีผลกระทบ 5 ตัว คือ ความเร็วรอบหมุน, อุณหภูมิของลมร้อนที่ใช้ ฟื้นฟูสภาพสารดูดซับ,ความเร็วเชิงมวลของอากาศชื้นภายในห้อง, ความเร็วเชิงมวลของลมร้อนที่ใช้ฟื้นฟูสภาพสารดูด ซับ และความยาวของโรเตอร์ ผลที่ได้แสดงว่าอุณหภูมิของลมร้อนที่ใช้ฟื้นฟูสภาพสารดูดซับที่ดีที่สุดสำหรับเครื่องดูด ซับแบบหมุนที่เคลือบด้วยซิลิกาเจลและซีโอไลท์-13X คือ 393 และ 453 เคลวิน ตามลำดับ อนึ่งความเร็วรอบหมุนที่ดี ที่สุดมีค่าประมาณ 6 ถึง 14 รอบต่อชั่วโมง ซึ่งจะขึ้นอยู่กับ ความยาวของโรเตอร์และความเร็วเชิงมวลของอากาศชื้น ณ เงื่อนไขที่ดีที่สุด การเพิ่มขึ้นของความเร็วเชิงมวลของอากาศชื้นจาก 4.05×10^{-3} เป็น 1.62×10^{-2} กิโลกรัมน้ำ/(ตารางเมตร ·วินาที) จะทำให้ประสิทธิภาพการลดความชื้นมีค่าลดลงจาก 95% เหลือเพียง 70% และจากเกือบ 100% เหลือเพียง 95% สำหรับกรณีของซิลิกาเจลและซีโอไลท์-13X ตามลำดับ

นอกจากนี้ได้ทำการจำลองเครื่องลดความชื้นแบบหมุนทั้งที่เคลือบด้วยซิลิกาเจลและซีโอไลท์ร่วมกับห้อง กระบวนการปิดที่มีพื้นเปียกในโรงงานเครื่องดื่มที่ทันสมัยแห่งหนึ่งในประเทศไทยเพื่อที่จะทำการศึกษาและทำนาย สมรรถนะการลดความชื้นของกระบวนการเชิงจลน์ที่สภาวะต่างๆ พร้อมทั้งนำผลไปเปรียบเทียบกับกรณีของลิเทียม คลอไรด์ด้วย (Prawarnpit, 1997) ผลที่ได้แสดงให้เห็นว่าสารดูดความชื้นแบบลิเทียมคลอไรด์ ซิลิกาเจล และซีโอไลท์ สามารถทำให้พื้นห้องแห้งภายใน 10 ชั่วโมง 6 ชั่วโมง และ 3 ชั่วโมง ตามลำดับ

ภาควิชา ....วิศวกรรมเคมี.............. ลายมือชื่อ
สาขาวิชา ....วิศวกรรมเคมี.............. ลายมือชื่ออาจารย์ที่
ปี ลายมือชื่ออาจารย์ที่ปรึกษา

In this thesis a simple dynamic model for the rotary honeycomb lithium chloride coated absorption-type dehumidifier consisting of ordinary differential equations has been modified and extended to the case of silica gel and zeolite-13X coated adsorption-type dehumidifiers. Dubinin-Astakhov equation is employed to correlate the equilibrium adsorption isotherm for water vapor on both silica gel and zeolite-13X coated ceramic fiber sheet. The reliability of the model is validated against detailed experimental data published by Kodama, A. et al. (1993,1994). The present model is shown to accurately predict the dehumidification performance and the local phenomena of simultaneous heat and mass transfer inside honeycomb of the dehumidifier. The air temperature and humidity profiles inside the rotary dehumidifier are compared and found to agree well with the experimental results.

Next five factors, i.e. the rotational speed of the rotor, regenerative air temperature, mass velocity of humid room air, mass velocity of hot regenerative air and length of the rotor are investigated. The results show that the optimal regenerative air temperatures are 393 K and 453 K for silica gel and zeolite-13X coated dehumidifiers, respectively. Meantime, the optimal rotational speed is approximately 6-14 rph which depends on the length of the rotor and the mass velocity of humid room air. At the optimal condition, increasing the mass velocity of the humid room air from 4.05×10^{-3} to 1.62×10^{-2} $kg_w/(m^2 \cdot s)$ decreases the dehumidification efficiency from 95% to 70% and from nearly 100% to 95% for the cases of silica gel and zeolite-13X, respectively.

Furthermore, both of silica gel and zeolite-13X coated rotary dehumidifiers are simulated in conjunction with a closed process room with wet floor in a modern beverage factory in Thailand in order to investigate and predict the dehumidification performance and the dynamic process of the water evaporation at various conditions as well as to compare the results with the case of lithium chloride absorbent (Prawarnpit, 1997). The results show that the lithium chloride, silica gel and zeolite-13X sorbents can dry out water on the wet floor within 10 hr, 6 hr and 3 hr, respectively.

Department . Chemical Engineering.   Student's signature ....

Field of study. Chemical Engineering.   Advisor's signature ....

Academic year …....…2001……..…   Co-advisor's signature ....

ACKNOWLEDGEMENT

CONTENTS

CHAPTER 3 LITERATURE REVIEW

CHAPTER 4 MATHEMATICAL MODELING AND SIMULATION

CHAPTER 5 VALIDATION OF ADSORPTION ISOTHERMS AND
    DYNAMIC MODELS

CHAPTER 6 RESULTS AND DISCUSSION

CHAPTER 7 CONCLUSIONS AND RECOMMENDATION

LIST OF TABLES

LIST OF FIGURES

NOMENCLATURE

a	=	Specific surface area, m^2/m^3
A	=	Cross sectional area, m^2
C_p	=	Specific heat, $kJ/(kg \cdot K)$
D	=	Diameter of rotor, m
D_h	=	Hydraulic diameter, m
D_p	=	Pore diameter, m
E	=	Enthalpy, kJ/kg
G	=	Mass velocity of dry air, $kg_{dry\ air}/(m^2 \cdot s)$
G_w	=	Mass velocity of humid air, $kg_{water\ vapor}/(m^2 \cdot s)$
H	=	Air humidity, $kg_{water\ vapor}/kg_{dry\ air}$
ΔH_{ads}	=	Heat of adsorption, $kJ/kg_{adsorbate}$
h_c	=	Convective-film heat transfer coefficient, $kJ/(m^2 \cdot K \cdot s)$
k_c	=	Convective-film mass transfer coefficient, $kg_{\Delta H}/(m^2 \cdot s)$
K_R	=	Number of completely mixed compartments for a room, (-)
L	=	Axial length (thickness) of the honeycomb dehumidifier, m
L_R	=	Total length of the room, m
MW	=	Molecular weight, kg/kmol
N	=	Number of completely mixed cells in a slot, (-)
Nu	=	Nusselt number, (-) $(= h \cdot D/k)$
P	=	Pressure, kPa
Pr	=	Prandtl number, (-) $(= C_p \cdot \mu/k)$
P_{sat}	=	Saturated vapor pressure, kPa
R	=	Gas constant, $(= 8.314\ kJ/kmol \cdot K)$,
RH	=	Relative humidity (%) or relative pressure (-)
R_{ads}	=	Rate of adsorption, $kg_{water\ vapor}/(kg_{adsorbent} \cdot s)$
R_{reg}	=	Rate of regeneration, $kg_{water\ vapor}/(kg_{adsorbent} \cdot s)$
R_k	=	Rate of evaporation, $kg_{water}/(m^2 \cdot s)$
Re	=	Reynolds Number, (-) $(= \rho \cdot V \cdot d/\mu)$
r_p	=	Pore radius, m
V	=	Velocity, m/s
V_H	=	Specific volume of humid air, $m^3/kg_{dry\ air}$
W	=	Amount adsorbed, $kg_{water\ vapor}/kg_{adsorbent}$ or water on the floor, $kg_{water\ vapor}/m^2$
t	=	Time, sec
t_f	=	Final simulation time, sec
Δt	=	Step size of integration, sec
T	=	Temperature, K
Z	=	Dimensionless length, (-)

GREEK LETTERS

ρ	=	Density, kg/m^3
λ	=	Latent heat of vaporization, kJ/kg
φ	=	Rotational speed, h^{-1} (rph)
ε	=	Void fraction of honeycomb, $(m^3 void/m^3 honeycomb)$

μ	=	Viscosity, kg/m·s
θ	=	Angle of the rotor, degree

SUBSCRIPT

a	=	Air
ads	=	Adsorption
c	=	Cells
cond	=	Conduction
da	=	Dry air
g	=	Gas phase
i	=	Cell no. i
in	=	Inlet condition
j	=	Slot no. j
k	=	Compartment no. k
o	=	Reference temperature (= 273.15 K) or initial condition
out	=	Outlet condition
R	=	Room
reg	=	Regeneration
s	=	Solid phase
sat	=	Saturated state
sb	=	Adsorbent
sh	=	Fiber sheet
ss	=	Slot wall including adsorbent and fiber sheet
thick	=	The equivalent number of closed slots compared to the width of the stationary partition plate between the adsorption and regeneration zones
v	=	Water vapor
w	=	Liquid water

SUPERSCRIPT

o	=	Reference temperature (= 273.15 K)

CHAPTER 1

INTRODUCTION

1.1 Background

High air humidity is a direct cause of various problems on the operation, products, materials, and instruments in a factory. These problems include the corrosion of iron materials that occurs at relative humidity, RH, higher than 40%, and the rapid reduction of the electrical resistance of insulation when relative humidity increases, say, its resistance lowered by 10,000 times when relative humidity increases from 50% to 90% (Prawarnpit, 1997). For several industries, such as petrochemical, food, chemical, medicine factories and so on, good air drying systems for process rooms are necessary for achieving high quality of products. In an air-conditioning system, increased humidity directly leads to higher energy consumption and higher operating costs. Accordingly, a dehumidifier has taken an important role in commercial buildings and even residential units. Various dehumidifying techniques, such as using solid desiccant to dry air via an adsorption process, using lithium chloride to dehumidify the air via an absorption process and so on, have long been developed.

Since air dehumidification is a purification process used in the confined space of a room or chamber of either a factory or building, the compactness and high sorption-capacity of the continuous honeycomb rotary type dehumidifier is of interest. In comparison with the packed column, a honeycomb structure has adequate sorption-capacity, light weight, low pressure drop, and is suited to continuous operation. Consequently, the honeycomb rotary dehumidifier that was pioneered by Munters et al. (1961), Hemstreet (1967), Macriss et al. (1977), J. Fishcher (1988), Kuma et al. (1989) and so on, has continuously been investigated. For examples, there are experimental study published by Kodama et al. (1993, 1994, 1995), and modeling efforts in which many

numerical approaches were adopted to predict the dehumidifying performance (Holmberg (1979), Jurinak et al. (1984), Banks (1985), Van den Bulck et al. (1985), Schultz et al. (1989), Chant et al. (1995), Worek et al. (1993), Elsayed et al. (1997) and Simonson et al.(1999)).

In recent years, Particle Technology and Materials Processing Lab in collaboration with Thai Powder Technology Center (TPTC), Chulalongkorn University, has developed a simple dynamic mathematical model for the absorption-type rotary dehumidifier used in a modern beverage factory (Prawarnpit, 1997). The model can realistically predict the dynamic behavior, such as dehumidifying efficiency, outlet air temperature, remaining water layer on the floor and air humidity in the process room at various operating conditions. In the present work, the dynamic mathematical model of the lithium-chloride absorption-type rotary dehumidifier (W. Tanthapanichakoon and A. Prawarnpit (1997, 2000)) will be modified and extended to the case of adsorption-type rotary dehumidifier, in which either silica gel or zeolites are used as desiccant.

1.2 Objectives of the thesis

1. To modify the existing mathematical of the lithium-chloride absorption rotary dehumidifier model in order to predict the dynamic behavior and performance of the adsorption-type honeycomb rotary dehumidifier.

2. To determine the significant factors affecting the dehumidifying performance and find out the optimal operating condition using the modified adsorption model.

1.3 Scope of the thesis

1. The adsorption isotherms for water vapor adsorption on silica gel and zeolite-13X will be correlated using the published experimental equilibrium data.

2. The existing mathematical model for the honeycomb rotary absorption-type dehumidifier will be modified and extended to predict the dynamic behavior and performance of the adsorption-type honeycomb rotary dehumidifier.

3. For the validation of the modified model, the simulation results will be compared with published experimental data for the adsorption of humidity on a silica gel coated honeycomb rotary dehumidifier.

4. The investigated factors affecting the dehumidifying performance of either silica gel or zeolite-13X coated honeycomb rotary dehumidifier are:

- Inlet air humidity into the adsorption section, which ranges from 30 to 60 % RH.
- Mass velocity of humid room air and hot regeneration air, which ranges from 0.5 to 2.0 $kg_{da}/(m^2s)$.
- Regeneration temperature, which ranges from 353 to 433 K for silica gel and 413 to 523 K for zeolite-13X.
- Rotational speed of the rotor, which ranges from 5 to 20 rph (h^{-1}).
- Axial length of the rotor, which ranges from 0.10 to 0.25 m.

5. The dehumidifying performance of two different dessicants, silica gel and zeolite-13X, operated optimally in the same process room will be compared with the case of solid lithium chloride absorbent.

1.4 Expected benefits

1. The extended model will be an accurate and handy tool for the design of the honeycomb rotary adsorber which can be used to remove humidity and/or inorganic air pollutants (CO_2, VOC) in a factory, a residential or commercial building.

2. The dynamic mathematical model can be used to predict the transient and steady-state behavior of the simultaneous adsorption and desorption within the honeycomb rotary dehumidifier and find out the optimal operating conditions for the dehumidifier.

CHAPTER 2

GAS ADSORPTION THEORY

2.1 Introduction

Ever since the observation of C.W. Scheele in 1773 and Abbè F. Fontanna in 1777 on the adsorption of gases by charcoal, there have been attempts to evolve a theoretical basis for the complex phenomena. Were adsorption to confine only to gases, the matter could be greatly simplified. In 1785, Lowitz discovered that charcoal could effectively remove from liquid solutions coloring matters which were organic compounds. While a far greater amount of the theoretical work has been done on the adsorption of gases, the greatest volume and weight of industrial adsorbents are employed in the treatment of solutions (Mantell, 1945). As expected, systems of gas adsorption are much more simpler than that of adsorption in solutions.

Jasra and Bhat (1998) said that nearly 40% of the total cost of a chemical process lies in its separation processes. Consequently, development in separation technology has been almost parallel to the growth of the chemical industry. Separation may be defined as a process that transforms a mixture of substances into two or more products that differ from one another in composition. The process is difficult to achieve because it is the opposite of mixing which is a process favored by the second law of thermodynamics (Yang, 1987).

Understanding of engineering design methods of adsorption systems is an important aspect of process engineering design not only in the chemical industry but also in the field of environmental pollution control and energy utilization. Moreover, adsorption is coming to be regarded as a practical separation method for purification or bulk separation in newly developed material production processes, for example, high-

technology materials and biochemical products which tend to decompose to other compounds in a distillation column under high temperature (Suzuki, 1990).

2.2 Fundamental principles

Adsorption is a phenomenon in which molecules in the fluid phase (referred as the adsorbate) adhere to the surface of a solid (referred as the adsorbent). When adsorbed, the molecules lose much of their molecular mobility, releasing heat often in the same order of magnitude of the corresponding heat of condensation. Desorption is a reverse phenomenon, so heat must be supplied to the adsorbent. This phenomenon, usually called regeneration, is quite important in the overall process. Firstly, desorption allows recovery of the adsorbates in those separation processes where the adsorbates are valuable; and secondly, it permits reuse of the adsorbent for further cycles. In a few cases, desorption is not practical, and the adsorbate must be removed by thermal destruction or another chemical reaction, or the adsorbent loaded with the adsorbate is simply discarded (Keller II, Anderson, and Yon, 1987).

Adsorption may be classified as either chemisorption or physical adsorption, depending on the nature of the surface forces. In physical adsorption the forces are relatively weak, involving mainly van der Waals (induced dipole - induced dipole) interactions, supplemented in many cases by electrostatic contributions from field gradient - dipole or - quadrupole interactions. By contrast, in chemisorption there is significant electron transfer, equivalent to the formation of a chemical bond between the sorbate and the solid surface. Such interactions are both stronger and more specific than the forces of physical adsorption and are obviously limited to monolayer coverage. The differences in the general features of physical sorption and chemisorption systems as shown in Table 2.1 can be understood on the basis of this difference in the nature of the surface forces.

Table 2.1 The general features of physical adsorption and chemisorption

Parameter	Physical adsorption	Chemisorption
Heat of adsorption	Low, < 1-5 times latent heat of evaporation	High, > 1-5 times latent heat of evaporation
Specificity	Nonspecific	Highly specific
Nature of adsorbed phase	Monolayer or multi-layer, no dissociation of adsorbed species	Monolayer only, may involve dissociation
Temperature range	Only significant at relatively low temperatures	Possible over a wide range of temperature
Forces of adsorption	No electron transfer, although polarization of sorbate may occur	Electron transfer leading to bond formation between sorbate and surface
Reversibility	Rapid, nonactivated, reversible	Activated, may be slow and irreversible

Heterogeneous catalysis generally involves chemisorption of the reactants, but most applications of adsorption in separation and purification processes depend on physical adsorption. Chemisorption is sometimes used in trace impurity removal since very high selectivities can be achieved. However, in most situations the low capacity imposed by the monolayer limit and the difficulty of regenerating the spent adsorbent more than out-weigh this advantage. The higher capacities achievable in physical adsorption result from multilayer formation and this is obviously critical in such applications as gas storage, but it is also an important consideration in most adsorption separation processes since the process cost is directly related to the adsorbent capacity.

In very small pores the molecules never escape from the force field of the pore wall even at the center of the pore. In this situation the concepts of monolayer and multiplayer sorption become blurred and it is more useful to consider adsorption simply as pore filling. The molecular volume in the adsorbed phase is similar to that of the saturated liquid sorbate, so a rough estimate of the saturation capacity can be obtained simply from the quotient of the specific micropore volume and the molar volume of the saturated liquid.

2.3 Adsorbent

Adsorbents have been developed for a wide range of separations. Commercial materials are provided usually as pellets, granules, or beads; although powders are used occasionally. The selection of a proper adsorbent for a given separation is a complex problem. The following factors are important for adsorbent selection (Yang, 1987):

1. Capacity of the adsorbent, within a range of operating pressure and temperature
2. A method for adsorbent regeneration such as increasing the temperature and/or decreasing the pressure
3. Separation factor

Commercial adsorbents are divided into two major classes: hydrophilic and hydrophobic surface classes. The most common hydrophilic adsorbents are molecular-sieve zeolites, activated alumina and silica gel. Since water is a highly polar molecule, it is strongly adsorbed on the polar surface of hydrophilic adsorbents. In contrast, the hydrophobic adsorbents such as activated carbon and silicalite can adsorb organic species more strongly than water. The general feature and application of both adsorbents are shown in Table 2.2.

For a practical application, the aluminum rich zeolites (4A or 13X) and silica gel which have a highly polar surface and a high specific area (small pores) have been widely used in dehumidification system. Thus the detailed properties of these adsorbents are presented below.

Table 2.2 The general features and application of hydrophilic and hydrophobic adsorbents

Adsorbent	Characteristics	Commercial uses	Strengths	Weaknesses
Activated carbon	-Hydrophobic surface -Favors organics over air or water	Removal of organic pollutants from aqueous and gaseous effluents	Cheapest hydrophobic adsorbent, workhorse of the pollution-control business	Difficult to regenerate if fouling occurs, sometimes can catch fire during regeneration
Silica gel	-Hydrophilic surface -High capacity	Primarily, drying of gas streams, sometimes used for polar hydrocarbon removal from gases	Higher capacity than zeolites	Not as effective as zeolites in removing traces of H_2O from gas
Activated alumina	-Hydrophilic surface -High capacity	Primarily, drying of gas streams	Higher capacity than zeolites	Not as effective as zeolites in removing traces of H_2O from gas
Zeolite	-Hydrophilic surface -Regular channels	Dehydration, air separations, geometry-based separations, many others	Can make selective separations based both on polarity and geometry	Lower total capacity than many other adsorbents
Silicalite	-Hydrophobic surface -Favors organics over air or water	Removal of organics from gas streams	Sorbates can be burned off more easily than the case of activated carbon	More costly than activated carbon

2.3.1 Molecular-sieve zeolites

Molecular-sieve zeolites are crystalline aluminosilicates of alkaline, alkaline earth or mixed alkaline and alkaline earth elements such as sodium, potassium, magnesium and calcium-zeolites are represented by the stoichiometry (Yang, 1987):

$$M_{x/n}\left[(AlO_2)_x(SiO_2)_y\right]\cdot zH_2O$$
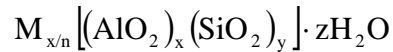
where x, y are integers with y/x equals to or greater than unity, n is the valence of cation M, and z is the number of water molecules in each unit cell. The cations are necessary to balance the electrical charge of aluminium atoms. The skeleton is a regular structure of cages, which is usually interconnected by six windows in each cage. The size of the window apertures, which can be controlled by fixing the type and number of cations, ranges from 3Å to 10Å. Besides surface characteristics, the sorption may occur with great selectivity because of the size of the aperture, hence the name molecular sieve. The primary structural units of zeolites are the tetrahedral of silicon SiO_4 and aluminium AlO_4. These units are assembled into secondary polyhedral building units such as cubes, hexagonal prisms, octahedra, and truncated octahedra. The adjacent silicon-aluminium atoms and silicon-silicon atoms located at the corners of the polyhedra are jointed by a shared oxygen. The final zeolites structure consists of assemblages of the secondary units in a regular three-dimensional crystalline framework. The ratio of silicon atoms to aluminium atoms (Si/Al) must be greater than unity.

Zeolites were first recognized as a new type of mineral in 1756. Studies of the gas-adsorption properties of dehydrated natural zeolite crystals more than 60 years ago led to the discovery of their molecular-sieve behavior. As microporous solids with uniform pore sizes that range from 0.3 to 0.8 nm, these materials can selectively adsorb or reject molecules based on their molecular shape and size. This effect, with commercial overtones leading to novel processes for separation of materials, inspired attempts to duplicate the natural materials by synthesis. Many new crystalline zeolites have been synthesized. More than 150 synthetic zeolite types and 40 zeolite minerals are known. The most important molecular-sieve zeolite adsorbents are the synthetic type A, type X, type Y, synthetic mordenite, and their ion-exchanged variations, as well as the mineral zeolites, chabacite, and mordenite (Kerller II, Anderson, and Yon, 1987).

2.3.2 Silica gel

Silica gel adsorbents are composed of a rigid three-dimensional network of spherical particles of amorphous colloidal silica (SiO_2). They were reported as early as 1640 and commercial production was begun around 1919. The surface area is generated by the very fine size of the colloidal particles. They exhibit surface areas from as little as 100 m^2/g for the "aerogels" to over 800 m^2/g. The product is provided in both granular and spherical forms. The silica gel surface has an affinity for water and organics, although water is preferred. The surface of the silica gel can be in a fully hydroxylated form (Si-O-H) or a dehydrated siloxane form (Si-O-Si). The former is the result of drying the gel or precipitate below 150 ∘C, and the surface is readily wetted with water. The dehydration of the fully hydroxylated form by heating from 300 to 1000 ∘C results in the siloxane-type surface. The most common preparation is by mixing a sodium silicate solution with a mineral acid such as hydrochloric acid. The reaction produces a concentrated dispersion of finely divided particles of hydrated SiO_2, known as silica hydrosol or silicic acid (Ruthven, 1984; Yang,1987).

$$Na_2SiO_3 + 2HCl + nH_2O \longrightarrow \qquad 2NaCl + SiO_2 \cdot nH_2O + H_2O$$

Various silica gels with a wide range of characteristics, such as surface area and pore-size distribution, can be made by varying the silica concentration and pH of solution. Silica gel is a desirable adsorbent for drying fluid stream, containing small amount of moisture, because of the hydrophilic surface.

2.4 Adsorption equilibrium

In practical operations, the maximum capacity of an adsorbent cannot be fully utilized due to mass transfer effects involved in actual fluid-solid contacting processes. In order to estimate practical or dynamic adsorption capacity, however, it is essential to have information on adsorption equilibrium (Suzuki, 1990). For a given gas and an amount of a given adsorbent, the amount of gas adsorbed at equilibrium is a function of the final pressure and temperature only (Mantell, 1945).

$$q = f(p, T) \qquad\qquad (2.1)$$

When the partial pressure of the gas is varied and the temperature is kept constant, an expression of the amount adsorbed versus the pressure is called the "adsorption isotherm".

$$q = f(p) \qquad \text{(constant T)} \qquad (2.2)$$

When the partial pressure of the gas is constant and temperature is varied, the resulting relationship is called the "adsorption isobar".

$$q = f(T) \qquad \text{(constant p)} \qquad (2.3)$$

The relationship of the variation of equilibrium pressure with respect to temperature at a fixed amount of the adsorbed is called the "adsorption isostere".

$$p = f(T) \qquad \text{(constant q)} \qquad (2.4)$$

2.4.1 Types of adsorption isotherms

Brunauer et al. (1940) divided isotherms of physical adsorption into five types as shown in Figure 2.1.
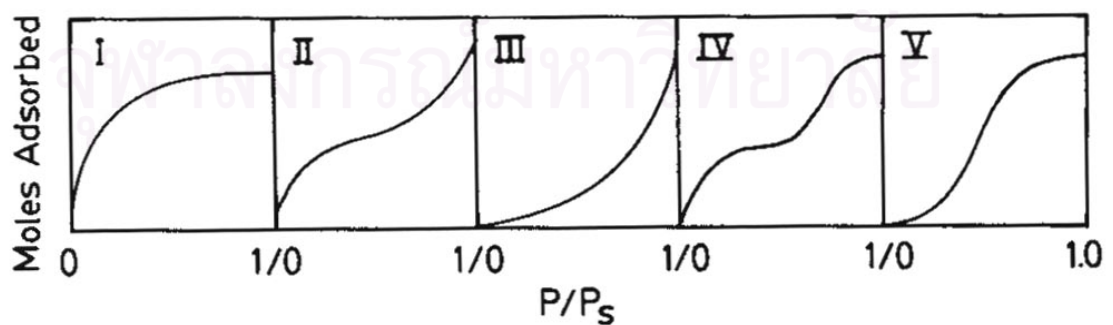
Figure 2.1 The five types of pure-component gas adsorption isotherms in the classification of Brunaure, Deming, Deming and Teller (Ruthven, 1980)

Type I isotherm represents unimolecular adsorption and applies to microporous adsorbents with small pore sizes (not significantly greater than the molecular diameter of the adsorbate). Adsorbents with type II or III isotherms are characterized by a wide range of pore sizes such that adsorption may extend from monolayer to multilayer and ultimately to capillary condensation. For example, adsorption of nitrogen on silica gel displays type II behavior. In this regard, it should be noted that both the potential theory and the capillary condensation theory deal with multilayer adsorption, but neither accounts for these isotherm shapes. An isotherm of type IV suggests that adsorption causes the formation of two surface layers. Type V isotherm behavior is found in the adsorption of water vapor on activated carbon.

To so-called "multimolecular adsorption theory" represents an attempt by earlier investigators to develop a general expression that incorporates all the characteristics displayed by these five types of isotherms. In terms of present understanding of adsorption, such an attempt is neither necessary nor particularly useful. In establishing isotherm equations for data representation, only two factors are of practical importance: (1) the accuracy of the representation, and (2) the ease with which the equation may be incorporated into adsorption calculation. The following discussion examines several isotherm equations commonly used for single-component gas-adsorption data.

2.4.2 Adsorption isotherm expressions

2.4.2.1 Linear isotherms: Henry's law

For physical adsorption there is no change in molecular state upon adsorption (i.e., no association or dissociation). It follows that for adsorption on a uniform surface at sufficiently low concentrations such that all molecules are isolated from their nearest neighbors, the equilibrium relationship between the partial pressure of the adsorbate in the gas phase and the amount adsorbed in the adsorbed phase will be linear.

$$q = Kp \qquad\qquad (2.5)$$

Equation (2.5) which represents the linear isotherms is analogous to the Henry's law of dilute solution. Hence K is called adsorption Henry constant. The temperature dependence of the Henry constant obeys vant Hoff equation:

$$\frac{d\ln K}{dT} = \frac{\Delta H}{RT^2}$$ (2.6)

where ΔH represents the difference in enthalpy between the adsorbed phase and the gas phase or the heat of adsorption. The Henry constant is given in equation (2.7) by integrating equation (2.6).

$$K = K_o e^{-\Delta H/RT}$$ (2.7)

2.4.2.2 The Langmuir isotherm

When a large number of adsorbate molecules are adsorbed on the adsorbent surface, the isotherm tends to be nonlinear. With an increase in the partial pressure of the adsorbate, the amount adsorbed usually approaches a certain value which represents the maximum amount directly adsorbed on the surface or the monolayer adsorbed amount. Under certain circumstances, the amount adsorbed is limited of this value which is known as the saturated value. The simplest and still the most useful isotherm for the monolayer adsorption is the Langmuir isotherm. This model was originally developed to represent adsorption on surface in which localized adsorption take place on an energetically uniform surface without any interaction between adsorbed molecules.

The basic assumptions on which Langmuir model was based are (Ruthven, 1984):

1. Molecules are adsorbed at a certain number of well-defined localized sites.
2. Each site can hold only one adsorbate molecule.
3. All sites are energetically equivalent.
4. There is no interaction between molecules adsorbed at neighboring sites.

When surface coverage or fractional filling of micropores is θ (=q/q_s) and the partial pressure in the gas phase, p, the adsorption rate is expressed as $k_a p(1-\theta)$ assuming

first order kinetics whereas the desorption rate is expressed as $k_d\theta$. Then equilibration of adsorption rate and desorption rate gives the Langmuir equilibrium relation as

$$\frac{q}{q_s} = \frac{K_L p}{1 + K_L p} \tag{2.8}$$

where q_s is the maximum adsorbed amount on the selected adsorbent and $K_L = k_a/k_d$ is called the Langmuir adsorption equilibrium constant. The limitation of the adsorbed amount corresponds to monolayer adsorption. The Langmuir isotherm is useful for practical purposes because it fits Type I and the initial portion of Type II isotherm in Figure 2.1, which are frequently encountered.

2.4.2.3 The Freundlich isotherm

When an adsorbate molecule can be adsorbed either on an adsorbent surface or on the molecules adsorbed on the surface, saturation of adsorption never occurs with an increase in the partial pressure of the adsorbate. An expression of this isotherm can be written as

$$q = K_F p^{1/n_f} \tag{2.9}$$

Parameter n_f is a constant which is not unity. If the parameter n_f is greater than unity, equation (2.9) is known as Freundlich isotherm which is an empirical expression. Although the expression provides similar results to Langmuir's model, the amount adsorbed is not limited. Equation (2.9) can represent multilayer adsorption.

2.4.2.4 The BET isotherm

When adsorption takes place in multilayers, adsorption directly on the adsorbent surface and above the adsorbed molecules is considered to be based on different attractive forces. Monolayer adsorption is formed by the same concept as the Langmuir type adsorption while adsorption above monolayers is equivalent to condensation of the adsorbate molecules, giving rise to the BET (Bruanauer, Emmett, and Teller, 1938) equation as shown in equation (2.10).

$$\frac{q}{q_s} = \frac{K_{BET}p_r}{[(1-p_r)(1-p_r+K_{BET}p_r)]} \quad ; \quad p_r \equiv p/p_s \qquad (2.10)$$

where p_r is the relative pressure and p_s is the saturation vapor pressure of the saturated liquid sorbate at that temperature. This expression, which has the general form of a type II isotherm in Brunauer's classification, has been found to provide a good representation of experimental physical adsorption isotherms. However, it is commonly used to determine the surface area of a selected adsorbent instead of determination of adsorption equilibria as other expressions mentioned above. For instance, in gaseous nitrogen adsorption at liquid nitrogen temperature, the surface area of the adsorbent is determined by converting q_s to the surface area. In most cases, q_s is obtained from the BET plot of the adsorption data. It gives a straight line in the range of $0.005<p_r<0.35$ and q_s is readily determined. Then by multiplying nitrogen surface area (3,480 m^2/g) with q_s, specific surface area of the adsorbent based on nitrogen adsorption is calculated (Suzuki, 1990).

2.4.2.5 The Dubinin-Polanyi isotherm

The original potential theory for the correlation of adsorption equilibria for microporous adsorbents has been developed by Polanyi (1914). It is based on the assumption that adsorption is due to long-range attractive forces extending out from the surface of the adsorbent. In micropores of size comparable to the size of the adsorbate molecules, adsorption takes place by attractive force from the wall surrounding the micropores, and the adsorbate molecules start to fill the micropore volumetrically. This phenomenon is similar to capillary condensation that occurs in large pores at high partial pressure, although the adsorbed phase in micropores is different because of the effect of the force field of the pore wall. Schematic representation of adsorption according to the Polanyi potential theory is shown in Figure 2.3.
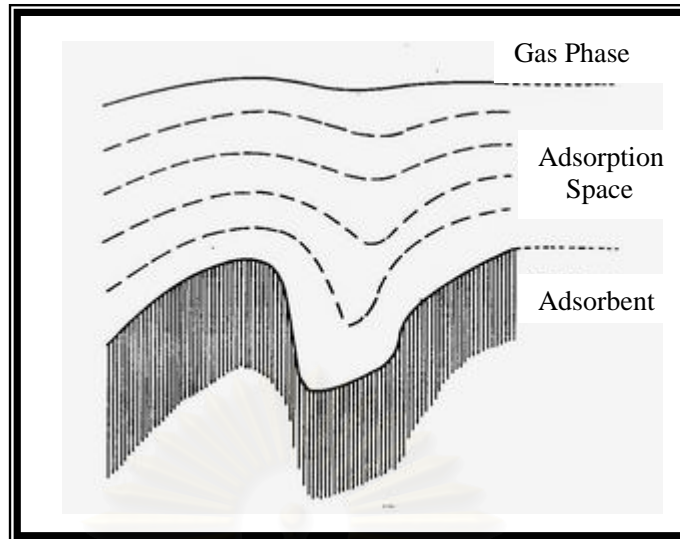
Figure 2.2 Schematic representation of adsorption according to the Polanyi potential theory (Tien, 1994)

In this type of adsorption, the adsorption equilibrium relation for a given adsorbate-adsorbent combination can be expressed independent of temperature by using the adsorption potential.

$$W(A) = q / \rho \tag{2.11}$$

where W is the volume of micropore filled by the adsorbate and ρ is the density of the adsorbed phase.

The adsorbed species within the micropores is considered to behave as a liquid although, due to the effect of the force field of the adsorbent, the properties of this liquid phase may differ from the properties of the bulk liquid at the same temperature. The difference in free energy between the adsorbed phase and the saturated liquid sorbate at the same temperature, which may be calculated directly from the ratio of the equilibrium pressure and the saturation vapor pressure, is referred to as the adsorption potential, A:

$$A = -RT\ln\left(\frac{p}{p_s}\right) \tag{2.12}$$

where p_s and p refer to the saturation pressure for the liquid sorbate and the corresponding equilibrium pressure for the adsorbed phase, respectively, and A is defined as the difference in free energy between the adsorbed phase and the saturated liquid.

Dubinin (1960) assumed a distribution of the Gaussian type for the characteristic curve and derived the following expression, which is called Dubinin-Radushkevich equation.

$$W = W_0 \exp\left(-kA^2\right) \tag{2.13}$$

Later this equation was generalized by Dubinin and Astakhov (1970) to the following form.

$$W = W_0 \exp\left[-\left(\frac{A}{E}\right)^n\right] \tag{2.14}$$

In this expression E is the characteristic energy of adsorption obtained from adsorption potential A at $W/W_0 = e^{-1}$. The parameter n in the Dubinin-Astakhov equation was originally considered to have an integer value, and n =1,2 and 3, respectively, corresponds to adsorption on the surface, in micropores and ultramicropores where adsorbed molecules lose one, two or three degrees of freedom.

Kawazoe and Kawai (1974) tried to examine applicability of the Dubinin-Astakhov (D-A) equation to equilibrium data of molecular sieve carbon (MSC). Since the D-A equation can be written as

$$\ln\left(\ln(W_0/W)\right) = n(\ln A - \ln E) \tag{2.15}$$

It is possible to determine n and E by plotting the left hand side of equation (2.15) versus ln A provided W_0 is known. W_0 can be estimated from the limit of adsorption and is considered to correspond to the micropore volume of the adsorbent.

2.5 Adsorption kinetics

For adsorption on a single adsorbent, an adsorbate molecule in bulk gas has to travel across gas film surrounding the adsorbent particle and subsequently travels through stagnant gas contained in the pore volume of the adsorbent in order to reach the gas adsorbed phase interface, as illustrated in Figure 2.3.
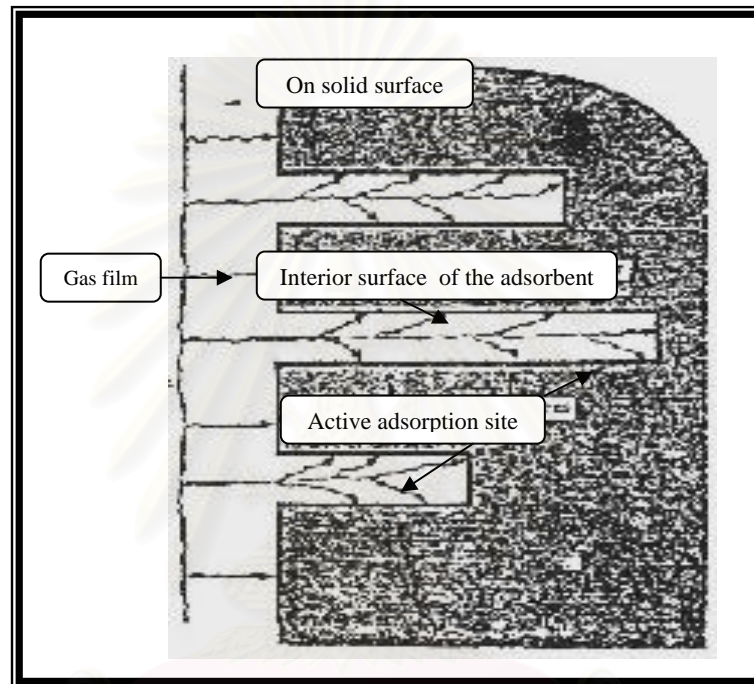
Figure 2.3 Mass-transfer steps in adsorption by porous adsorbent (Prawarnpit, 1997)

Consequently, the mechanism of adsorption can be divided mainly into 3 consecutive steps, i.e. the external film mass transfer, the pore diffusion, and the surface adsorption. The slowest mechanism thus controls the rate of adsorption depending on the particular system and the conditions.

2.5.1 External film resistance

In practice, the rate of adsorption, which is the rate of mass transfer across the film, can be expressed in terms of a film mass-transfer coefficient, k_f, as follows:

$$R_{ads} = k_f a(p - p_e) \tag{2.16}$$

where p and p_e is partial pressure in the gas phase and in the solid (adsorbed) phase, respectively. For spherical non-porous adsorbent, the interfacial area per unit volume, *a*, equals to $6/D_p$ or $3/R_p$.

The film mass transfer coefficient can be determined from an appropriate correlation of Sherwood number (Sh) with Reynolds number (Re) and Schmidt number (Sc). For a packed bed of uniform size of adsorbent particles with radius, R_p, an appropriate correlation for the determination of the external mass transfer coefficient was developed by Wakes and Funazki (Ruthven, 1984; Yang, 1987) and written as

$$Sh = k_f \frac{2R_p}{D_m} = 2.0 + 1.1 Sc^{1/3} Re^{1/2} \qquad (2.17)$$

2.5.2 The pore diffusion

Pore diffusion may occur by several different mechanisms depending on the pore size, the adsorbate concentration, and other conditions [Ruthven, 1984], such as the mean free path of adsorbate molecules. Thus, the diffusion in the pore volume of the selected adsorbent also depends on the collision frequency among adsorbate molecules and that between adsorbate molecules and the pore surface area. If the collision frequency among adsorbate molecules is much higher than the other, the pore diffusion can be represented by the "molecular or ordinary diffusion" in open space. Otherwise, the pore diffusion has been known as "Knudsen diffusion" (Ruthven, 1984). A common criteria for identification of diffusion in pore volume is the ratio of the average pore diameter of the selected adsorbent to the mean free path of the adsorbate. If the ratio is greater than unity, the pore diffusion is equivalent to the molecular diffusion. Otherwise, it becomes Knudsen diffusion. In order to increase the specific surface area, the average pore diameter tends to be relatively small so that the diffusion in the pore volume should be Knudsen type. In this circumstance, the rate of adsorption relates to Knudsen diffusivity, which can be estimated from the following expression:

$$D_k = \frac{2\sqrt{8RTr_p}}{3\sqrt{\pi MW}} = 9700 r_p \left(\frac{T}{MW} \right)^{1/2} \qquad (2.18)$$

where MW is the molecular weight of a diffusing gas and r_p is the pore radius of the adsorbent. Consequently, the pore diffusivity, D_p, of a porous adsorbent is equivalent to D_k and D_M for "Knudsen diffusion" and "molecular diffusion", respectively. The rate of adsorption, which is controlled by pore diffusion, thus can be expressed as follows:

$$R_{ads} = \left(\frac{15\varepsilon_p D_p}{R_p^2} \right)(p - p_e) \tag{2.19}$$

Alternatively, the rate of adsorption may be expressed in terms of the pore mass transfer coefficient (k_p), defined as

$$k_p a_s = \frac{15\varepsilon_p D_p}{R_p^2} \tag{2.20}$$

Instead of determination of the rate of pore diffusion, the effective rate of adsorption is determined practically in terms of overall mass-transfer coefficient (k_0) which is defined as:

$$R_{ads} = k_0 (p - p_e) \tag{2.21}$$

where

$$\frac{1}{k_0} = \left(\frac{1}{k_f a} + \frac{1}{k_p a_s} \right) = \left(\frac{1}{k_f a} + \frac{R_P^2}{15\varepsilon_p D_P} \right) \tag{2.22}$$

The overall mass-transfer coefficient is a combined mass-transfer coefficient of the external film and the pore mass-transfer coefficient. Equation 2.22 has been known as "linear driving force rate of adsorption."

2.6 Adsorption dynamics

Actual adsorption processes are in many cases associated with adsorption in a column as shown in Figure 2.4. Adsorbent particles are packed in the column and fluid that contains one or more components of adsorbates flows through the bed. Adsorption takes place from the inlet of the column and proceeds up to the exit.
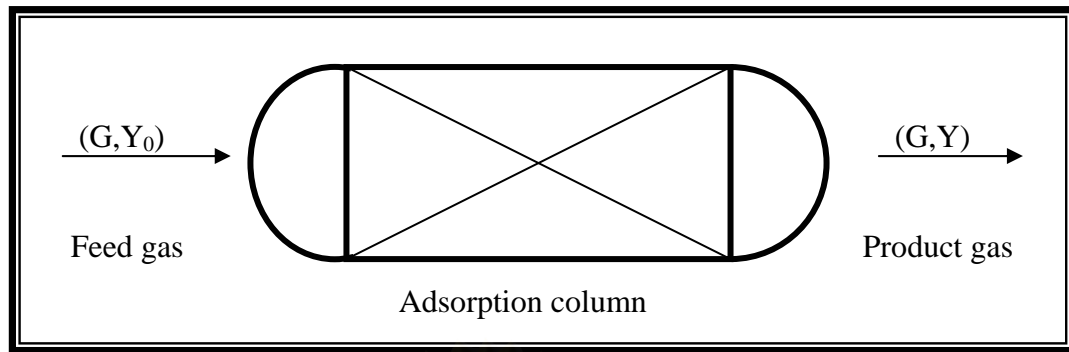
Figure 2.4 Schematic diagram of a fixed-bed adsorption column

In fixed-bed adsorption, the concentrations in the fluid phase, Y, and the solid phase, X, change with time, θ, as well as with position in the bed, L. At first, most of the mass transfer takes place near the inlet of the bed, where the fluid first contacts the adsorbent. After a few minutes, a saturated zone is formed near the inlet of the column, and most of the mass transfer takes place further downstream from the inlet. This saturated region is called "Equilibrium zone". If the solid contains no adsorbate, X_0, at the start, the amount of the adsorbed or concentration in the solid phase drops exponentially with distance from the equilibrium zone to zero before the end of the bed is reached. The S-shaped concentration profile in Figures 2.5b and 2.5c is the region where most of the change in concentration occurs. It is called "the mass-transfer zone (MTZ)". With time, the mass transfer zone moves down the bed, as shown in Figures 2.5d and 2.5g.

Mass transfer from the fluid to the adsorbent continuously occurs. Seepage of the adsorbable components is observed in the effluent stream when the mass transfer zone approaches the exit of the bed and the so-called "breakthrough curve" will be obtained as illustrated in Figure 2.5h to 2.5n. It is the curve of concentration vs. time for the fluid leaving the bed. Initially, the exit concentration is practically zero. Then when the exit concentration reaches some limiting permissible value or break point, the flow is either stopped or diverted to a fresh adsorbent bed. The break point, θ_b, is often taken as a relative concentration of $0.05Y_0$ or $0.10Y_0$. If adsorption were continued beyond the break point, the concentration would rise rapidly to nearly the inlet concentration, Y_0, in the final stage as shown by curves i to k in Figure 2.5.

Time(θ)	Concentration profile in bed	Breakthrough curve
$\theta < \theta_0$	a)	h)
$\theta = \theta_0$	b)	i)
$\theta = \theta + \Delta\theta$	c)	j)
$\theta = \theta_b$	d)	k)
$\theta = \theta_s$	e)	l)
$\theta = \theta_e$	f)	m)
$\theta > \theta_e$	g)	n)
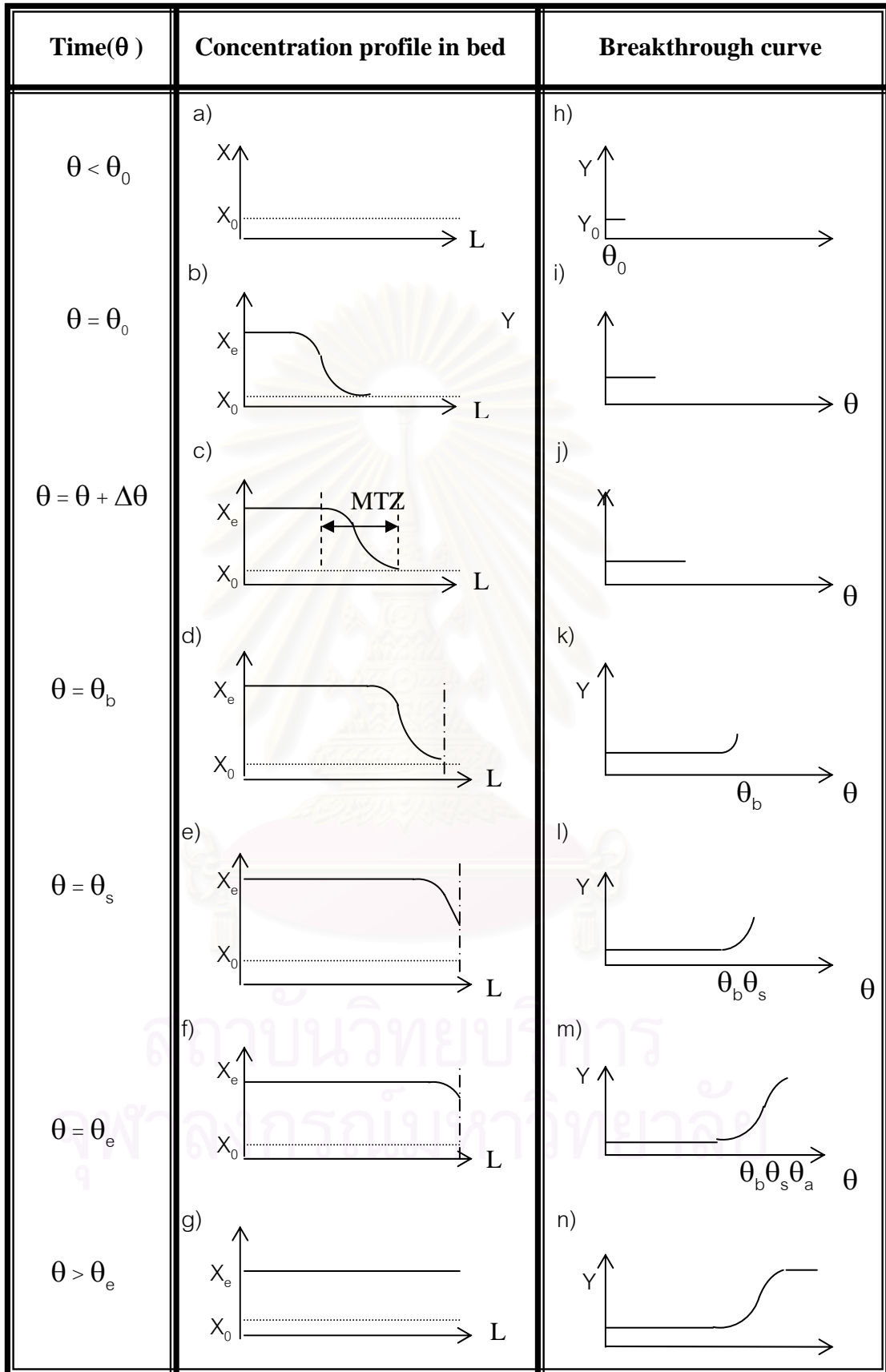
Figure 2.5 Phenomena of the dynamics of adsorption column

2.7 Adsorption processes

Adsorption processes are often identified by their method of regeneration. For gas separation and purification processes, two strategies, i.e., decreasing pressure and increasing temperature are the most frequently used. The method of altering the partial pressure of the adsorbate in the gas phase is called "pressure swing adsorption" (PSA). In contrast, the method of changing the temperature of the adsorbent is called "temperature swing adsorption" or "thermal-swing adsorption" (TSA).

2.7.1 Pressure swing adsorption (PSA)

The most frequent application of PSA involves the bulk separation of gases, particularly air separation to recover oxygen or nitrogen, and hydrogen purification; some new uses are springing up for recovery of contaminants in vent streams. A schematic diagram of a simple PSA process is shown in Figure 2.6. The feed step is operated at a relatively high pressure, and the regeneration step at a lower pressure. A fraction of the adsorbate-free product is used to purge the low-pressure bed; so, the regeneration step in fact uses a total-pressure reduction and an adsorbate-concentration reduction to effect the partial-pressure reduction that facilitates desorption. The heat of adsorption is stored in the bed and is available for the subsequent desorption step.

The use of part of the adsorbate-free stream for purging greatly limits the application of PSA. First, only a fraction of the adsorbate-free stream is recovered, and then the adsorbate-rich purge stream is contaminated with non-adsorbate. To minimize (but not completely eliminate) this problem, much more complex flowsheets than that shown in Figure 2.6. have been devised, with many different types of gas exchanges between the beds. These flowsheets, although they increase the percent recovery of the non-adsorbed stream and reduce the energy requirements for the process, nevertheless carry an inevitable investment penalty due to their greater complexity.
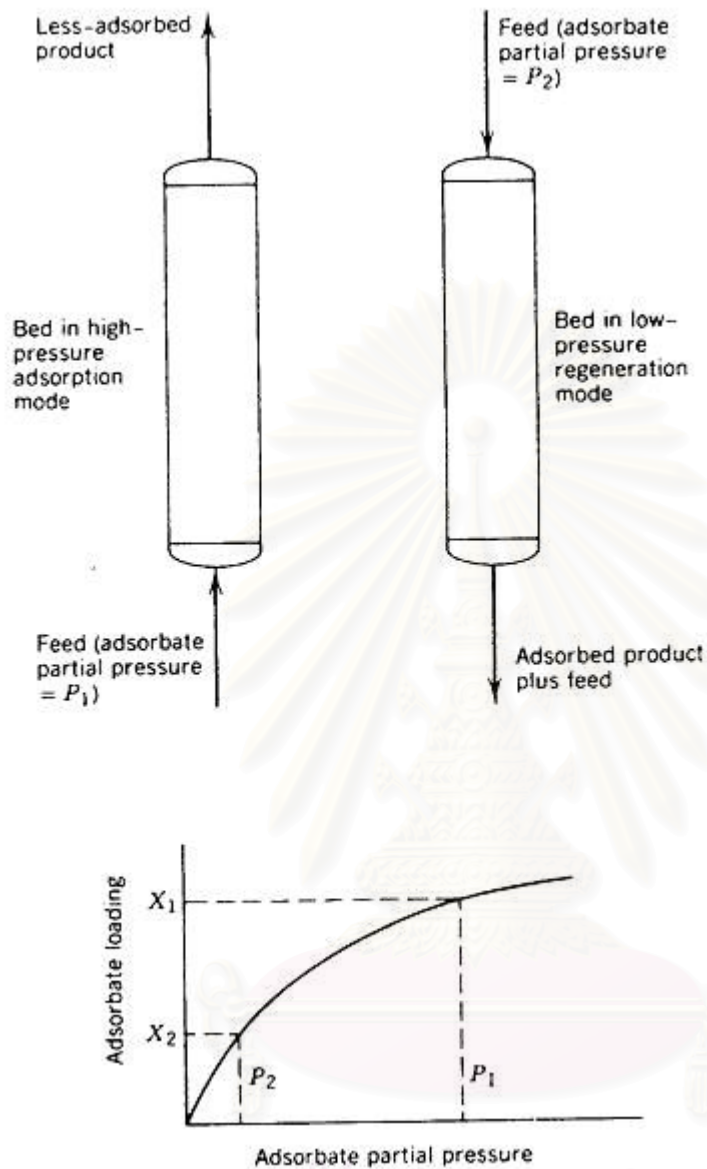
Figure 2.6 Schematic diagram of pressure swing adsorption cycle

2.7.2 Temperature swing adsorption (TSA)

Figure 2.7 provides a simple schematic diagram of a TSA process. The bed operates nearly isothermally during the adsorption step and a significant amount of heat, which is about the order of two to three times the heat of vaporization of the adsorbate is

released. During the regeneration step, the bed is heated, most often directly by a hot gas or steam rather than indirectly through the wall or via coils in the bed. The heat both warms the bed and supplies the energy necessary to desorb the adsorbate. The hot gas or steam not only provides heat but also dilutes the concentration of adsorbate in the fluid and thereby provides an additional incentive for desorption.

At the end of the regeneration step, a cool gas stream usually is fed for a short period to bring the bed back to the adsorption temperature. Extra steps are included when the feed is a liquid vapor phase.
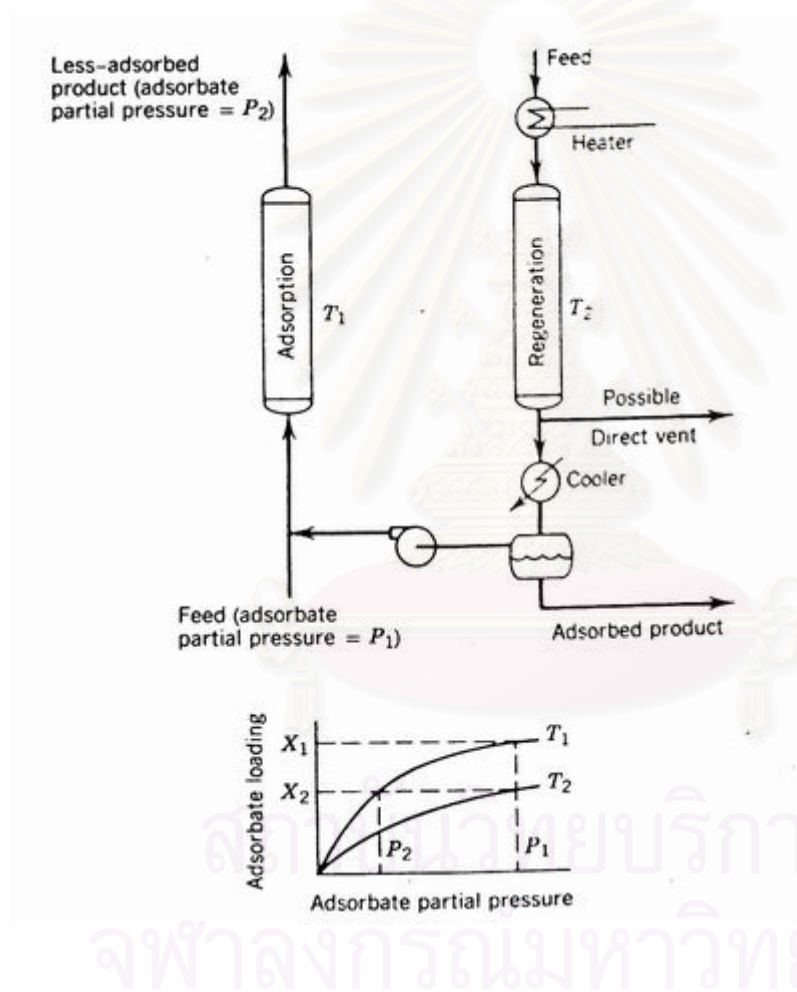
Figure 2.7 Schematic diagram of temperature swing adsorption cycle

2.7.3 Wheel temperature swing adsorption (Wheel TSA)

Heating and then cooling of an adsorbent bed require much more time than changing the pressure of the gas in contact with a bed as shown in Figure 2.8. Clearly, PSA

processes generally have cycle times of a few seconds to a few minutes, while TSA processes have ones of a few to many hours. This fact limits TSA processes to purifications because if adsorbate concentrations were high in the feed as they are in bulk separations, then the feed part of the cycle would be very short compared to the regeneration part. This would require a large number of beds in parallel, with all of the attendant economic handicaps. Accordingly, the new adsorbent-wheel processes, which are based on TSA have been developed to reduce the cycle time of TSA processes and to operate the processes continuously.
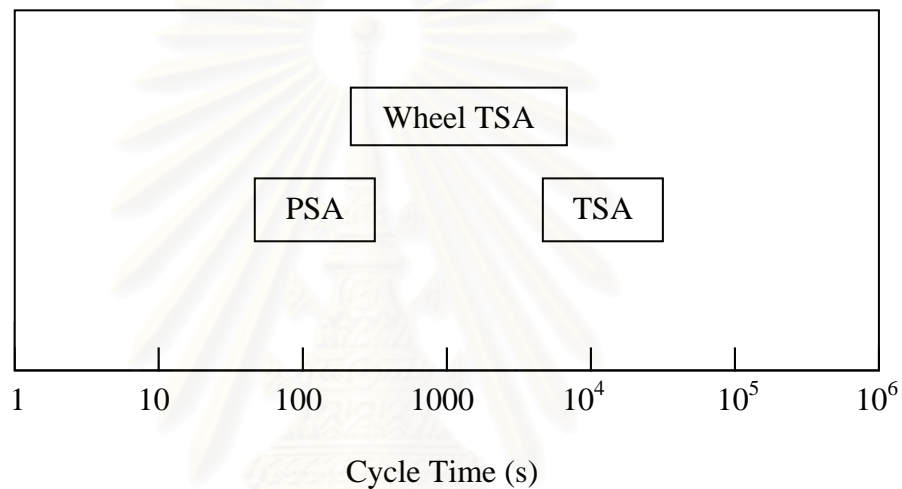
Figure 2.8 Comparison of cycle time of various adsorption processes (Keller II, 1995)

Figure 2.9 The series of the commercial rotary adsorber for dehumidification process manufactured by Munters Zeol AB of Sweden

A radically different approach to continuous adsorption processes also has been commercialized recently as shown in Figure 2.9. In it, the adsorbent is contained in a monolithic structure resembling a wheel or rotor as illustrated in Figure 2.10. The wheel rotates so that each segment passes through a zone in which adsorption takes place, and then through a second zone in which the adsorbent is heated, regenerated, and sometimes cooled down to the adsorption temperature before passing back into the adsorption zone. This second zone typically requires much less than half of the wheel's cycle. A purge gas, which can be either part of the purified gas or another gas, flows through the wheel during the regeneration part of the cycle. In typical processes, the adsorbate concentrating effect can be used to send a much more concentrated stream to an incinerator, or, alternatively, it may be possible in some cases to recover the adsorbate by condensing it from the purge-gas stream. If that stream still contains a significant amount of adsorbate after the condensation, then the purge-gas stream can be combined and fed with the feed gas to complete the removal.
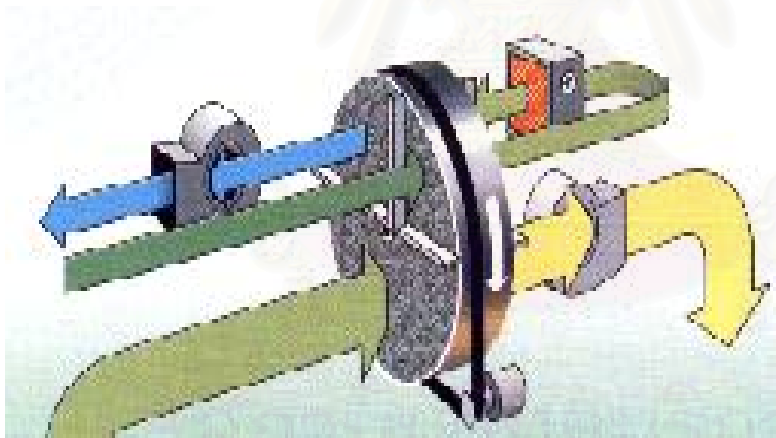
Figure 2.10 Schematic diagram of rotary adsorber

The diameters of commercial wheels range from about 0.2 m (~8 in.) to at least 4.2 m (nearly 14 ft). The largest wheels can process up to 60,000 m^3/h (2.1 million ft^3/h) of feed gas. Presently, the process is offered by Munters Zeol, Lurgi in Germany, and Seibu Giken Co., in Japan.

Adsorbent wheels, in addition to incorporating the process simplifications associated with continuous operation, have another major plus: a very low pressure drop – on the order of 0.2-0.4 kPa (about one in. of water). This feature often is very important in treating vent streams whose pressure is close to atmospheric, because the higher pressure drops that can occur in packed beds can lead to substantially higher investment and operating costs in compression equipment. Accordingly, adsorbent wheels primarily are used for removal of organic contaminants from vent streams – typical organic concentrations in streams fed to wheels are 1,000 ppm or less – and for dehumidification of air and other gases as illustrated in Figure 2.11.
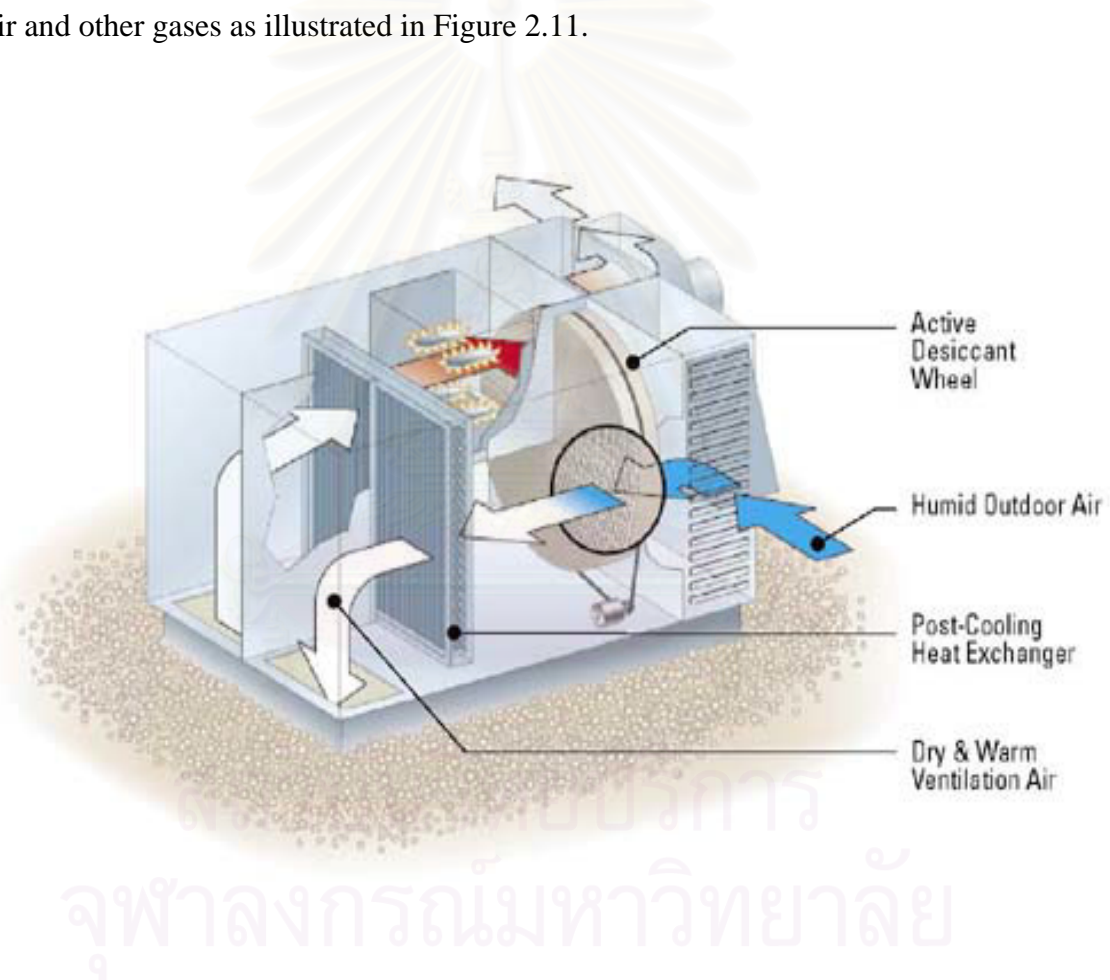
Figure 2.11 Schematic of dehumidification system consisting of rotary adsorber, blower and heat exchange

CHAPTER 3

LITERATURE REVIEW

A honeycomb rotary dehumidifier using solid adsorbent is the most widely employed in air-conditioning and industrial air-drying systems because the honeycomb shape of the adsorbent-coated rotor will increase the dynamic adsorption capacity and reduces the heat capacity for rapid thermal response. In addition, it allows a compact design and ensures minimal pressure drops. Consequently, many researchers have attempted to understand and improve the performance of the continuous rotary dehumidifier by adopting experimental and/or theoretical approaches.

3.1 Experimental study

A rotary dehumidifier was originally introduced by Munters et al. (1960). Subsequently, many researchers, e.g. Hemstreet (1967), Macris et al. (1977), Kuma et al. (1989), Masanori (1992) and Kodama et al. (1993,1994,1998), have developed and modified their production methods, the construction of honeycomb rotor, materials, and adsorption process to obtain high dehumidifying performance.

Hemstreet (1967) proposed adsorbent-coated thermal panels, specifically non-porous panels coated with thin layers of adsorbent adapted for rapid heating and cooling. The panels may be made of metal, preferably aluminum, stainless steel, or copper, coated with a molecular sieve zeolite. The adsorbent is bonded to the panel wall using an inorganic binder (e.g., a clay substantially free of any organic binder). In the case of zeolites, gases that can be adsorbed include water, carbon dioxide, and vaporized organic liquids (Hemstreet, 1967).

Macris et al. (1977) introduced the honeycomb rotor that consists of thin sheets or layers of fibrous material containing about 10 to 90% by weight of a finely divided crystalline X-type molecular sieve material for air cleaning purpose. For a four-compartmented rotor, moisture and one or more undesirable gases such as NO_x, SO_x and CO_2 are continuously adsorbed on the molecular sieve in compartment I to produce dry pollutant-free air. While hot air is passed counter flow through compartment II and III for regeneration, a portion of the clean air is passed through compartment IV in the opposite direction for cooling the rotor. Regeneration temperature for this system is in the range of 250-350 °F (121-176 °C) (Macris et al., 1977).

Kuma et al. (1989) extensively investigated the construction of a honeycomb that is coated with an adsorbent for removing the ultra-low concentration of an active gas, such as water vapor from air. The element is produced by laminating low density papers composed of inorganic fibers to form a matrix in the form of a gas adsorbing element having numerous small channels penetrating through opposite surfaces, impregnating the matrix with water glass in which type 4A synthesized zeolite powder is dispersed, and soaking the matrix in aqueous solution of aluminum salts, magnesium salts or calcium salts, and so on, to form metal silicate hydrogel on the paper and in the apertures between the fibers of the papers, finally washing and drying the matrix and the metal silicate hydrogel to obtain the honeycomb element. When the rotary dehumidifier was tested under various operating conditions, it was found that the optimal regeneration temperature is approximately 453 K to 473 K (Kuma et al., 1989).

Masanori (1992) focused on the improvement of the regeneration efficiency and on the long-term continuous use without lowering the dehumidifying performance by installing a cooling zone between the dehumidifying zone and the regeneration zone.

Kodama et al. (1993,1994,1998) investigated the optimal operation of a thermal-swing honeycomb rotor adsorber with a thin layer of silica gel as adsorbent. The effect of the rotational speed of the rotor on dehumidifying performance under various operating conditions was investigated in order to obtain an empirical correlation for the optimal rotational speed of the rotor. The results show that the optimal rotational speed depends on the bulk density of the rotor, the gas velocity through the regeneration zone and the width

of the rotor, and that the dehumidification efficiency can reach 80-90% at the optimal operating conditions (Kodama et al, 1993). In addition, the two-dimensional temperature profiles along the honeycomb axis and the rotational angle were extensively measured at various operating conditions in order to simultaneously investigate the adsorption and desorption phenomena (Kodama et al, 1994). Moreover, they applied the silica gel coated honeycomb rotary dehumidifier to an air conditioning system, which consists of a heat exchanger, heater and evaporative cooler. High efficiency of dehumidification was confirmed at a regeneration temperature as low as 353 K when the rotation speed or cycle time was adjusted to the optimal value (Kodama et al, 1995).

3.2 Modeling study

Since modeling and simulation are a handy and effective tool, attempts to predict efficiency, outlet conditions and energy consumption, and to understand the simultaneous heat and mass transfer phenomena using mathematical models have grown rapidly. Using the analogy from that of a thermal regenerator transferring heat alone, Maclaine-Cross and Banks (1972) and Banks (1985) could predict the dehumidifying performance of a rotary dehumidifier in which heat and mass transfer simultaneously occur. Equal overall transfer coefficients for heat and mass transfer as well as convective transfer controlling were assumed. For a heat recovery regenerator, the linear analogy method was shown to be satisfactory, while a nonlinear method was required for a rotary dehumidifier. In their analogy approach, the number of transfer units (NTU) of the dehumidifier was transformed into analogous dimensionless transfer coefficients (Maclaine-Cross and Banks and Banks (1972,1985)).

Jurinak et al. (1984) proposed an explicit-finite difference model of a counter-flow rotary dehumidifier for their investigation on the effect of matrix properties on dehumidifying performance. The matrix properties considered are the shape of the sorption isotherm, the maximum sorbent water content, the heat of sorption, the matrix thermal capacitance, matrix moisture diffusivity, and sorption isotherm hysteresis. The isotherm shapes and the sorption parametric values are selected to be representative of available insoluble desiccants. The results of the finite difference calculations show that the shape of the isotherm has a greater effect on dehumidification than the maximum water content, and

that hysteresis in the adsorption isotherm significantly impairs dehumidifier performance. Furthermore, a large adsorption heat effect or matrix thermal capacitance has a detrimental impact on dehumidification (Jurinak et al., 1984).

Van den Bulck et al. (1985, 1986) theoretically studied the model of rotary heat and mass exchangers with infinite and finite transfer coefficients. The continuity and energy conservation equations for one-dimensional transient flow were established and analyzed. For the ideal dehumidifier model, the overall heat and mass transfer coefficients are assumed to be infinite. Solutions to that case were obtained by both the method of characteristics and the shock wave method (Van den Bulck et al., 1985). Either method provided a set of analytical equations that allow performance prediction of the rotary dehumidifier with infinite transfer coefficients. In contrast, a finite-difference model was used to solve the equations for performance prediction of rotary dehumidifiers with finite transfer coefficients. Correlations of the moisture and enthalpy effectiveness of a silica gel rotary dehumidifier with finite transfer coefficients were given as functions of the number of transfer units (NTU). Moreover, they further investigated the use of rotary dehumidifiers in gas-fired open-cycle desiccant cooling systems by analyzing the performance of the rotary heat exchanger-rotary dehumidifier subsystem. The results show that the optimal values for rotational speed and regeneration flow rate are functions of the regeneration air inlet temperature and the process air inlet humidity ratio (Van den Bulck et al.,1986).

Worek et al. (1993,1995) proposed and applied an implicit-finite difference technique to the numerical simulation of a solid desiccant dehumidifier (Worek et al., 1993). The effect of the rotational speed on the performance of an adiabatic rotary dehumidifier was parametrically studied, and the optimal rotational speed was determined by examining the outlet adsorption-side humidity profiles and the humidity wave fronts inside the desiccant dehumidifier. It was found that there exists an optimum rotational speed for desiccant rotor operation. They further studied some advanced desiccant materials to improve the performance of the rotary dehumidifier and cooling systems. The effect of the isotherm shape, maximum desiccant matrix moisture, moisture uptake and number of transfer units, NTU, of the desiccant rotor on the dehumidification performance was investigated. It was found that the rotational speed is a key control parameter to achieve optimal dehumidifier performance (Worek et al., 1995).

Chant et al. (1995) alternatively applied a parabolic and a quartic concentration profile assumption to the model of the diffusion resistance inside the desiccant particle for the mass transfer rate equation. An implicit periodic steady-state solution for the parabolic concentration profile model with a linearized adsorption isotherm was developed, which utilized a sparse matrix solving routine to vastly reduce computational time. The quartic concentration profile assumption yielded a 2.8 percent average improvement in prediction error over the parabolic model (Chant et al., 1995).

Elsayed et al. (1997) proposed an alternative model to predict the steady periodic performance of a radial flow type rotary dehumidifier. The model was expressed in terms of the same dimensionless parameters that are commonly used in modeling the conventional axial flow type rotary dehumidifier. In addition, a dimensionless geometrical ratio of the volume of the matrix to the volume of the wheel core was found to affect the dehumidification performance of the wheel. An implicit finite difference technique employing a staggered grid was used to discretize the governing dimensionless equations. The discretized equations were solved to predict the performance of the rotary dehumidifier (Elsayed et al., 1997).

Tanthapanichkoon et al. (2000) developed a simple dynamic model consisting of a set of nonlinear ordinary differential equations for a honeycomb rotary absorption-type dehumidifier installed in a process room with wet floor. The 4-th order Runge Kutta method was used to integrate those equations simultaneously. The model was validated experimentally using the transient measurement data on the air properties at the outlets of both the dehumidification and regeneration sections in a beverage factory. Moreover, they extensively investigated the effects of the regeneration temperature, air velocity of the room and regeneration air, inlet room air humidity, rotational speed of the rotor, quantity of water remaining on the wet floor, and the condition of ambient air on the dehumidifying performance. The optimal operating condition was also determined by considering the dehumidifying efficiency, the energy consumption of the air heater and the time to dry out the wet floor overnight (Prawarnpit, 1997).

CHAPTER 4

MATHEMATICAL MODELING AND SIMULATION

4.1 Modeling concept for dynamic dehumidification system

Modeling of the dynamic dehumidification system in this work is divided to two categories, i.e. dehumidifier model and process room model. The dehumidifier model is used to predict and quantify in details the heat and mass transfer phenomena and to estimate the performance of various adsorbent-coated honeycomb rotary dehumidifiers, whereas the room model is employed to calculate the quantity of water remaining on the wet floor, the humidity and temperature of room air and so on. The two models may be simulated independently or coupled to simulate the dynamic dehumidification behavior in an industrial process room. The continuous dehumidification in a closed process room with wet floor in a beverage factory in Thailand has been investigated experimentally and theoretically with the aid of a simple dynamic model (Prawarnpit, 1997). In this case, the water remaining on the wet floor of the process room after cleaning and mopping is a main cause of humidity in the process room, in which the relative humidity should be controlled between 30-50%. In conclusion, the model of the dynamic dehumidification system may incorporate only the rotary dehumidifier model or the coupled dehumidifier-room model depending on the purpose and scope of investigation.

4.2 Mathematical model of a honeycomb rotary dehumidifier

An adsorption-type honeycomb rotary dehumidifier consisting of thin coats of an adsorbent such as silica gel, zeolite, etc., is to be modeled and simulated. The rotor is

typically divided into two sectors by two stationary partition plates as shown in Figure 4.1. One sector represents an adsorption zone ($0°$-$\theta°_{ads}$), in which moisture is removed from the feed air (recycled room air). The other represents a regeneration zone ($\theta°_{ads}$-$360°$), through which an ambient air stream heated by an external heat source is sent to regenerate the adsorbent coated on the interior walls of the honeycomb. The two air streams pass through the honeycomb rotor in counter flow paths. While the dehumidified air or dry air is supplied (recycled) to the air-conditioned space, the exhaust air from the regeneration sector is vented to the outdoor.
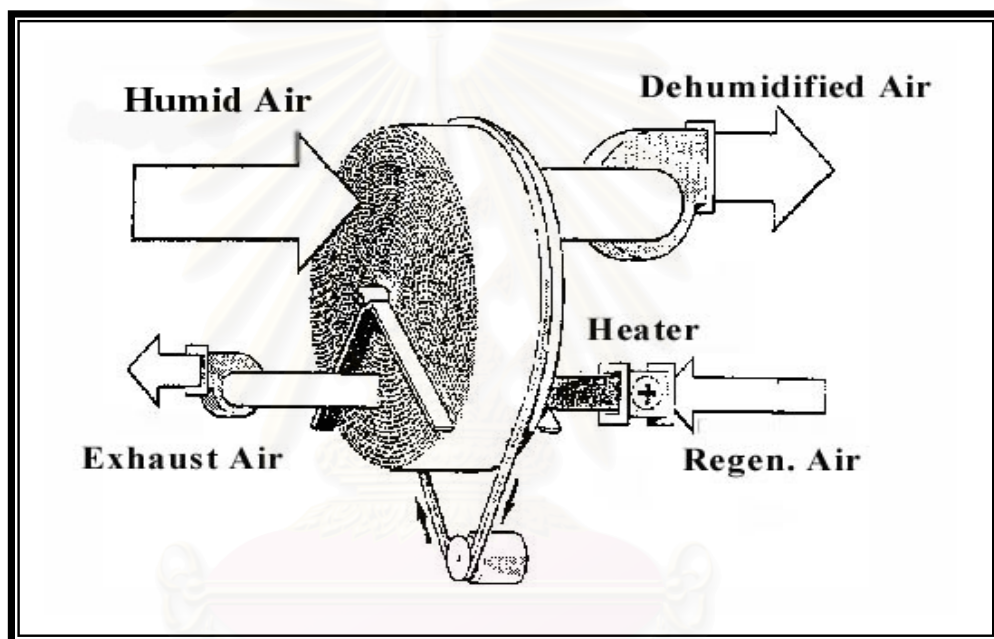
Figure 4.1 Schematic of a honeycomb rotary dehumidifier
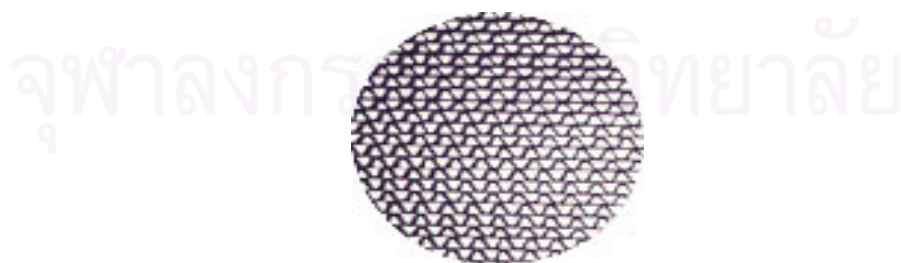
Figure 4.2 Schematic of an adsorbent coated honeycomb

As shown in Figure 4.2, the honeycomb rotor consists of thousands of essentially identical narrow straight slots uniformly distributed over its rotor cross section. Figure 4.3 illustrates the air stream flowing through a portion of the slots of a honeycomb rotor. Because of geometric similarity (see Figure 4.1), the multiple annular layers of straight slots in the dehumidification and the regeneration section can be represented performance-wise by a single "representative annulus" of thickness Δr equaling one slot height.

Figure 4.3 Schematic of the air stream flowing through the slots of a honeycomb rotor

In this way, the three cylindrical coordinates (r,θ,z), i.e., the radial, angular and axial directions, respectively, in the rotary dehumidifier model can rationally be reduced to two independent spatial coordinates (θ,z). By taking into account each constituent slot within the total M identical slots in the θ–direction spanning the entire cross section of the representative annulus, the remaining spatial variable is only z. For example, M = 120 slots with 90 consecutive slots of the rotating rotor representing the adsorption section and the remaining 30 slots representing the regeneration section. Of course, one more independent variable in the dynamic model is the time t. In other words, the dynamic behavior of the honeycomb rotary dehumidifier can be simulated by following the transient or dynamic changes occurring in the z-direction within each of the M slots as the rotor slowly turns.

4.2.1 Assumptions used in the rotary honeycomb dehumidifier model

For simplicity, the rotary dehumidifier model incorporates the following assumptions.

1. Dehumidified air flow is uniformly distributed across the adsorption cross-section, and so is the hot air across the regeneration cross-section.

2. The air stream flowing through each identical slot is assumed to be plug or piston flow. In the plug flow model, variation does not exist in the radial direction or the direction perpendicular to the slot flow, but exists only in the axial or z-direction. Theoretically and conceptually, the plug flow model can be and has been shown to be equivalent to the model of a series of equal-volume CSTR's in which an infinitely large number of completely mixed cells, each of infinitely small thickness, are connected in series. For practical reason, the plug flow model of each slot in this study will be approximated as a serial CSTR model consisting of N cells in series as shown in Figure 4.2, N being a sufficiently large integer of, say, 10, 20 or 30.

3. Gas-phase heat conduction and water vapor diffusion in the axial direction are negligibly small compared to their convective effects in the same slot.

4. Each slot is adiabatic and heat conduction in the axial direction along the slot wall may also be neglected.

5. Interphase moisture transfer rate between the gas and adjacent solid adsorbent phases in each slot is controlled by gas-phase film resistance. This is reasonable since the thickness of the adsorbent coat is quite thin and all internal pore volumes of the adsorbent are close to the gas-solid interface.

6. Enthalpy change of the moisture between the gas and liquid (adsorbed) phases is defined as heat of adsorption that can be estimated using Clausius-Clapeyron equation in conjunction with the equilibrium isotherm since partial pressure is a function of both temperature and adsorbed moisture.

A schematic diagram of a typical slot in the adsorption and regeneration sections of the honeycomb rotary dehumidifier model based on the above assumptions is shown in Figure 4.4.
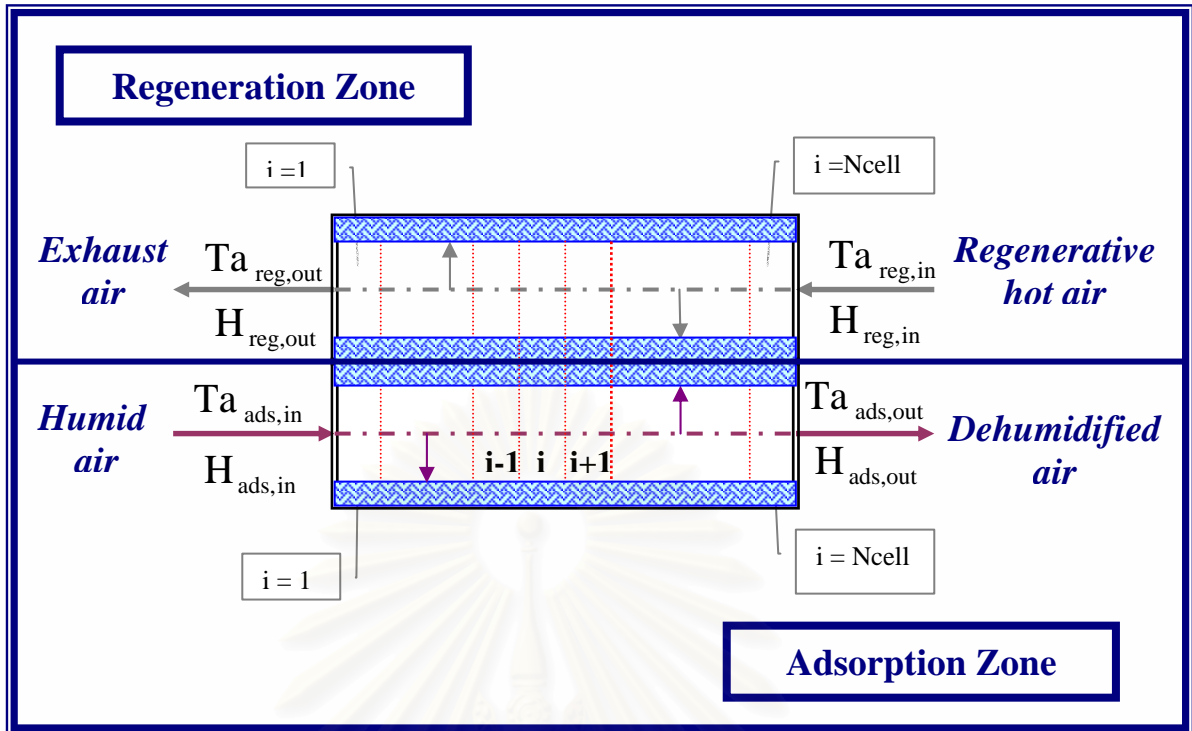
Figure 4.4 Schematic diagram of a representative slot of the honeycomb rotor in the adsorption and the regeneration zone

4.2.2 Moisture and enthalpy balances of the rotary dehumidifier model in the adsorption zone

Consider slot no. j in the adsorption zone. The unsteady-state moisture and enthalpy balances for cell no. i (i =1,2,…,N) in this particular slot are presented below. A schematic diagram of the interface mass and heat transfer in cell no. i of slot no. j in the adsorption zone is shown in Figure 4.5. For simplicity the subscript j for slot no. j is omitted here.
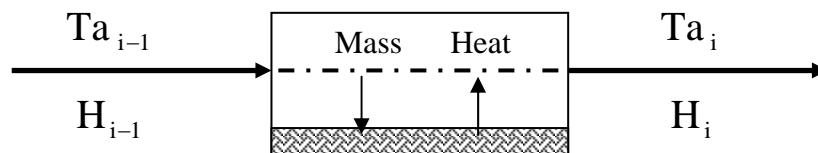
Figure 4.5 Schematic diagram of mass and heat transfer in cell no. i of slot no. j in the adsorption zone

4.2.2.1 Gas-phase moisture balance in cell no. i:

$$
\left\{
\begin{array}{c}
\text{Rate of} \\
\text{accumulation of} \\
\text{moisture within} \\
\text{gas phase of cell}
\end{array}
\right\}
=
\left\{
\begin{array}{c}
\text{Rate of} \\
\text{convective flow} \\
\text{of moisture into} \\
\text{gas phase of cell}
\end{array}
\right\}
-
\left\{
\begin{array}{c}
\text{Rate of convective} \\
\text{flow of moisture} \\
\text{out of gas phase} \\
\text{of cell}
\end{array}
\right\}
-
\left\{
\begin{array}{c}
\text{Rate of} \\
\text{adsorption of} \\
\text{moisture into solid} \\
\text{phase of cell}
\end{array}
\right\}
$$

$$
\frac{d}{dt}\left(\frac{1}{V_{H,i}}\left(\frac{\varepsilon A_c L}{N} \right) H_i \right) = \varepsilon A_c G_{i-1} H_{i-1} - \varepsilon A_c G_i H_i - R_{ads,i}\, \rho_{sb}\left(\frac{A_{ss} L}{N} \right) \tag{4.1}
$$

From mass conservation of dry air flow through the slot:

$$
\varepsilon A_c G_{i-1} = \varepsilon A_c G_i = \varepsilon A_c G_{in} \tag{4.2}
$$

Thus the flow rate of dry air for all cells is:

$$
G_{i-1} = G_i = G_{in} \tag{4.3}
$$

Substitute equation (4.3) in (4.1) and divide both sides of the equation by $\left(\dfrac{\varepsilon A_c L}{N} \right)$ to obtain

$$
\frac{d}{dt}\left(\frac{H_i}{V_{H,i}} \right) = \frac{NG_{in}}{L}\left(H_{i-1} - H_i \right) - R_{ads,i}\, \rho_{sb}\left(\frac{A_{ss}}{\varepsilon A_c} \right)
$$

$$
\left(\frac{1}{V_{H,i}}\frac{dH_i}{dt} - \frac{H_i}{V_{H,i}^2}\frac{dV_{H,i}}{dt} \right) = \frac{NG_{in}}{L}\left(H_{i-1} - H_i \right) - R_{ads,i}\, \rho_{sb}\left(\frac{A_{ss}}{\varepsilon A_c} \right)
$$

$$
\frac{dH_i}{dt} = \frac{V_{H,i}NG_{in}}{L}\left(H_{i-1} - H_i \right) - R_{ads,i}\, \rho_{sb}\left(\frac{V_{H,i} A_{ss}}{\varepsilon A_c} \right) + \frac{H_i}{V_{H,i}}\frac{dV_{H,i}}{dt} \tag{4.4}
$$

Since the gas film resistance is assumed to be the rate-controlling step, the rate of adsorption can be calculated as follows:

$$
R_{ads,i} = \frac{k_{c,i}\, a\left(H_i - H_{s,i} \right)}{\rho_{sb}} \tag{4.5}
$$

Replace $R_{ads,i}$ in equation (4.4) by (4.5) to get

$$\frac{dH_i}{dt} = \frac{V_{H,i}NG_{in}}{L}\left(H_{i-1} - H_i\right) - \frac{k_{c,i}aA_{ss}V_{H,i}}{\varepsilon A_c}\left(H_i - H_{s,i}\right) + \frac{H_i}{V_{H,i}}\frac{dV_{H,i}}{dt} \qquad (4.6)$$

4.2.2.2 Solid-phase moisture balance in cell no. i:

$$\left\{\begin{array}{c}\text{Rate of}\\\text{accumulation of}\\\text{moisture within}\\\text{solid phase of cell}\end{array}\right\} = \left\{\begin{array}{c}\text{Rate of convective}\\\text{flow of moisture}\\\text{into solid phase of}\\\text{cell}\end{array}\right\} - \left\{\begin{array}{c}\text{Rate of convective}\\\text{flow of moisture}\\\text{out of solid phase}\\\text{of cell}\end{array}\right\} + \left\{\begin{array}{c}\text{Rate of adsorption}\\\text{of moisture into}\\\text{solid phase of cell}\end{array}\right\}$$

$$\frac{d}{dt}\left(\rho_{sb}\left(\frac{A_{ss}L}{N}\right)W_i\right) = 0 - 0 + R_{ads,i}\rho_{sb}\left(\frac{A_{ss}L}{N}\right)$$

$$\frac{dW_i}{dt} = R_{ads,i} \qquad (4.7)$$

Making use of equation (4.5), the solid-phase moisture balance in cell no. i becomes

$$\frac{dW_i}{dt} = \frac{k_{c,i}a\left(H_i - H_{s,i}\right)}{\rho_{sb}} \qquad (4.8)$$

4.2.2.3 Gas-phase enthalpy balance in cell no. i :

$$\left\{\begin{array}{c}\text{Rate of accumulation}\\\text{of enthalpy within gas}\\\text{phase of cell}\end{array}\right\} = \left\{\begin{array}{c}\text{Rate of convective}\\\text{flow of enthalpy into}\\\text{gas phase of cell}\end{array}\right\} - \left\{\begin{array}{c}\text{Rate of convective}\\\text{flow of enthalpy out}\\\text{of gas phase of cell}\end{array}\right\}$$

$$+ \left\{\begin{array}{c}\text{Rate of heat transfer}\\\text{from solid phase to}\\\text{gas phase of cell}\end{array}\right\} - \left\{\begin{array}{c}\text{Rate of enthalpy transfer}\\\text{associated with mass}\\\text{transfer from gas phase to}\\\text{solid phase by adsorption}\end{array}\right\}$$

$$\frac{d}{dt}\left(\frac{1}{V_{H,i}}\left(\frac{\varepsilon A_c L}{N}\right)E_{a,i}\right) = \varepsilon A_c G_{i-1} E_{a,i-1} - \varepsilon A_c G_i E_{a,i} + h_{c,i} a\left(\frac{A_{ss} L}{N}\right)(T_{s,i} - T_{a,i})$$

$$- R_{ads,i} \rho_{sb} \Delta H_{ads,i}\left(\frac{A_{ss} L}{N}\right) \qquad (4.9)$$

Divide both sides of equation (4.9) by $\left(\dfrac{\varepsilon A_c L}{N}\right)$ and using the equation (4.3) to obtain

$$\frac{1}{V_{H,i}}\frac{dE_{a,i}}{dt} - \frac{E_{a,i}}{V_{H,i}^2}\frac{dV_{H,i}}{dt} = \left(\frac{NG_{in}}{L}\right)(E_{a,i-1} - E_{a,i}) + h_{c,i} a\left(\frac{A_{ss}}{\varepsilon A_c}\right)(T_{s,i} - T_{a,i})$$

$$- \left(\frac{\rho_{sb} A_{ss}}{\varepsilon A_c}\right)R_{ads,i} \Delta H_{ads,i} \qquad (4.10)$$

For the gas phase, the enthalpy term of the humid air consists of latent heat and sensible heat as follows:

$$E_{a,i} = \left(C_{p,da} + C_{p,v} H_i\right)\left(T_{a,i} - T_a^0\right) + \lambda_0 H_i \qquad (4.11)$$

Differentiation of the gas-phase energy term gives

$$\frac{dE_{a,i}}{dt} = \left(C_{p,da} + C_{p,v} H_i\right)\frac{dT_{a,i}}{dt} + \left(C_{p,v}\left(T_{a,i} - T_a^0\right) + \lambda_0\right)\frac{dH_i}{dt} \qquad (4.12)$$

From equations (4.11) and (4.12), equation (4.10) becomes

$$\left(\frac{C_{p,da} + C_{p,v} H_i}{V_{H,i}}\right)\frac{dT_{a,i}}{dt} + \left(\frac{C_{p,v}\left(T_{a,i} - T_a^0\right) + \lambda_0}{V_{H,i}}\right)\frac{dH_i}{dt}$$

$$- \left(\frac{\left(C_{p,da} + C_{p,v} H_i\right)\left(T_{a,i} - T_a^0\right) + \lambda_0 H_i}{V_{H,i}^2}\right)\frac{dV_{H,i}}{dt}$$

$$= \left(\frac{NG_{in}}{L}\right)\left(\left(C_{p,da}\right)\left(T_{a,i-1} - T_{a,i}\right) + C_{p,v}\left(H_{i-1}\left(T_{a,i-1} - T_a^0\right) - H_i\left(T_{a,i} - T_a^0\right)\right)\right)$$

$$+ h_{c,i} a\left(\frac{A_{ss}}{\varepsilon A_c}\right)\left(T_{s,i} - T_{a,i}\right) + \left(\frac{NG_{in}}{L}\right)\left(\lambda_0\left(H_{i-1} - H_i\right)\right) - \left(\frac{\rho_{sb} A_{ss}}{\varepsilon A_c}\right)R_{ads,i} \Delta H_{ads,i}$$

From equations (4.5) and (4.6), the above equation becomes

$$\left(\frac{C_{p,da}+C_{p,v}H_i}{V_{H,i}}\right)\frac{dT_{a,i}}{dt}+\left(\frac{NG_{in}}{L}\right)\!\left(C_{p,v}\left(T_{a,i}-T_a^0\right)+\lambda_0\right)\!\left(H_{i-1}-H_1\right)$$

$$-\left(\frac{k_{c,i}aA_{ss}}{\varepsilon A_c}\right)\!\left(C_{p,v}\left(T_{a,i}-T_a^0\right)+\lambda_0\right)\!\left(H_i-H_{s,i}\right)-\left(\frac{C_{p,da}\left(T_{a,i}-T_a^0\right)}{V_{H,i}^2}\right)\frac{dV_{H,i}}{dt}$$

$$=\left(\frac{NG_{in}}{L}\right)\!\left(\left(C_{p,da}\right)\!\left(T_{a,i\text{-}1}-T_{a,i}\right)+C_{p,v}\left(H_{i\text{-}1}\left(T_{a,i\text{-}1}-T_a^0\right)-H_i\left(T_{a,i}-T_a^0\right)\right)\right)$$

$$+\left(\frac{h_{c,i}aA_{ss}}{\varepsilon A_c}\right)\!\left(T_{s,i}-T_{a,i}\right)+\left(\frac{NG_{in}}{L}\right)\!\left(\lambda_0\left(H_{i-1}-H_i\right)\right)-\left(\frac{k_{c,i}aA_{ss}}{\varepsilon A_c}\right)\Delta H_{ads,i}\left(H_i-H_{s,i}\right)$$

$$\left(\frac{C_{p,da}+C_{p,v}H_i}{V_{H,i}}\right)\frac{dT_{a,i}}{dt}-\left(\frac{C_{p,da}\left(T_{a,i}-T_a^0\right)}{V_{H,i}^2}\right)\frac{dV_{H,i}}{dt}$$

$$=\left(\frac{NG_{in}}{L}\right)\!\left(C_{p,da}+C_{p,v}H_{i-1}\right)\!\left(T_{a,i\text{-}1}-T_{a,i}\right)+\left(\frac{h_{c,i}aA_{ss}}{\varepsilon A_c}\right)\!\left(T_{s,i}-T_{a,i}\right) \qquad (4.13)$$

$$-\left(\frac{k_{c,i}aA_{ss}}{\varepsilon A_c}\right)\!\left(\Delta H_{ads,i}-C_{p,v}\left(T_{a,i}-T_a^0\right)-\lambda_0\right)\!\left(H_i-H_{s,i}\right)$$

4.2.2.4 Solid-phase enthalpy balance in cell no i :

$$\left\{\begin{array}{c}\text{Rate of accumulation}\\\text{of enthalpy within}\\\text{solid phase of cell}\end{array}\right\}=\left\{\begin{array}{c}\text{Rate of convective}\\\text{flow of enthalpy into}\\\text{solid phase of cell}\end{array}\right\}-\left\{\begin{array}{c}\text{Rate of convective}\\\text{flow of enthalpy out}\\\text{of solid phase of cell}\end{array}\right\}$$

$$-\left\{\begin{array}{c}\text{Rate of heat transfer}\\\text{from solid phase to}\\\text{gas phase of cell}\end{array}\right\}+\left\{\begin{array}{c}\text{Rate of enthalpy transfer}\\\text{associated with mass}\\\text{transfer from gas phase to}\\\text{solid phase by adsorption}\end{array}\right\}$$

$$\frac{d}{dt}\!\left(\left(\frac{\rho_{ss}A_{ss}L}{N}\right)E_{ss,i}\right)=0-0-h_{c,i}a\!\left(\frac{A_{ss}L}{N}\right)\!\left(T_{s,i}-T_{a,i}\right)+R_{ads,i}\rho_{sb}\Delta H_{ads,i}\!\left(\frac{A_{ss}L}{N}\right) \quad (4.14)$$

Dividing both sides of the above equation by $\left(\dfrac{A_{ss}L}{N}\right)$ to obtain

$$\frac{d}{dt}\!\left(\rho_{ss}E_{ss,i}\right)=-h_{c,i}a\!\left(T_{s,i}-T_{a,i}\right)+R_{ads,i}\,\rho_{sb}\Delta H_{ads,i} \qquad (4.15)$$

For the solid phase, the enthalpy term of the adsorbent coated wall consists of sensible heat of the support, adsorbent and adsorbed moisture as follows:

$$E_{ss,i} = \left(\frac{\rho_{sh}}{\rho_{ss}} C_{p,sh} + \frac{\rho_{sb}}{\rho_{ss}} C_{p,sb} + \frac{\rho_{sb}}{\rho_{ss}} C_{p,w} W_i \right) \left(T_{s,i} - T_s^0 \right) \tag{4.16}$$

Using equation (4.16), equation (4.15) is rearranged as follows:

$$\frac{d}{dt} \left(\left(\rho_{sh} C_{p,sh} + \rho_{sb} \left(C_{p,sb} + C_{p,w} W_i \right) \right) \left(T_{s,i} - T_s^0 \right) \right) = -h_{c,i} a \left(T_{s,i} - T_{a,i} \right) + R_{ads,i} \, \rho_{sb} \Delta H_{ads}$$

$$\left(\rho_{sh} C_{p,sh} + \rho_{bh} \left(C_{p,sb} + C_{p,w} W_i \right) \right) \frac{d T_{s,i}}{dt} = -h_{c,i} a \left(T_{s,i} - T_{a,i} \right) + R_{ads,i} \, \rho_{sb} \Delta H_{ads,i}$$
$$- \left(\rho_{sb} C_{p,w} \right) \left(T_{s,i} - T_s^0 \right) \frac{dW_i}{dt}$$

Replace R_{ads} and $\dfrac{dW_i}{dt}$ by equation (4.5) and (4.8), respectively and the above equation becomes

$$\left(\rho_{sh} C_{p,sh} + \rho_{bh} \left(C_{p,sb} + C_{p,w} W_i \right) \right) \frac{d T_{s,i}}{dt} = \left(k_{c,i} a \right) \left(\Delta H_{ads,i} - C_{p,w} \left(T_{s,i} - T_s^0 \right) \right) \left(H_i - H_{s,i} \right)$$
$$- h_{c,i} a \left(T_{s,i} - T_{a,i} \right) \tag{4.17}$$

4.2.3 Moisture and enthalpy balances of the rotary dehumidifier in the regeneration zone
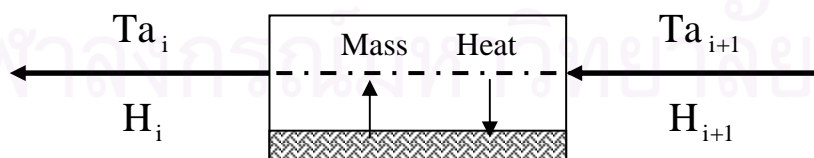
Figure 4.6 Schematic diagram of mass and heat transfer in cell no. i of slot no. j of the regeneration zone

Consider slot no. j in the regeneration zone. For simplicity the subscript j will be omitted throughout this section. Note that the air flow direction is reversed and cell no. I=1 means the outlet of a slot in this zone.

4.2.3.1 Gas-phase moisture balance in cell no. i:

$$\left\{\begin{array}{c}\text{Rate of} \\ \text{accumulation of} \\ \text{moisture within} \\ \text{gas phase of cell}\end{array}\right\} = \left\{\begin{array}{c}\text{Rate of} \\ \text{convective flow} \\ \text{of moisture into} \\ \text{gas phase of cell}\end{array}\right\} - \left\{\begin{array}{c}\text{Rate of} \\ \text{convective flow} \\ \text{of moisture out} \\ \text{of gas phase of} \\ \text{cell}\end{array}\right\} + \left\{\begin{array}{c}\text{Rate of} \\ \text{desorption of} \\ \text{moisture into gas} \\ \text{phase of cell}\end{array}\right\}$$

$$\frac{d}{dt}\left(\frac{1}{V_{H,i}}\left(\frac{\varepsilon A_c L}{N}\right)H_i\right) = \varepsilon A_c G_{i+1} H_{i+1} - \varepsilon A_c G_i H_i + R_{reg,i}\,\rho_{sb}\left(\frac{A_{ss}L}{N}\right) \tag{4.18}$$

Substitute equation (4.3) in (4.18) and divide both sides of the equation by $\left(\dfrac{\varepsilon A_c L}{N}\right)$ to obtain

$$\frac{d}{dt}\left(\frac{H_i}{V_{H,i}}\right) = \frac{NG_{in}}{L}\left(H_{i+1} - H_i\right) + R_{reg,i}\,\rho_{sb}\left(\frac{A_{ss}}{\varepsilon A_c}\right)$$

$$\left(\frac{1}{V_{H,i}}\frac{dH_i}{dt} - \frac{H_i}{V_{H,i}^2}\frac{dV_{H,i}}{dt}\right) = \frac{NG_{in}}{L}\left(H_{i+1} - H_i\right) + R_{reg,i}\,\rho_{sb}\left(\frac{A_{ss}}{\varepsilon A_c}\right)$$

$$\frac{dH_i}{dt} = \frac{V_{H,i}NG_{in}}{L}\left(H_{i+1} - H_i\right) + R_{reg,i}\,\rho_{sb}\left(\frac{V_{H,i}\,A_{ss}}{\varepsilon A_c}\right) + \frac{H_i}{V_{H,i}}\frac{dV_{H,i}}{dt} \tag{4.19}$$

Similar to the adsorption rate, the desorption rate can be calculated as follows:

$$R_{reg,i} = \frac{k_{c,i}a\left(H_{s,i} - H_i\right)}{\rho_{sb}} \tag{4.20}$$

Note that the values of $k_{c,i}$, $H_{s,i}$, etc. are different from that of the adsorption zone.

Replace $R_{reg,i}$ in equation (4.20) by (4.5) to get

$$\frac{dH_i}{dt} = \frac{V_{H,i}NG_{in}}{L}\left(H_{i+1} - H_i\right) + \frac{k_{c,i}aA_{ss}V_{H,i}}{\varepsilon A_c}\left(H_{s,i} - H_i\right) + \frac{H_i}{V_{H,i}}\frac{dV_{H,i}}{dt} \qquad (4.21)$$

4.2.3.2 Solid-phase moisture balance in cell no. i:

$$\left\{\begin{array}{c}\text{Rate of}\\\text{accumulation of}\\\text{moisture within}\\\text{solid phase of cell}\end{array}\right\} = \left\{\begin{array}{c}\text{Rate of convective}\\\text{flow of moisture}\\\text{into solid phase of}\\\text{cell}\end{array}\right\} - \left\{\begin{array}{c}\text{Rate of convective}\\\text{flow of moisture}\\\text{out of solid phase}\\\text{of cell}\end{array}\right\} - \left\{\begin{array}{c}\text{Rate of}\\\text{desorption of}\\\text{moisture from}\\\text{solid phase of cell}\end{array}\right\}$$

$$\frac{d}{dt}\left(\rho_{sb}\left(\frac{A_{ss}L}{N}\right)W_i\right) = 0 - 0 - R_{reg,i}\rho_{sb}\left(\frac{A_{ss}L}{N}\right)$$

$$\frac{dW_i}{dt} = -R_{reg,i} \qquad (4.22)$$

Using equation (4.20), the solid-phase moisture balance in cell no. i becomes

$$\frac{dW_i}{dt} = \frac{k_{c,i}a\left(H_i - H_{s,i}\right)}{\rho_{sb}} \qquad (4.23)$$

4.2.3.3 Gas-phase enthalpy balance in cell no. i :

$$\left\{\begin{array}{c}\text{Rate of accumulation}\\\text{of enthalpy within gas}\\\text{phase of cell}\end{array}\right\} = \left\{\begin{array}{c}\text{Rate of convective}\\\text{flow of enthalpy into}\\\text{gas phase of cell}\end{array}\right\} - \left\{\begin{array}{c}\text{Rate of convective}\\\text{flow of enthalpy out}\\\text{of gas phase of cell}\end{array}\right\}$$

$$- \left\{\begin{array}{c}\text{Rate of heat transfer}\\\text{from gas phase to}\\\text{solid phase of cell}\end{array}\right\} + \left\{\begin{array}{c}\text{Rate of enthalpy transfer}\\\text{associated with moisture}\\\text{transfer from solid phase to}\\\text{gas phase by desorption}\end{array}\right\}$$

$$\frac{d}{dt}\left(\frac{1}{V_{H,i}}\left(\frac{\varepsilon A_c L}{N}\right)E_{a,i}\right) = \varepsilon A_c G_{i+1}E_{a,i+1} - \varepsilon A_c G_i E_{a,i} - h_{c,i}a\left(\frac{A_{ss}L}{N}\right)\left(T_{a,i} - T_{s,i}\right)$$
$$+ R_{reg,i}\rho_{sb}\Delta H_{reg,i}\left(\frac{A_{ss}L}{N}\right) \qquad (4.24)$$

Divide both sides of equation (4.24) by $\left(\dfrac{\varepsilon A_c L}{N}\right)$ and make use of equation (4.3) to obtain

$$\frac{1}{V_{H,i}}\frac{dE_{a,i}}{dt} - \frac{E_{a,i}}{V_{H,i}^2}\frac{dV_{H,i}}{dt} = \left(\frac{NG_{in}}{L}\right)\left(E_{a,i+1} - E_{a,i}\right) - h_{c,i}a\left(\frac{A_{ss}}{\varepsilon A_c}\right)\left(T_{a,i} - T_{s,i}\right)$$
$$+ \left(\frac{\rho_{sb}A_{ss}}{\varepsilon A_c}\right)R_{reg,i}\Delta H_{reg,i} \tag{4.25}$$

From equations (4.11) and (4.12), equation (4.25) becomes

$$\left(\frac{C_{p,da} + C_{p,v}H_i}{V_{H,i}}\right)\frac{dT_{a,i}}{dt} + \left(\frac{C_{p,v}\left(T_{a,i} - T_a^0\right) + \lambda_0}{V_{H,i}}\right)\frac{dH_i}{dt}$$
$$- \left(\frac{\left(C_{p,da} + C_{p,v}H_i\right)\left(T_{a,i} - T_a^0\right) + \lambda_0 H_i}{V_{H,i}^2}\right)\frac{dV_{H,i}}{dt}$$
$$= \left(\frac{NG_{in}}{L}\right)\left(\left(C_{p,da}\right)\left(T_{a,i+1} - T_{a,i}\right) + C_{p,v}\left(H_{i+1}\left(T_{a,i+1} - T_a^0\right) - H_i\left(T_{a,i} - T_a^0\right)\right)\right)$$
$$- h_{c,i}a\left(\frac{A_{ss}}{\varepsilon A_c}\right)\left(T_{a,i} - T_{s,i}\right) + \left(\frac{NG_{in}}{L}\right)\left(\lambda_0\left(H_{i+1} - H_i\right)\right) + \left(\frac{\rho_{sb}A_{ss}}{\varepsilon A_c}\right)R_{reg,i}\Delta H_{reg,i}$$

From equations (4.5) and (4.6), the above equation becomes

$$\left(\frac{C_{p,da} + C_{p,v}H_i}{V_{H,i}}\right)\frac{dT_{a,i}}{dt} + \left(\frac{NG_{in}}{L}\right)\left(C_{p,v}\left(T_{a,i} - T_a^0\right) + \lambda_0\right)\left(H_{i+1} - H_1\right)$$
$$- \left(\frac{k_{c,i}aA_{ss}}{\varepsilon A_c}\right)\left(C_{p,v}\left(T_{a,i} - T_a^0\right) + \lambda_0\right)\left(H_i - H_{s,i}\right) - \left(\frac{C_{p,da}\left(T_{a,i} - T_a^0\right)}{V_{H,i}^2}\right)\frac{dV_{H,i}}{dt}$$
$$= \left(\frac{NG_{in}}{L}\right)\left(\left(C_{p,da}\right)\left(T_{a,i+1} - T_{a,i}\right) + C_{p,v}\left(H_{i+1}\left(T_{a,i+1} - T_a^0\right) - H_i\left(T_{a,i} - T_a^0\right)\right)\right)$$
$$+ \left(\frac{h_{c,i}aA_{ss}}{\varepsilon A_c}\right)\left(T_{s,i} - T_{a,i}\right) + \left(\frac{NG_{in}}{L}\right)\left(\lambda_0\left(H_{i+1} - H_i\right)\right) + \left(\frac{k_{c,i}aA_{ss}}{\varepsilon A_c}\right)\Delta H_{reg}\left(H_{s,i} - H_i\right)$$

$$\left(\frac{C_{p,da}+C_{p,v}H_i}{V_{H,i}}\right)\frac{dT_{a,i}}{dt}-\left(\frac{C_{p,da}\left(T_{a,i}-T_a^0\right)}{V_{H,i}^2}\right)\frac{dV_{H,i}}{dt}$$

$$=\left(\frac{NG_{in}}{L}\right)\left(C_{p,da}+C_{p,v}H_{i+1}\right)\left(T_{a,i+1}-T_{a,i}\right)+\left(\frac{h_{c,i}aA_{ss}}{\varepsilon A_c}\right)\left(T_{s,i}-T_{a,i}\right) \qquad (4.26)$$

$$-\left(\frac{k_{c,i}aA_{ss}}{\varepsilon A_c}\right)\left(\Delta H_{reg,i}-C_{p,v}\left(T_{a,i}-T_a^0\right)-\lambda_0\right)\left(H_i-H_{s,i}\right)$$

4.2.3.4 Solid-phase enthalpy balance in cell no i :

$$\left\{\begin{array}{c}\text{Rate of accumulation}\\\text{of enthalpy within}\\\text{solid phase of cell}\end{array}\right\}=\left\{\begin{array}{c}\text{Rate of convective}\\\text{flow of enthalpy into}\\\text{solid phase of cell}\end{array}\right\}-\left\{\begin{array}{c}\text{Rate of convective}\\\text{flow of enthalpy out}\\\text{of solid phase of cell}\end{array}\right\}$$

$$+\left\{\begin{array}{c}\text{Rate of heat transfer}\\\text{from gas phase to}\\\text{solid phase of cell}\end{array}\right\}-\left\{\begin{array}{c}\text{Rate of enthalpy transfer}\\\text{associated with moisture}\\\text{transfer from solid phase to}\\\text{gas phase by desorption}\end{array}\right\}$$

$$\frac{d}{dt}\left(\left(\frac{\rho_{ss}A_{ss}L}{N}\right)E_{ss,i}\right)=0-0+h_{c,i}a\left(\frac{A_{ss}L}{N}\right)\left(T_{a,i}-T_{s,i}\right)-R_{reg,i}\rho_{sb}\Delta H_{reg,i}\left(\frac{A_{ss}L}{N}\right) \qquad (4.27)$$

Divide both sides of the above equation by $\left(\dfrac{A_{ss}L}{N}\right)$ to obtain

$$\frac{d}{dt}\left(\rho_{ss}E_{ss,i}\right)=h_{c,i}a\left(T_{a,i}-T_{s,i}\right)-R_{reg,i}\,\rho_{sb}\Delta H_{reg,i} \qquad (4.28)$$

Making use of equation (4.16), equation (4.28) is rearranged as follows:

$$\frac{d}{dt}\left(\left(\rho_{sh}C_{p,sh}+\rho_{sb}\left(C_{p,sb}+C_{p,w}W_i\right)\right)\left(T_{s,i}-T_s^0\right)\right)=-R_{reg,i}\,\rho_{sb}\Delta H_{reg,i}+h_{c,i}a\left(T_{a,i}-T_{s,i}\right)$$

$$\left(\rho_{sh}C_{p,sh}+\rho_{bh}\left(C_{p,sb}+C_{p,w}W_i\right)\right)\frac{dT_{s,i}}{dt}=-R_{reg,i}\,\rho_{sb}\Delta H_{reg,i}+h_{c,i}a\left(T_{a,i}-T_{s,i}\right)$$

$$-\left(\rho_{sb}C_{p,w}\right)\left(T_{s,i}-T_s^0\right)\frac{dW_i}{dt}$$

Replace R_{reg} and $\dfrac{dW_i}{dt}$ by equations (4.5) and (4.8), respectively, the above equation

becomes

$$\left(\rho_{sh}C_{p,sh} + \rho_{bh}\left(C_{p,sb} + C_{p,w}W_i\right)\right)\frac{dT_{s,i}}{dt} = \left(k_{c,i}a\right)\left(\Delta H_{reg,i} - C_{p,w}\left(T_{s,i} - T_s^0\right)\right)\left(H_i - H_{s,i}\right)$$
$$- h_{c,i}a\left(T_{s,i} - T_{a,i}\right) \qquad (4.29)$$

4.3 Mathematical model for air circulation in a process room

The process room in the above-mentioned beverage factory, including the process equipment in the room, is washed and cleaned up at the end of each work day. Then the room is closed and the dehumidifier units are left to run overnight in order to dry up all water layer remaining on the wet floor by the start of the following work day. As dehumidified room air circulates through the process room, it picks up moisture from the wet concrete floor, thus gradually drying out the floor. Air circulation during the night inside the closed room can be approximated as a series of K_R imaginary completely mixed compartments ($K_R = 2\sim4$). Here R is the number of imaginary compartments in the process room. A schematic diagram of the two-coupled models, the rotary dehumidifier and process room model, is given in Figure 4.7.
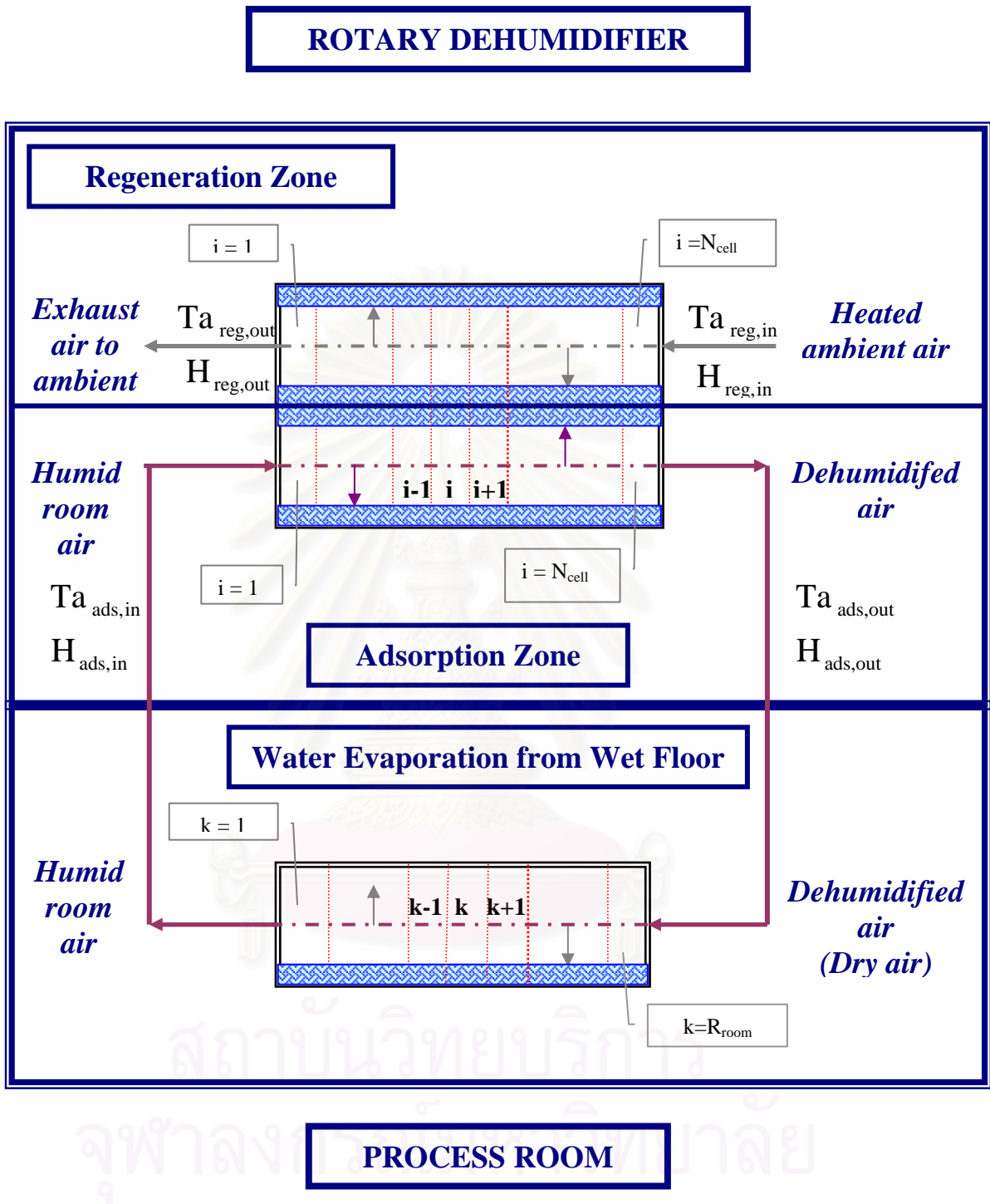
Figure 4.7 Schematic diagram of the rotary dehumidifier (showing a representative slot of each zone) and the process room

4.3.1 Assumptions used in the process room model

For simplicity, the process room model is based on the following assumptions.

1. The flow pattern and mixing effect of room air circulation in the closed process room are equivalent to a series of R imaginary completely mixed compartments. Typically, R is an integer between 2 and 4, though any suitable integer larger then 2 may be used. Dehumidified air from the rotary dehumidifier enters the Rth compartment. After picking up moisture from the wet floor in each compartment, the humid room air in compartment no.1 returns to the adsorption section of the rotary dehumidifier.

2. Gas-phase heat conduction and moisture diffusion in the air flow direction are negligibly small compared to the convective effects.

3. Each room compartment is adiabatic and heat conduction along the floor, ceiling and room walls may be neglected.

4.3.2 Moisture and enthalpy balances in the process room
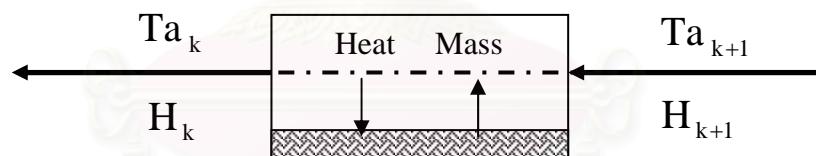
Figure 4.8 Mass and heat transfer for cell no. k of the humid room

Consider compartment no.k of the process room. Figure 4.8 illustrates simultaneous heat and mass transfer in this compartment.

4.3.2.1 Gas-phase moisture balance in compartment no. k:

$$\left\{\begin{array}{c}\text{Rate of accumulation}\\\text{of moisture within gas}\\\text{phase of compartment}\end{array}\right\}=\left\{\begin{array}{c}\text{Rate of flow}\\\text{of moisture}\\\text{into gas phase}\\\text{of compartment}\end{array}\right\}-\left\{\begin{array}{c}\text{Rate of flow}\\\text{of moisture}\\\text{out of gas phase}\\\text{of compartment}\end{array}\right\}+\left\{\begin{array}{c}\text{Rate of water}\\\text{evaporation into}\\\text{gas phase of}\\\text{compartment}\end{array}\right\}$$

$$\frac{d}{dt}\left(\frac{1}{V_{H_k}}\left(\frac{A_R L_R}{K_R}\right)H_k\right) = A_R G_{k+1} H_{k+1} - A_R G_k H_k + R_k\left(\frac{A_f}{K_R}\right) \tag{4.30}$$

From mass conservation of dry air flow through the process room:

$$A_R G_{k+1} = A_R G_k = A_R G_{in} \tag{4.31}$$

Thus the flow rate of dry air for all compartments is:

$$G_{k-1} = G_k = G_{in} \tag{4.32}$$

Substitute equation (4.32) in (4.30) and divide both sides of the equation by $\left(\dfrac{A_R L_R}{K_R}\right)$ to obtain

$$\frac{d}{dt}\left(\frac{H_k}{V_{H_k}}\right) = \frac{K_R G_{in}}{L_R}\left(H_{k+1} - H_k\right) + R_k\left(\frac{A_f}{A_R L_R}\right)$$

$$\left(\frac{1}{V_{H_k}}\frac{dH_k}{dt} - \frac{H_k}{V_{H_k}^2}\frac{dV_{H_k}}{dt}\right) = \frac{K_R G_{in}}{L_R}\left(H_{k+1} - H_k\right) + R_k\left(\frac{A_f}{A_R L_R}\right)$$

$$\frac{dH_k}{dt} = \frac{V_{H_k} K_R G_{in}}{L_R}\left(H_{k+1} - H_k\right) + R_k\left(\frac{V_{H_k} A_f}{A_R L_R}\right) + \frac{H_k}{V_{H_k}}\frac{dV_{H_k}}{dt} \tag{4.33}$$

Rate of evaporation of water on the floor is given as follow:

$$R_k = k_{c,k}\left(H_{w,k} - H_k\right) \cdot f(W_k) \tag{4.34}$$

Here $f(W_k)$ is defined in section 4.3.3. Then

$$\frac{dH_k}{dt} = \frac{V_{H_k} K_R G_{in}}{L_R}\left(H_{k+1} - H_k\right) + \left(\frac{k_{c,k} V_{H_k} A_f}{A_R L_R}\right)\left(H_{w,k} - H_k\right) \cdot f(W_k) + \frac{H_k}{V_{H_k}}\frac{dV_{H_k}}{dt} \tag{4.35}$$

4.3.2.2 Liquid-phase (floor) moisture balance in compartment no. k:

$$\left\{ \begin{array}{c} \text{Rate of} \\ \text{accumulation of} \\ \text{moisture within} \\ \text{liquid phase of} \\ \text{compartment} \end{array} \right\} = \left\{ \begin{array}{c} \text{Rate of flow} \\ \text{of moisture} \\ \text{into liquid phase} \\ \text{of compartment} \end{array} \right\} - \left\{ \begin{array}{c} \text{Rate of flow} \\ \text{of moisture} \\ \text{out of liquid phase} \\ \text{of compartment} \end{array} \right\} - \left\{ \begin{array}{c} \text{Rate of water} \\ \text{evaporation into} \\ \text{gas phase of} \\ \text{compartment} \end{array} \right\}$$

$$\frac{dW_k}{dt} = 0 - 0 - R_k$$

$$\frac{dW_k}{dt} = -R_k \tag{4.36}$$

Using the equation (4.34), the liquid-phase moisture balance in compartment no. k is

$$\frac{dW_k}{dt} = -k_{c,k}\left(H_{w,k} - H_k\right) \cdot f(W_k) \tag{4.37}$$

4.3.1.3 Gas-phase enthalpy balance in compartment no. k :

$$\left\{ \begin{array}{c} \text{Rate of} \\ \text{accumulation of} \\ \text{enthalpy within} \\ \text{gas phase of} \\ \text{compartment} \end{array} \right\} = \left\{ \begin{array}{c} \text{Rate of convective} \\ \text{flow of enthalpy} \\ \text{into gas phase of} \\ \text{compartment} \end{array} \right\} - \left\{ \begin{array}{c} \text{Rate of convective} \\ \text{flow of enthalpy out} \\ \text{of gas phase of} \\ \text{compartment} \end{array} \right\}$$

$$+ \left\{ \begin{array}{c} \text{Enthalpy gain} \\ \text{associated with the} \\ \text{evaporation of water} \\ \text{into gas phase of} \\ \text{compartment} \end{array} \right\} - \left\{ \begin{array}{c} \text{Rate of heat} \\ \text{transfer from gas} \\ \text{phase to liquid} \\ \text{phase of} \\ \text{compartment} \end{array} \right\}$$

$$\frac{d}{dt}\left(\frac{1}{V_{H_k}}\left(\frac{A_R L_R}{K_R} \right) E_{a,k} \right) = A_R G_{k+1} E_{a,k+1} - A_R G_k E_{a,k} + R_k \lambda_w \left(\frac{A_f}{K_R} \right)$$

$$- h_R \left(\frac{A_f}{K_R} \right)\left(T_{a,k} - T_{w,k} \right) \tag{4.38}$$

Divide both sides of the equation (4.35) by $\left(\dfrac{A_R L_R}{K_R} \right)$ and make use of equation (4.32) to

obtain

$$\frac{1}{V_{H_k}}\frac{dE_{a,k}}{dt} - \frac{E_{a,k}}{V_{H_k}^2}\frac{dV_{H_k}}{dt} = \left(\frac{K_R G_{in}}{L_R}\right)\left(E_{a,k+1} - E_{a,k}\right) + \left(\frac{R_k A_f \lambda_w}{A_R L_R}\right)$$
$$+ \left(\frac{A_f h_R}{A_R L_R}\right)\left(T_{w,k} - T_{a,k}\right) \tag{4.39}$$

For the gas phase, the enthalpy term of the humid room air consists of latent heat and sensible heat as follows:

$$E_{a,k} = \left(C_{p,da} + C_{p,v} H_k\right)\left(T_{a,k} - T_a^0\right) + \lambda_0 H_k \tag{4.40}$$

Differentiation of the gas-phase enthalpy term gives

$$\frac{dE_{a,k}}{dt} = \left(C_{p,da} + C_{p,v} H_k\right)\frac{dT_{a,k}}{dt} + \left(C_{p,v}\left(T_{a,k} - T_a^0\right) + \lambda_0\right)\frac{dH_k}{dt} \tag{4.41}$$

From equations (4.40) and (4.41), equation (4.39) becomes

$$\left(\frac{C_{p,da} + C_{p,v} H_k}{V_{H_k}}\right)\frac{dT_{a,k}}{dt} + \left(\frac{C_{p,v}\left(T_{a,k} - T_a^0\right) + \lambda_0}{V_{H_k}}\right)\frac{dH_k}{dt}$$
$$- \left(\frac{\left(C_{p,da} + C_{p,v} H_k\right)\left(T_{a,k} - T_a^0\right) + \lambda_{0,} H_k}{V_{H_k}^2}\right)\frac{dV_{H_k}}{dt}$$
$$= \left(\frac{K_R G_{in}}{L_R}\right)\left(\left(C_{p,da}\right)\left(T_{a,k+1} - T_{a,k}\right) + C_{p,v}\left(H_{k+1}\left(T_{a,k+1} - T_a^0\right) - H_k\left(T_{a,k} - T_a^0\right)\right)\right)$$
$$+ \left(\frac{K_R G_{in}}{L_R}\right)\left(\lambda_0\left(H_{k+1} - H_k\right)\right) + \left(\frac{R_k A_f \lambda_w}{A_R L_R}\right) + \left(\frac{h_R A_f}{A_R L_R}\right)\left(T_{w,k} - T_{a,k}\right)$$

From equation (4.35), the above equation becomes

$$\left(\frac{C_{p,da} + C_{p,v} H_k}{V_{H_k}}\right)\frac{dT_{a,k}}{dt} - \left(\frac{C_{p,da}\left(T_{a,k} - T_a^0\right)}{V_{H_k}^2}\right)\frac{dV_{H_k}}{dt}$$
$$= \left(\frac{K_R G_{in}}{L_R}\right)\left(\left(C_{p,da} + C_{p,v} H_{k+1}\right)\left(T_{a,k+1} - T_{a,k}\right)\right) + \left(\frac{h_R A_f}{A_R L_R}\right)\left(T_{w,k} - T_{a,k}\right) \tag{4.42}$$
$$+ \left(\frac{R_k A_f}{A_R L_R}\right)\left(\lambda_w - \lambda_0 - C_{p,v}\left(T_{a,k} - T_a^0\right)\right)$$

The enthalpy of hot air can be computed using the relation of ideal mixed gas as follows:

$$\lambda_0 + C_{p,v} T_{a,k} = C_{p,w} T_{w,k} + \lambda_w + C_{p,v}\left(T_{a,k} - T_{w,k}\right) \tag{4.43}$$

Therefore,

$$
\left(\frac{C_{p,da} + C_{p,v} H_k}{V_{H_k}}\right)\frac{dT_{a,k}}{dt} - \left(\frac{C_{p,da}\left(T_{a,k} - T_a^0\right)}{V_{H_k}^2}\right)\frac{dV_{H_k}}{dt}
$$
$$
= \left(\frac{K_R G_{in}}{L_R}\right)\left(\left(C_{p,da} + C_{p,v} H_{k+1}\right)\left(T_{a,k+1} - T_{a,k}\right)\right) + \left(\frac{h_R A_f}{A_R L_R}\right)\left(T_{w,k} - T_{a,k}\right) \tag{4.44}
$$
$$
- \left(\frac{R_k A_f}{A_R L_R}\right)\left(C_{p,w} T_{w,k} + C_{p,v}\left(T_{a,k} - T_{w,k}\right)\right)
$$

From equation (4.34), the above equation is rearranged as follows:

$$
\left(\frac{C_{p,da} + C_{p,v} H_k}{V_{H_k}}\right)\frac{dT_{a,k}}{dt} - \left(\frac{C_{p,da}\left(T_{a,k} - T_a^0\right)}{V_{H_k}^2}\right)\frac{dV_{H_k}}{dt}
$$
$$
= \left(\frac{K_R G_{in}}{L_R}\right)\left(\left(C_{p,da} + C_{p,v} H_{k+1}\right)\left(T_{a,k+1} - T_{a,k}\right)\right) + \left(\frac{h_R A_f}{A_R L_R}\right)\left(T_{w,k} - T_{a,k}\right) \tag{4.45}
$$
$$
- \left(\frac{k_{c,k} A_f}{A_R L_R}\right)\left(C_{p,w} T_{w,k} + C_{p,v}\left(T_{a,k} - T_{w,k}\right)\right)\left(H_{w,k} - H_k\right) \cdot f\left(W_k\right)
$$

4.3.2.4 Liquid-phase enthalpy balance in compartment no. k :

$$
\left\{\begin{array}{c}\text{Rate of}\\ \text{accumulation of}\\ \text{enthalpy within}\\ \text{liquid phase of}\\ \text{compartment}\end{array}\right\} = \left\{\begin{array}{c}\text{Rate of convective}\\ \text{flow of enthalpy}\\ \text{into liquid phase of}\\ \text{compartment}\end{array}\right\} - \left\{\begin{array}{c}\text{Rate of convective}\\ \text{flow of enthalpy out}\\ \text{of liquid phase of}\\ \text{compartment}\end{array}\right\}
$$
$$
- \left\{\begin{array}{c}\text{Enthalpy loss}\\ \text{associated with the}\\ \text{evaporation of water}\\ \text{out of liquid phase of}\\ \text{compartment}\end{array}\right\} + \left\{\begin{array}{c}\text{Rate of heat}\\ \text{transfer from gas}\\ \text{phase to liquid}\\ \text{phase of}\\ \text{compartment}\end{array}\right\}
$$

$$\frac{d}{dt}\left(E_{w,k}\right) = -R_k\left(\lambda_w\right) + h_{R,k}\left(T_{a,k} - T_{w,k}\right) \tag{4.46}$$

Where
$$E_{w,k} = C_{p,w} W_k \left(T_{w,k} - T_w^0\right) \tag{4.47}$$

So,
$$\frac{dE_{w,k}}{dt} = C_{p,w} W_k \frac{dT_{w,k}}{dt} + C_{p,w}\left(T_{w,k} - T_w^0\right)\frac{dW_k}{dt} \tag{4.48}$$

$$C_{p,w} W_k \frac{dT_{w,k}}{dt} + C_{p,w}\left(T_{w,k} - T_w^0\right)\frac{dW_k}{dt} = -R_k\left(\lambda_w\right) + h_R\left(T_{a,k} - T_{w,k}\right) \tag{4.49}$$

Using equations (4.34) and (4.37) gives

$$C_{p,w} W_k \frac{dT_{w,k}}{dt} = -k_{c,k}\left(\lambda_w - C_{p,w}\left(T_{w,k} - T_w^0\right)\right)\left(H_{w,k} - H_k\right)\cdot f\left(W_k\right) + h_R\left(T_{a,k} - T_{w,k}\right) \tag{4.50}$$

4.3.3 Evaporation rate of water remaining on the wet floor of the process room

A function $f(W_k)$ is used to define the evaporation rate in compartment no. k. If evaporation occurs at a constant rate, then we define

$$f(W_k) = 1 \tag{4.51}$$

If evaporation occurs at a falling rate, then $f\left(W_k\right)$ is defined as follows:

$$f\left(W_k\right) = \left(\frac{W_k - W_E}{W_C - W_E}\right) \qquad W_E < W_k < W_C \tag{4.52}$$

If no more water remains on the floor, then we define

$$f(W_k) = 0 \tag{4.53}$$

4.4 Simulation algorithm for the present dynamic dehumidification system

Simulation is a powerful technique for solving a wide variety of problems. To simulate is to imitate the behavior of a system or phenomenon under study. The basic idea behind dynamic simulation is simple, namely, to model the given system by means of mathematical equations, and then determine its time-dependent behavior. The simplicity of the approach, when combined with the computational power of a high-speed digital computer, makes simulation a powerful tool. Normally, simulation is used when either an exact analytic expression for the behavior of the system under investigation is not available, or the analytic solution is to time-consuming or costly to obtain.

In this section the simulation algorithm for determining the simultaneous heat and mass transfer phenomena of the rotary honeycomb dehumidifier is presented and its simplified flow chart is illustrated in Figures 4.9 through 4.11. The simulation is carried out according to the following steps:

1. Input data, including values of relevant parameters, i.e. properties of air, adsorbent, dehumidifier and process room, as well as the inlet and initial conditions, i.e. humidity, temperature and amount of adsorbed water in the adsorption and regeneration sections.
2. Display the values of parameters, inlet and initial conditions on the screen and write them on to a designated file.
3. For the investigation on combined air dehumidification and floor moisture removal in a process room, the amount of adsorbed water in the solid-phase, solid-phase temperature, air humidity and air temperature of both the adsorption and regeneration zones of the rotary dehumidifier model as well as the quantity of water remaining on the floor, temperature of water on the floor, air humidity and air temperature in the process room of the room model are simultaneously integrated for a small time step using the 4-th order Runge-Kutta method. In this step, the set of $4(N \cdot M_{slot}+R)$ ordinary differential equations consisting of equations (4.6), (4.8), (4.13) and (4.17) for the $(N \cdot M_{ads})$ cells in the adsorption zone, equations (4.21), (4.23), (4.26) and (4.29) for the $(N \cdot M_{reg})$ cells in the

regeneration zone and equations (4.35), (4.37), (4.45) and (4.50) for the R compartments of the process room are integrated simultaneously. However, if the investigation focuses only on the isolated operation of the rotary dehumidifier, this integration process will be the same as the above except that the room model will be excluded from the calculation. In short, the 4-th order Runge-Kutta method is used to integrate the set of $4(N \cdot M_{slot})$ equations simultaneously.

4. Calculate the thermal energy input to the heater, which is required to heat the ambient air to the desired temperature in the regeneration process, as well as calculate the cumulative energy consumption.

5. Check if it is the time to display the results. If it is, go to the next step. If not, skip to step 7.

6. Write the output data onto the designated file.

7. Check if it is time to rotate the honeycomb. If it is the time instant for slot rotation, go to the next step. If not, skip to step 9.

8. Slot no. j will rotate to replace the next slot j+1 successively in circle (j = 1,2,…,M_{slot}-1), and finally slot no. M_{slot} will replace slot no.1.

9. Check if it is time to display additional results. If it is, go to next step. If not, skip to step 11.

10. Write the output data after slot rotation onto the file and also display air humidity and temperature on the screen.

11. If the final time has been reached, the simulation is ended. Otherwise, return to step 3 after calculating the derivative values of the specific volume of the air in the rotary dehumidifier and process room, respectively.

It should be noted that a sufficiently small but not excessively small integration time stepsize should be used since the present RUNGE subroutine uses only a fixed stepsize. However, the stepsize must also be chosen so that the linear distance traveled by the rotor will exactly equal the size of a honeycomb slot after an integer number of time steps. In addition the total number of slots in the representative annulus of the honeycomb rotor must not be less than 50 or 60. The higher the total number of slots, the more accurate the simulation results become. However, the required computational time will be nearly proportional to the total slot number.

MAIN PROGRAM

```
                    ( START )
                        |
                        v
     Read parameters, inlet and initial
                conditions
                        |
                        v
    Print parameters, inlet and initial data
      on screen and write them onto file
                        |
                        v
                   icount = 0
                        |
   (2) ----------------> |
                         v
              t  = t0 + (icount)dt
                        |
                        v
                  CALL  RUNGE
                        |
                        v
                 < t = tprint? > ---- No
                        |
                       Yes
                        |
                        v
      Write output data, i.e. air temperature,
      humidity, amount of adsorbed and solid
      temperature, at present time onto file
                        |
                        v
                       (1)
```

①

t = trotate?

No

Yes

CALL ROTATE

t = tprint?

Yes

Write output data, i.e. air temperature, humidity, amount of adsorbed and solid temperature, at present time onto file

②

icount = icount + 1 ← Yes ← t < tfinal?

No

STOP

RUNGE SUBROUTINE

START

Assign step size (h)

mm = max no. of the integrated variables

Xold(m) = X(m)
for m = 1 to mm

n = 1

CALL ODE OF
- ADSORPTION PROCESS
- DESORPTION PROCESS
- ROOM PROCESS

$K_n(m) = F(m)*h$
for m = 1 to mm

n = 4 ? — Yes

No

n < 3 ? — Yes / No

$X(m) = X(m)+(K_n(m))/2$
for m = 1 to mm

$X(m) = X(m)+K_n(m)$
for m = 1 to mm

n = n + 1

$X(m) = Xold + (K_1(m)+2*K_2(m)+2*K_3(m)+K_4(m))/6$
for m = 1 to mm

RETURN

ROTATE SUBROUTINE

```
START
```

$j = Mslot$

$i = 0$

$i = i+1$

$NN = 4*(i-1)$
$MM = NN+Ncell*4*(j-1)$

$S(NN+1) = X(MM+1)$
$S(NN+2) = X(MM+2)$
$S(NN+3) = X(MM+3)$
$S(NN+4) = X(MM+4)$

$i = Ncell$? — No

Yes

$j = j-1$

$i = 0$

$i = i+1$

$S(Ncell*4+MM+1) = X(MM+1)$
$S(Ncell*4+MM+2) = X(MM+2)$
$S(Ncell*4+MM+3) = X(MM+3)$
$S(Ncell*4+MM+4) = X(MM+4)$

$i = Ncell$? — No

Yes

$j = 1$?

$i = 0$

$i = i+1$

$X(NN+1) = S(NN+1)$
$X(NN+2) = S(NN+2)$
$X(NN+3) = S(NN+3)$
$X(NN+4) = S(NN+4)$

$i = Ncell$? — No

Yes

```
RETURN
```

CHAPTER 5

VALIDATION OF ADSORPTION ISOTHERMS AND
DYNAMIC MODELS

The reliability of the adsorption isotherms and mathematical models used to predict simultaneous heat and mass transfer in the rotary dehumidifier and process room is the most important requirement for the simulation work. As shown in appendix A, a correlation for the adsorption isotherms and air properties. Consequently, the first section of this chapter is dedicated to the validation of the obtained correlations for water vapor adsorption isotherms on silica gel and zeolites against published experimental data. Then the validation of the mathematical model of the rotary-honeycomb dehumidifier described in section 4.2 through 4.3 will be carried out by comparing the computed results with published experimental data of Kodama et al. (1993, 1994).

The reliability of the process room model for water evaporation and room air circulation has been investigated and confirmed by Prawarnwit (1997) in conjunction with the development of a dynamic model for the absorption-type rotary honeycomb dehumidifier by comparison with experimental data obtained from an existing process room in a modern beverage. Therefore, the reliability of the process room model for use in the same process room is omitted here.

5.1 Validation of adsorption isotherms

The potential theory for adsorption equilibrium is applied to water vapor adsorption on silica gel coated on a ceramic fiber sheet and on zeolite-13X. For micropore adsorption, Dubinin-Astakhov relation can precisely predict the adsorption equilibrium as described in the following section. The details of the determination of the equilibrium correlations for both silica gel and zeolite-13X, however, are expressed in Appendix A.1.

5.1.1 Water vapor adsorption on silica gel coated on ceramic fiber sheet

The equilibrium adsorption isotherms obtained in the present study for water vapor adsorption on silica gel coated on ceramic fiber sheet have been compared with experimental data of Wolf and Schlünder (1999) at the reported temperatures of 288, 303, 318 and 333 K, respectively. The isotherms are presented not only in terms of partial pressure in Figure 5.1a but also in terms of relative humidity (RH) as shown in Figure 5.1b.
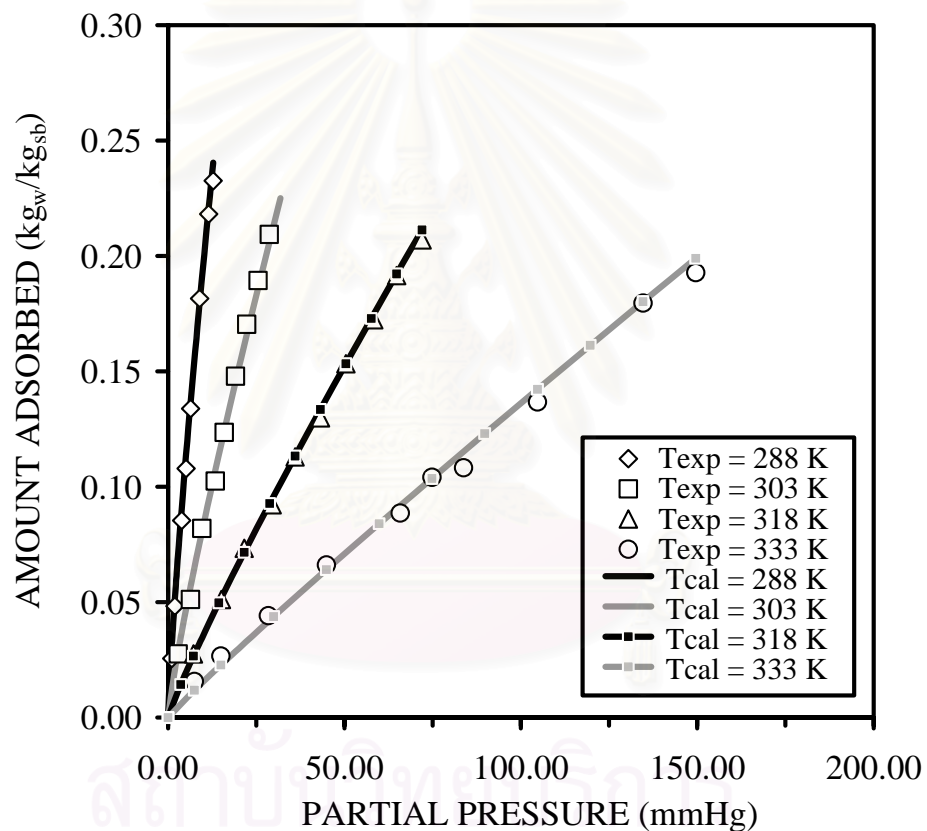
Figure 5.1a Comparison of adsorption isotherms of water vapor on silica gel coated on ceramic fiber sheet between experimental and calculated data (amount adsorbed vs. partial pressure of water vapor)
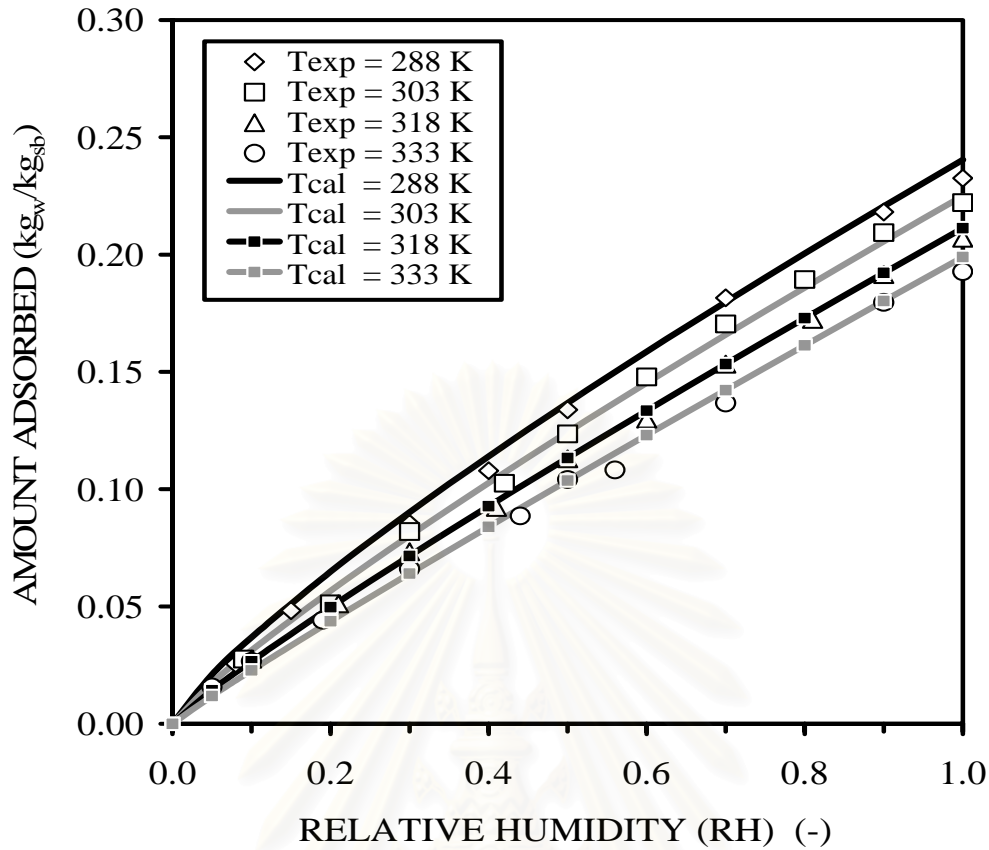
Figure 5.1b Comparison of adsorption isotherms of water vapor on silica gel coated on ceramic fiber sheet between experimental and calculated data (amount adsorbed vs. relative humidity)

In Figure 5.1a and 5.1b, it is seen that the amount of water adsorbed on silica gel increases nearly linearly as partial pressure of steam or relative humidity of air increases. In addition, the adsorbed amount rapidly decreases substantially when temperature rises above 318 K. The obtained Dubinin-Astakov correlation for water vapor adsorption on silica gel gives accurate prediction, although the relative errors are higher at very low adsorption level, as shown in Tables 5.1-5.4.

Table 5.1 Comparison of water vapor adsorption isotherm on silica gel coated on ceramic
fiber sheet at 288 K

Partial pressure (mmHg)	Total amount adsorbed (kg$_w$/kg$_{da}$)		Relative error (%)
	Experimental data	Calculated data	
1.917	0.04824	0.05165	7.07
3.834	0.08541	0.08978	5.11
5.112	0.10791	0.11293	4.66
6.390	0.13385	0.13494	0.81
8.946	0.18159	0.17648	-2.82
11.502	0.21816	0.21565	-1.15
12.780	0.23257	0.23455	0.85

Table 5.2 Comparison of water vapor adsorption isotherm on silica gel coated on ceramic
fiber sheet at 303 K

Partial pressure (mmHg)	Total amount adsorbed (kg$_w$/kg$_{da}$)		Relative error (%)
	Experimental data	Calculated data	
2.869	0.02756	0.02911	5.62
6.376	0.05116	0.05690	7.21
9.564	0.08197	0.07996	-2.45
13.390	0.10251	0.10605	3.46
15.940	0.12358	0.12276	-0.67
19.128	0.14790	0.14305	-3.28
22.316	0.17042	0.16281	-4.47
25.504	0.18934	0.18212	-3.81
28.692	0.20933	0.20104	-3.96
31.880	0.22213	0.21962	-1.13

Table 5.3 Comparison of water vapor adsorption isotherm on silica gel coated on ceramic
fiber sheet at 318 K

Partial pressure (mmHg)	Total amount adsorbed (kg_w/kg_{da})		Relative error (%)
	Experimental data	**Calculated data**	
7.20	0.02756	0.02713	- 1.56
15.12	0.05116	0.05215	1.94
21.60	0.07332	0.07140	- 2.62
29.52	0.09224	0.09402	1.93
36.01	0.11300	0.11197	- 0.87
43.21	0.12990	0.13148	1.22
50.41	0.15330	0.15059	- 1.77
58.33	0.17240	0.17125	- 0.67
64.81	0.19150	0.18790	- 1.88
72.01	0.20700	0.20618	- 0.39

Table 5.4 Comparison of water vapor adsorption isotherm on silica gel coated on ceramic
fiber sheet at 333 K

Partial pressure (mmHg)	Total amount adsorbed (kg_w/kg_{da})		Relative error (%)
	Experimental data	**Calculated data**	
14.96	0.02666	0.02322	-12.90
28.42	0.04414	0.04196	- 4.92
44.88	0.06612	0.06395	- 3.28
65.82	0.08863	0.09104	2.72
74.80	0.10413	0.10243	- 1.63
83.78	0.10822	0.11372	5.08
104.72	0.13673	0.13970	2.17
134.64	0.17961	0.17614	- 1.93
149.60	0.19276	0.19412	0.71

5.1.2 Water vapor adsorption on zeolite-13X coated on ceramic fiber sheet

Similarly, Dubinin-astakhov correlation is applied to the equilibrium adsorption isotherms of water vapor on molecular sieve zeolite-13X. The experimental data of Hines and Ghosh of Gas Research Institute, United State (Hines and Ghosh, 1993) are used for comparison with calculated data at 288, 298 and 308 K. The relations between the amount of adsorbed water and partial pressure or relative humidity are presented in Figures 5.2a and 5.2b, respectively.
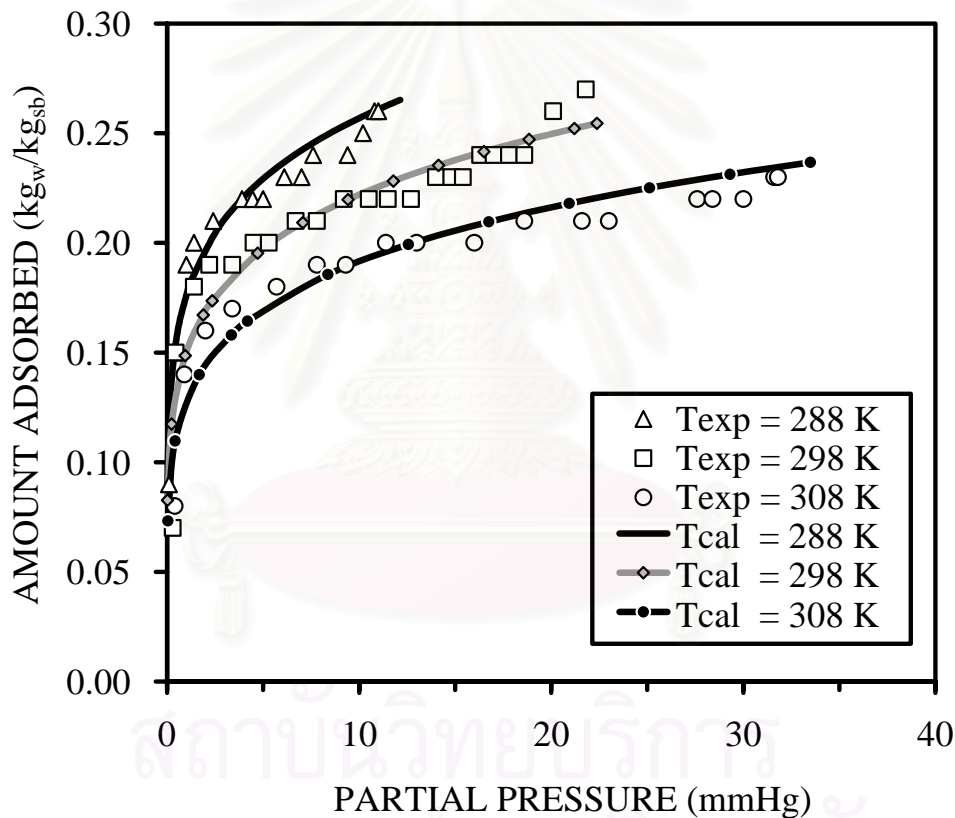
Figure 5.2a Comparison of adsorption isotherms of water vapor on zeolite-13X between experimental and calculated data (amount adsorbed vs. partial pressure of water vapor)
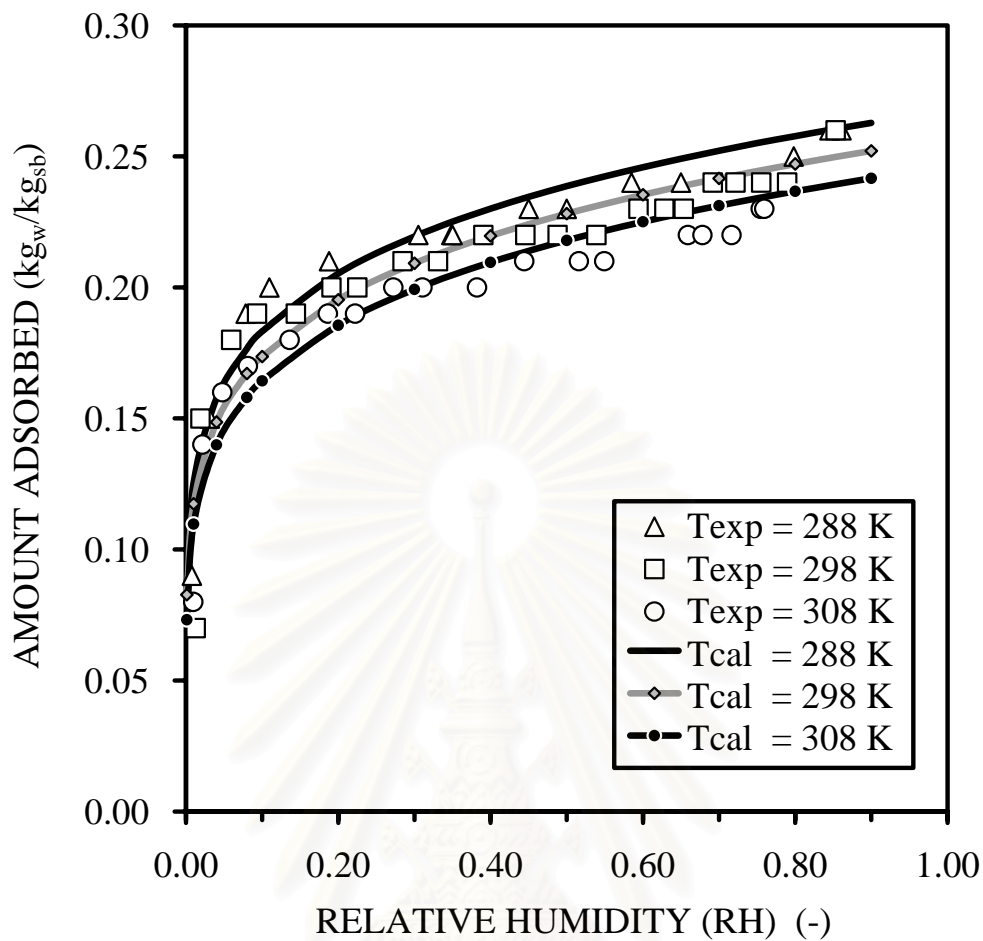
Figure 5.2b Comparison of adsorption isotherms of water vapor on zeolite-13X between experimental and calculated data (amount adsorbed vs. relative humidity)

From Figure 5.2a and 5.2b, it is seen that the shape of each isotherm belongs to Type I isotherm as classified by Brunauer (1940) in chapter 2. Here the amount of adsorbed water increases rapidly when relative humidity is below 10% and then gradually approaches saturated value. As expected, a temperature increase reduces the adsorption capacity of zeolite-13X. The consistency between the calculated isotherm data and experimental data are within an average relative error of ± 10%. Tables 5.6 to 5.7 list their numerical values and relative errors.

Table 5.5 Comparison of water vapor adsorption isotherm on zeolite-13X at 288 K

Partial pressure (mmHg)	Total amount adsorbed (kg_w/kg_{da})		Relative error (%)
	Experimental data	Calculated data	
0.40	0.15	0.1514	0.95
1.00	0.19	0.1760	- 7.37
1.40	0.20	0.1860	- 7.00
2.40	0.21	0.2032	- 3.24
3.90	0.22	0.2201	0.03
4.45	0.22	0.2249	2.22
5.00	0.22	0.2292	4.19
6.10	0.23	0.2368	2.97
7.00	0.23	0.2422	5.32
7.60	0.24	0.2455	2.31
9.40	0.24	0.2543	5.94
10.20	0.25	0.2577	3.07

Table 5.6 Comparison of water vapor adsorption isotherm on zeolite-13X at 298 K

Partial pressure (mmHg)	Total amount of adsorbed (kg_w/kg_{da})		Relative error (%)
	Experimental data	Calculated data	
0.45	0.15	0.1309	- 12.74
2.20	0.19	0.1714	- 9.79
3.40	0.20	0.1845	- 7.73
4.50	0.20	0.1935	- 3.23
5.30	0.20	0.1990	- 0.50
6.70	0.21	0.2071	- 1.39
7.80	0.21	0.2125	1.19
9.20	0.22	0.2185	- 0.66
12.70	0.22	0.2308	4.93
14.00	0.23	0.2347	2.04
15.40	0.23	0.2385	3.71
16.30	0.24	0.2408	0.35
17.00	0.24	0.2426	1.07
18.60	0.24	0.2463	2.63

Table 5.7 Comparison of water vapor adsorption isotherm on zeolite-13X at 308 K

Partial pressure (mmHg)	Total amount adsorbed (kg_w/kg_{da})		Relative error (%)
	Experimental data	Calculated data	
0.90	0.14	0.1255	- 10.39
2.00	0.16	0.1443	- 9.79
3.40	0.17	0.1584	- 6.81
5.70	0.18	0.1735	- 3.63
7.80	0.19	0.1833	- 3.53
9.30	0.19	0.1890	- 0.51
11.40	0.20	0.1959	- 2.04
13.00	0.20	0.2005	0.24
16.00	0.20	0.2079	3.97
18.60	0.21	0.2135	1.67
21.60	0.21	0.2192	4.37
23.00	0.21	0.2216	5.53
27.60	0.22	0.2288	4.01
28.40	0.22	0.2300	4.53
30.00	0.22	0.2322	5.54
31.60	0.23	0.2343	1.88
31.80	0.23	0.2346	1.99

5.2 Validation of the rotary honeycomb dehumidifier model

In this section, validation of the dehumidifier model in the case of silica gel coated honeycomb rotor is carried under various operating conditions. The simulation results are validated against experimental data. Kodama et al. (1993,1994) published in Chemical Engineering Journal of Japan. In their experiments, a commercial rotary honeycomb dehumidifier made by Seibu Giken Co., Ltd., Japan, was used. The parameters and properties of the rotary dehumidifier and humid air for validation in this chapter are detailed in Table 5.8.

Table 5.8 Parameters and properties of the silica gel coated honeycomb rotary dehumidifier used for validation

SIZE OF THE ROTARY DEHUMIDIFIER		
Diameter of rotor (D)	0.32	m
Length of rotor (L)	0.2	m
Cross sectional area of a slot (A_c)	3.49×10^{-6}	m^2
Cross sectional area of the gas phase in a slot (A_g)	2.88×10^{-6}	m^2
Cross sectional area of the solid phase in a slot (A_{ss})	6.11×10^{-7}	m^2
Hydraulic diameter of a slot	1.44×10^{-3}	m
PROPERTIES OF HONEYCOMB ROTOR		
Specific heat of adsorbent (Cp_{sb})	0.92	$kJ/(kg_{da} \cdot K)$
Specific heat of water (Cp_w)	4.187	$kJ/(kg_{da} \cdot K)$
Specific heat of ceramic fiber (Cp_{sh})	1.20	$kJ/(kg_{da} \cdot K)$
Bulk density of rotor (ρ_{sb})	250	kg/m^3
Density of ceramic fiber (ρ_{sh})	185	kg/m^3
Mass fraction of adsorbent	0.70	(-)
Specific surface area of the honeycomb (*a*)	3000	m^2/m^3
Void fraction of the honeycomb (ε)	0.825	(-)
PROPERTIES OF HUMID AIR		
Specific heat of dry air (Cp_{da})	1.005	$kJ/(kg_{da} \cdot K)$
Specific heat of water vapor (Cp_v)	1.820	$kJ/(kg_{da} \cdot K)$
Latent heat of vaporization at 273 K (λ_0)	2501.3	$kJ/(kg_{da} \cdot K)$

Since humid air of constant humidity is fed through the dehumidifier at a constant rate, the simulated outlet air properties soon approach the same steady state regardless of the assumed initial conditions. The results are then compared with the experimental data of Kodama et al. which also at the steady state. At first, section 5.2.1, is earmarked at showing the typical manner of steady state approach for dehumidification using the honeycomb rotor. In order to minimize computational time while and providing sufficient accuracy in the prediction, the effect of the main model parameters, i.e. the thickness of a stationary partition plate between the adsorption and regeneration zones (M_{thick}), and the number of cells (N_{cell}) in each slot are next investigated. Then relevant results are presented and discussed in section 5.2.2. Finally detailed validation of the dynamic rotary dehumidifier model, which are divided into three parts, that is, validation of the average outlet air humidity of the adsorption zone, the angular profile of the air humidity and the temperature distribution in the dehumidifier are carried out in section 5.2.3-5.2.5, respectively.

5.2.1 The manner of steady state approach for the dehumidifier model

A typical case used to illustrate the manner in which the steady state of the model is approached employs the simulation parameters, and the initial and inlet conditions listed in Tables 5.9 and 5.10, respectively.

Table 5.9 Model parameters used to illustrate the steady-state approach of a silica gel coated honeycomb rotary dehumidifier

SIMULATION PARAMETERS		
The number of cells in each slot (N_{cell})	10	cell
Total number of slots (M_{slot})	120	slot
Number of slots for the adsorption zone (M_{ads})	90	slot
Number of slots for the regeneration zone (M_{reg})	30	slot
Step size (Δt) of integration	0.006	sec
Display time interval	300	sec
Final simulation time (t_f)	3600	sec

Table 5.10 Operating conditions used to illustrate the steady-state approach of a silica gel
coated honeycomb rotary dehumidifier

INITIAL CONDITIONS		
Local amount of moisture adsorbed in the adsorbent (W_0)	0.001	kg_w/kg_{sb}
Local air humidity in the slots (H_0)	0.0001	kg_w/kg_{da}
Local solid temperature in the slots(Ts_0)	293.15	K
Local gas temperature in the slots (Ta_0)	293.15	K
INLET CONDITIONS		
Inlet humidity of the adsorption zone ($H_{in,ads}$)	4.5×10^{-3}	kg_w/kg_{da}
Inlet gas temperature of the adsorption zone ($Ta_{in,ads}$)	297.30	K
Inlet humidity of the regeneration zone ($H_{in,reg}$)	5×10^{-4}	kg_w/kg_{da}
Inlet gas temperature of theregeneration zone ($Ta_{in,reg}$)	413.15	K
Inlet air velocity of the adsorption zone ($V_{in,ads}$)	1.0	m/s
Inlet air velocity of the regeneration zone ($V_{in,reg}$)	1.0	m/s
Rotational speed of the rotor (φ)	3.3	rph

The simulation results on the steady state approach are illustrated as a function of
time in Figures 5.3 through 5.5. It is seen that the average amount of adsorbed moisture
and average humidity of the dehumidified air, i.e. the outlet air of the adsorption zone,
increase almost linearly from their initial values to the steady state in approximately 800
seconds. In contrast, the average temperature of the dehumidified air increases rapidly and
overshoots in approximately 200 seconds and then gradually decreases to the steady state
in about 800 seconds. Since fresh adsorbent is used and the initial air and adsorbent
temperatures are low, the initial high adsorption rate and massive release of heat of
adsorption in the adsorption zone causes an abrupt increase in the average air temperature.
Then a continuous accumulation of the amount of adsorbed moisture not only decrease the
rate of adsorption but also results in higher air humidity and gradual decline in the air
temperature at the outlet of the adsorption zone. In conclusion, the above-mentioned
transient behavior is typical of the start-up of the honeycomb rotary dehumidifier with
fresh adsorbent.
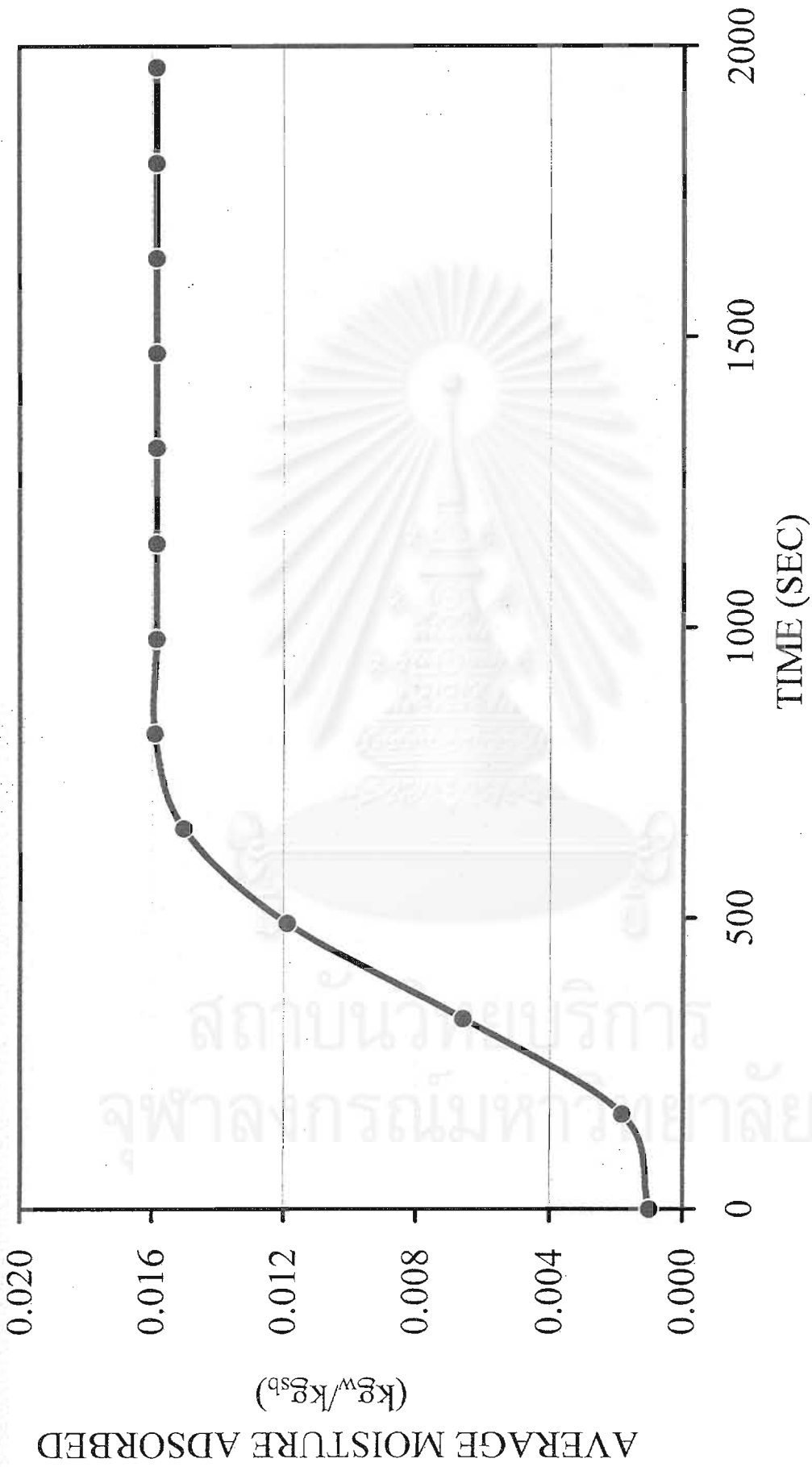
Figure 5.3 The average amount of adsorbed moisture in the adsorption zone vs. simulation time
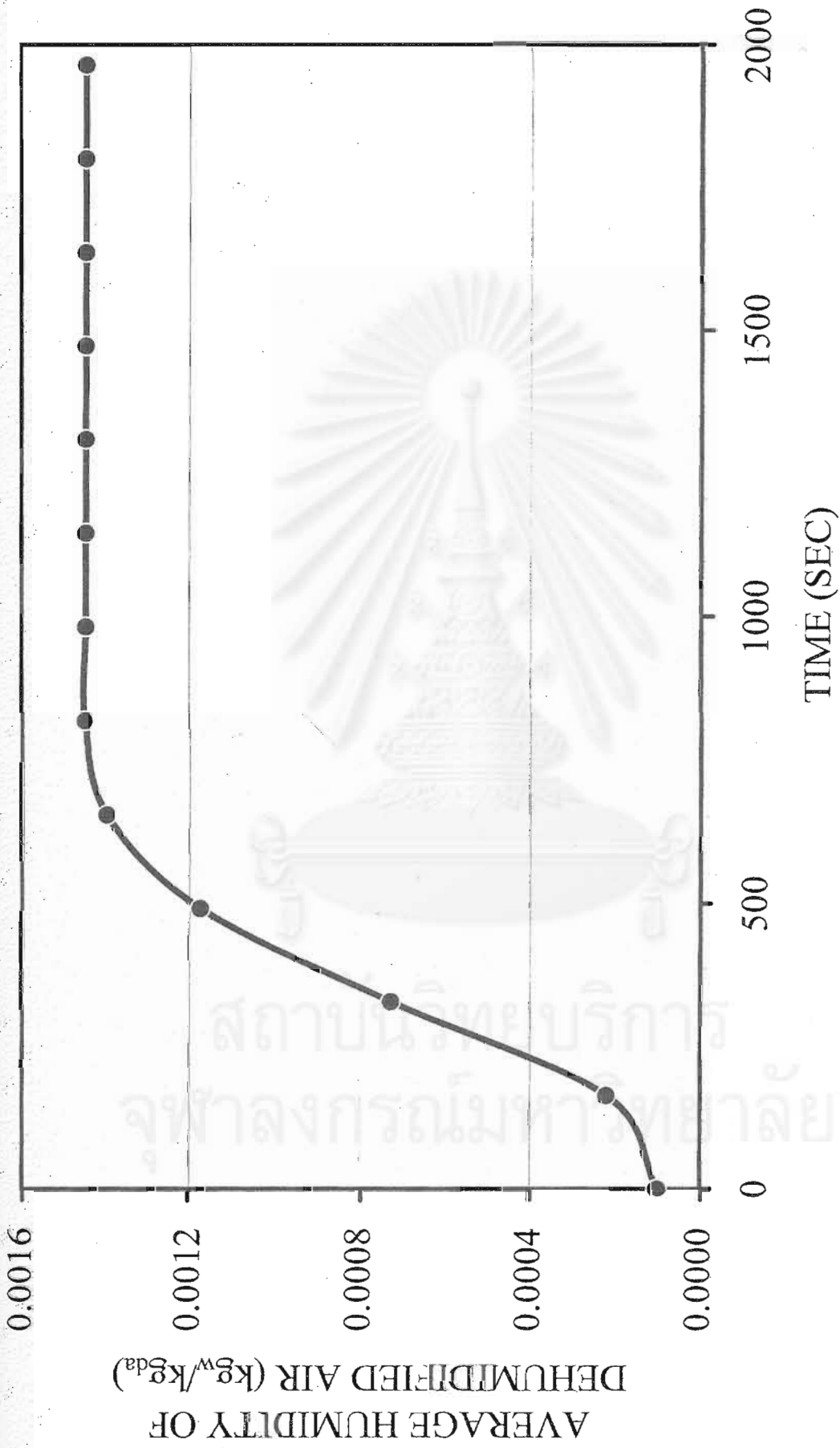
Figure 5.4 The average outlet air humidity of the adsorption zone vs. simulation time
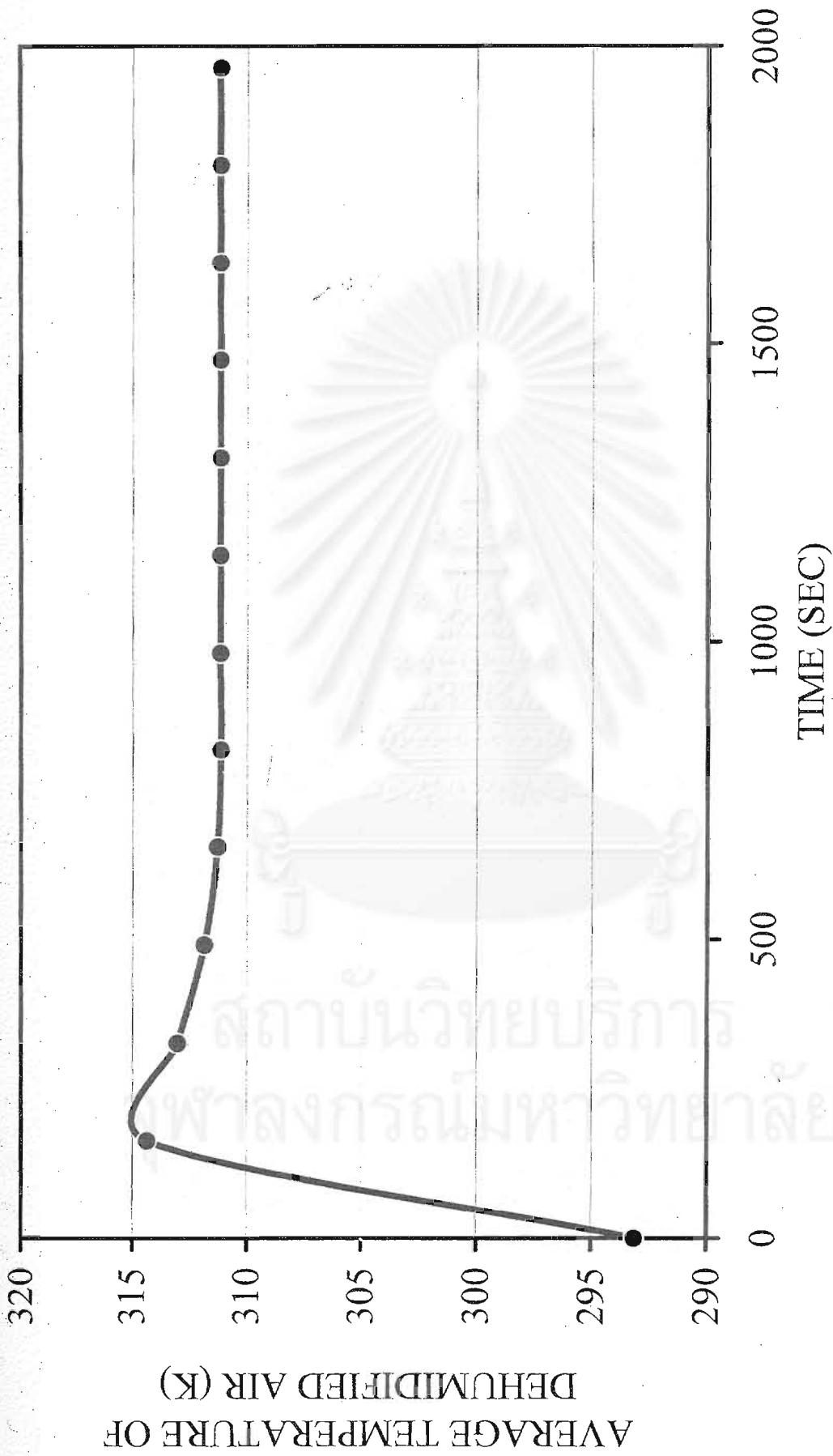
Figure 5.5 The average outlet air temperature of the adsorption zone vs. simulation time

5.2.2 Effect of main model parameters

The investigated model parameters which are the thickness of a stationary partition plate between the adsorption and regeneration zones, and the number of cells in each slot are presented and discussed in sections 5.2.2.1 and 5.2.2.2, respectively. Both parameters are investigated independently using the same operating conditions as listed in Table 5.11.

Table 5.11 Operating conditions used to investigate the effect of model parameters on the silica gel coated honeycomb rotary dehumidifier

INITIAL CONDITIONS		
Local amount of moisture adsorbed in the adsorbent (W_0)	0.001	kg_w/kg_{sb}
Local air humidity in the slots (H_0)	0.0001	kg_w/kg_{da}
Local solid temperature in the slots (Ts_0)	293.15	K
Local gas temperature in the slots (Ta_0)	293.15	K
INLET CONDITIONS		
Inlet humidity of the adsorption zone $(H_{in,ads})$	4.5×10^{-3}	kg_w/kg_{da}
Inlet gas temperature of the adsorption zone $(Ta_{in,ads})$	297.30	K
Inlet humidity of the regeneration zone $(H_{in,reg})$	5×10^{-4}	kg_w/kg_{da}
Inlet gas temperature of theregeneration zone $(Ta_{in,reg})$	413.15	K
Inlet air velocity of the adsorption zone $(V_{in,ads})$	1.0	m/s
Inlet air velocity of the regeneration zone $(V_{in,reg})$	1.0	m/s
Rotational speed of the rotor (φ)	6.6	rph

5.2.2.1 Thickness of the stationary partition plate between the adsorption and regeneration zone

In this section the effect of the thickness of the stationary partition plate between the adsorption and regeneration zone is investigated. In certain designs of the rotary dehumidifier, a small number of the slots between the adsorption and regeneration zone do not allow any air to pass through. For the sake of simplicity in simulation, the number of these "dead" may be assumed to be negligible, that is, $M_{thick} = 0$. Nevertheless, the validity of the assumption will be examined by comparing the results between $M_{thick} = 0$ and with $M_{thick} = 4$ as well as with experimental data. The model parameters used in the case of $M_{thick} = 0$ and $M_{thick} = 4$ are listed in Tables 5.12 and 5.13, respectively.

Table 5.12 Model parameters used to investigate the effect of M_{thick} on the silica gel coated honeycomb rotary dehumidifier with $M_{thick} = 0$

MODEL PARAMETERS FOR $M_{THICK} = 0$		
The number of cells in each slot (N_{cell})	20	cell
Total number of slots (M_{slot})	120	slot
Number of slots for the adsorption zone (M_{ads})	90	slot
Number of slots for the regeneration zone (M_{reg})	30	slot
Closed Slot (M_{thick})	0	slot
Step size (Δt) of integration	0.006	sec
Display time interval	300	sec
Final simulation time (t_f)	3600	sec

Table 5.13 Model parameters used to investigate the effect of M_{thick} on the silica gel coated honeycomb rotary dehumidifier with $M_{thick} = 4$

SIMULATION PARAMETERS FOR $M_{THICK} = 4$		
The number of cells in each slot (N_{cell})	20	Cell
Total number of slots (M_{slot})	120	slot
Number of slots for the adsorption zone (M_{ads})	90	slot
Number of slots for the regeneration zone (M_{reg})	26	slot
Closed Slot (M_{thick})	4	slot
Step size (Δt) of integration	0.006	sec
Display time interval	300	sec
Final simulation time (t_f)	3600	sec

The results of the two cases of simulation are compared with the experimental data (Kodama et al., 1994) in Figures 5.6 and 5.7. In Figure 5.6, the angular profiles of the air humidity at the outlet of the adsorption zone for $M_{thick} = 0$ and $M_{thick} = 4$ are represented by solid and dotted lines, respectively. Graphically, both simulated profiles show a close resemblance. In addition, the close agreement of the angular profiles of the air temperature at the outlet of the adsorption zone between $M_{thick} = 0$ and $M_{thick} = 4$ as well as with the experimental data are observed in Figure 5.7. Accordingly, M_{thick} will be set as zero in all subsequent simulations of the rotary dehumidifier.
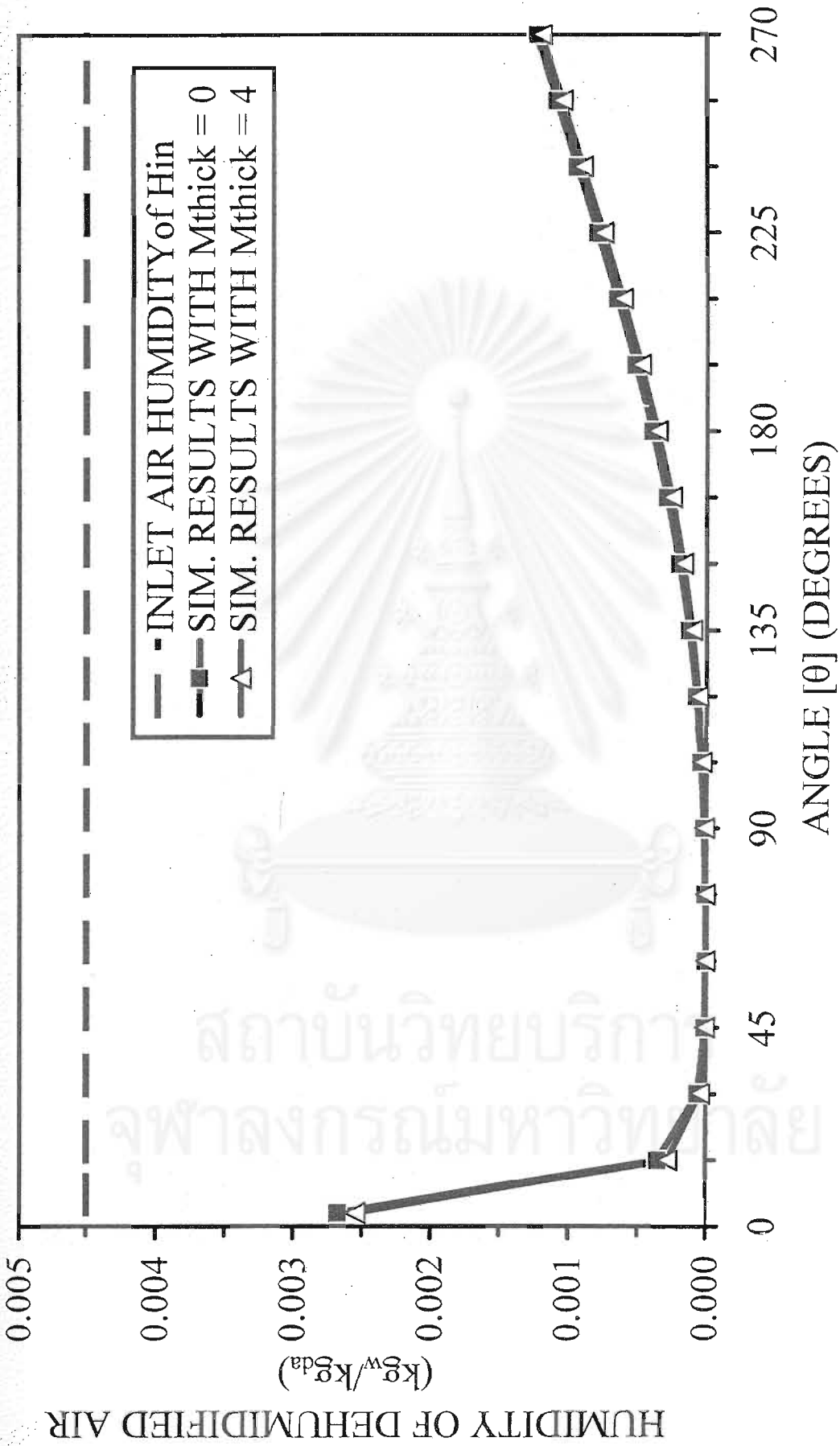
Figure 5.6 Comparison the angular profiles of outlet air humidity from the adsorption zone between the two simulation results ($M_{thick} = 0$ and 4)
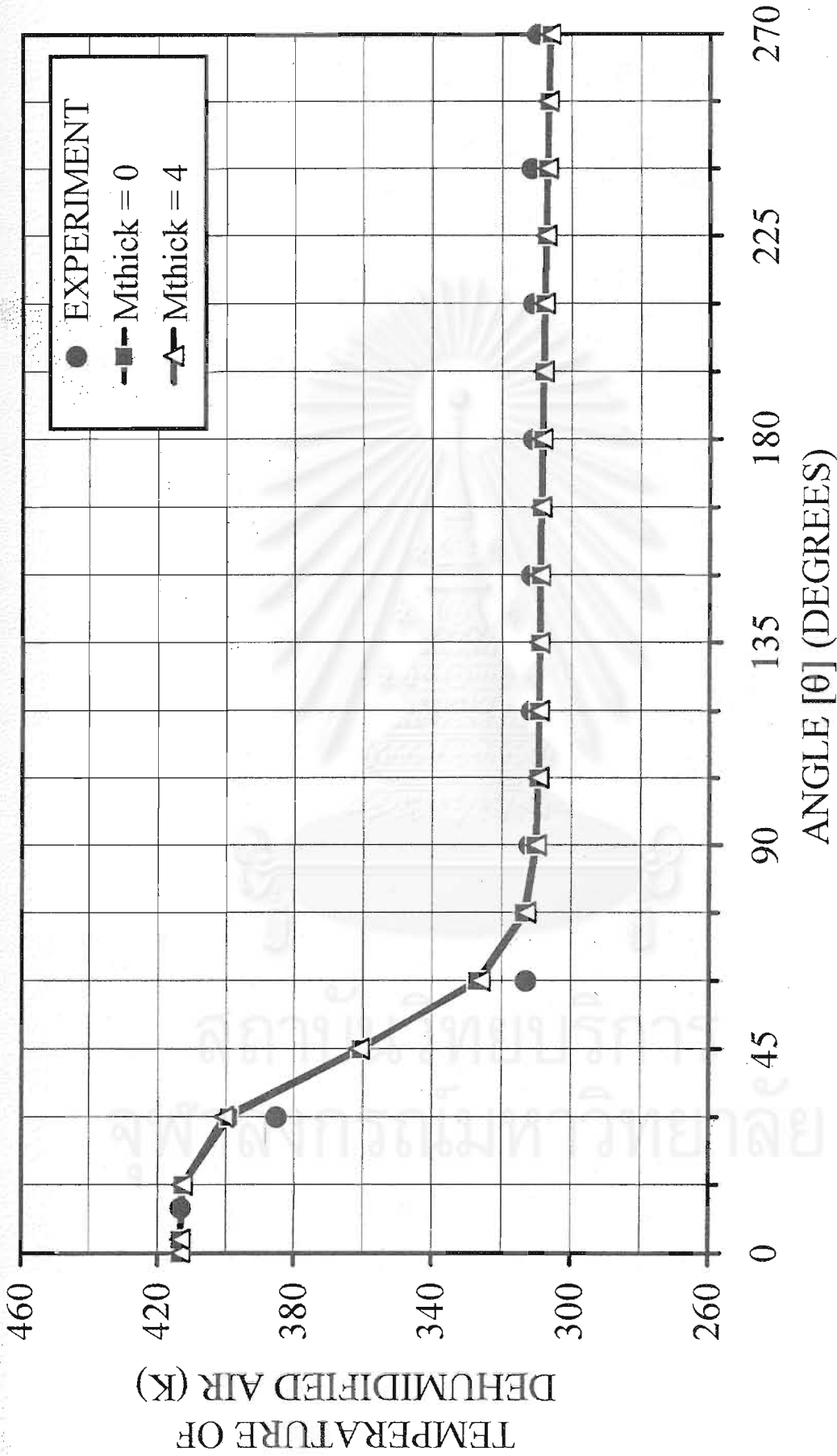
Figure 5.7 Comparison of the angular profiles of outlet air temperature from the adsorption zone between the experimental data and the two simulated results ($M_{thick} = 0$ and 4)

5.2.2.2 The number of cells in each slot

Theoretically and conceptually, the plug flow model has been shown to be equivalent to the model of a series of equal-volume CSTR's in which an infinitely large number of completely mixed cells, each of infinitely small thickness, are connected in series. For practical reason, the plug flow model of each slot will be approximated in this study by an equivalent CSTR model consisting of a finite number of N cells in series. To minimize computational time while maintaining sufficiently accurate prediction, the appropriate value N_{cell} (10, 20 and 25) will be obtained by comparison with experimental results (Kodama et al., 1994) in this section. The model parameters used to investigate the effect of N_{cell} (N_{cell} = 10, 20 and 25) are listed in Tables 5.14 through 5.16, respectively.

The simulated results for the case of N_{cell} = 10, 20 and 25 are shown and compared in Figures 5.8, 5.9 and 5.10. Figure 5.8 presents the comparison of the angular profiles of the outlet air humidity from the adsorption zone for the three cases of N_{cell}. The humidity profile for N_{cell} = 10 cells is obviously a bit different from the profiles for N_{cell} = 20 and 25. Similarly, in Figure 5.9, the angular profile of the air temperature at the outlet of the adsorption zone for N_{cell} = 10 shows a slight difference from the profiles for N_{cell} = 20 and 25. However, all of the three simulated profile in Figure 5.9 are consistent with the experimental data. In addition, the close resemblance between the three simulated results and the experimental data of the angular temperature profiles in the axial or flow direction in the slots of the dehumidifier are observed in Figure 5.10. Since N_{cell} = 10 gives results that only slightly differ from the cases of N_{cell} = 20 and 25 but agree equally well with the experimental results, N_{cell} 10 will be adopted in all subsequent simulations of the rotary dehumidifier.

Table 5.14 Model parameters used to investigate the effect of N_{cell} on the honeycomb
rotary dehumidifier ($N_{cell} = 10$)

MODEL PARAMETERS FOR $N_{CELL} = 10$		
The number of cells in each slot (N_{cell})	10	cell
Total number of slots (M_{slot})	120	slot
Number of slots for the adsorption zone (M_{ads})	90	slot
Number of slots for the regeneration zone (M_{reg})	30	slot
Step size (Δt) of integration	0.006	sec
Display time interval	300	sec
Final simulation time (t_f)	3600	sec

Table 5.15 Model parameters used to investigate the effect of N_{cell} on the honeycomb
rotary dehumidifier ($N_{cell} = 20$)

MODEL PARAMETERS FOR $N_{CELL} = 20$		
The number of cells in each slot (N_{cell})	20	cell
Total number of slots (M_{slot})	120	slot
Number of slots for the adsorption zone (M_{ads})	90	slot
Number of slots for the regeneration zone (M_{reg})	30	slot
Step size (Δt) of integration	0.006	sec
Display time interval	300	sec
Final simulation time (t_f)	3600	sec

Table 5.16 Model parameters used to investigate the effect of N_{cell} on the honeycomb
rotary dehumidifier ($N_{cell} = 25$)

SIMULATION PARAMETERS FOR $N_{CELL} = 25$		
The number of cells in each slot (N_{cell})	25	cell
Total number of slots (M_{slot})	120	slot
Number of slots for the adsorption zone (M_{ads})	90	slot
Number of slots for the regeneration zone (M_{reg})	30	slot
Step size (Δt) of integration	0.006	sec
Display time interval	300	sec
Final simulation time (t_f)	3600	sec
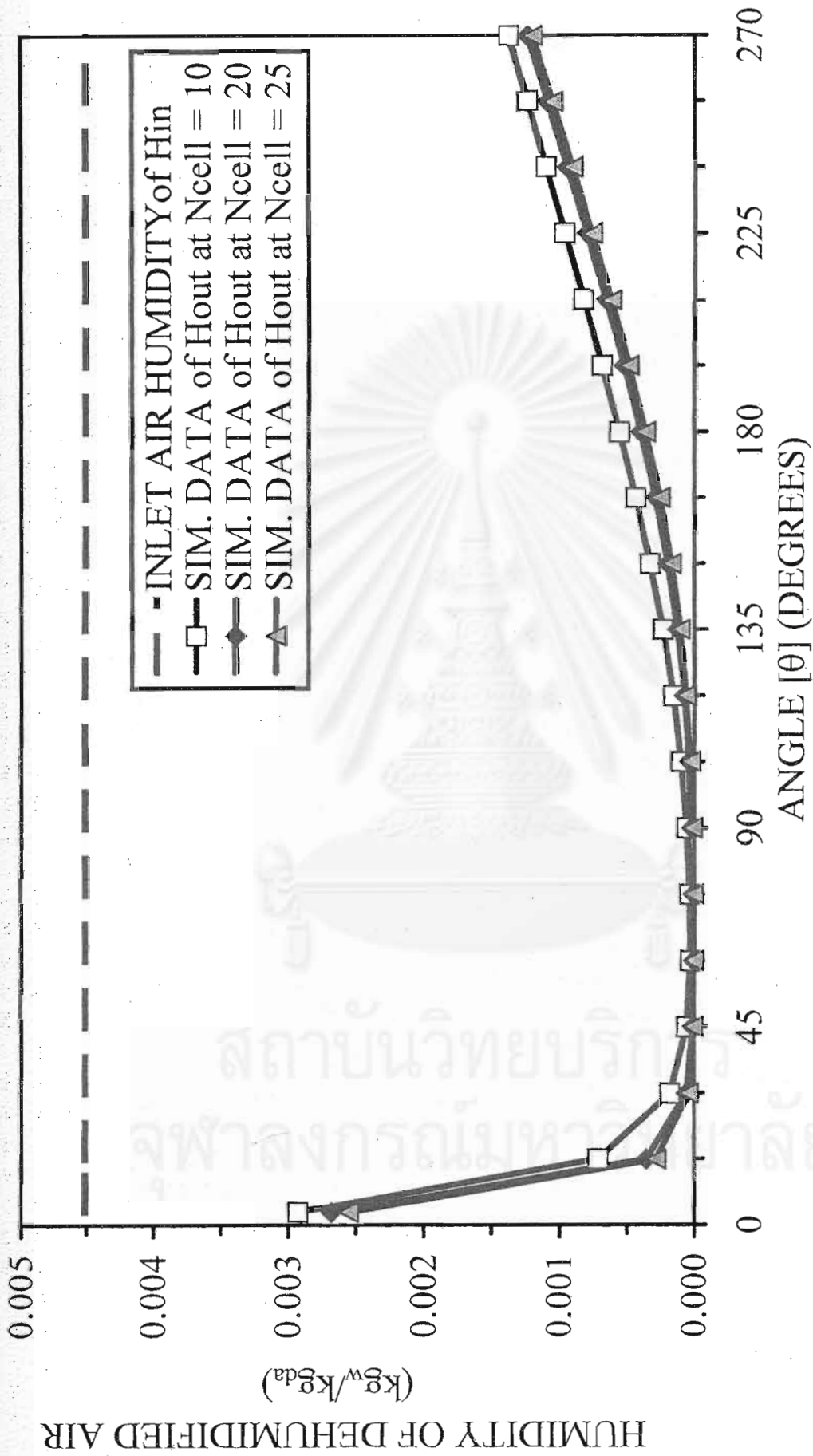
Figure 5.8 Comparison of the angular profiles of outlet air humidity from the adsorption zone between $N_{cell} = 10$, 20 and 25
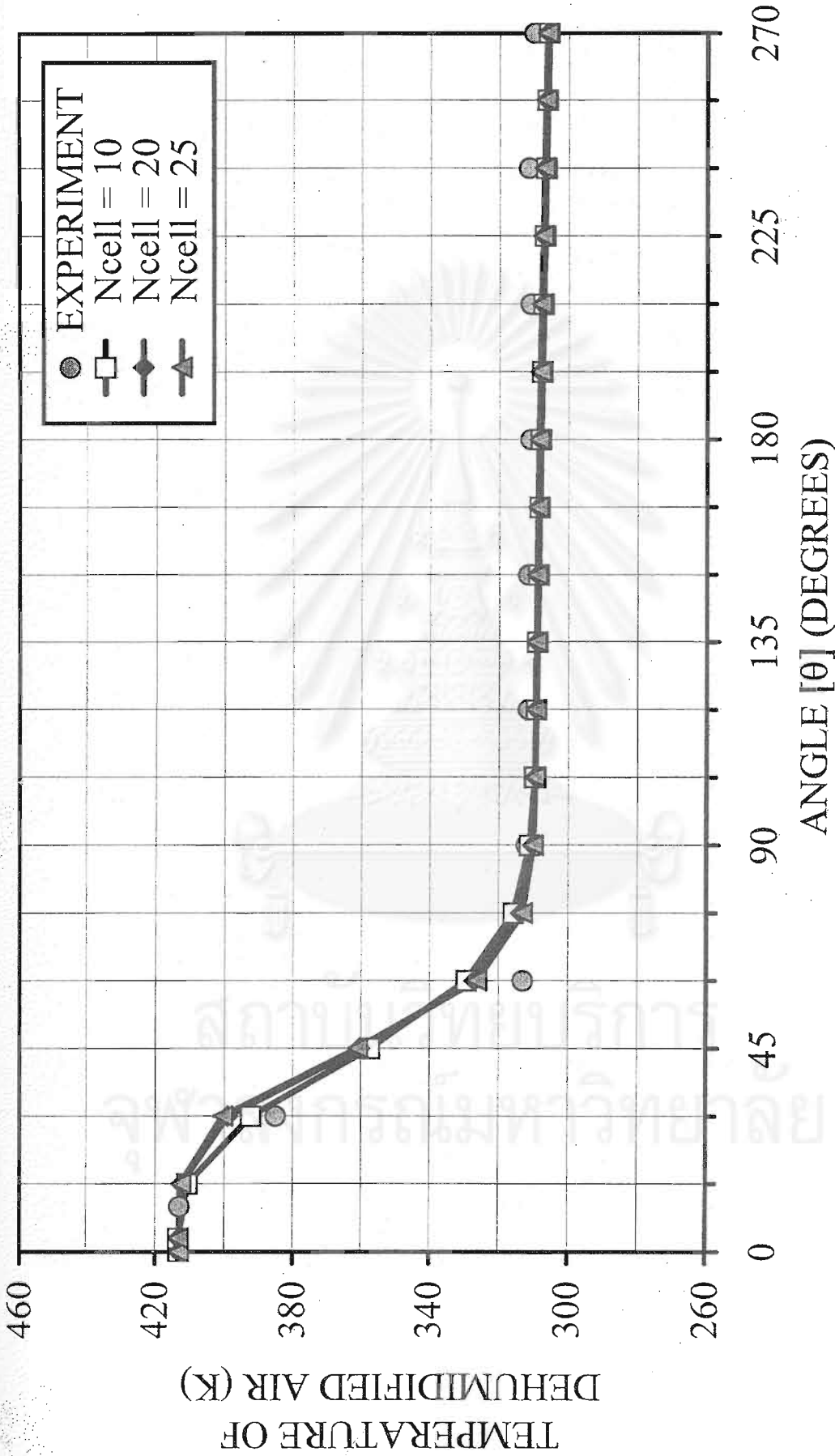
Figure 5.9 Comparison of the angular profiles of outlet air temperature from the experimental data and the 3 simulated results (N_{cell} = 10, 20 and 25)
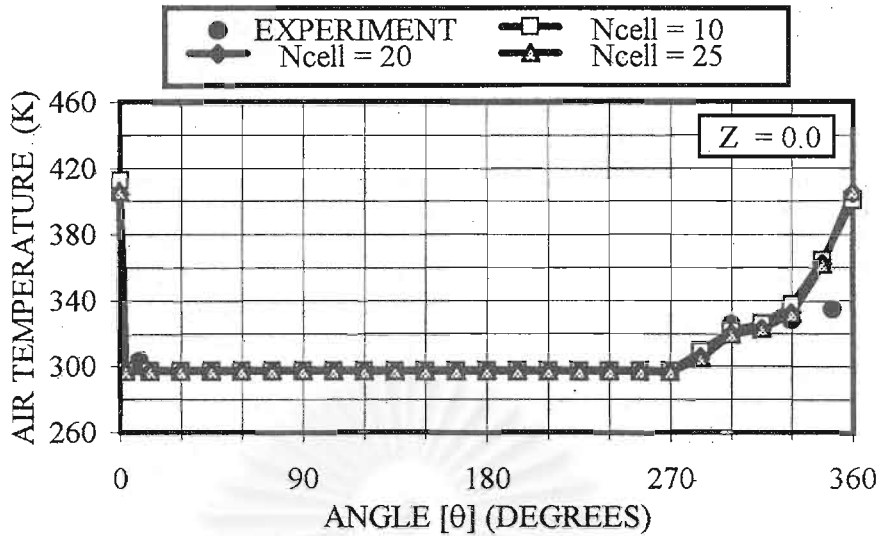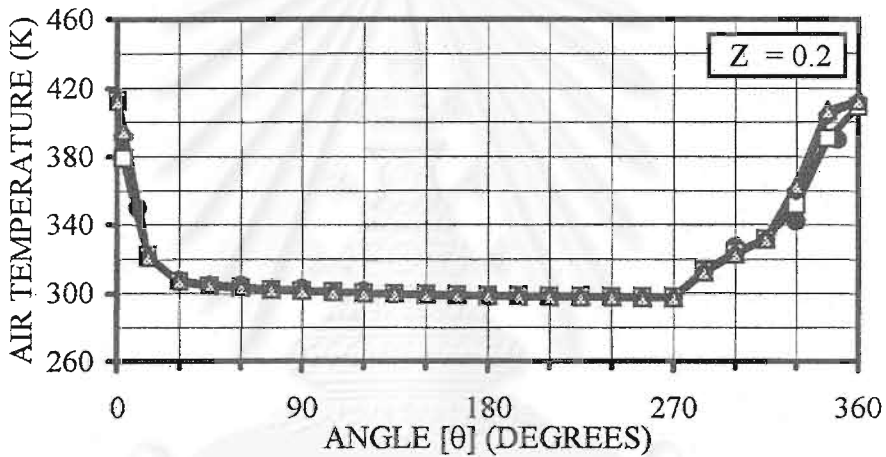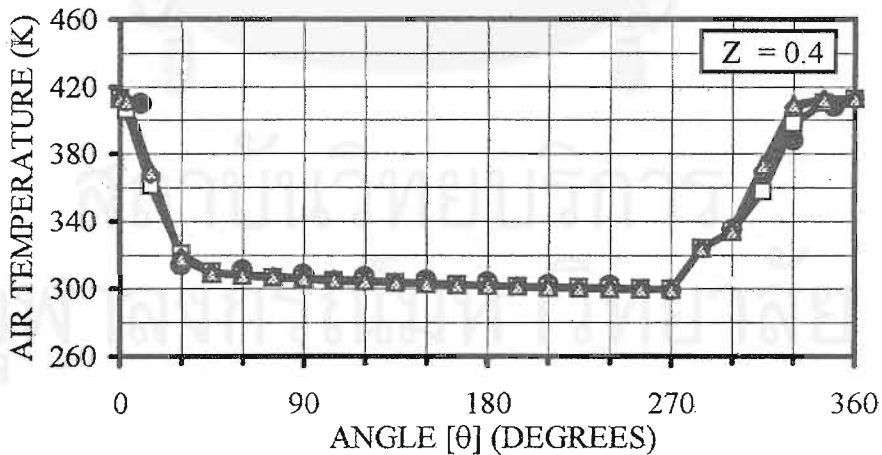
Figure 5.10 Comparison of the angular profiles of slot air temperature between the experimental data and the 3 simulated results (N=10, 20 and 25) at various dimensionless lengths a) Z = 0.0, b) Z= 0.2, c) Z = 0.4, d) Z = 0.6, e) Z = 0.8 and f) Z = 1.0
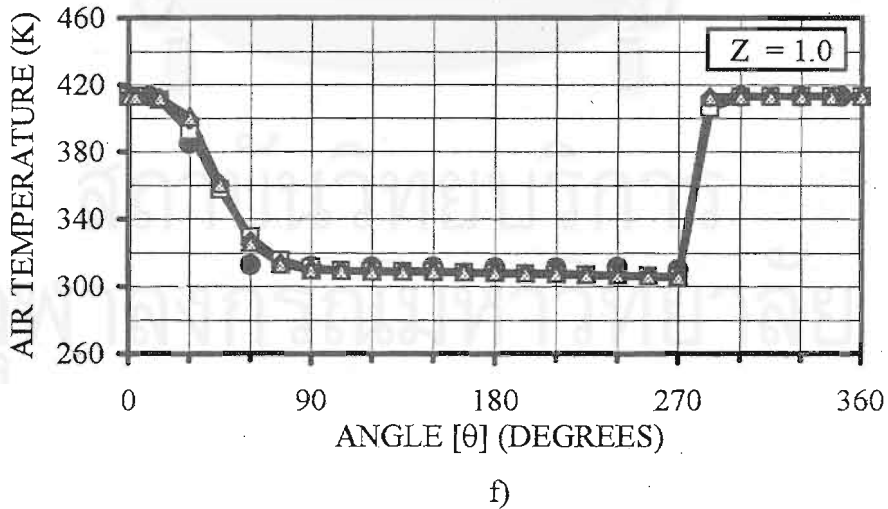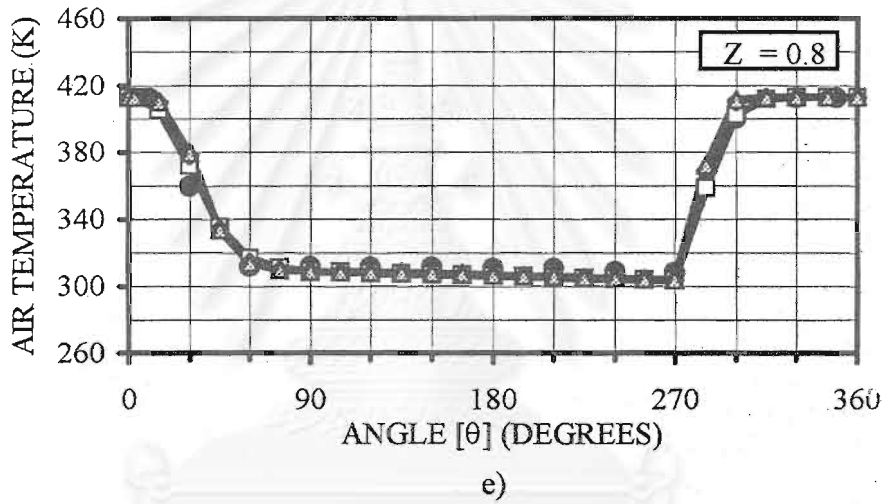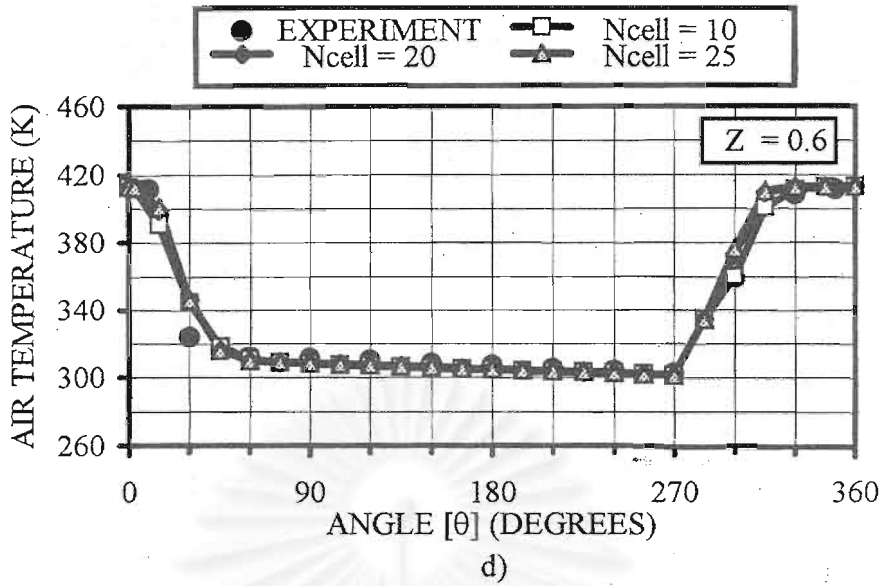
Figure 5.10(cont.) Comparison of the angular profiles of slot air temperature between the experimental data and the 3 simulated results (N=10, 20 and 25) at various dimensionless lengths a) Z = 0.0, b) Z= 0.2, c) Z = 0.4, d) Z = 0.6, e) Z = 0.8 and f) Z = 1.0

5.2.3 Validation of the average humidity of the dehumidified air

In this section, the simulation results for the three cases of the rotational speed, i.e. 3.3, 6.6 and 13.2 rph, have been substantiated against the corresponding experimental data. The average humidity of the dehumidified air and the air humidity profile at the outlet of the adsorption zone for the three rotational speeds are shown in Figures 5.11 to 5.13, respectively. Next the effect of the rotational speed on the average humidity of the dehumidified air and the dehumidification efficiency is illustrated in Figures 5.14 and 5.15, respectively. All simulation cases in this section use the same operating conditions, except the rotational speed, as listed in Table 5.17.

Table 5.17 Operating conditions used to validate the average humidity of the dehumidified air from the silica gel coated honeycomb rotary dehumidifier

INITIAL CONDITIONS		
Local amount of moisture adsorbed in the adsorbent (W_0)	0.001	kg_w/kg_{sb}
Local air humidity in the slots (H_0)	0.0001	kg_w/kg_{da}
Local solid temperature in the slots (Ts_0)	293.15	K
Local gas temperature in the slots (Ta_0)	293.15	K
INLET CONDITIONS		
Inlet humidity of the adsorption zone $(H_{in,ads})$	4.5×10^{-3}	kg_w/kg_{da}
Inlet gas temperature of the adsorption zone $(Ta_{in,ads})$	297.30	K
Inlet humidity of the regeneration zone $(H_{in,reg})$	5×10^{-4}	kg_w/kg_{da}
Inlet gas temperature of the regeneration zone $(Ta_{in,reg})$	413.15	K
Inlet air velocity of the adsorption zone $(V_{in,ads})$	1.0	m/s
Inlet air velocity of the regeneration zone $(V_{in,reg})$	1.0	m/s

In Figures 5.11 to 5.13, it is seen that sufficiently good accuracy of the predicted average humidity of the dehumidified air is obtained at each rotational speed because the relative errors with respect to the inlet humidity are small. To confirm this assertion, the average humidity of the dehumidified air and the dehumidification efficiency vs. the rotational speed are compared with their experimental results in Figures 5.14 and 5.15, respectively. In addition to their close agreement, an optimal value of the rotational speed, which ranges from 6 to 8 rph, is obtained. At the optimal value, the efficiency can reach 90% or higher. On the other hand, an efficiency as low as 70% will be obtained when the rotational speed is too slow as seen in Figure 5.15. Further investigation into the effect of the rotational speed will be carried out and discussed in the next chapter.
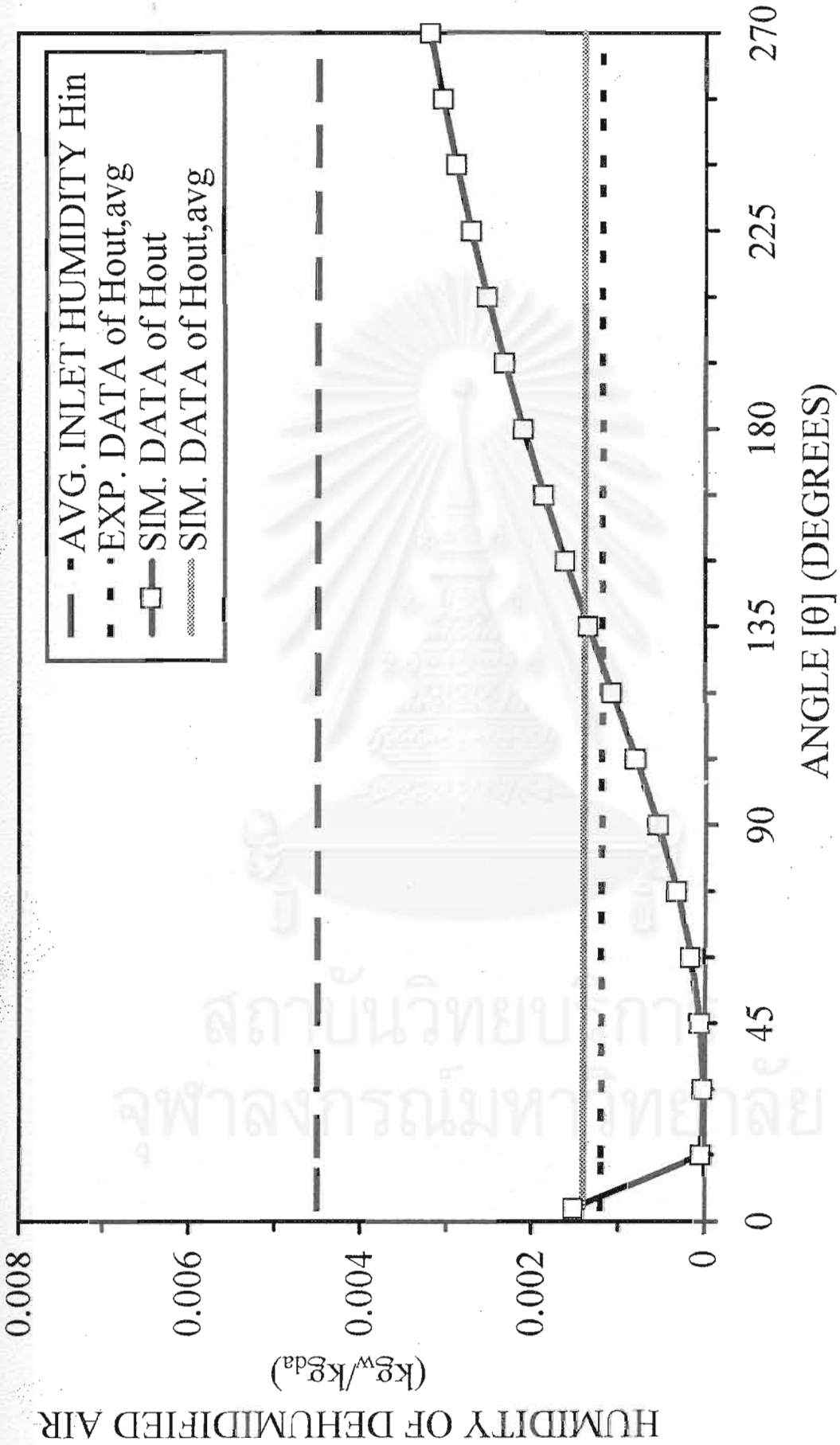
Figure 5.11 Comparison of average humidity of dehumidified air between experimental and simulated results at 3.3 rph
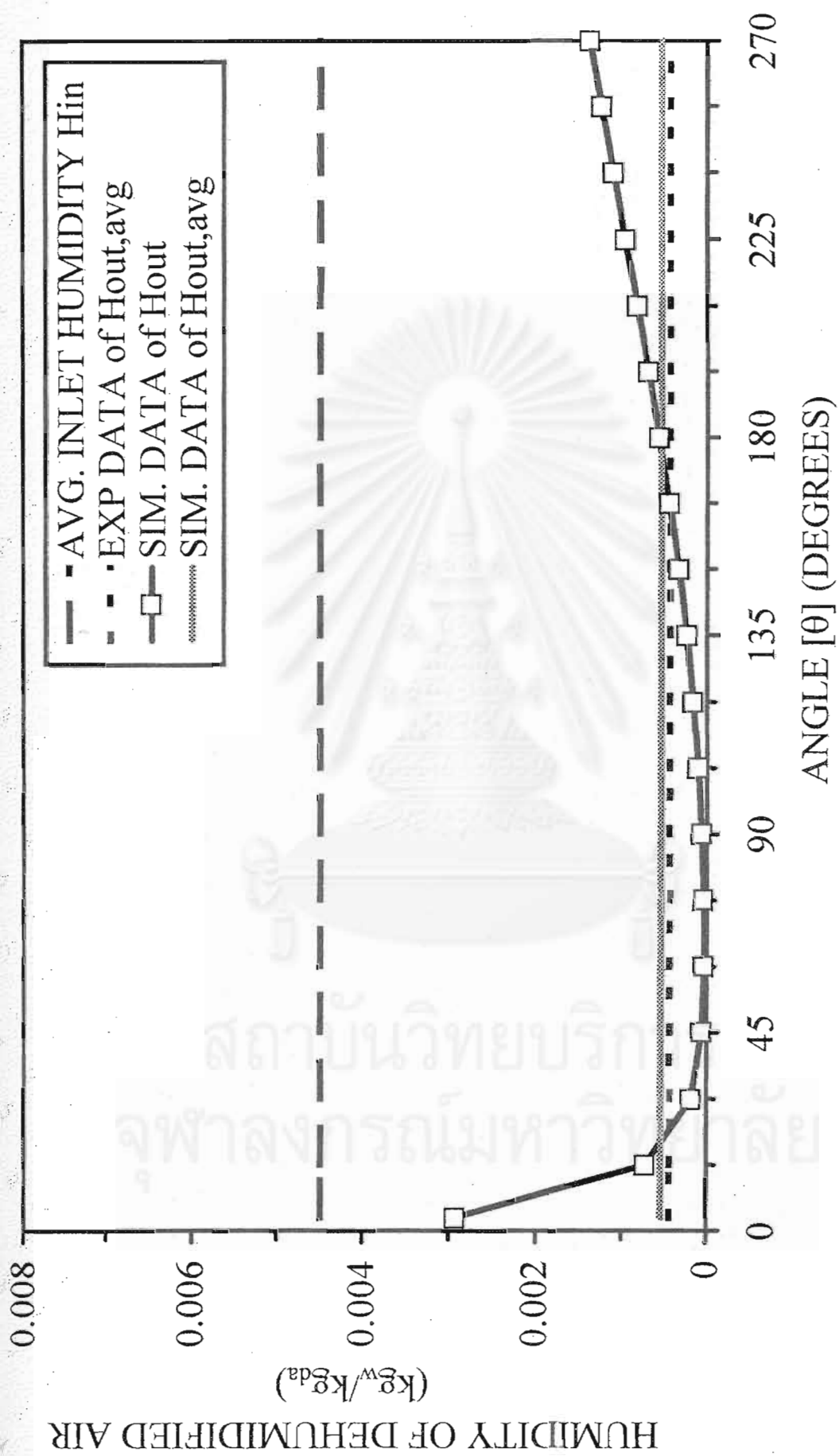
Figure 5.12 Comparison of average humidity of dehumidified air between experimental and simulated results at 6.6 rph
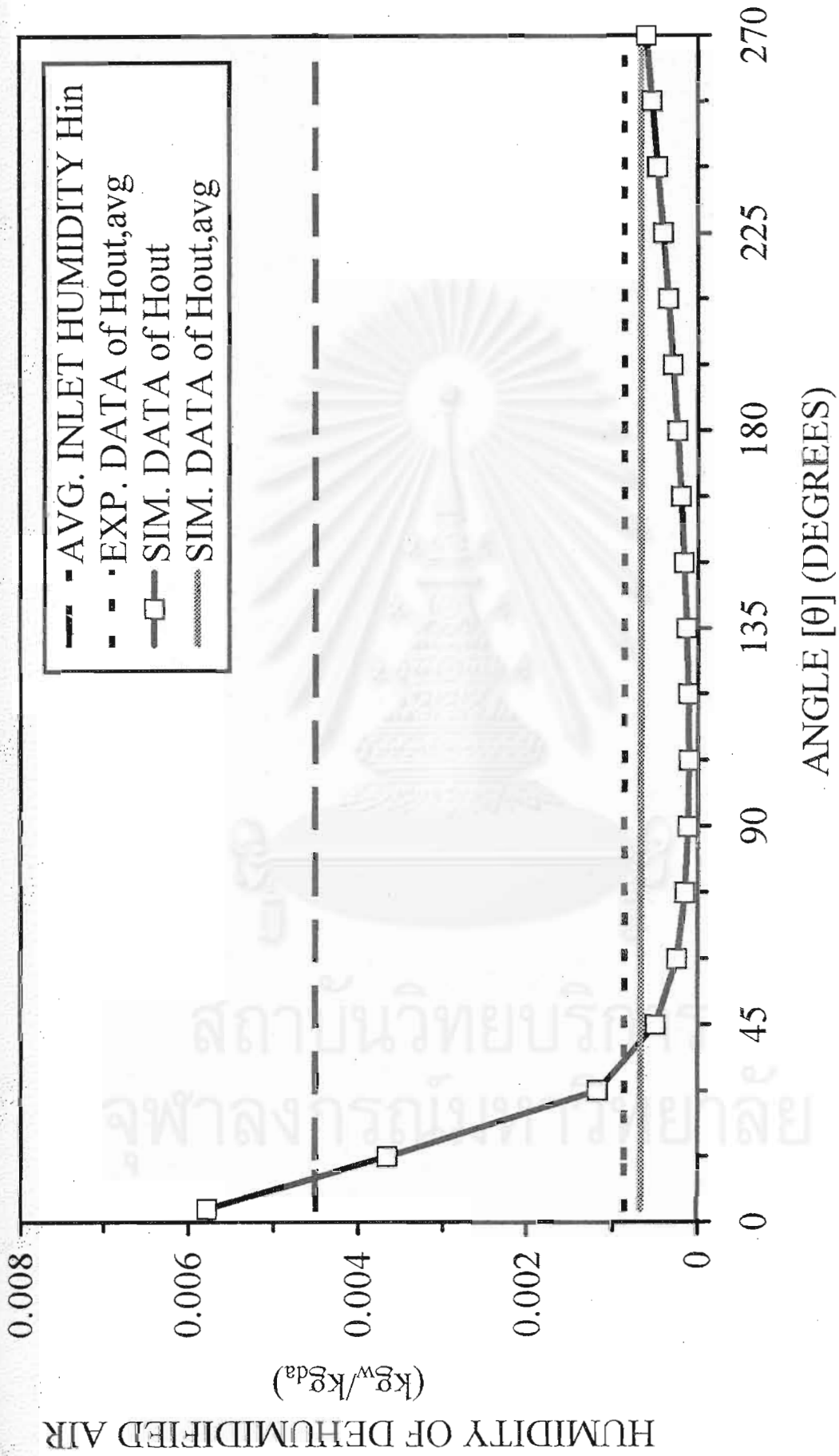
Figure 5.13 Comparison of average humidity of dehumidified air between experimental and simulated results at 13.2 rph
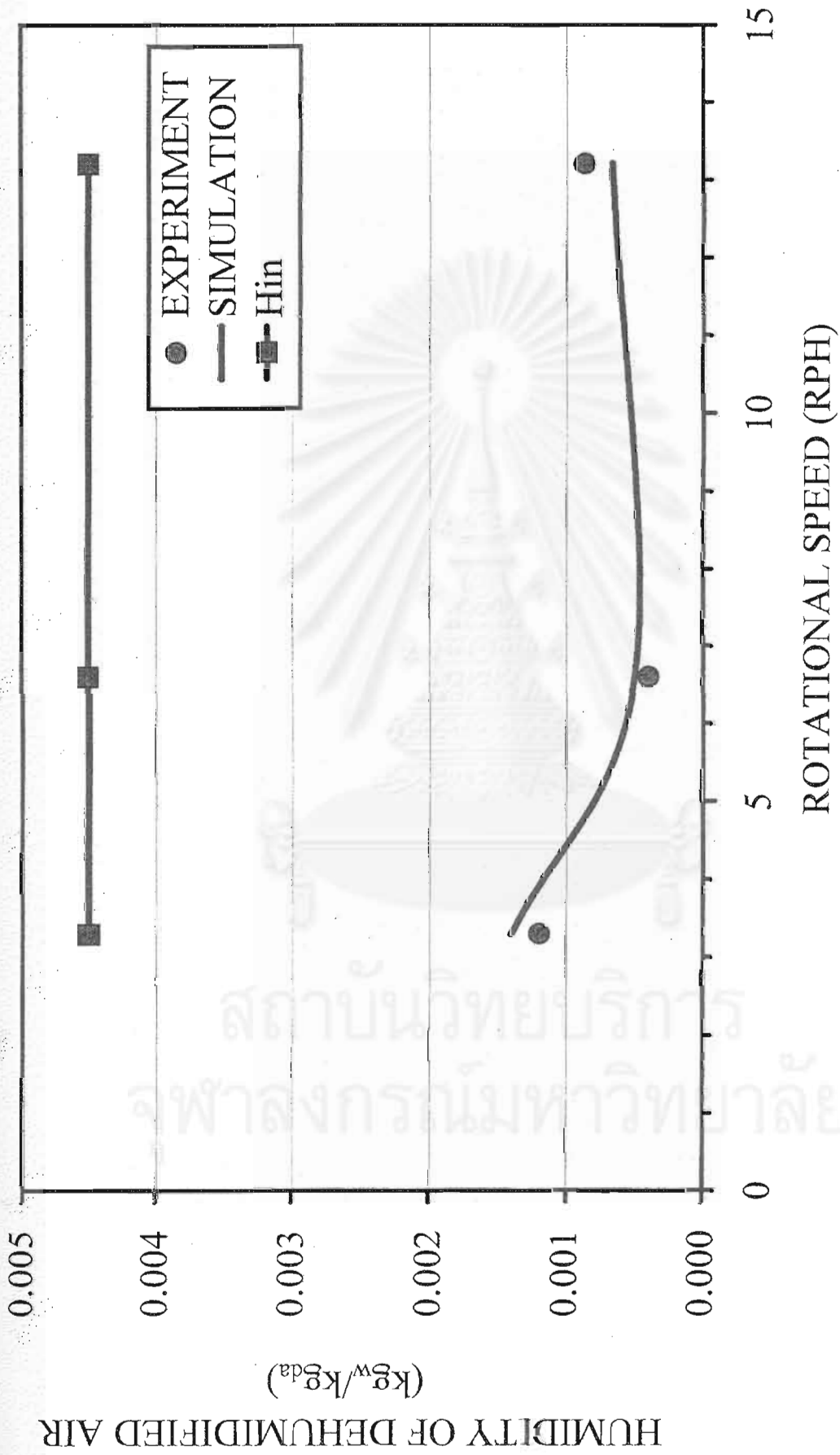
Figure 5.14 Comparison of average humidity of dehumidified air vs. rotational speed between experimental and simulated results
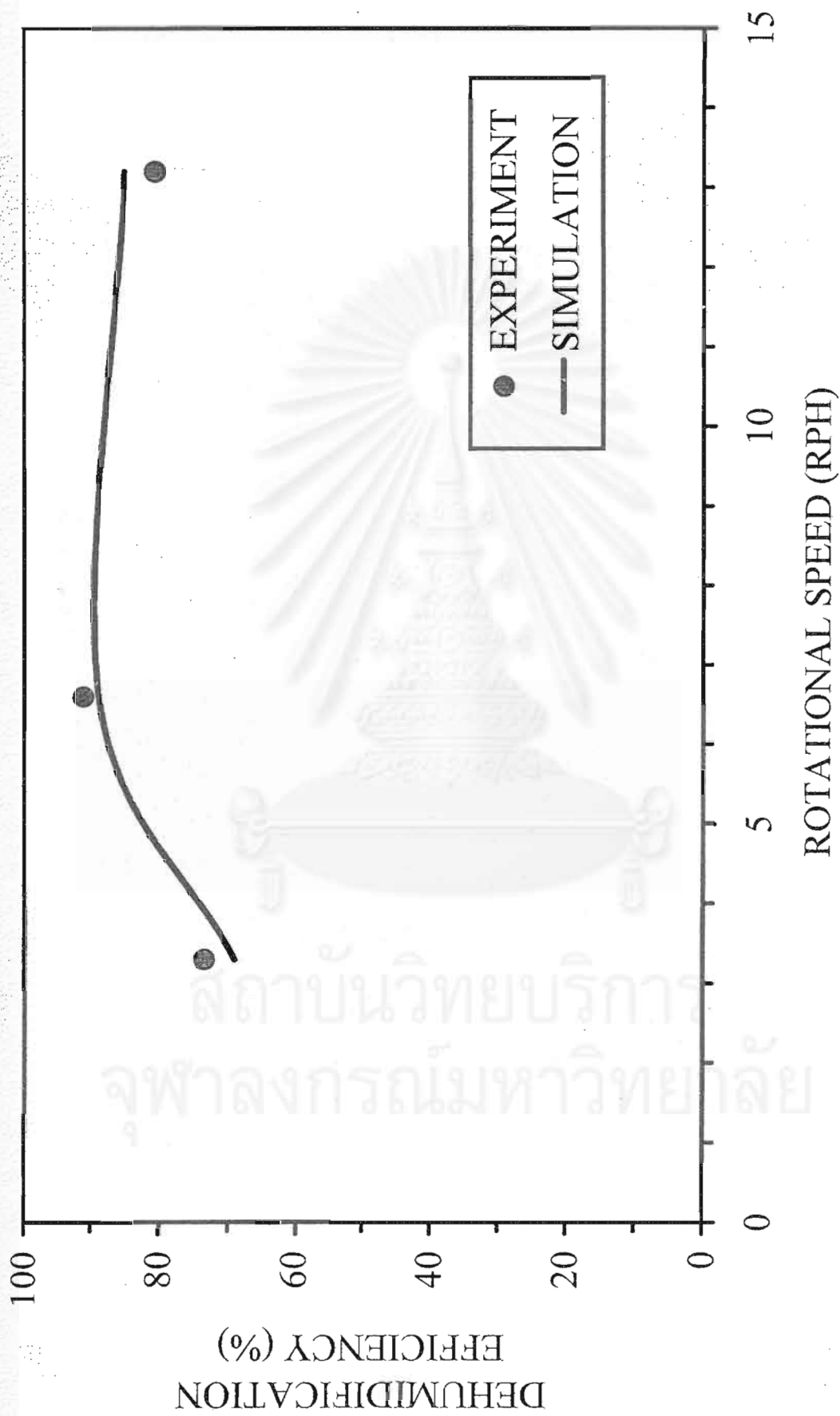
Figure 5.15 Comparison of dehumidification efficiency vs. rotational speed between experimental and simulated results
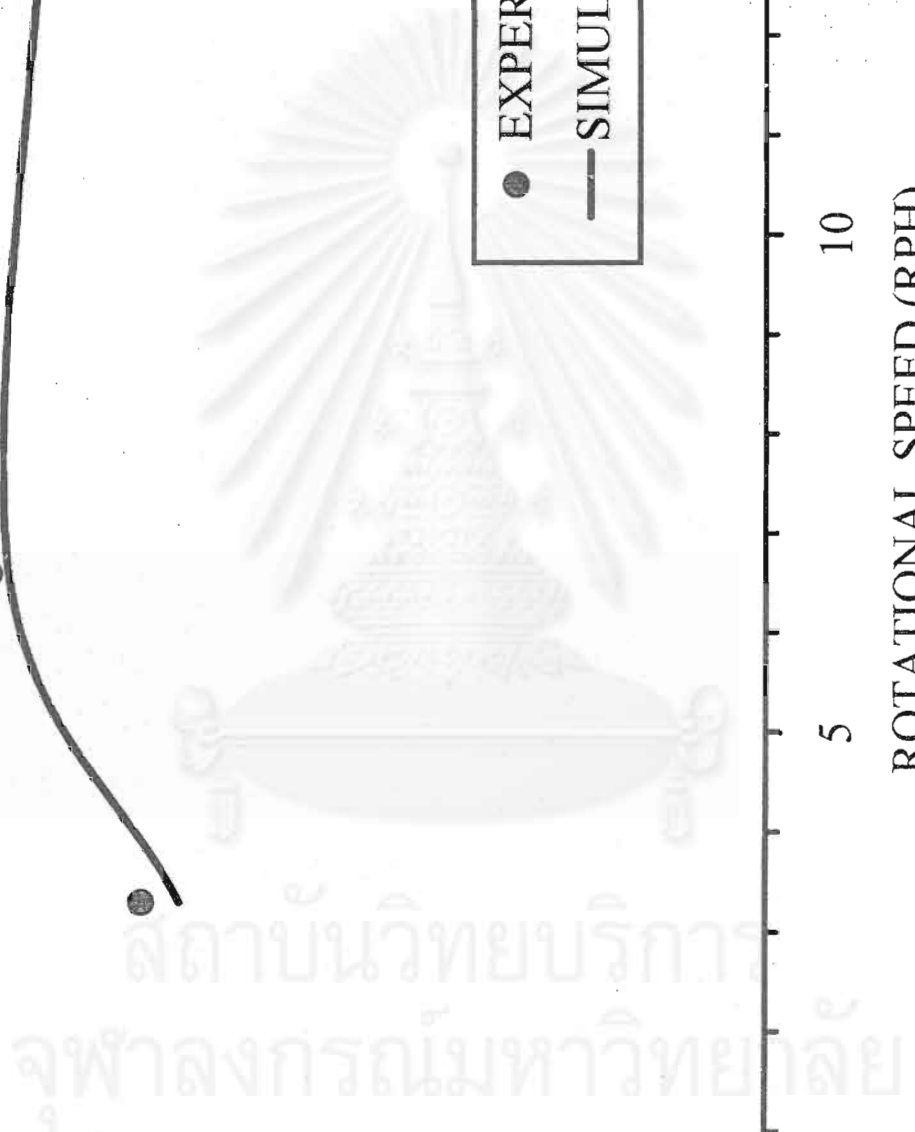
5.2.4 Validation of the two-dimensional distribution of the slot air temperature in the rotary dehumidifier

In this section, two-dimensional distributions of the slot air temperature in the angular and axial directions in the rotary dehumidifier are validated with the published experimental data (Kodama et al., 1994). The operating conditions are as listed in section 5.2.3 and the simulated distributions for the rotational speeds of 3.3, 6.6 and 13.2 rph are presented in Figure 5.16 and 5.18, respectively. The θ angle ranges from $0°$ to $270°$ and $270°$ to $360°$, for the adsorption and regeneration zone respectively. Here, Z denotes the dimensionless length of the rotor or slot.

As seen in Figures 5.16 to 5.18, consistently good agreements between the simulated results (solid lines) and the experimental results (dots) are observed for all of the cases. However, some apparently significant discrepancies are noticeable at the outlet of the regeneration section ($Z = 0$) when the experimental data at the outlet of regeneration zone are always less than the simulated results. The discrepancies may be ascribed to the mixing gas of the exhaust and the much cooler ambient air in the experiments, thus, resulting in lower measured values of the outlet air temperature. In addition, the properties of the silica gel used in the experiments are not identical to those used in the simulation. In conclusion, no matter what the causes of the local discrepancies are, the present dehumidifier model still predicts accurate local values for the entire adsorption zone as well as gives accurate predictions for the overall performance of the rotary dehumidifier.

To understand the local heat transfer phenomena in the rotary dehumidifier, let's consider and discuss Figure 5.17 in more detail. As seen in Figures 5.17a) to 5.17f) for the case of 6.6-rph rotational speed, the angular distribution of the air temperature in the adsorption section is essentially flat at the inlet of the adsorption section ($Z = 0$) except at the borderline between the adsorption and regeneration sections. As the rotor slowly turns, the remaining hot air carried over from the regeneration section will gradually be replaced by the cooler humid room air. The time required for the replacement process is the time it takes the rotor to turns from $0°$-$10°$. This explains why the sharp temperature gradient at Z $= 0$ and θ close to zero begins to gradually broaden up to $\theta = 10°$ as Z increases to unity or

the outlet. As expected, the higher the rotational speed, the broader the temperature gradient as Z approaches unity.

Similarly, it is seen from Figures 5.17a) to 5.17f) that the angular temperature distribution of the hot regeneration air at 413.15 K is essentially flat at the inlet of the regeneration section (Z = 1) except at $\theta = 270°–285°$. As the rotor slowly turns from $\theta = 270°$, the remaining relatively cool air carried over from the adsorption section will gradually be replaced by the hot regeneration air while its thermal energy is used to desorb the moisture from the adsorbent. The large amount of heat of desorption required explains why the temperature of the regeneration air drops significantly as it approaches the outlet (Z = 0). To ensure adequate desorption of the adsorbed moisture the outlet air temperature at $\theta = 360°$ should remain sufficiently high. If the rotational speed is too fast, there will not be enough time to achieve adequate desorption of the moisture and the dehumidification efficiency will start to decrease. On the contrary, if the rotational speed is too slow, then the adsorbent will become saturated before it reaches the regeneration section. As a result the dehumidification efficiency again decreases.
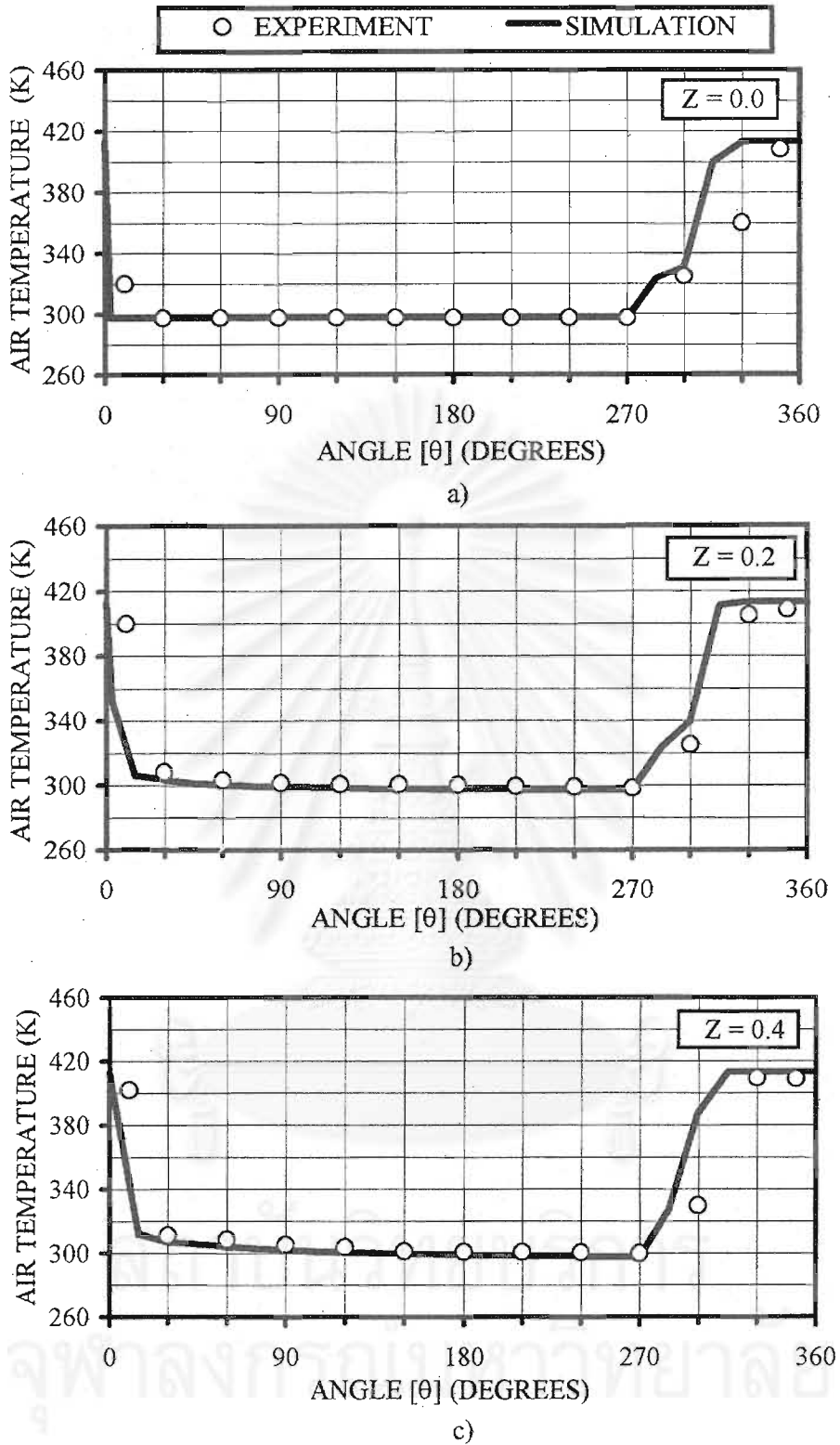
Figure 5.16 Comparison of the angular distributions of the slot air temperature between the experimental and simulated results at 3.3 rph and various dimensionless lengths: a) Z = 0.0, b) Z= 0.2, c) Z = 0.4, d) Z = 0.6, e) Z = 0.8 and f) Z = 1.0
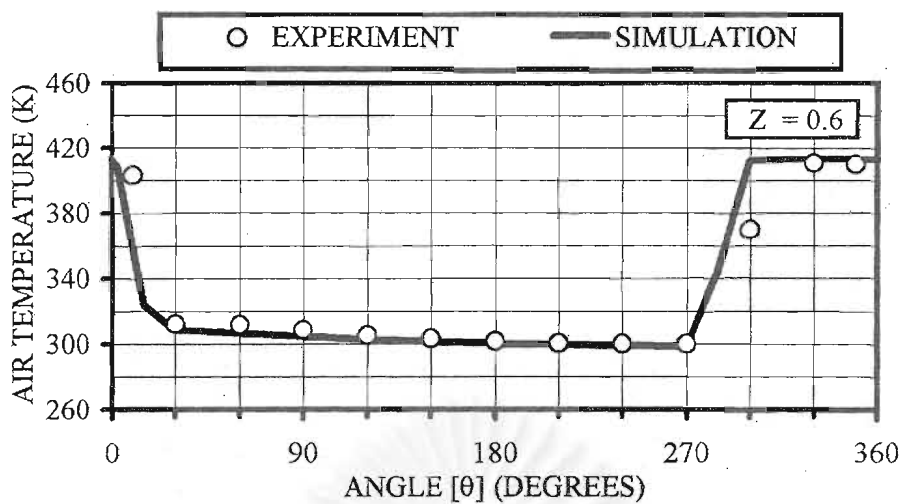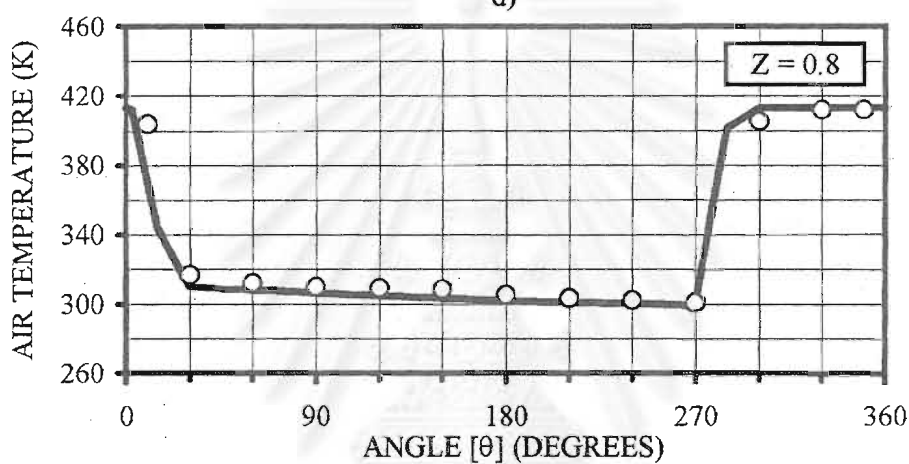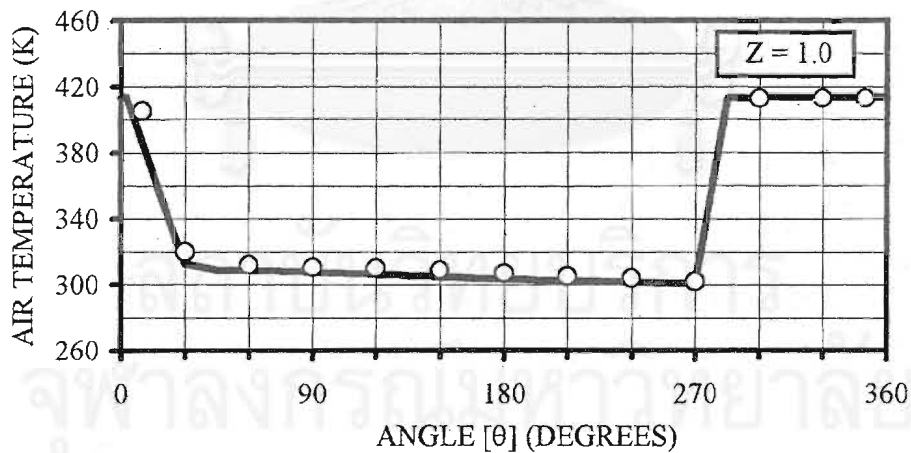
Figure 5.16(cont.) Comparison of the angular distributions of the slot air temperature between the experimental and simulated results at 3.3 rph and various dimensionless lengths: a) Z = 0.0, b) Z= 0.2, c) Z = 0.4, d) Z = 0.6, e) Z = 0.8 and f) Z = 1.0
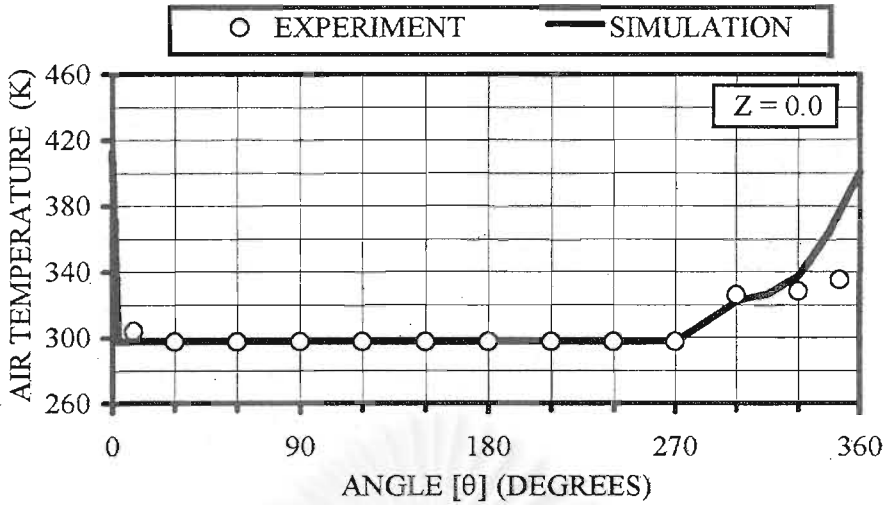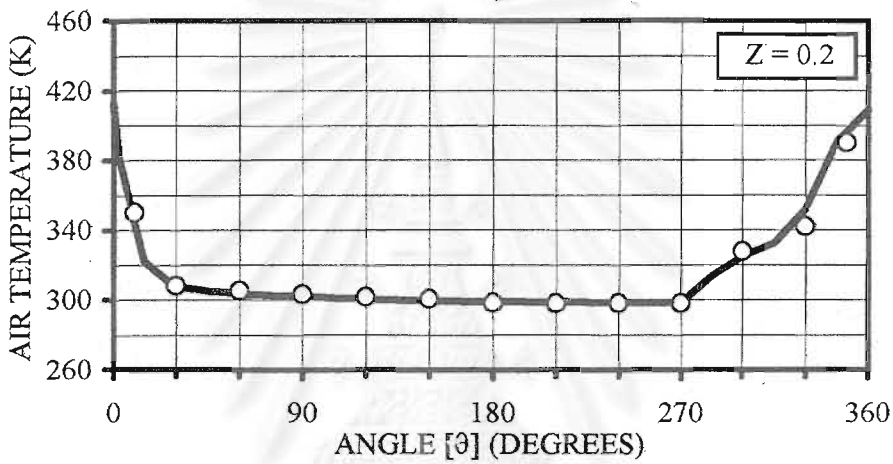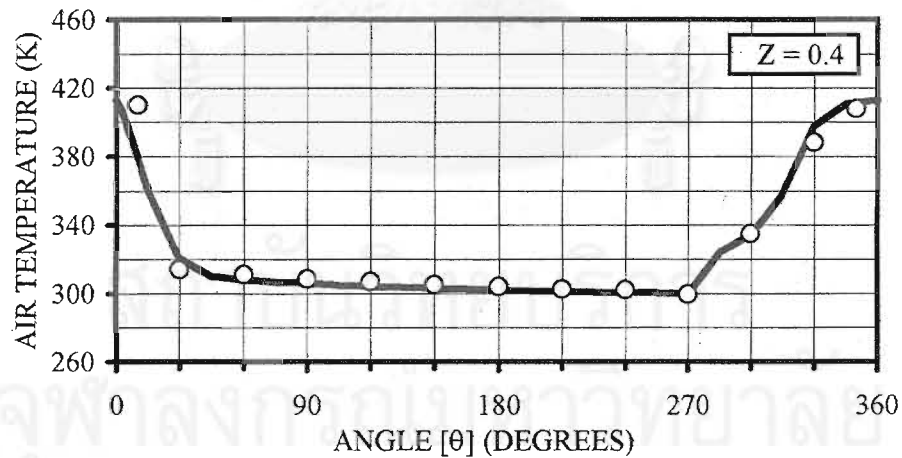
Figure 5.17 Comparison of the angular distributions of the slot air temperature between the experimental and simulated results at 6.6 rph and various dimensionless lengths: a) Z = 0.0, b) Z= 0.2, c) Z = 0.4, d) Z = 0.6, e) Z = 0.8 and f) Z = 1.0
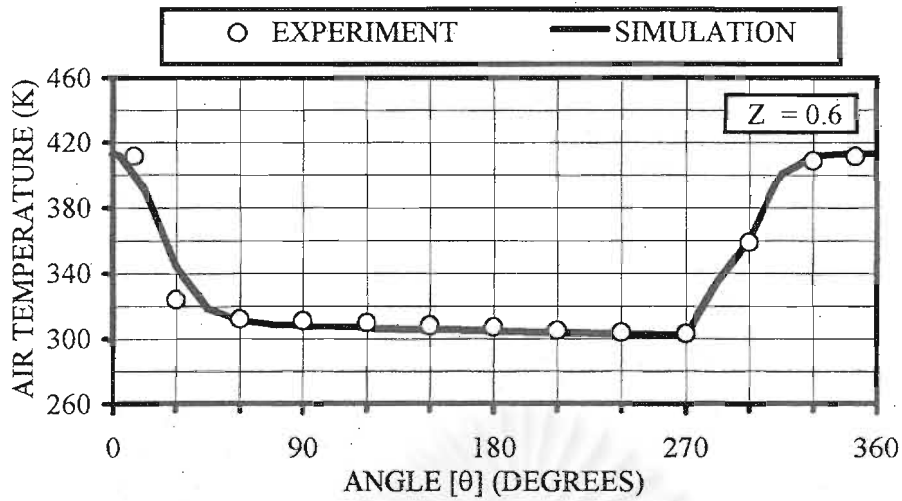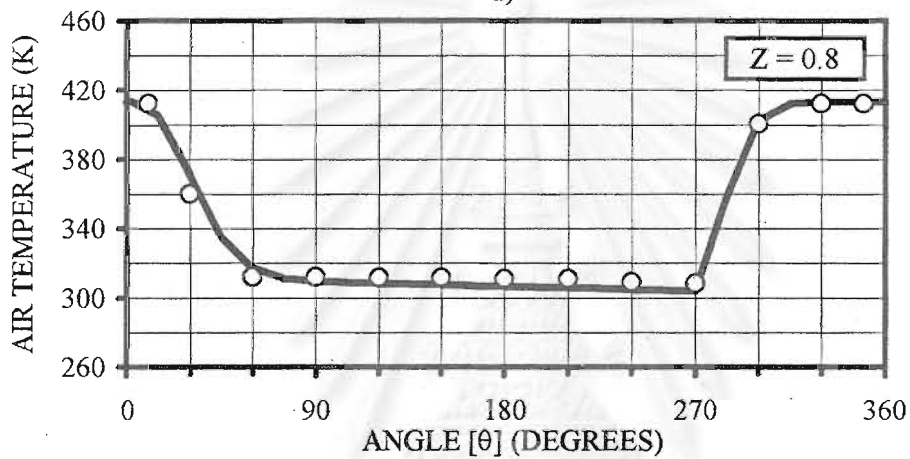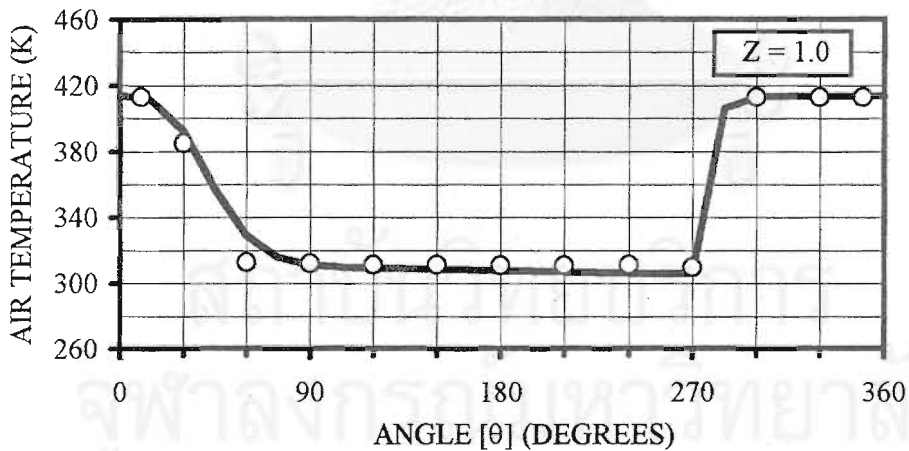
Figure 5.17(cont.) Comparison of the angular distributions of the slot air temperature between the experimental and simulated results at 6.6 rph and various dimensionless lengths: a) Z = 0.0, b) Z= 0.2, c) Z = 0.4, d) Z = 0.6, e) Z = 0.8 and f) Z = 1.0
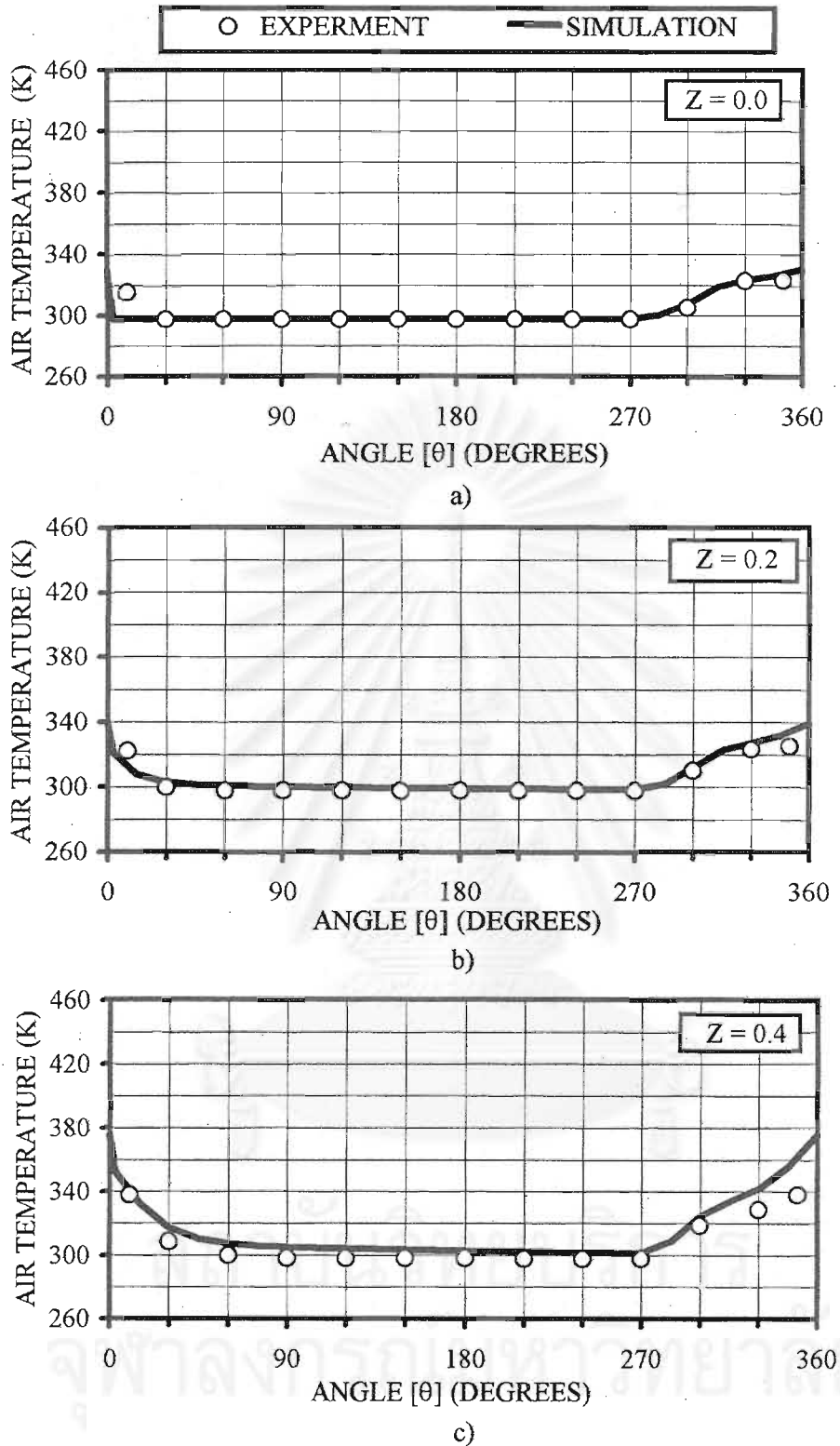
Figure 5.18 Comparison of the angular distributions of the slot air temperature between the experimental and simulated results at 13.2 rph and various dimensionless lengths: a) Z = 0.0, b) Z= 0.2, c) Z = 0.4, d) Z = 0.6, e) Z = 0.8 and f) Z = 1.0
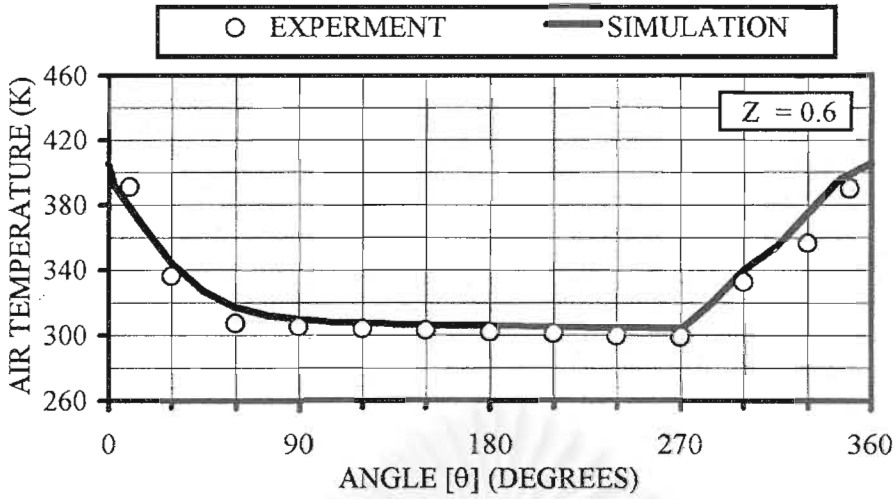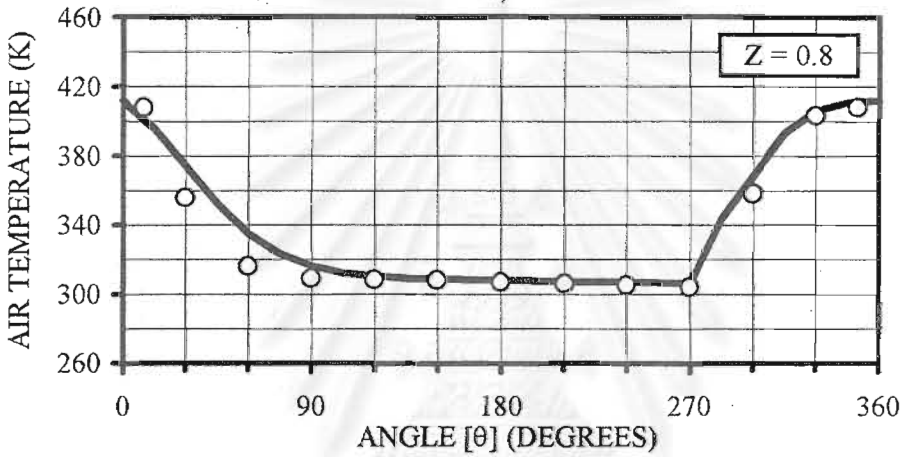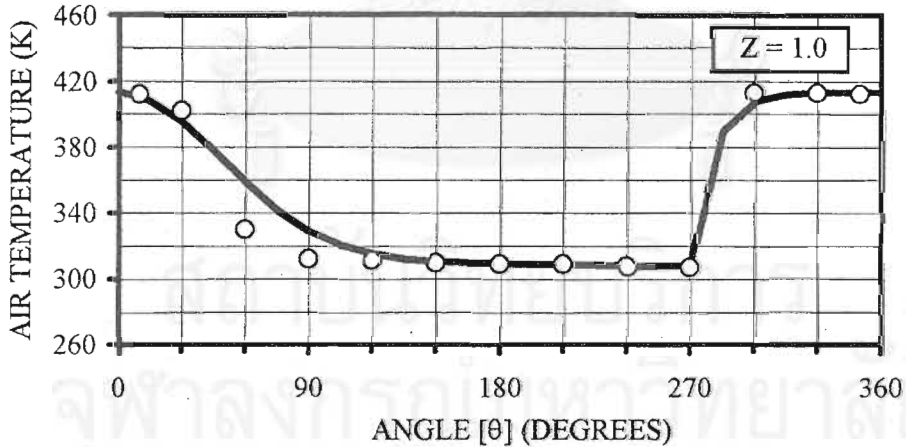
Figure 5.18(cont.) Comparison of the angular distributions of the slot air temperature between the experimental and simulated results at 13.2 rph and various dimensionless lengths: a) Z = 0.0, b) Z= 0.2, c) Z = 0.4, d) Z = 0.6, e) Z = 0.8 and f) Z = 1.0

5.2.5 Validation of angular distributions of the temperature and humidity of the dehumidified air

To ensure high accuracy and reliability of the model, the simulation results on the angular distribution of the temperature and humidity of the dehumidified air are also validated with the detailed experimental data of Kodama et al.(1993) in this section. Two main factors are investigated. One is the variation of the rotational speed in the range of 3.5 to 28 rph as shown in Figures 5.19 to 5.28. The other is the variation of the inlet air humidity in the range of 0.0030 to 0.0142 kg_w/kg_{da} as shown in Figures 5.29 to 5.36. In the Figures, the solid lines represent the simulation results and the dots the experimental results. The initial conditions used are summarized in Table 5.18. The inlet conditions for the rotational speed and the inlet air humidity are listed in Tables 5.19 and 5.20, respectively.

Table 5.18 Initial conditions used to validate the effect of the rotational speed and the inlet air humidity on the silica gel coated honeycomb rotary dehumidifier

INITIAL CONDITIONS		
Local amount of moisture adsorbed in the adsorbent (W_0)	0.001	kg_w/kg_{sb}
Local air humidity in the slots (H_0)	0.0001	kg_w/kg_{da}
Local solid temperature in the slots(Ts_0)	293.15	K
Local gas temperature in the slots (Ta_0)	293.15	K

Table 5.19 Inlet conditions used to validate the effect of the rotational speed on the silica gel coated honeycomb rotary dehumidifier

INLET CONDITIONS		
Inlet humidity of the adsorption zone ($H_{in,ads}$)	4.5×10^{-3}	kg_w/kg_{da}
Inlet gas temperature of the adsorption zone ($Ta_{in,ads}$)	297.30	K
Inlet humidity of the regeneration zone ($H_{in,reg}$)	5×10^{-4}	kg_w/kg_{da}
Inlet gas temperature of the regeneration zone ($Ta_{in,reg}$)	413.15	K
Inlet air velocity of the adsorption zone ($V_{in,ads}$)	1.0	m/s
Inlet air velocity of the regeneration zone ($V_{in,reg}$)	1.0	m/s

Table 5.20 Inlet conditions used to validate the effect of inlet air humidity on the silica gel
coated honeycomb rotary dehumidifier

INLET CONDITIONS		
Inlet gas temperature of the adsorption zone ($Ta_{in,ads}$)	297.30	K
Inlet humidity of the regeneration zone ($H_{in,reg}$)	5×10^{-4}	kg_w/kg_{da}
Inlet gas temperature of the regeneration zone ($Ta_{in,reg}$)	413.15	K
Inlet air velocity of the adsorption zone ($V_{in,ads}$)	1.0	m/s
Inlet air velocity of the regeneration zone ($V_{in,reg}$)	1.0	m/s
Rotational speed (φ)	6.0	rph

As seen in Figures 5.19 to 5.36, the simulated results on both the angular distribution
of the temperature and humidity of the dehumidified air agree reasonably very well with the
corresponding experimental data. Since the properties of the silica gel used in the
experiments and the simulations may not be identical, some discrepancies in the angular
distributions are not unusual.

Considering the angular humidity profiles of the dehumidified air, high values of the
outlet humidity are always observed in range of $\theta = 0°$ to $15°$, sometimes, extending to $30°$.
As the rotor slowly turns, the relatively hot humid air carried over from the regeneration
section will gradually be replaced by the cooler humid room air. The adsorption capacity of
the adsorbent decreases as the temperature increases. Since the air replacement and cooling
process take some time to achieve, the outlet air humidity remains relatively high in the
region of small θ. Such behavior depends on the rotational speed of the rotor as shown in
Figures 5.19 to 5.28. For instance, high air humidity the region of small θ values extends to
approximately $90°$ in the case of 28-rph rotational speed in spite of only $15°$ for the 3.5-rph
rotational speed. In addition, the gradual broadening of the high humidity region in terms of
θ is pronounced especially at high inlet humidity and low rotational speed. Accordingly, the
dehumidification efficiency will significantly decrease if the operating conditions are not
suitable.

The effect of the rotational speed on the angular profile of the temperature of the
dehumidified air has already been discussed and will be omitted here.
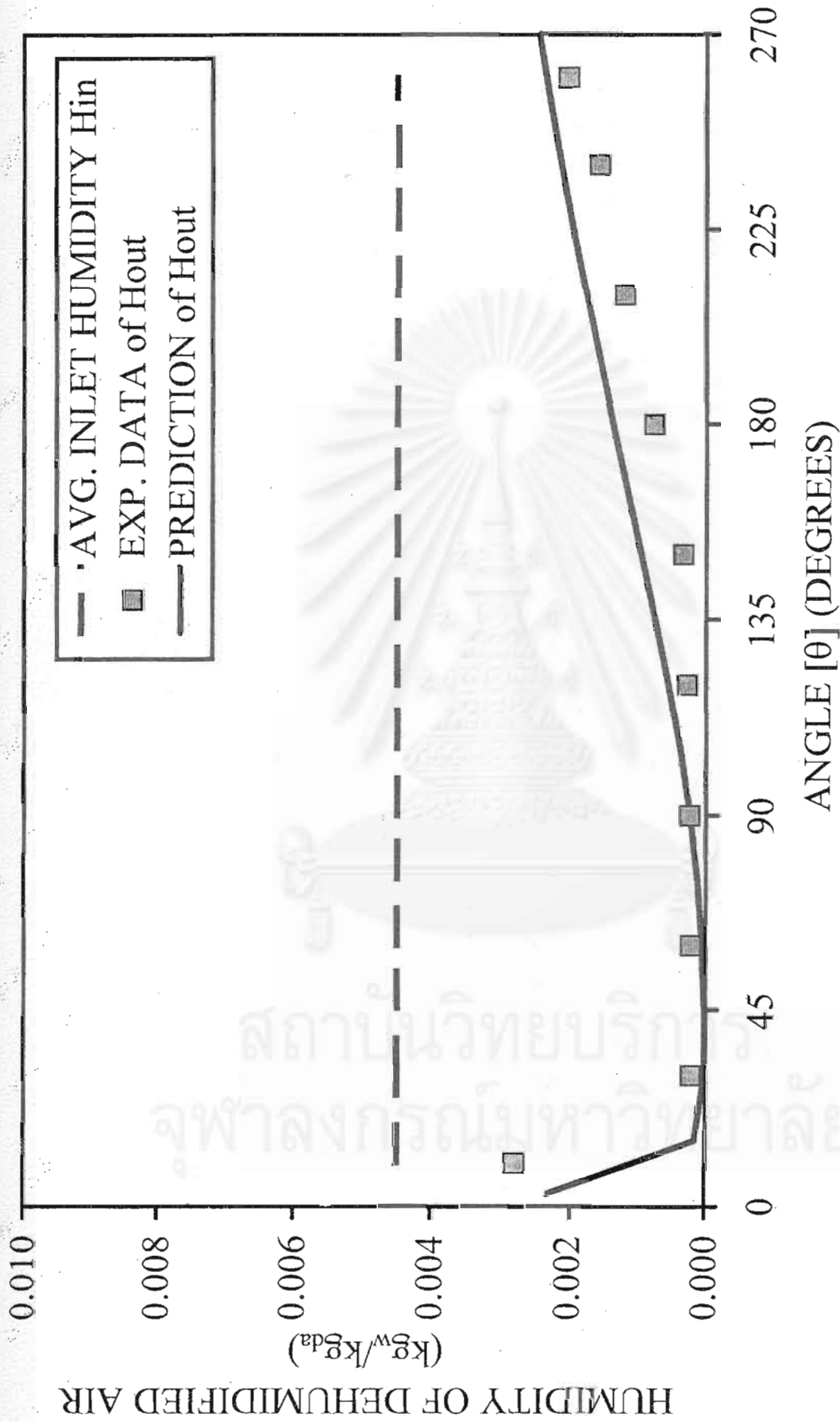
Figure 5.19 Comparison of angular distribution of the humidity of the dehumidified air between experimental and simulated results at 3.5 rph
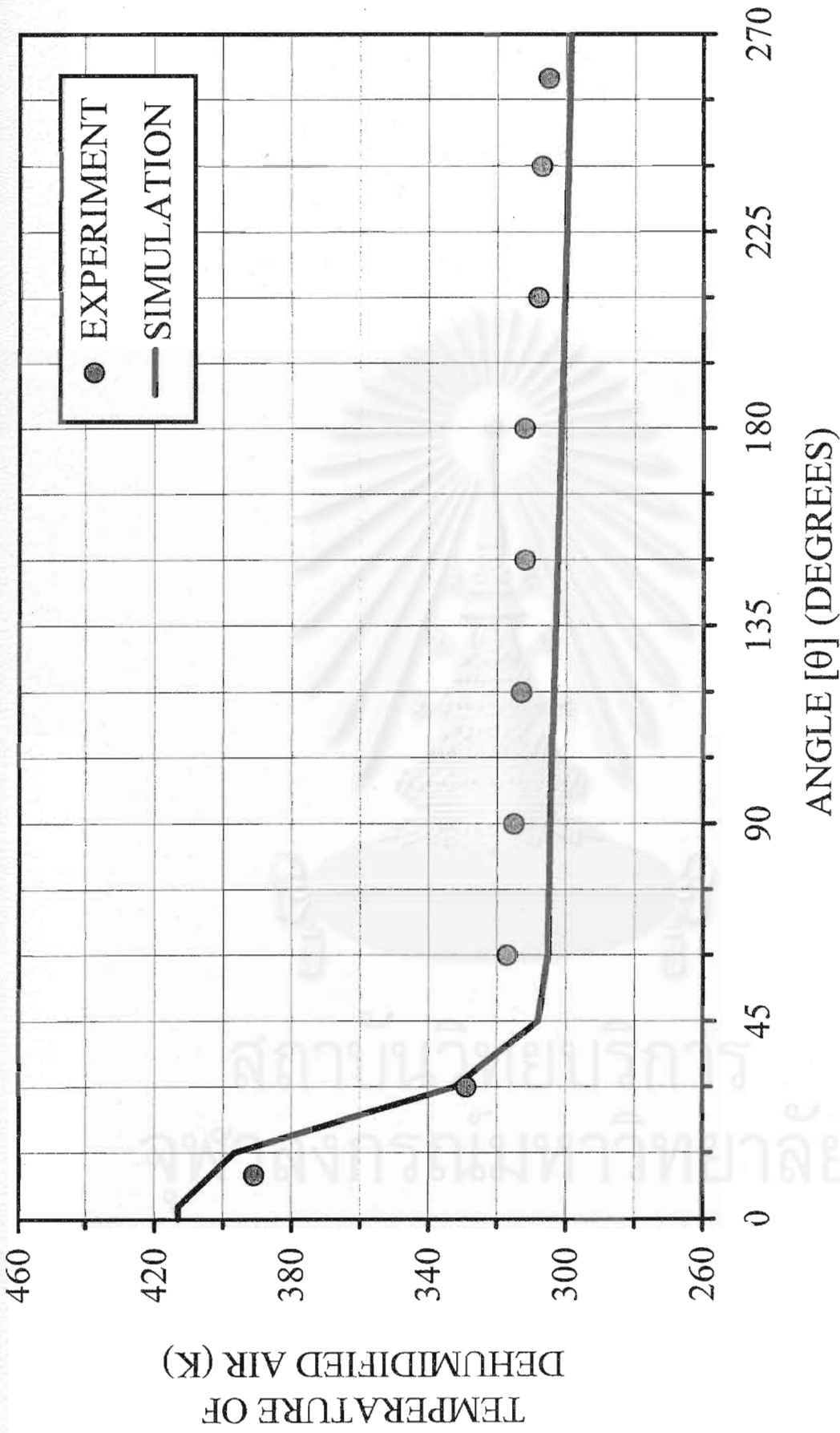
Figure 5.20 Comparison of angular distribution of the temperature of the dehumidified air between experimental and simulated results at 3.5 rph
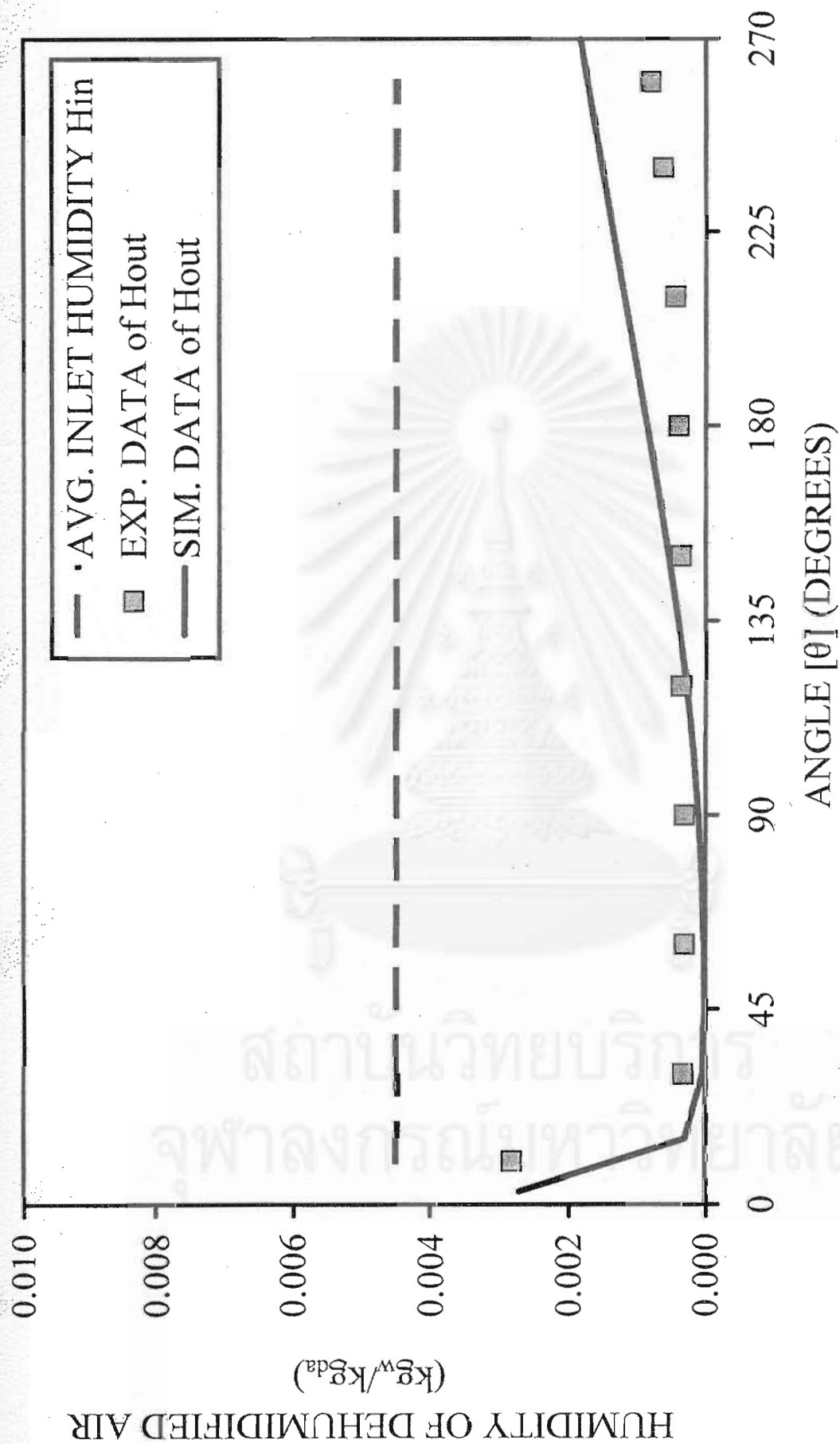
Figure 5.21 Comparison of angular distribution of the humidity of the dehumidified air between experimental and simulated results at 4.4 rph
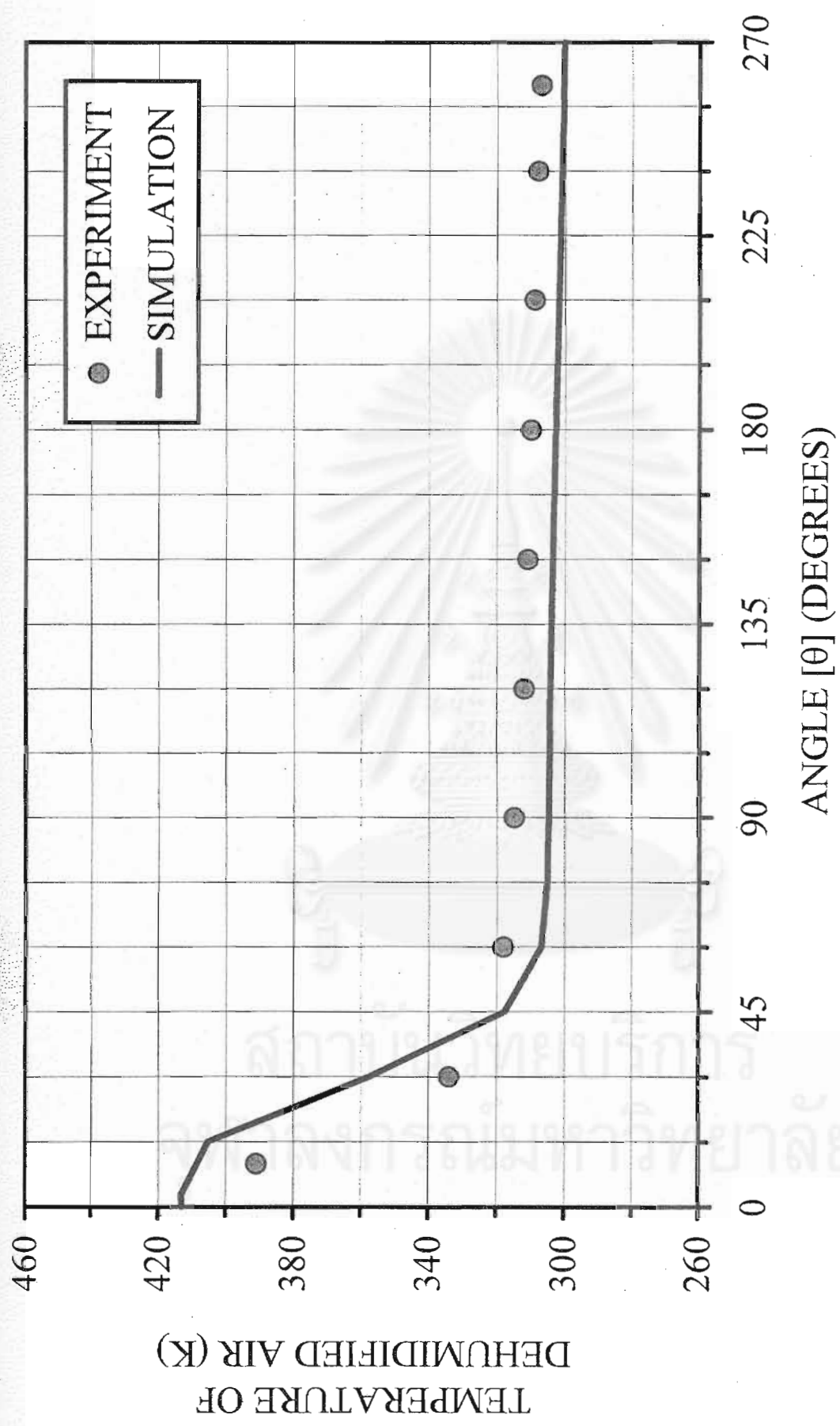
Figure 5.22 Comparison of angular distribution of the temperature of the dehumidified air between experimental and simulated results at 4.4 rph
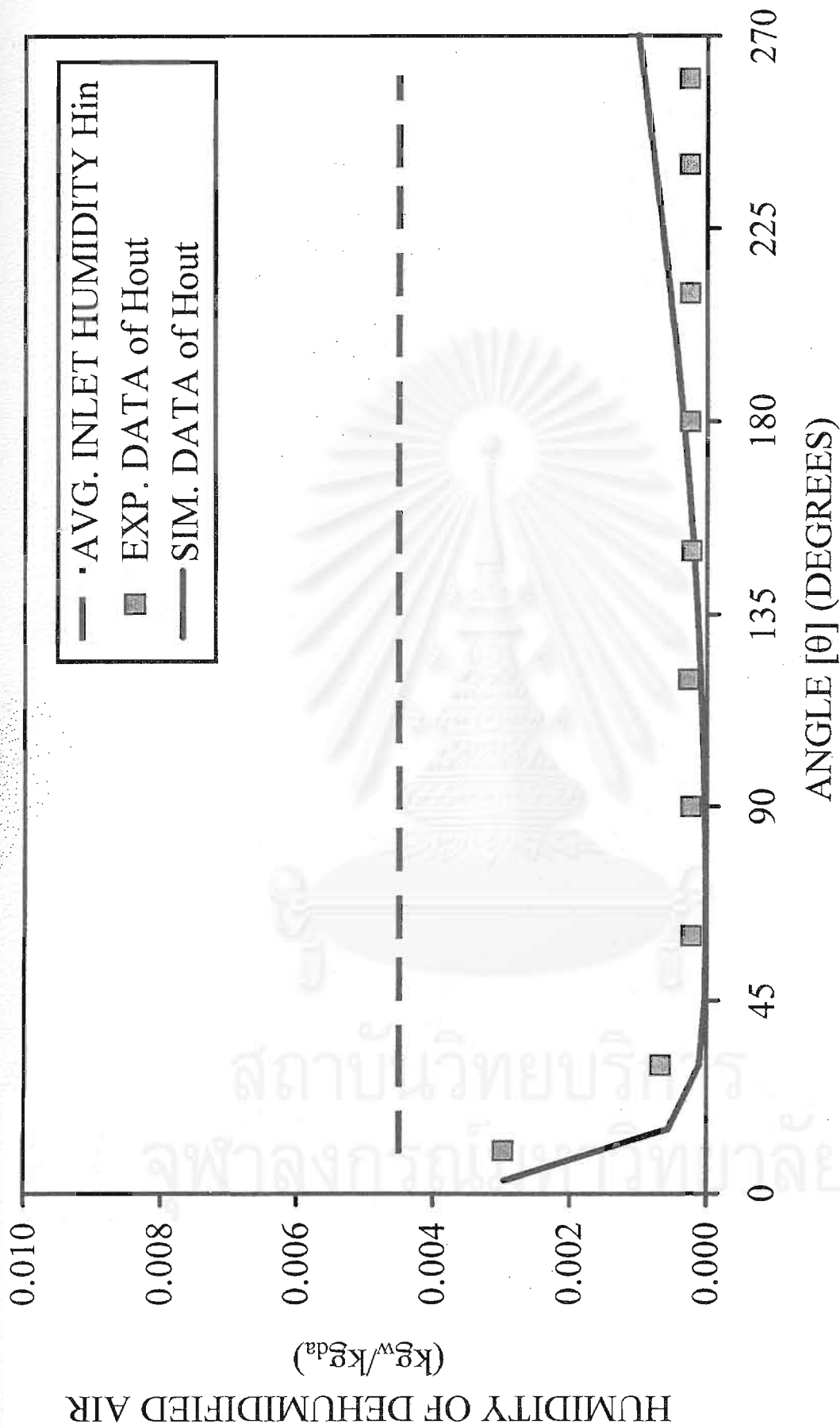
Figure 5.23 Comparison of angular distribution of the humidity of the dehumidified air between experimental and simulated results at 6.2 rph
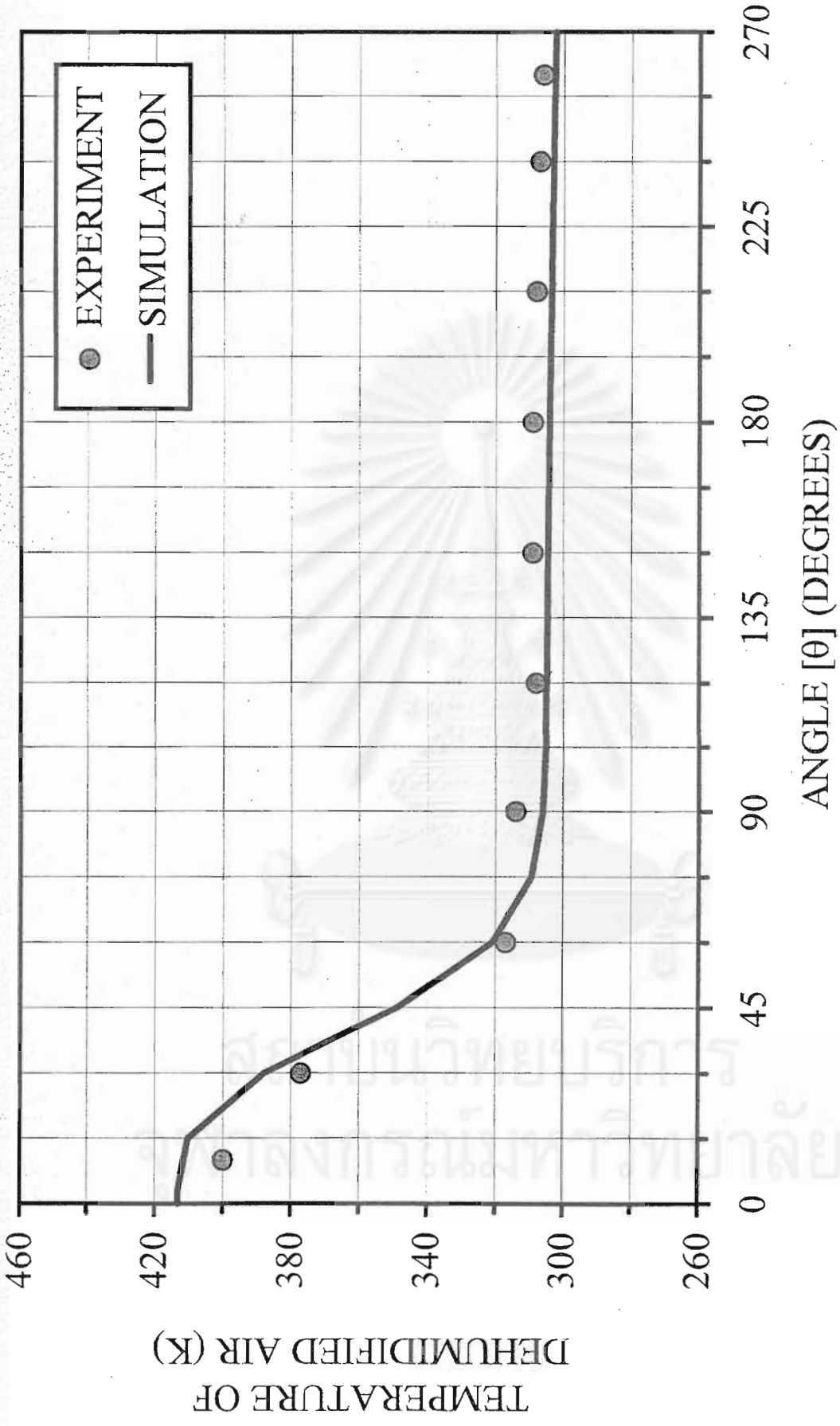
Figure 5.24 Comparison of angular distribution of the temperature of the dehumidified air between experimental and simulated results at 6.2 rph
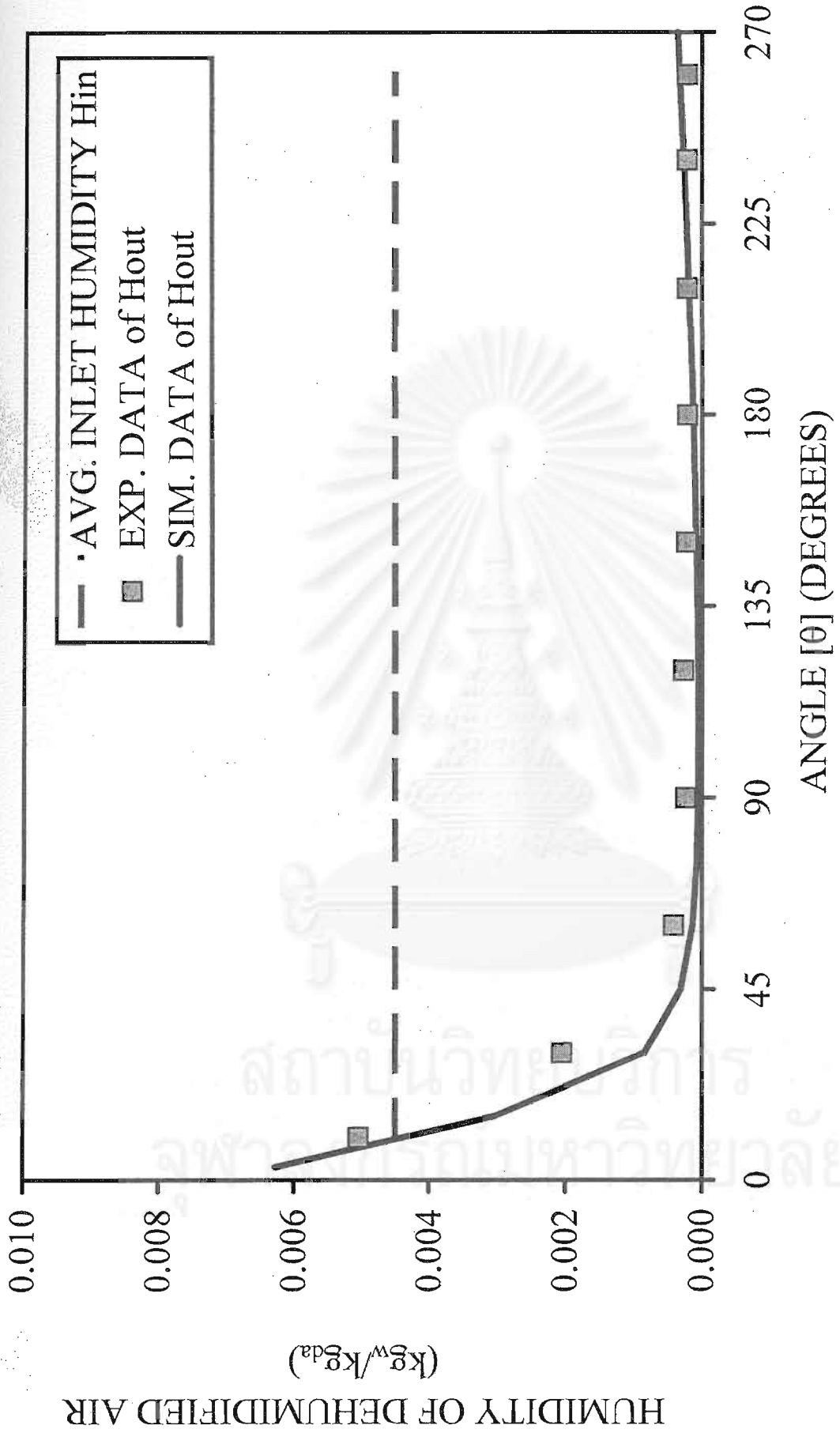
Figure 5.25 Comparison of angular distribution of the humidity of the dehumidified air between experimental and simulated results at 12.5 rph
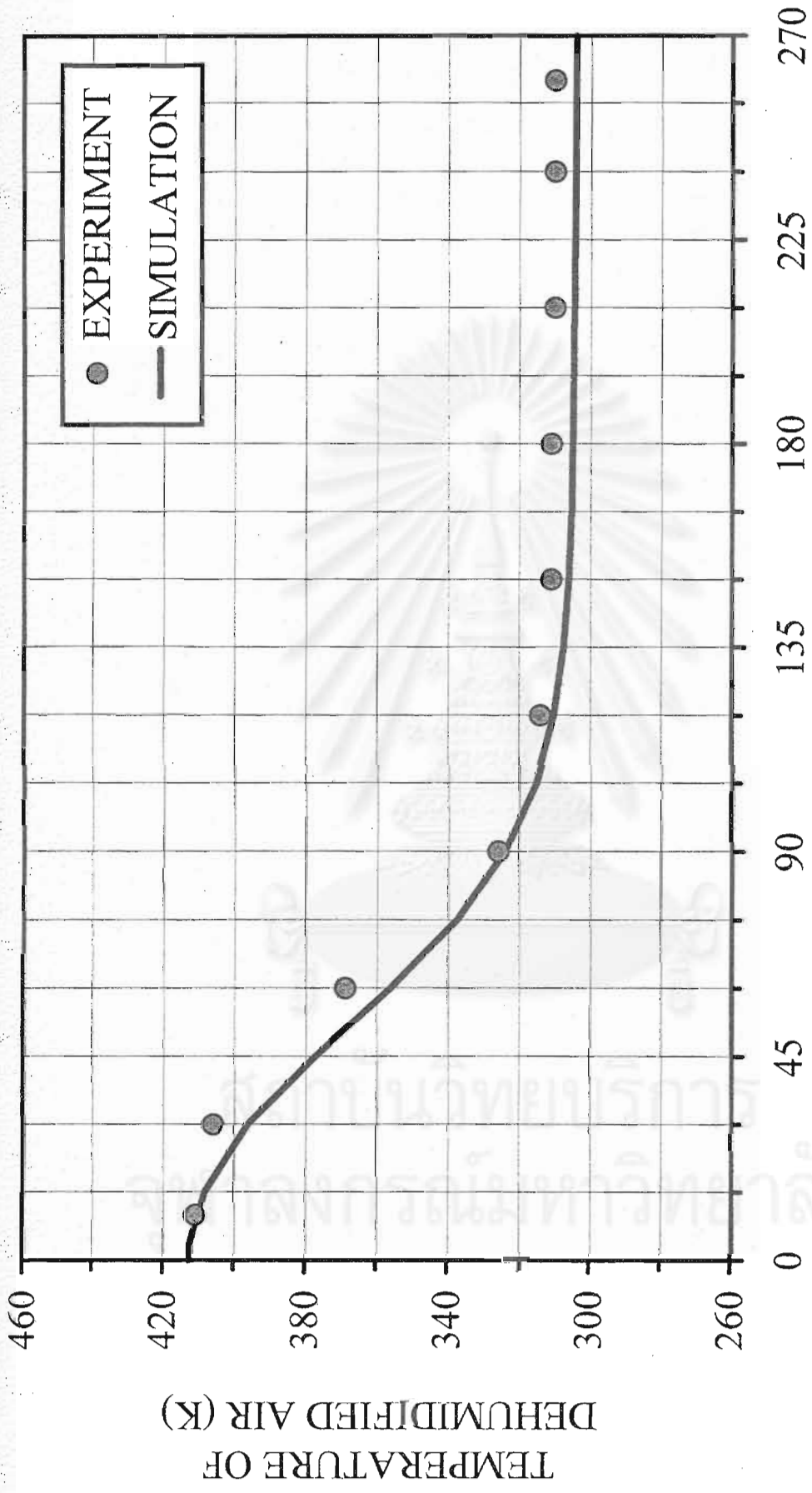
Figure 5.26 Comparison of angular distribution of the temperature of the dehumidified air between experimental and simulated results at 12.5 rph
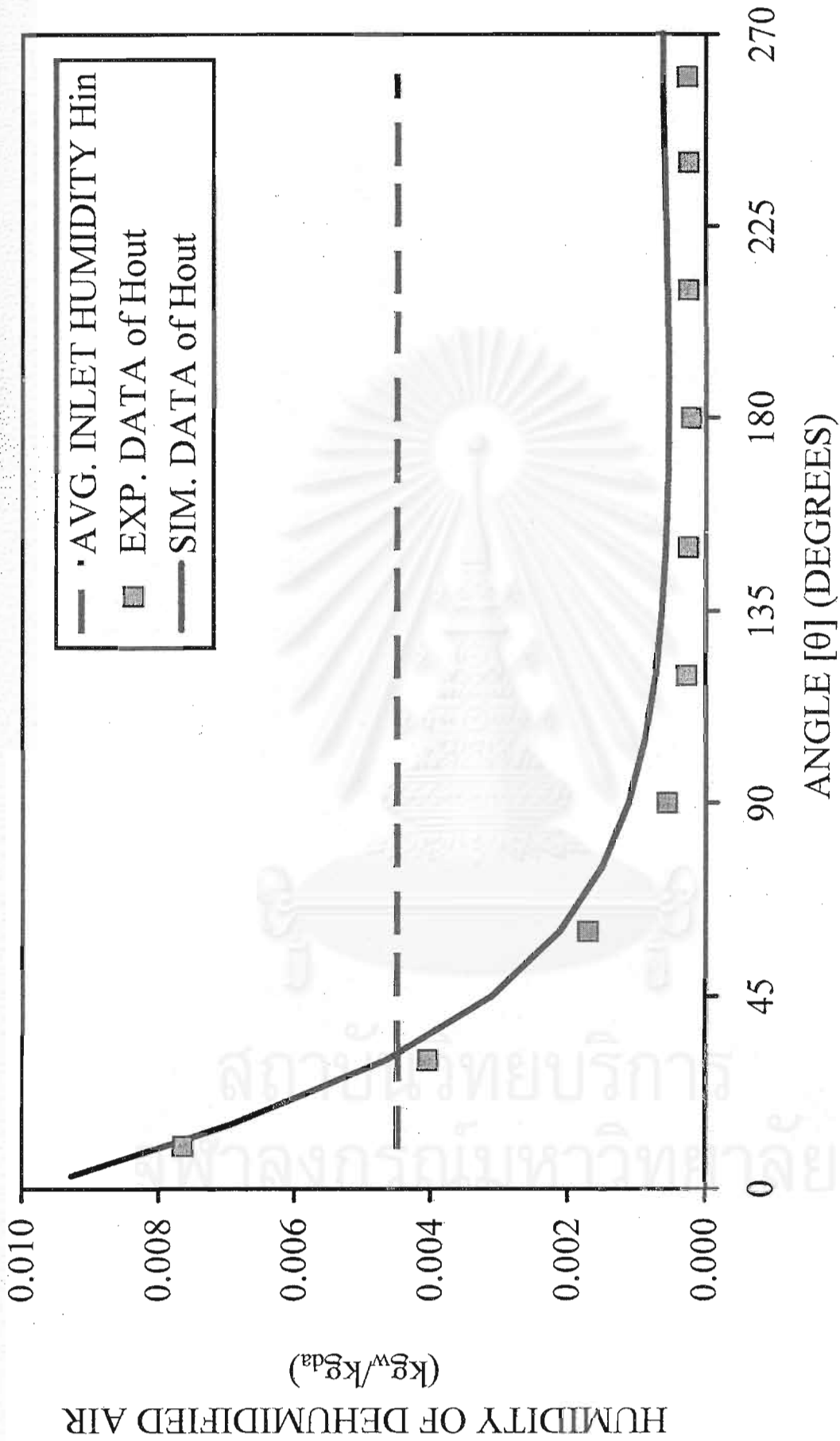
Figure 5.27 Comparison of angular distribution of the humidity of the dehumidified air between experimental and simulated results at 28 rph
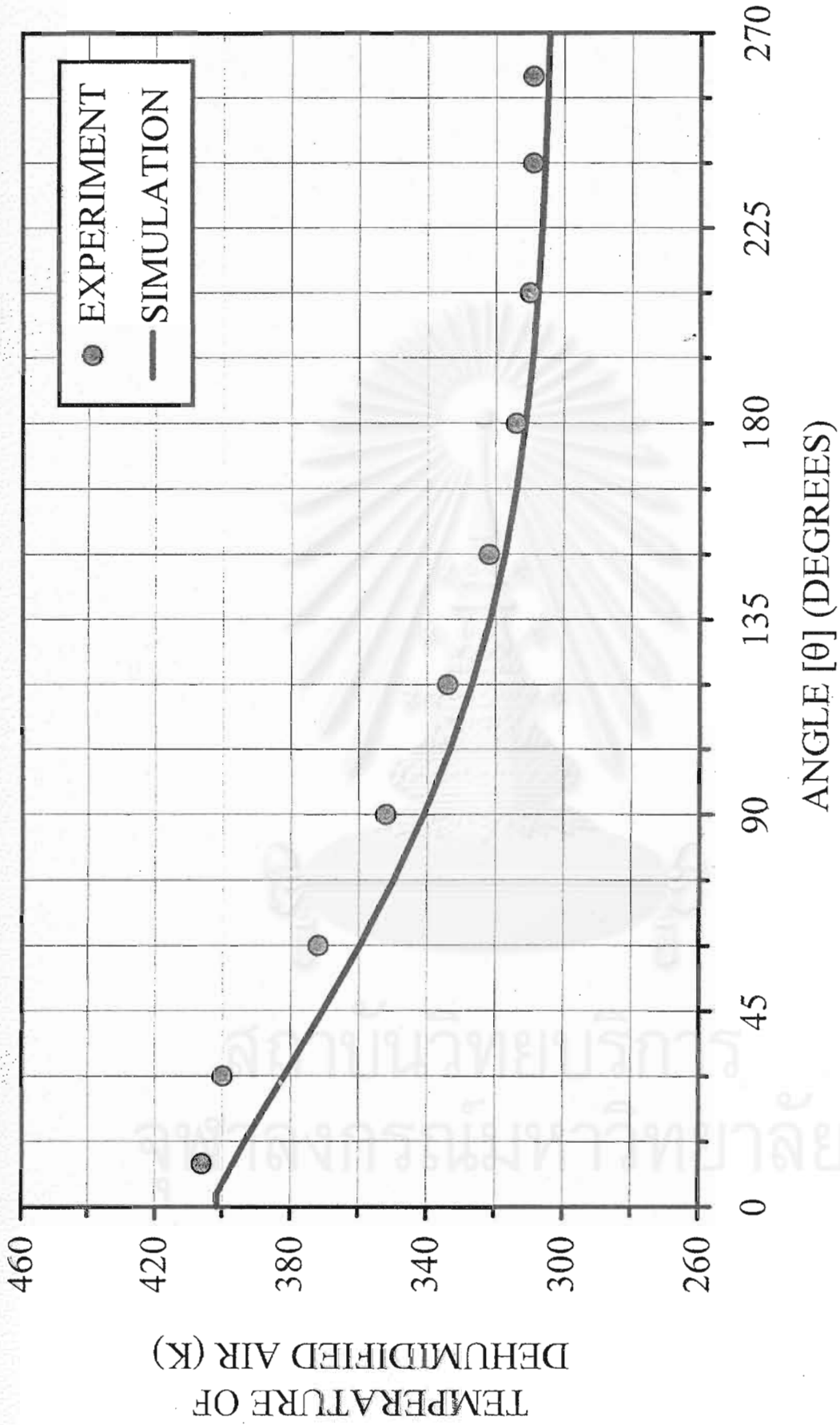
Figure 5.28 Comparison of angular distribution of the temperature of the dehumidified air between experimental and simulated results at 28 rph
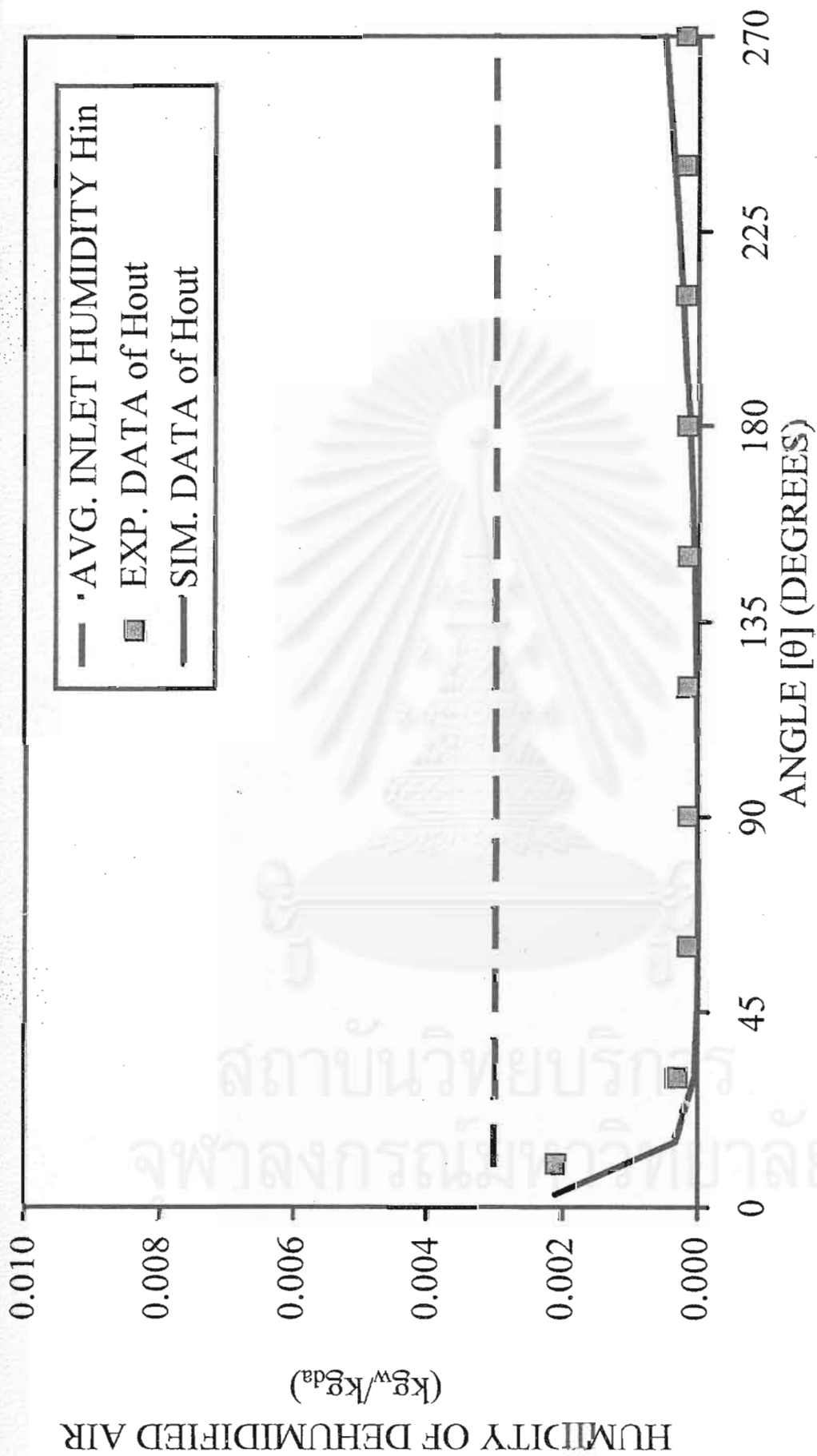
Figure 5.29 Comparison of angular distribution of the humidity of the dehumidified air between experimental and simulated results at $H_{in} = 0.003 \text{ kg}_w/\text{kg}_{da}$
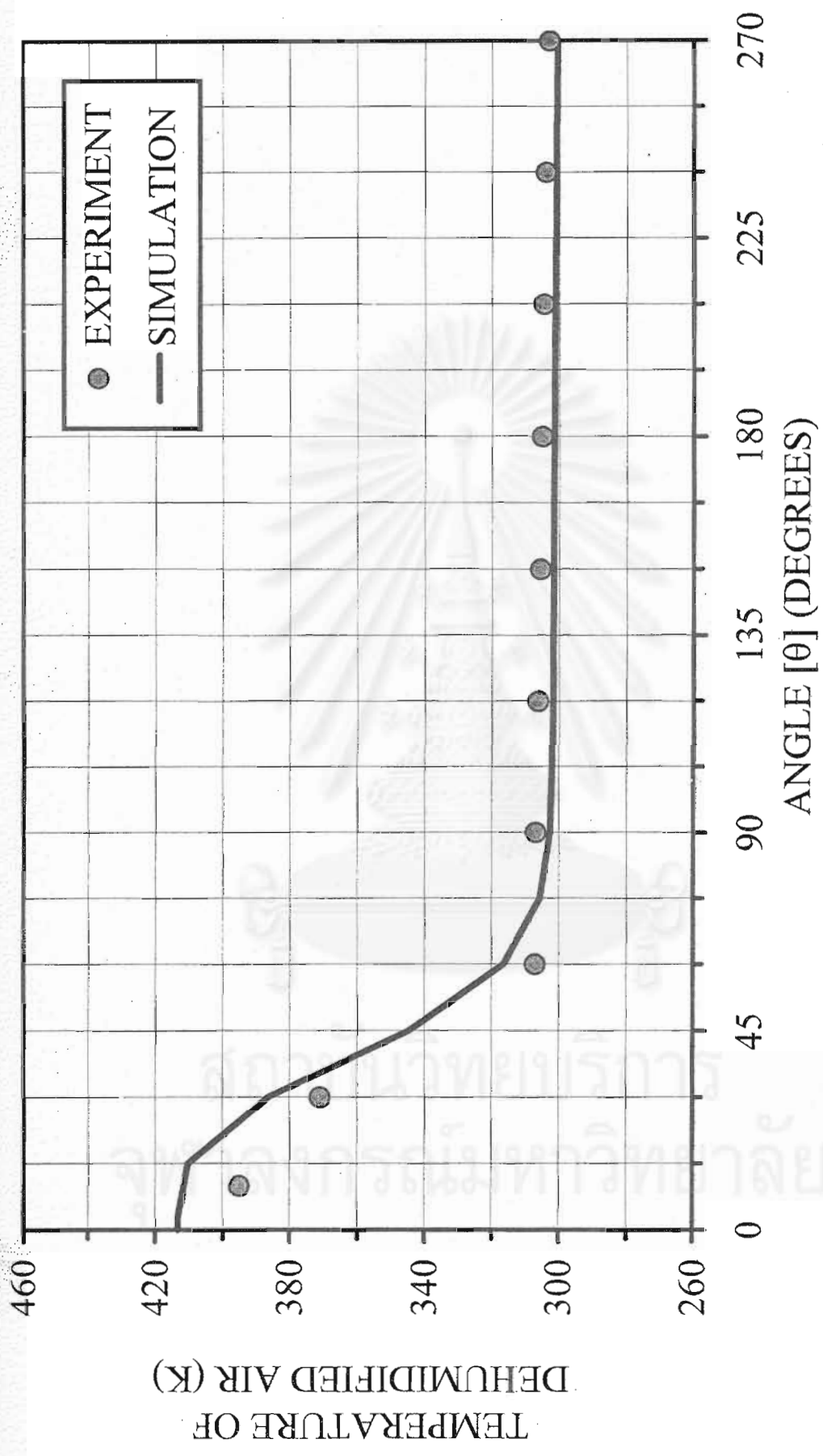
Figure 5.30 Comparison of angular distribution of the temperature of the dehumidified air between experimental and simulated results at $H_{in} = 0.003 \text{ kg}_w/\text{kg}_{da}$
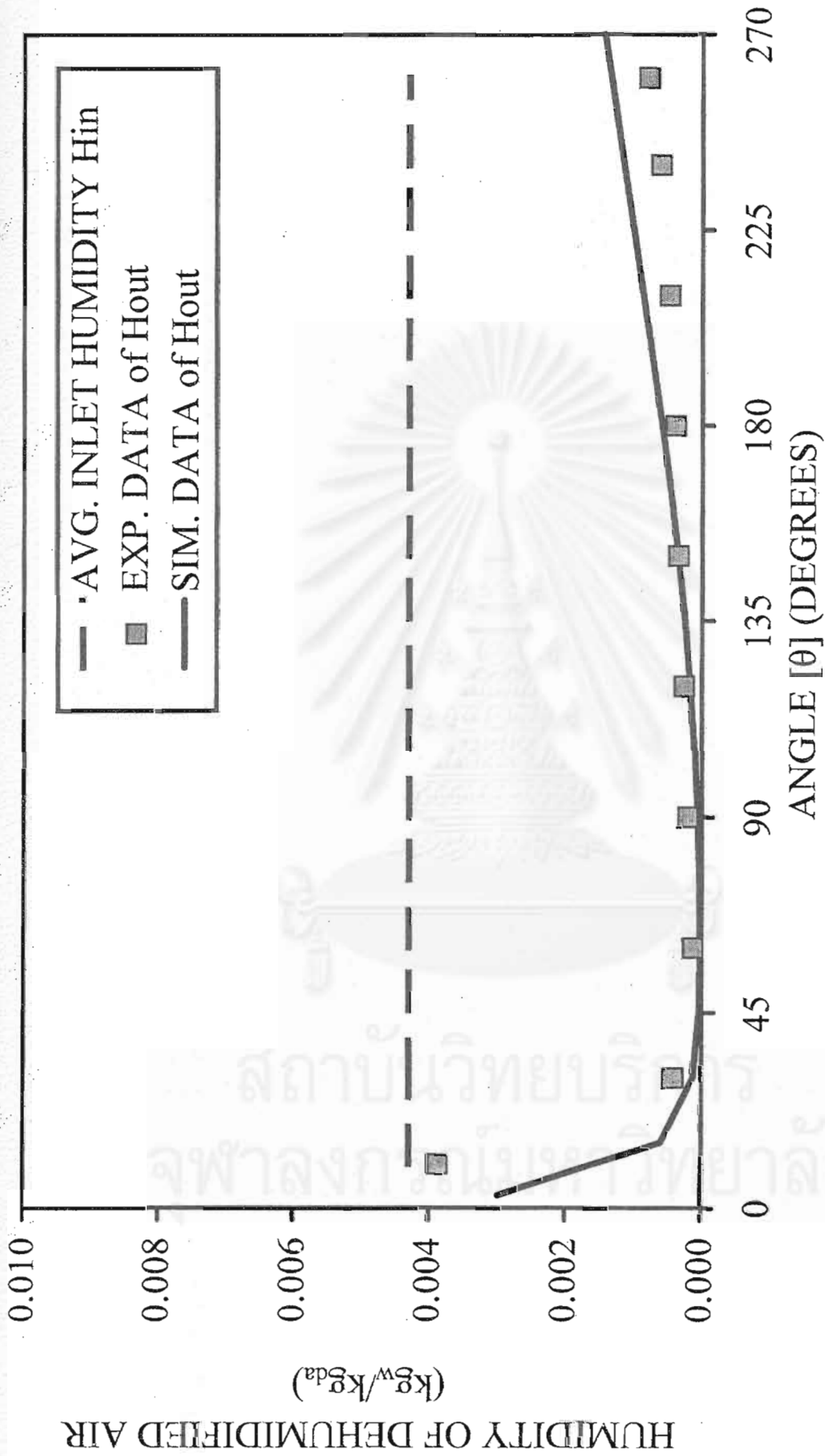
Figure 5.31 Comparison of angular distribution of the humidity of the dehumidified air between experimental and simulated results at H_{in} = 0.0043 kg$_w$/kg$_{da}$
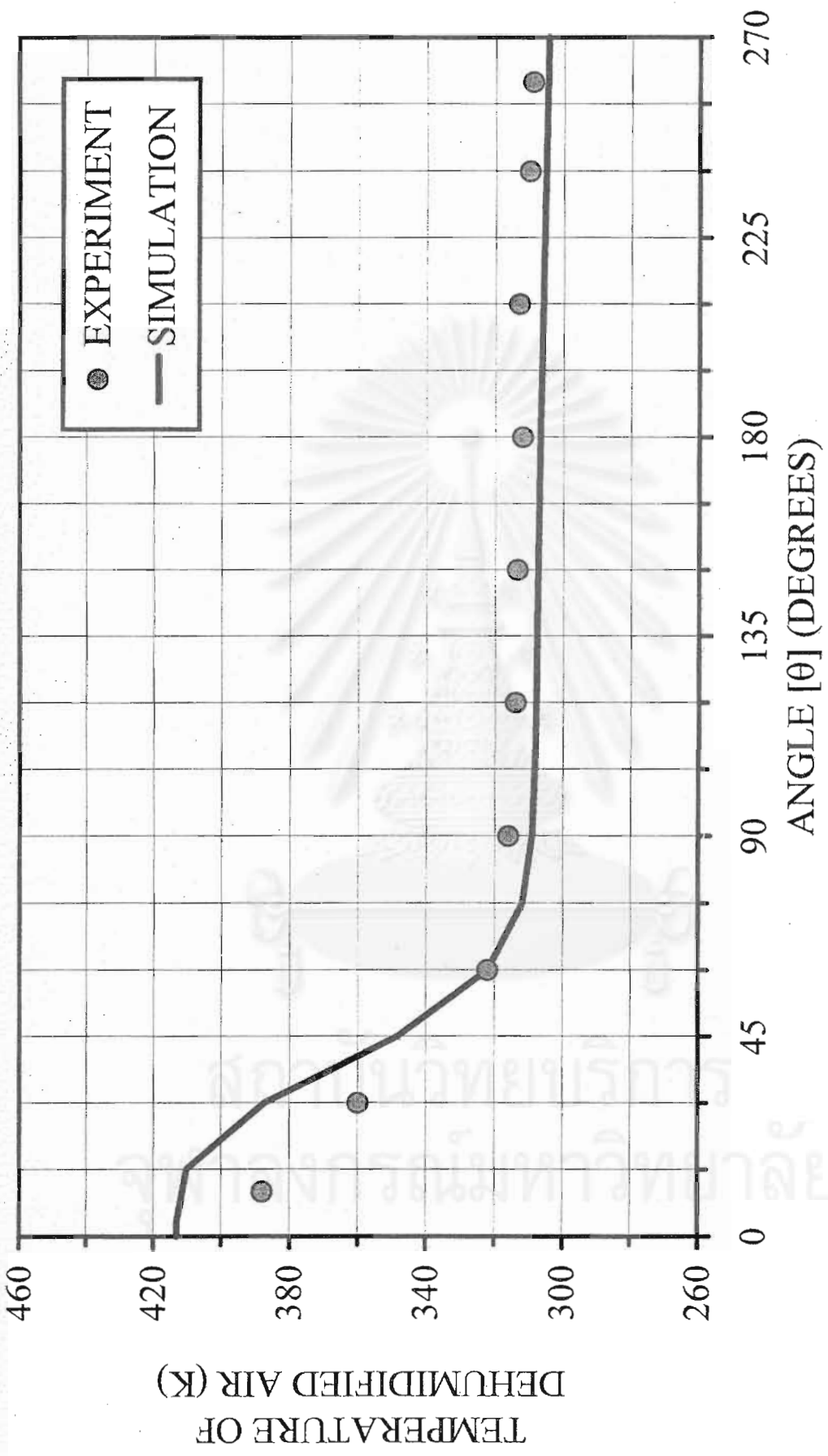
Figure 5.32 Comparison of angular distribution of the temperature of the dehumidified air between experimental and simulated results at H_{in} = 0.0043 kg$_w$/kg$_{da}$
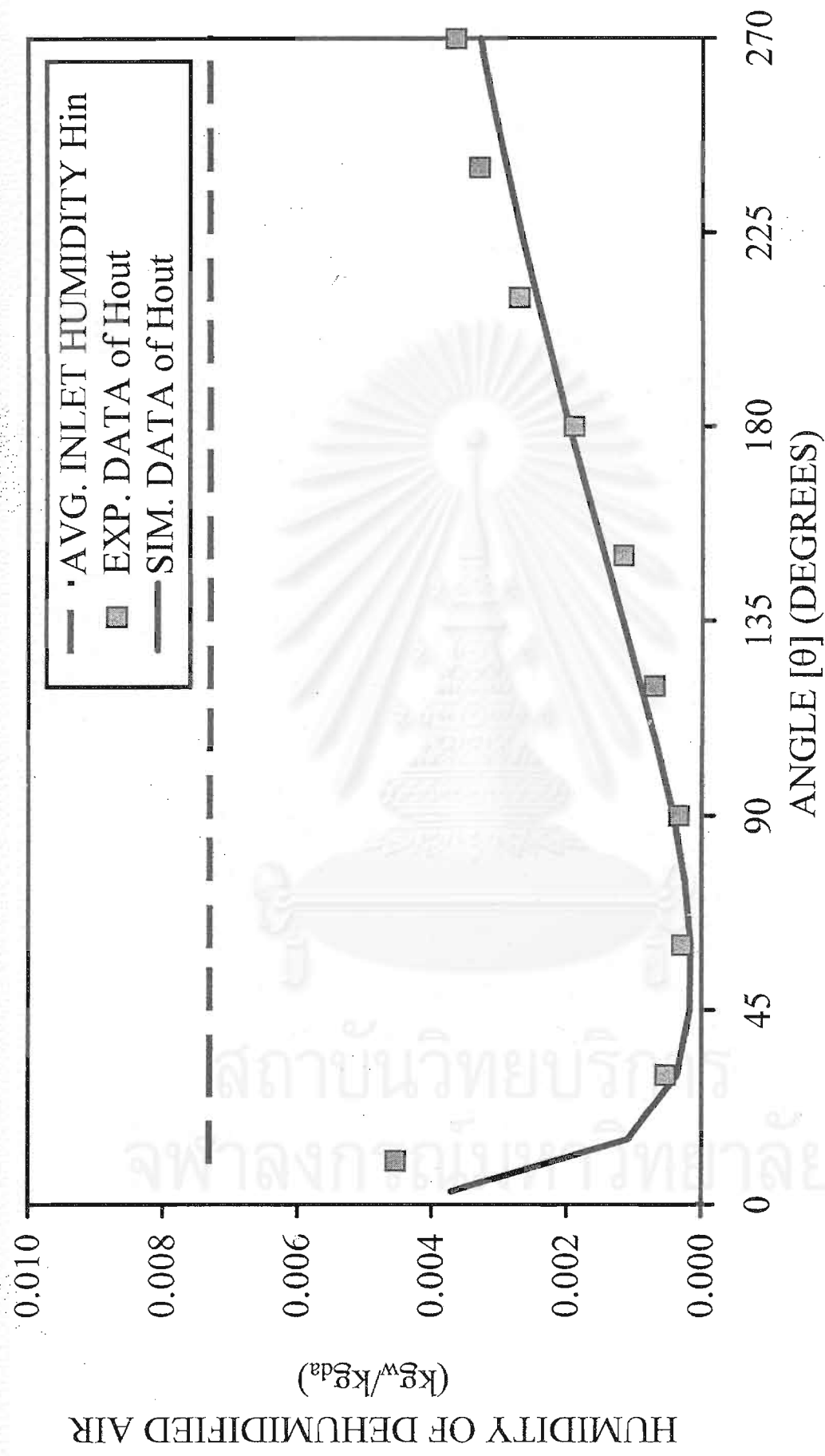
Figure 5.33 Comparison of angular distribution of the humidity of the dehumidified air between experimental and simulated results at H_{in} = 0.0073 kg_w/kg_{da}
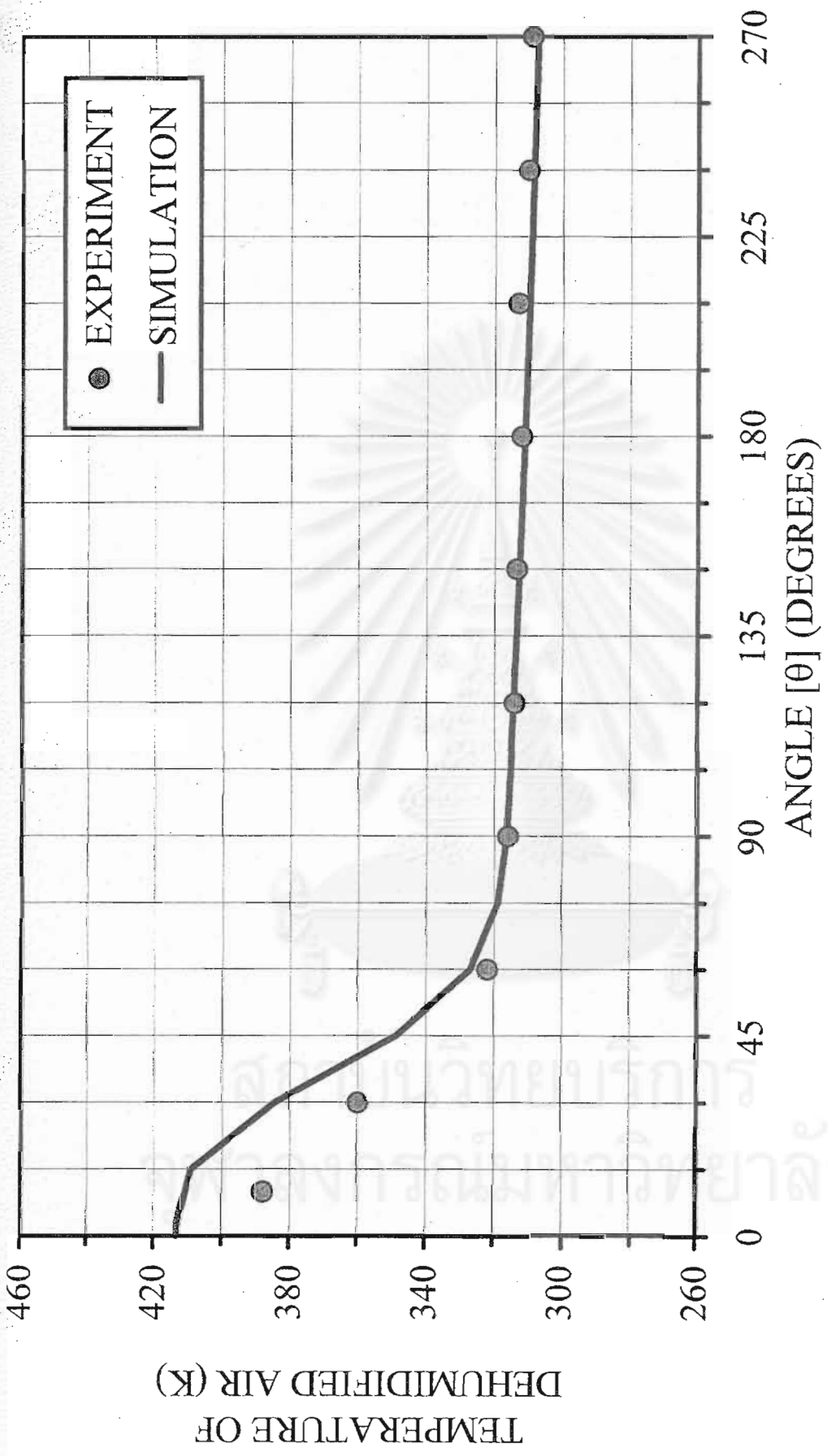
Figure 5.34 Comparison of angular distribution of the temperature of the dehumidified air between experimental and simulated results at H_{in} = 0.0073 kg$_w$/kg$_{da}$
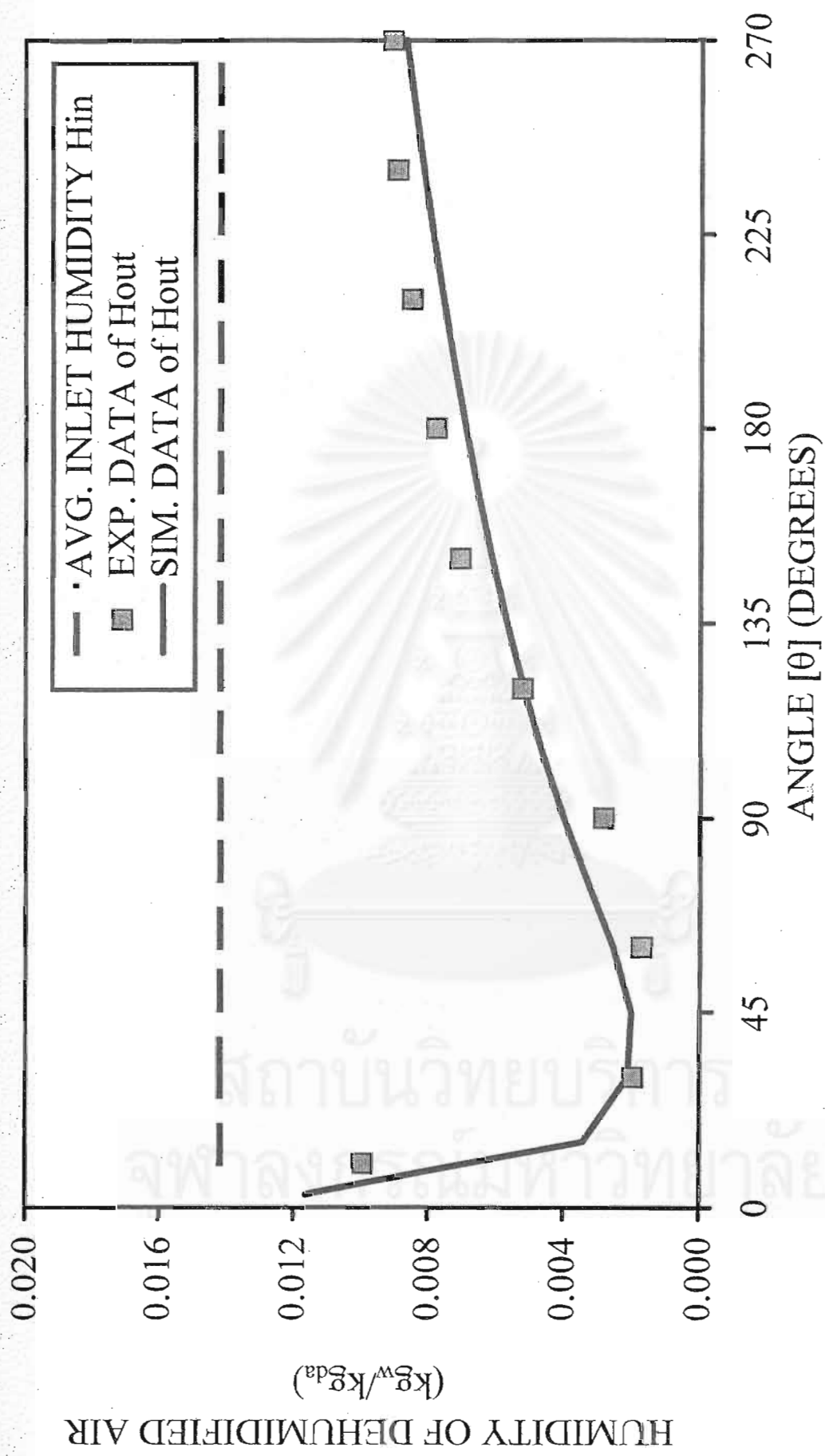
Figure 5.35 Comparison of angular distribution of the humidity of the dehumidified air between experimental and simulated results at H_{in} = 0.0142 kg_w/kg_{da}
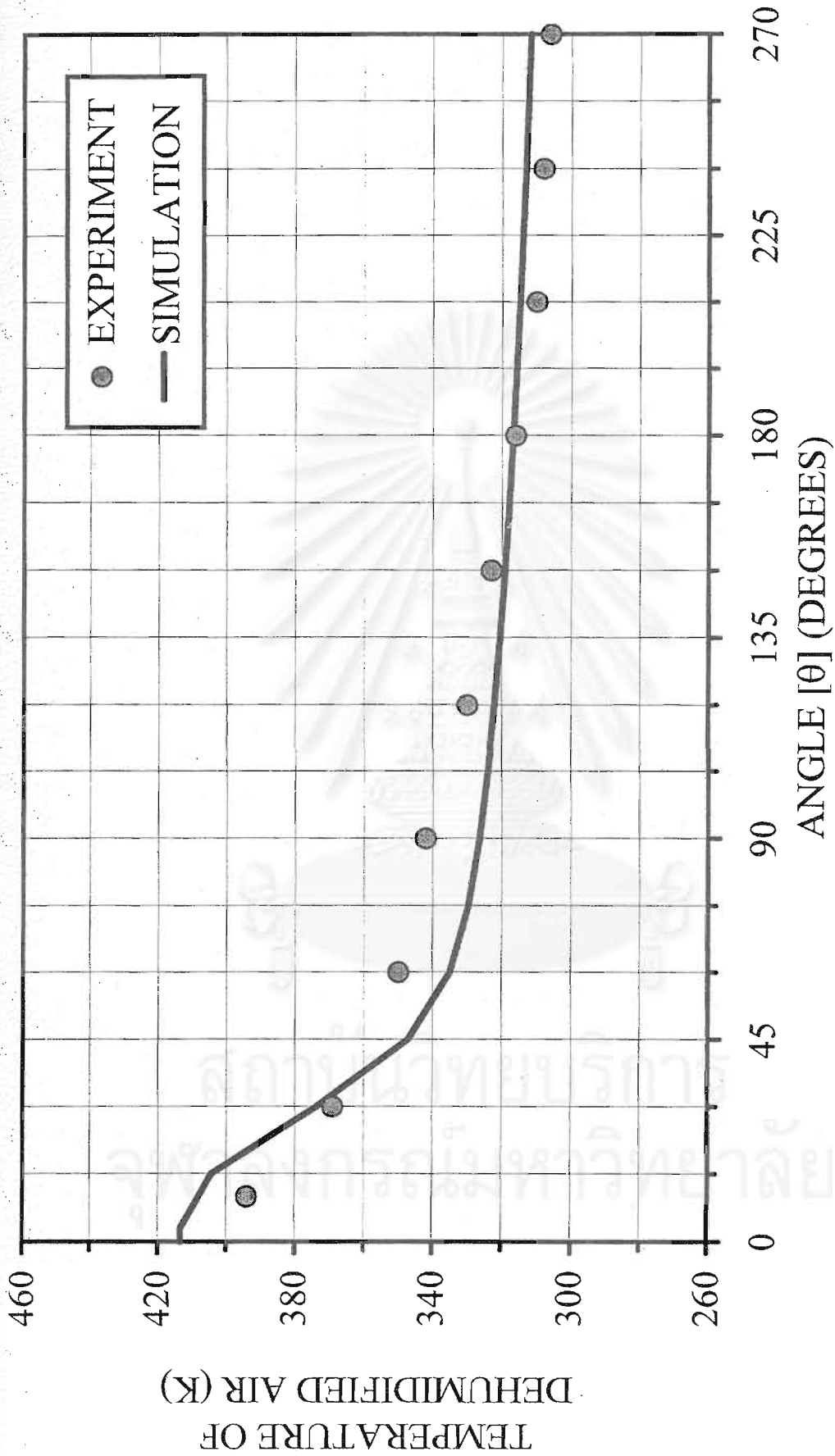
Figure 5.36 Comparison of angular distribution of the temperature of the dehumidified air between experimental and simulated results at $H_{in} = 0.0142$ kg$_w$/kg$_{da}$

CHAPTER 6

RESULTS AND DISCUSSION

The investigation on the effects of rotational speed, regenerative temperature, mass velocity of humid room air, mass velocity of hot regenerative air and axial length of the rotor on the performance of the rotary honeycomb dehumidifier is presented in this chapter. In the first section, the principle of the experimental design described in appendix D is used to identify the significant effects. Then the performance of both the rotary silica gel and zeolite-13X coated honeycomb dehumidifier and the phenomena of simultaneous heat and mass transfer inside the rotary honeycomb dehumidifier under various conditions will be presented in section 6.2 and 6.3. Consequently, the optimal operating conditions of both the rotary silica gel and zeolite-13X coated honeycomb dehumidifiers are determined. Moreover, the application of the silica gel and zeolite-13X coated honeycomb rotary dehumidifier in the process room of a modern beverage factory in Thailand has been proposed and compared with the lithium chloride coated honeycomb rotor in the last section.

6.1 Identification of significant effects

Since the number of factors considered in this experiment is moderately large, say k ≥ 4, the number of runs required for the analysis is large even though using the principle of the 2^k factorial experiment. Thus the fractional factorial design is useful for this situation. The screening experiments are performed at early stage in order to identify the factors that have little or no effect.

In this study, we have investigated 5 main effects as follows:
- Rotational speed of rotor (φ)
- Regenerative temperature (T_{reg})
- Mass velocity of humid air (Gw_{ads})

- Mass velocity of regenerative hot air (Gw_{reg})
- Length of rotor (L)

where

$$Gw_{ads} \quad = \quad H_{in,ads}*Ga_{ads} \qquad (kg_w/m^2 \cdot s) \qquad (6.1)$$

$$Gw_{reg} \quad = \quad H_{in,reg}*Ga_{reg} \qquad (kg_w/m^2 \cdot s) \qquad (6.2)$$

The ranges of such main effects are shown in Table 6.1

Table 6.1 Maximum and minimum values of main effects

Range	Main effect				
	$A = \varphi$	$B = T_{reg}$	$C = Gw_{ads}$	$D = Gw_{reg}$	$E = L$
Minimum (-)	4.4	373	0.00405	0.00045	0.10
Maximum (+)	28.0	433	0.01620	0.00150	0.25

At first, the one-half of factorial design method has been used to get the significant variables. Thus only a half of 2^5 treatment combination or 16 runs, say, the case of *a*, *b*, *c*, *d*, *e*, *abc*, *abd*, *abe*, *acd*, *ace*, *ade*, *bcd*, *bce*, *bde*, *cde* and *abcde*, are tested. As experimental design principle (Mongomery, 1984), the name of treatment combination such as *a*, *b*, *abc*, *abcde*, etc. is indicated that the presented corresponding a capital Latin letter is maximum or high value and the other are minimum or low value. For example, the case of *a* consists of maximum value of A factor, minimum value of B, C, D and E factor.

To investigate the significant effects, parameters and properties used in this section are summarized in Table 6.2.

Table 6.2 Parameters and properties used to investigate the factors influencing the dehumidification performance of the silica gel coated honeycomb rotary dehumidifier.

SIZE OF A SILICA GEL COATED HONYCOMB ROTARY DEHUMIDIFIER		
Diameter of rotor (D)	0.32	m
Length of rotor (L)	0.20	m
Cross sectional area of a slot (A_c)	3.49×10^{-6}	m^2
Cross sectional area of the gas phase in a slot (A_g)	2.88×10^{-6}	m^2
Cross sectional area of the solid phase in a slot (A_{ss})	6.11×10^{-7}	m^2
Hydraulic diameter of a slot	1.44×10^{-3}	m
PROPERTIES OF HONEYCOMB ROTOR		
Specific heat of adsorbent (Cp_{sb})	0.92	$kJ/(kg_{da}{\cdot}K)$
Specific heat of water (Cp_w)	4.187	$kJ/(kg_{da}{\cdot}K)$
Specific heat of ceramic fiber (Cp_{sh})	1.20	$kJ/(kg_{da}{\cdot}K)$
Bulk density of rotor (ρ_{sb})	250	kg/m^3
Density of ceramic fiber (ρ_{sh})	185	kg/m^3
Mass fraction of adsorbent	0.70	(-)
Specific surface area of honeycomb (*a*)	3000	m^2/m^3
Void fraction of the honeycomb (ε)	0.825	(-)
PROPERTIES OF HUMID AIR		
Specific heat of dry air (Cp_{da})	1.005	$kJ/(kg_{da}{\cdot}K)$
Specific heat of water vapor (Cp_v)	1.820	$kJ/(kg_{da}{\cdot}K)$
Latent heat of vaporization at 273 K (λ_0)	2501.3	$kJ/(kg_{da}{\cdot}K)$
SIMULATION PARAMETERS		
The number of cells in each slot (N_{cell})	10	cell
Total number of slots (M_{slot})	120	slot
Number of slots for the adsorption zone (M_{ads})	90	slot
Number of slots for the regeneration zone (M_{reg})	30	slot
Step size (Δt) of integration	0.006	sec
Display time interval	300	sec
Final simulation time (t_f)	3600	sec
INITIAL CONDITIONS		
Local amount of moisture adsorbed in the adsorbent (W_0)	0.001	kg_w/kg_{sb}
Local air humidity in the slots (H_0)	0.0001	kg_w/kg_{da}
Local solid temperature in the slots (Ts_0)	291.15	K
Local gas temperature in the slots (Ta_0)	292.15	K

For the simulated results, the dehumidification efficiency of the silica gel coated honeycomb rotor in the case of the *a*, *b*, *c*, *d*, *e*, *abc*, *abd*, *abe*, *acd*, *ace*, *ade*, *bcd*, *bce*, *bde*, *cde* and *abcde* treatment combination, the so-called 2^{5-1} factorial design, are shown in Table 6.3.

Table 6.3 Dehumidification efficiency of the silica gel coated on honeycomb rotor in the case of the one-half of fractional treatment combinations

Treatment combinations	Dehumidification efficiency (%)
A	63.44
B	70.76
C	35.97
D	72.51
E	90.98
Abc	73.72
Abd	77.89
Abe	36.89
Acd	62.91
Ace	48.13
Ade	35.56
Bcd	37.27
Bce	65.84
Bde	95.90
Cde	66.40
Abcde	62.44

For the analysis of significant effects, the estimation of the treatment effects on normal probability paper has been easily applied in this study. Principally, the estimated effects are ordered from the smallest to the largest effects as presented in Table 6.4 for the 2^{5-1} factorial design of the dehumidification using the silica gel coated honeycomb rotor. To clearly observe, the plot of the probability of each effect against the estimated effects, which is calculated using equation (D.15), on the normal probability paper are then illustrated in Figure 6.1.

Table 6.4 Ordered effects of the 2^{5-1} factorial design

Order (q)	P_q	Treatment effects	Estimated effects (l_i)
1	0.0333	BCD+AE	-24.70
2	0.1000	C+ABDE	-11.40
3	0.1667	A+BCDE	-9.33
4	0.2333	ABE+CD	-1.81
5	0.3000	ACD+BE	-0.60
6	0.3667	ADE+BC	0.87
7	0.4333	E+ABCD	0.96
8	0.5000	BCE+AD	1.01
9	0.5667	ABC+DE	1.47
10	0.6333	D+ABCD	3.14
11	0.7000	ACE+BD	3.43
12	0.7667	CDE+AB	4.62
13	0.8333	B+ACDE	5.60
14	0.9000	ABD+CE	7.28
15	0.9667	BDE+AC	19.76
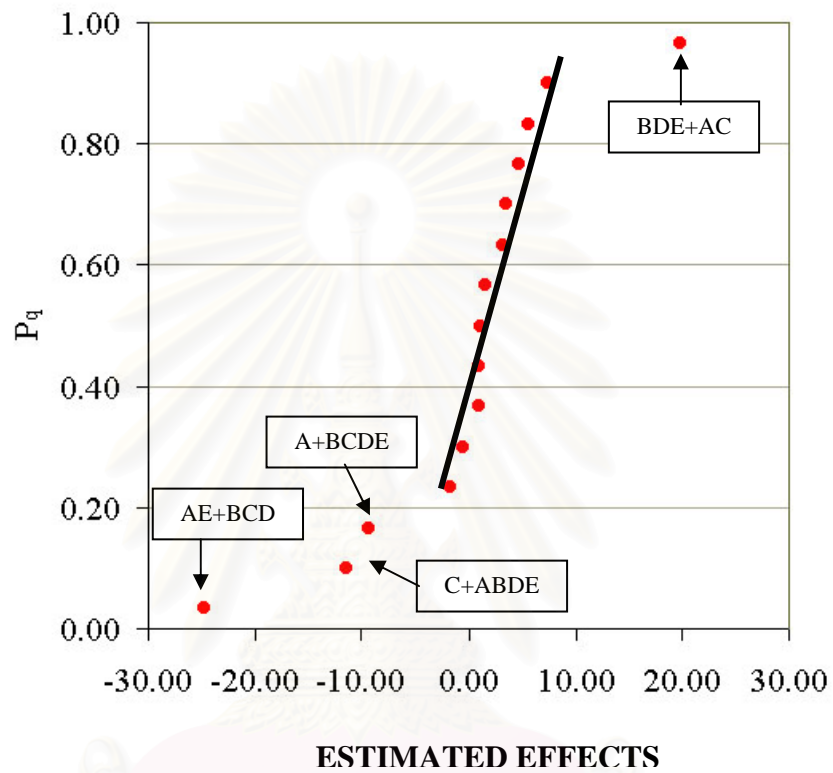
Figure 6.1 The plot of the ordered effects on the dehumidification efficiency of the silica gel coated honeycomb rotor on normal probability paper in the case of the 2^{5-1} factorial design

For the one-half fractional factorial design, each point represents the combined two-effects and significant effects will not lie along the straight line (Montgomery, 1984). Since high order interaction is negligible as mentioned in appendix D.2.2, only A, C and AC interaction effects are, of course, significant. However, the AE and BCD interaction effects are ambiguous. Consequently, we have tested the other half of the 2^5 factorial design. The results of that test are shown in Table 6.5 and 6.6 including Figure 6.2. For simplicity, the estimated effects can be calculated using Yate's method as presented in appendix E. As similar to the 2^{5-1} design, it is found that A and C main effects as well as AC and AE interactions are significant effects. However, CE interaction is probably a significant effect.

In conclusion, rotational speed, mass velocity of the humid air, the interaction of rotational speed and mass velocity of the humid air, rotational speed and length of the rotor are significant effects on the dehumidification performance of the silica gel coated honeycomb rotor. In contrast, the interaction of mass velocity of the humid air and length of the rotor is probably a minor effect on such a system. Of course, mass velocity of regenerative hot air and regenerative temperature insignificantly effect on the system. Accordingly, only three variables have been studied. Moreover, the analysis of variance, the so-called ANOVA, is ensured the investigation as described in appendix F. Preferably, it can indicate the flexible significant effect depending on the situation or significance of system.

Table 6.5 Dehumidification efficiency of the silica gel coated honeycomb rotor in the
case of the 2^5 factorial design

Number of run	Treatment combinations	Dehumidification efficiency (%)
1	*(1)*	70.53
2	*a*	63.44
3	*b*	70.76
4	*c*	35.97
5	*d*	72.51
6	*e*	90.98
7	*ab*	75.80
8	*ac*	59.23
9	*ad*	66.02
10	*ae*	35.49
11	*bc*	36.19
12	*bd*	72.76
13	*be*	94.78
14	*cd*	37.01
15	*ce*	63.84
16	*de*	92.78
17	*abc*	73.72
18	*abd*	77.89
19	*abe*	36.89
20	*acd*	62.91
21	*ace*	48.13
22	*ade*	35.56
23	*bcd*	37.27
24	*bce*	65.84
25	*bde*	95.90
26	*cde*	66.40
27	*abcd*	78.62
28	*abce*	60.73
29	*abde*	36.47
30	*acde*	49.30
31	*bcde*	67.96
32	*abcde*	62.44

Table 6.6 Ordered effects on the dehumidification performance of the silica gel coated honeycomb rotor for the 2^5 factorial design

Order (q)	P_q	Treatment effects	Estimated effects (l_i)
1	0.0161	AE	-24.88
2	0.0484	C	-11.44
3	0.0806	A	-9.30
4	0.1129	ABE	-2.24
5	0.1452	BE	-1.05
6	0.1774	ADE	-0.76
7	0.2097	DE	-0.58
8	0.2419	ACDE	-0.27
9	0.2742	BDE	-0.12
10	0.3065	ABCDE	-0.06
11	0.3387	BCDE	-0.03
12	0.3710	BD	-0.02
13	0.4032	ABDE	0.03
14	0.4355	ABD	0.12
15	0.4677	AD	0.13
16	0.5000	ABCD	0.16
17	0.5323	CDE	0.18
18	0.5645	BCD	0.19
19	0.5968	CD	0.44
20	0.6290	ACD	0.45
21	0.6613	E	0.80
22	0.6935	BCE	0.88
23	0.7258	ABCE	1.30
24	0.7581	BC	1.63
25	0.7903	D	1.84
26	0.8226	ABC	2.05
27	0.8548	ACE	3.45
28	0.8871	AB	4.44
29	0.9194	B	5.87
30	0.9516	CE	7.16
31	0.9839	AC	19.88
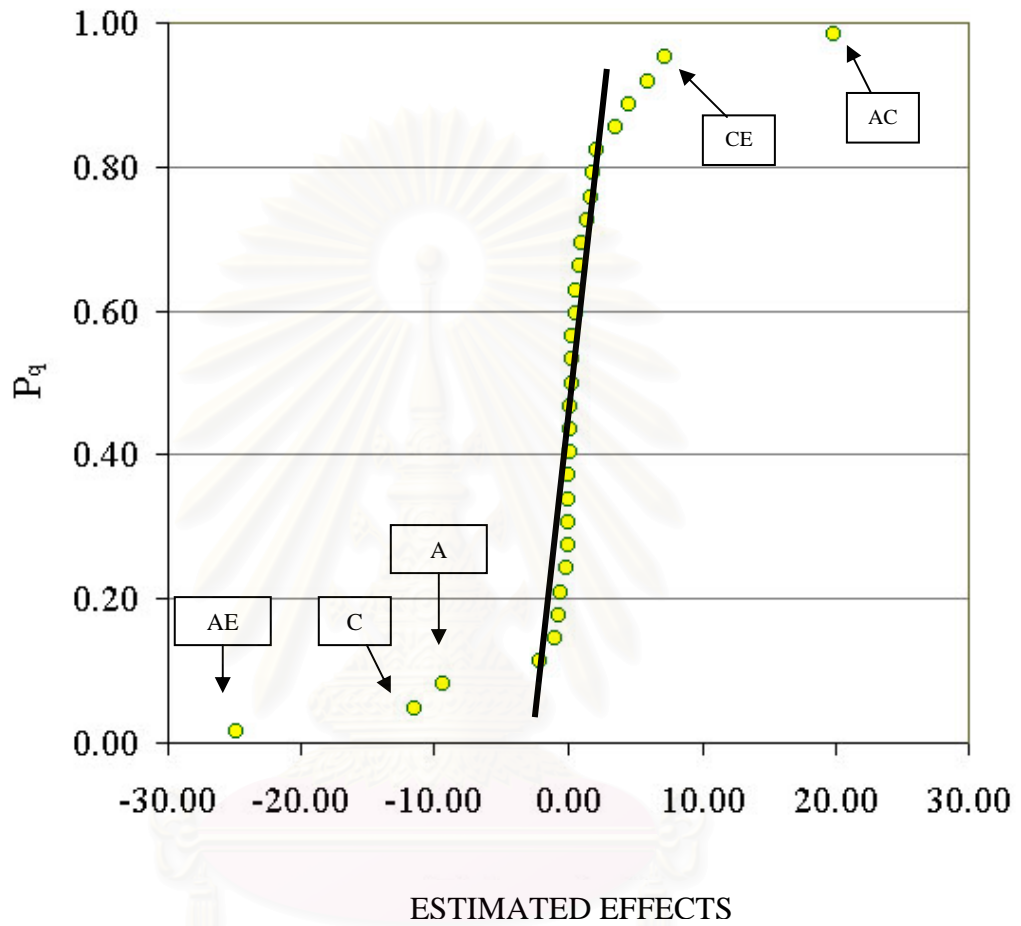
Figure 6.2 The plot of the ordered effects on the dehumidification performance of the silica gel coated honeycomb rotor on normal probability paper in the case of the 2^5 factorial design

6.2 Effect of significant factors

Three significant factors, i.e. rotational speed, mass velocity of the humid air and length of the rotor, as well as their interactions are investigated in this section. The operating conditions for all cases are listed in Table 6.7. In this study, the humid air with $H_a = 0.0045$ kg_w/kg_{da} is sent through the adsorption section of the rotor and the regenerative hot air entering the inlet of the regeneration section are kept constant at 413 K and 4.25×10^{-4} kg_w/m^2s, respectively, since the regenerative temperature in the range of 393 to 433 K and the mass velocity of the hot air in the range of 3.2×10^{-4} to 1.28×10^{-3} kg_w/m^2s are insignificant effect on the dehumidification as illustrated in appendix G.

Table 6.7 Operating conditions used to investigate the significant factors influencing the dehumidification performance of the silica gel coated honeycomb rotary dehumidifier.

CASE	ROTATIONAL SPEED (RPH)	MASS VELOCITY OF HUMID AIR ($\times 10^3$ kg_w/m^2s)	LENGTH OF THE ROTOR (m)	FILE NAME (filename.dat)
Speed-SG-Effect	3.5	5.40	0.20	SG-CASE-01
	6.2	5.40	0.20	SG-CASE-02
	12.5	5.40	0.20	SG-CASE-03
	28.0	5.40	0.20	SG-CASE-04
Gads-SG-Effect	6.2	4.05	0.20	SG-CASE-05
	6.2	5.40	0.20	SG-CASE-02
	6.2	6.75	0.20	SG-CASE-06
	6.2	8.10	0.20	SG-CASE-07
Length-SG-Effect	6.2	5.40	0.10	SG-CASE-08
	6.2	5.40	0.15	SG-CASE-09
	6.2	5.40	0.20	SG-CASE-02
	6.2	5.40	0.25	SG-CASE-10
Speed& Gads-SG-Effect	3.5	4.05	0.20	SG-CASE-11
	6.2	4.05	0.20	SG-CASE-05
	12.5	4.05	0.20	SG-CASE-12
	28.0	4.05	0.20	SG-CASE-13
	3.5	5.40	0.20	SG-CASE-01
	6.2	5.40	0.20	SG-CASE-02
	12.5	5.40	0.20	SG-CASE-03
	28.0	5.40	0.20	SG-CASE-04
	3.5	6.75	0.20	SG-CASE-14
	6.2	6.75	0.20	SG-CASE-15
	12.5	6.75	0.20	SG-CASE-16

Table 6.7(cont.) Operating conditions used to investigate the significant factors influencing the dehumidification performance of the silica gel coated honeycomb rotary dehumidifier.

CASE	ROTATIONAL SPEED (RPH)	MASS VELOCITY OF HUMID AIR ($\times 10^3$ kg$_w$/m^{2}s)	LENGTH OF THE ROTOR (m)	FILE NAME (filename.dat)
Speed& Gads-SG- Effect	28.0	6.75	0.20	SG-CASE-17
	3.5	8.10	0.20	SG-CASE-18
	6.2	8.10	0.20	SG-CASE-19
	12.5	8.10	0.20	SG-CASE-20
	28.0	8.10	0.20	SG-CASE-21
Speed& Length-SG- Effect	3.5	5.40	0.10	SG-CASE-22
	6.2	5.40	0.10	SG-CASE-08
	12.5	5.40	0.10	SG-CASE-23
	28.0	5.40	0.10	SG-CASE-24
	3.5	5.40	0.15	SG-CASE-25
	6.2	5.40	0.15	SG-CASE-26
	12.5	5.40	0.15	SG-CASE-27
	28.0	5.40	0.15	SG-CASE-28
	3.5	5.40	0.20	SG-CASE-01
	6.2	5.40	0.20	SG-CASE-02
	12.5	5.40	0.20	SG-CASE-03
	28.0	5.40	0.20	SG-CASE-04
	3.5	5.40	0.25	SG-CASE-29
	6.2	5.40	0.25	SG-CASE-30
	12.5	5.40	0.25	SG-CASE-31
	28.0	5.40	0.25	SG-CASE-32
Gads& Length-SG- Effect	6.2	4.05	0.10	SG-CASE-33
	6.2	5.40	0.10	SG-CASE-08
	6.2	6.75	0.10	SG-CASE-34
	6.2	8.10	0.10	SG-CASE-35
	6.2	4.05	0.15	SG-CASE-36
	6.2	5.40	0.15	SG-CASE-26
	6.2	6.75	0.15	SG-CASE-37
	6.2	8.10	0.15	SG-CASE-38
	6.2	4.05	0.20	SG-CASE-05
	6.2	5.40	0.20	SG-CASE-02
	6.2	6.75	0.20	SG-CASE-06
	6.2	8.10	0.20	SG-CASE-07
	6.2	4.05	0.25	SG-CASE-39
	6.2	5.40	0.25	SG-CASE-10
	6.2	6.75	0.25	SG-CASE-40
	6.2	8.10	0.25	SG-CASE-41

6.2.1 Effect of rotational speed

In Figures 6.3 and 6.4, they show the optimal value of rotational speed for the silica gel coated honeycomb rotary dehumidifier that ranges from 6 to 10 rph. At optimal value, the dehumidification efficiency can reach more than 90%. Below 6 rph the efficiency rapidly decreases as the rotational speed decreases and becomes as low as 35% at 3.5 rph since the moisture loading in the region $\theta = 150°$- $270°$ exceeds the maximum adsorption capacity as seen in Figure 6.7. In contrast, above 10 rph the efficiency gradually decreases and becomes as low as 55% at 28 rph since the range of the cooling down the hot, newly regenerated adsorbent at faster rotating is wider from only 45° at 3.5-rph to 225° at 28-rph as seen in Figure 6.8. So the ineffective area caused by high temperature increases with the rotational speed of the rotor that ranges from 3.5 rph to 28.0 rph. Consequently, the average temperature of the dehumidified air significantly increases with the rotational speed, particularly, in the range of 3 to 10 rph as shown in Figure 6.5. In this case, the power required by heater at various the rotational speeds are constant as shown in Figure 6.6 because the regenerative temperature and the mass velocities of the hot air are kept constant at 413 K and 4.25×10^{-4} kg$_w$/m^{2}s, respectively.

Furthermore, the phenomena of heat and mass transfer inside the silica gel coated rotary dehumidifier at different rotational speed are investigated as shown in Figures 6.9 to 6.20. These figures illustrate the two-dimensional angular distributions of the air humidity, the air temperature, the adsorbed moisture and the solid-phase temperature for 3.5, 6.2, 12.5 rph of the rotational speed. The simultaneous adsorption and desorption process of the rotary dehumidifier are represented in the region $\theta = 0°$- $270°$ and $270°$- $360°$, respectively. In the adsorption zone, the humid air is sent to the dehumidifier at $Z = 0$ and most of the humidity is then adsorbed at nearly inlet. Thus the adsorbed moisture in each slot gradually decreases with the depth of the slot as seen in the region $\theta = 0°$- $270°$ of Figures 6.15 to 6.17. In the regeneration zone ($\theta = 270°$- $360°$), the hot regenerative air is counter flow to the dehumidifier at $Z = 1.0$ in order for driving out the adsorbed moisture. Thus the adsorbed moisture gradually decreases from $\theta = 270°$ to $360°$ as seen in Figure 6.15 to 6.17. However, the rotational speed effects on the two-dimensional distributions of adsorbed moisture on silica gel coated honeycomb rotary dehumidifier. At 3.5-rph of rotational speed, most of the adsorbed moisture is driven out in the region $\theta = 270°$- $330°$

as shown in Figure 6.15. It can indicate that the rotational speed is too low since some useless slot in the region $\theta = 330°- 360°$ are observed. In the case of 6.2 rph, the adsorbent through the rotor are sufficiently dried in the region $\theta = 270°- 360°$ as shown in Figure 6.16. It can be assure the optimum condition. For high rotational speed as seen in Figure 6.17, it is seen that the adsorbent could not be adequate for driving out the adsorbed moisture. So it indicates that the rotational speed is too high. Similar to the angular distributions of the slot-adsorbed moisture, the air humidity in the slot of the regeneration zone of the rotary dehumidification are dried out within the region $\theta = 270°- 330°$ at 3.5 rph and in the region $\theta = 270°- 360°$ at 6.2 rph. Whereas, at 12.5 rph, the regenerative slot at $\theta = 360°$ is still humid.

Since the angular distributions of the slot-air temperature in Figures 6.12 to 6.14 and the solid-phase temperature in Figures 6.18 to 6.20 are resemblant at the same as rotational speed of the rotor, only the air temperature profiles are discussed here in details. From Figure 6.12, it is seen that the temperature in the early region, i.e. $\theta = 0°- 45°$, for all depth ($Z = 0$-1) is very high because of the hot, newly regenerated adsorbent. Whereas little increasing the air temperature as the depth of the slot for adsorption zone is caused by heat of adsorption. For the regeneration zone, the air temperature decreases from the inlet side ($Z = 1$) to the outlet side ($Z = 0$) since it is used to drive out the adsorbed moisture on the adsorbent. In this case, at 3.5 rph, the temperatures for all depth at the region $\theta = 330°-360°$ are constant at the inlet value, 413 K, since the slots are dry. It indicates that the rotational speed is too low. At the optimal rotational speed as shown in Figure 6.13, the temperatures for all depth are equal only at $\theta = 360°$. For too high rotational speed, the temperature at $\theta = 360°$ still decreases from the inlet side ($Z = 1$) to the outlet side ($Z = 0$) as shown in Figure 6.14.
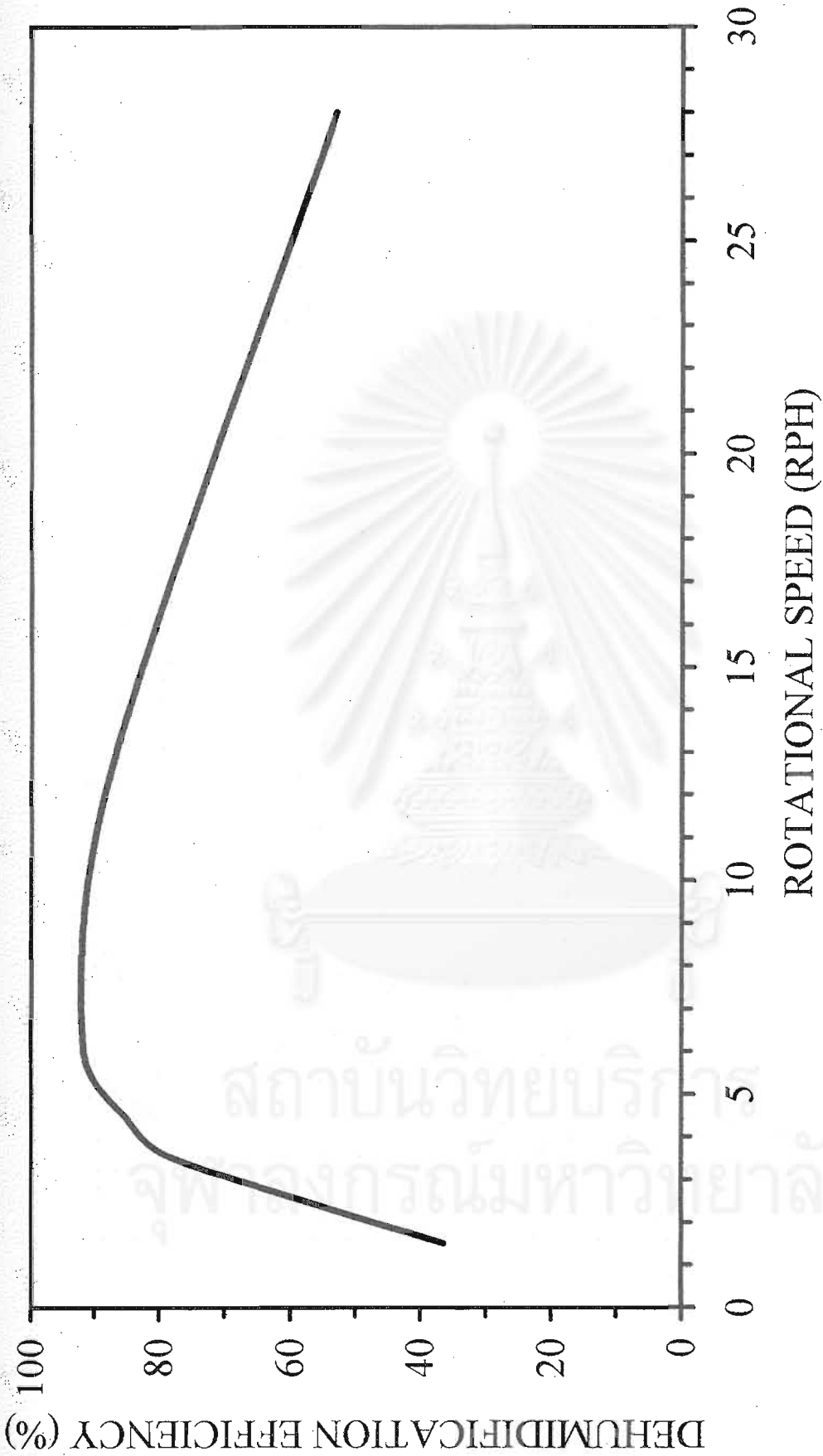
Figure 6.3 Effect of rotational speed on the dehumidification efficiency of the silica gel coated honeycomb rotary dehumidifier (Speed-SG-Effect condition)
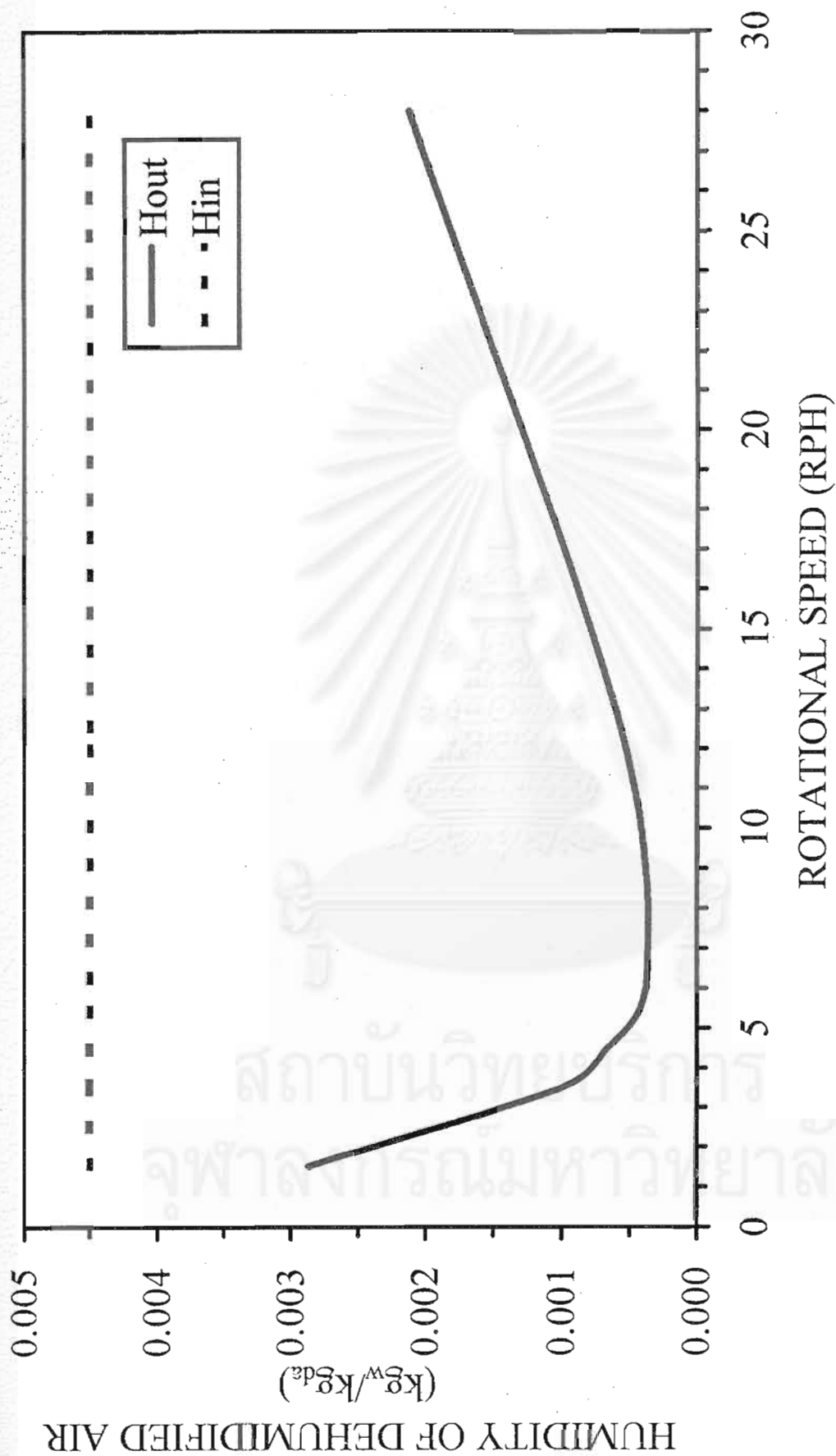
Figure 6.4 Effect of rotational speed on the average humidity of the dehumidified air from the silica gel coated honeycomb rotary dehumidifier (Speed-SG-Effect Condition)
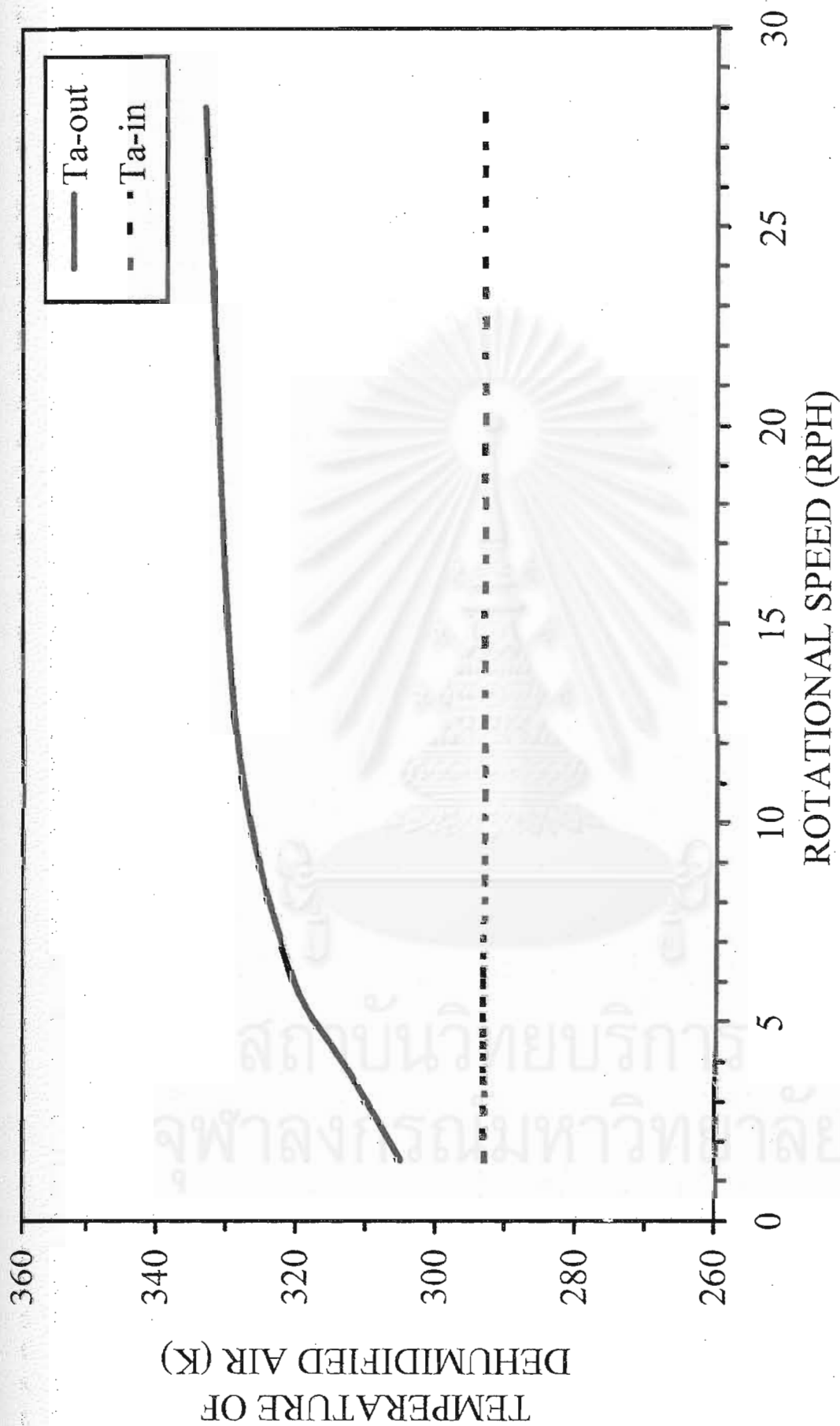
Figure 6.5 Effect of rotational speed on the average temperature of the dehumidified air from the silica gel coated honeycomb rotary dehumidifier (Speed-SG-Effect Condition)
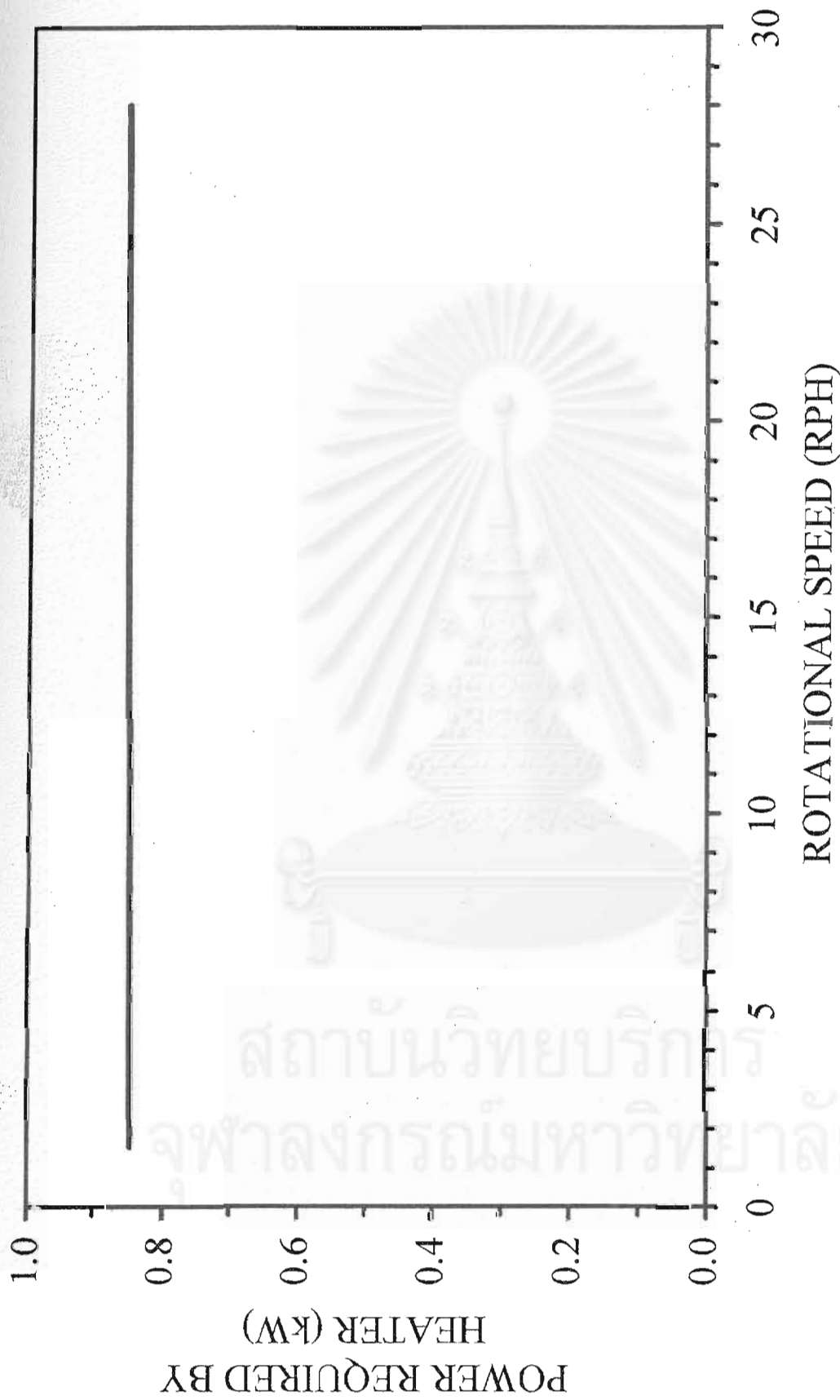
Figure 6.6 Power required by heater at various rotational speeds for the silica gel coated honeycomb rotary dehumidifier (Speed-SG-Effect Condition)
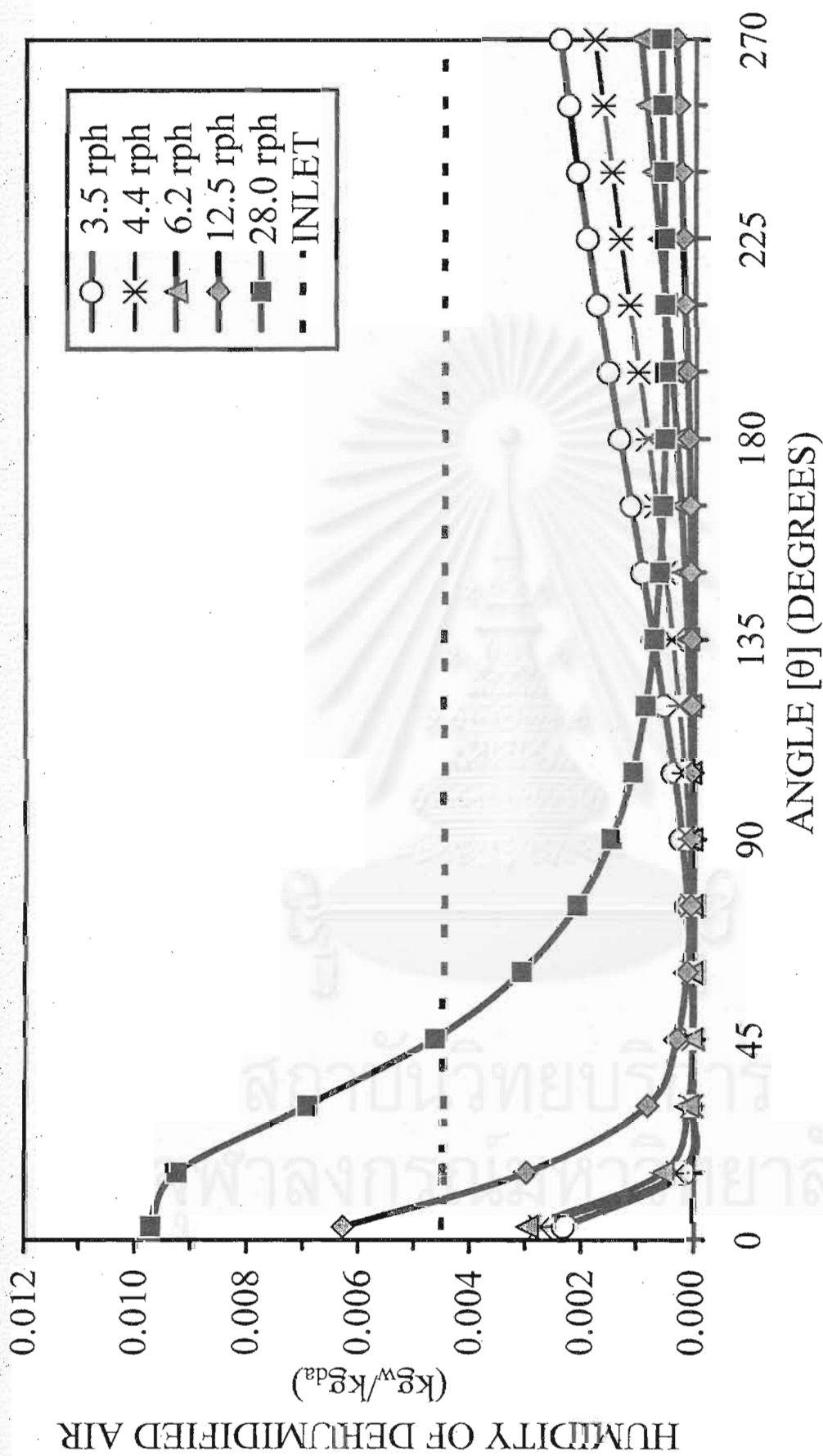
Figure 6.7 The angular distributions of the humidity of the dehumidified air from the silica gel coated honeycomb rotary dehumidifier at various rotational speeds (Speed-SG-Effect Condition)
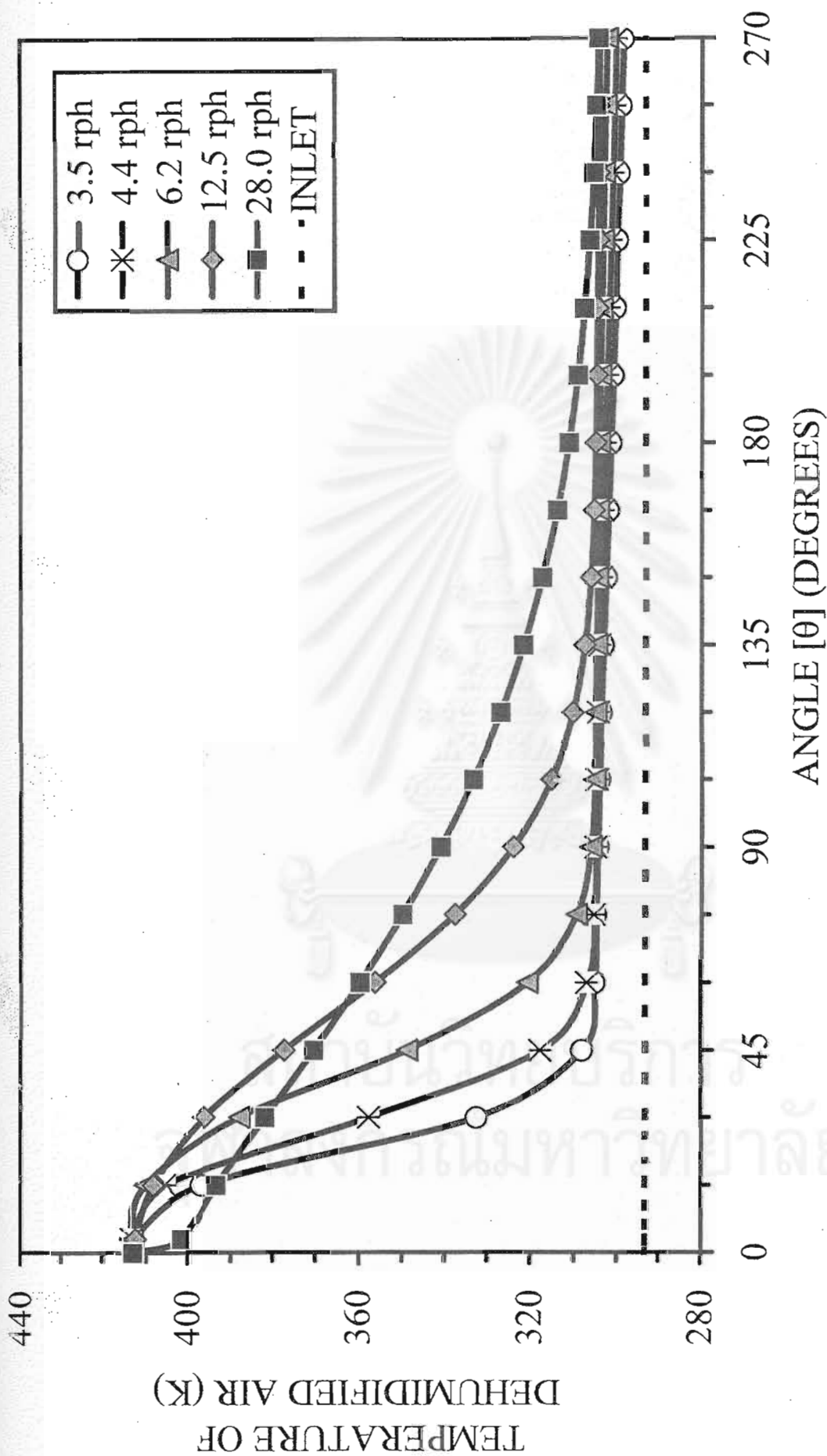
Figure 6.8 The angular distributions of the temperature of the dehumidified air from the silica gel coated honeycomb rotary dehumidifier at various rotational speeds (Speed-SG-Effect Condition)
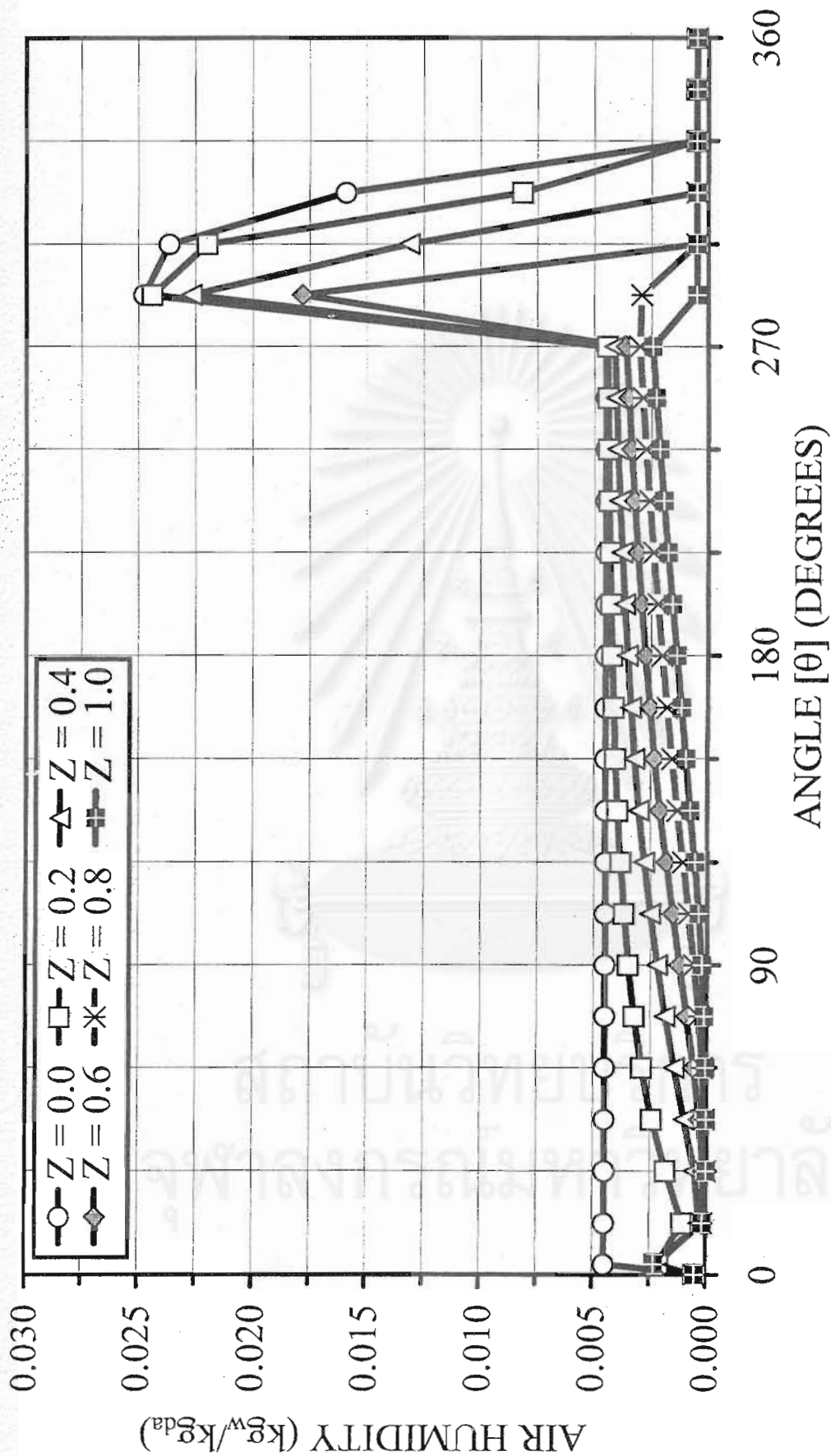
Figure 6.9 The two-dimensional distributions of the slot air humidity in the silica gel coated honeycomb rotary dehumidifier at 3.5 rph (Speed-SG-Effect Condition)
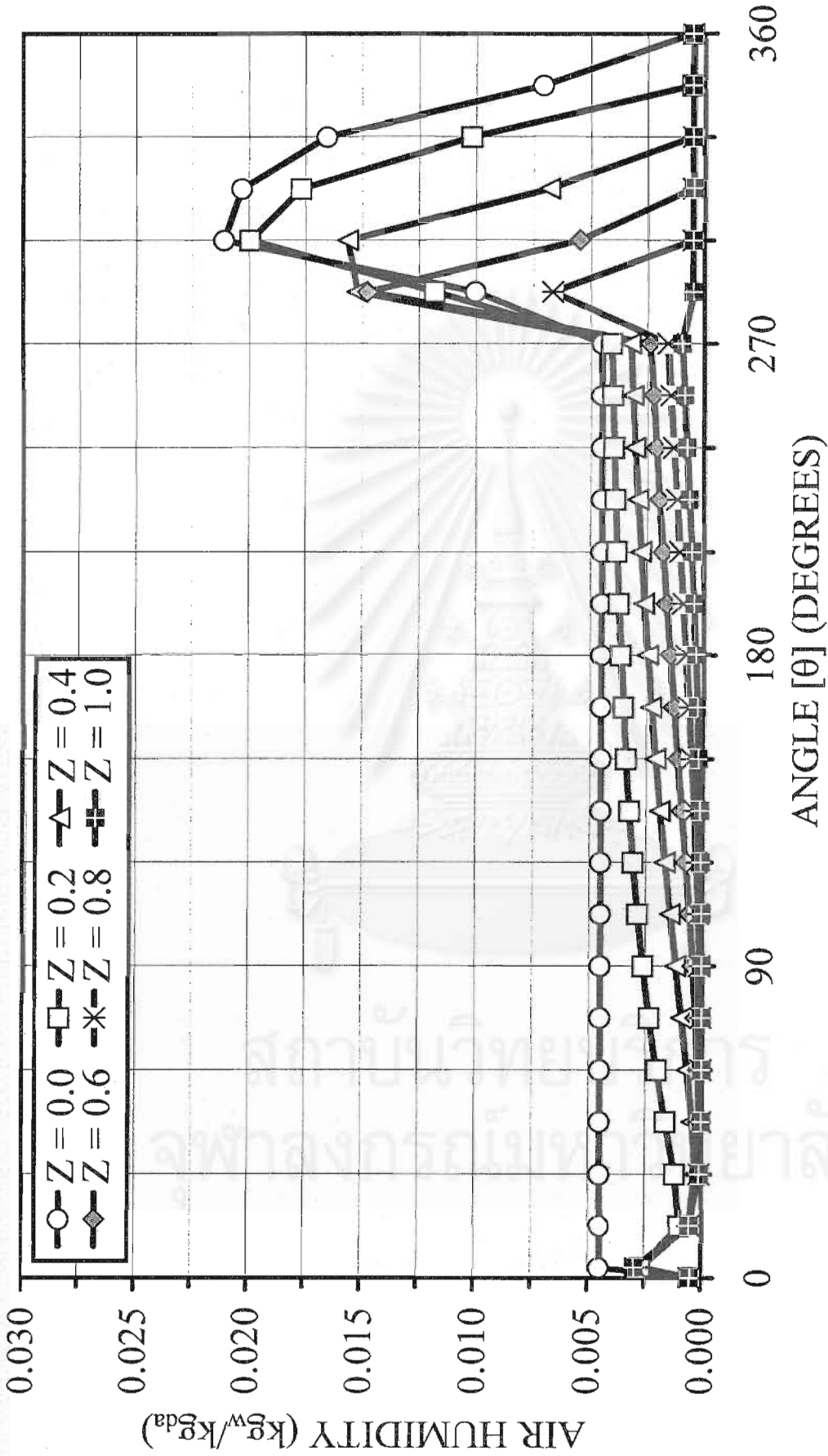
Figure 6.10 The two-dimensional distributions of the slot air humidity in the silica gel coated honeycomb rotary dehumidifier at 6.2 rph (Speed-SG-Effect Condition)
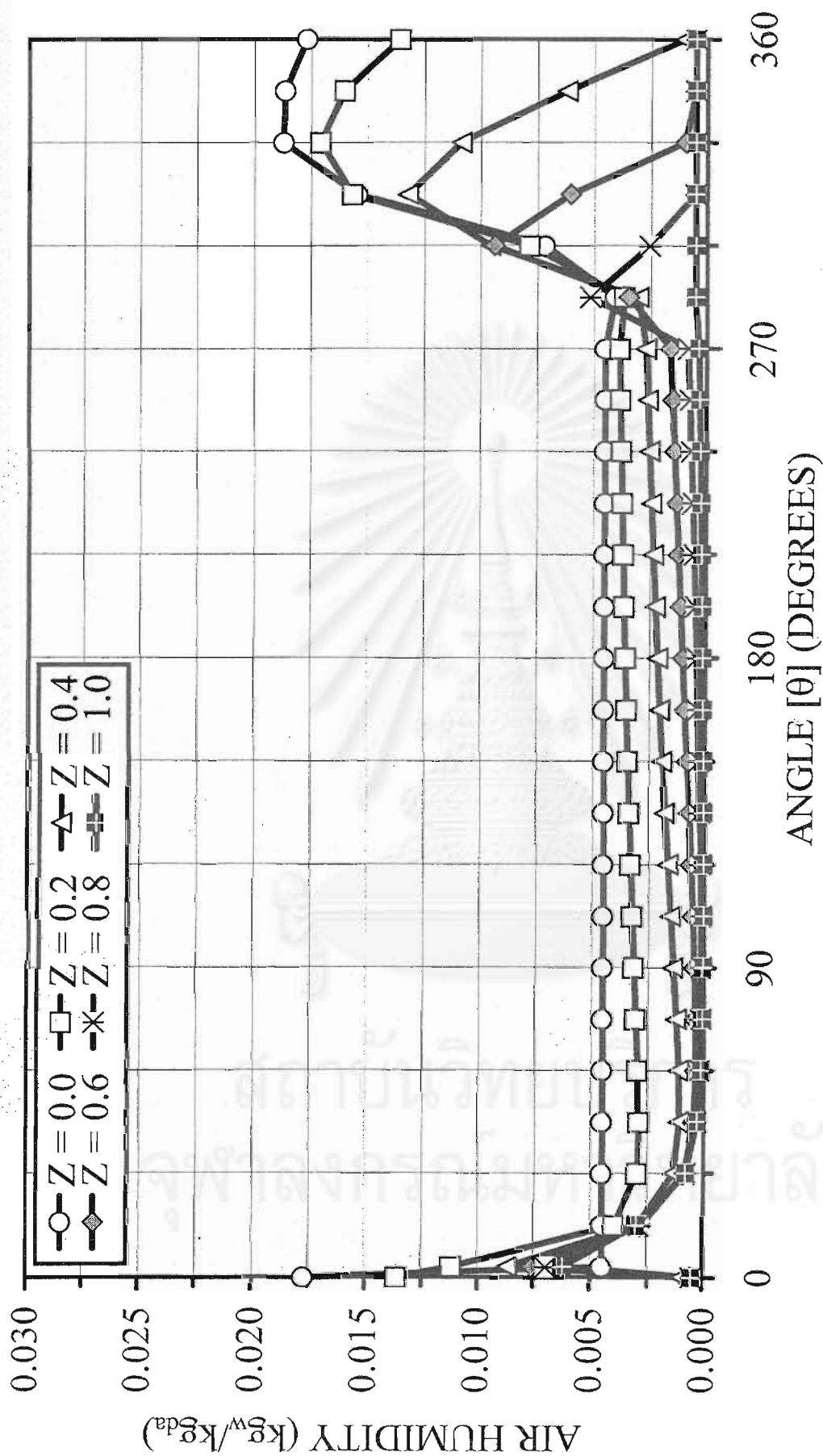
Figure 6.11 The two-dimensional distributions of the slot air humidity in the silica gel coated honeycomb rotary dehumidifier at 12.5 rph (Speed-SG-Effect Condition)
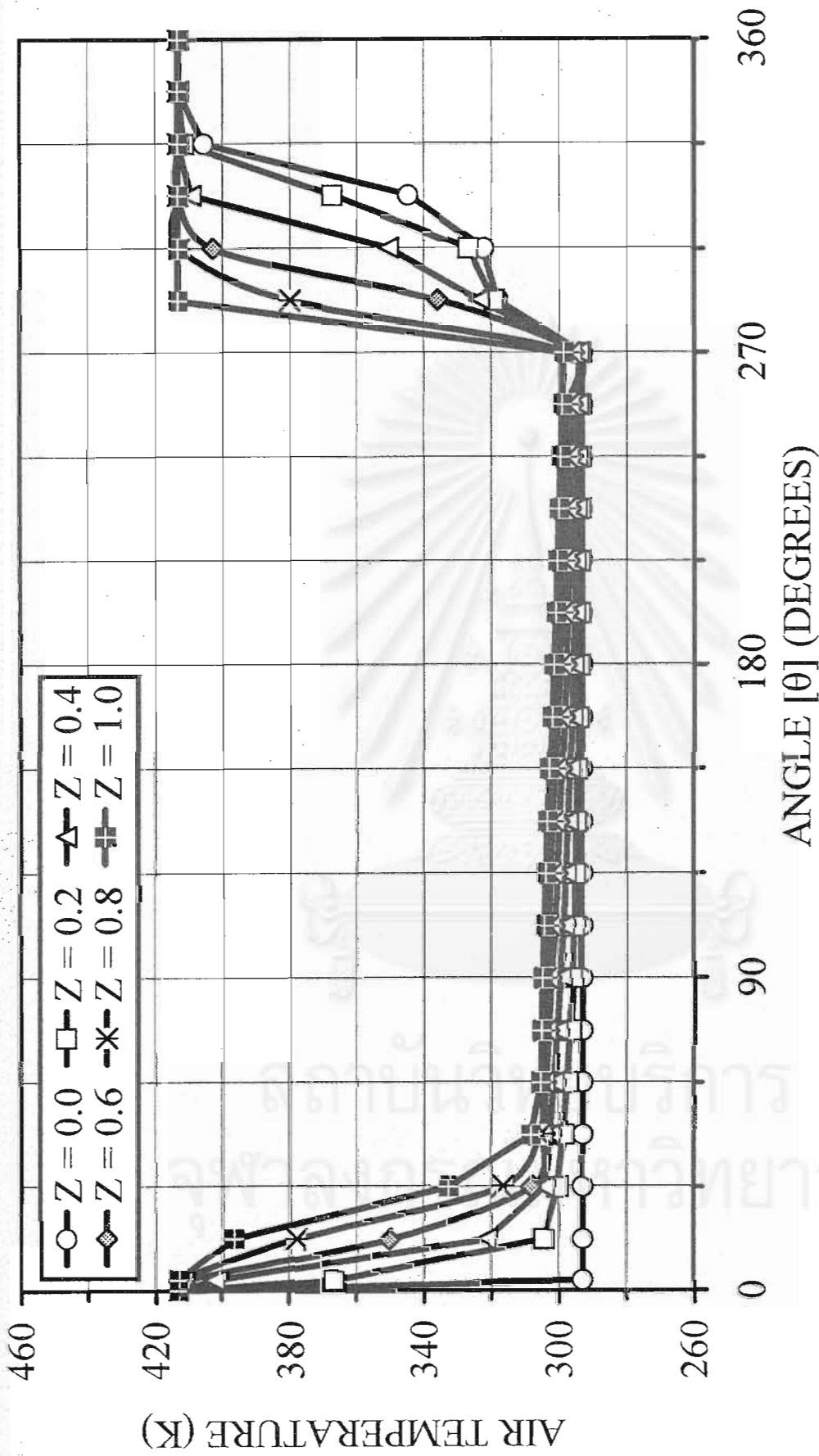
Figure 6.12 The two-dimensional distributions of the slot air temperature in the silica gel coated honeycomb rotary dehumidifier at 3.5 rph (Speed-SG-Effect Condition)
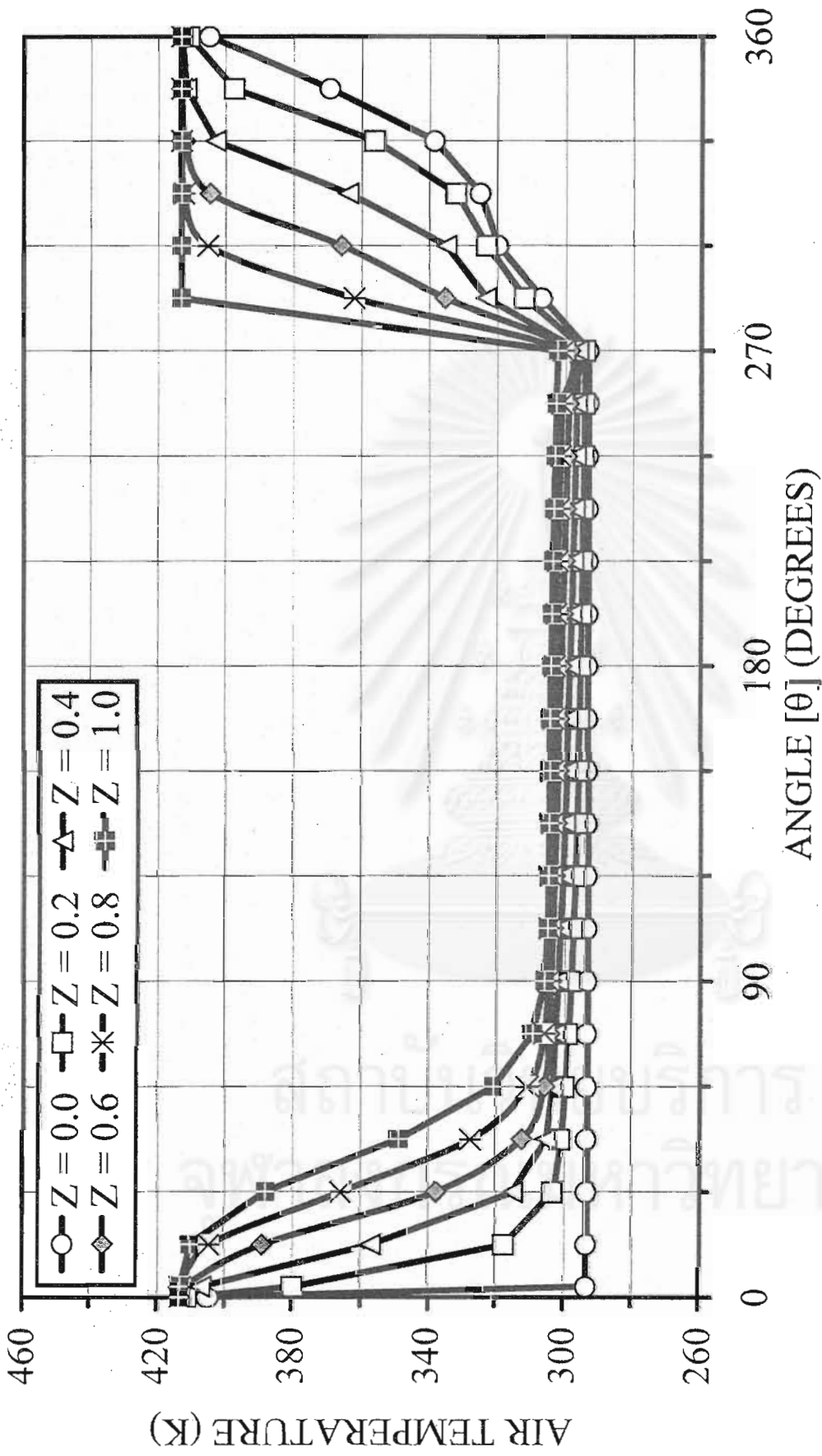
Figure 6.13 The two-dimensional distributions of the slot air temperature in the silica gel coated honeycomb rotary dehumidifier at 6.2 rph (Speed-SG-Effect Condition)
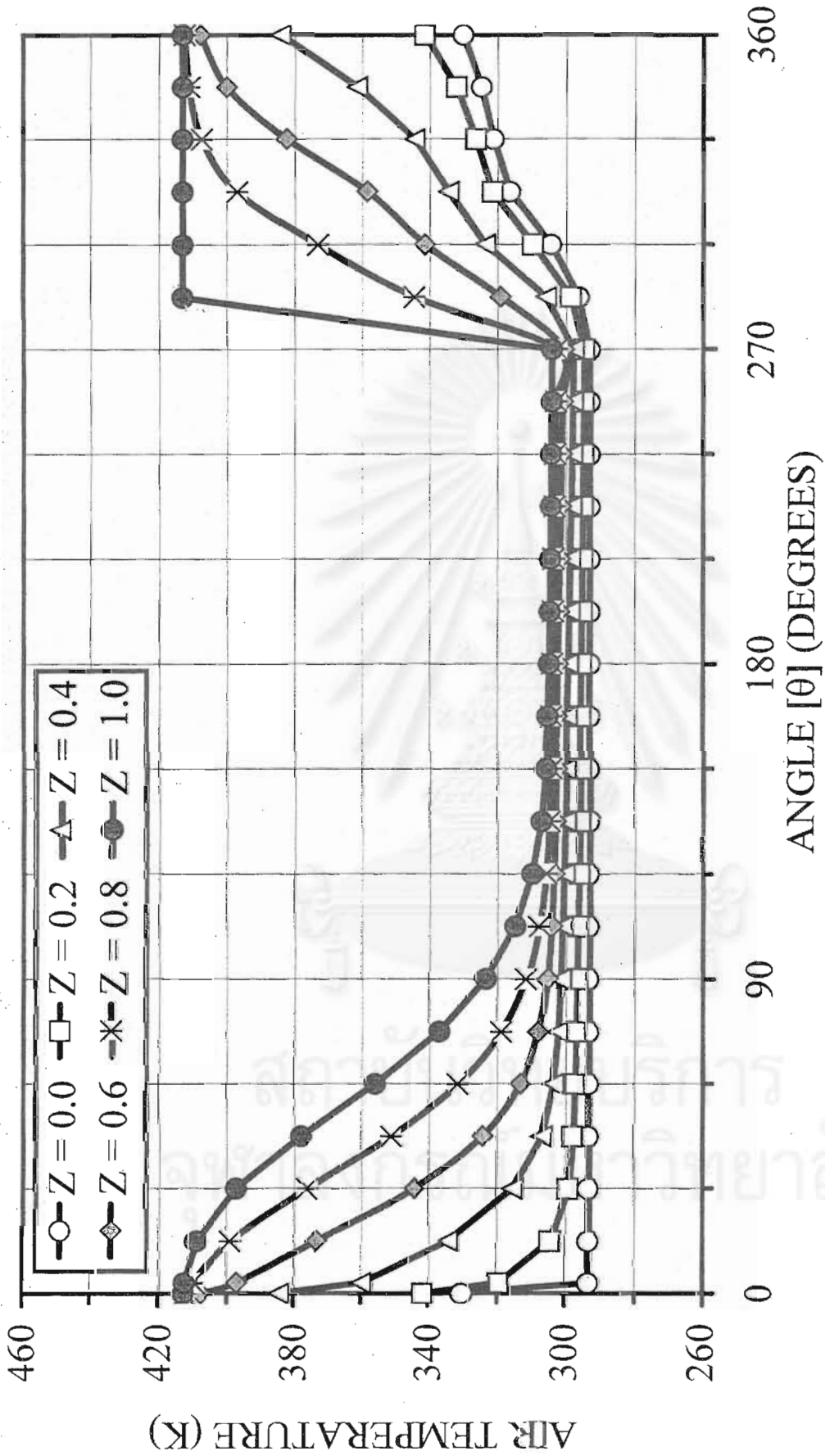
Figure 6.14 The two-dimensional distributions of the slot air temperature in the silica gel coated honeycomb rotary dehumidifier at 12.5 rph (Speed-SG-Effect Condition)
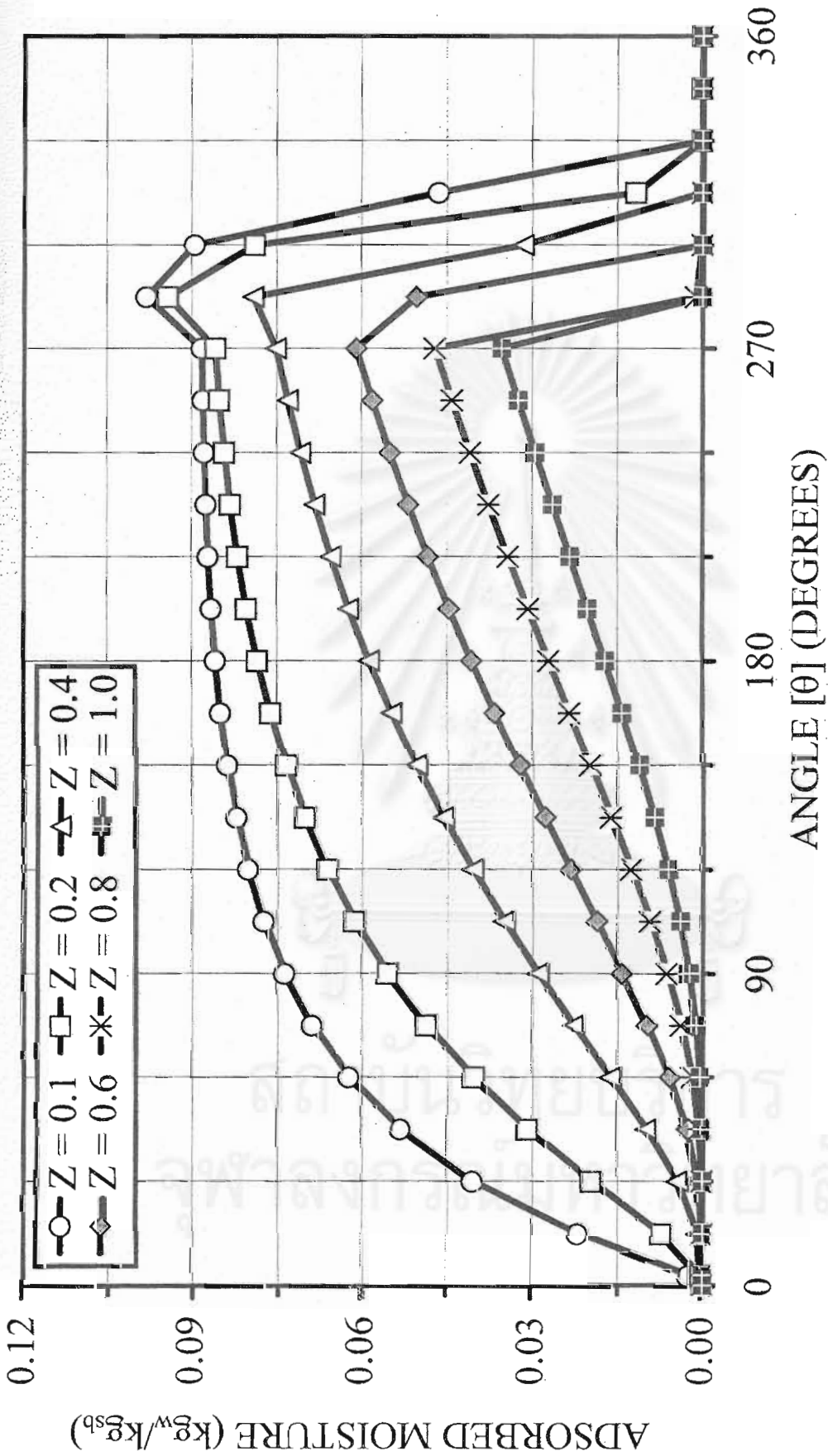
Figure 6.15 The two-dimensional distributions of the adsorbed moisture on silica gel coated honeycomb rotary dehumidifier at 3.5 rph (Speed-SG-Effect Condition)
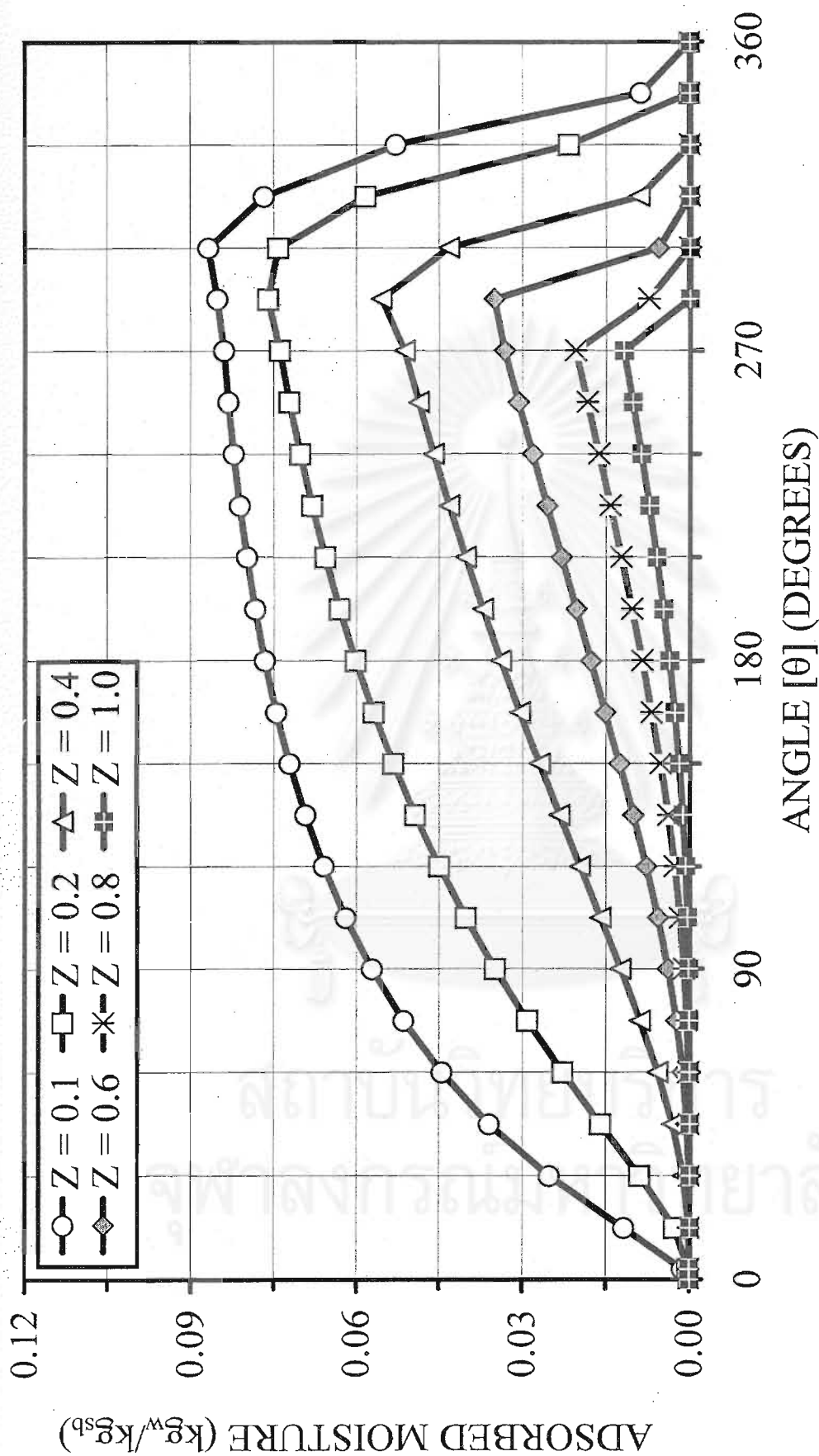
Figure 6.16 The two-dimensional distributions of the adsorbed moisture on silica gel coated honeycomb rotary dehumidifier at 6.2 rph (Speed-SG-Effect Condition)
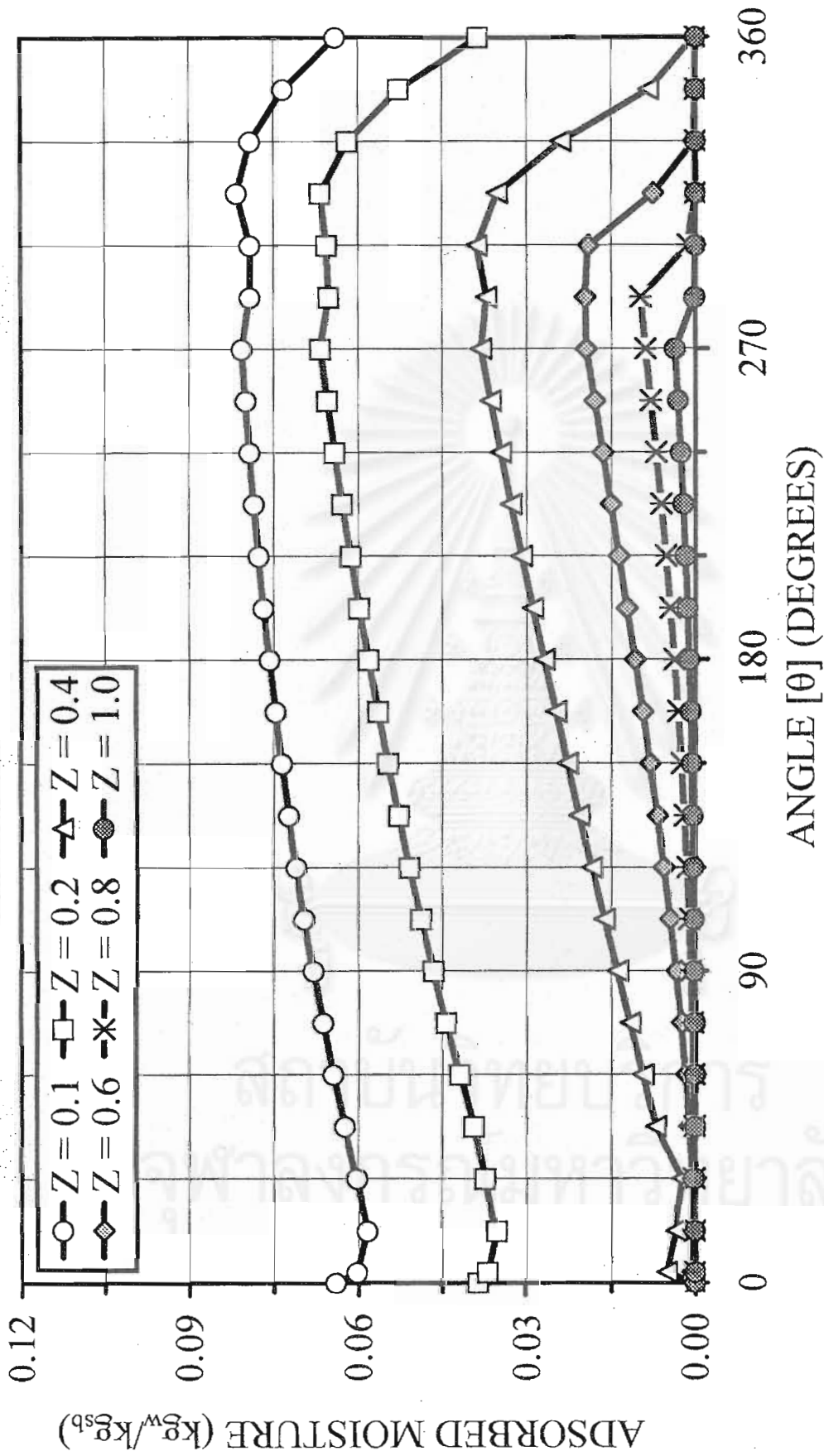
Figure 6.17 The two-dimensional distributions of the adsorbed moisture on silica gel coated honeycomb rotary dehumidifier at 12.5 rph (Speed-SG-Effect Condition)
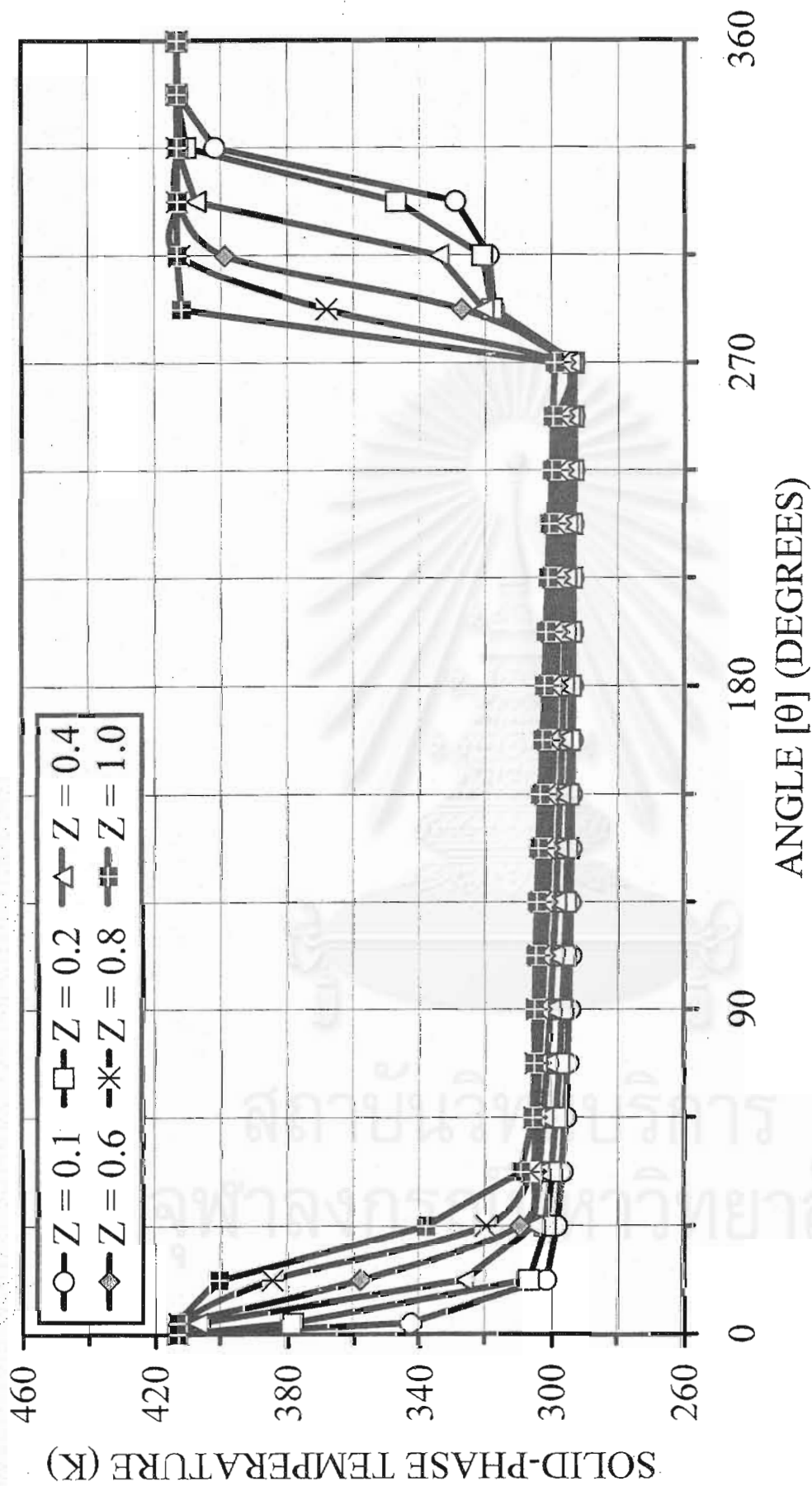
Figure 6.18 The two-dimensional distributions of the solid-phase temperature in the silica gel coated honeycomb rotary dehumidifier at 3.5 rph (Speed-SG-Effect Condition)
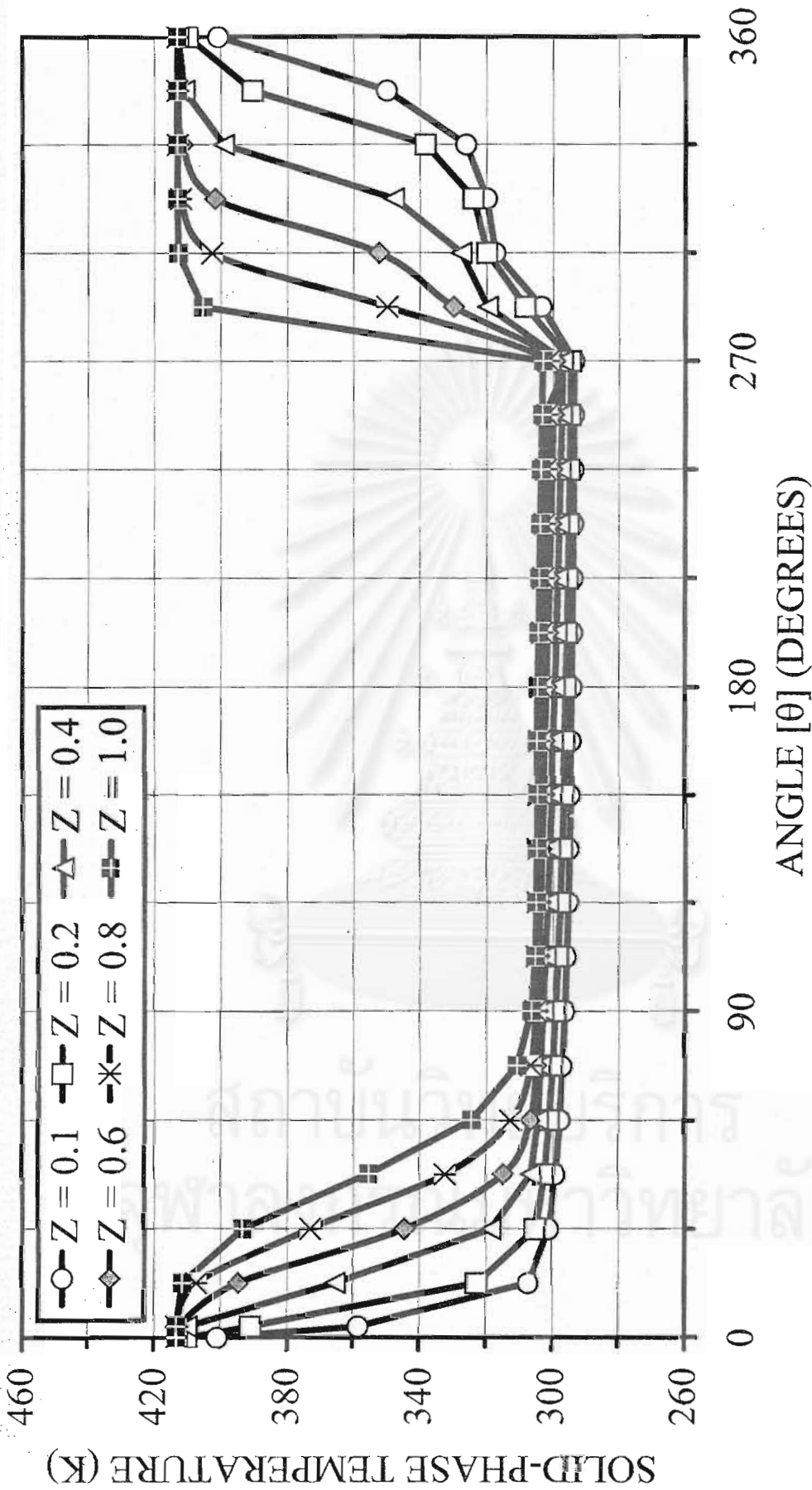
Figure 6.19 The two-dimensional distributions of the solid-phase temperature in the silica gel coated honeycomb rotary dehumidifier at 6.2 rph (Speed-SG-Effect Condition)
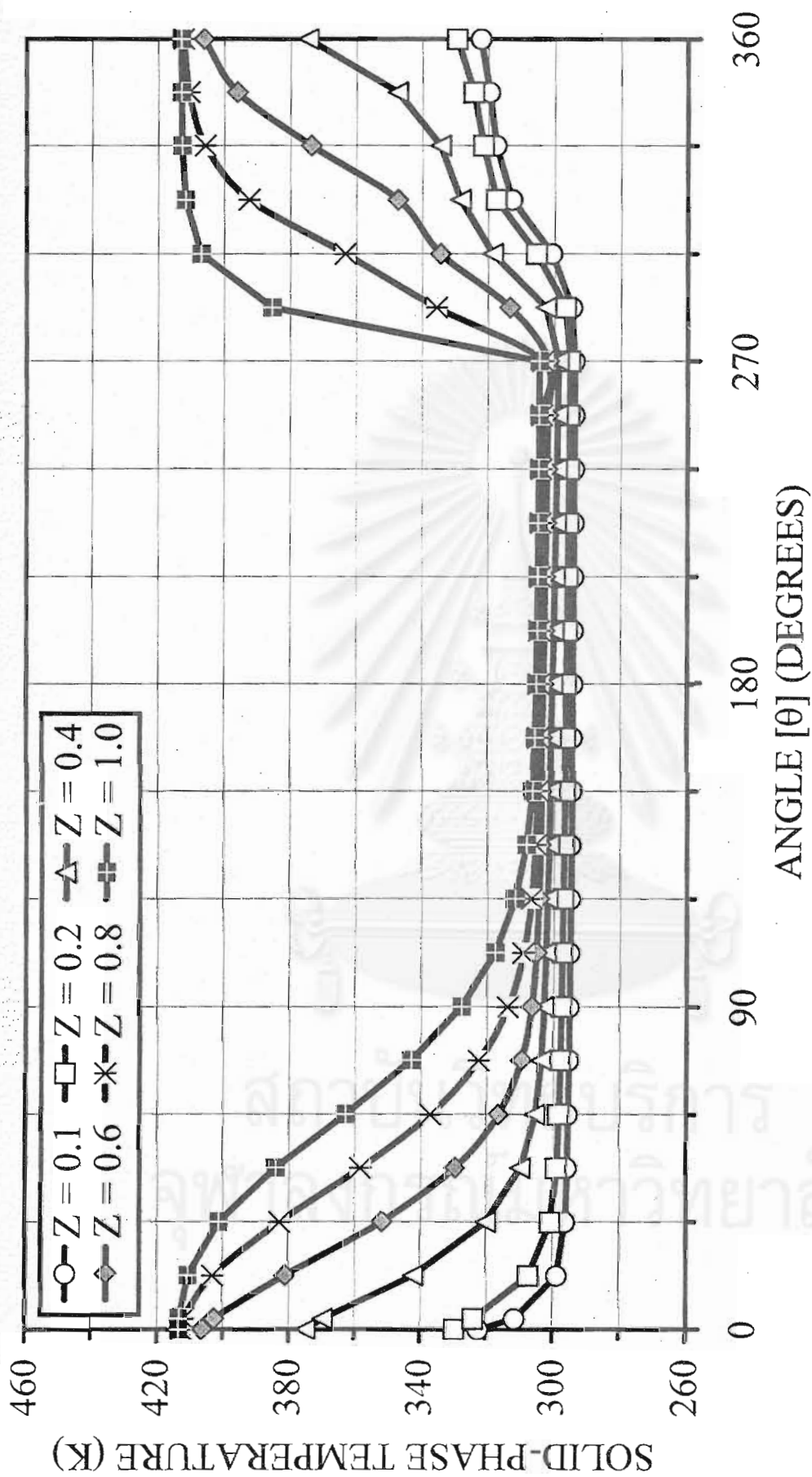
Figure 6.20 The two-dimensional distributions of the solid-phase temperature in the silica gel coated honeycomb rotary dehumidifier at 12.5 rph (Speed-SG-Effect Condition)

6.2.2 Effect of mass velocity of humid air

As expected, one significant factor influencing the dehumidification efficiency is the mass velocity of the humid air, which is proportional to the moisture loading. In Figure 6.21, it is seen that the efficiency nearly linearly decreases from 95 to 70 % approximately as the air mass velocity G_w increases from 4.05×10^{-3} to 1.62×10^{-2} $kg_w/(m^2 s)$. As the moisture loading increases, it begins to exceed the maximum adsorption capacity of the dehumidifier and the dehumidification efficiency drops linearly with G_w. The slight drop in the outlet air temperature in Figure 6.23 can be attributed to the higher capacity of the air stream as G_w increases. While the power required by heater at various mass velocities of the humid air are constant as shown in Figure 6.24 since the regenerative temperature and the mass velocities of the hot air are kept constant at 413 K and 4.25×10^{-4} $kg_w/m^2 s$, respectively.

Figure 6.25 illustrates how the local humidity of the dehumidified air changes with θ at various mass velocities of the room air. Similarly, Figure 6.26 shows the angular profile of the dehumidified air temperature at different mass velocities. In Figure 6.25 the local humidity profile of dehumidified air at 4.05×10^{-3} $kg_w/(m^2 s)$ is essentially zero over the region $\theta = 45°\text{-}135°$ because the adsorption capacity of the dehumidifier is big enough for the applied moisture loading. In addition, increasing the mass velocity of the humid air at 8.10×10^{-3} $kg_w/(m^2 s)$, the zero region of the local humidity profile of the dehumidified air reduces to $\theta = 45°\text{-}60°$. In Figure 6.26 the outlet air temperature drops more rapidly in the region $\theta = 0°\text{-}60°$ as G_w increases because the air has higher heat capacity to cool down the hot, newly regenerated adsorbent while little moisture adsorption takes place at relatively high adsorbent temperature.

Moreover, the phenomena of the heat and mass transfer in the rotary dehumidifier at various mass velocities of the humid air can easily be investigated in details as shown in Figures 6.27 - 6.34 that illustrate the two-dimensional angular distributions of the air humidity, the air temperature, the adsorbed moisture and the solid-phase temperature inside the rotor for $G_w = 4.05 \times 10^{-3}$ and 8.10×10^{-3} $kg_w/(m^2 s)$. In the adsorption zone ($\theta = 0°\text{-}270°$), the hot adsorbent initially has to be cooled down in order for dehumidification to become effective.
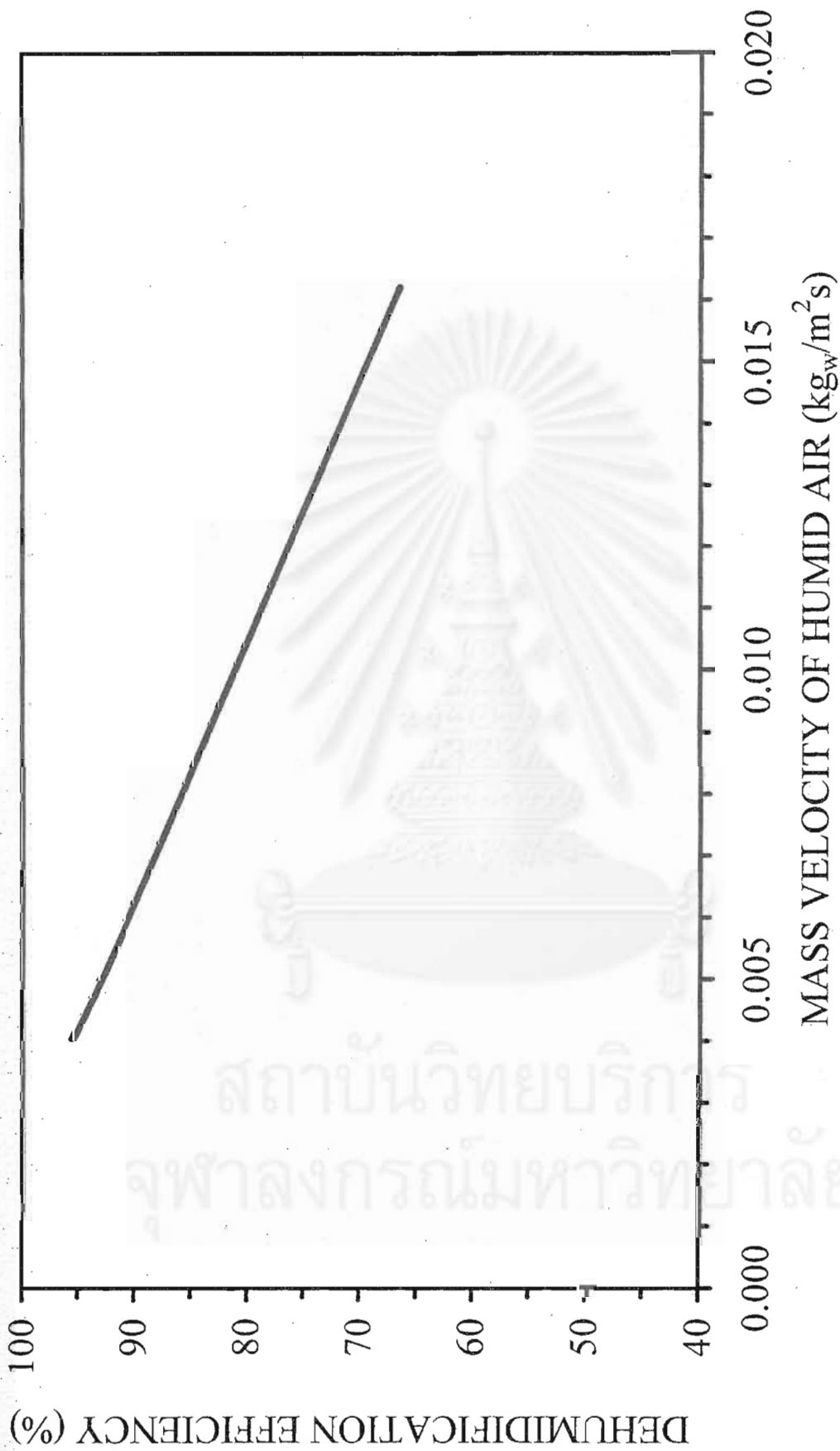
Figure 6.21 Effect of mass velocity of humid air on the dehumidification efficiency of the silica gel coated honeycomb rotary dehumidifier (Gads-SG-Effect condition)
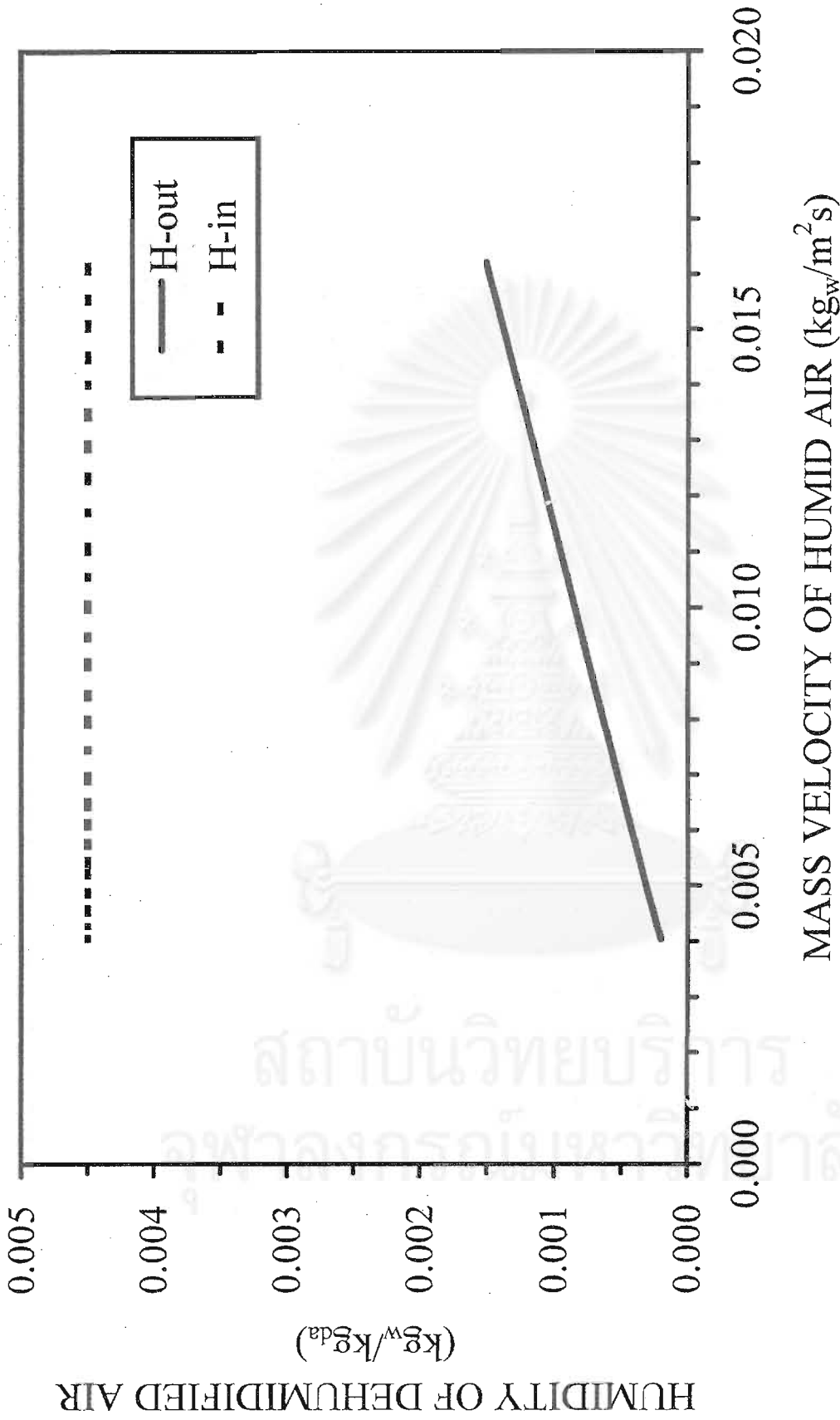
Figure 6.22 Effect of mass velocity of humid air on the average humidity of the dehumidified air from the silica gel coated honeycomb rotary dehumidifier (Gads-SG-Effect Condition)
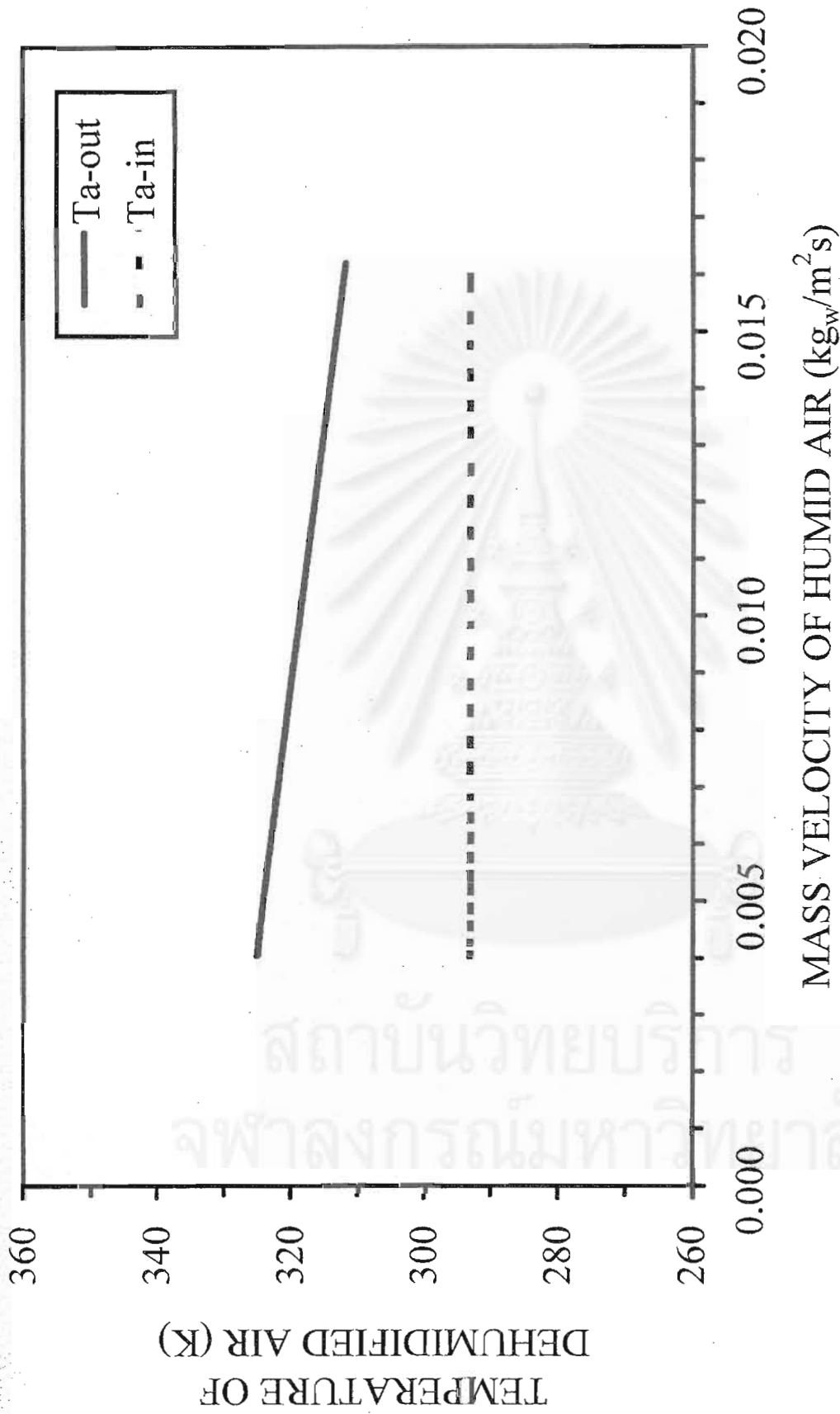
Figure 6.23 Effect of mass velocity of humid air on the average temperature of the dehumidified air from the silica gel coated honeycomb rotary dehumidifier (Gads-SG-Effect Condition)
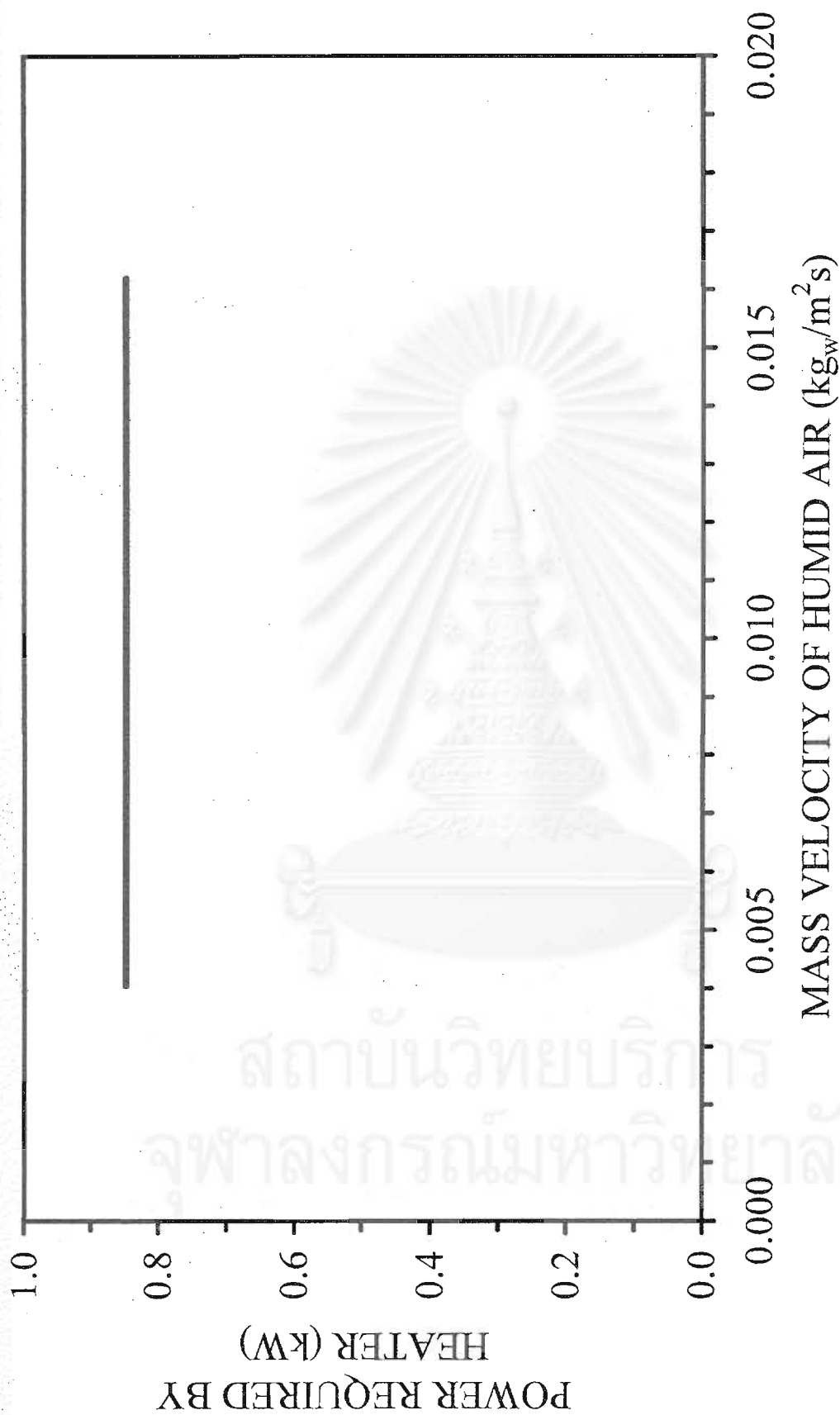
Figure 6.24 Power required by heater at various mass velocities of humid air for the silica gel coated honeycomb rotary dehumidifier (Gads-SG-Effect Condition)
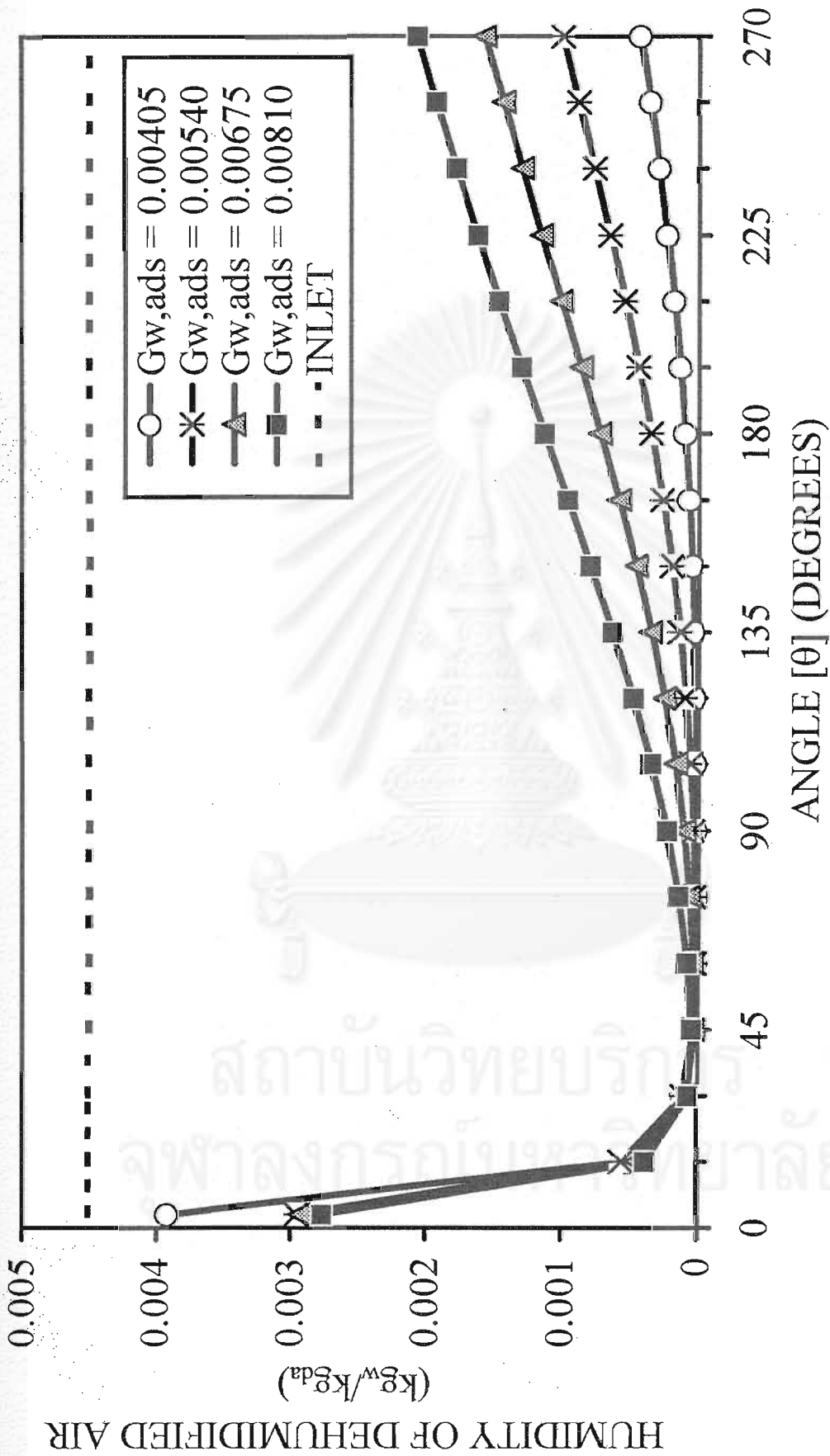
Figure 6.25 The angular distributions of the humidity of the dehumidified air from the silica gel coated honeycomb rotary dehumidifier at various mass velocities of humid air (Gads-SG-Effect Condition)
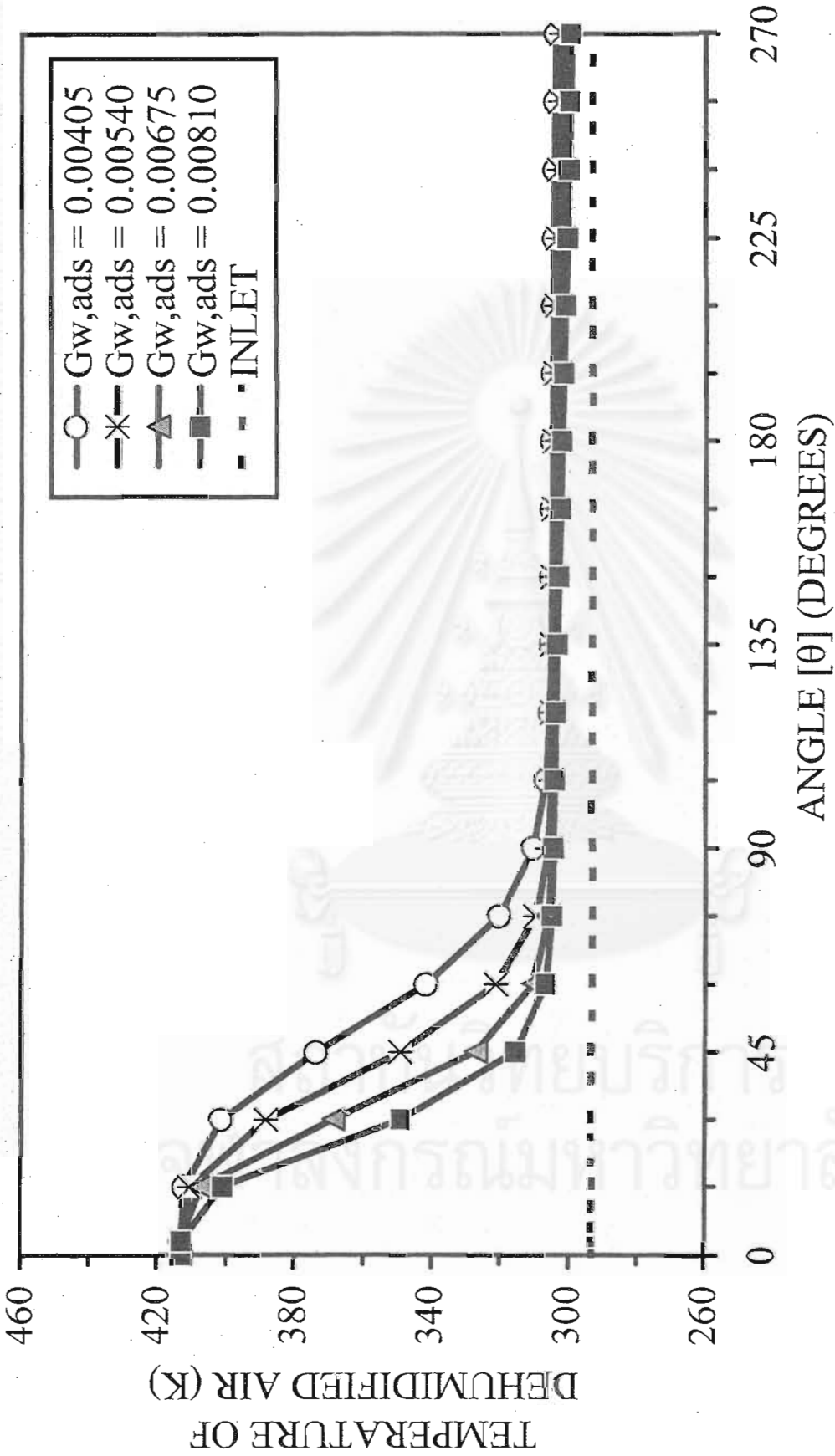
Figure 6.26 The angular distributions of the temperature of the dehumidified air from the silica gel coated honeycomb rotary dehumidifier at various mass velocities of humid air (Gads-SG-Effect Condition)
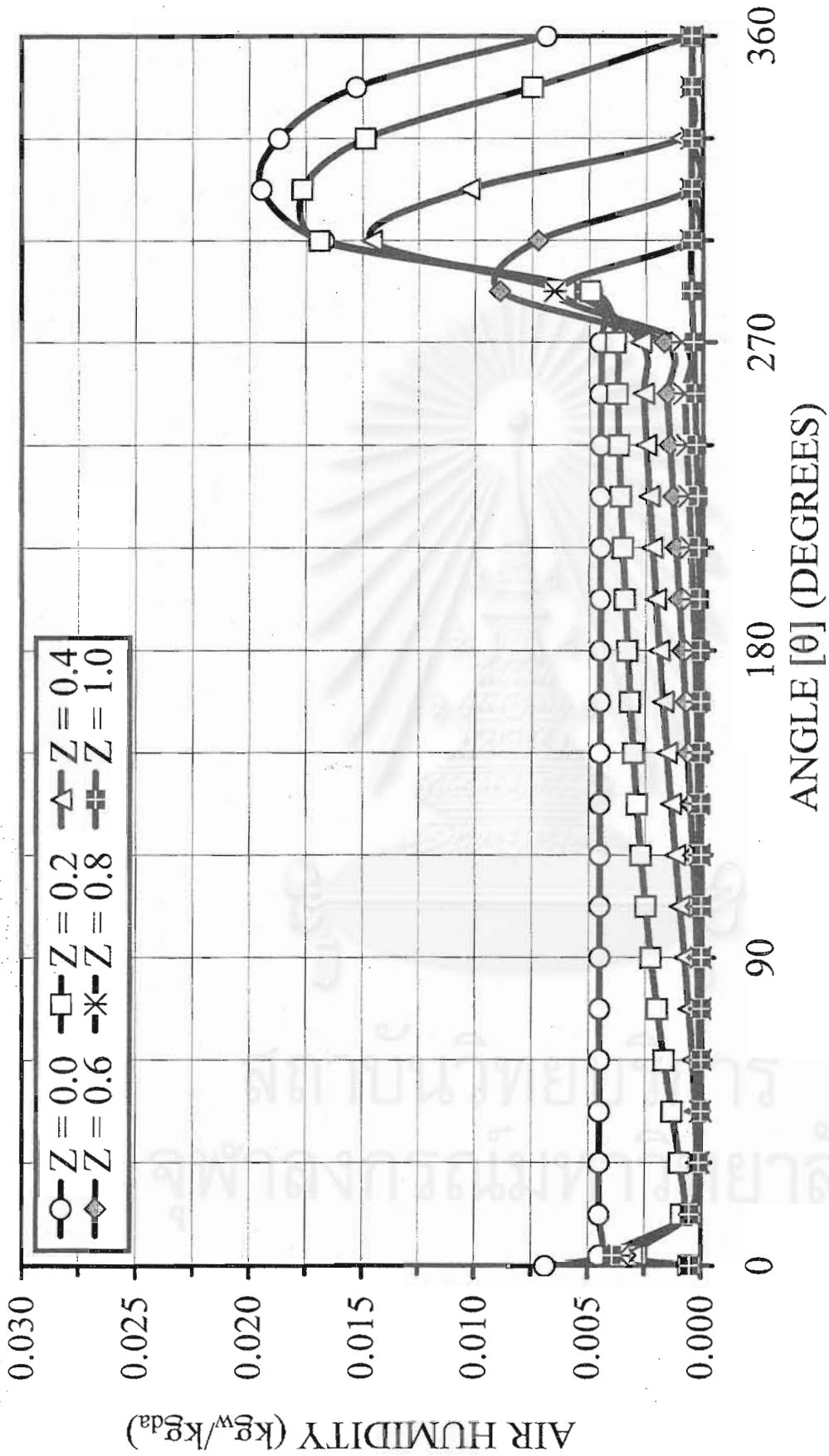
Figure 6.27 The two-dimensional distributions of the slot air humidity in the silica gel coated honeycomb rotary dehumidifier at 0.00405 kg$_w$/(m^{2}s) of mass velocity of humid air (Gads-SG-Effect Condition)
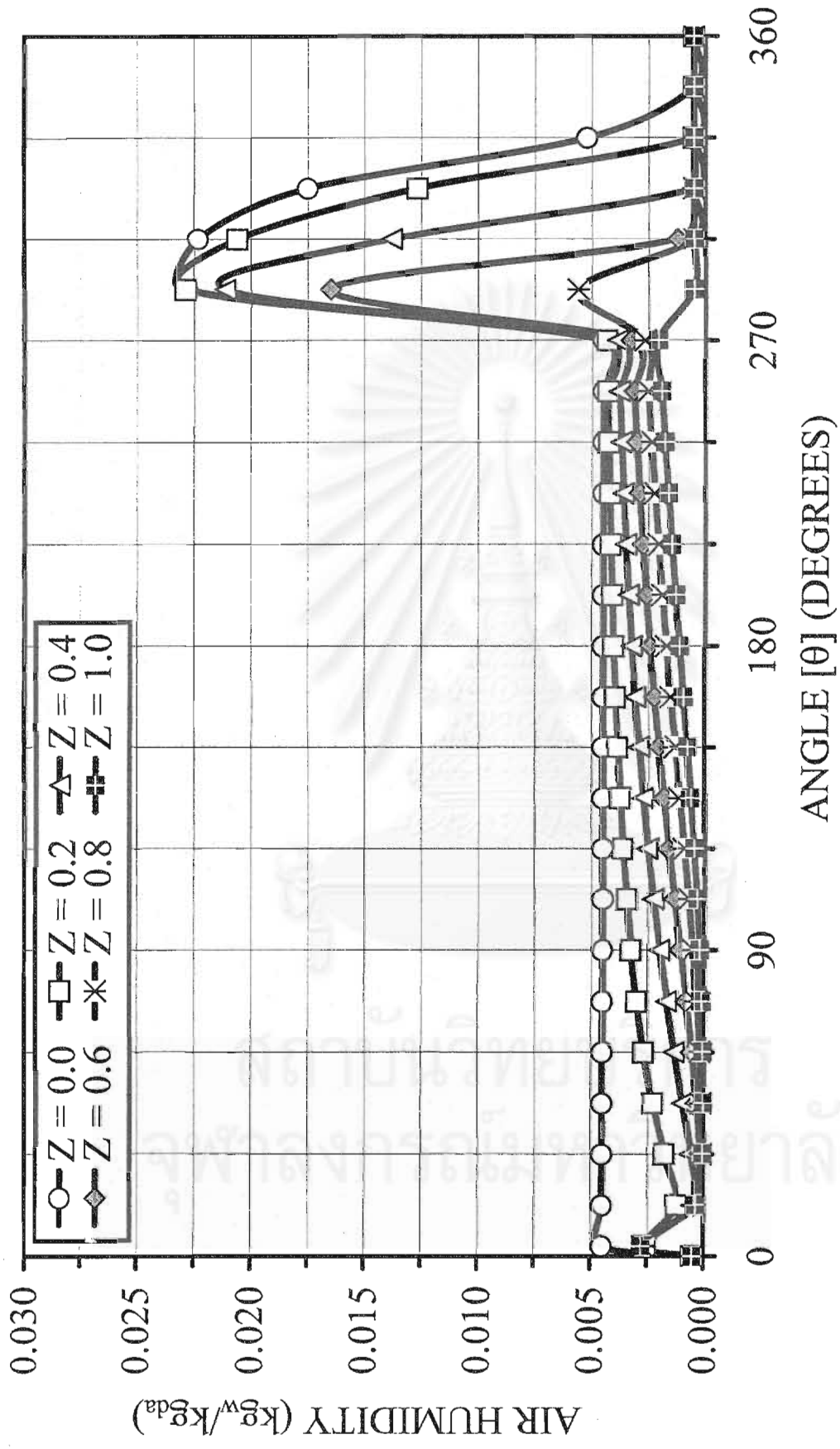
Figure 6.28 The two-dimensional distributions of the slot air humidity in the silica gel coated honeycomb rotary dehumidifier at 0.0081 kg$_w$/ (m^{2}s) of mass velocity of humid air (Gads-SG-Effect Condition)
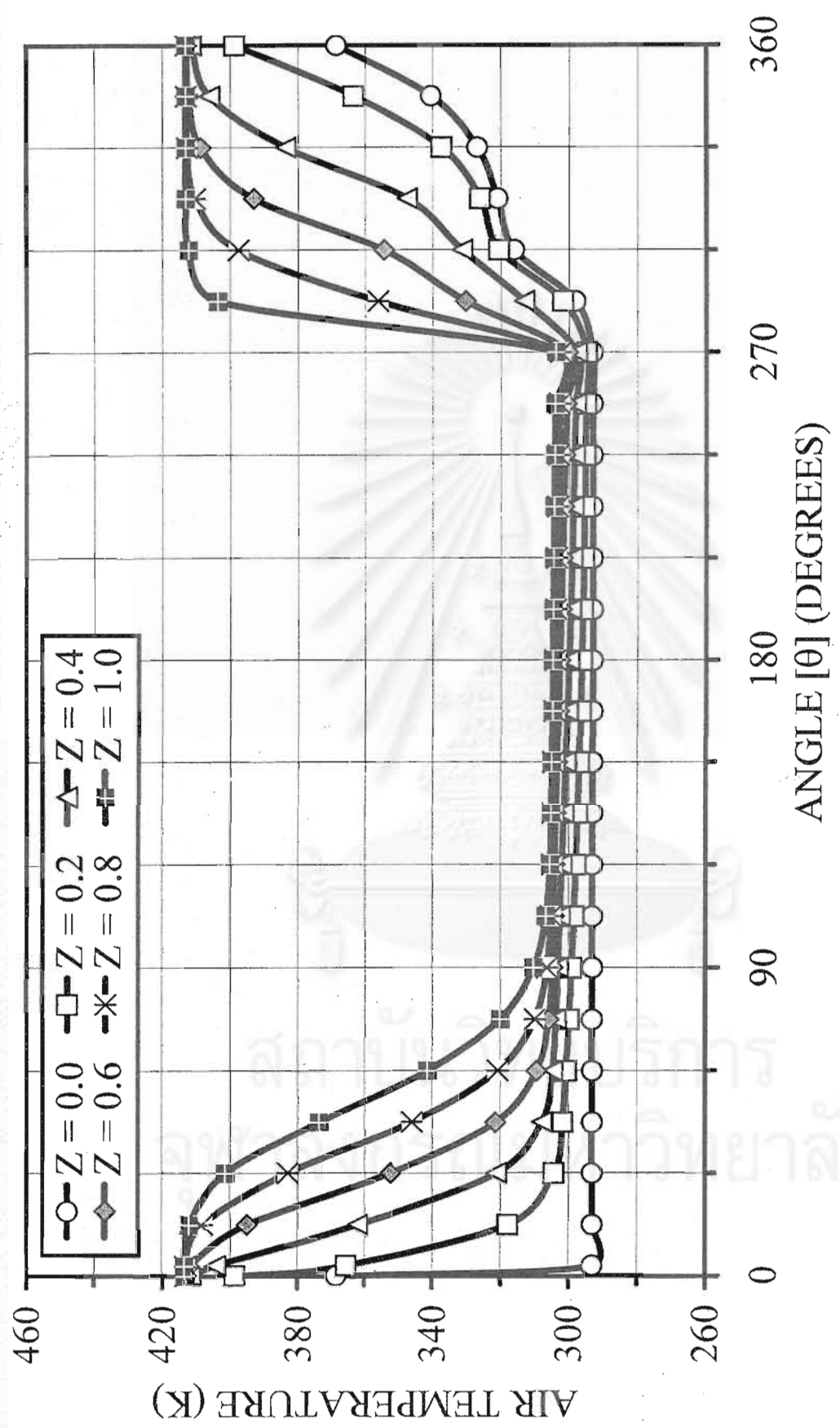
Figure 6.29 The two-dimensional distributions of the slot air temperature in the silica gel coated honeycomb rotary dehumidifier at 0.00405 kg$_w$/ (m^{2}s) of mass velocity of humid air (Gads-SG-Effect Condition)
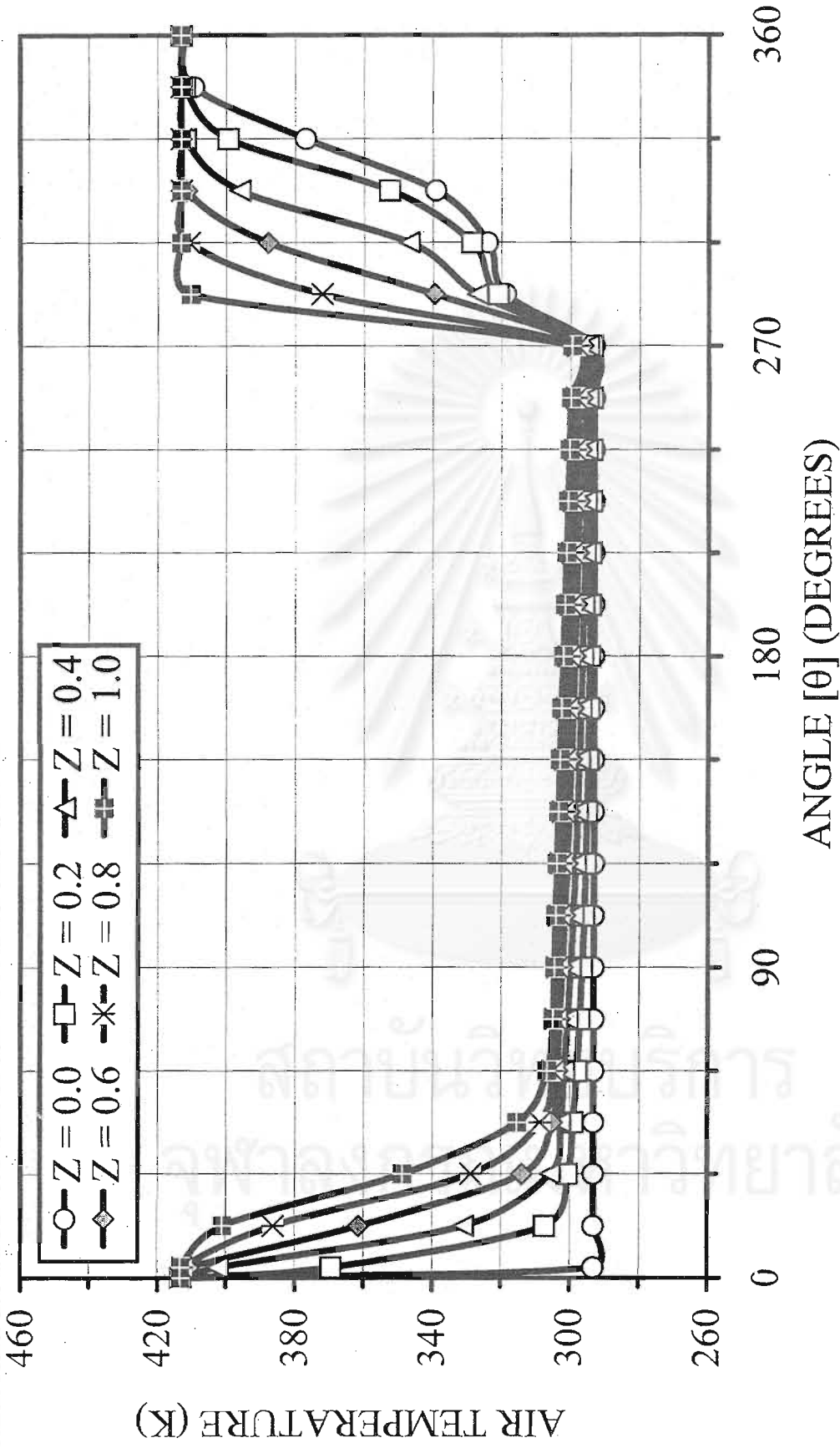
Figure 6.30 The two-dimensional distributions of the slot air temperature in the silica gel coated honeycomb rotary dehumidifier at 0.0081 kg$_w$/(m^{2}s) of mass velocity of humid air (Gads.-SG-Effect Condition)
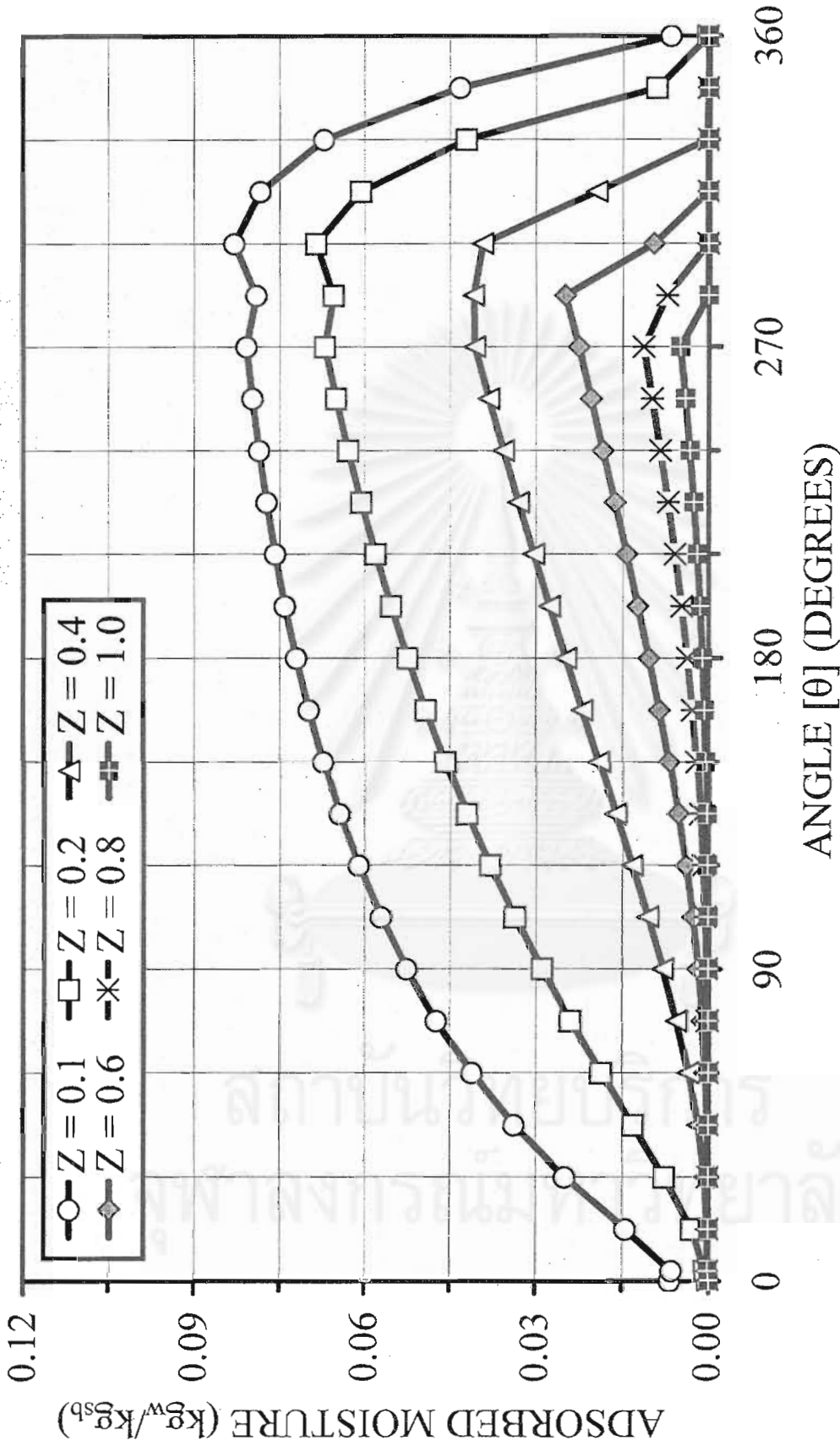
Figure 6.31 The two-dimensional distributions of the adsorbed moisture on silica gel coated honeycomb rotary dehumidifier at 0.00405 kg$_w$/(m^{2}s) of mass velocity of humid air (Gads-SG-Effect Condition)
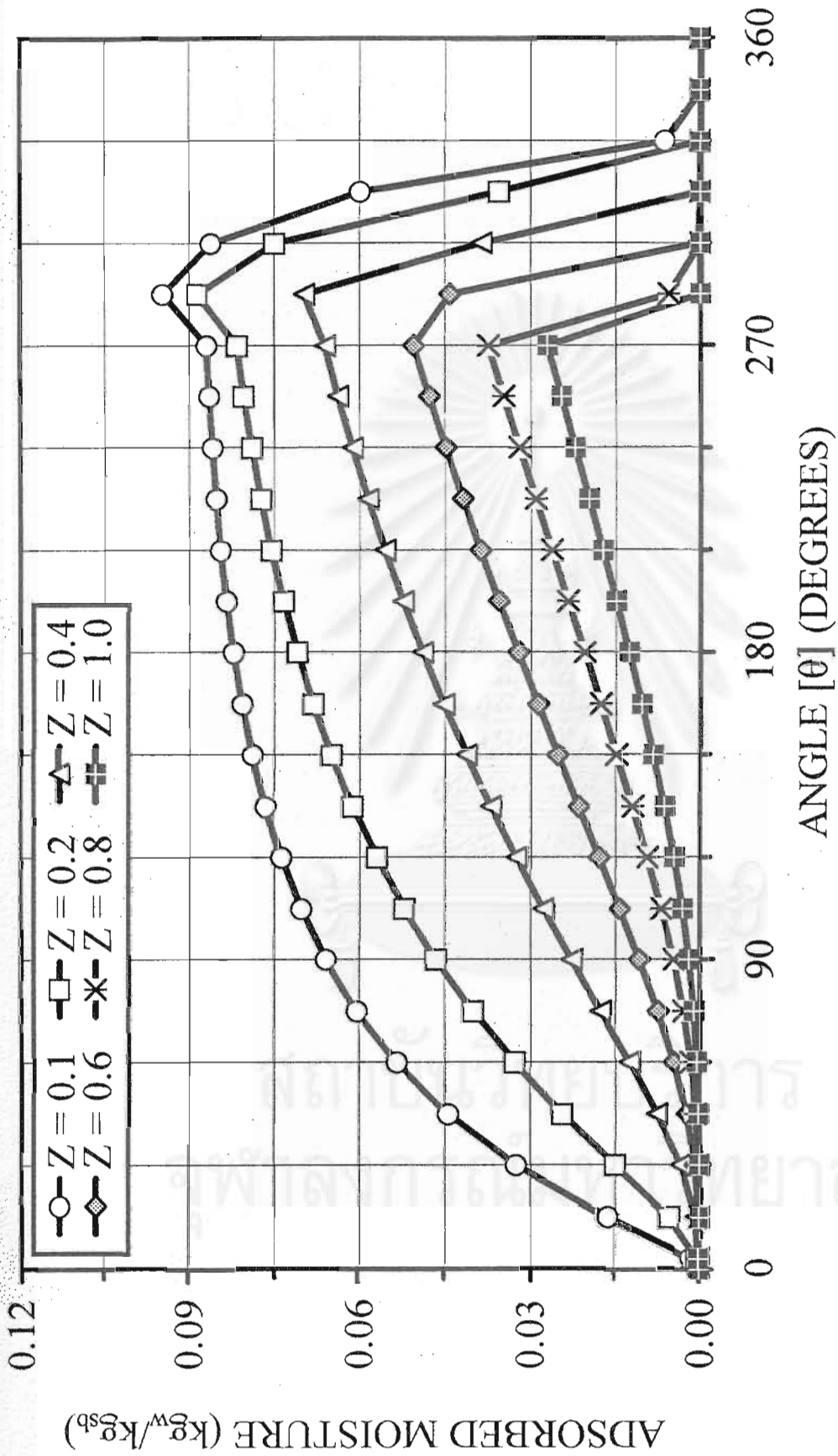
Figure 6.32 The two-dimensional distributions of the adsorbed moisture on silica gel coated honeycomb rotary dehumidifier at 0.0081 $kg_w/(m^2s)$ of mass velocity of humid air (Gads-SG-Effect Condition)
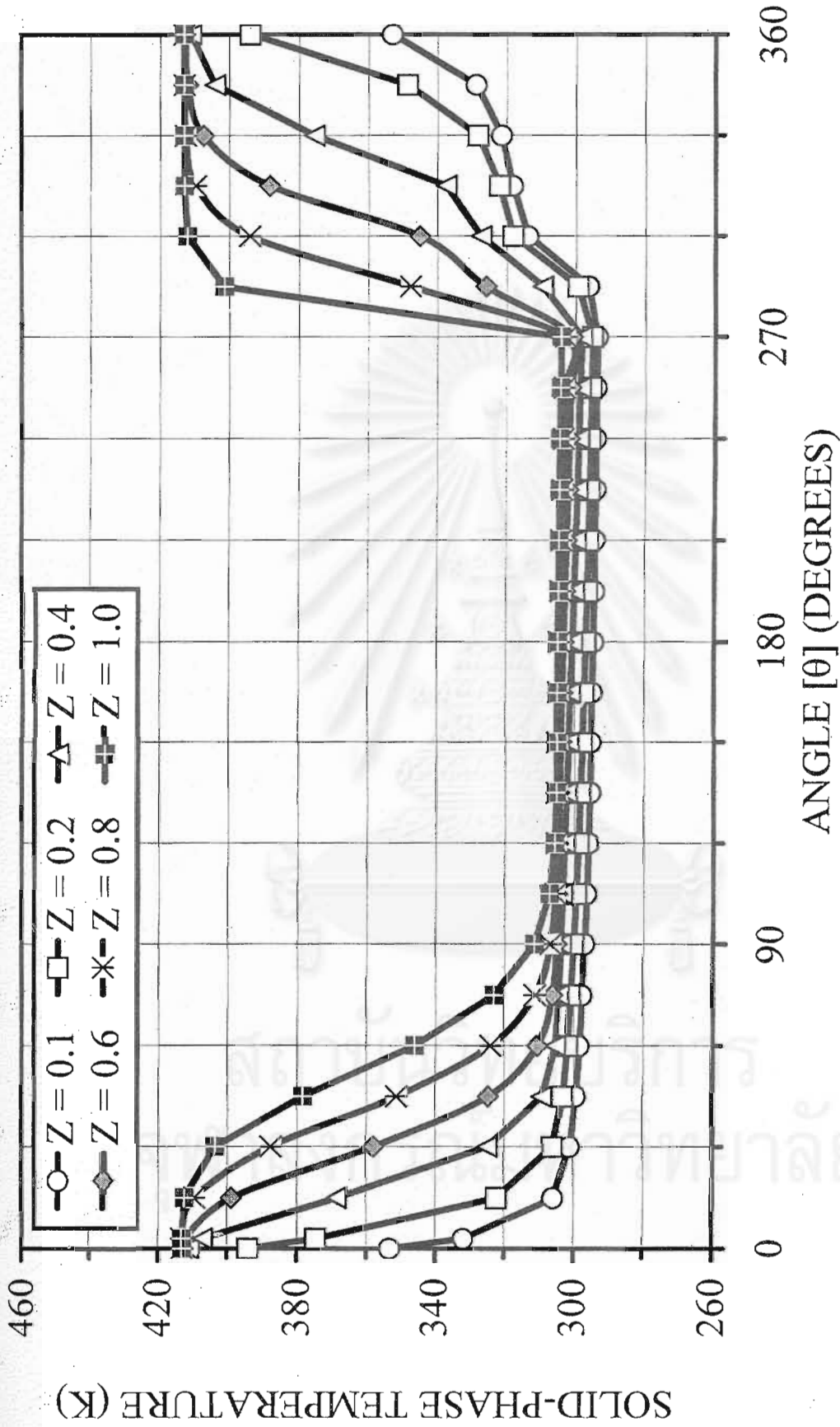
Figure 6.33 The two-dimensional distributions of the solid-phase temperature in the silica gel coated honeycomb rotary dehumidifier at 0.00405 kg$_w$/(m²s) of mass velocity of humid air (Gads-SG-Effect Condition)
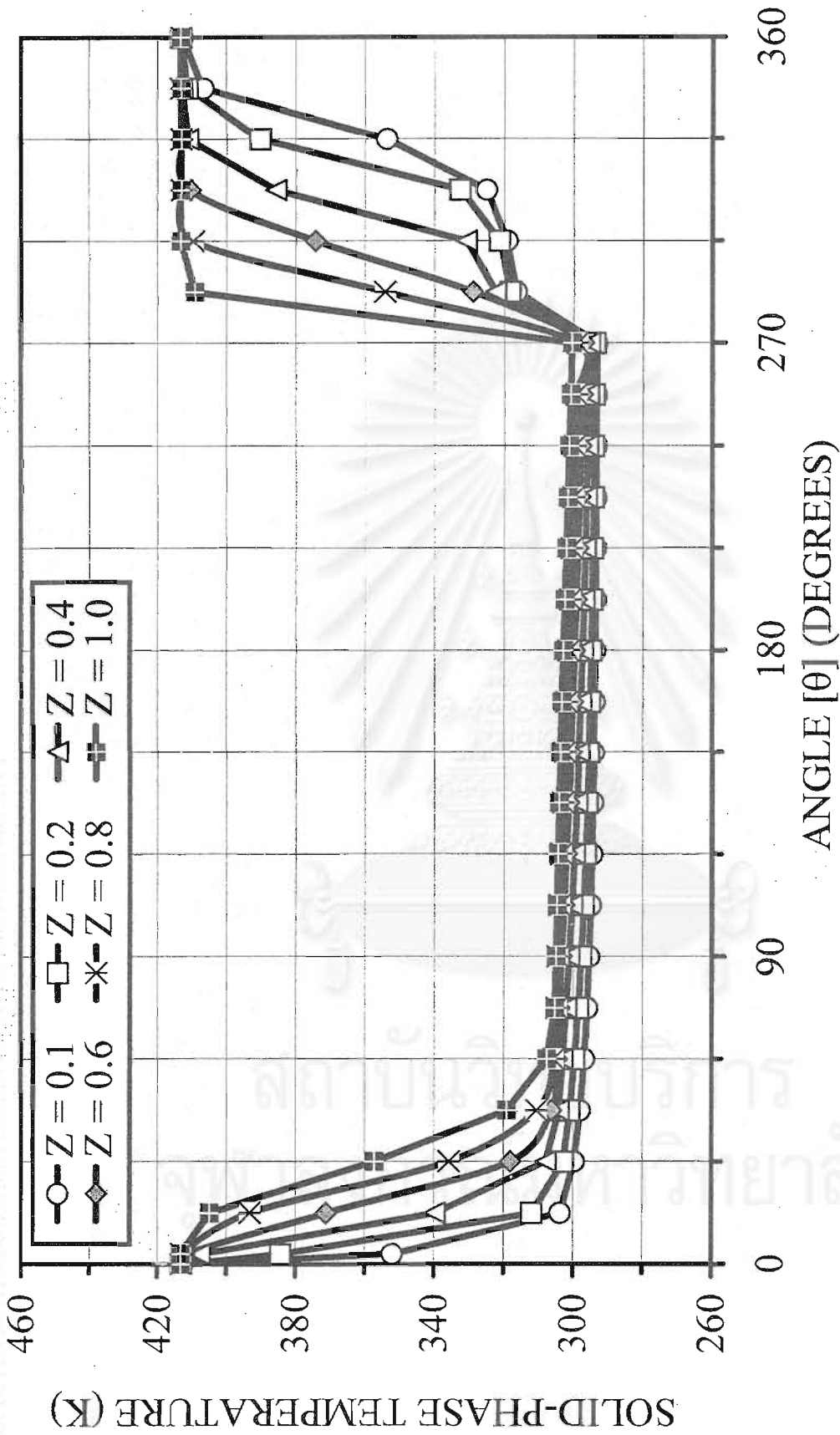
Figure 6.34 The two-dimensional distributions of the solid-phase temperature in the silica gel coated honeycomb rotary dehumidifier at 0.0081 $kg_w/(m^2s)$ of mass velocity of humid air (Gads-SG-Effect Condition)

6.2.3 Effect of length of the rotor

In Figure 6.35, it is seen that increasing length of the rotor, L, from 0.10 to 0.25 m. rapidly increases the dehumidification efficiency from 70 to 95 %. While the temperature of the dehumidified air linearly increase from 310 to 325 K as shown in Figure 6.37. The higher temperature of the dehumidified air is caused by the extending of the cooling region in the adsorption zone as shown in Figure 6.39. As expected, longer rotor takes long time to cool down the hot, newly regenerated adsorbent through the rotor. However, the regions are slightly different, say, $\theta = 0°- 45°$ for the 0.10-m and $\theta = 0°- 90°$ for 0.25-m. Since longer rotor gives higher adsorption capacity, the nearly zero region of the local humidity profile of the dehumidified air in Figure 6.38 are extended from $\theta = 45°$ to $\theta = 150°$.

The two-dimensional profiles of the air humidity, the air temperature, the adsorbed moisture and the solid-phase temperature inside the silica gel coated rotary dehumidifier are shown in Figures 6.40 to 6.51 in order to investigate the phenomena of the heat and mass transfer in the rotary dehumidifier at different lengths of rotor. If the air humidity and adsorbed moisture profiles in the regeneration zone ($\theta = 270°- 360°$) as shown in Figure 6.40 and 6.46, respectively, drops to zero before $\theta = 360°$, then it means the rotor is too short. In contrast, if the profiles drop to zero at $\theta = 360°$ as shown in Figure 6.41 and 6.47, then it means the rotor has the optimal length.
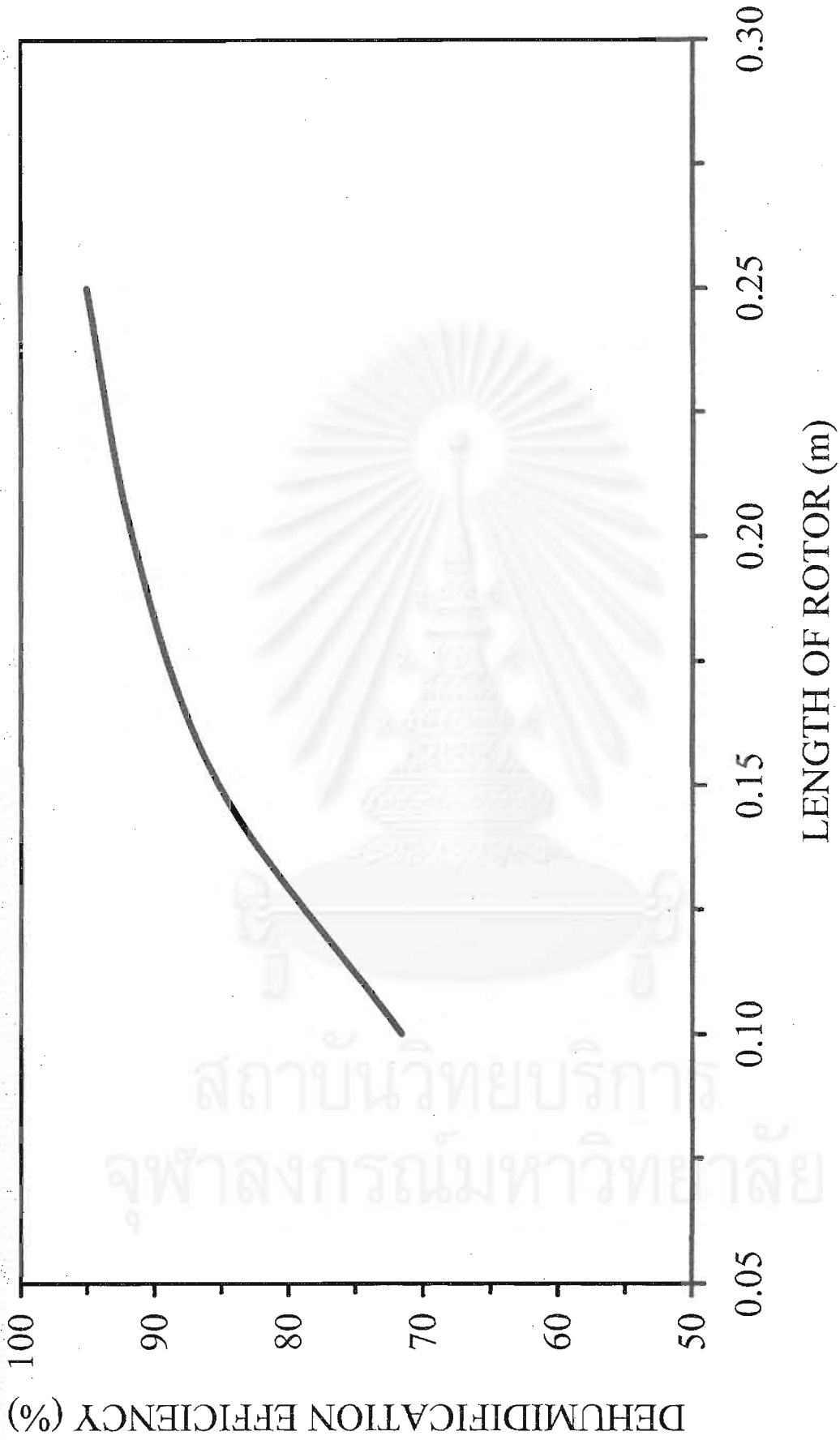
Figure 6.35 Effect of axial length of the rotor on the dehumidification efficiency of the silica gel coated honeycomb rotary dehumidifier (Length -SG-Effect condition)
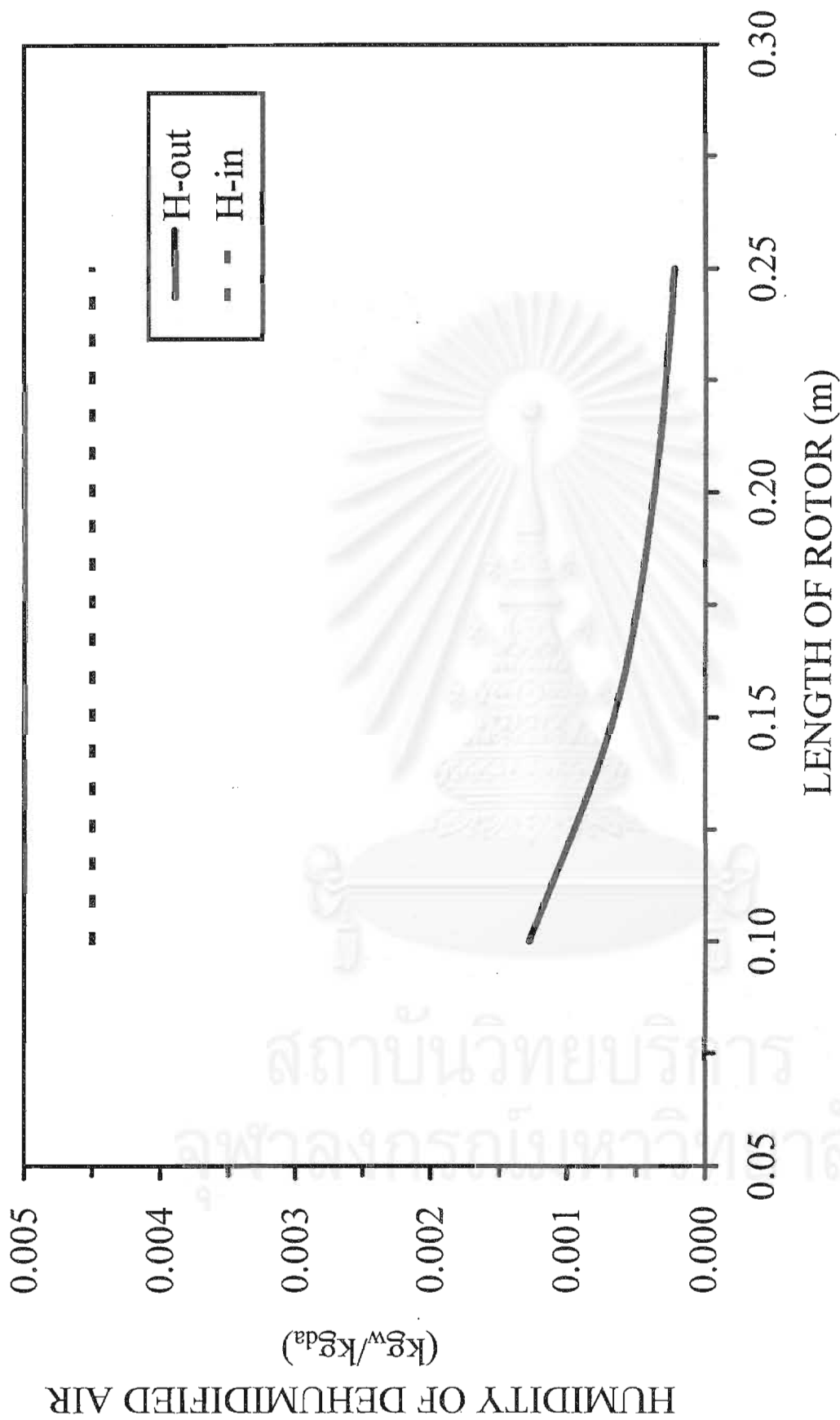
Figure 6.36 Effect of axial length of the rotor on the average humidity of the dehumidified air from the silica gel coated honeycomb rotary dehumidifier (Length-SG-Effect condition)
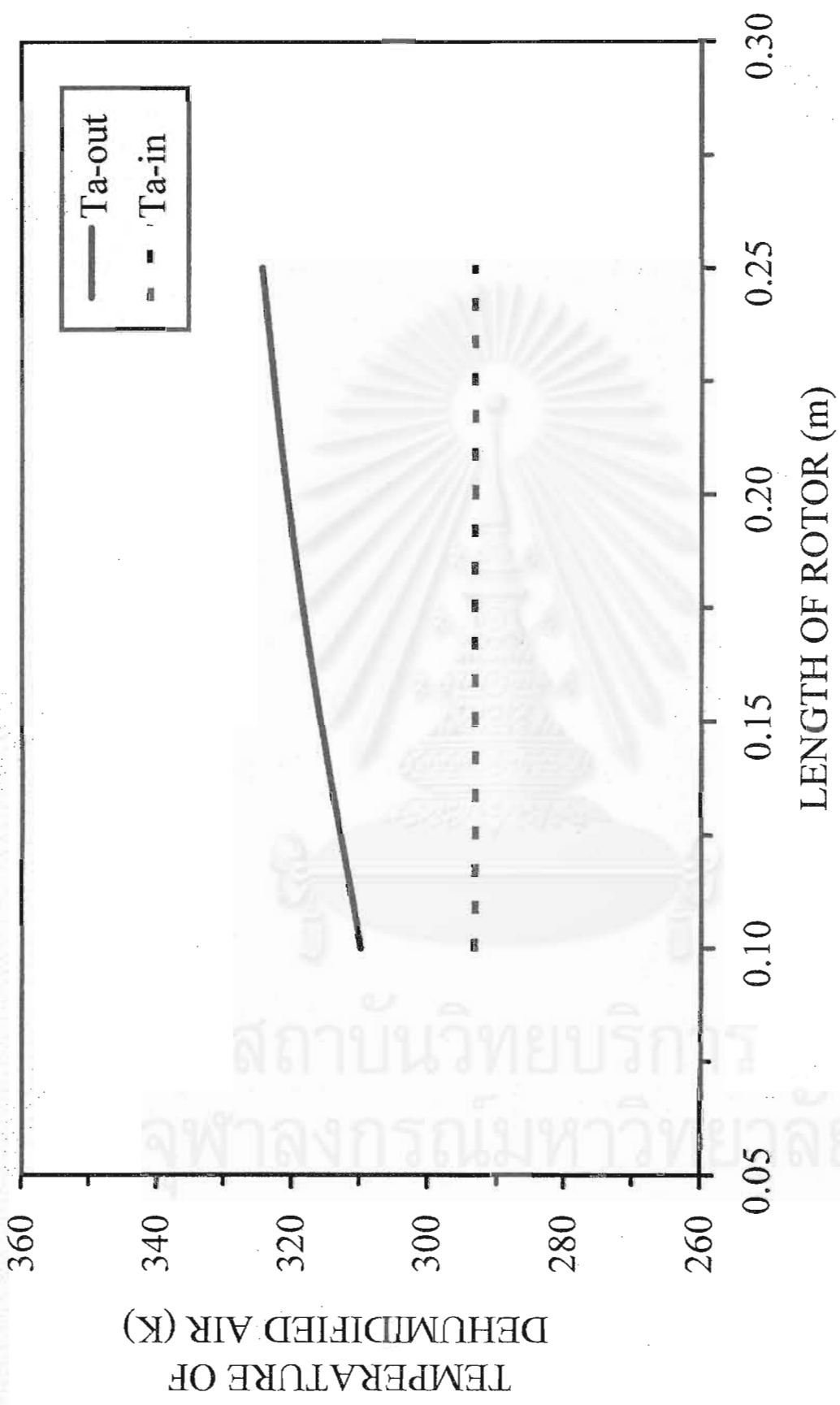
Figure 6.37 Effect of axial length of the rotor on the average temperature of the dehumidified air from the silica gel coated honeycomb rotary dehumidifier (Length-SG-Effect condition)
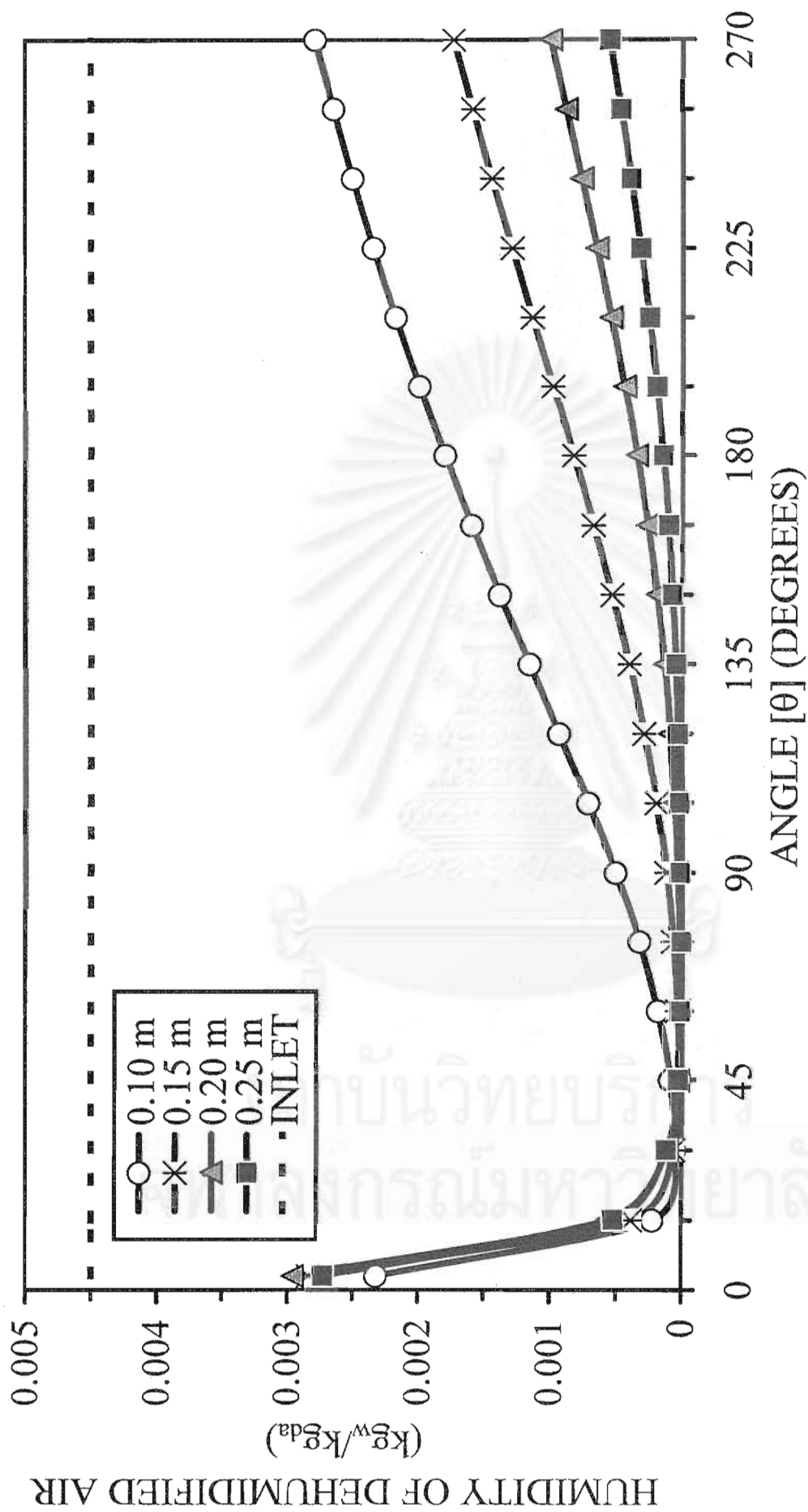
Figure 6.38 The angular distributions of the humidity of the dehumidified air from the silica gel coated honeycomb rotary dehumidifier at various axial lengths of the rotor (Length-SG-Effect Condition)
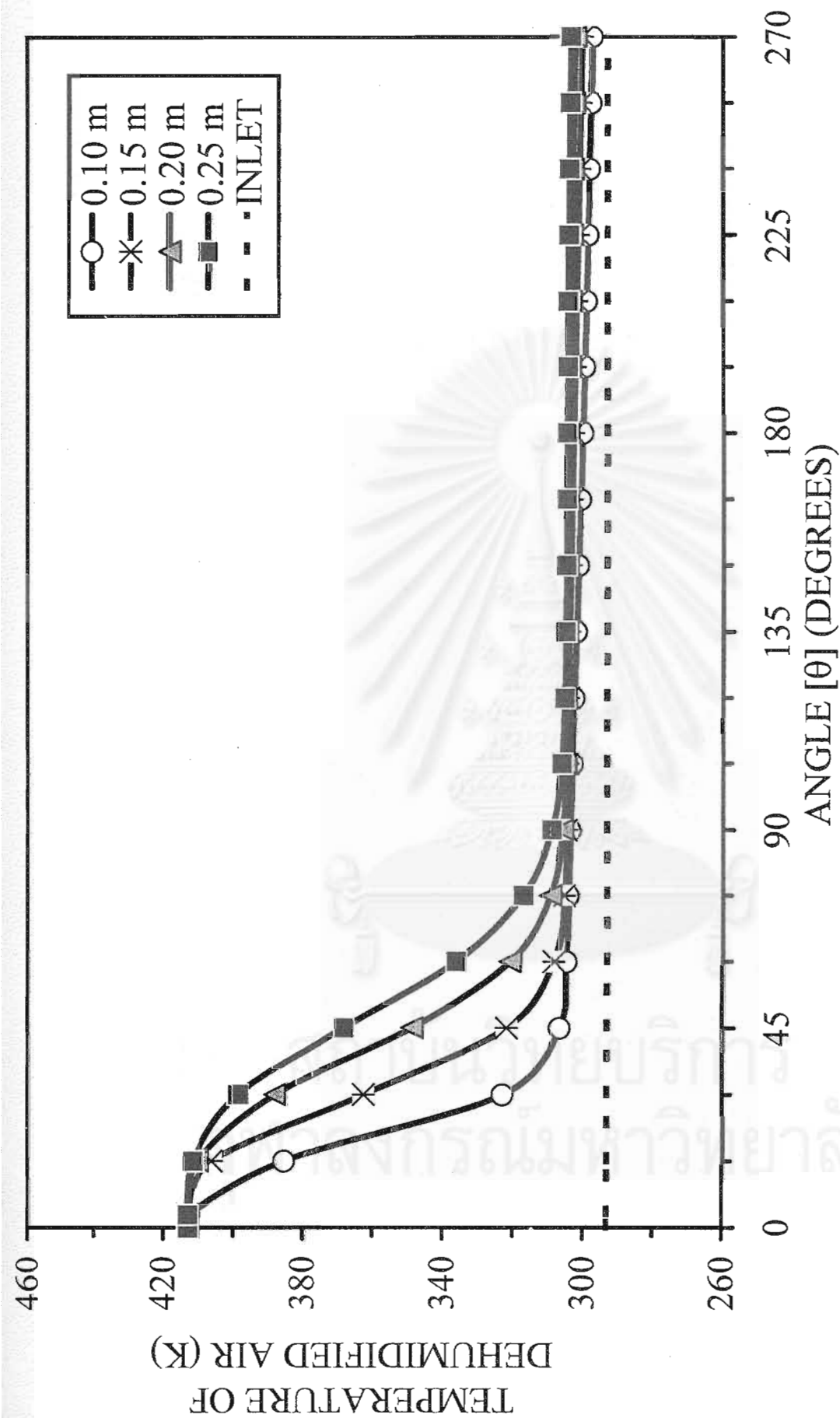
Figure 6.39 The angular distributions of the temperature of the dehumidified air from the silica gel coated honeycomb rotary dehumidifier at various axial lengths of the rotor (Length-SG-Effect Condition)
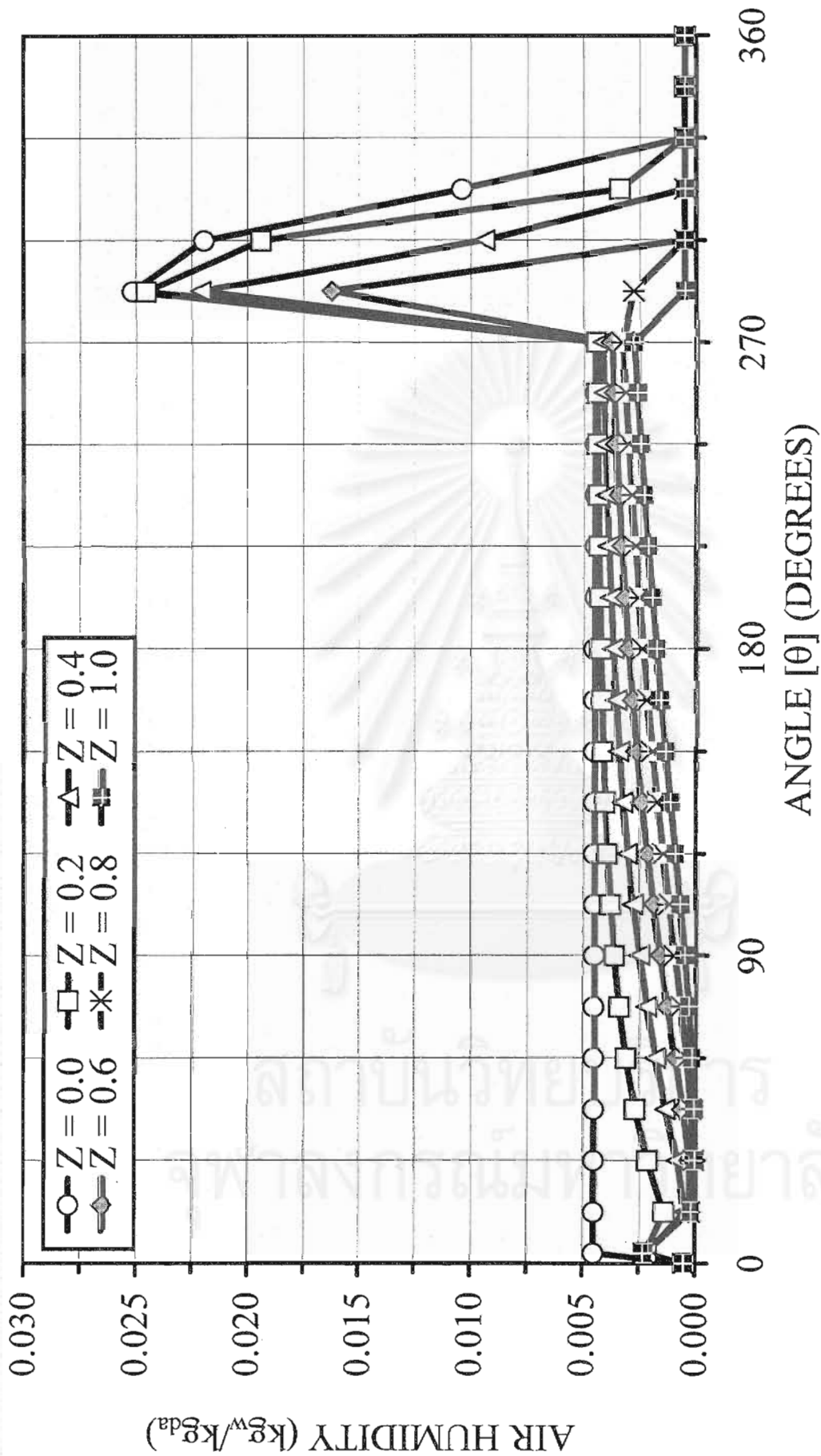
Figure 6.40 The two-dimensional distributions of the slot air humidity in the silica gel coated honeycomb rotary dehumidifier at L = 0.10 m (Length-SG-Effect Condition)
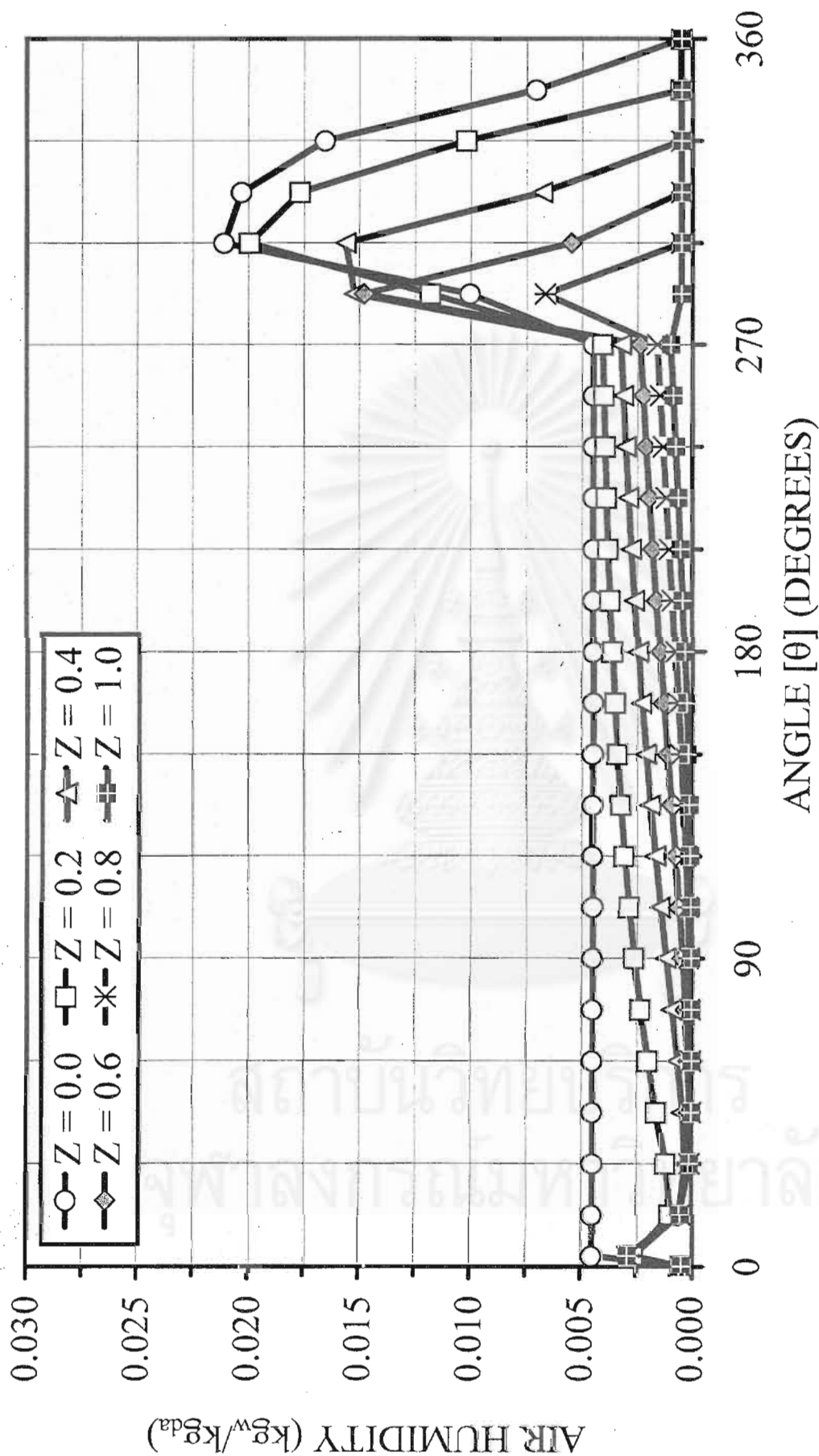
Figure 6.41 The two-dimensional distributions of the slot air humidity in the silica gel coated honeycomb rotary dehumidifier at L = 0.20 m (Length-SG-Effect Condition)
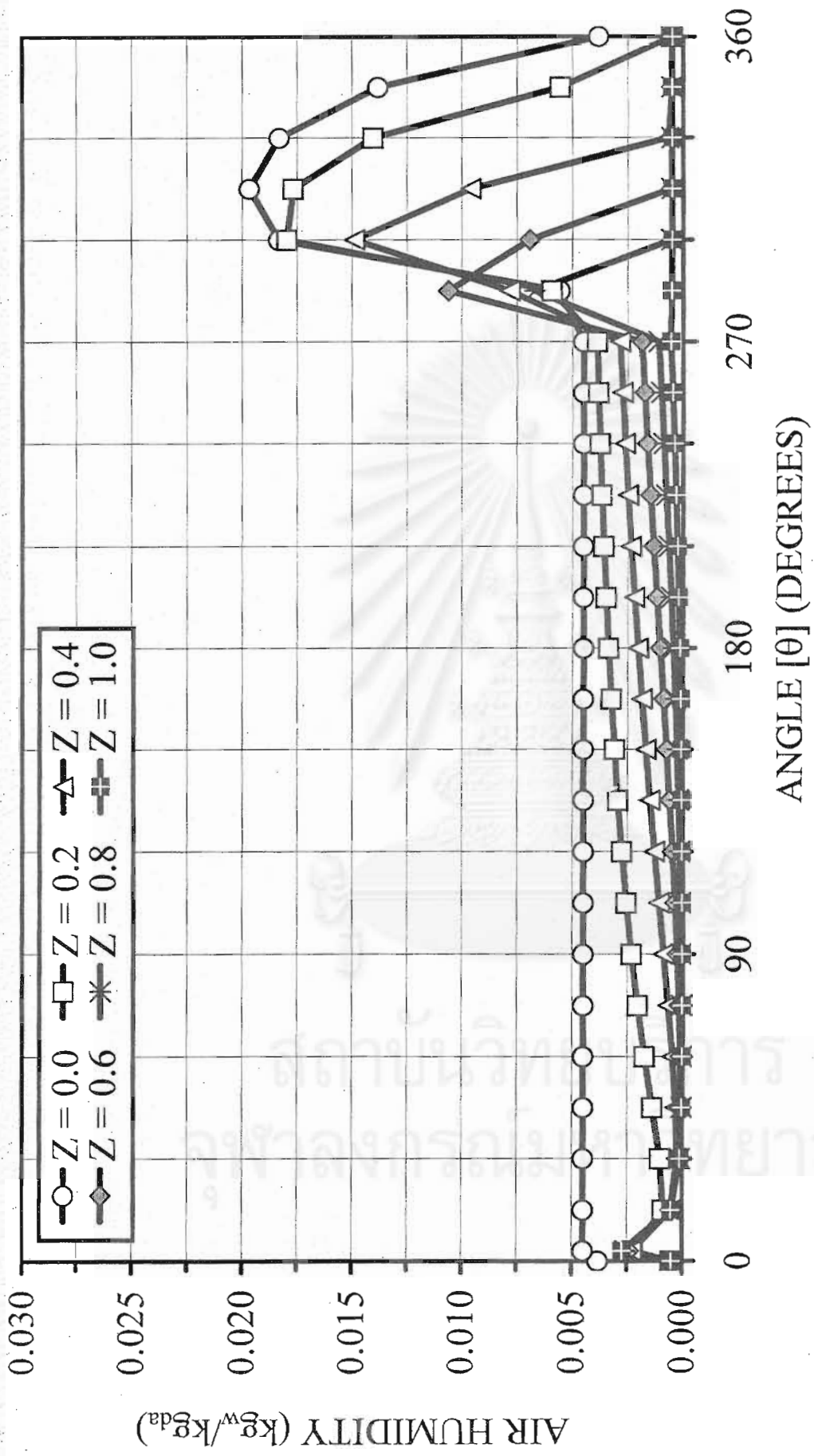
Figure 6.42 The two-dimensional distributions of the slot air humidity in the silica gel coated honeycomb rotary dehumidifier at L = 0.25 m (Length-SG-Effect Condition)
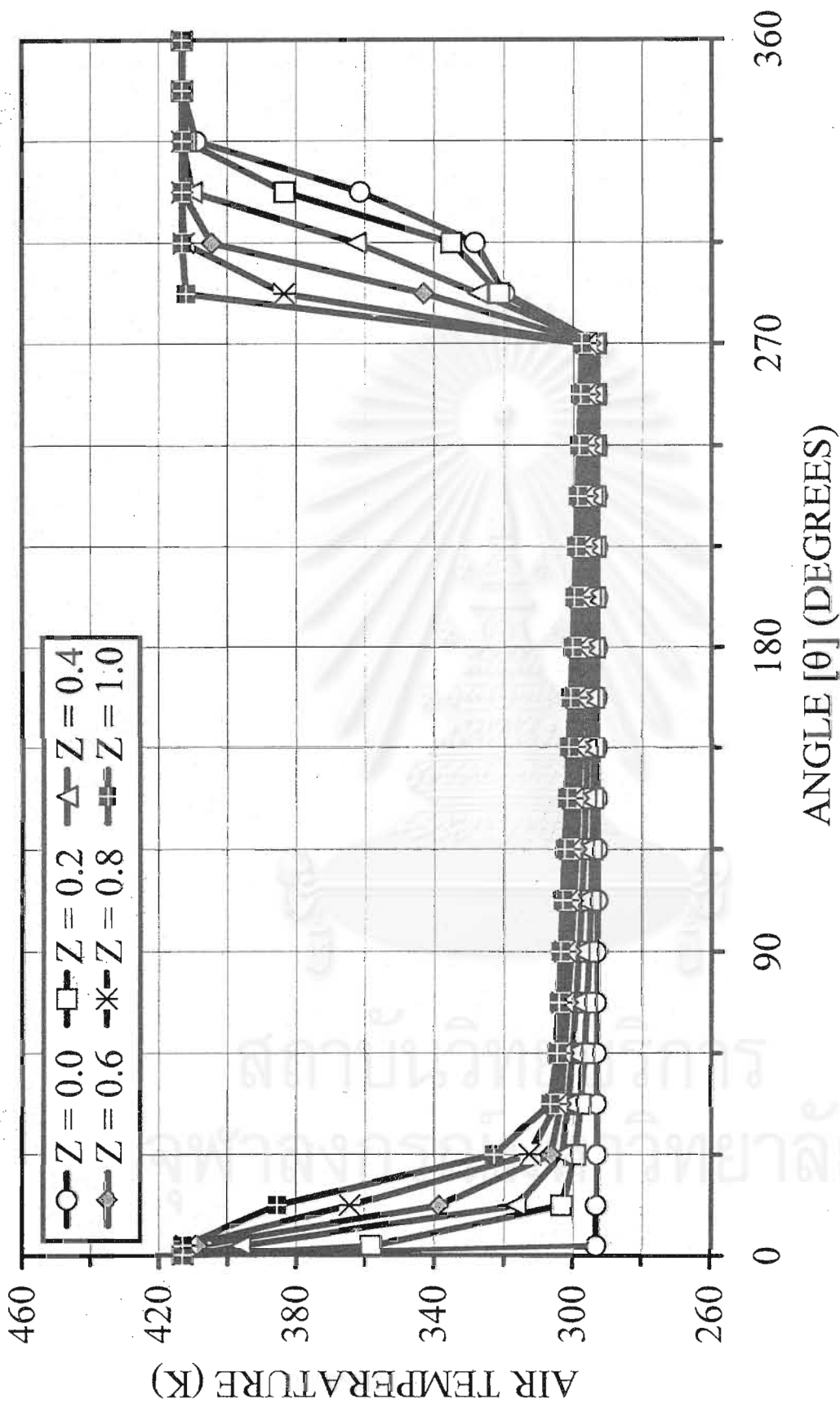
Figure 6.43 The two-dimensional distributions of the slot air temperature in the silica gel coated honeycomb rotary dehumidifier at L = 0.10 m (Length-SG-Effect Condition)
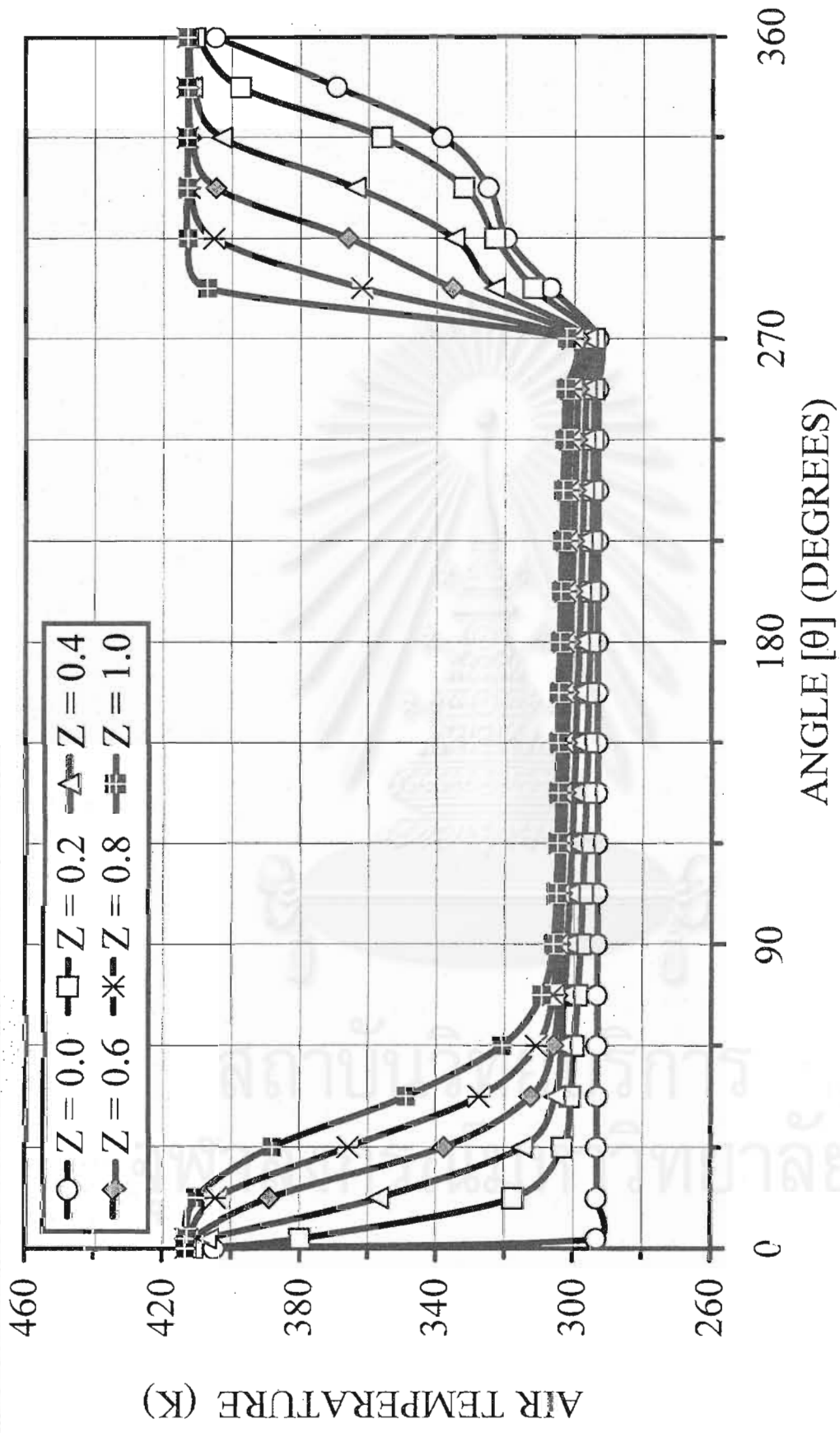
Figure 6.44 The two-dimensional distributions of the slot air temperature in the silica gel coated honeycomb rotary dehumidifier at L = 0.20 m (Length-SG-Effect Condition)
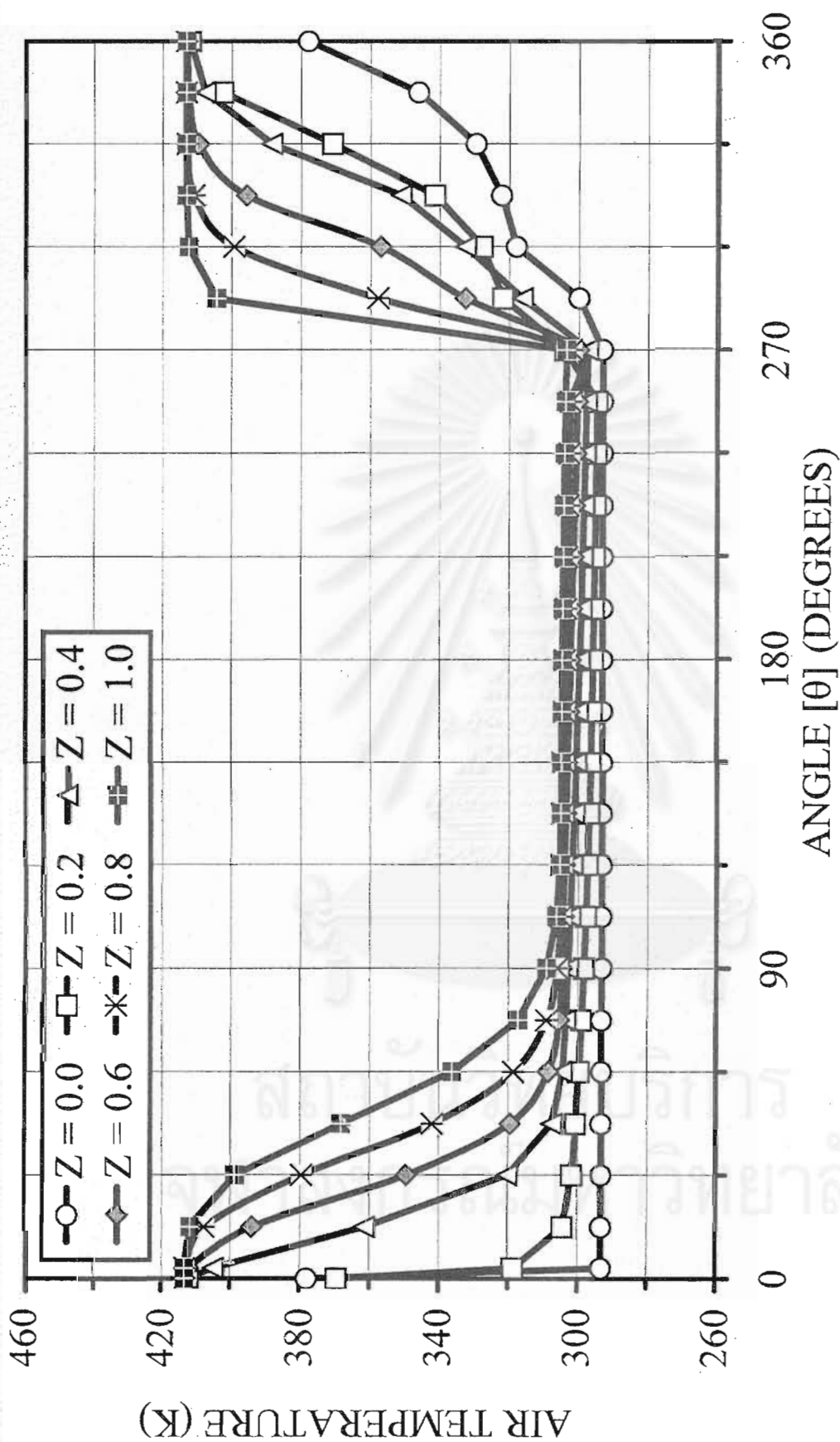
Figure 6.45 The two-dimensional distributions of the slot air temperature in the silica gel coated honeycomb rotary dehumidifier at L = 0.25 m (Length-SG-Effect Condition)

Figure 6.46 The two-dimensional distributions of the adsorbed moisture on silica gel coated honeycomb rotary dehumidifier at L = 0.10 m (Length-SG-Effect Condition)
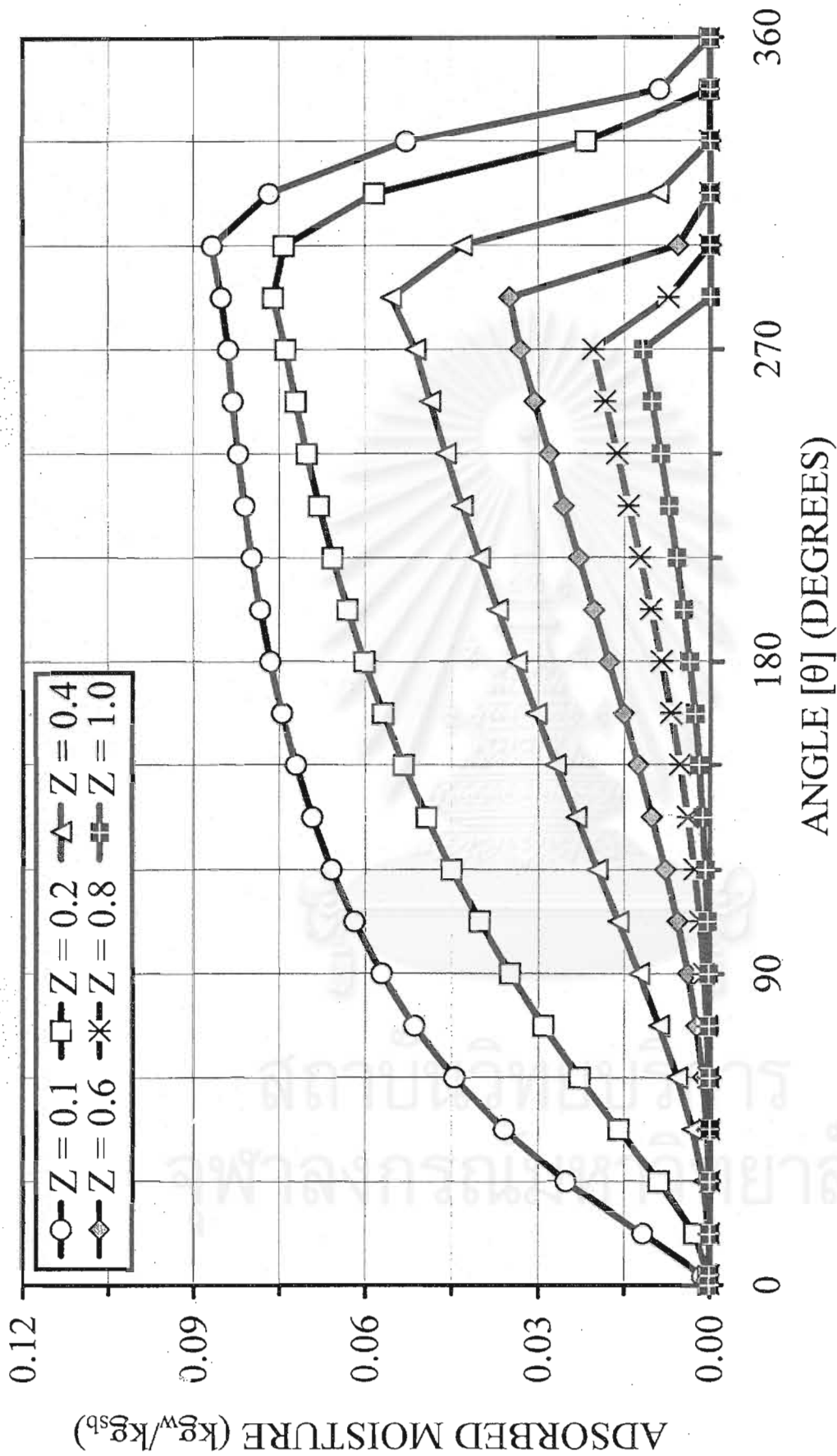
Figure 6.47 The two-dimensional distributions of the adsorbed moisture on silica gel coated honeycomb rotary dehumidifier at L = 0.20 m (Length-SG-Effect Condition)

Figure 6.48 The two-dimensional distributions of the adsorbed moisture on silica gel coated honeycomb rotary dehumidifier at L = 0.25 m (Length-SG-Effect Condition)

Figure 6.49 The two-dimensional distributions of the solid-phase temperature in the silica gel coated honeycomb rotary dehumidifier at L = 0.10 m (Length-SG-Effect Condition)

Figure 6.50 The two-dimensional distributions of the solid-phase temperature in the silica gel coated honeycomb rotary dehumidifier at L = 0.20 m (Length-SG-Effect Condition)

Figure 6.51 The two-dimensional distributions of the solid-phase temperature in the silica gel coated honeycomb rotary dehumidifier at L = 0.25 m (Length-SG-Effect Condition)

6.2.4 Interaction-effect of rotational speed and mass velocity of humid air

Figure 6.52 illustrates that increasing the mass velocity of the humid air increases the optimal rotational speed of the rotor because the adsorbent at high moisture loading requires less time to reach the maximum capacity. Consequently, at high rotational speed, the dehumidification efficiency increases with the mass velocity of the humid air. In contrast, at low rotational speed, higher the air mass velocity decreases the efficiency as low as 60% approximately. While the dehumidification efficiency reach 95% at the optimal operating condition. Such a relation can be briefly presented in Table 6.8.

Table 6.8 The relation of the optimal rotational speed and mass velocity of the humid air for the silica gel coated rotary dehumidifier

MASS VELOCITY OF HUMID AIR (kg_w/m^2s)	OPTIMAL ROTATIONAL SPEED (RPH)
0.00405	6-7
0.00540	6-10
0.00675	10-13
0.00810	11-14

Since the rotational speed is proportional to the mass velocity of the humid air, the correlation between (G_w/φ) and the dehumidification efficiency is established as shown in Figure 6.53. In Figure 6.54, the average temperatures of the dehumidified air are considered for various conditions. As mentioned above, cooling times for the varied rotational speeds of the rotor are significantly different. It means that high rotational speed may require the long region ($\theta = 0° - 225°$) for cooling down the hot regenerated adsorbent that being turn to the adsorption zone and low rotational speed may merely require short region ($\theta = 0° - 45°$). Accordingly, the average temperature of the dehumidified air at low rotational speed is always less than high rotational speed at constant the air mass velocity. In contrast, increasing the air mass velocity decreases the average temperature of the dehumidified air because of the higher heat capacity.
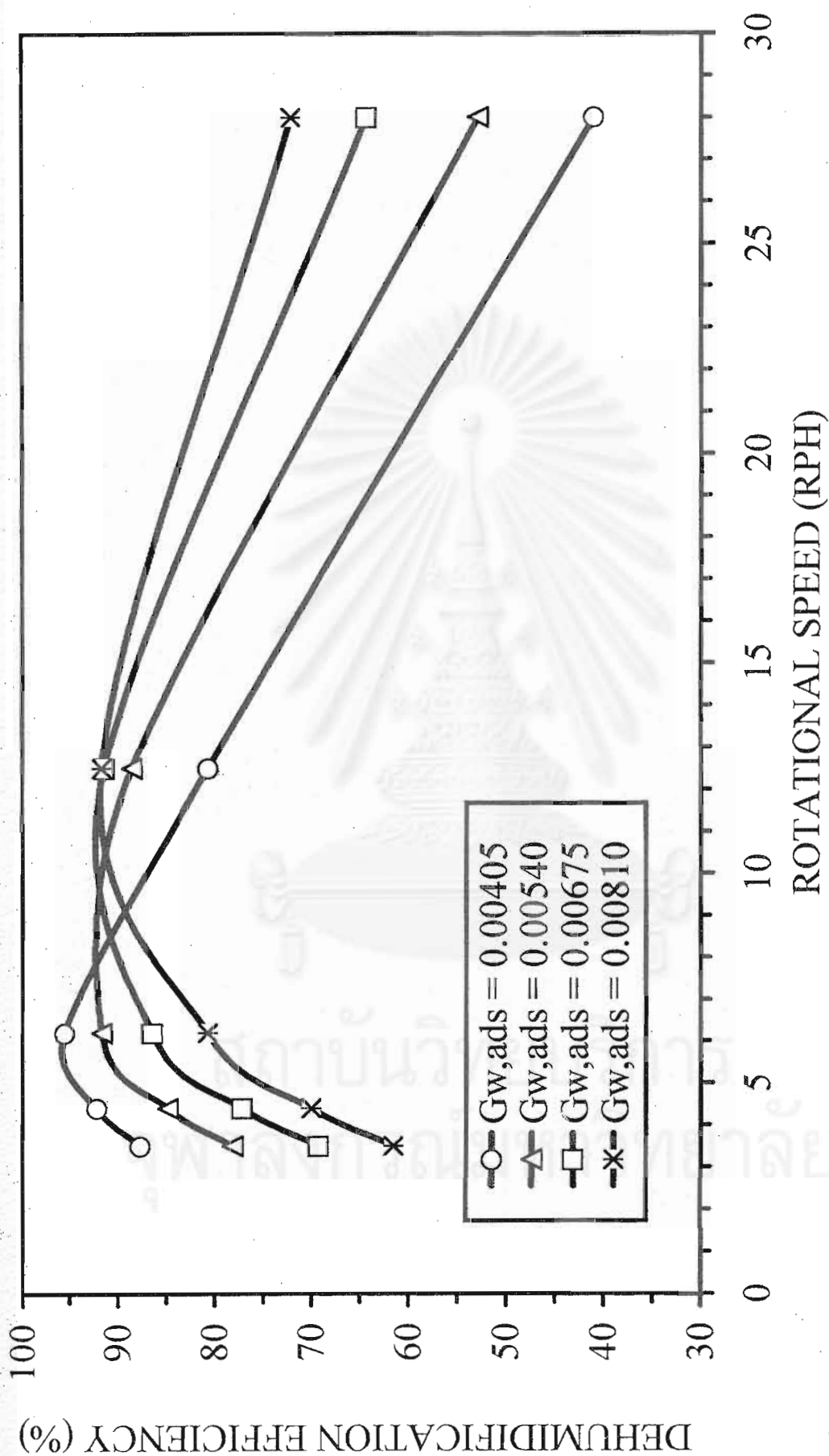
Figure 6.52 Effect of rotational speed on the dehumidification efficiency of the silica gel coated honeycomb rotary dehumidifier at various mass velocities of humid air

$y = -2E+19x^6 + 2E+17x^5 - 7E+14x^4 + 1E+12x^3 - 1E+09x^2 + 583244x - 23.234$
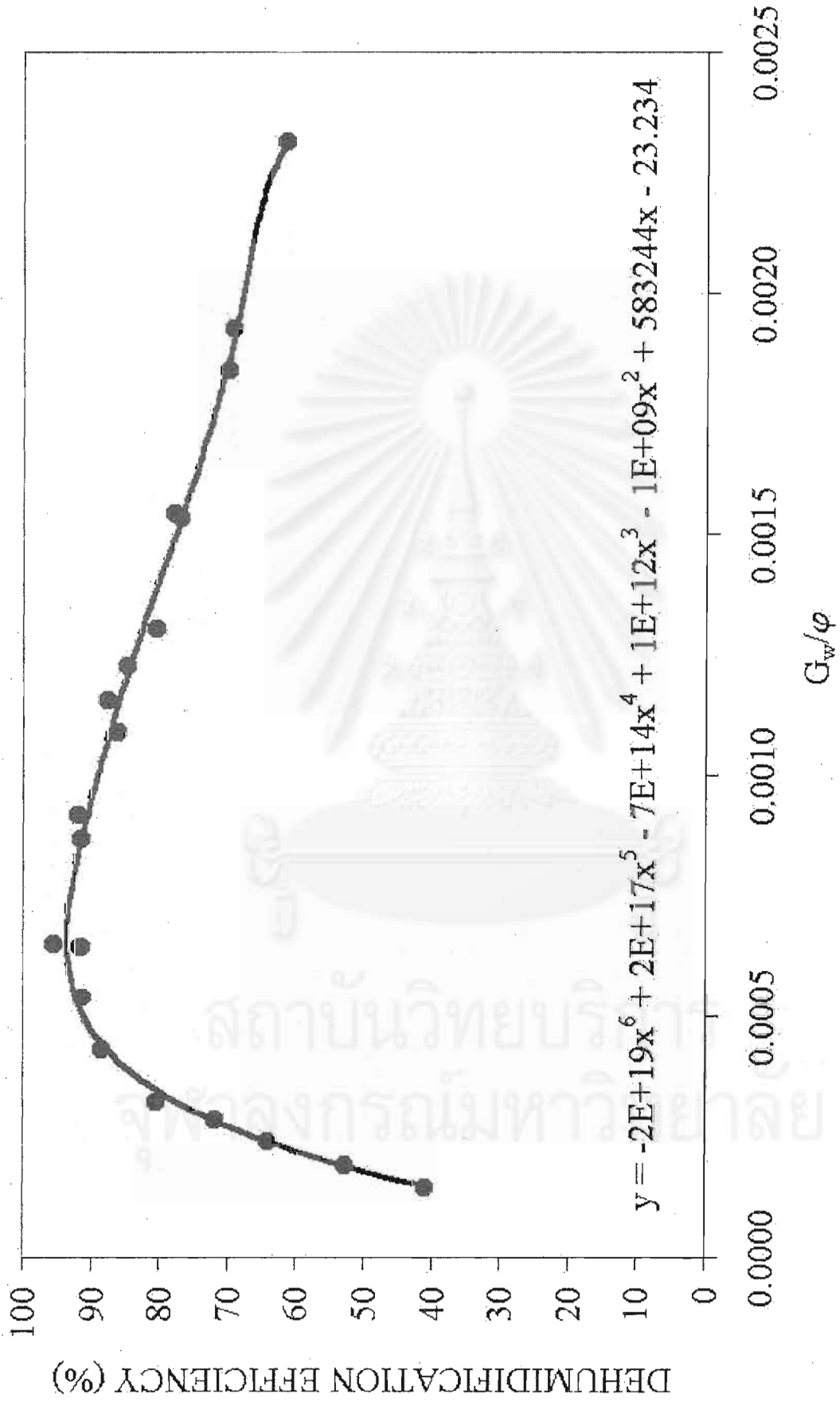
Figure 6.53 The correlation of (G_w/φ) and the dehumidification efficiency for the silica gel coated honeycomb rotary dehumidifier

Figure 6.54 Effect of rotational speed on the average temperature of the dehumidified air from the silica gel coated honeycomb rotary dehumidifier at various mass velocities of humid air

6.2.5 Interaction-effect of rotational speed and length of the rotor

Figure 6.55 shows the interaction-effect of the rotational speed and length of the rotor on the dehumidification efficiency of the silica gel coated honeycomb rotary dehumidifier. It is seen that the optimal rotational speed will be higher when the rotor is shorter as concluded in Table 6.9. At the optimal rotational speed, the dehumidification efficiency is more than 90% and especially reaches 95% at L = 0.25 m. Since the length of the rotor is proportional to rotational speed, the correlation between $1/(L \cdot \varphi)$ and the dehumidification efficiency is established as shown in Figure 6.56. Figure 6.57 illustrates that increasing length of the rotor increases the temperature of the dehumidified air.

Table 6.9 The relation of the optimal rotational speed and length of the rotor for the silica gel coated rotary dehumidifier

LENGTH OF ROTOR (m)	OPTIMAL ROTATIONAL SPEED (RPH)
0.10	11 - 14
0.15	10 - 13
0.20	6 - 10
0.25	6 - 7

Figure 6.55 Effect of rotational speed on the dehumidification efficiency of the silica gel coated honeycomb rotary dehumidifier at various axial lengths of the rotor

Figure 6.56 The correlation of $(L \cdot \phi)^{-1}$ and the dehumidification efficiency for the silica gel coated honeycomb rotary dehumidifier
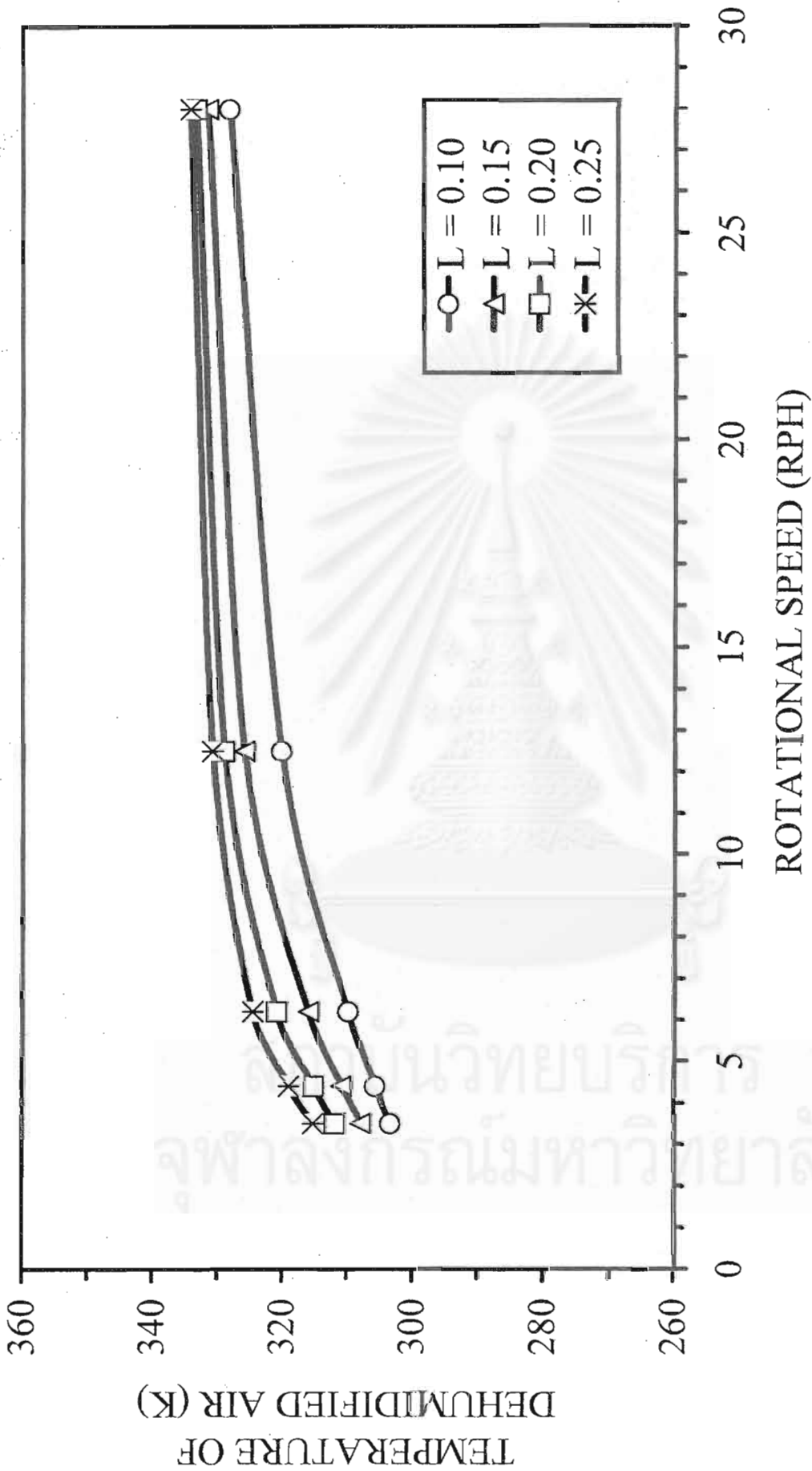
Figure 6.57 Effect of rotational speed on the average temperature of the dehumidified air from the silica gel coated honeycomb rotary dehumidifier at various axial lengths of the rotor

6.2.6 Interaction-effect of mass velocity of humid air and length of rotor

In Figure 6.58, it is seen that the dehumidification efficiency linearly drops when mass velocity increases. The efficiency decreases rapidly from 80% to 55% for the short rotor and decreases gradually from 95% to 90% for the long rotor. In conclusion, the air mass velocity has significant effect on the efficiency when the rotor is too short. In contrast, at very long rotor, the efficiency decreases from approximately 95% to 90% when the air mass velocity increases from 0.00405 to 0.0081 kg_w/m^2s. Thus the short rotor is ineffective at high air mass velocity. In Figure 6.59, the effects of mass velocity of the humid air and the length of the rotor on the efficiency can be correlated as (G_w/L) vs. the efficiency. In addition, the relation of the average temperature of the dehumidified air and mass velocity of the humid air at various lengths of the rotor is presented in Figure 6.60. It is seen that the temperature only depends on axial length of the rotor.

In conclusion, three factors, say, L, G_w and φ significantly effect on the dehumidification efficiency. Thus their correlation is established in general term in order to easily obtain the optimal rotational speed at various operating condition as shown in the Figure 6.61.
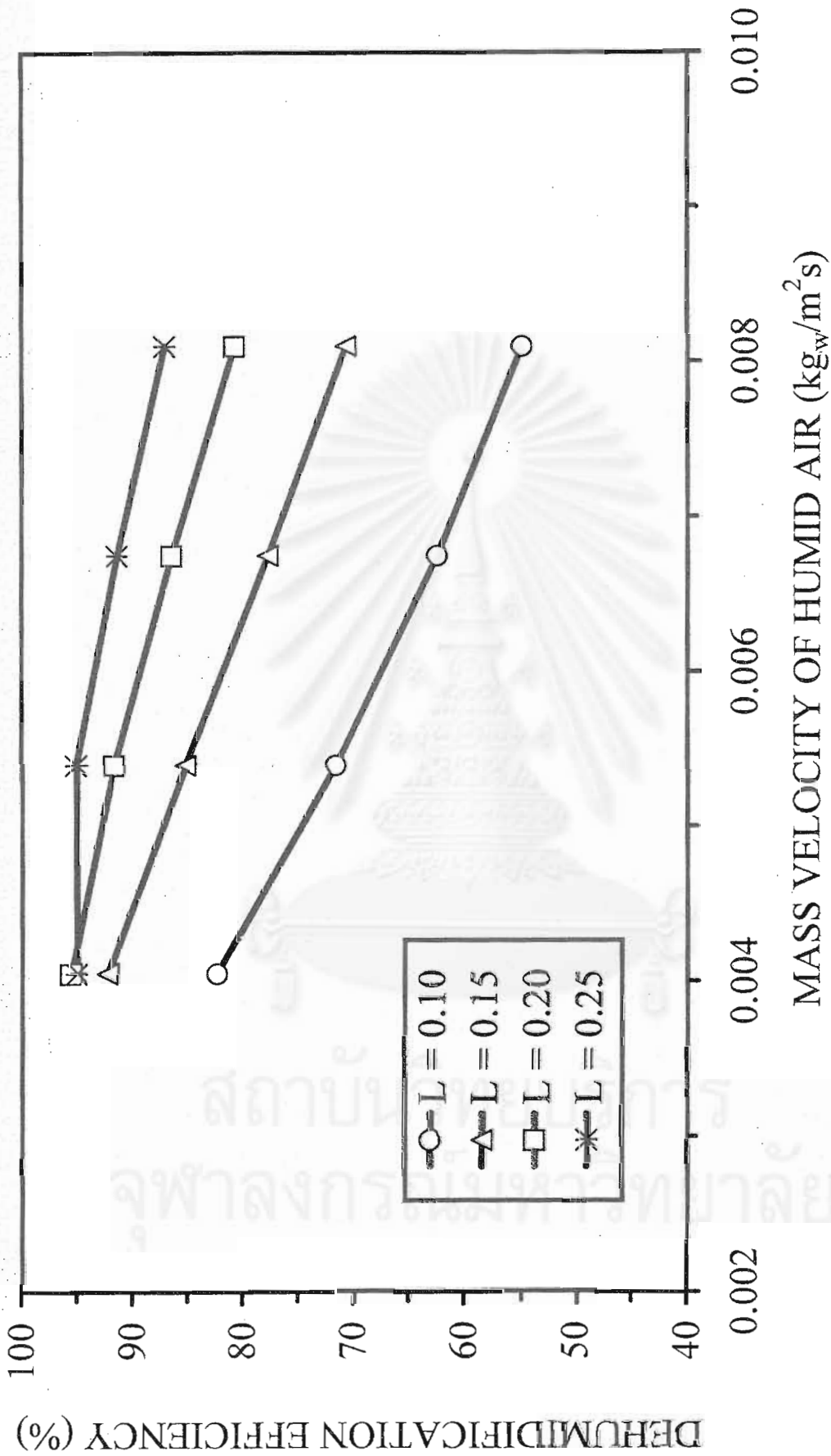
Figure 6.58 Effect of mass velocity of humid air on the dehumidification efficiency at various lengths of the silica gel coated honeycomb rotary dehumidifier

$$y = -700.78x + 110.03$$
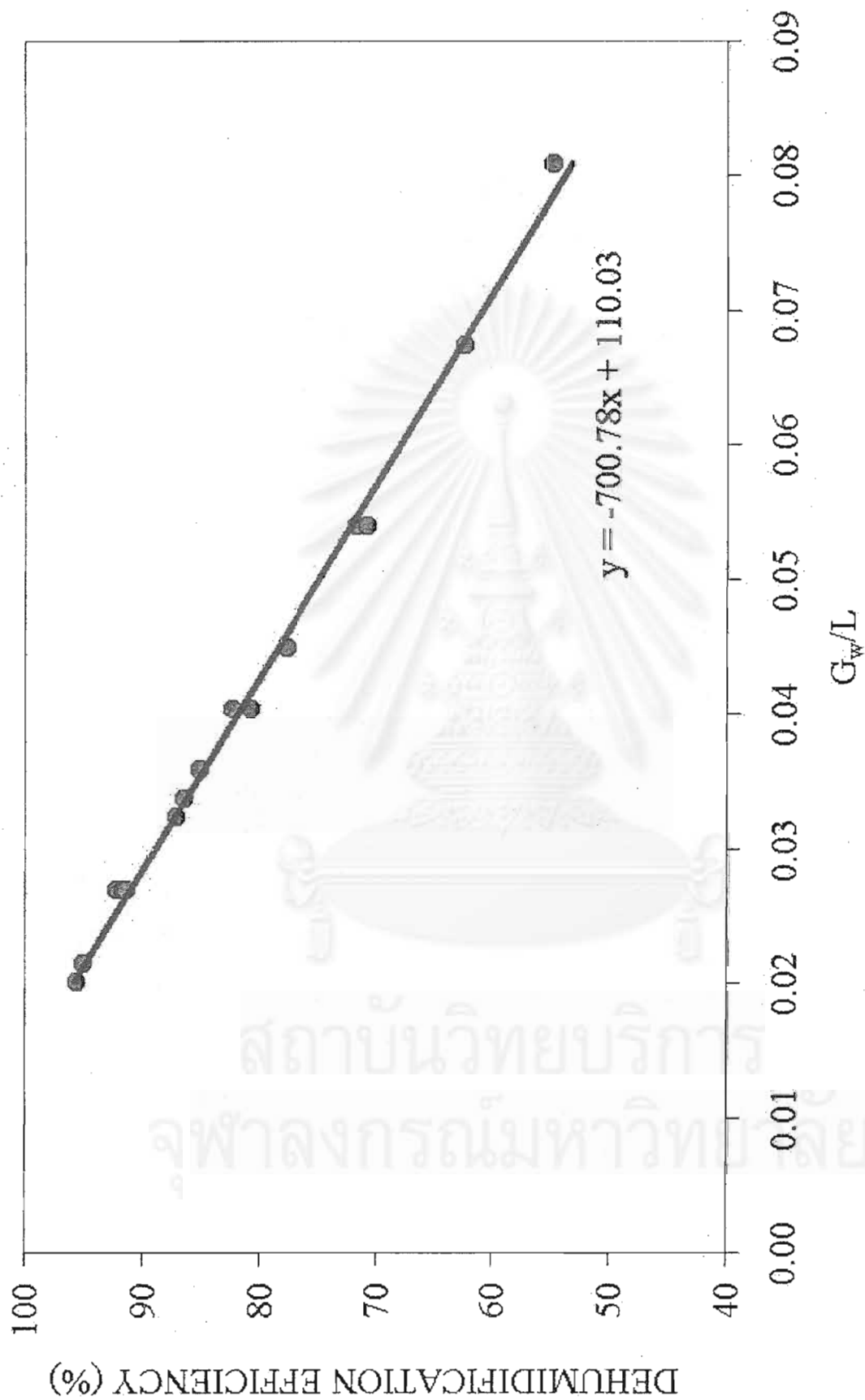
Figure 6.59 The correlation of (G_w/L) and the dehumidification efficiency for the silica gel coated honeycomb rotary dehumidifier
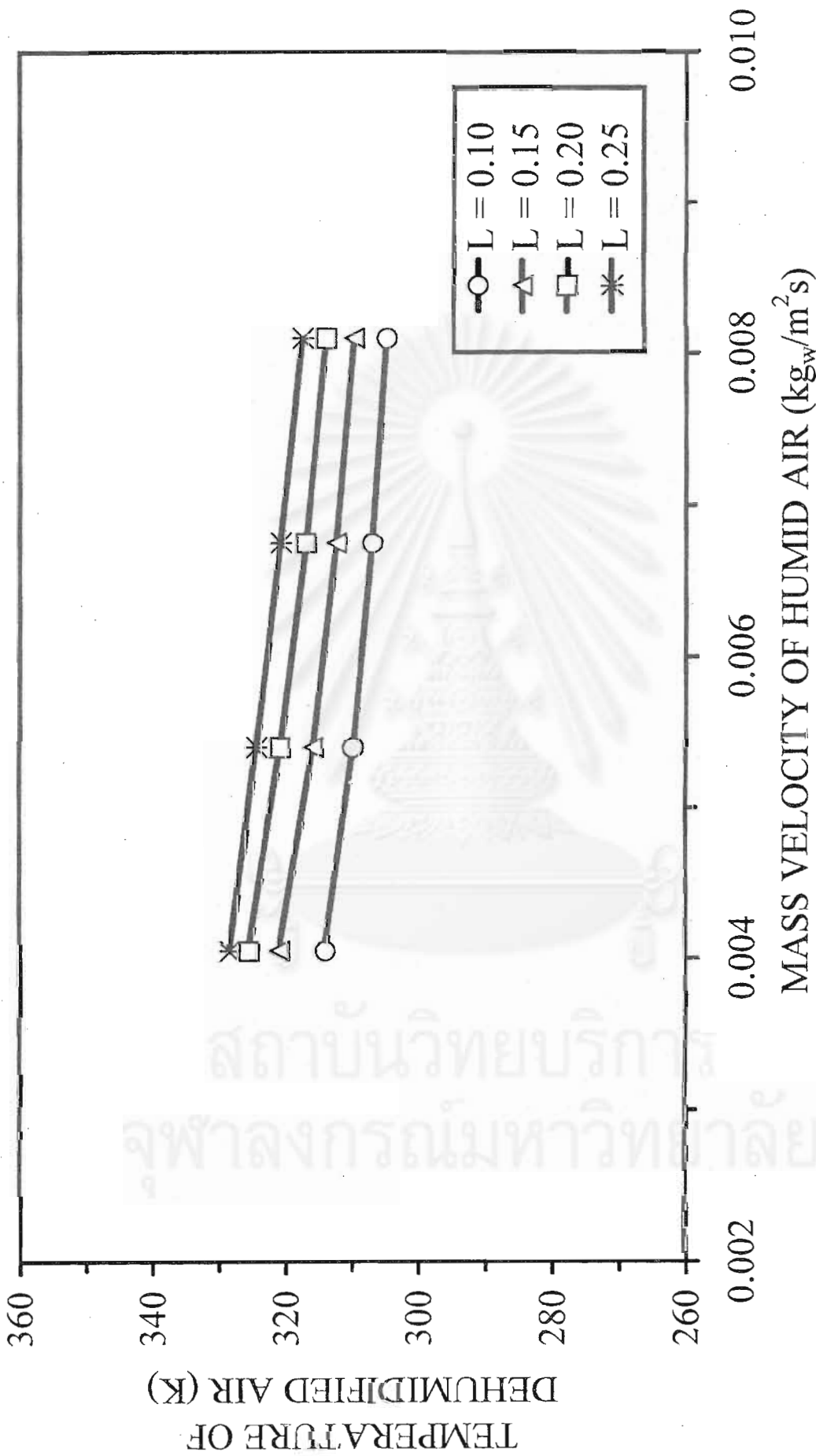
Figure 6.60 Effect of mass velocity of humid air on the average temperature of the dehumidified air at various lengths of the silica gel coated honeycomb rotary dehumidifier

$y = -6E-08x^6 + 1E-05x^5 - 0.0014x^4 + 0.0689x^3 - 1.7759x^2 + 21.402x$
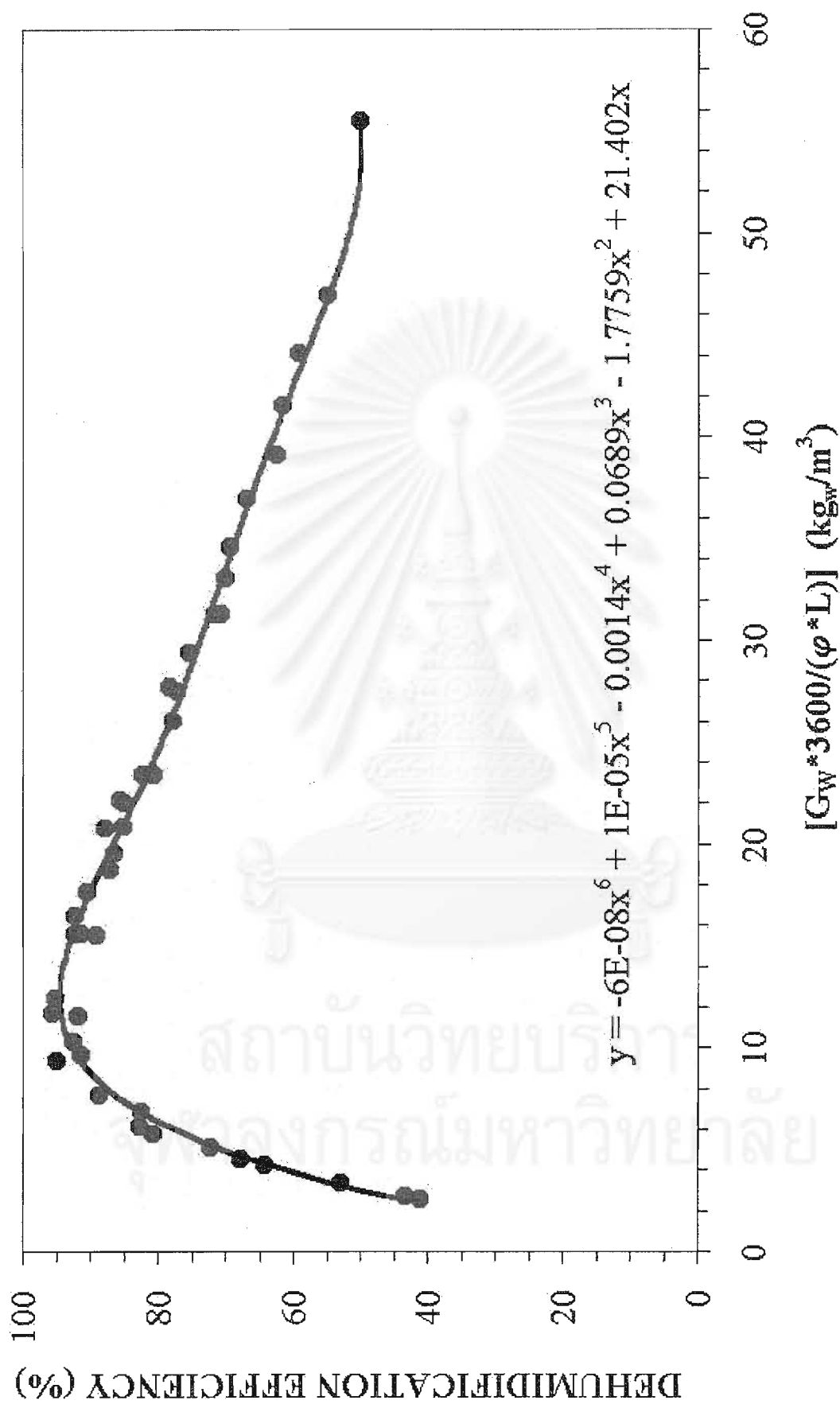
Figure 6.61 The correlation of $(G_w/(L \cdot \varphi))$ and the dehumidification efficiency for the silica gel coated honeycomb rotary dehumidifier

6.3 Effect of adsorbent

Another significant factor investigated in this study is the adsorptive capacity, which depends on the type of adsorbent. In air-conditioning and -drying systems, both of silica gel and zeolites are well known as a commercial solid-desiccant, even though their structures, pore size and adsorptive capacity are different as mentioned in section 2.3. To obtain high dehumidification performance as well as low operating cost, zeolite-13X and silica gel that are type I and IV isotherm of Brunauer, respectively (Ruthven, 1984) have been carried out under various conditions. Since all above investigation uses silica gel as desiccant, the optimal operating condition and the dehumidification performance of a zeolite-13X coated rotary dehumidifier is only presented in this section.

In the case of the zeolite-13X coated rotary dehumidifier, the regenerative temperature, the rotational speed and the mass velocity of the humid air are varied to get the optimal operating condition. The operating conditions used for investigation the zeolite-13X coated honeycomb rotary dehumidifier are listed in Table 6.10. In this study, the humid air is sent through the adsorption section of the 20-m of rotor at 293.15 K and hot air entering the inlet of the regeneration section is kept constant at 4.25×10^{-4} kg_w/m^2s.

Table 6.10 Operating conditions used for investigation the zeolite-13X coated honeycomb rotary dehumidifier.

CASE	REGENERATIVE TEMPERATURE (K)	ROTATIONAL SPEED (RPH)	MASS VELOCITY OF HUMID AIR ($\times 10^3$ kg_w/m^2s)	FILE NAME (filename.dat)
Treg-ZE-Effect	413	6	10.8	ZE-CASE-01
	453	6	10.8	ZE-CASE-02
	523	6	10.8	ZE-CASE-03
Speed-ZE-Effect	453	3	10.8	ZE-CASE-04
	453	6	10.8	ZE-CASE-02
	453	12	10.8	ZE-CASE-05
	453	18	10.8	ZE-CASE-06
Gads-ZE-Effect	453	6	5.04	ZE-CASE-07
	453	6	10.8	ZE-CASE-02
	453	6	16.2	ZE-CASE-08

Table 6.10(cont.) Operating conditions used for investigation the zeolite-13X coated honeycomb rotary dehumidifier.

CASE	REGENERATIVE TEMPERATURE (K)	ROTATIONAL SPEED (RPH)	MASS VELOCITY OF HUMID AIR (x10^3 kg$_w$/m^{2}s)	FILE NAME (filename.dat)
Treg& Speed -ZE-Effect	413	3	5.04	ZE-CASE-09
	453	3	5.04	ZE-CASE-10
	523	3	5.04	ZE-CASE-11
	413	6	5.04	ZE-CASE-12
	453	6	5.04	ZE-CASE-07
	523	6	5.04	ZE-CASE-13
	413	12	5.04	ZE-CASE-14
	453	12	5.04	ZE-CASE-15
	523	12	5.04	ZE-CASE-16
	413	18	5.04	ZE-CASE-17
	453	18	5.04	ZE-CASE-18
	523	18	5.04	ZE-CASE-19
Treg& Gads-ZE-Effect	413	6	5.04	ZE-CASE-12
	453	6	5.04	ZE-CASE-07
	523	6	5.04	ZE-CASE-13
	413	6	10.8	ZE-CASE-01
	453	6	10.8	ZE-CASE-02
	523	6	10.8	ZE-CASE-03
	413	6	16.2	ZE-CASE-20
	453	6	16.2	ZE-CASE-08
	523	6	16.2	ZE-CASE-21
Gads& Speed -ZE-Effect	453	3	5.04	ZE-CASE-10
	453	3	10.8	ZE-CASE-04
	453	3	16.2	ZE-CASE-22
	453	6	5.04	ZE-CASE-07
	453	6	10.8	ZE-CASE-02
	453	6	16.2	ZE-CASE-08
	453	12	5.04	ZE-CASE-15
	453	12	10.8	ZE-CASE-05
	453	12	16.2	ZE-CASE-23
	453	18	5.04	ZE-CASE-18
	453	18	10.8	ZE-CASE-06
	453	18	16.2	ZE-CASE-24

In Figure 6.62, the dehumidification efficiency linearly increases as the regenerative temperature increases from 413 to 453 K and is nearly constant at 98% approximately when the regenerative temperature is above 453 K. However, both the dehumidified air temperature and power required by heater are higher when the regenerative temperature increases as seen in Figure 6.64 and 6.65. Consequently, the optimal regenerative temperature for the case of zeolite-13X is approximately 453 K, which is consistent with the commercial data of NCI MFG Inc., Scottsboro, Alabama USA (www.ncifg.com). From Figures 6.68 to 6.79, the two-dimensional profiles of the air humidity, the air temperature, the adsorbed moisture and the solid-phase temperature are presented to investigate the performance of the zeolite-13X coated honeycomb rotary dehumidifier under various the regenerative temperatures.

For the effect of the rotation speed, Figures 6.80 and 6.81 show the optimal value of the zeolite-13X rotor, which is approximately 3-6 rph. The optimal rotational speed in this case is a few less than the case of the silica gel rotor. At optimal condition, the dehumidification efficiency reaches nearly 100% for the zeolite-13X honeycomb rotor while the silica gel honeycomb rotor gives approximately 90% as shown in Figure 6.4. However, the power required by heater of the case of zeolite-13X is higher than the case of the silica gel rotor since the optimal regenerative temperature of the zeolite-13X rotor is as high as 453 K. Figure 6.83 shows that the zeolite-13X rotary dehumidifier requires the power about 1.4 kW. While the silica gel rotary dehumidifier requires only 0.85 kW as shown in Figure 6.6. In addition, the average temperature of the dehumidified air of the case of the zeolite-13X rotor is more than the case of the silica gel at the optimal condition as shown in Figure 6.82 and 6.5. Similar to the silica gel rotor, the angular distributions of the humidity and the temperature of the dehumidified air under various rotational speeds are illustrated in Figure 6.84 to 6.85, respectively.

Figure 6.86 illustrates that above 0.010 kg_w/m^2s increasing the mass velocity of the humid air decreases the dehumidification efficiency. Although the air mass velocity is very high, the efficiency is still more than 95%, which is much more than the case of the silica gel rotor as shown in Figure 6.26. Consequently, the zeolite-13X coated rotary dehumidifier should be applied when moisture loading is large. In addition, the angular distributions of the dehumidified air humidity and temperature under various the mass velocities are shown in Figures 6.90 and 6.91, respectively.

Figure 6.92 shows the interaction effect of the regenerative temperature and the rotational speed on the dehumidification efficiency. It is seen that the regenerative temperature insignificantly effects on the efficiency at low rotational speed. In contrast, decreasing the regenerative temperature ranges from 523 to 413 K rapidly drops the efficiency from 90% to 70% at 18-rph. Similarly, it effects on the dehumidified air temperature at high rotational speed as shown in Figure 6.93. At 18 rph, increasing the regenerative temperature from 413 to 523 K increases the dehumidified air temperature from 330 to 370 K. Whereas the dehumidified air temperature are constantly about 320 K at 3-rph.

Figure 6.94 illustrates that the regenerative temperature significantly effects on the dehumidification efficiency when the mass velocity of the humid air is very high. At 0.0162 kg_w/m^2s, the efficiency rapidly drops from nearly 100% to approximately 80% as the regenerative temperature decreases from 523 to 413 K. The interaction effect of the regenerative temperature and the air mass velocity on the dehumidified air temperature is insignificant as shown in Figure 6.95.

Figure 6.96 shows the effect of the mass velocity of the humid air on the optimal rotational speed. At very high mass velocity, the range of the optimal rotational speed is narrower, say, the optimal value reduces from 3-6 rph at 0.0054 kg_w/m^2s to only 5-6 rph at 0.0162 kg_w/m^2s. In Figure 6.97, it is seen that increasing the air mass velocity increases the average temperature of the dehumidified air at below 9 rph whereas gradually decreases the temperature at above 9 rph. Since zeolite-13X has high adsorptive capacity, very high humid air can be effectively dried even though the rotational speed is low.

In conclusion, three factors, i.e., L, G_w and φ, significantly effect on the dehumidification efficiency of the zeolite-13X rotor. Similar to the case of the silica gel, their correlation is established in the general term, $(3600 \cdot G_w)/(L \cdot \varphi)$, in order to easily obtain the optimal rotational condition at various the operating condition as shown in Figure 6.98.

Figure 6.62 Effect of regenerative temperature on the dehumidification efficiency of the zeolite-13X coated honeycomb rotary dehumidifier (Treg-ZE-Effect Condition)
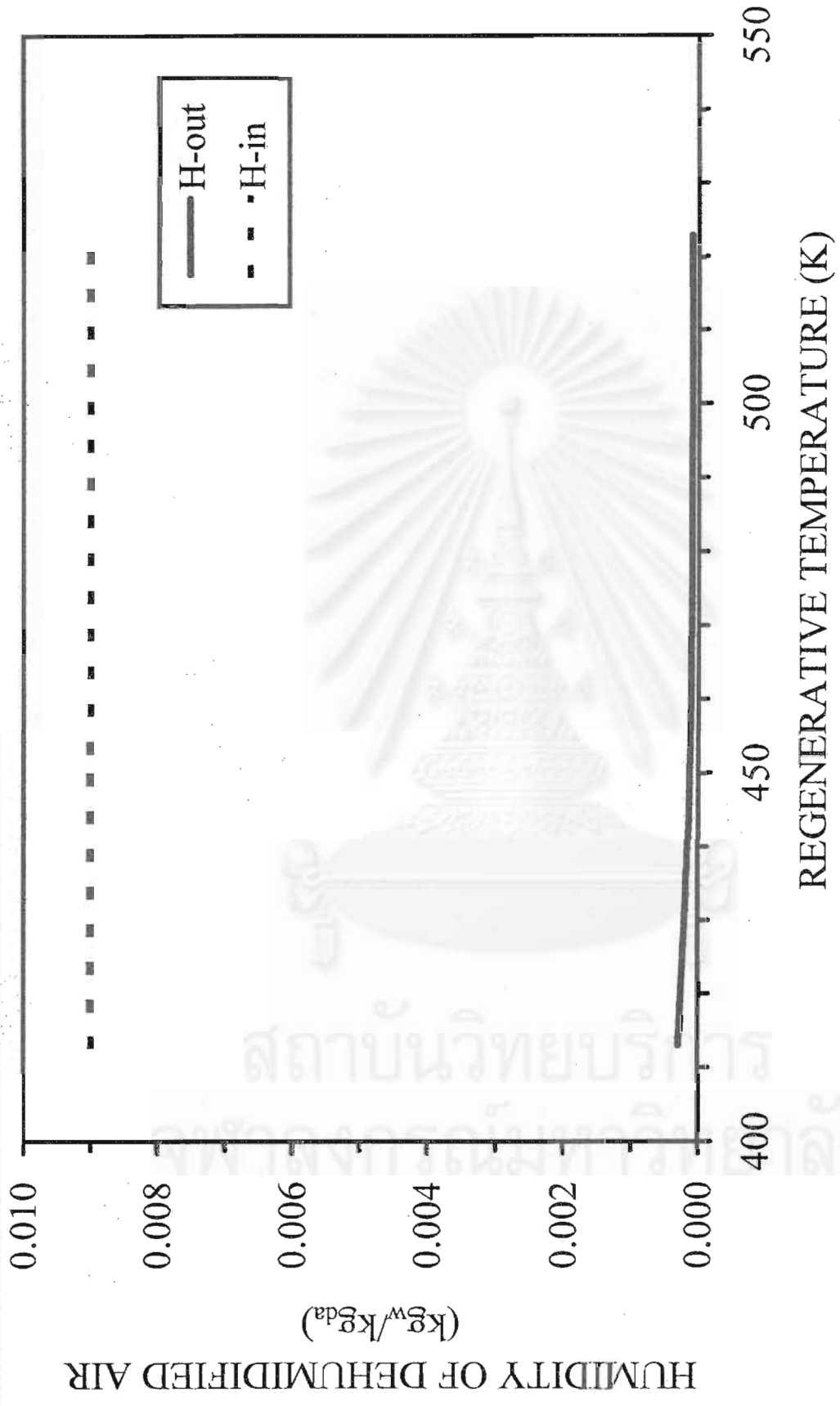
Figure 6.63 Effect of regenerative temperature on the average humidity of the dehumidified air of the zeolite-13X coated honeycomb rotary dehumidifier (Treg-ZE-Effect Condition)
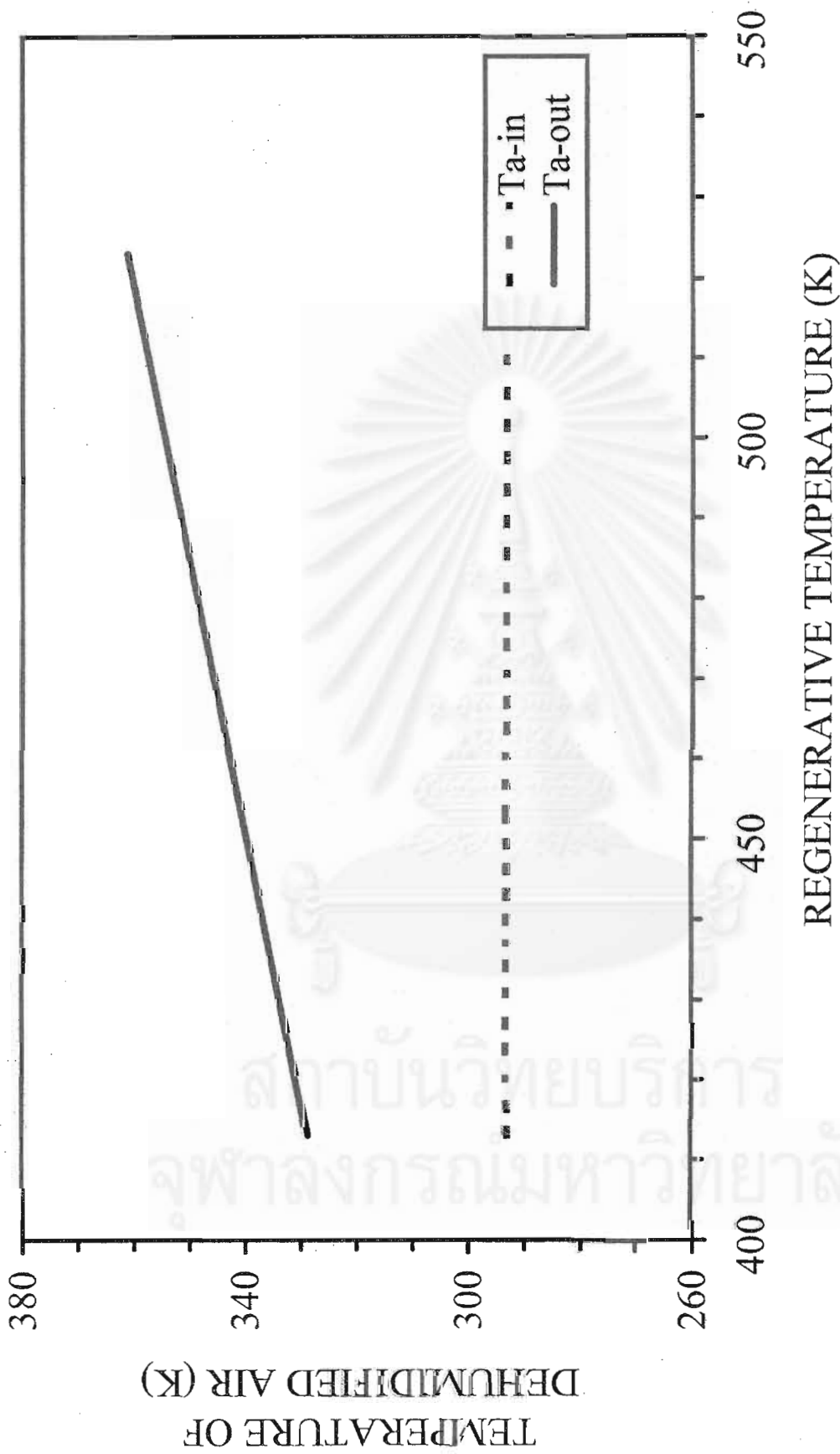
Figure 6.64 Effect of regenerative temperature on the average temperature of the dehumidified air from the zeolite-13X coated honeycomb rotary dehumidifier (Treg-ZE-Effect Condition)
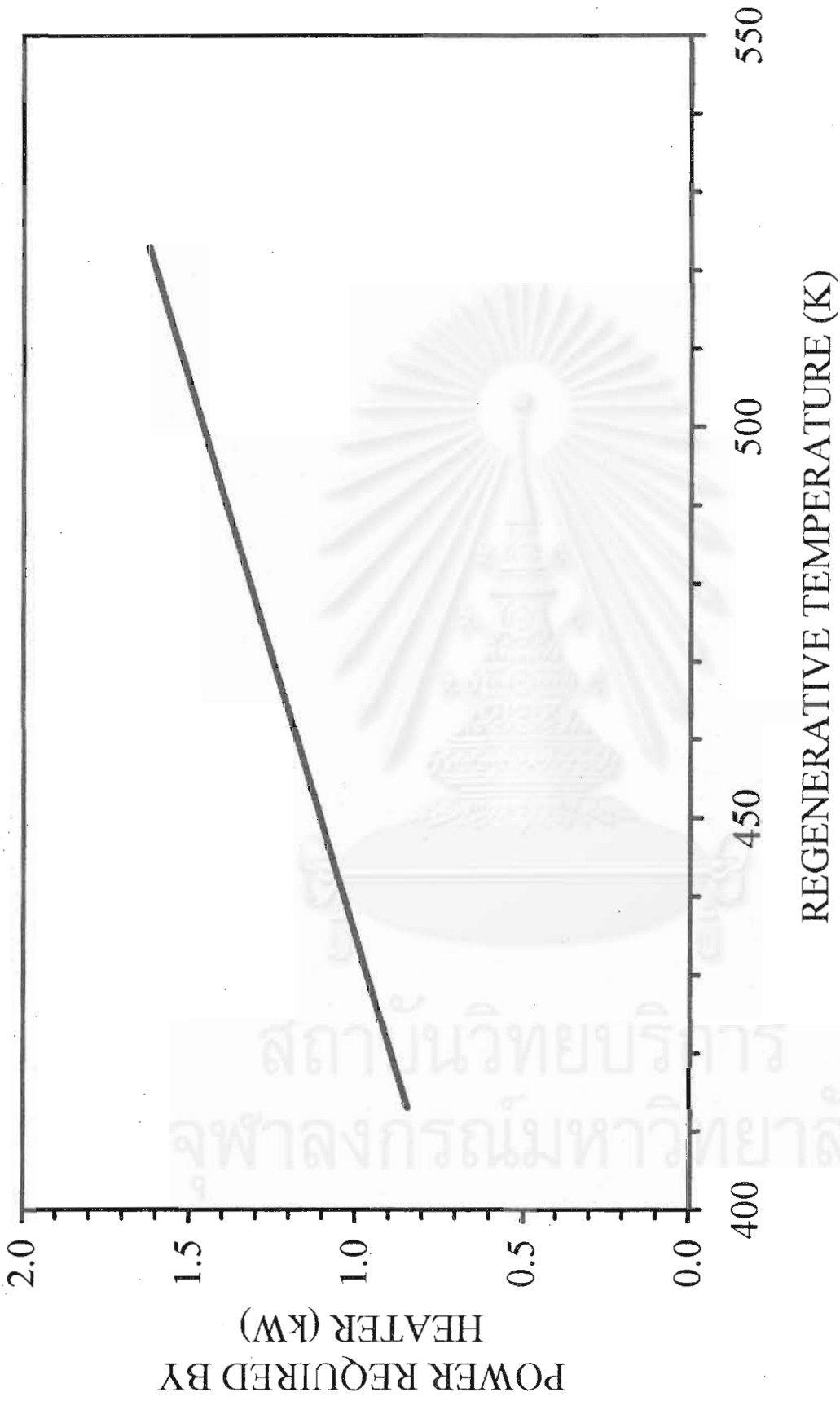
Figure 6.65 Power required by heater at various regenerative temperatures for the zeolite-13X coated honeycomb rotary dehumidifier (Treg-ZE-Effect Condition)
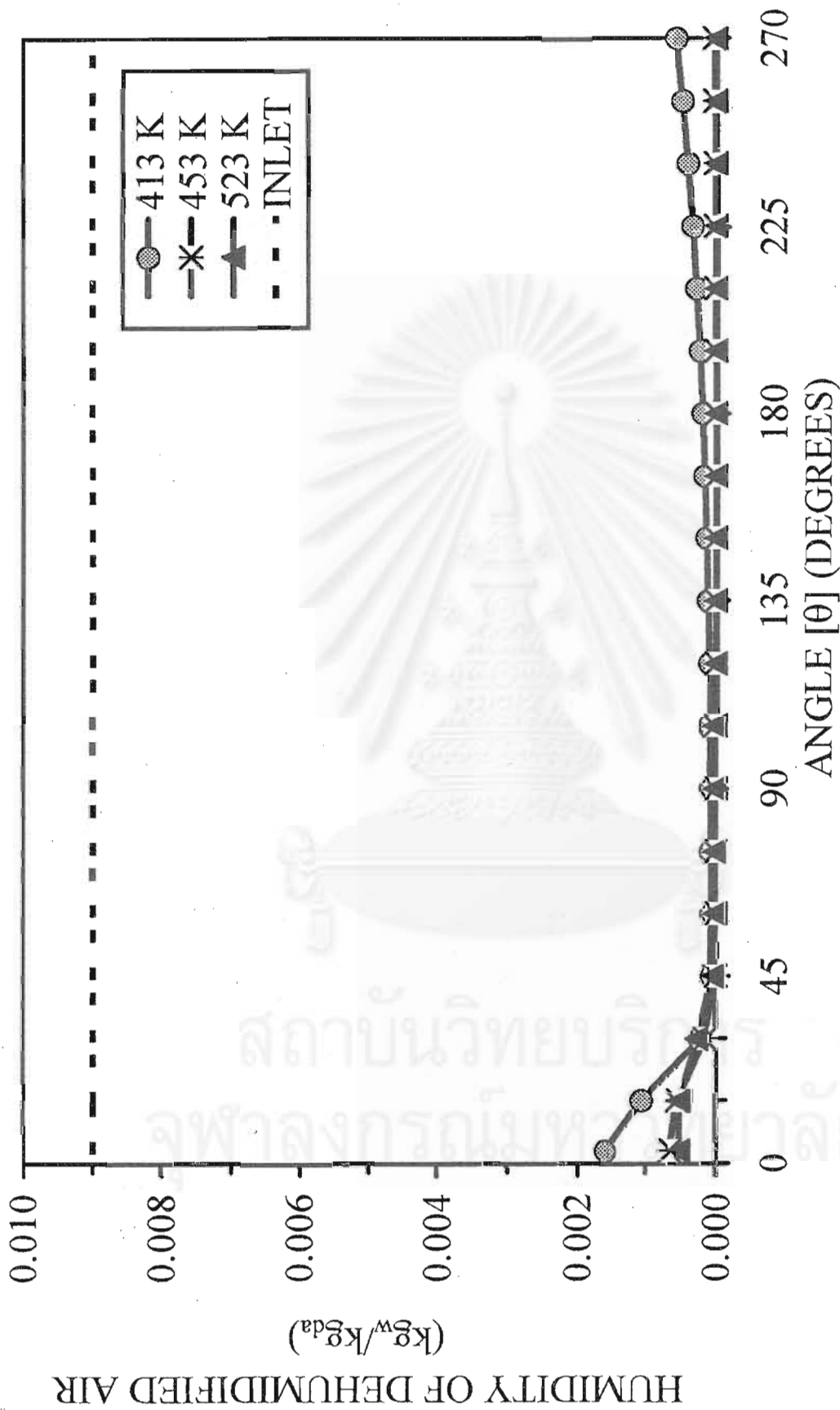
Figure 6.66 The angular distributions of the humidity of the dehumidified air from the zeolite-13X coated honeycomb rotary dehumidifier at various regenerative temperatures (Treg-ZE-Effect Condition)
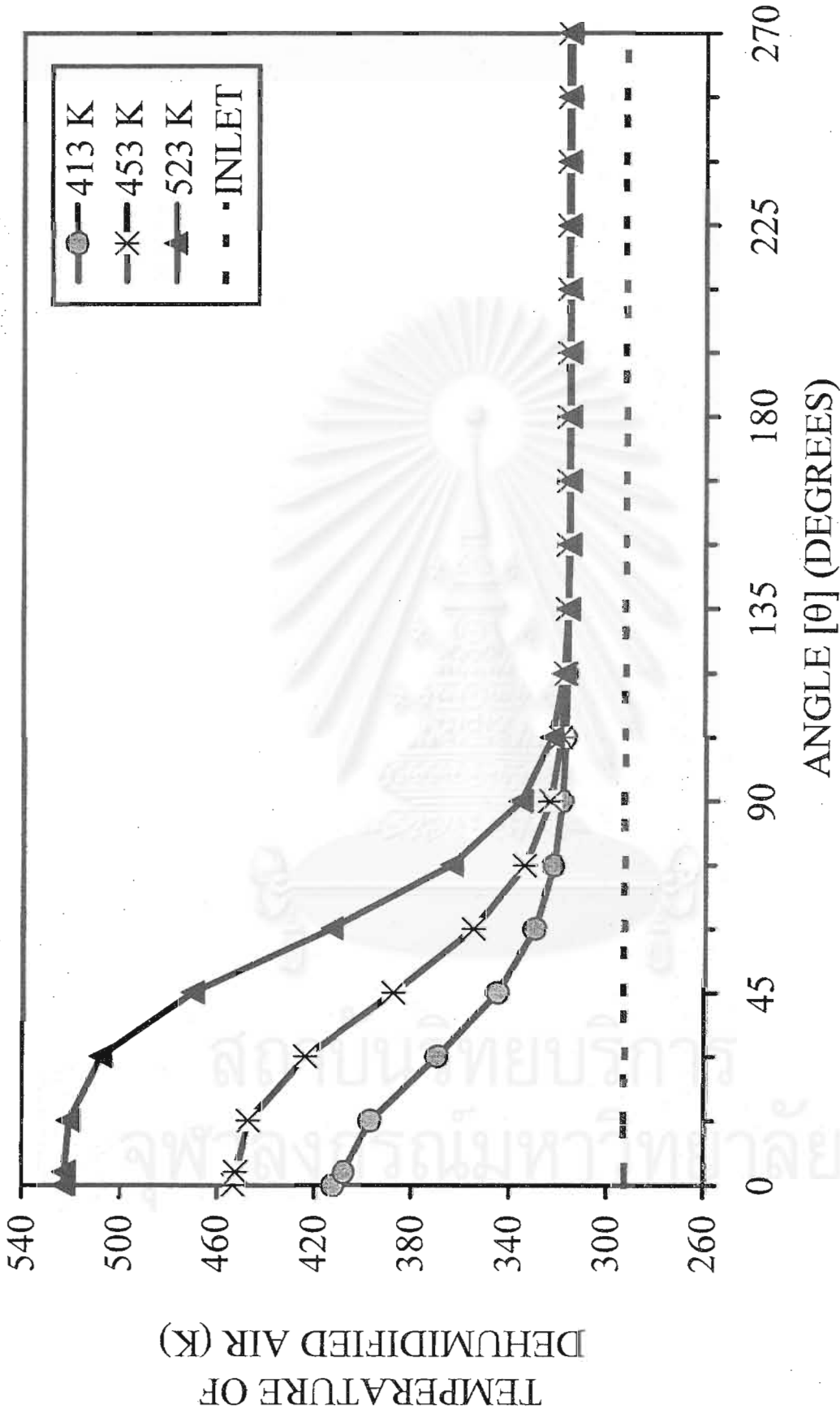
Figure 6.67 The angular distributions of the temperature of the deumidified air from the zeolite-13X coated honeycomb rotary dehumidifier at various regenerative temperatures (Treg-ZE-Effect Condition)
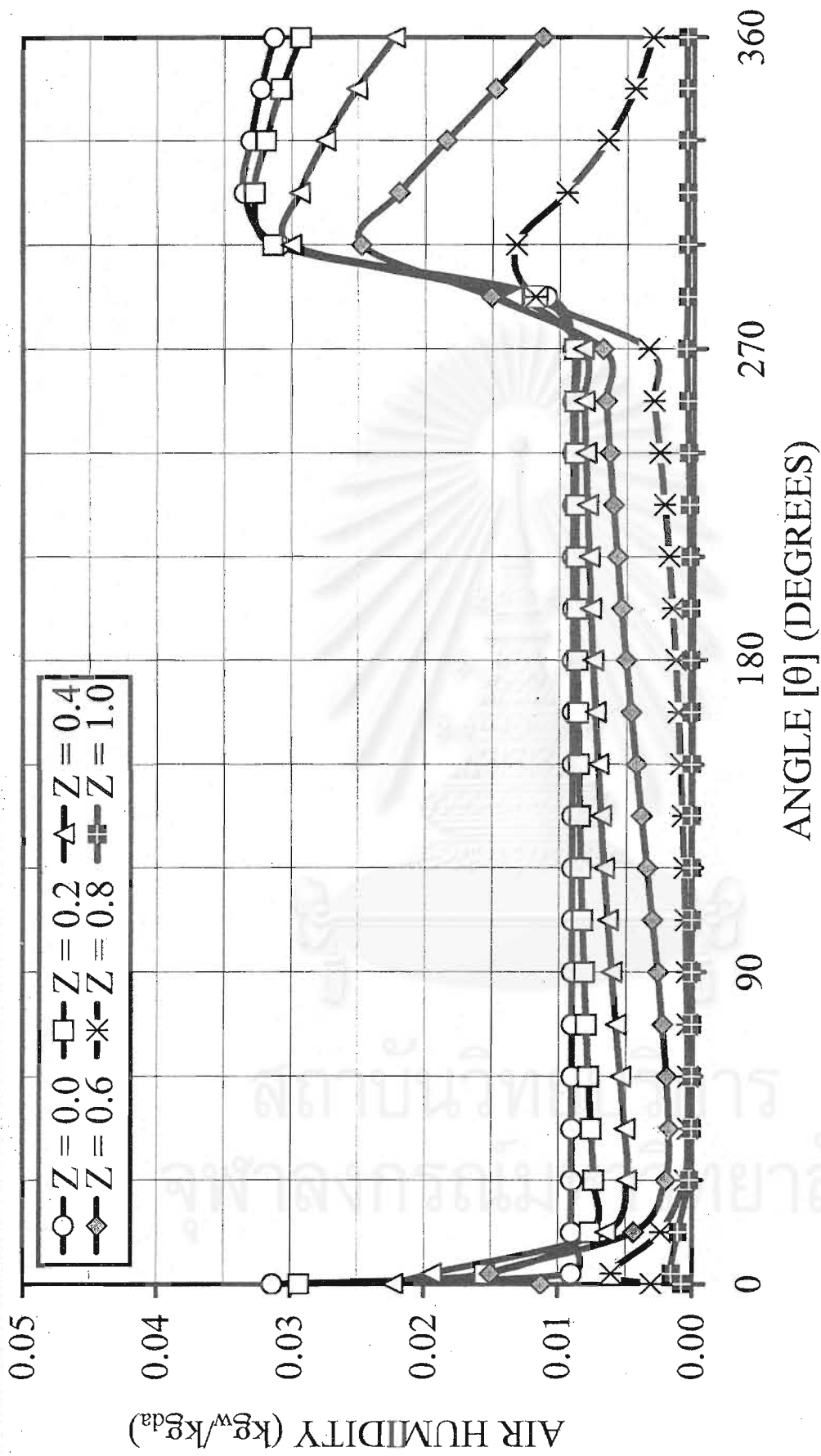
Figure 6.68 The two-dimensional distributions of the slot air humidity in the zeolite-13X coated honeycomb rotary dehumidifier at $T_{reg} = 413$ K (Treg-ZE-Effect Condition)
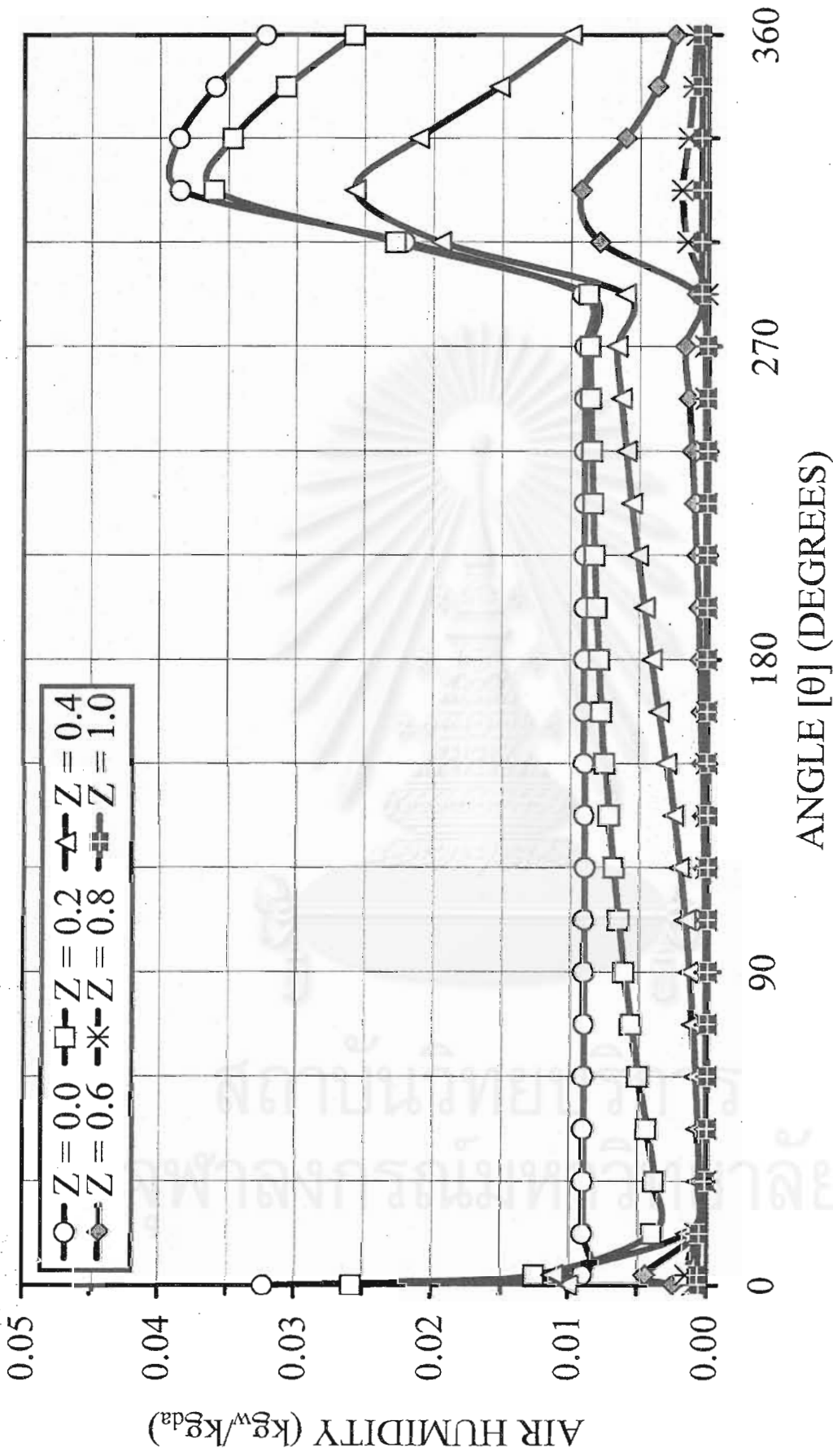
Figure 6.69 The two-dimensional distributions of the slot air humidity in the zeolite-13X coated honeycomb rotary dehumidifier at T_{reg} = 453 K (Treg-ZE-Effect Condition)
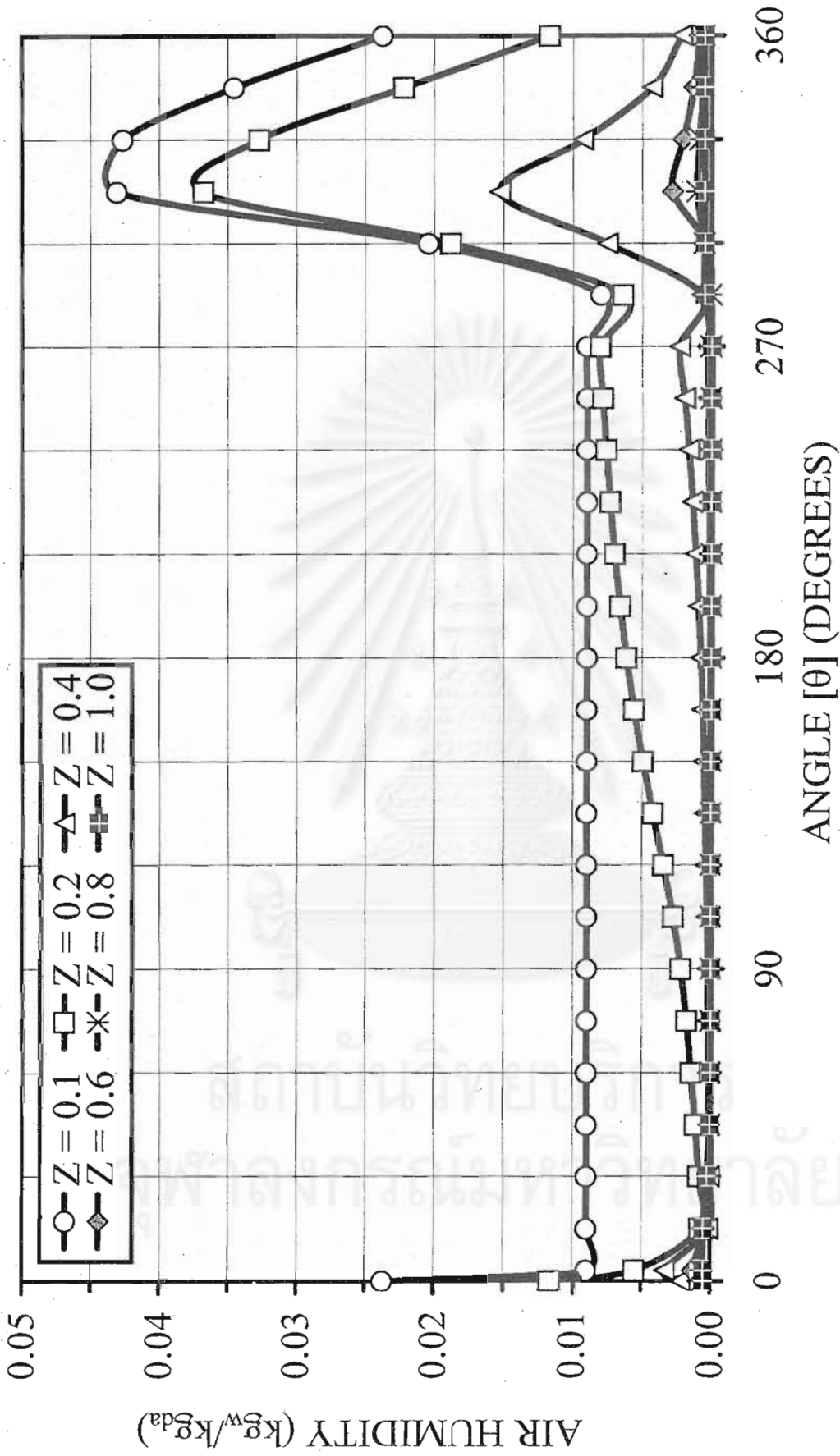
Figure 6.70 The two-dimensional distributions of the slot air humidity in the zeolite-13X coated honeycomb rotary dehumidifier at T_{reg} = 523 K (Treg-ZE-Effect Condition)
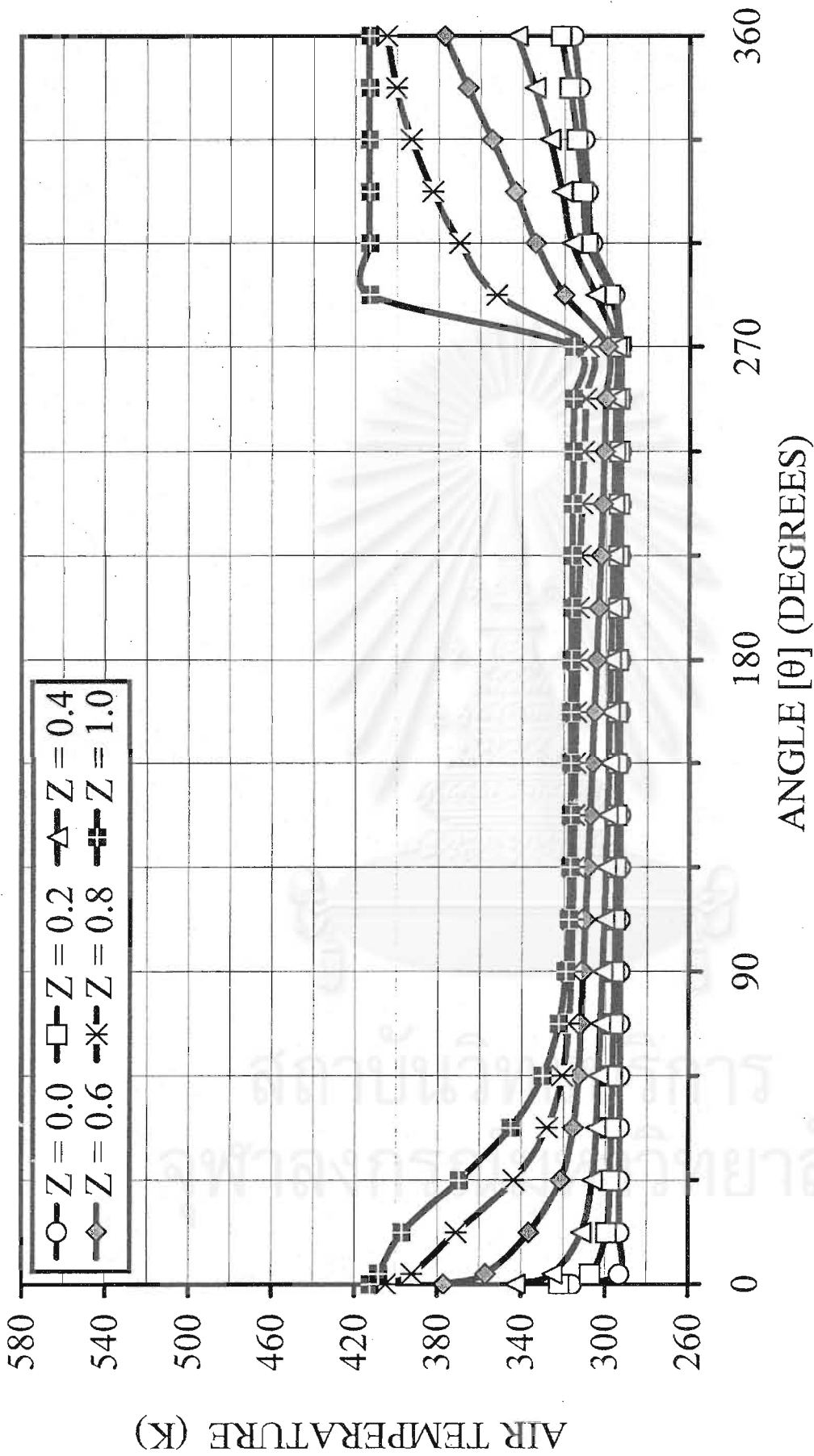
Figure 6.71 The two-dimensional distributions of the slot air temperature in the zeolite-13X coated honeycomb rotary dehumidifier at $T_{reg} = 413$ K (T_{reg}-ZE-Effect Condition)
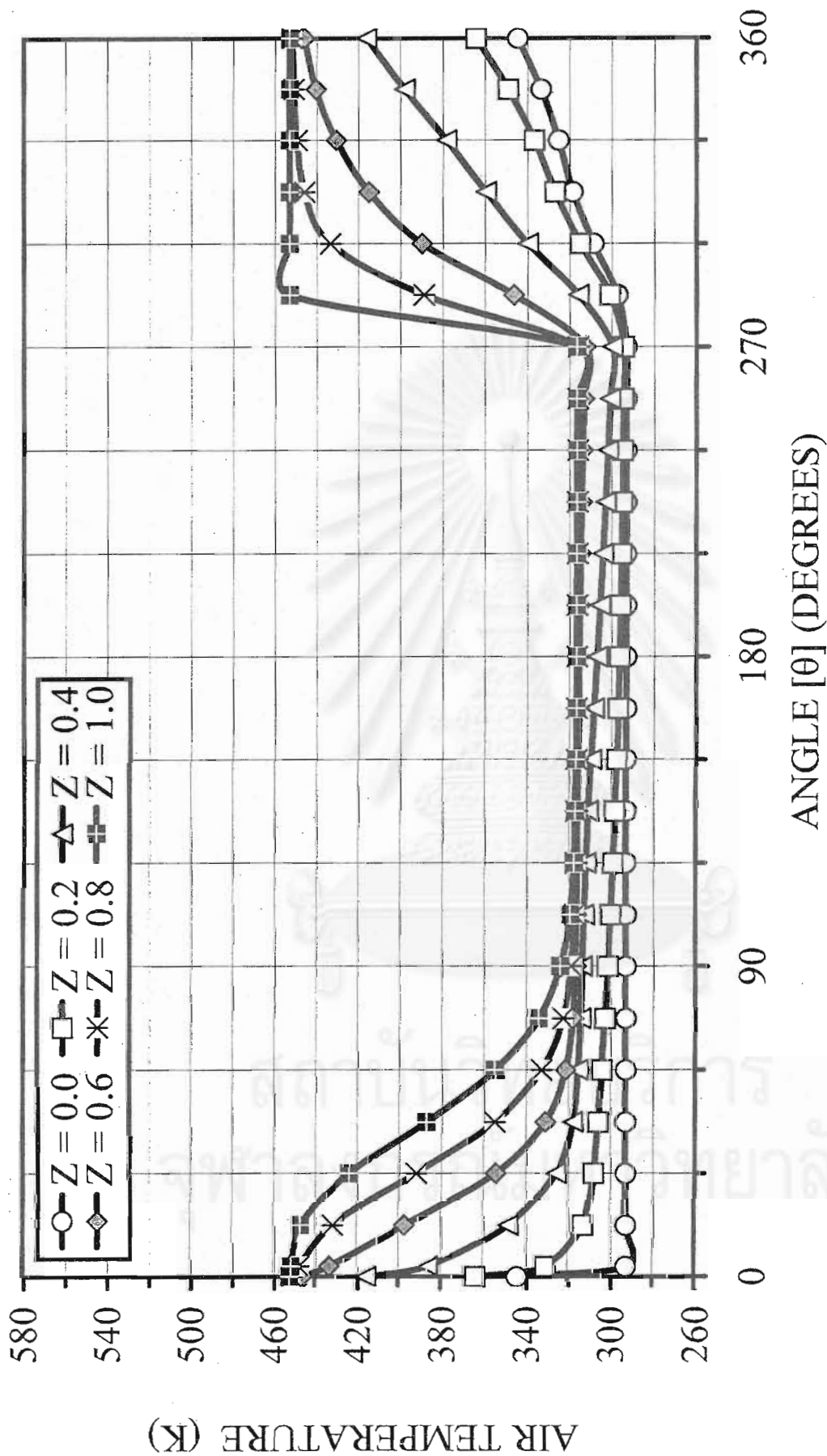
Figure 6.72 The two-dimensional distributions of the slot air temperature in the zeolite-13X coated honeycomb rotary dehumidifier at $T_{reg} = 453$ K (Treg-ZE-Effect Condition)
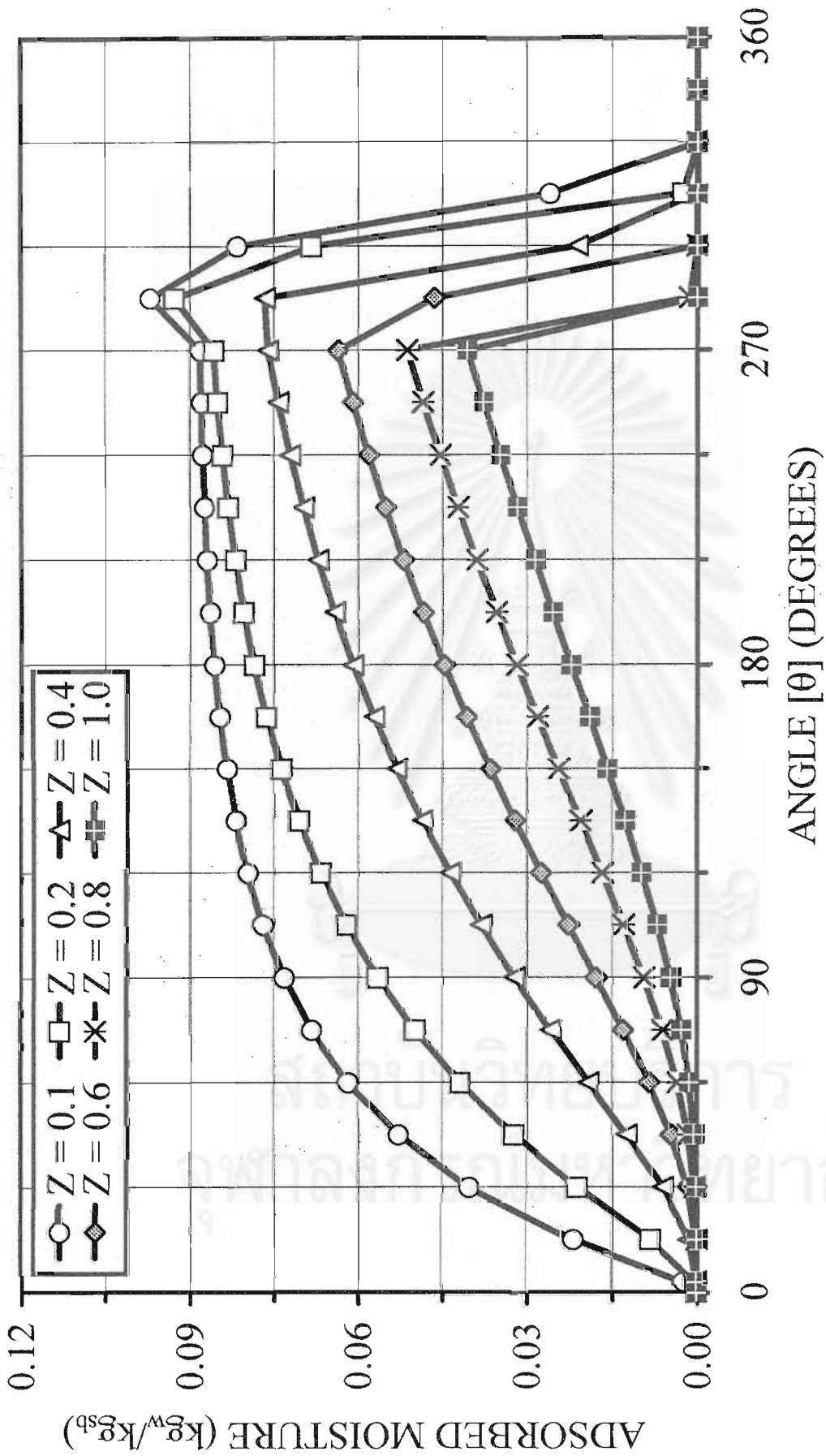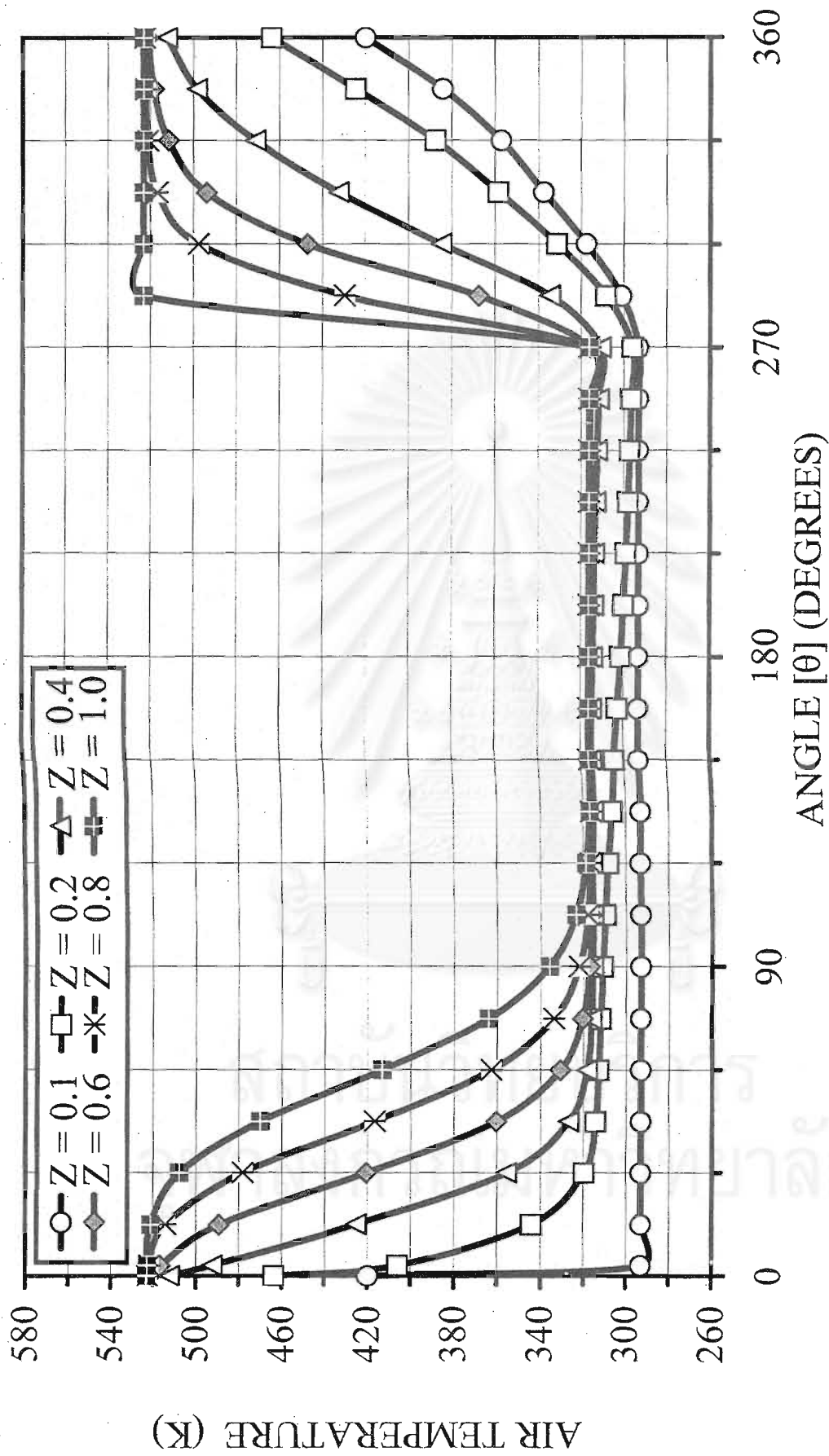
Figure 6.73 The two-dimensional distributions of the slot air temperature in the zeolite-13X coated honeycomb rotary dehumidifier at $T_{reg} = 523$ K (T_{reg}-ZE-Effect Condition)
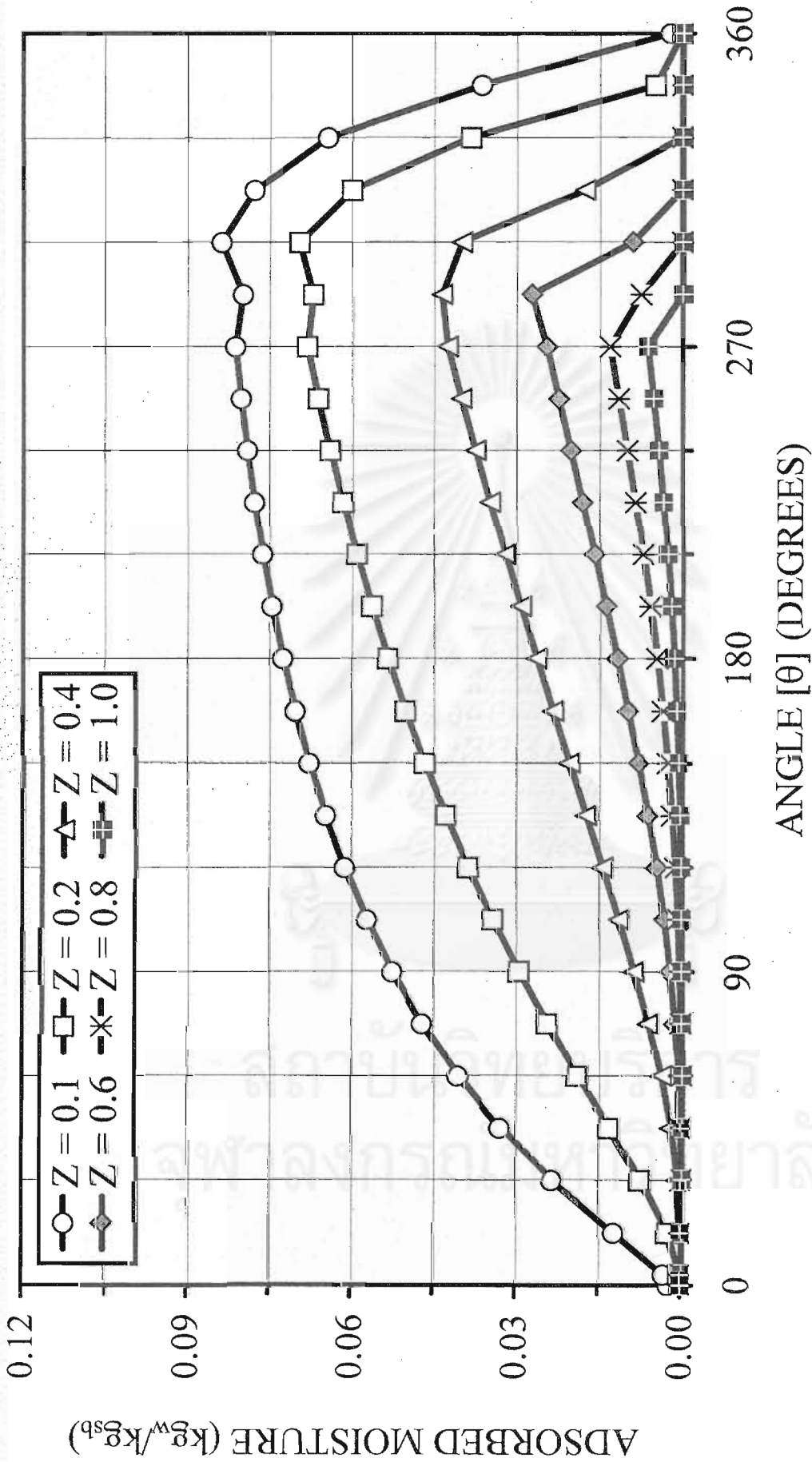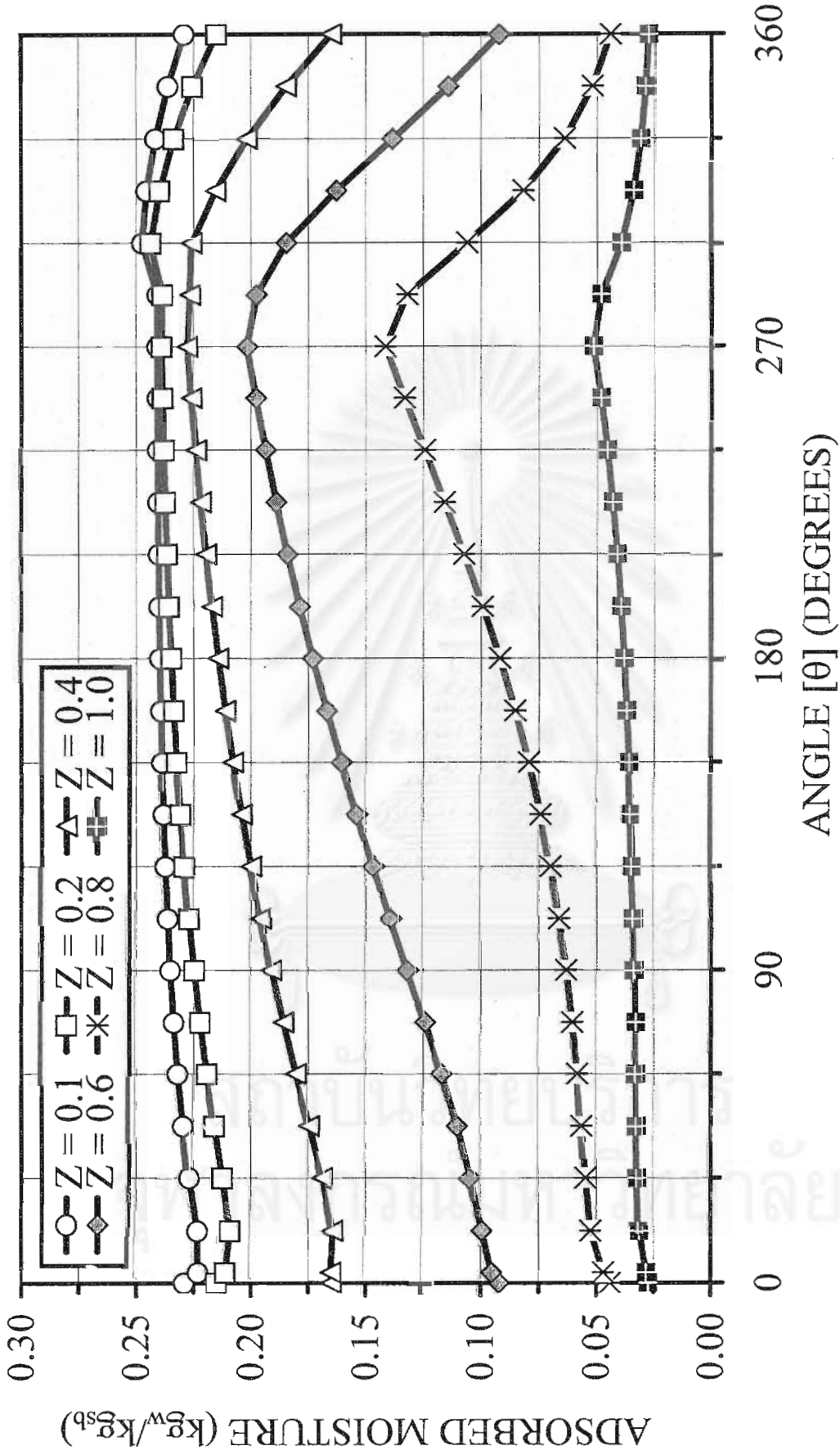
Figure 6.74 The two-dimensional distributions of the adsorbed moisture on zeolite-13X coated honeycomb rotary dehumidifier at $T_{reg} = 413$ K (Treg-ZE-Effect Condition)
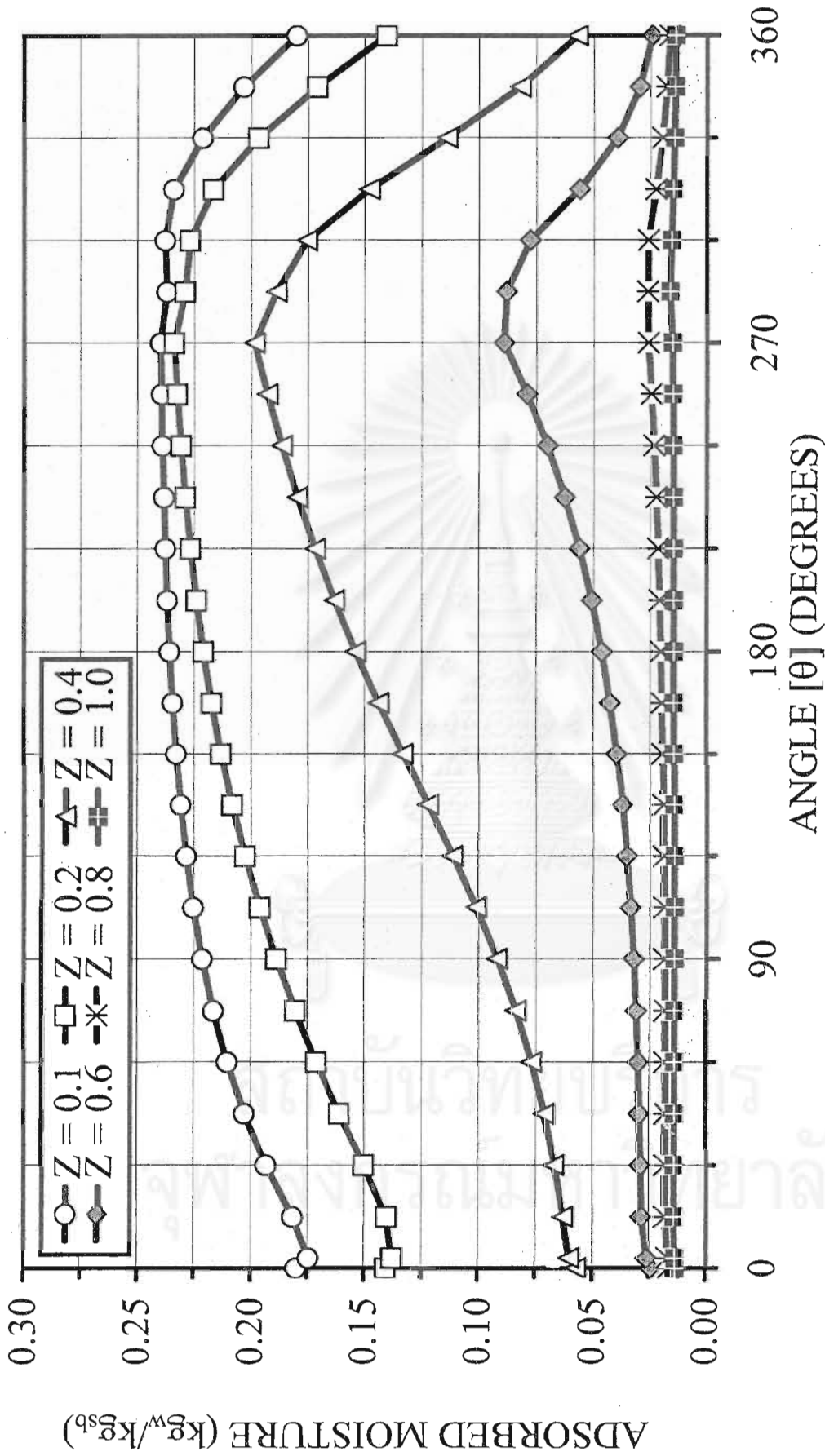
Figure 6.75 The two-dimensional distributions of the adsorbed moisture on zeolite-13X coated honeycomb rotary dehumidifier at T_{reg} = 453 K (Treg-ZE-Effect Condition)
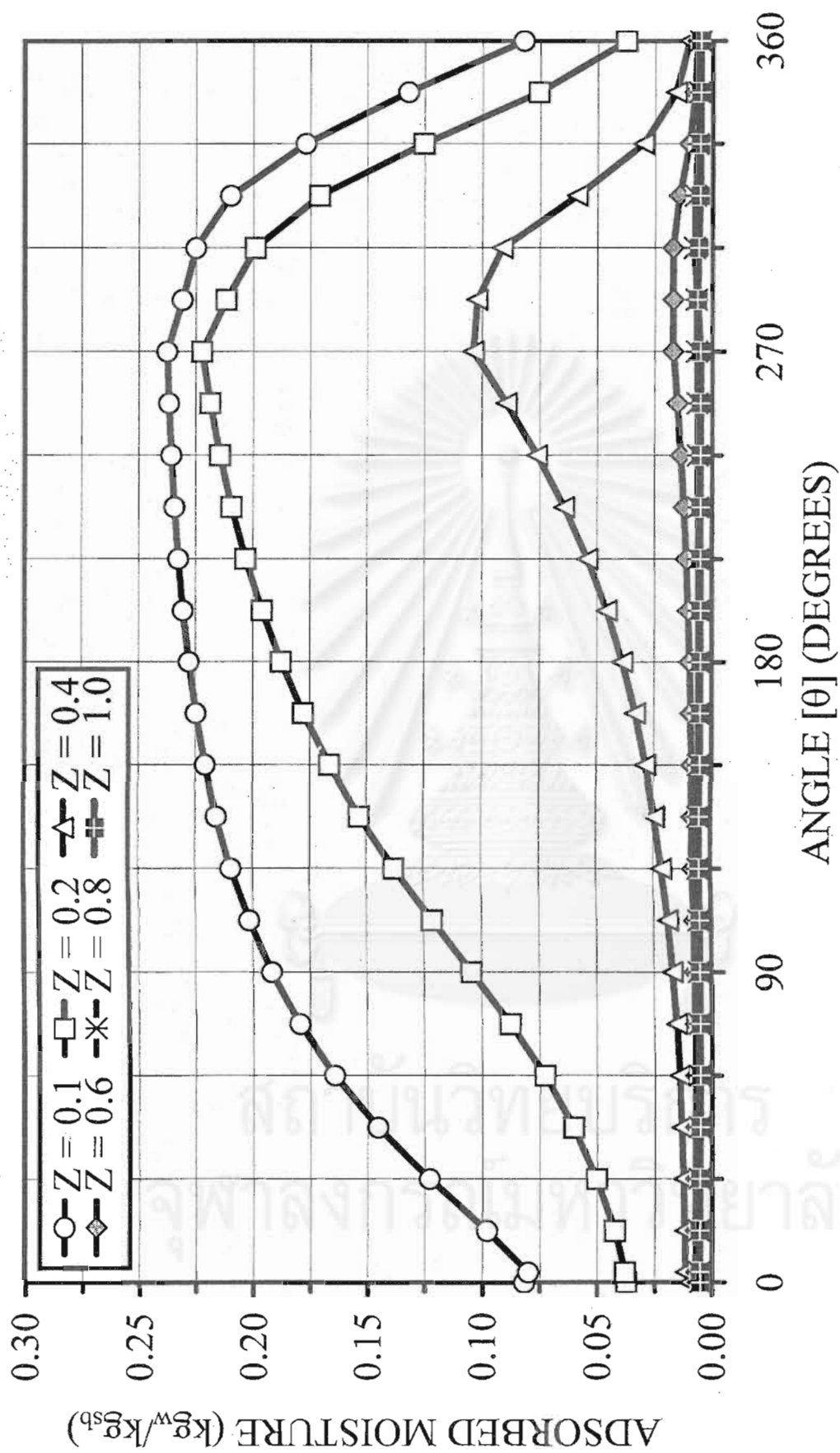
Figure 6.76 The two-dimensional distributions of the adsorbed moisture on zeolite-13X coated honeycomb rotary dehumidifier at T_{reg} = 523 K (Treg-ZE-Effect Condition)
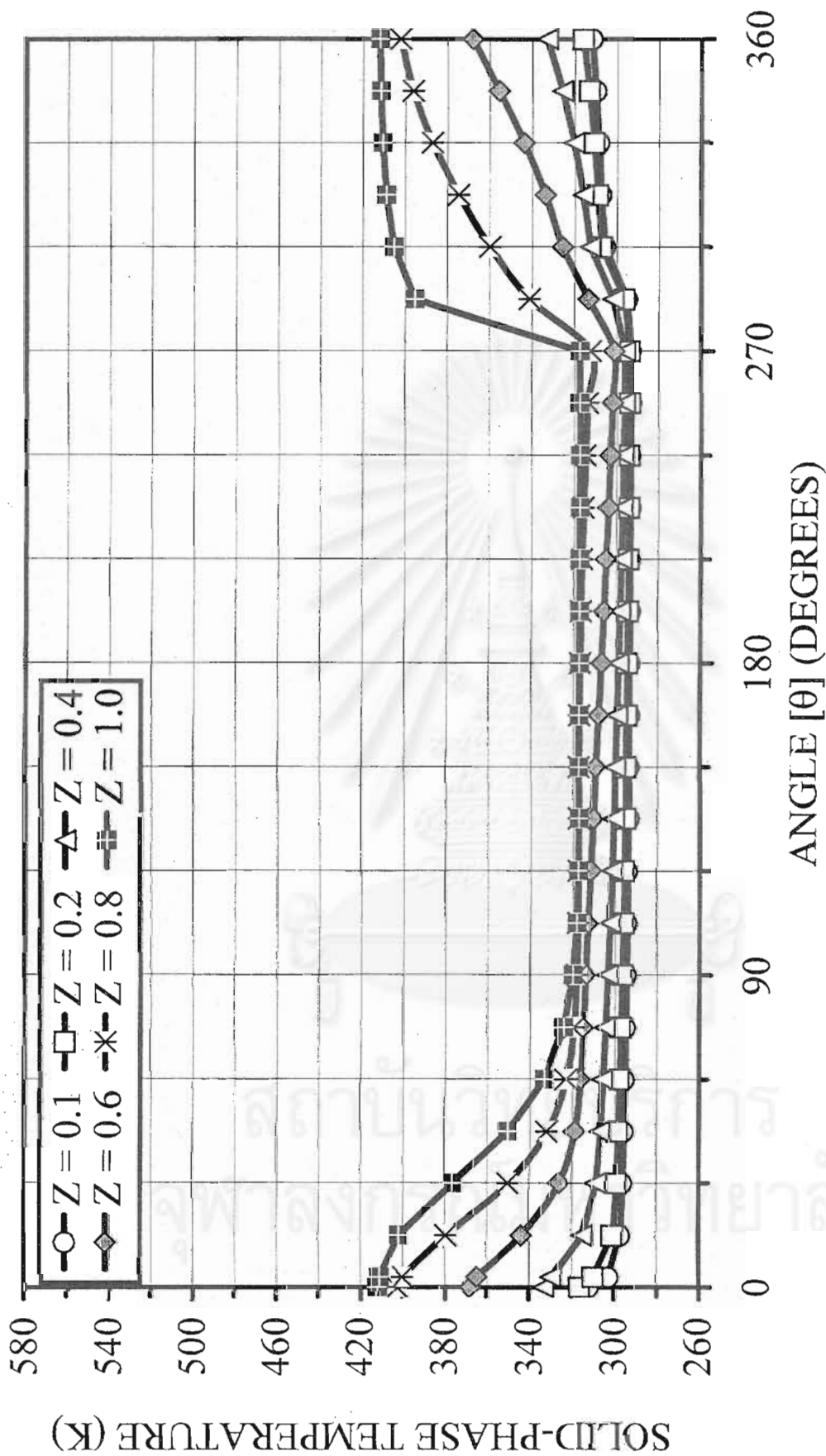
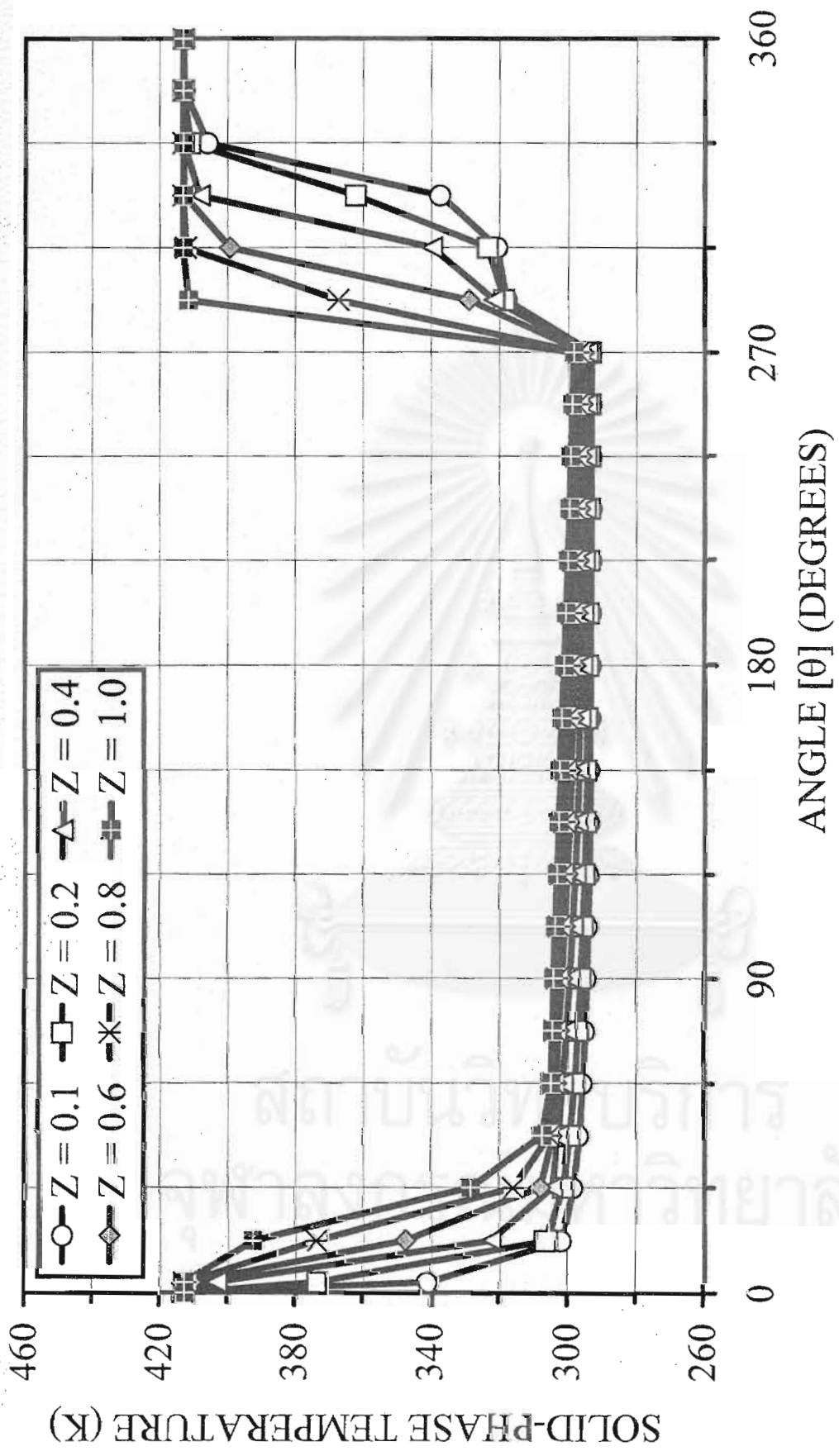**Figure 6.77** The two-dimensional distributions of the solid-phase temperature in the zeolite-13X coated honeycomb rotary dehumidifier at T_{reg} = 413 K (Treg-ZE-Effect Condition)
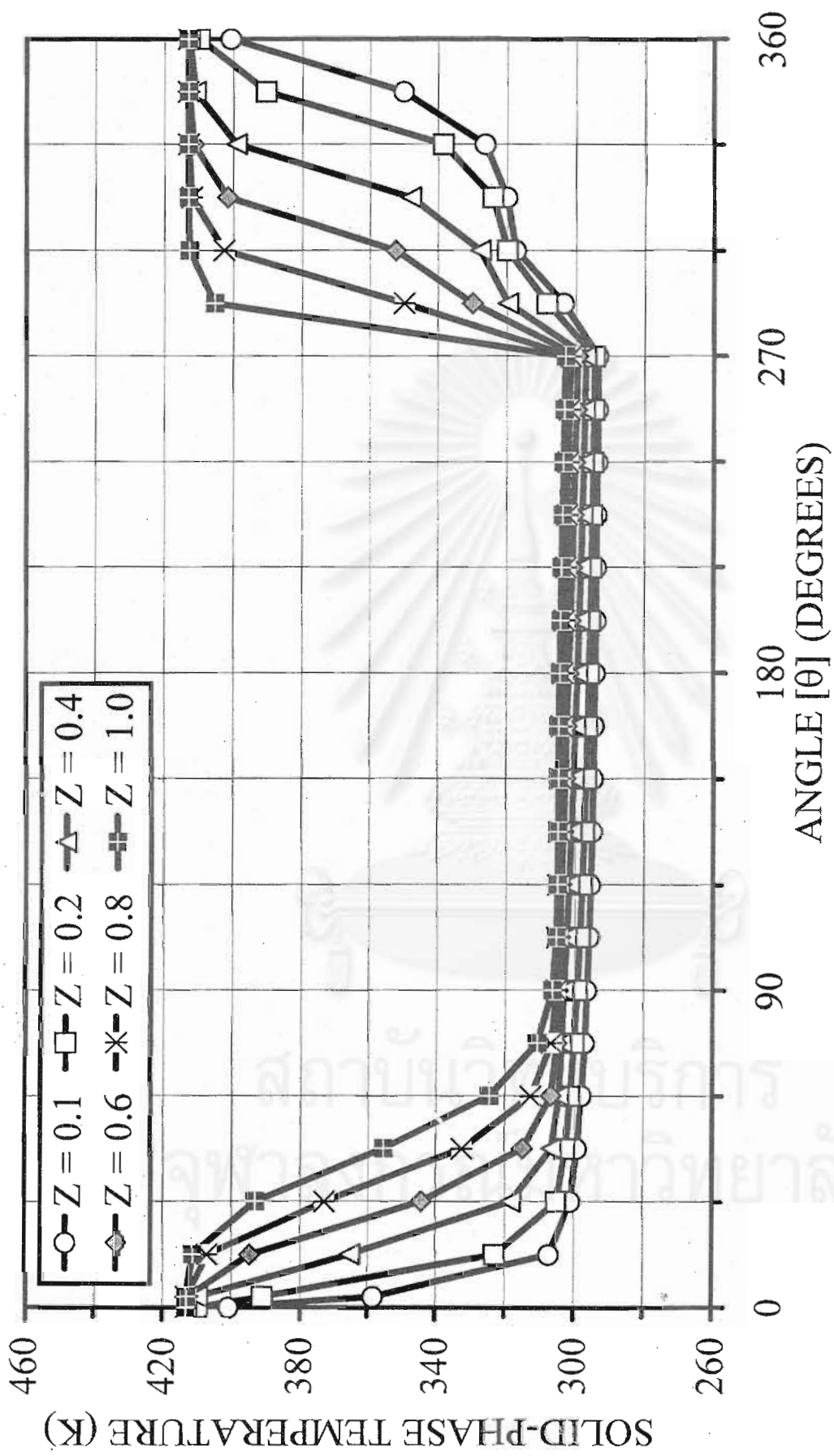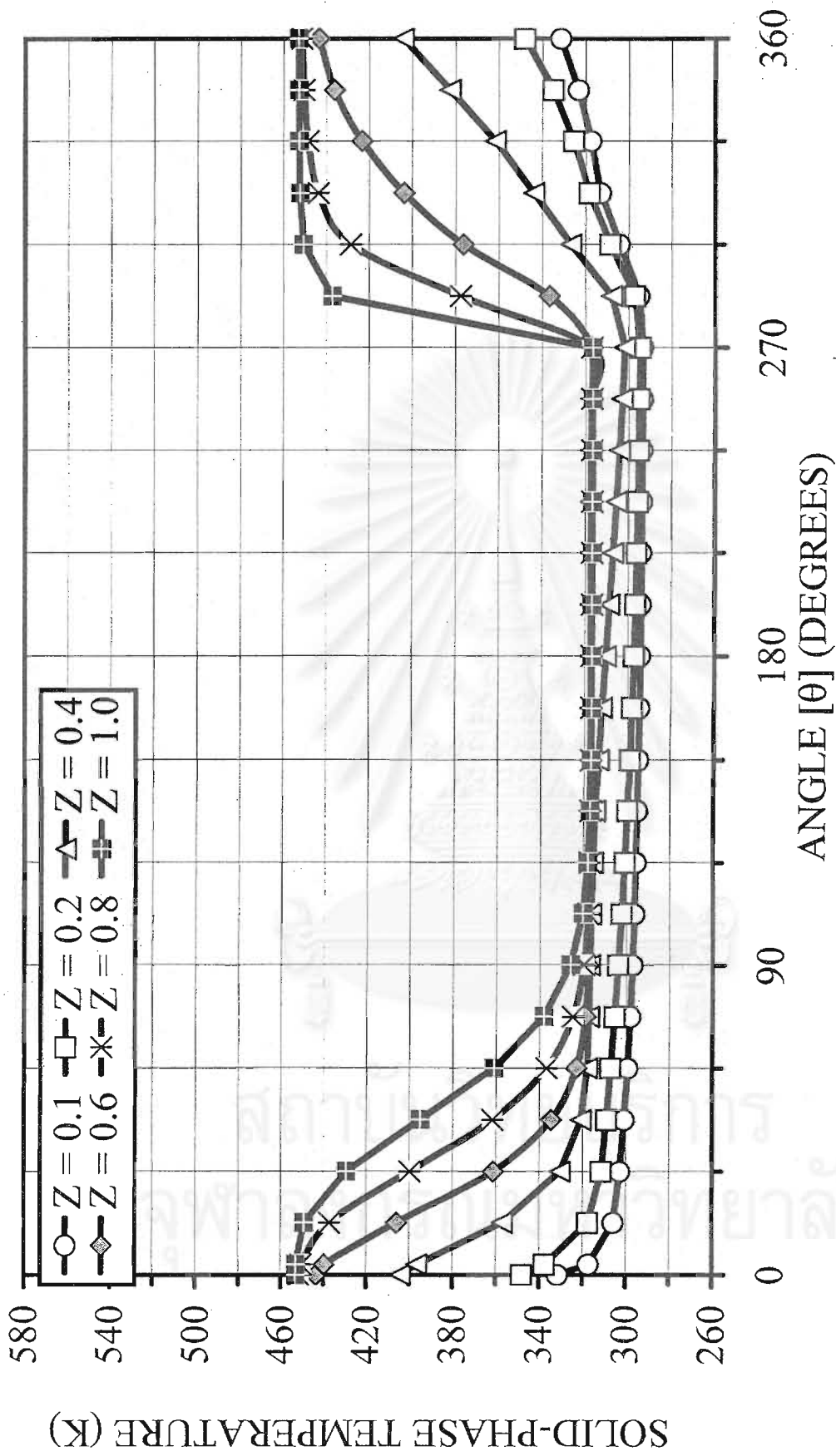
Figure 6.78 The two-dimensional distributions of the solid-phase temperature in the zeolite-13X coated honeycomb rotary dehumidifier at $T_{reg} = 453$ K (Treg-ZE-Effect Condition)
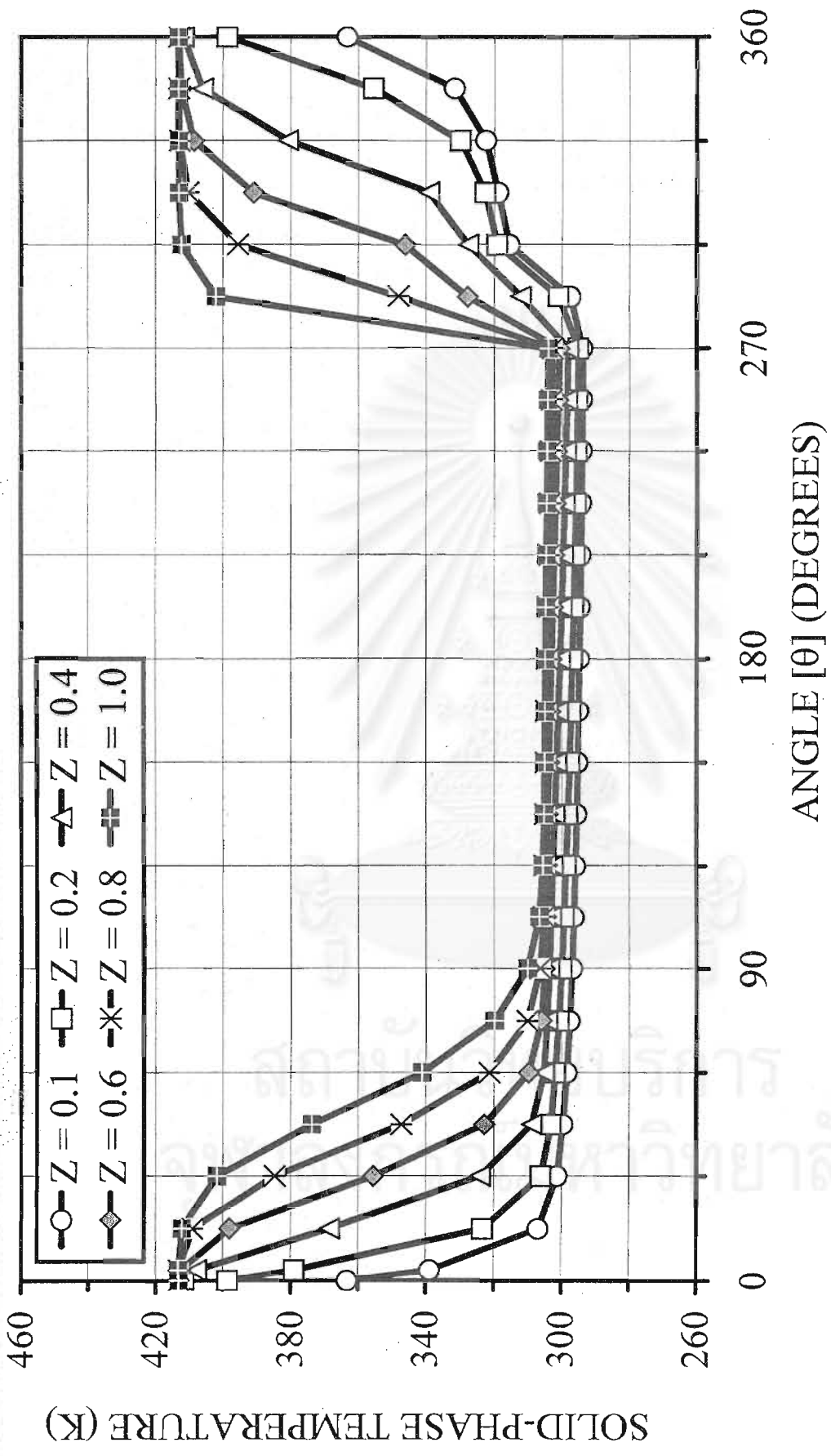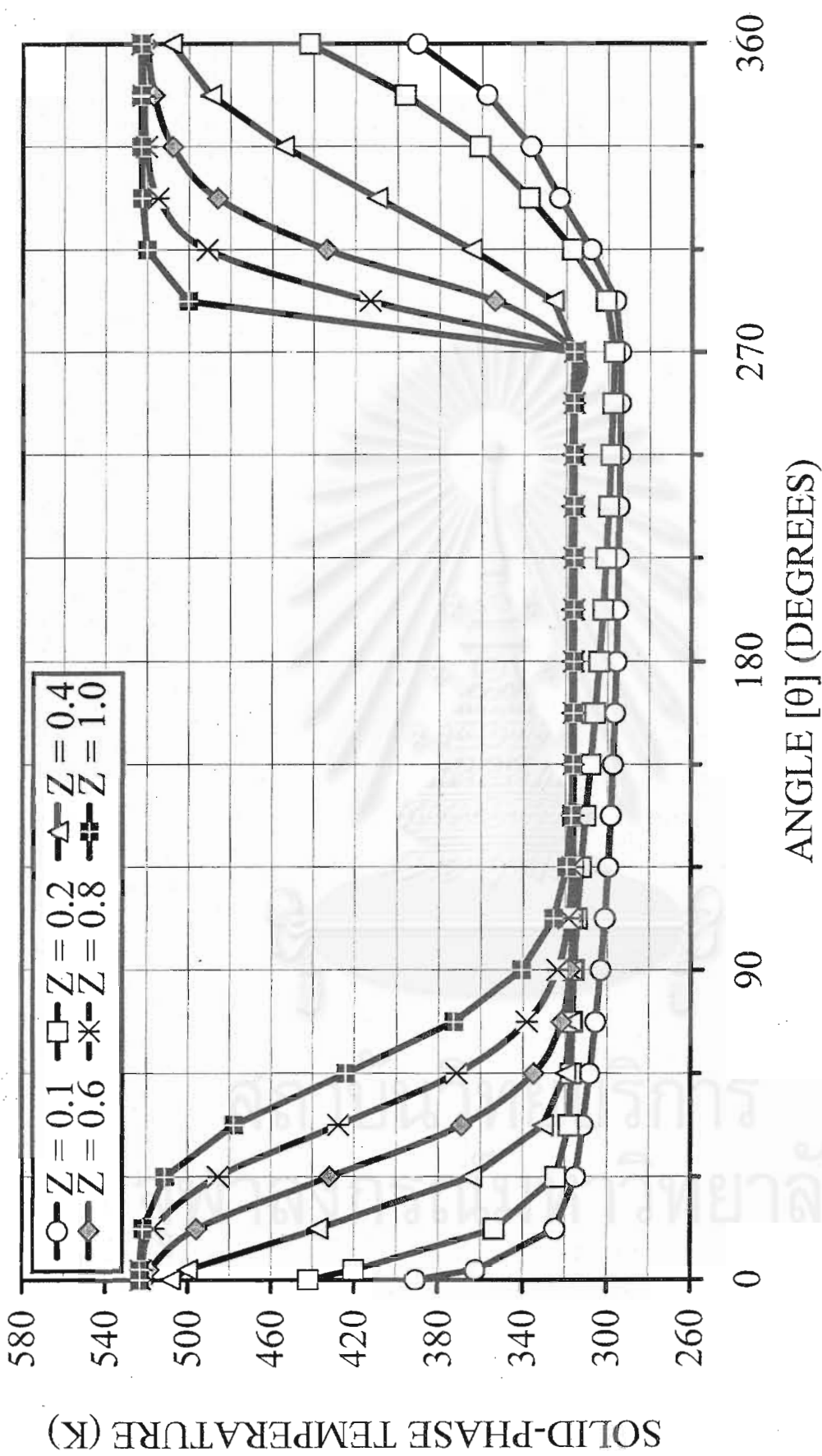
Figure 6.79 The two-dimensional distributions of the solid-phase temperature in the zeolite-13X coated honeycomb rotary dehumidifier at T_{reg} = 523 K (T_{reg}-ZE-Effect Condition)
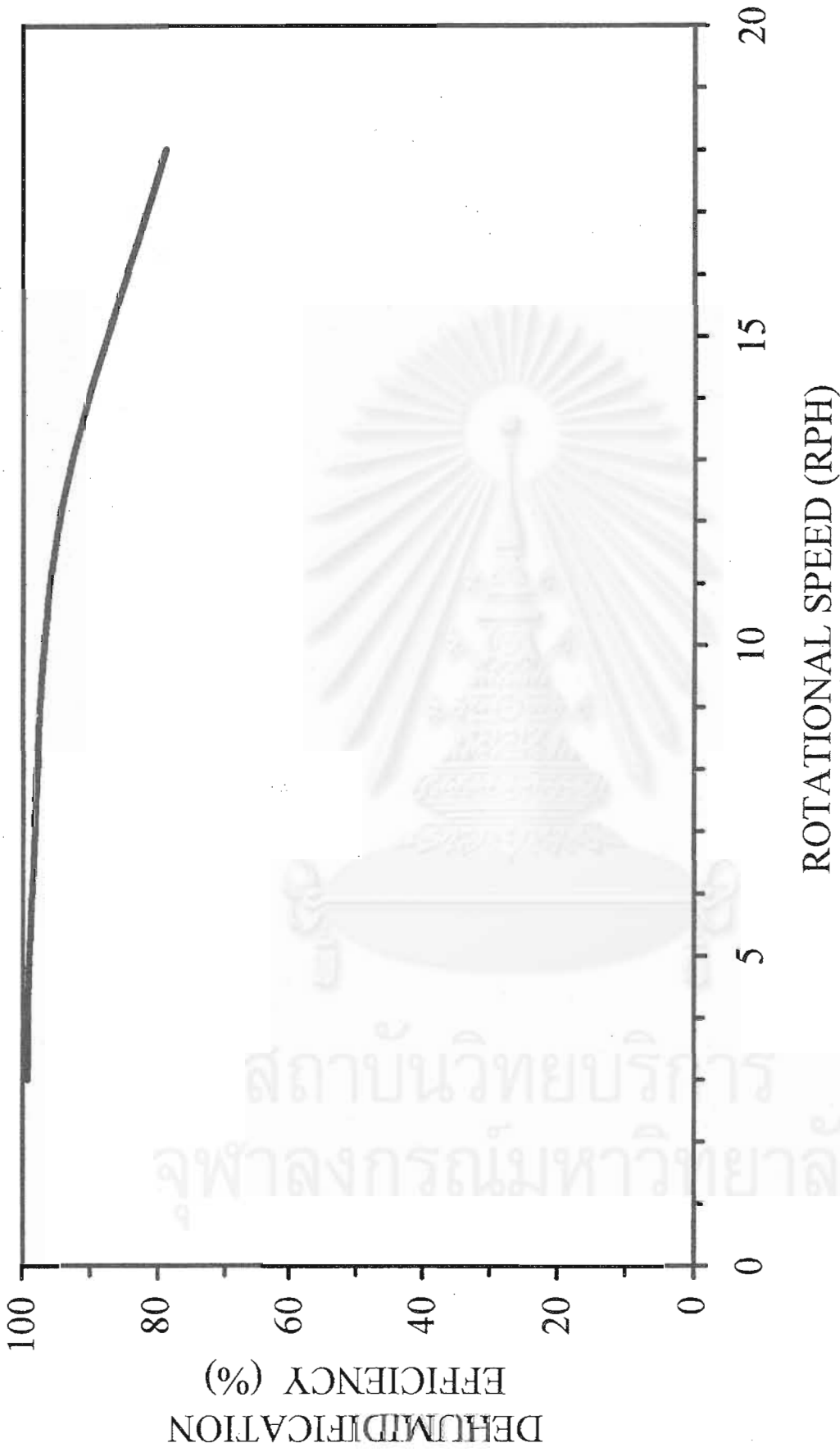
Figure 6.80 Effect of rotational speed on the dehumidification efficiency of the zeolite-13X coated honeycomb rotary dehumidifier (Speed-ZE-Effect condition)
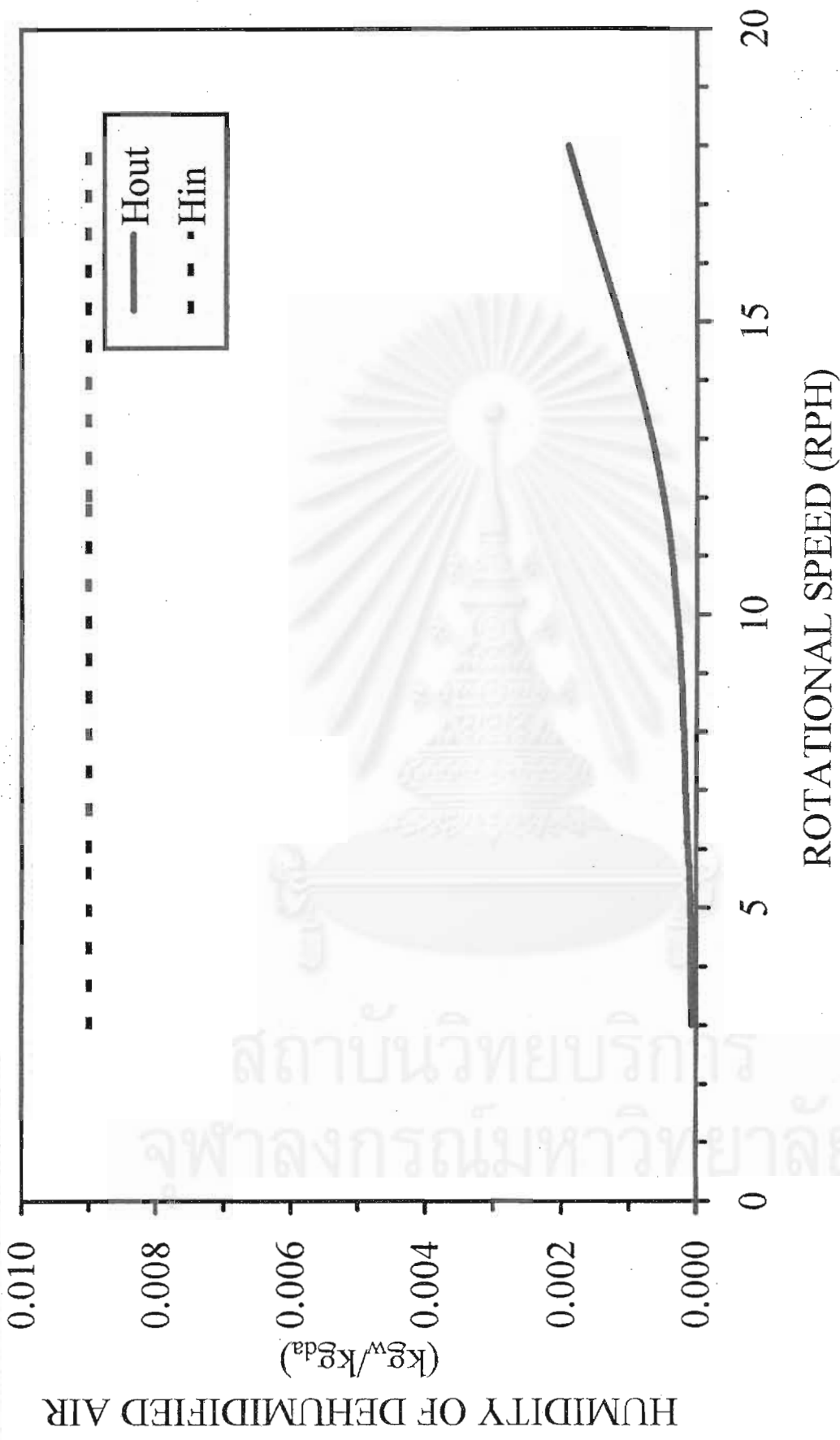
Figure 6.81 Effect of rotational speed on the average humidity of the dehumidified air from the zeolite-13X coated rotary dehumidifier (Speed-ZE-Effect Condition)
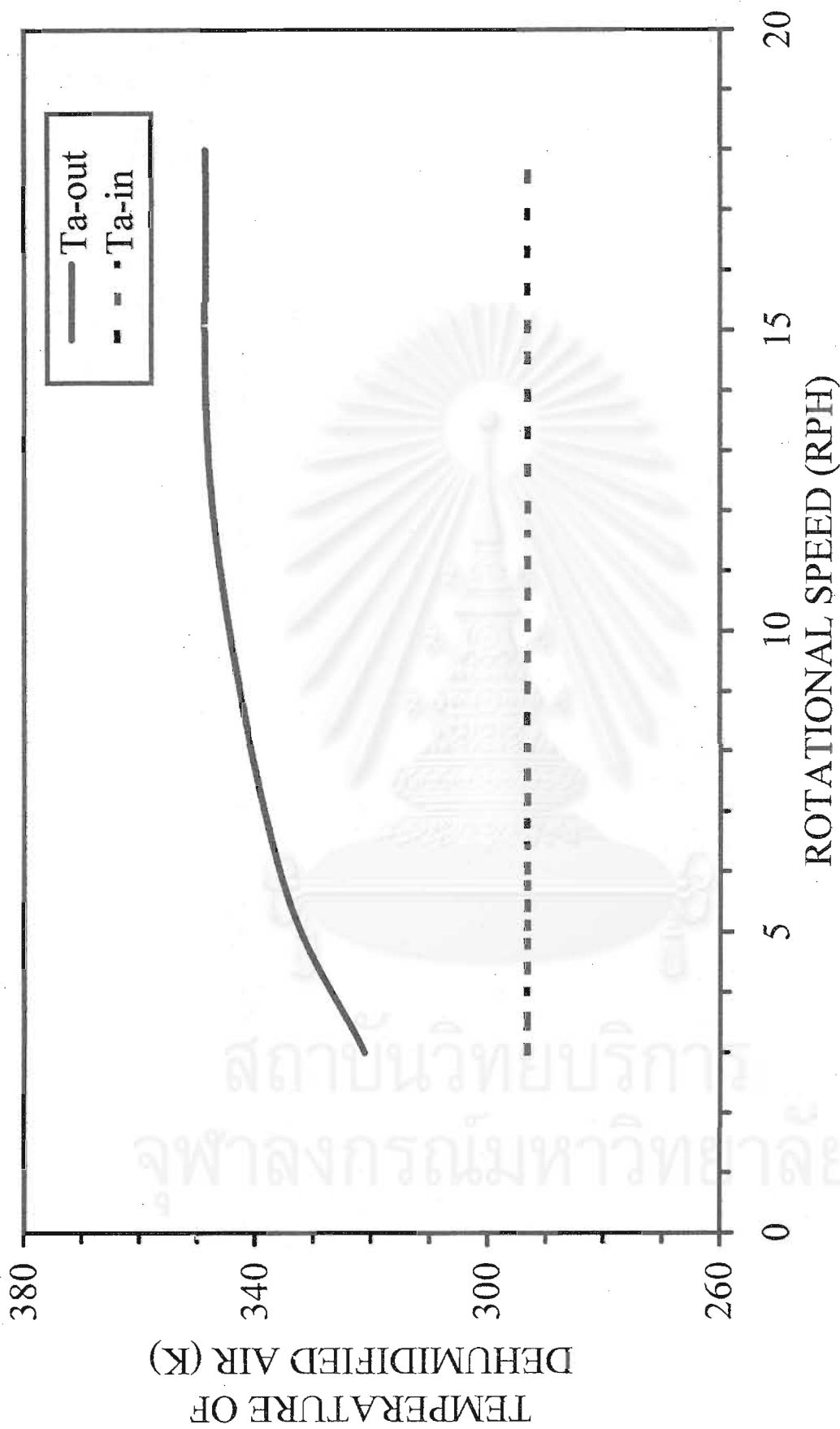
Figure 6.82 Effect of rotational speed on the average temperature of the dehumidified air from the zeolite-13X coated honeycomb rotary dehumidifier (Speed-ZE-Effect Condition)
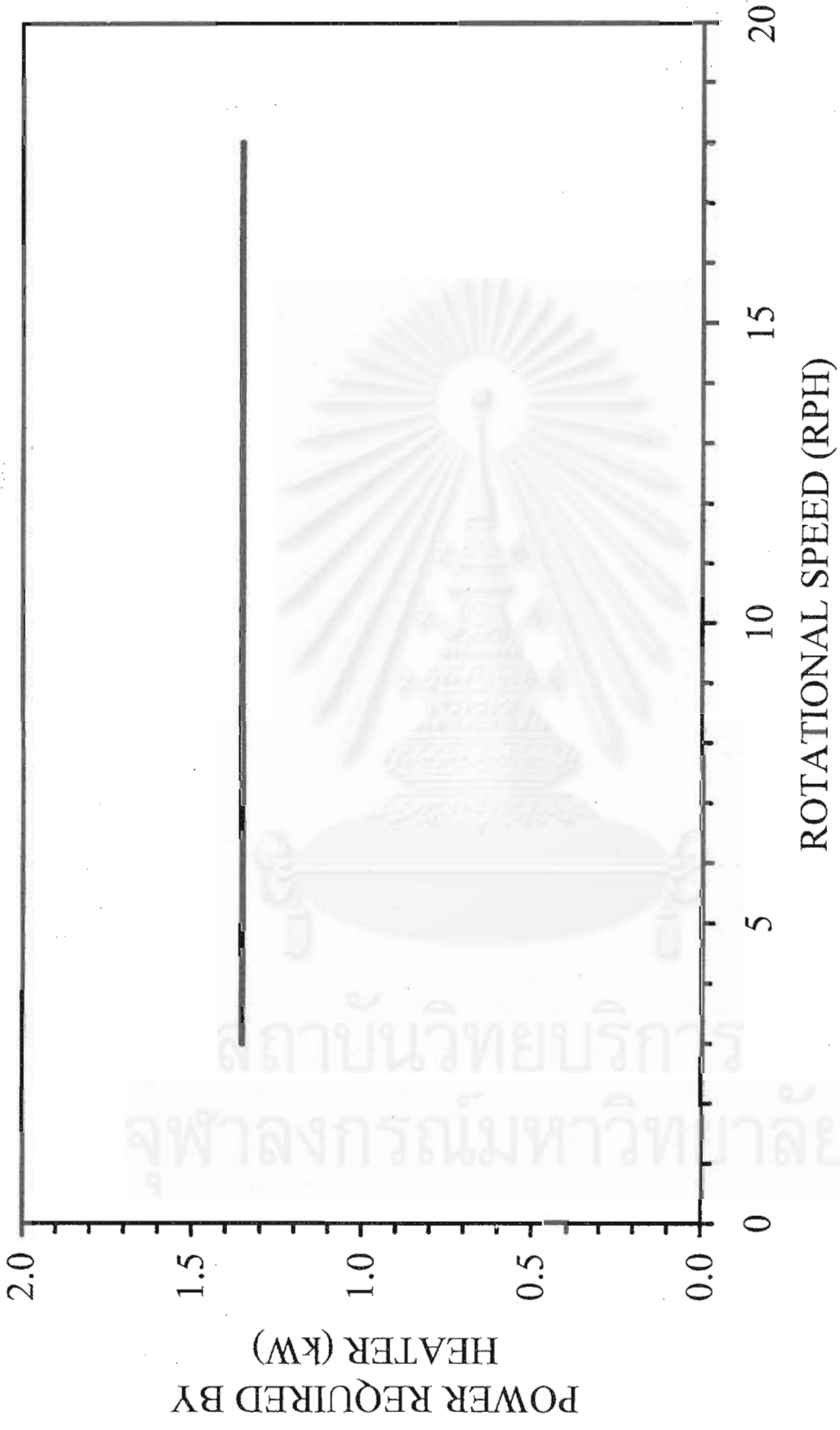
Figure 6.83 Power required by heater at various rotational speeds for the zeolite-13X coated honeycomb rotary dehumidifier (Speed-ZE-Effect Condition)
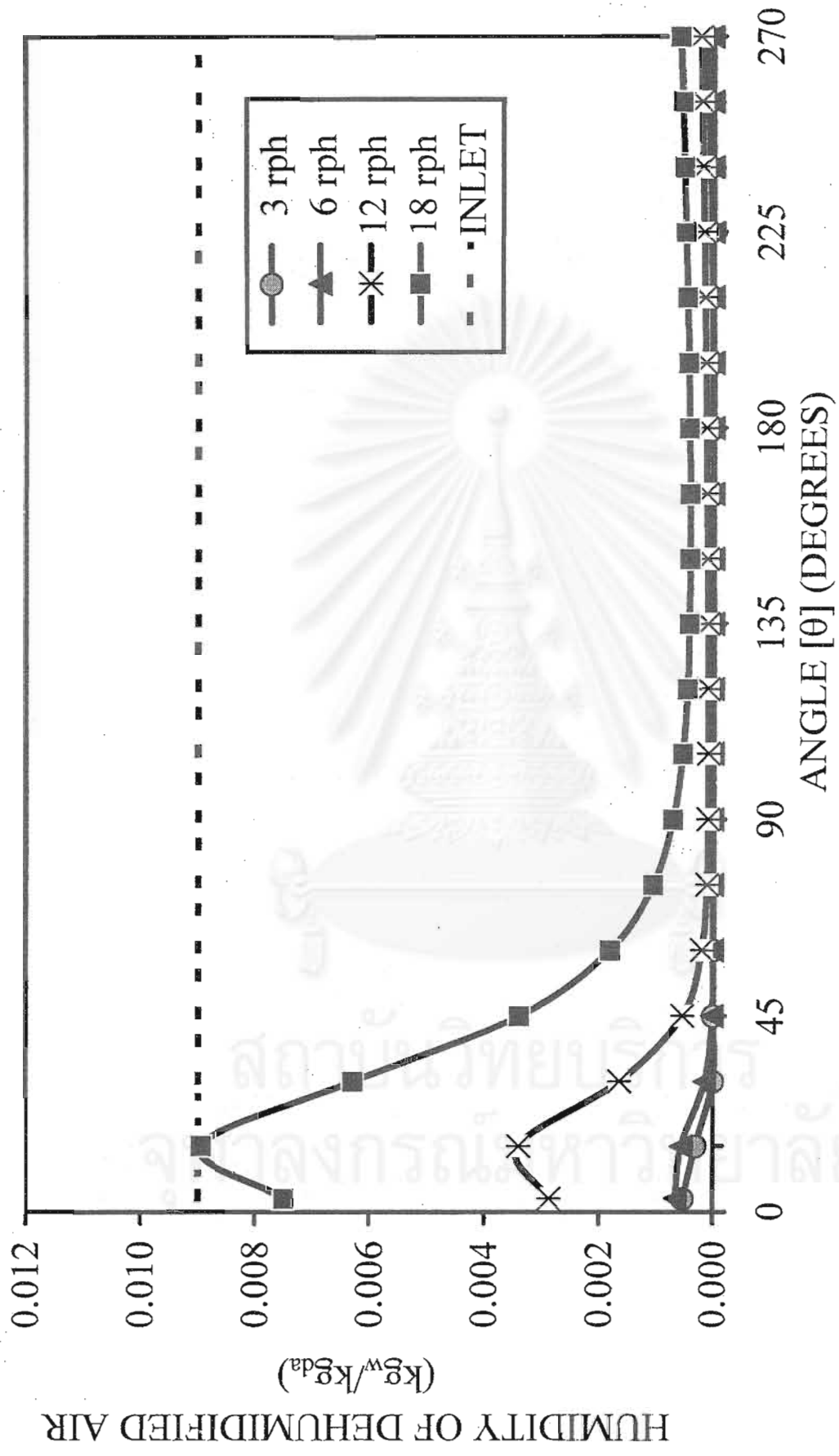
Figure 6.84 The angular distributions of the humidity of the dehumidified air from the zeolite-13X coated honeycomb rotary dehumidifier at various rotational speeds (Speed-ZE-Effect Condition)
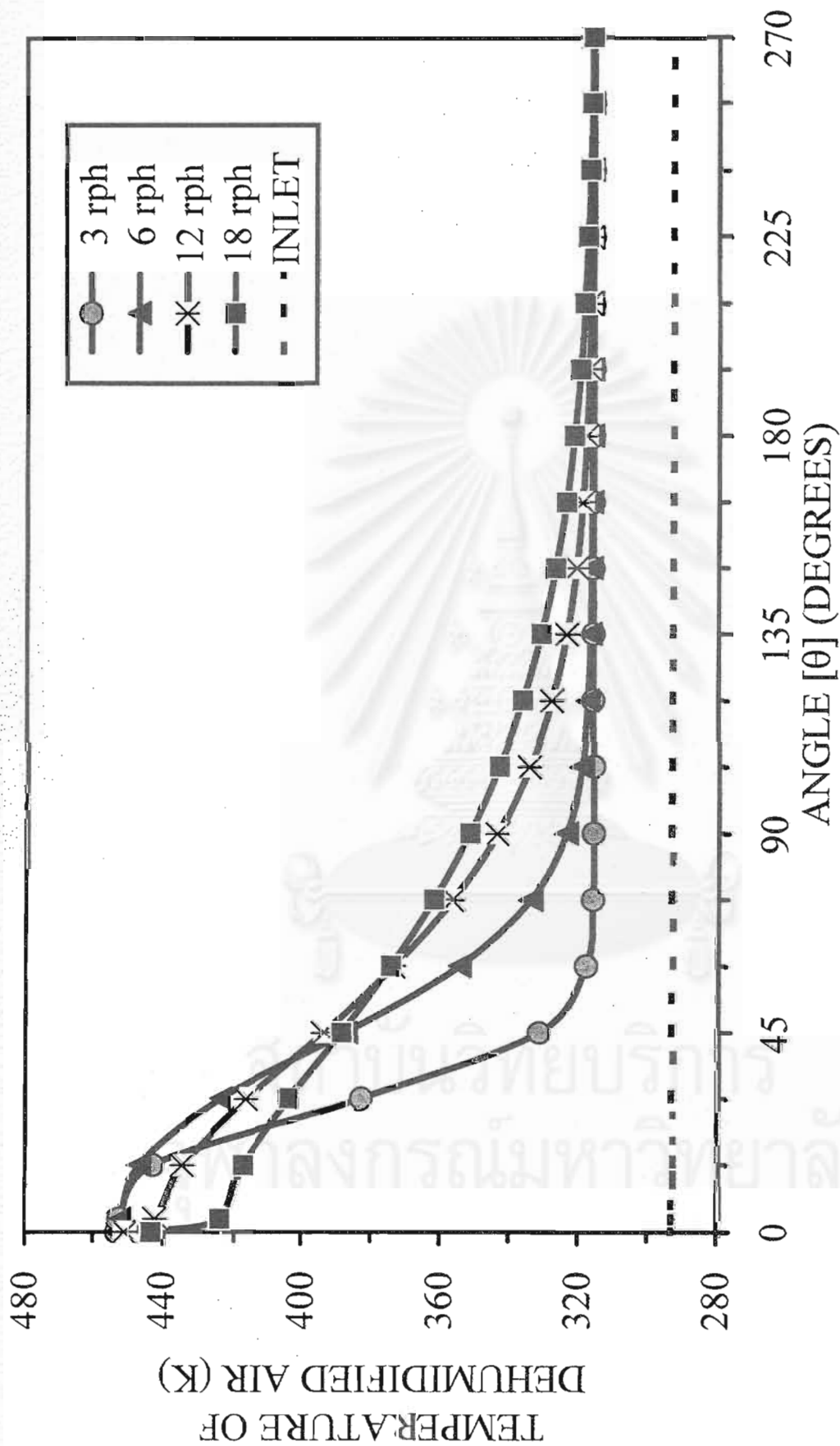
Figure 6.85 The angular distributions of the temperature of the dehumidified air from the zeolite-13X coated honeycomb rotary dehumidifier at various rotational speeds (Speed-ZE-Effect Condition)
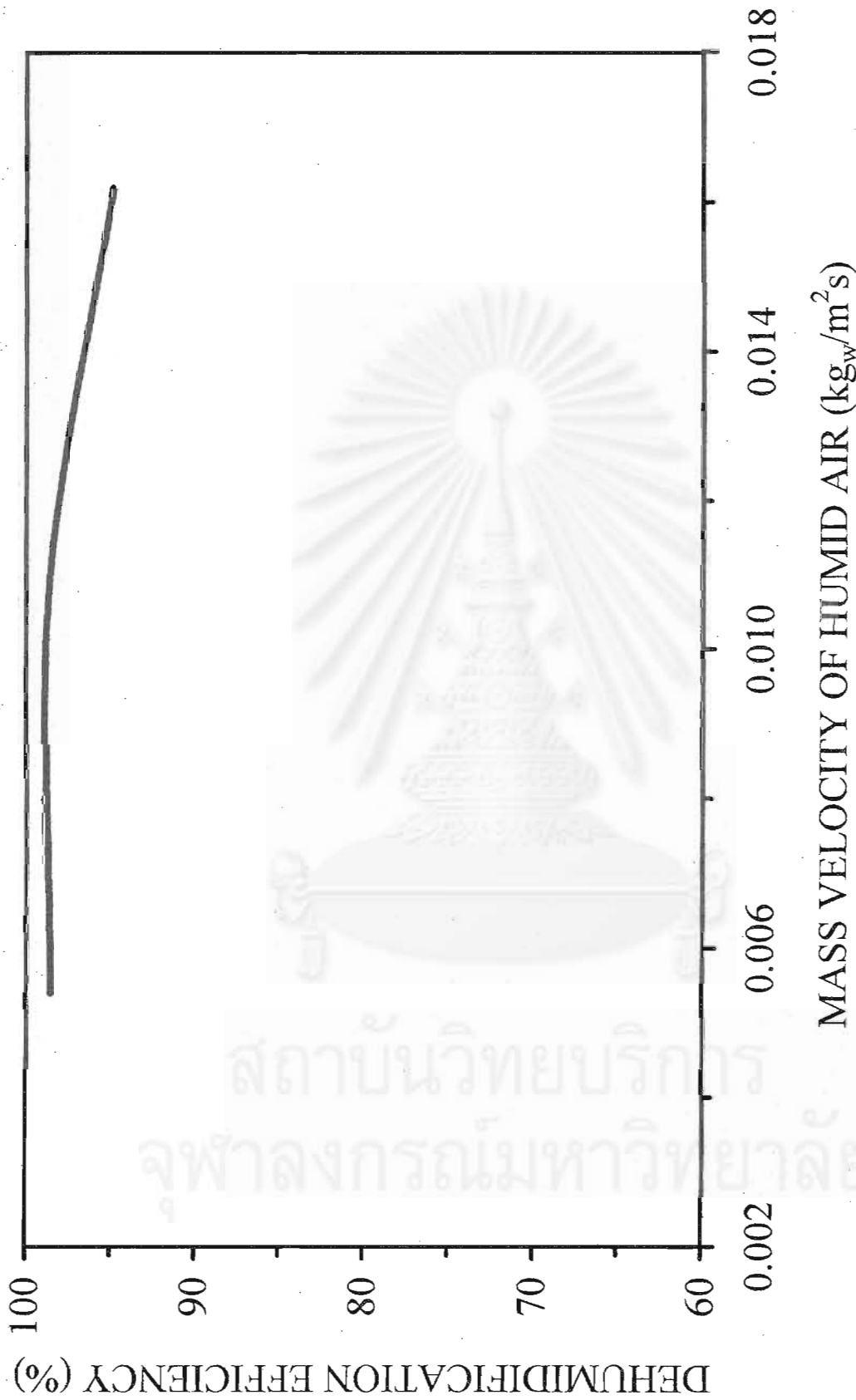
Figure 6.86 Effect of mass velocity of humid air on the dehumidification efficiency of the zeolite-13X coated honeycomb rotary dehumidifier (Gads-ZE-Effect Condition)
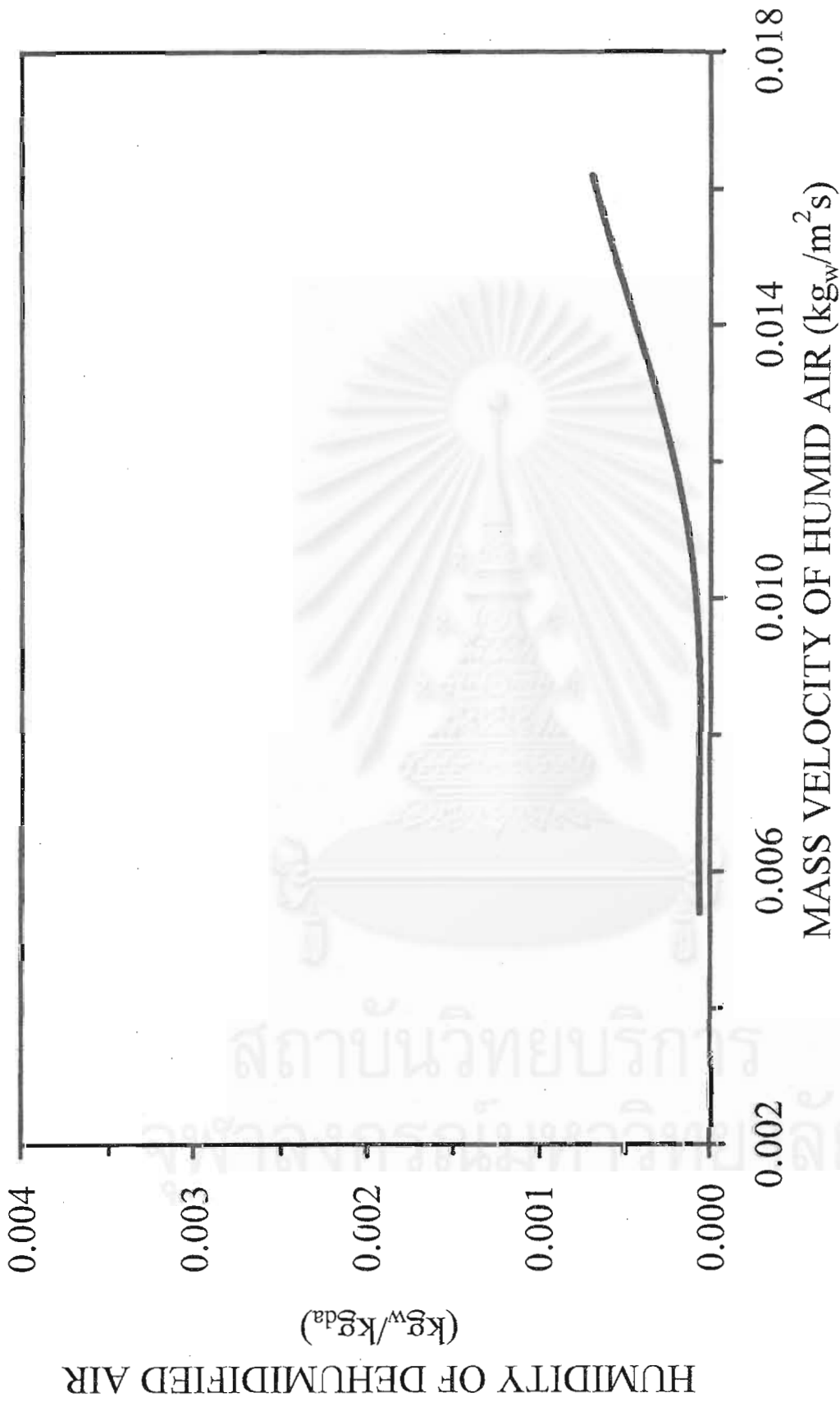
Figure 6.87 Effect of mass velocity of humid air on the average humidity of the dehumidified air from the zeolite-13X coated honeycomb rotary dehumidifier (Gads-ZE-Effect Condition)
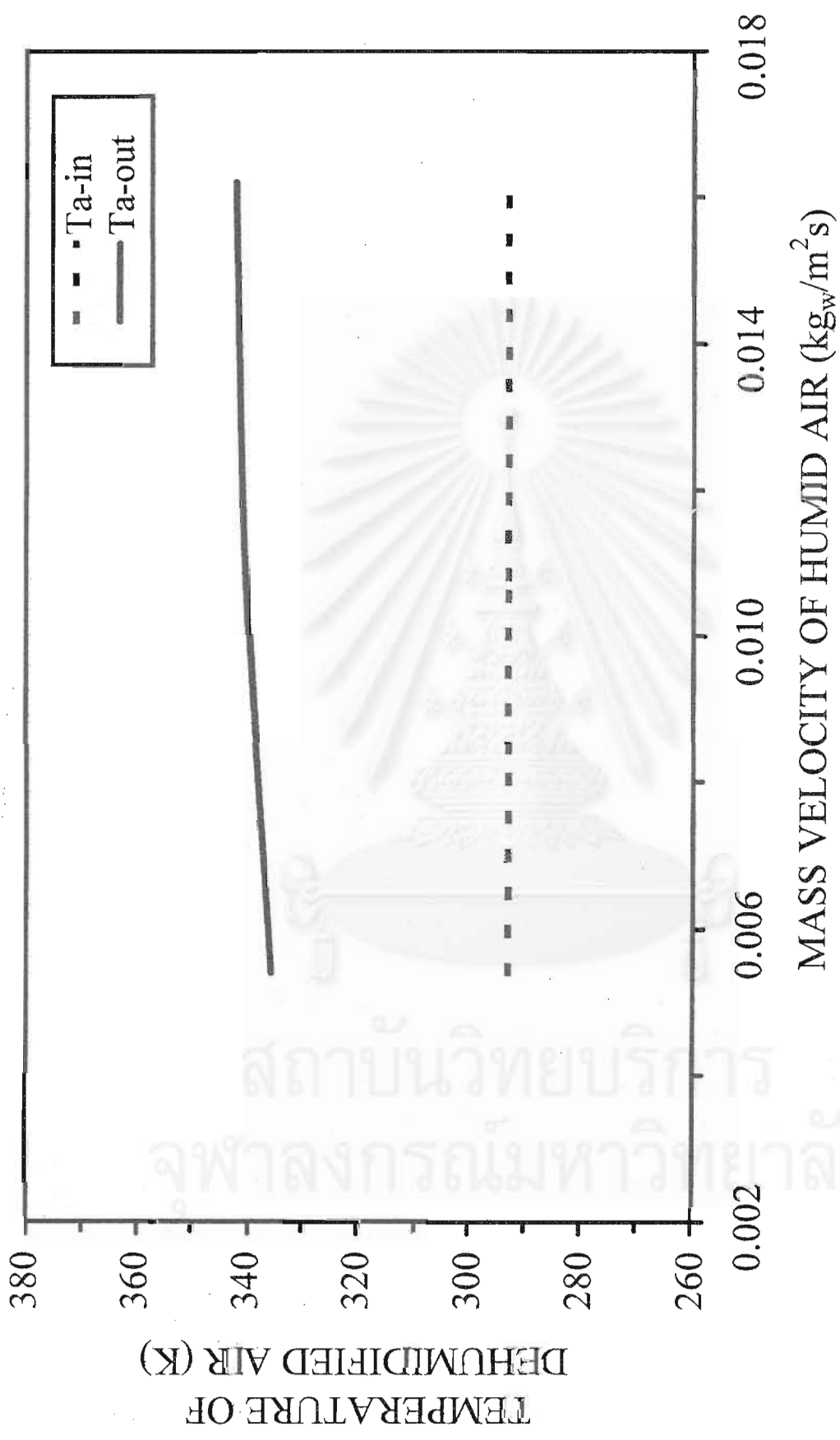
Figure 6.88 Effect of mass velocity of humid air on the average temperature of the dehumidified air from the zeolite-13X coated honeycomb rotary dehumidifier (Gads-ZE-Effect Condition)
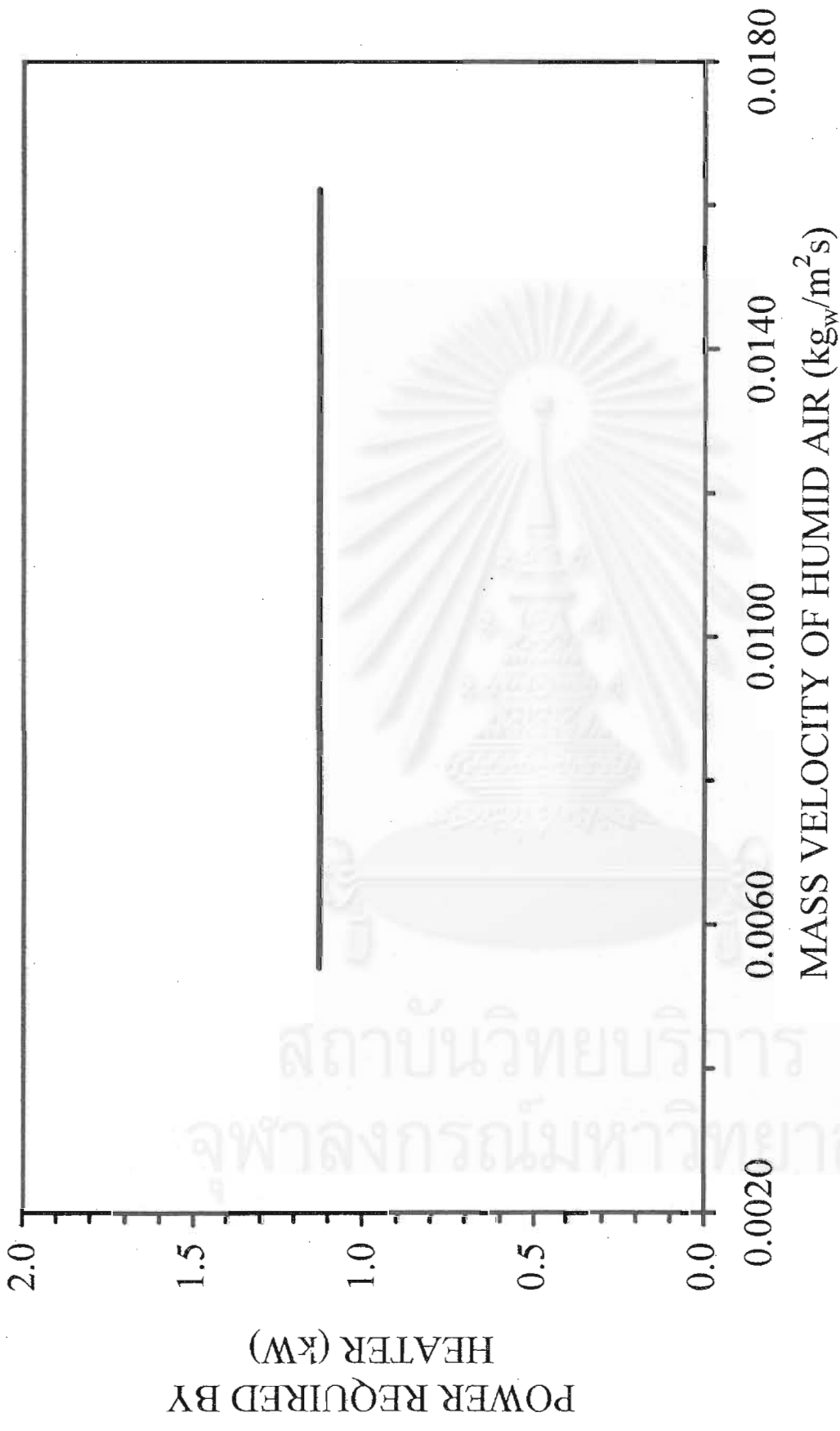
Figure 6.89 Power required by heater at various mass velocities of humid air for the zeolite-13X coated honeycomb rotary dehumidifier (Gads-ZE-Effect Condition)
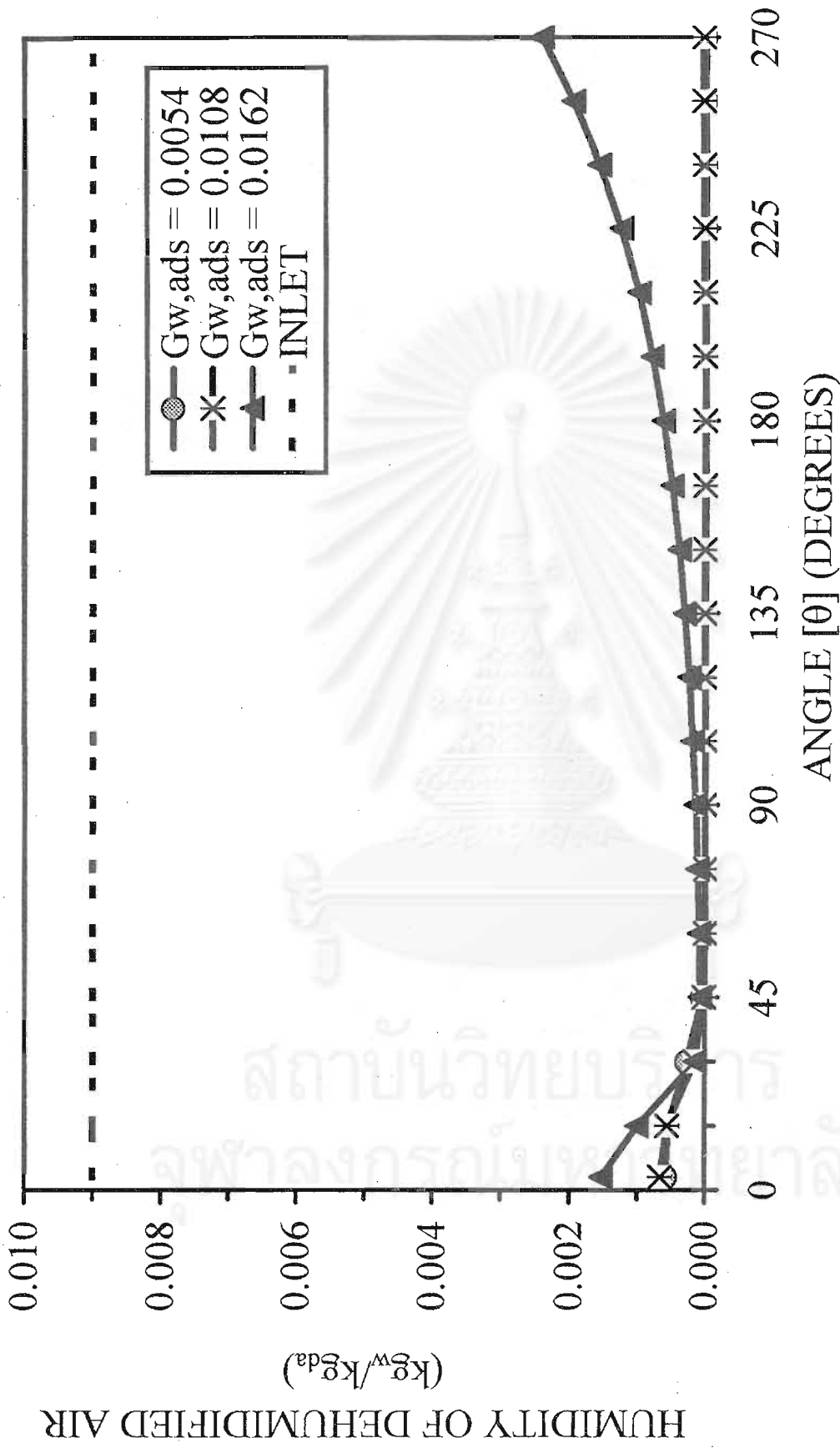
Figure 6.90 The angular distributions of the humidity of the dehumidified air from the zeolite-13X coated honeycomb rotary dehumidifier at various mass velocities of humid air (Gads-ZE-Effect Condition)
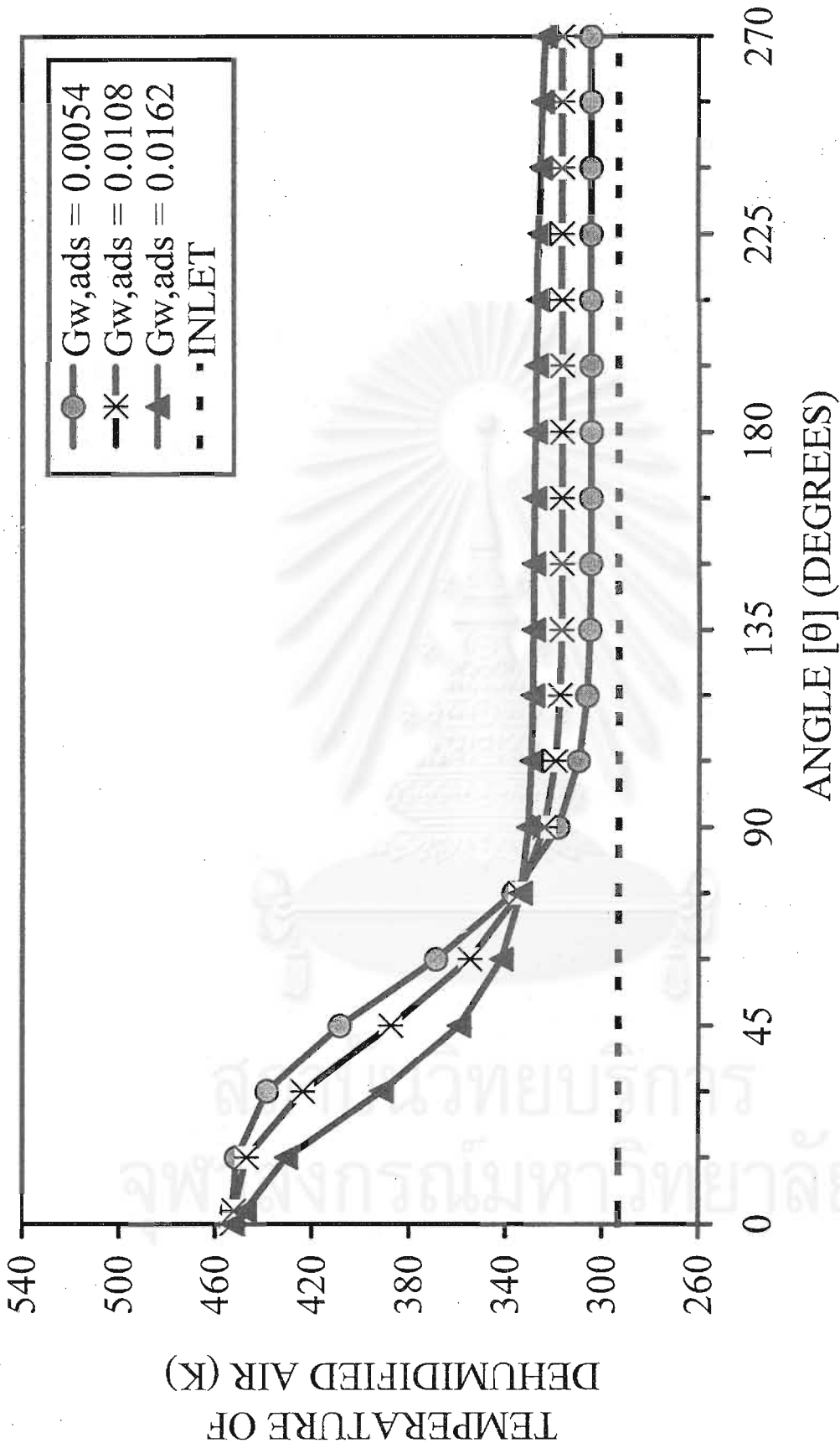
Figure 6.91 The angular distributions of the temperature of the dehumidified air from the zeolite-13X coated honeycomb rotary dehumidifier at various mass velocities of humid air (Gads-ZE-Effect Condition)
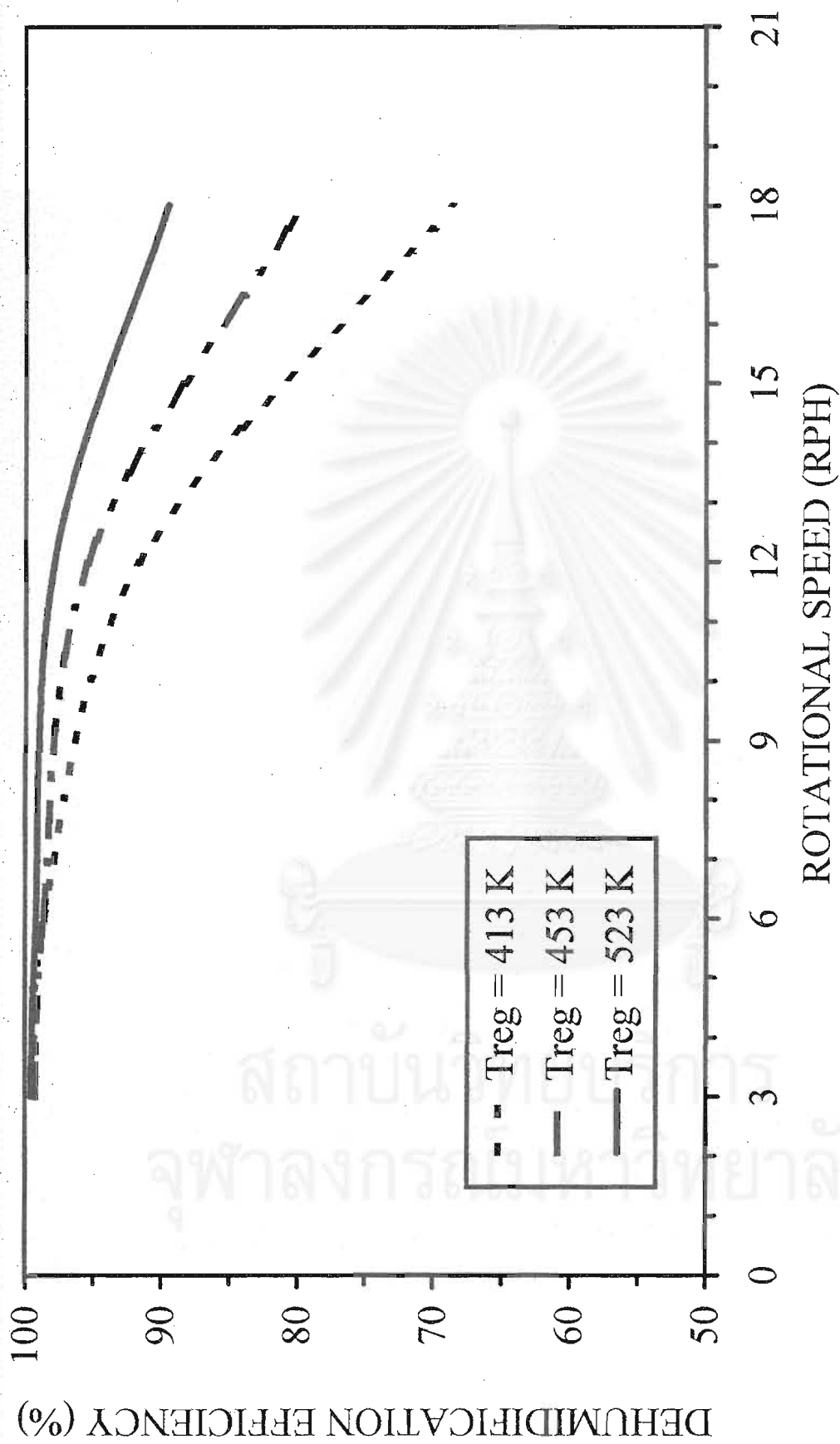
Figure 6.92 Effect of rotational speed on the dehumidification efficiency of the zeolite-13X coated honeycomb rotary dehumidifier at various regenerative temperatures
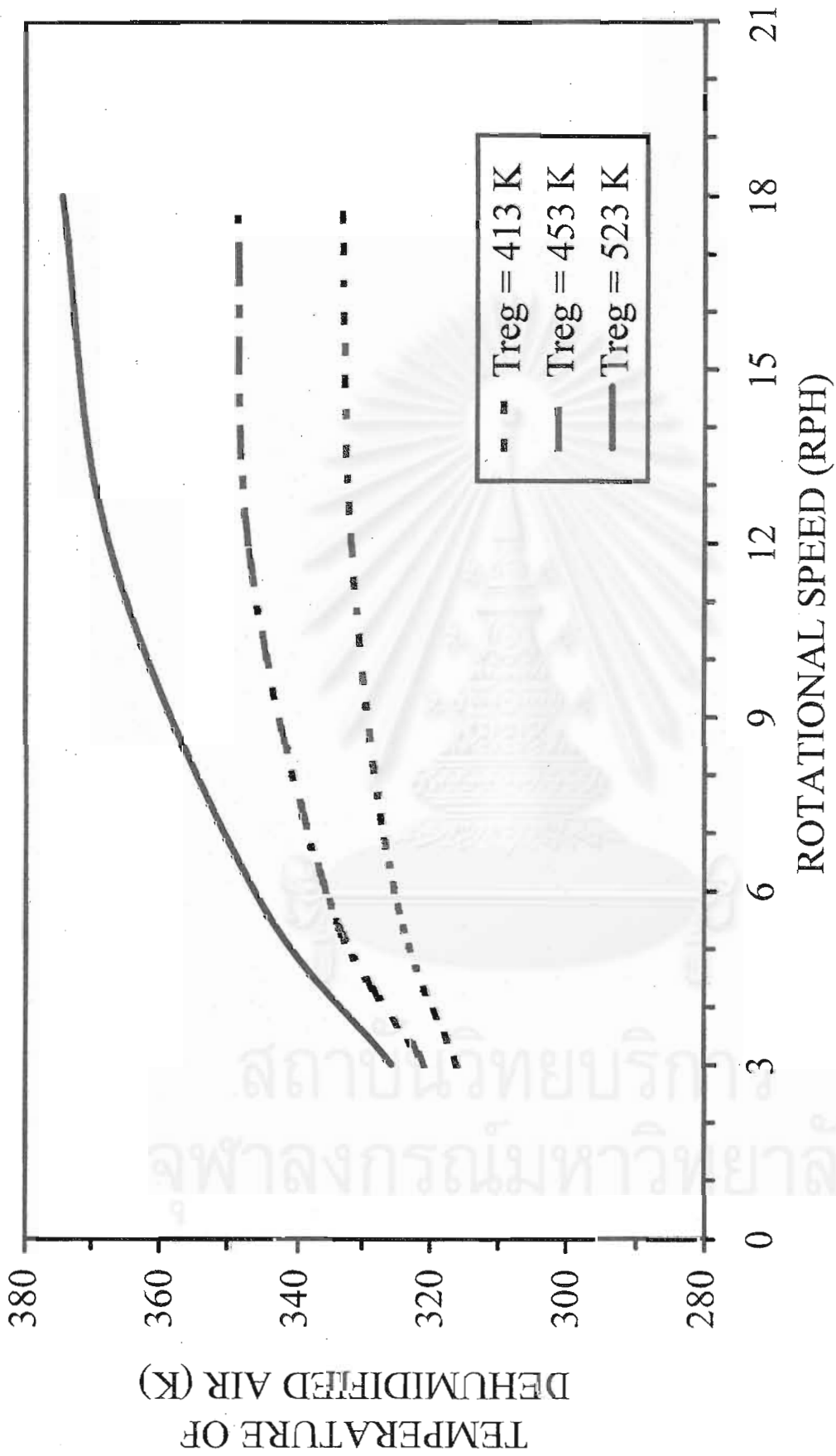
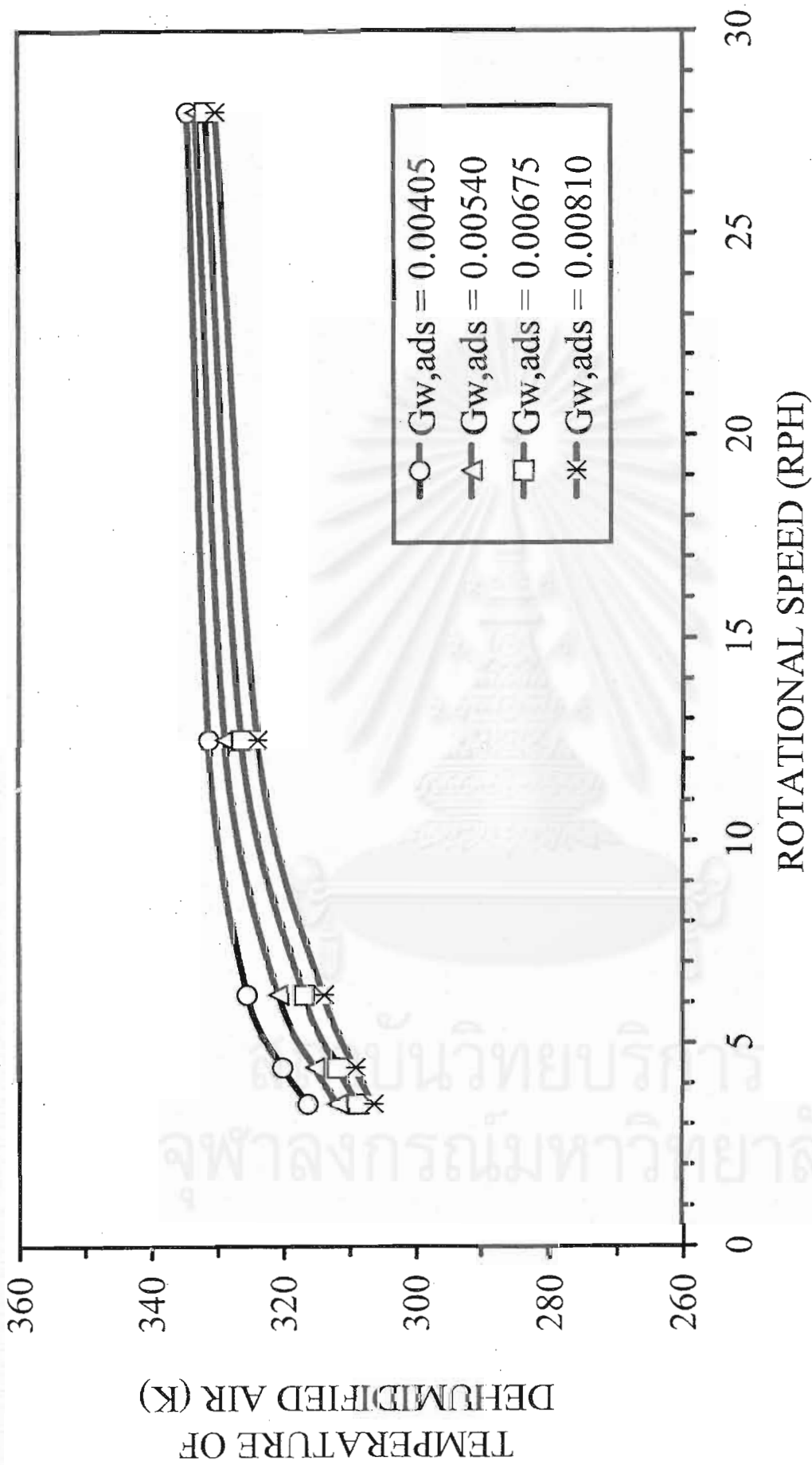**Figure 6.93** Effect of rotational speed on the average temperature of the dehumidified air from the zeolite-13X coated honeycomb rotary dehumidifier at various regenerative temperatures
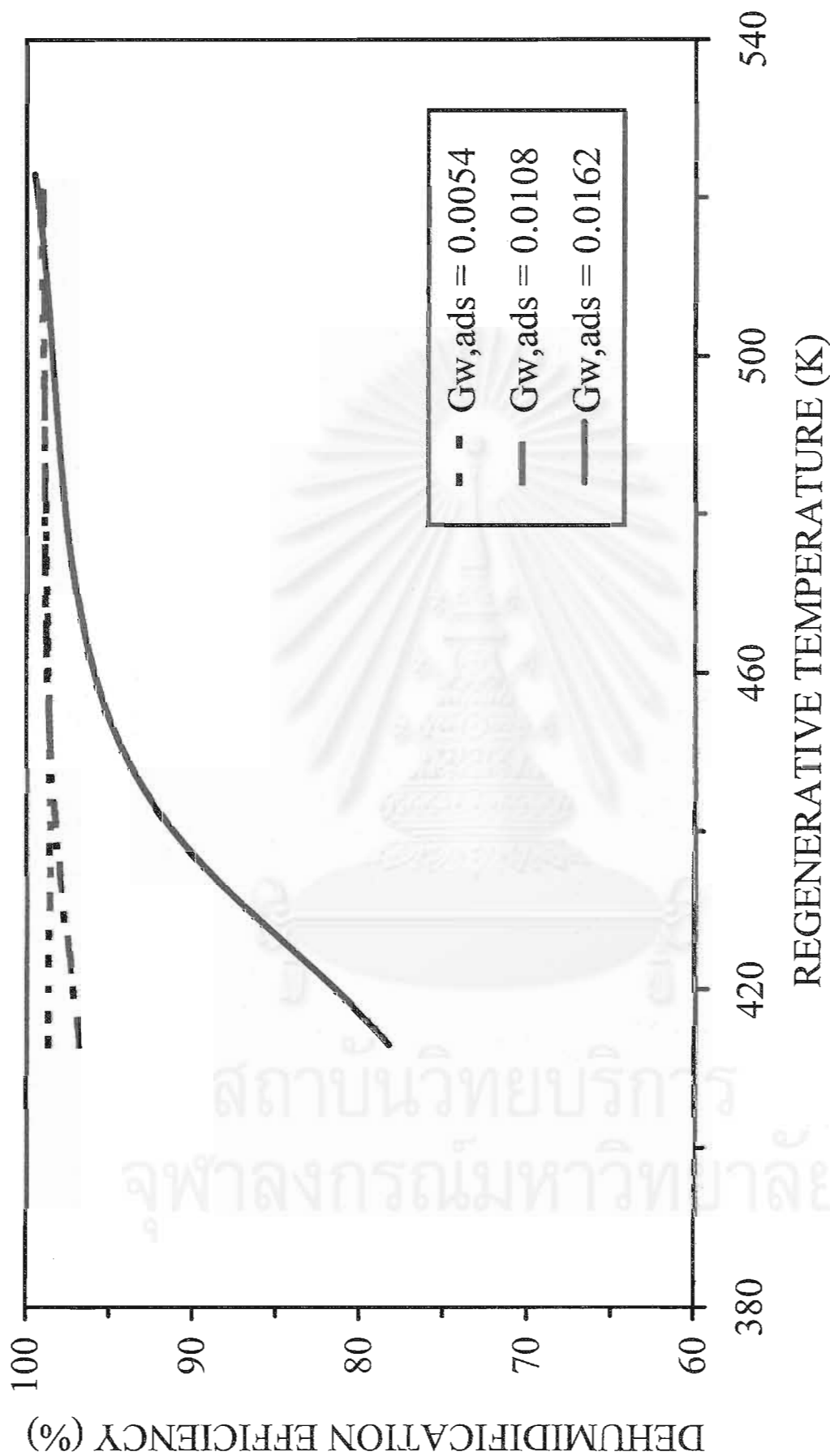
Figure 6.94 Effect of regenerative temperature on the dehumidification efficiency of the zeolite-13X coated honeycomb rotary dehumidifier at various mass velocities of humid air
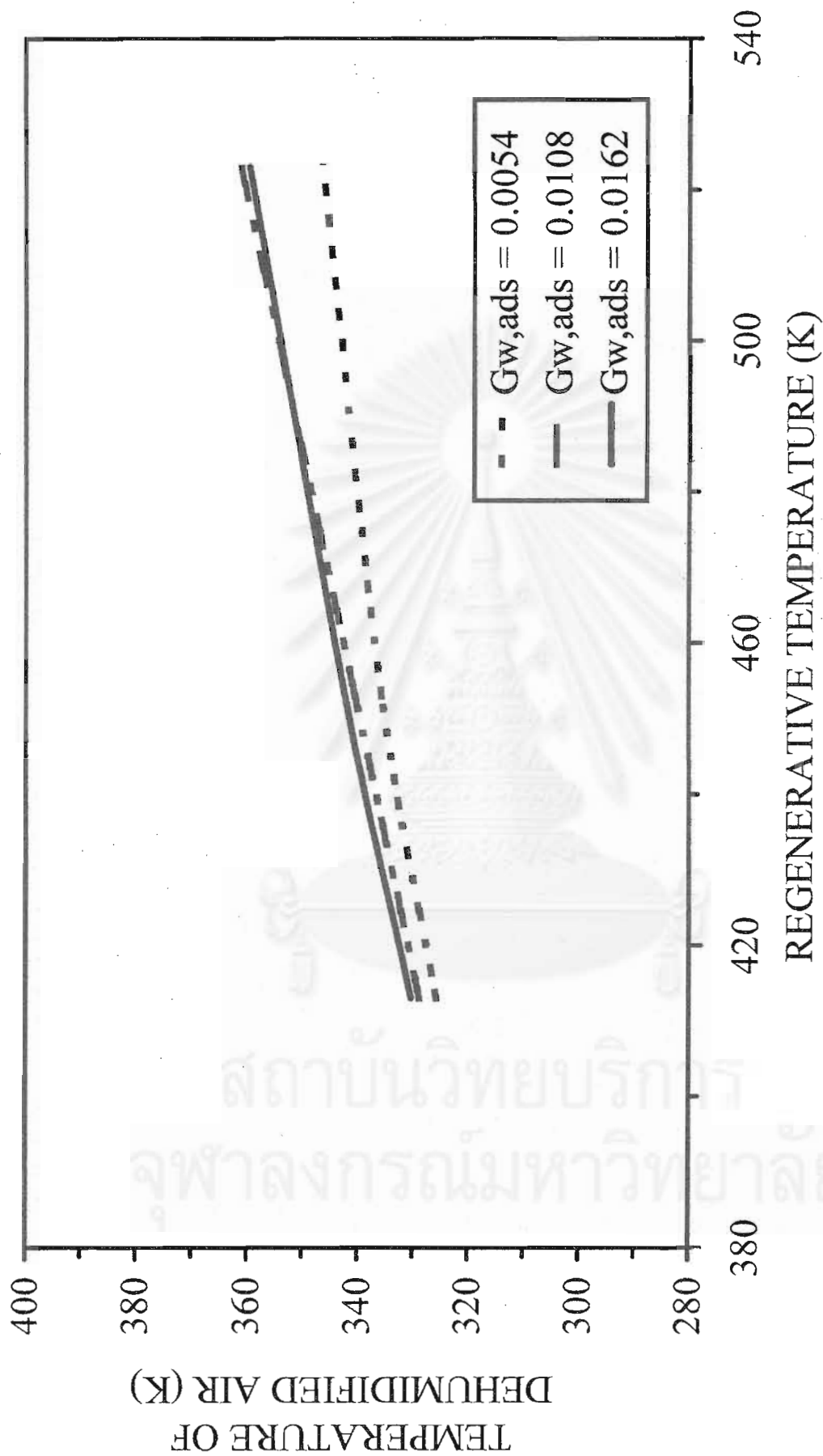
Figure 6.95 Effect of regenerative temperature on the average temperature of the dehumidified air from the zeolite-13X coated honeycomb rotary dehumidifier at various mass velocities of humid air
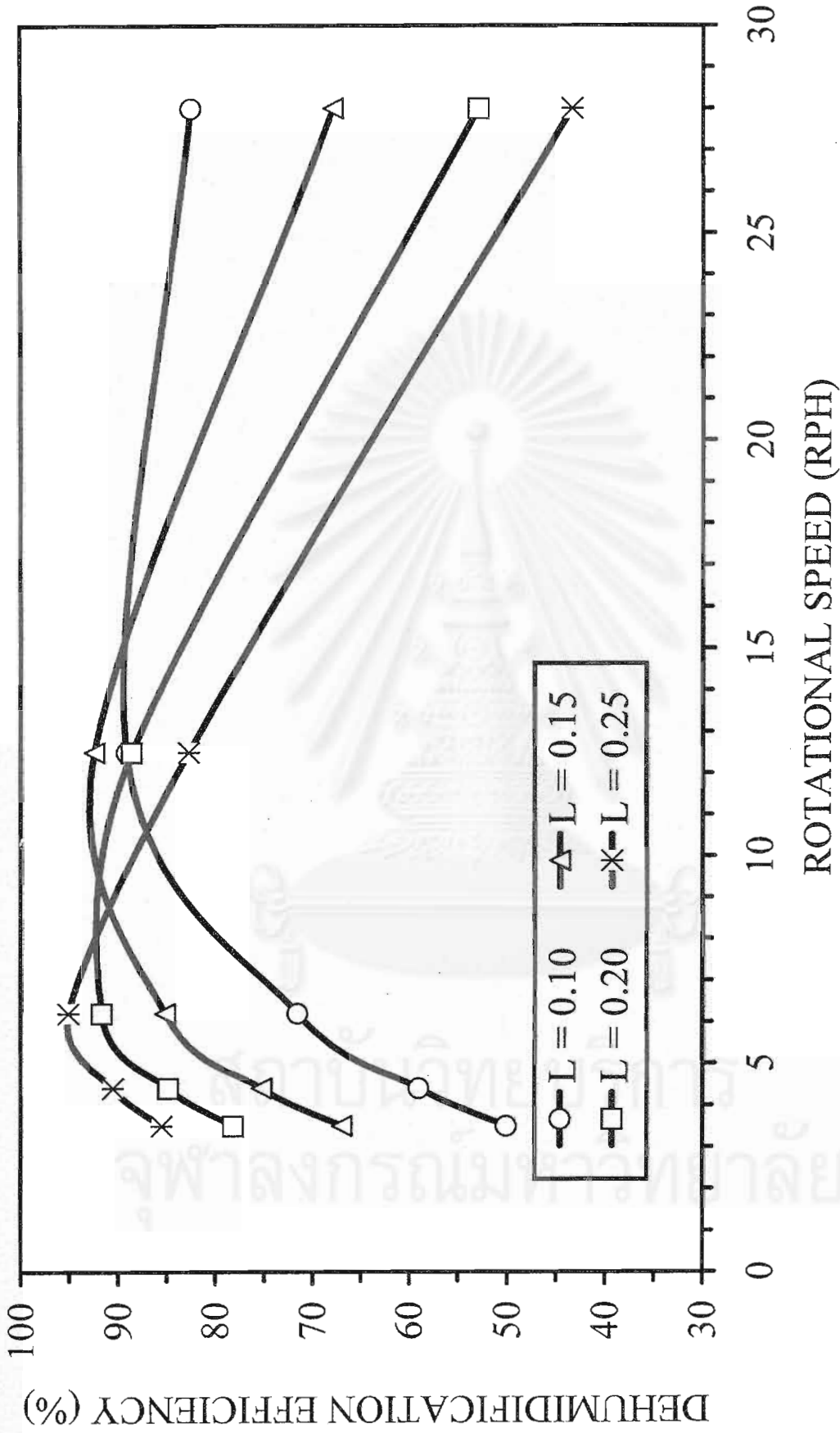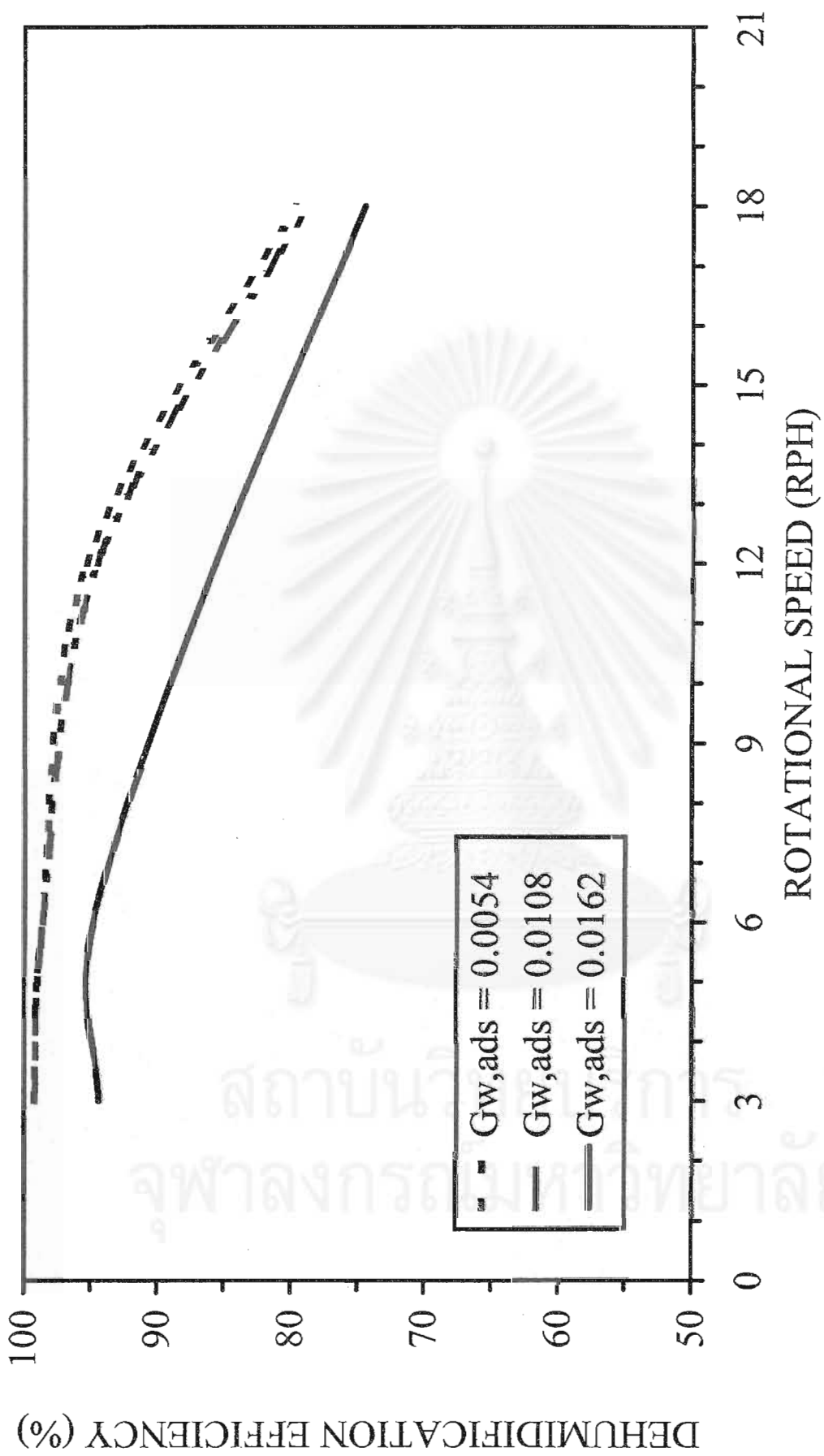
Figure 6.96 Effect of rotational speed on the dehumidification efficiency of the zeolite-13X coated honeycomb rotary dehumidifier at various mass velocities of humid air
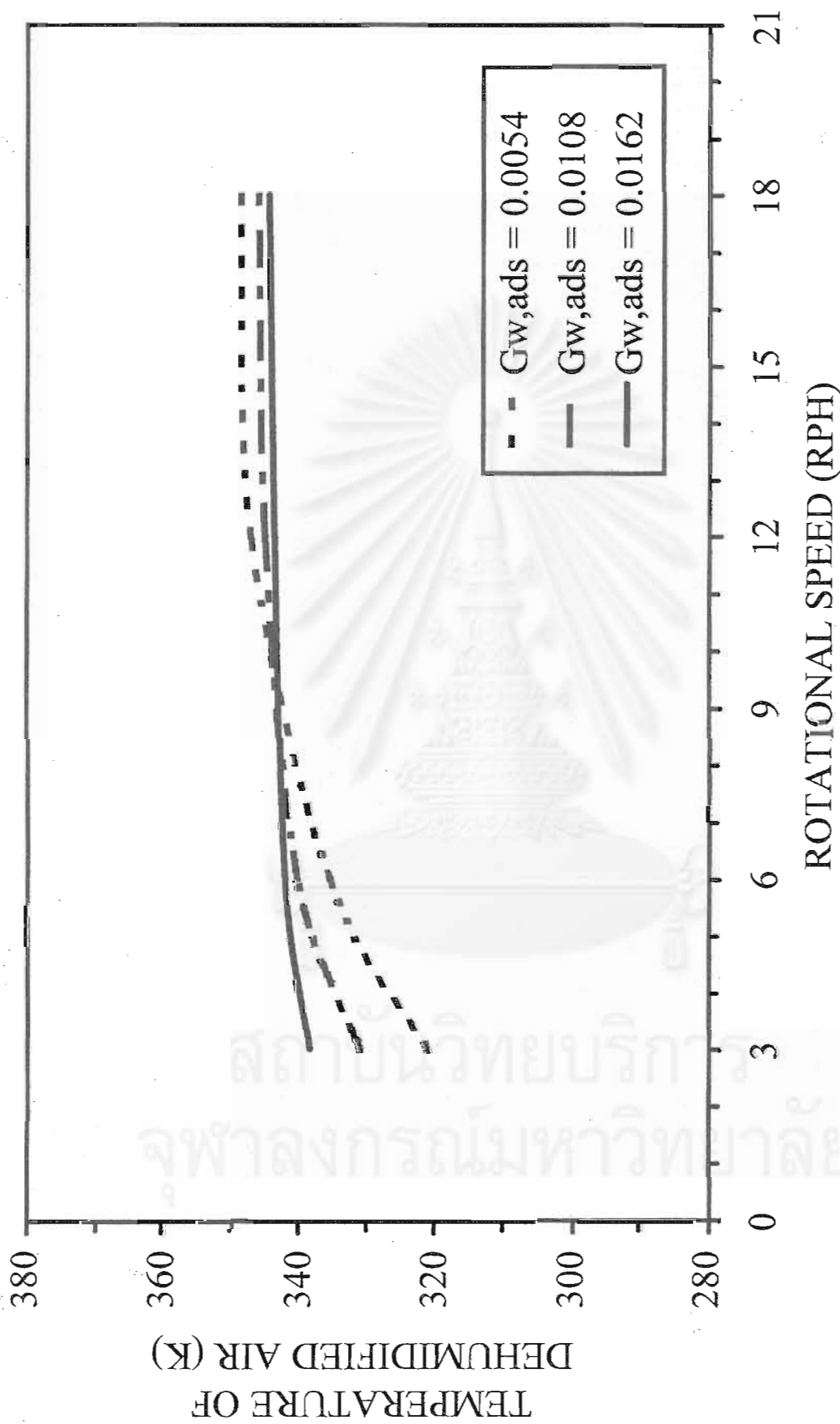
Figure 6.97 Effect of rotational speed on the average temperature of the dehumidified air from the zeolite-13X coated honeycomb rotary dehumidifier at various mass velocities of humid air
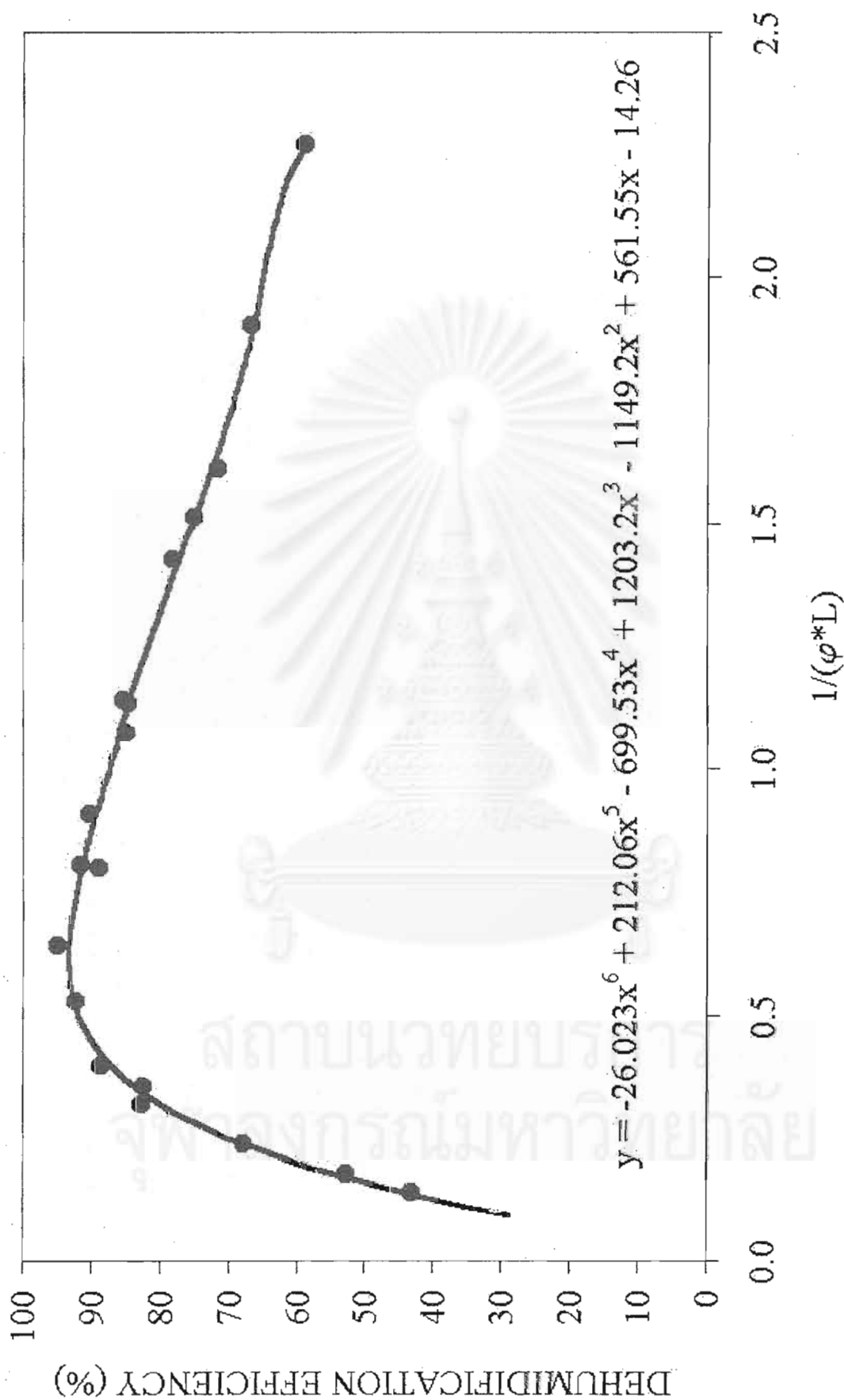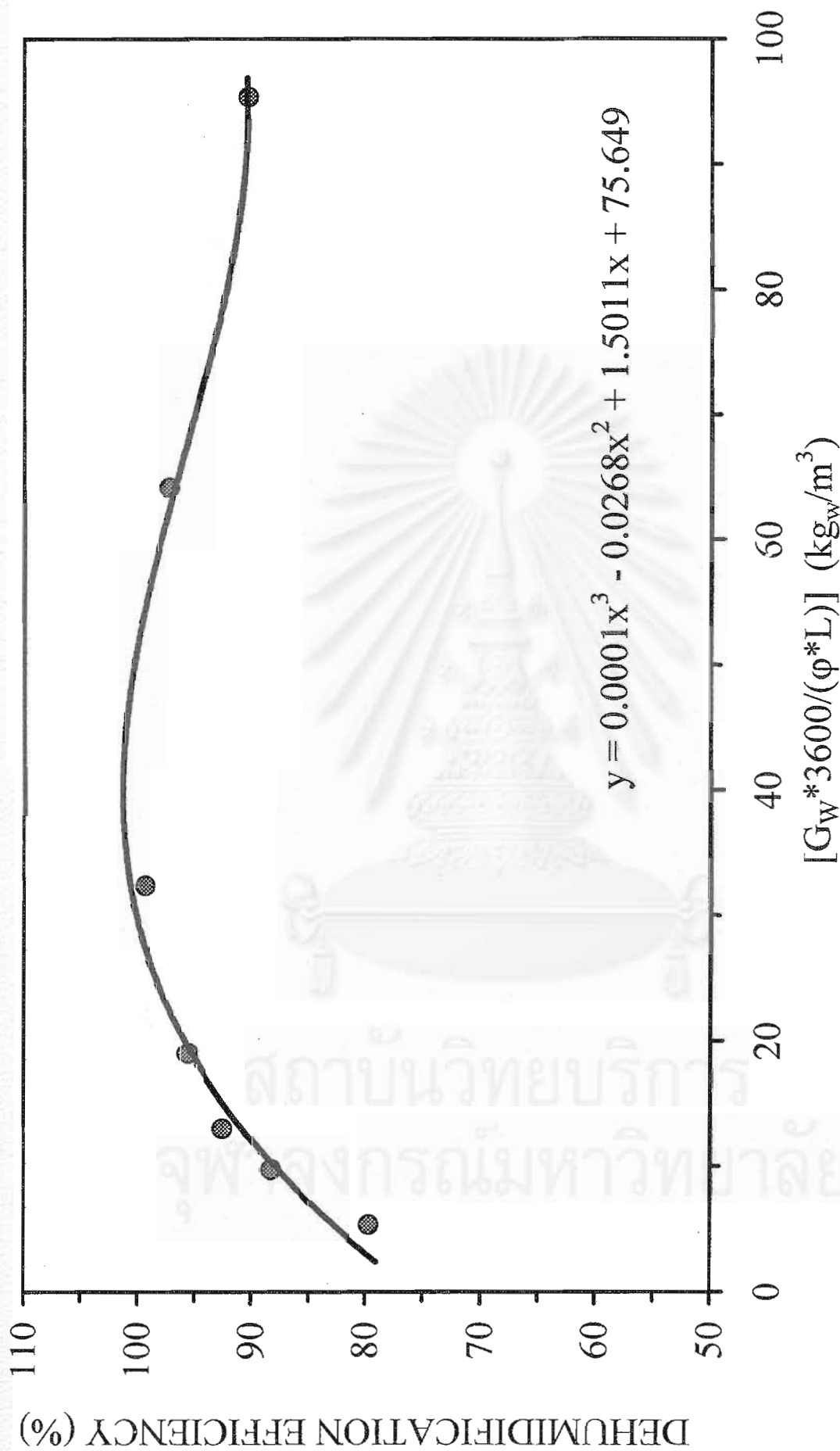
Figure 6.98 The correlation of ($G_w/(L \cdot \varphi)$) and the dehumidification efficiency for the zeolite-13X coated honeycomb rotary dehumidifier

6.4 Comparison of the performance of the silica gel, zeolite-13X and lithium chloride coated honeycomb rotor used in the dynamic dehumidification system

In commercial building and even residential unit, a rotary dehumidifier is used to dehumidify the humid room air continuously in the closed process room. Accordingly, the dynamic behavior of the sorbent-coated rotary dehumidifier has been investigated. In this section, the ambient conditions and the size of the room in a well-known beverage factory in Thailand (Prawarnpit, 1997) are necessary. Then the dehumidification performance of both of the silica gel and zeolite-13X coated honeycomb rotary dehumidifier are compared with the case of lithium chloride, which has been investigated by Tanthapanickoon and Prawarnpit (2000), under normal and rain condition.

The operating conditions for each rotor are listed in Table 6.11. Parameters and properties of the rotary dehumidifier and the closed process room used in the dynamic dehumidification system as well as the initial condition are presented in Table 6.12 and 6.13, respectively.

Table 6.11 Operating conditions of the silica gel and zeolite-13X coated honeycomb rotary dehumidifier used in the dynamic dehumidification system.

CASE	ROTATIONAL SPEED (RPH)	REGEN. TEMPERAUTE (K)	VELOCITY OF HUMID AIR (m/s)	VELOCITY OF HOT AIR (m/s)	FILE NAME (filename.dat)
SG-Normal	12	393	1.0	0.5	SG-Normal -Case
ZE-Normal	12	453	1.0	0.5	ZE-Normal -Case
SG-Rain	12	393	1.0	0.5	SG-Rain -Case
ZE-Rain	12	453	1.0	0.5	ZE-Rain -Case

Table 6.12 Parameters and properties of the rotary dehumidifier and the humid room used in the dynamic dehumidification system

SIZE OF THE ROOM WITH WET FLOOR		
Length of the room	7.50	m
Cross sectional area of the room	36.0	m^2
Surface area of the room	45.0	m^2
SIZE OF THE ROTARY DEHUMIDIFIER		
Length of rotor (L)	0.10	m
Cross sectional area of a slot (A_c)	2.90 x10^{-6}	m^2
Cross sectional area of the gas phase in a slot (A_g)	2.26 x10^{-6}	m^2
Cross sectional area of solid phase (A_{ss})	6.38 x10^{-7}	m^2
Hydraulic diameter of a slot	1.67 x10^{-3}	m
PROPERTIES OF HONEYCOMB ROTOR		
Specific heat of silica gel (Cp_{sb})	0.92	kJ/(kg$_{da}$·K)
Specific heat of zeolite-13X (Cp_{sb})	1.05	kJ/(kg$_{da}$·K)
Specific heat of water (Cp_w)	4.187	kJ/(kg$_{da}$·K)
Specific heat of ceramic fiber (Cp_{sh})	1.20	kJ/(kg$_{da}$·K)
Bulk density of rotor (ρ_{sb})	250	kg/m^3
Density of ceramic fiber (ρ_{sh})	185	kg/m^3
Mass fraction of adsorbent	0.70	(-)
Specific surface area of the honeycomb (*a*)	3000	m^2/m^3
Void fraction of the honeycomb (ε)	0.78	(-)
PROPERTIES OF HUMID AIR		
Specific heat of dry air (Cp_{da})	1.005	kJ/(kg$_{da}$·K)
Specific heat of water vapor (Cp_v)	1.820	kJ/(kg$_{da}$·K)
Latent heat of vaporization at 273 K (λ_0)	2501.3	kJ/(kg$_{da}$·K)
SIMULATION PARAMETERS		
The number of cells in each slot (N_{cell})	10	cell
Total number of slots (M_{slot})	120	slot
Number of slots for the adsorption zone (M_{ads})	90	slot
Number of slots for the regeneration zone (M_{reg})	30	slot
Step size (Δt) of integration	0.006	sec
Display time interval	900	sec
Final simulation time (t_f)	57600	sec

Table 6.13 Initial conditions for the dynamic dehumidification system

INITIAL CONDITIONS FOR THE ROOM		
Average amount of water on the floor (W_{0r})	0.46	kg_w/m^2
Average humidity in the room (H_{0r})	0.022	kg_w/kg_{da}
Temperature on the floor (Tw_{0r})	300.15	K
Gas temperature in the room (Ta_{0r})	301.15	K
Equilibrium water on the floor (W_{Er})	0.001	kg_w/m^2
Critical water on the floor (W_{Cr})	0.1	kg_w/m^2
Air velocity in the room (V_r)	0.06	m/s
INITIAL CONDITIONS FOR ROTARY DEHUMIDIFIER		
Local amount of moisture adsorbed in the adsorbent (W_0)	0.23	kg_w/kg_{sb}
Local air humidity in the slots (H_0)	0.022	kg_w/kg_{da}
Local solid temperature in the slots(Ts_0)	303.15	K
Local gas temperature in the slots (Ta_0)	302.15	K

Inlet air humidity and temperature at any time for normal and rain conditions (Prawarnpit, 1997) are illustrated in Figure 6.99 and 6.100, respectively.
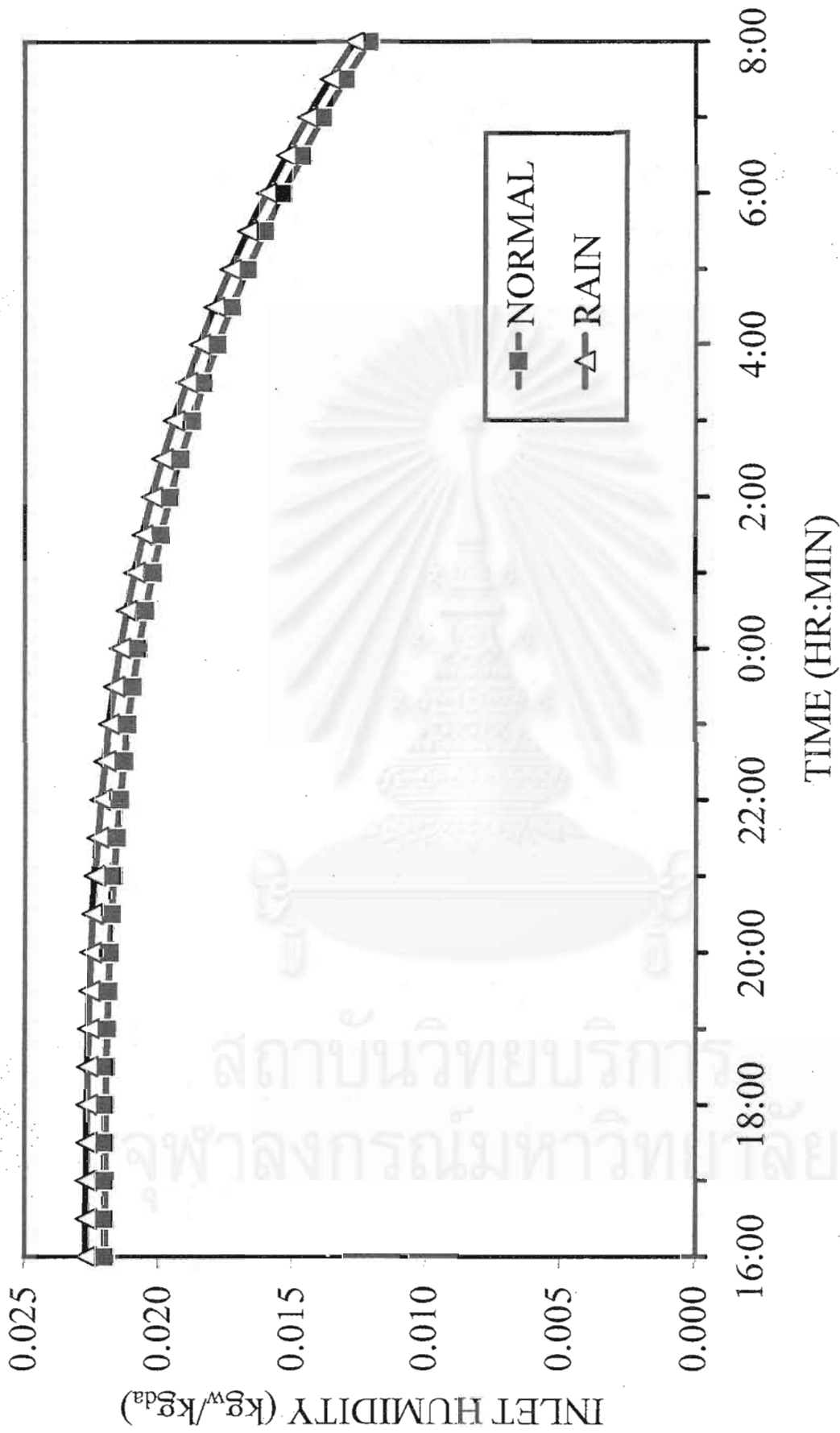
Figure 6.99 Relationship between the humidity of the ambient air vs. time for normal and rain conditions
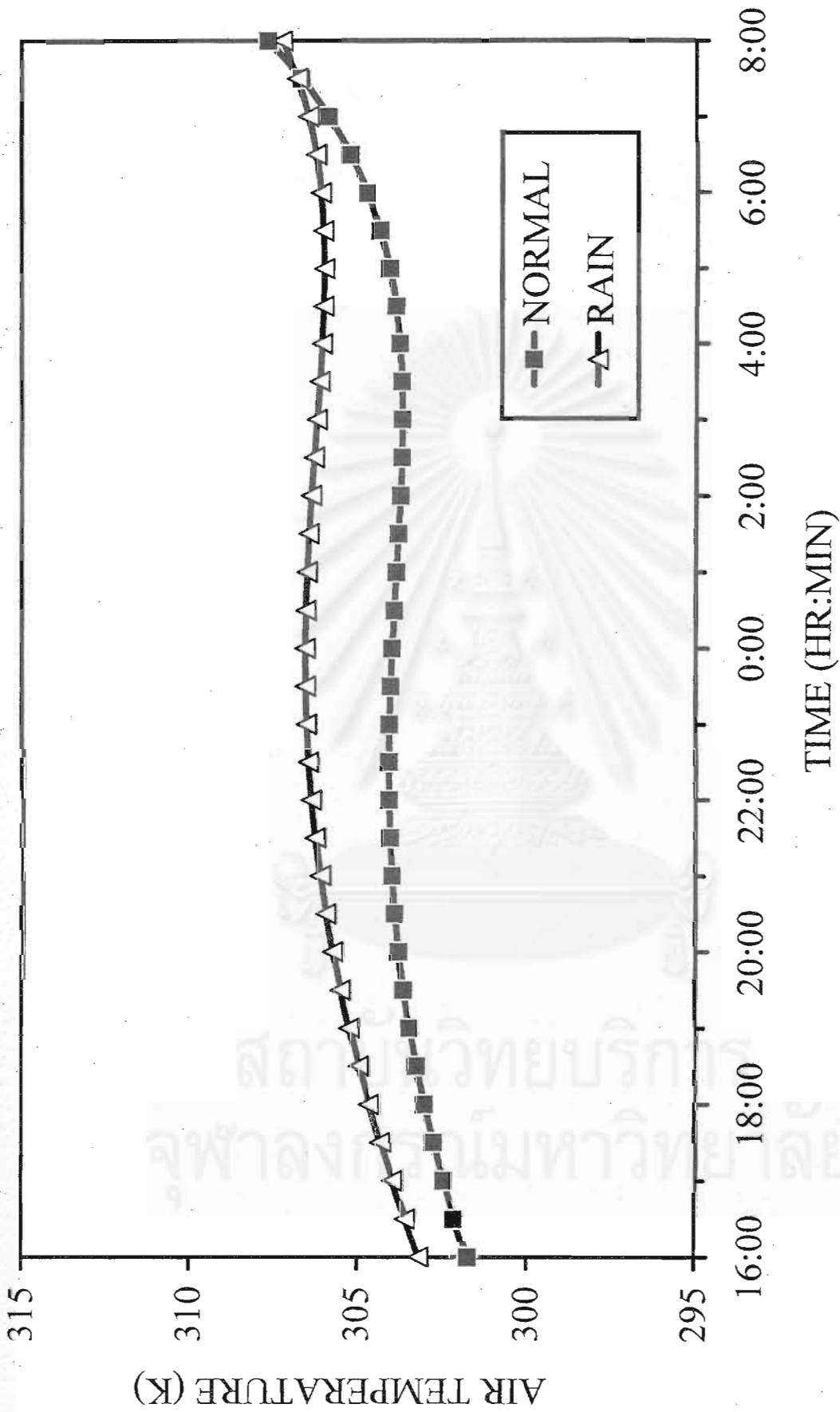
Figure 6.100 Relationship between the temperature of the ambient air vs. time for normal and rain conditions

From Figure 6.101, as time increases, the dehumidified air humidity gradually decreases until the floor becomes dry, and it then drops faster since the air humidity in room is lesser. Among the investigated honeycomb rotors, the zeolite-13X coated honeycomb rotary dehumidifier give the highest efficiency because of its very large adsorptive capacity. Since the temperature of hot air used for the regeneration of the zeolite-13X rotor is very high, say, 453 K, high temperature is observed in the early region of adsorption zone, $\theta \approx 0°$-$60°$. Consequently, the average temperature of the dehumidified air from the zeolite-13X rotor is the highest as shown in Figure 6.102. Similarly, as time increase, the humidity of the room air gradually decreases until the floor becomes dry. Then the profiles are rapidly drop as shown in Figure 6.103 and 6.104.

In Figure 6.105, it is seen that the water on the wet concrete floor linearly decreases until the floor becomes dry. The zeolite-13X coated rotary dehumidifier can quickly dry out the wet floor in the room within 3 hr while the silica gel and lithium chloride rotors require 6 and 10 hr, respectively. Since the optimal regeneration temperature in the case of zeolite-13X adsorption is the highest, the heater in this case consumes the highest power compared with the cases of silica gel and lithium chloride as seen in Figure 6.106. On the other hand, the times that the wet floor becomes completely dry are at 19.00 p.m., 22.00 p.m. and 2.00 a.m. for the zeolite-13X, silica gel and lithium chloride rotor, respectively. As the results, the minimum total energy consumption by the heater are 9800 kJ, 12100 kJ and 13670 kJ for the zeolite-13X, silica gel and lithium chloride rotor, respectively, as seen in Figure 6.103.

Figures 6.108 to 6.111 show the effect of ambient condition, i.e. normal and rain conditions on the dehumidification performance of the various honeycombs. It is seen that the rotary dehumidifiers used under the rain condition dry the wet floor in the process room slower than the normal condition approximately 30 minutes. However, the humidity and temperature profiles of the dehumidified air in both conditions are similar.
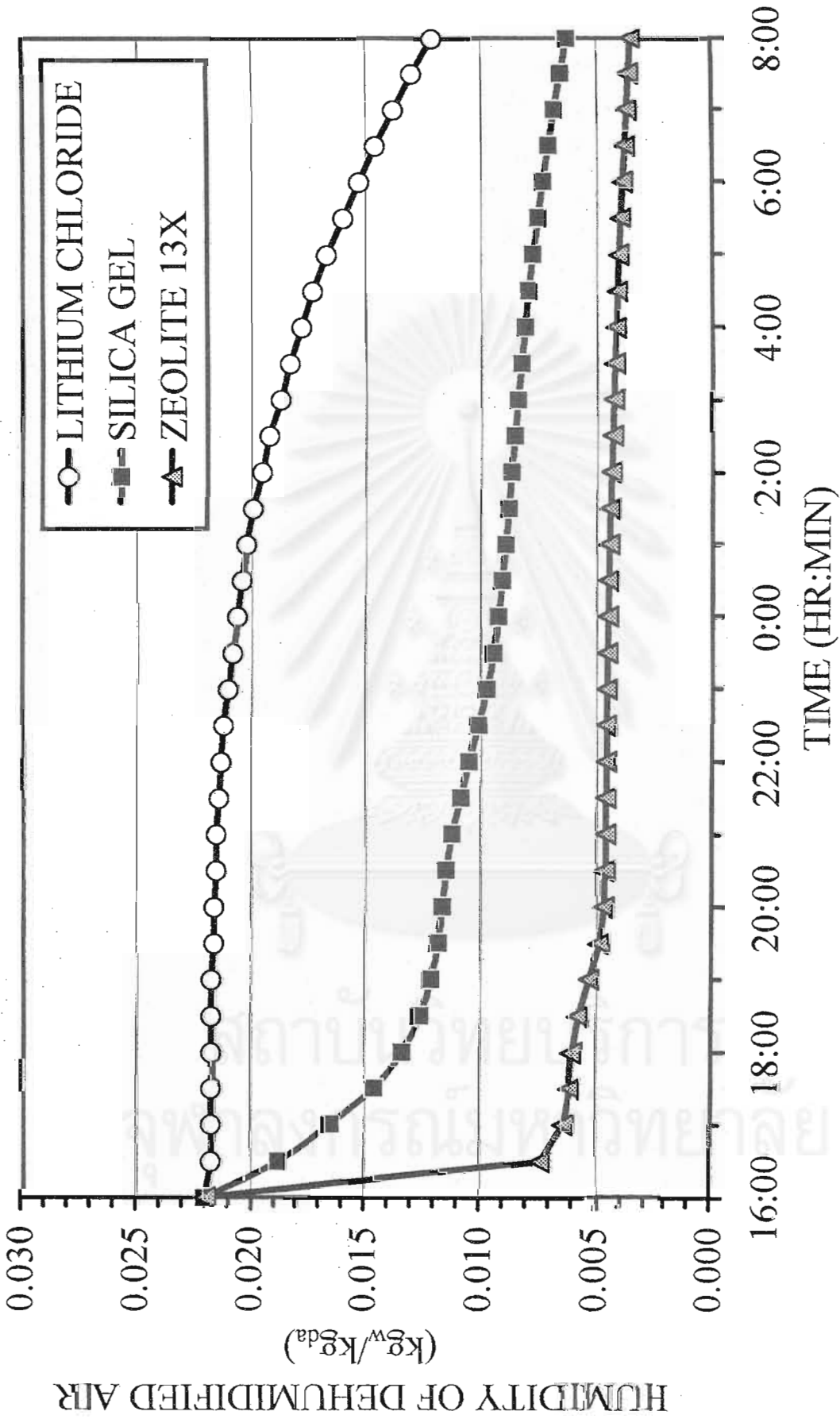
Figure 6.101 Relationship between the humidity of the dehumidified air vs. time for various rotary dehumidifiers
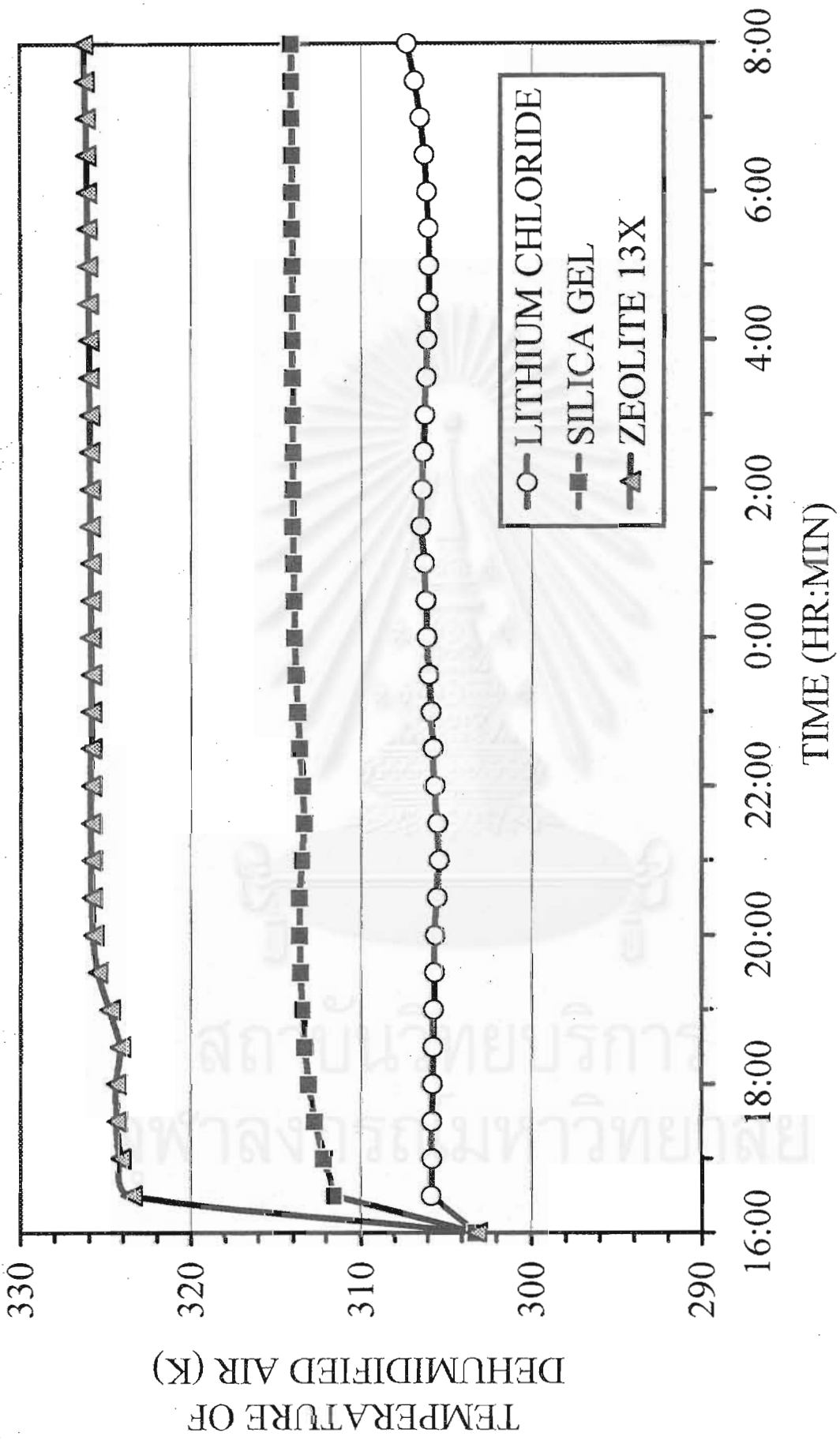
Figure 6.102 Relationship between the temperature of the dehumidified air vs. time for various rotary dehumidifiers
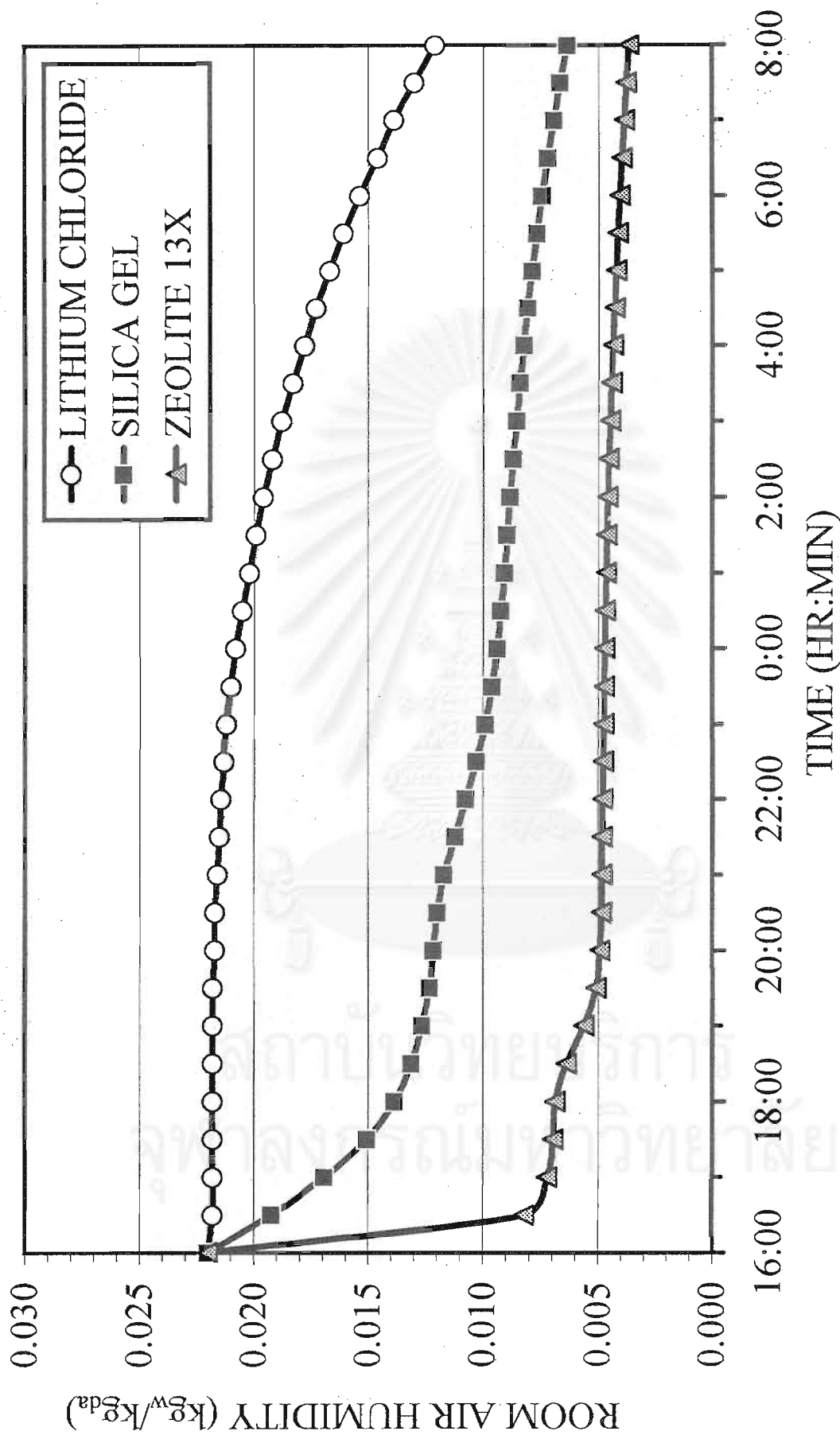
Figure 6.103 Relationship between the humidity of the room air vs. time for various rotary dehumidifiers
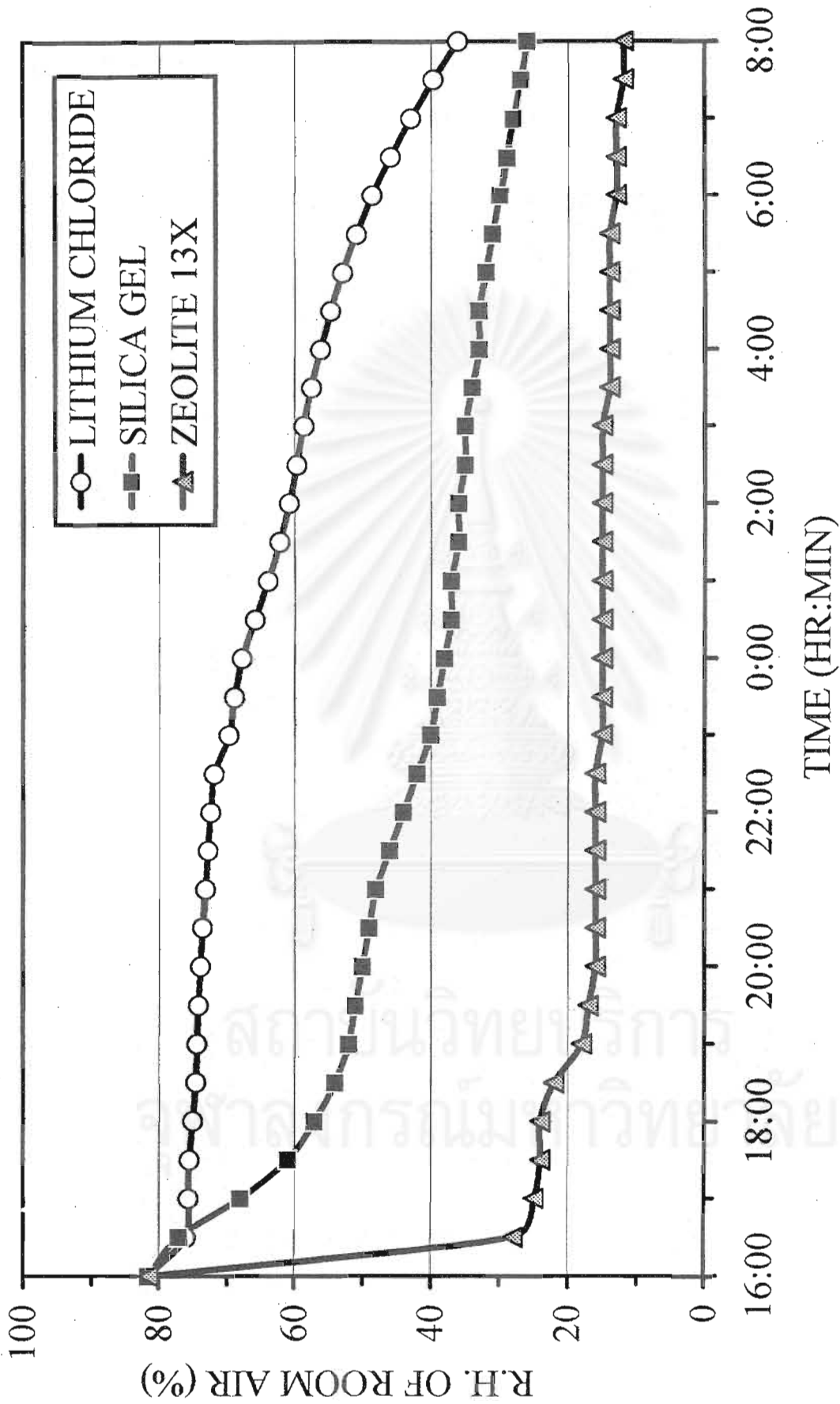
Figure 6.104 Relationship between the relative humidity of the room air vs. time for various rotary dehumidifiers
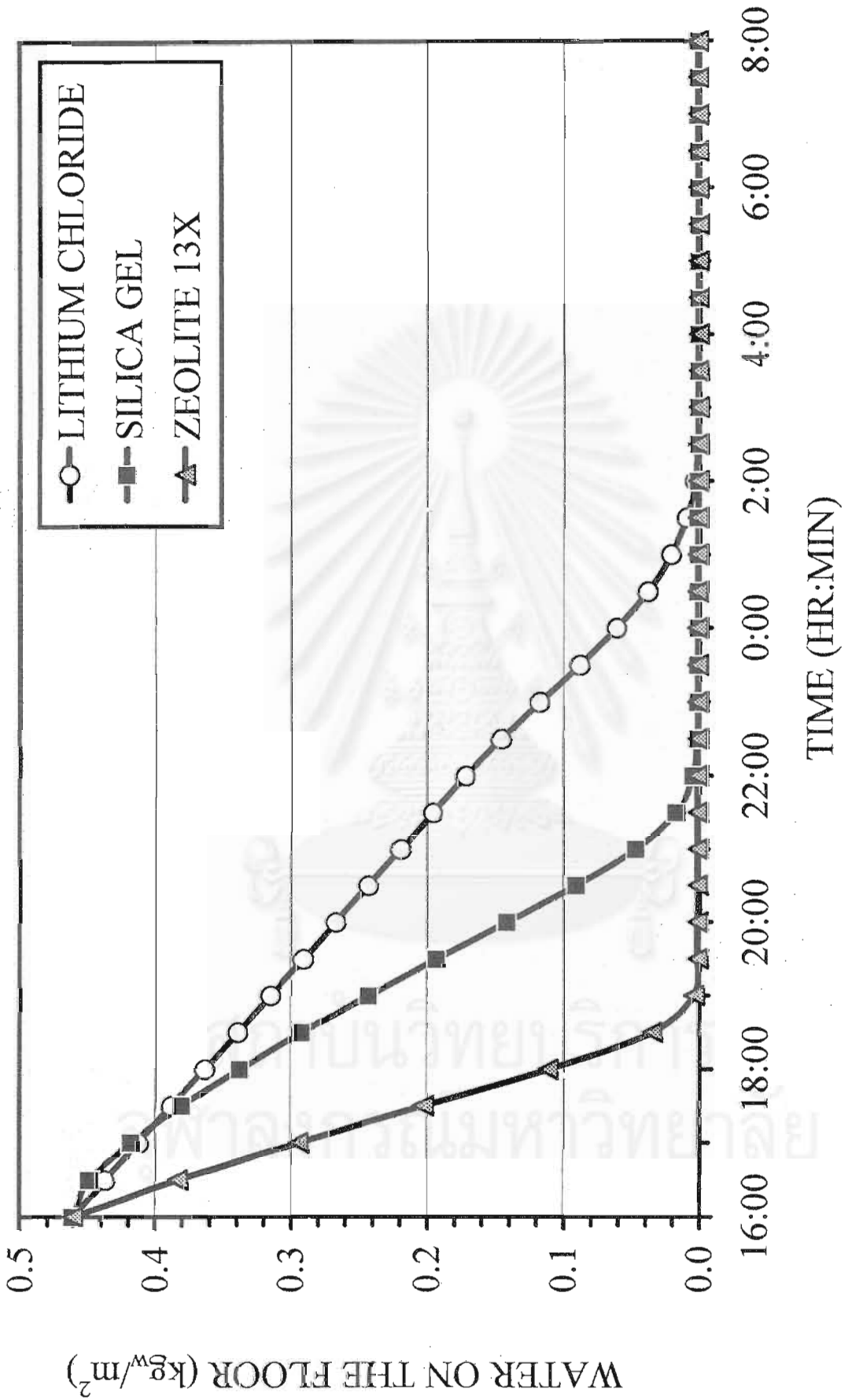
Figure 6.105 Relationship between the water on the floor vs. time for various rotary dehumidifiers
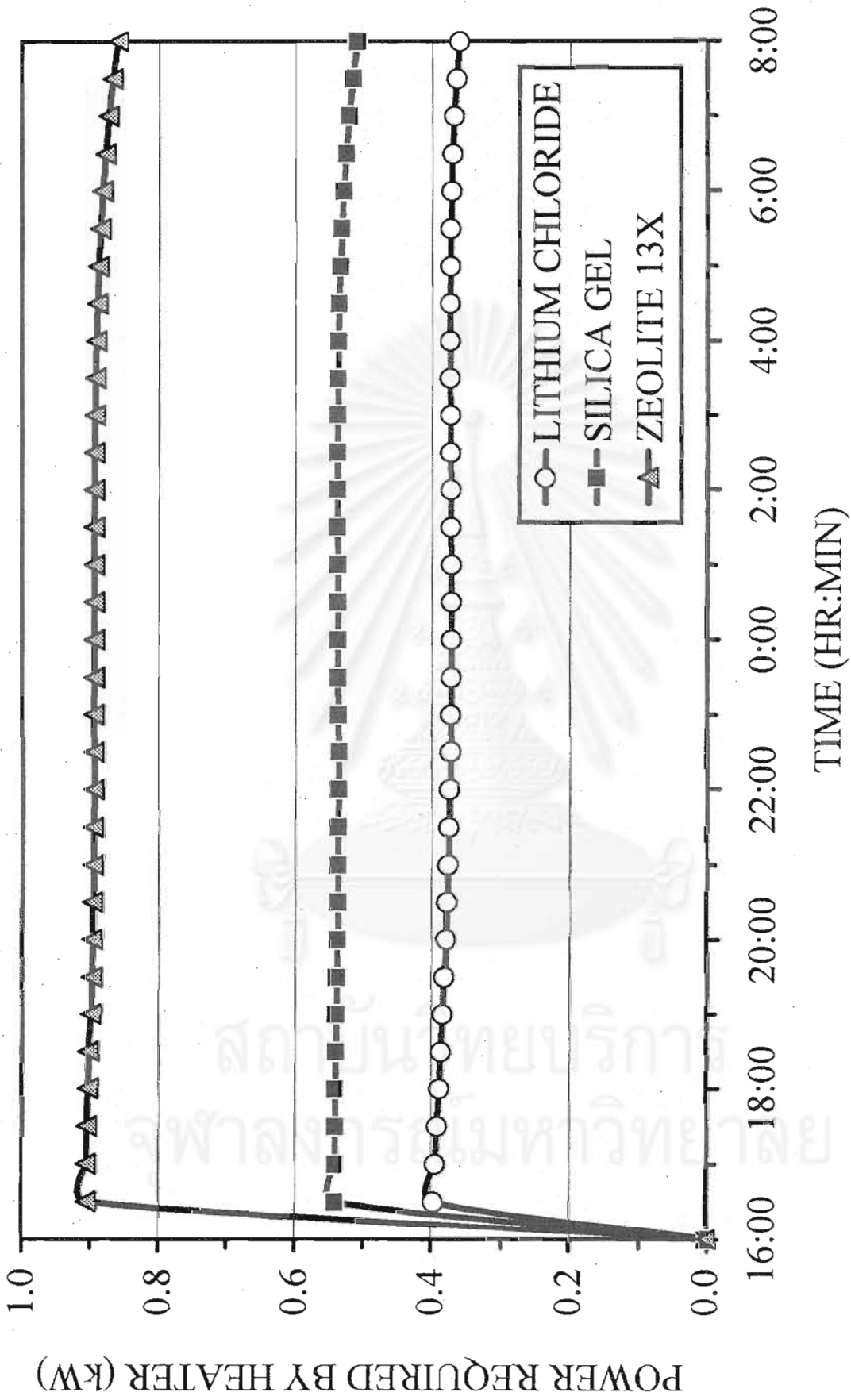
Figure 6.106 Relationship between power required by heater vs. time for various rotary dehumidifiers
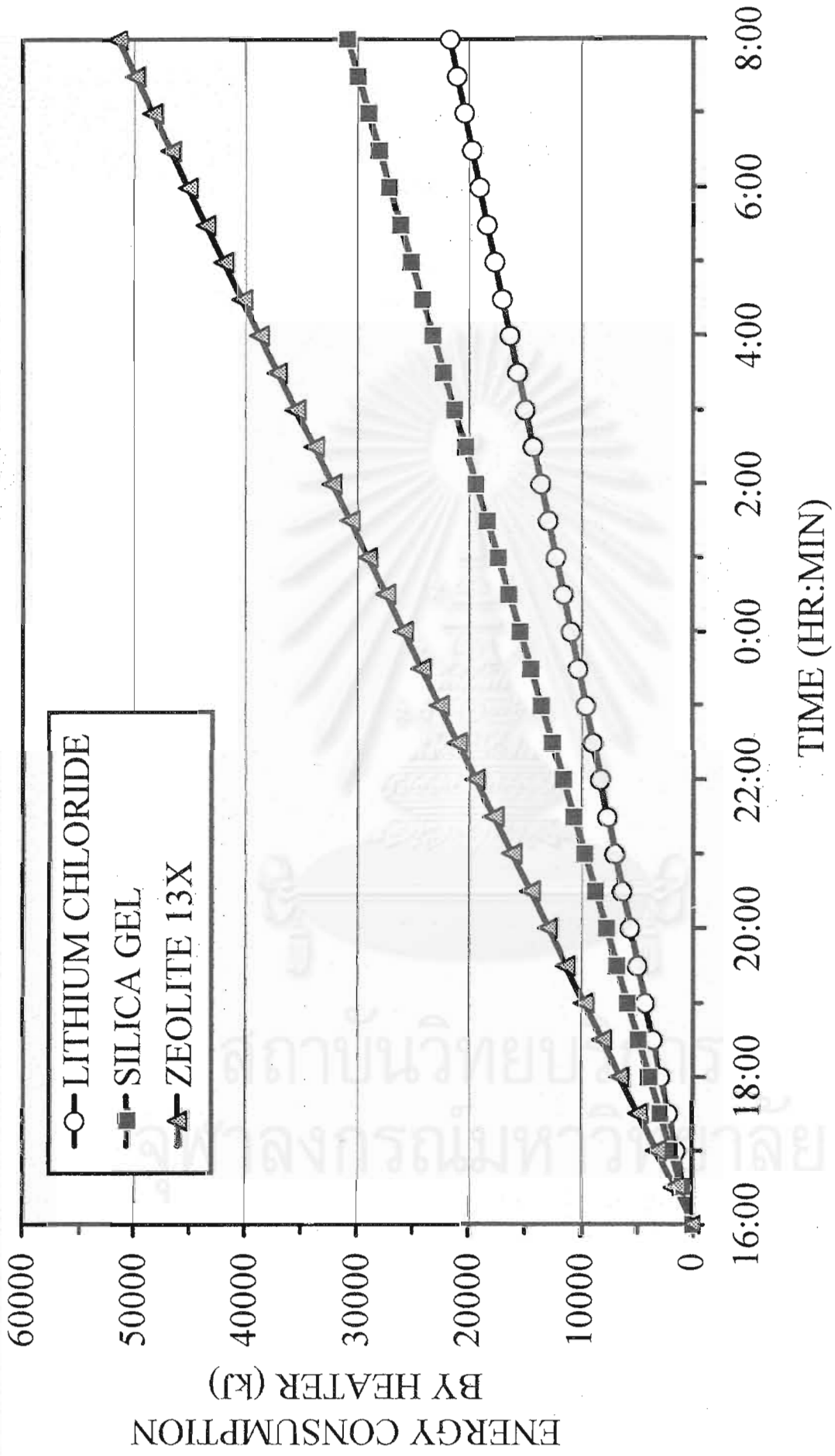
Figure 6.107 Relationship between energy consumption by heater vs. time for various rotary dehumidifiers
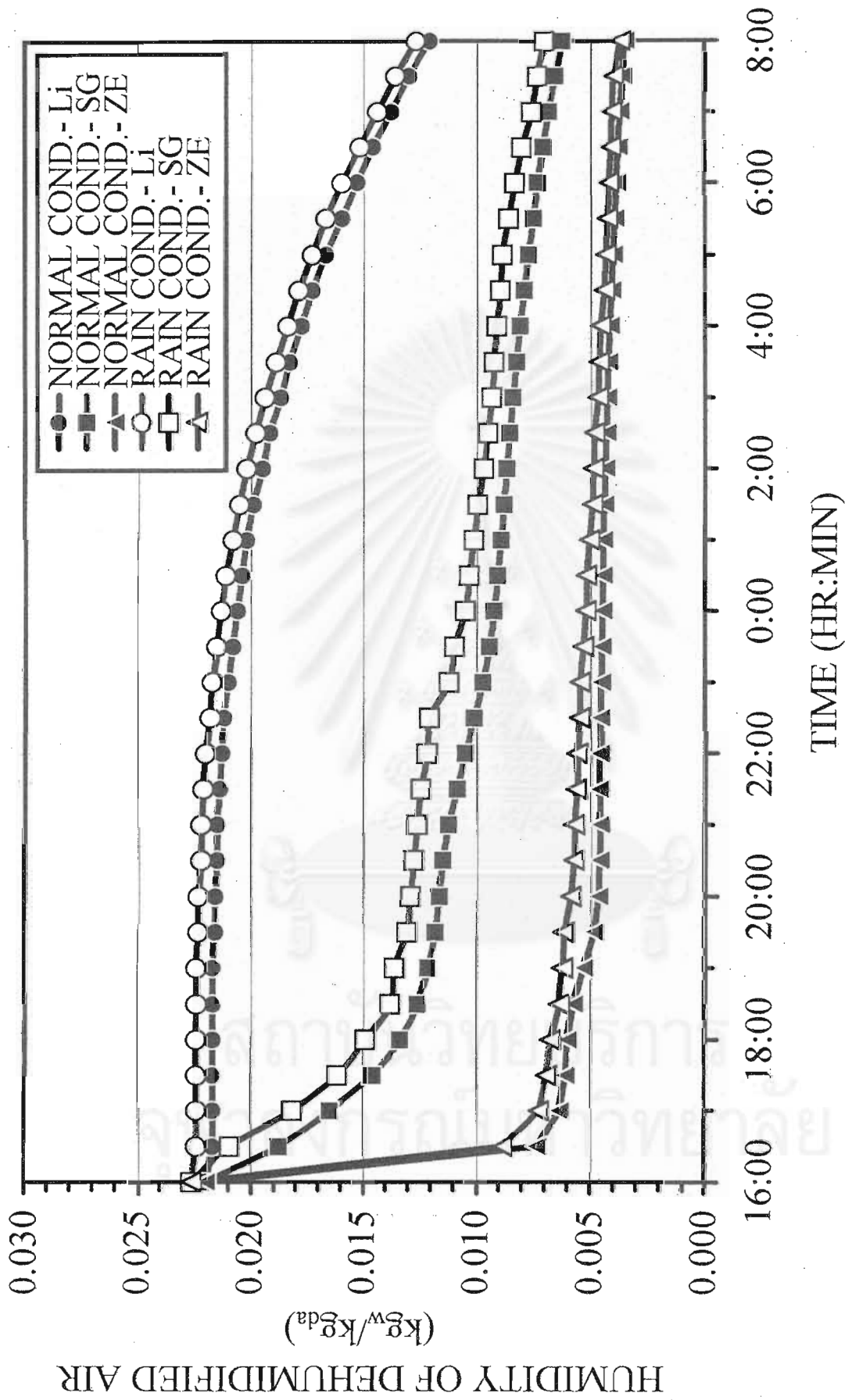
Figure 6.108 Effect of the ambient condition on the humidity of the dehumidified air for various rotary dehumidifiers
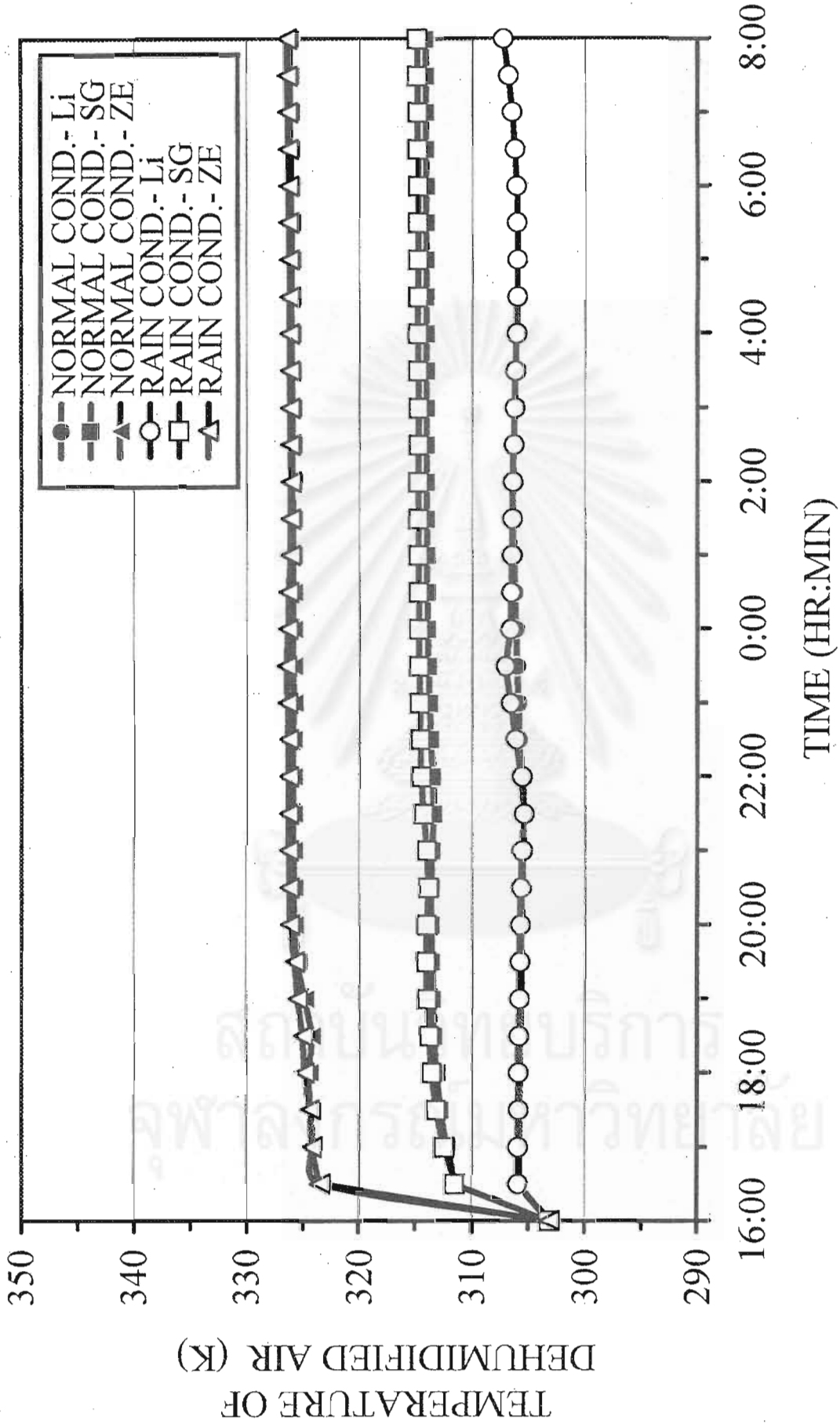
Figure 6.109 Effect of the ambient condition on the temperature of the dehumidified air for various rotary dehumidifiers
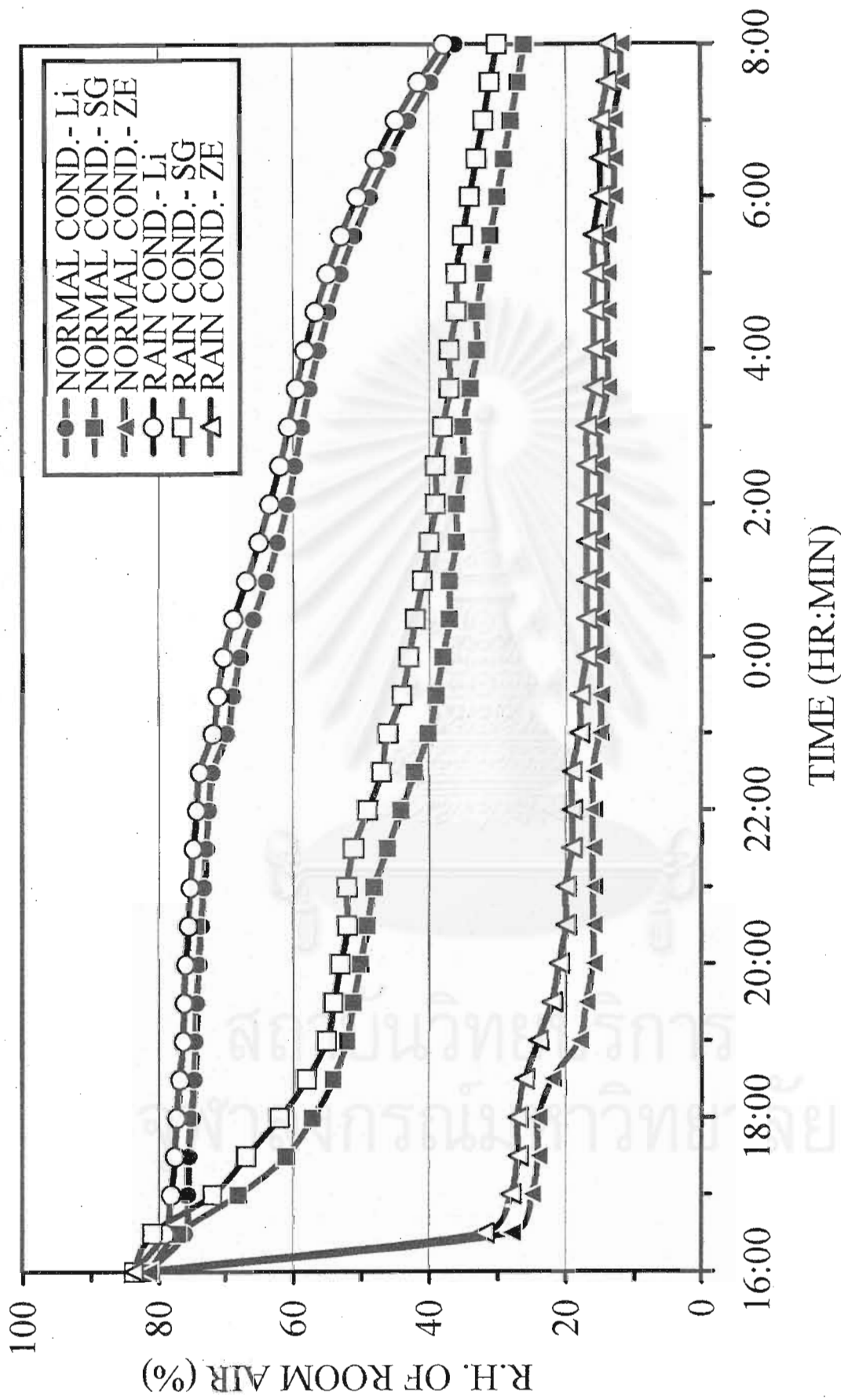
Figure 6.110 Effect of the ambient condition on the relative humidity of the room air for various rotary dehumidifiers
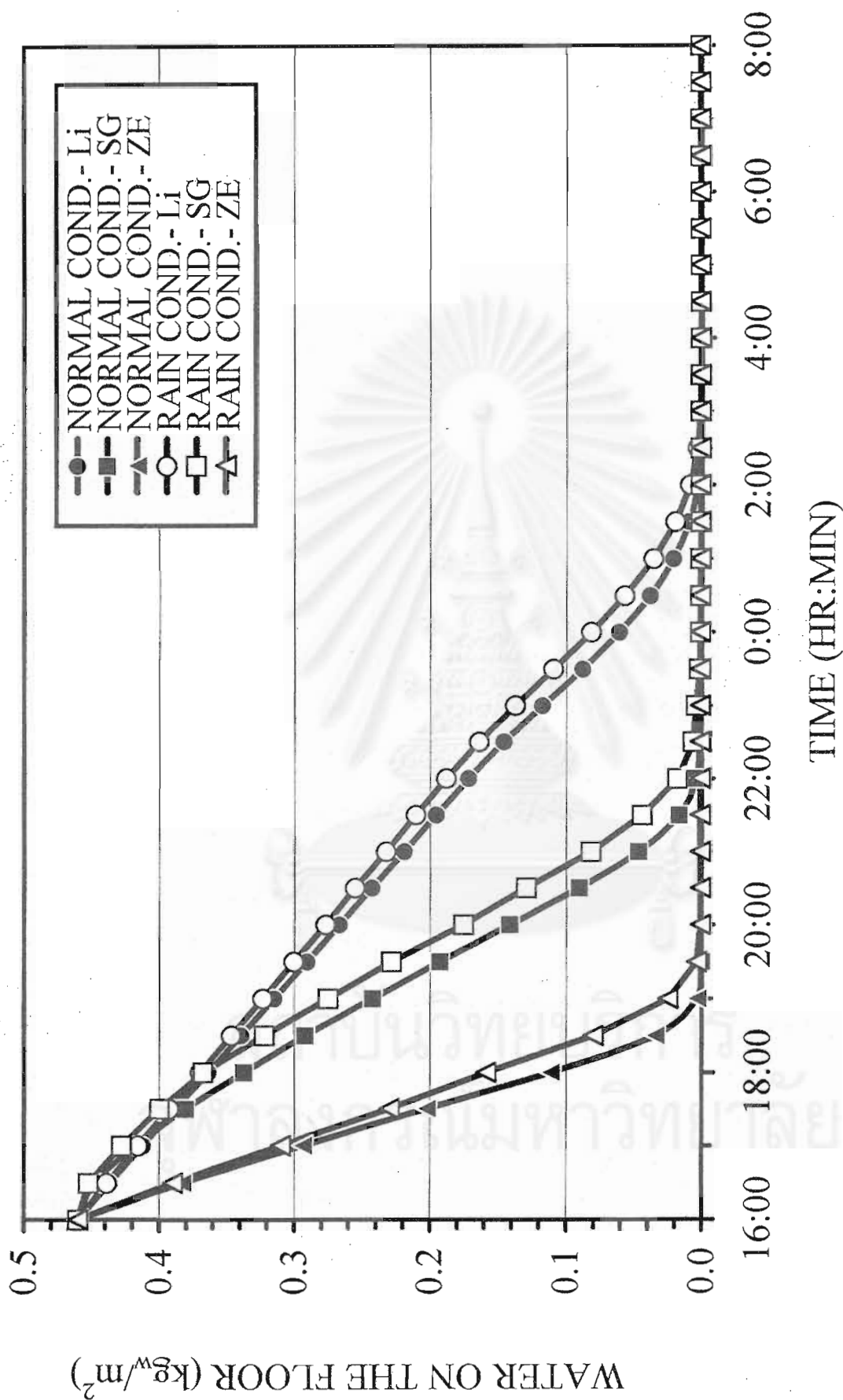
Figure 6.111 Effect of the ambient condition on the water on the floor for various rotary dehumidifiers

CHAPTER 7

CONCLUSIONS

7.1 Conclusions

A simple unsteady-state model for the rotary honeycomb lithium chloride coated absorption-type dehumidifier has successfully been extended to the case of adsorption using silica gel and zeolite coated honeycombs. The present model is shown to accurately predict not only the overall dehumidification performance but also the phenomena of simultaneous heat and mass transfer inside the honeycomb of the dehumidifier. The air temperature and humidity profiles inside the rotary dehumidifier are compared and found to agree well with experimental data published by Kodama, A. et al. (1993,1994).

Factors possibly influencing the dehumidification performance of the rotary adsorption-type dehumidifier are as follows:

1. Mass velocity of the hot regenerative air that ranges from 4.50×10^{-4} to 1.50×10^{-3} $kg_w/(m^2 \cdot s)$ has insignificant effect on the dehumidification efficiency.

2. For a silica gel coated rotary dehumidifier, the regenerative temperature that ranges from 373 to 433 K insignificantly affects the dehumidification efficiency. Particularly, the efficiency remains rather constant at approximately 90% when the temperature ranges from 393 to 433 K but rapidly decreases when the temperature drops below 373 K. Consequently, the optimal regenerative temperature for the case of silica gel is about 393 K. In contrast, the dehumidification efficiency for the zeolite-13X coated rotary dehumidifier reaches nearly 100% when using the optimal regenerative temperature of 453 K.

3. The dehumidification efficiency decreases rapidly below 5 rph and drops gradually above 15 rph. So the optimal rotational speed of the rotor is approximately 6 to 14 rph depending on the length of the rotor and mass velocity or humidity load of the humid air. As expected, the optimal rotational speed gradually increases when either the rotor becomes shorter or the air mass velocity becomes higher.

4. At the optimal condition, increasing the mass velocity of the humid room air from 4.05×10^{-3} to 1.62×10^{-2} $kg_w/(m^2 \cdot s)$ decreases the dehumidification efficiency almost linearly from 95% to 70% and from nearly 100% to 95% for the silica gel and zeolite-13X coated rotary dehumidifiers, respectively.

5. As the rotor becomes longer, the dehumidification efficiency rapidly increases from 75% at 0.10-m length to 95% at 0.25-m length. At low mass velocity of the humid air, the length of the rotor has insignificant effects on the efficiency, which varies from 80 to 95%. In contrast, the efficiency varies in a wide range from 55 to 90% at high mass velocity of the air

6. For each type of adsorbent, the dehumidification efficiency is found to be a function of the dimensional groups $(3600 \cdot G_w)/(L \cdot \varphi)$ and from Figures 6.61 and 6.98 the optimal operating rotational speed (φ) are approximately $(300 \cdot G_w/L)$ and $(100 \cdot G_w/L)$ for the silica gel rotor and the zeolite-13X rotor, respectively.

Finally, both of the silica gel and zeolite-13X coated honeycomb rotary dehumidifiers are simulated in conjunction with a closed process room with wet floor in a modern beverage factory in Thailand in order to investigate and predict the dehumidification performance and the dynamic evaporation process on the wet floor at various conditions as well as to compare the results with the case of lithium chloride absorbent (Prawarnpit, 1997). The results show that the lithium chloride, silica gel and zeolite-13X coated honeycomb rotor can dry out the water on the wet floor within 10 hr, 6 hr and 3 hr, respectively and the minimum total energy consumption by heater for the case of zeolite-13X adsorption is the lowest. Consequently, the zeolite-13X coated rotary dehumidifiers are suitable for drying out the wet floor in this study.

7.2 Recommendation

Both the original (Prawarnpit, 1997) and the present mathematical models are applicable only to the case of the adsorption of water vapor from a gas stream. So the author recommends some interesting extension of the model as follows:

1. Modify the model to cover the case of different single adsorbates, more specifically, a volatile organic compound (VOC), carbon dioxide (CO_2) and so on.

2. Extend the mathematical model to cover the case of simultaneous adsorption of the two adsorbates, for example, an air pollutant and water vapor.

REFERENCES

1. Banks, P.J. 1985. Prediction of heat and mass regenerator performance using nonlinear analogy method: Part 1- Basis. ASME J. Heat Transfer 107: 222-229.

2. Banks, P.J. 1985. Prediction of heat and mass regenerator performance using nonlinear analogy method: Part 2- Comparison of methods. ASME J. Heat Transfer 107: 230-238.

3. Cengel, Y.A., and M.A. Boles. 1994. Thermodynamics: An Engineering Approach 2nd ed. New York: McGraw-Hill.

4. Chant, E.E., and S.M. Jeter. 1995. On the use of the parabolic concentration profile assumption for a rotary desiccant cooling systems. ASME Journal of Solar Energy Engineering 117: 45-50.

5. Elsayed, M.M. and A.J. Chamkha. 1997. Analysis and performance of radial flow rotary desiccant dehumidifiers. Journal of Solar Energy Engineering 119: 35-43.

6. Harriman II, L.G., M. Czachorski, M.J. Witte, and D.R. Kosar. 1999. Evaluating active desiccant systems for ventilating commercial buildings. ASHRAE Journal 28-37.

7. Hines, A.L. and T.K. Ghosh. 1993. Investigation of co-sorption of gases and vapors as a means to enhance indoor air quality-phase 2: water vapor uptake and removal of chemical pollutants by solid adsorbents, Gas Research Institute Report GRI-92/0157.2 Gas Research Institute, Chicago, IL.

8. Hines, W.W.. and D.C. Montgomery. 1990. Probability and statistics in engineering and management science 3rd ed. Toronto: John Wiley & Sons.

9. Himmelbleu, D.M. and K.B. Bischoff. 1970. <u>Process Analysis and Simulation</u> New York: John Wiley& Sons.

10. Holmberg, R.B. 1979. Combined Heat and mass transfer in regenerators with hygroscopic materials. <u>ASME Journal of Heat Transfer</u> 101: 205-210.

11. Incropera, F.P., and D.P. DeWitt. 1985. <u>Fundamentals of Heat and Mass Transfer</u> 2nd ed. New York: John Wiley & Son.

12. Jurinak, J.J., and J.W. Mitchell. 1984. Effect of matrix properties on the performance of a counterflow rotary dehumidifier. <u>ASME J. of Heat Transfer</u> 106: 638-645.

13. Jasra, R.V. and Bhat, S.G.T. 1988. Adsorptive bulk separations by zeolite molecular sieves. <u>Separation Science and Technology</u> 23(10&11): 945-989.

14. Keller II, G.E., R.A. Anderson, and C.M. Yon 1987. Adsorption. <u>Handbook of Separation Process Technology</u> New York: John Wiley & Son 573-600.

15. Keller II, G. E. 1995. Adsorption: Building upon a solid foundation. <u>Chemical Engineering Progress</u> October: 56-67.

16. Knaebel, K.S. 1999. The basics of adsorber design. <u>Chemical Engineering</u> 92-103.

17. Kodama, A., M. Goto, T. Hirose and T. Kuma. 1993. Experimental study of optimal operation for a honeycomb adsorber operated with thermal swing. <u>Journal of Chemical Engineering of Japan</u> 26(5): 530-535.

18. Kodama, A., M. Goto, T. Hirose and T. Kuma. 1994. Temperature profile and optimal rotational speed of a honeycomb rotor adsorber operated with thermal swing. <u>Journal of Chemical Engineering of Japan</u> 27(5): 644-649.

19. Kodama, A., M. Goto, T. Hirose, and T. Kuma. 1995. Performance evaluation for a thermal swing honeycomb rotor adsorber operated with thermal swing. <u>Journal of Chemical Engineering of Japan</u> 28: 19-24.

20. Kodama, A., M. Goto, T. Hirose, and W. Jin. 1998. An adsorptive desiccant cooling using honeycomb rotor dehumidifier. Journal of Chemical Engineering of Japan 31(5): 706-713.

21. Kodama, A., M. Goto, T. Hirose, and T. Kuma. 1998. Thermally regenerative monolithic rotor dehumidifier for adsorption cooling system. Journal of Solar Energy Engineering 120: 45-50.

22. Kuma, T., H. Okano. 1989. Active gas adsorbing element and method of manufacturing. U.S. Patent. 4,886,769.

23. Luyben, W.L., 1973. Process Modeling, Simulation, and Control for Chemical Engineers International Student Edition. Tokyo: McGraw-Hill Kogakusha.

24. McCabe, W.L., J.C. Smith, and P. Harriott. 1993. Unit Operations of Chemical Engineering 5th ed. New York: McGraw-Hill.

25. Mantell, C.L. 1945. Adsorption 1st ed. New York: McGraw-Hill.

26. Maciss, R.A., W.F. Rush and S.A. Weil. 1977. Air cleaning adsorption process. U.S. Patent. 4,012,206.

27. Montgomery, D.C., 1984. Design and Analysis of Experiments 2th ed. New York: John Wiley & Sons.

28. Perry, J.H. 1958. Perry's Chemical Engineers' Handbook 3rd ed. New York: McGraw-Hill.

29. Prawarnpit A. 1997. Simulation of rotary adsorption dehumidifier system M.S. thesis, Department of Chemical Engineering, Chulalongkorn University.

30. Qi, S., K.J. Hay, M.J. Rood, and M. P. Cal. 2000. Equilibrium and heat of adsorption for water vapor and activated carbon. Journal of environmental engineering 126(3): 267-271.

31. Ruthven, D.M. 1984. <u>Principles of adsorption and adsorption processes</u> New York: Wiley Interscience.

32. Shan, Z., W.E.J. van Kooten, O.L. Oudshoorn, J.C. Jansen, H. van Bekkum, C.M. van den Bleek and H.P.A. Cailis. 2000. Optimization of the preparation of binderless ZSM-5 coatings on stainless steel monoliths by in situ hydrothermal synthesis. <u>Microporous and Mesoporous Materials</u> 34: 81-91.

33. Sullivan, T.P. 1999. Thermal desorption: The basics. <u>Chemical Engineering Progress</u>. 49-56.

34. Suzuki, M. 1990. <u>Adsorption Engineering</u> Tokyo: Kodansha Ltd., and Amsterdam, The Netherlands: Elsevier Science Publishers B.V.

35. Tien, C. 1994. <u>Adsorption Calculations and Modeling</u> Boston: Butterworth-Heinemann.

36. Van den Bulck, E. J.W. Mitchell and S.A. Klein. 1985. Design theory for rotary heat and mass exchangers-I Wave analysis of rotary heat and mass exchangers with infinite transfer coefficients. <u>Int. J. Heat Mass Transfer</u> 28(8): 1575-1586.

37. Van den Bulck, E. J.W. Mitchell and S.A. Klein. 1985. Design theory for rotary heat and mass exchangers-II Effectiveness-number-of-transfer-units method for rotary heat and mass exchangers. <u>Int. J. Heat Mass Transfer</u> 28(8): 1587-1595.

38. Van den Bulck, E. J.W. Mitchell and S.A. Klein. 1986. The use of dehumidifiers in desiccant coling and dehumidification systems. <u>Transactions of the ASME J. Heat Transfer</u> 108: 684-692.

39. Tanthapanichkoon, W. and A. Prawarnpit. 2000. New simple mathematical model of a honeycomb rotary absorption-type dehumidifier. <u>Proceedings of the 12th International Drying Symposium (IDS2000)</u>.

40. Wolf, H.E., and E.-U. Schlünder. 1999. Adsorption equilibrium of solvent mixtures on silica gel and silica gel coated ceramics. <u>Chemical Engineering and Processing</u> 38: 211-218.

41. Yang, R.T. 1987. <u>Gas Seperation by Adsorption Processes</u> London: Butterworths.

42. Zheng, W. and W.M. Worek. 1993. Numerical simulation of combined heat and mass transfer processes in a rotary dehumidifier. <u>Numerical Heat Transfer (Part A)</u> 23: 211-232.

43. Zheng, W., M. Worek and D. Novosel. 1993. Control and optimization of rotational speeds for rotary dehumidifiers. <u>ASHRAE Transaction: Symposia</u> Part 1. 99: 825-833.

44. Zheng, W., M. Worek and D. Novosel. 1995. Performance optimization of rotary dehumidifiers. <u>ASME Journal of Solar Energy Engineering</u> 117: 40-44.

45. Zheng, W., M. Worek and D. Novosel. 1995. Effect of operating conditions on optimal performance of rotary dehumidifiers. <u>Transactions of ASME Journal of Solar Energy Engineering</u> 117: 62-66.

APPENDIX A

BASIC CALCULATION

A.1 Calculation of adsorption equilibrium

A.1.1 Water vapor adsorption on silica gel

The total amount of adsorbed moisture on silica gel coated on ceramic fiber sheet at various temperatures that is predicted using the following correlation has been compared with experimental data of Wolf and Schlünder (1999) as shown in Figure A.1.1 and Table A.1.1. High accuracy of the correlation can be observed.

$$W_o = \frac{385.4}{T^{1.3074}} \tag{A.1.1}$$

Table A.1.1 Comparison of the total amount adsorbed on silica gel coated on ceramic fiber sheet between experimental and calculated data at various temperatures

Temperature (K)	Total amount adsorbed (kg_w/kg_{da})		Relative error (%)
	Experimental data	Calculated data	
288	0.2326	0.2347	0.9003
303	0.2221	0.2196	-1.1273
318	0.2070	0.2062	-0.3980
333	0.1928	0.1941	0.7050
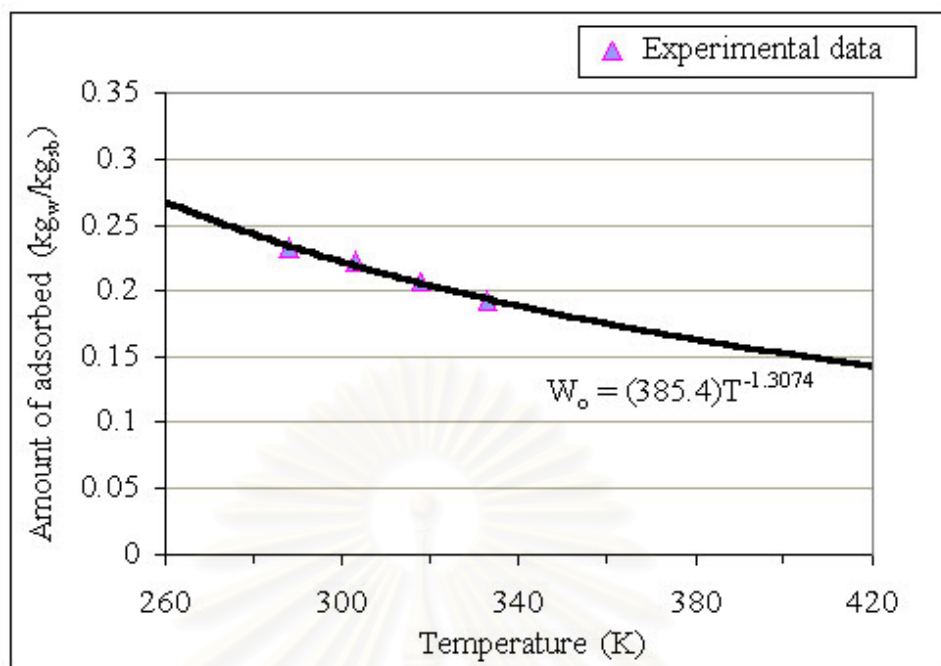
Figure A.1.1 Comparison of the relation of total amount adsorbed on silica gel coated on ceramic fiber sheet and temperatures between experimental and calculated data

For gas adsorption on micropore adsorbent, the Dubinin-Astakhov relations can be completely predicted. The amount of adsorbed moisture, W, is a function of adsorption potential (A), activation energy (E), temperature (T) and total amount of adsorbed moisture (W_o) as shown in equation A.1.2.

$$W = W_o \exp\left(-\frac{A}{E}\right)^m \tag{A.1.2}$$

and

$$A = -(RT)(\ln(RH)) \tag{A.1.3}$$

The parameters E and m, which depend on an adsorbate-adsorbent system, can be estimated as follows:

$$\ln\left(\ln\left(\frac{W_o}{W}\right)\right) = m(\ln A - \ln E) \tag{A.1.4}$$
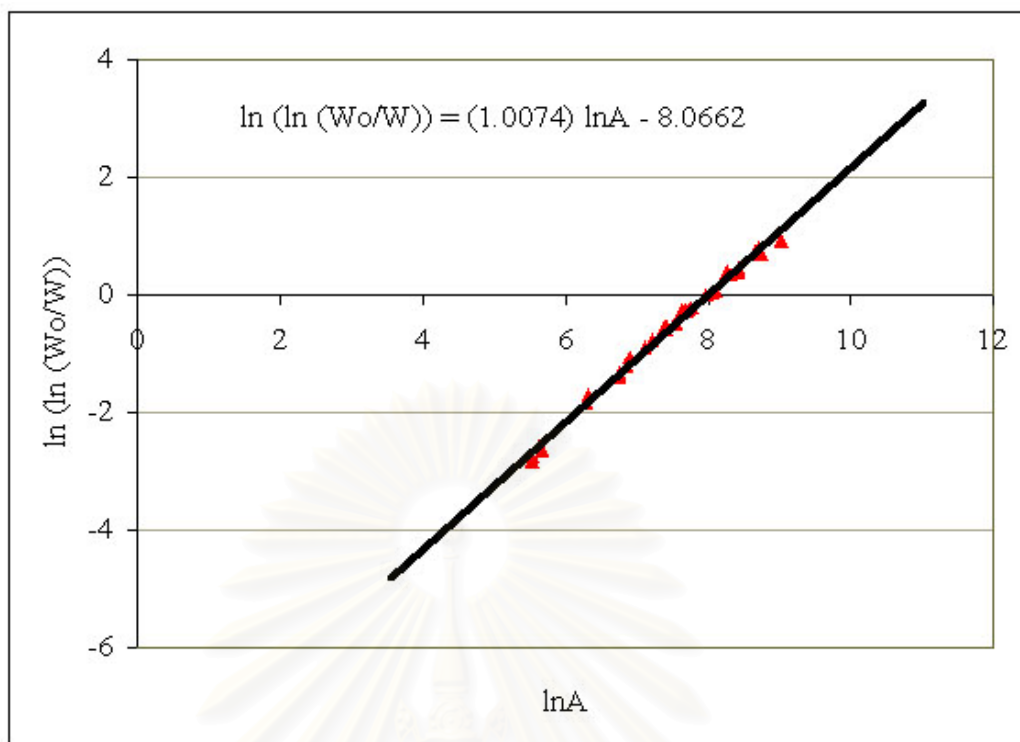
Figure A.1.2 The plot of ln (ln(Wo/W)) vs. ln A for water vapor adsorption on silica gel
coated on ceramic fiber sheet

From Figure A.1.2, it is seen that E and m are 3001.87 J/mole and approximated 1,
respectively. Thus, the isotherm of water vapor adsorption on silica gel coated on ceramic
fiber sheet is

$$W = W_o \exp\left(\frac{RT \ln(RH)}{E} \right) \tag{A.1.5}$$

$$W = \left(\frac{385.4 \left(\ln(RH) \right)^{(RT/3001.87)}}{T^{1.3074}} \right) \tag{A.1.6}$$

A.1.2 Water vapor adsorption on zeolite-13X

For zeolite-13X adsorption, the correlation of the total amount of adsorbed moisture on silica gel coated on ceramic fiber sheet is

$$W_o = \frac{285.05}{T^{1.2311}} \qquad (A.1.7)$$

Table A.1.2 Comparison of the total amount adsorbed on zeolite-13X between experimental and calculated data at various temperatures

Temperature (K)	Total amount adsorbed (kg_w/kg_{da})		Relative error (%)
	Experimental data	Calculated data	
288	0.26	0.2674	- 0.98
298	0.27	0.2564	5.04
308	0.23	0.2462	- 7.04
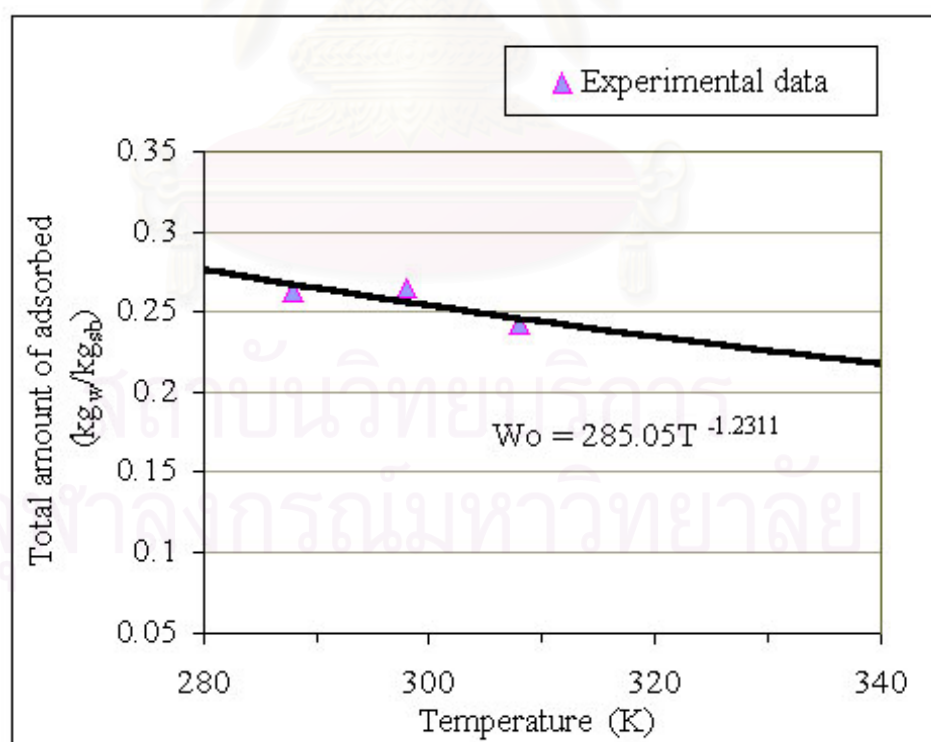
Figure A.1.3 Comparison the relation of the total amount adsorbed on zeolite-13X and temperature between experimental and calculated data

The prediction of the total amount adsorbed on silica gel coated on ceramic fiber sheet at various temperatures using equation A.1.7 has been compared with experimental data of Hines and Ghosh (1993) as shown in Figure A.1.1 and Table A.1.1. Although the relative errors are found at higher temperature, the accurate prediction is observed.

Since the Dubinin-Astakhov relation is used to determine the equilibrium adsorption isotherm of water vapor on zeolite-13X, the parameters E and m for this system are estimated using Figure A.1.4.
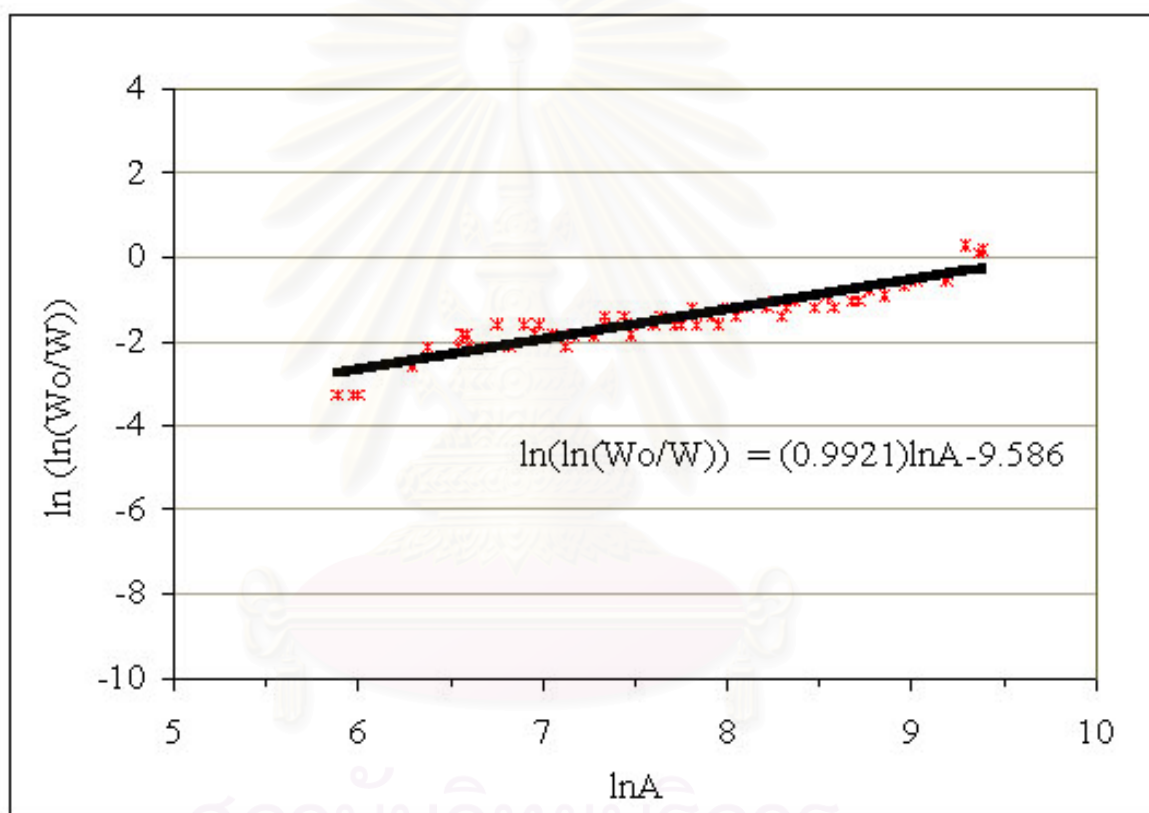
Figure A.1.4 The plot of ln(ln(Wo/W)) vs. ln A for water vapor adsorption on zeolite-13X

From Figure A.1.4, it is seen that E is 14586.0 J/mole and m is approximated 1. Consequently, the correlation of the equilibrium adsorption isotherm of water vapor on zeolite-13X is given in equation A.1.8

$$W = \left(\frac{285.05 \left(\ln(RH)\right)^{(RT/14586)}}{T^{1.2311}} \right)$$

(A.1.8)

A.2 Calculation of heat and mass transfer coefficient

A.2.1 Heat transfer coefficient

For flowing though very small slot of rotary dehumidifier, heat transfer coefficient (h_f) is estimated using the correlation for internal flow with low Reynold number (Re) (Incropera, 1985) as follows:

$$Nu = 1.86 * \left(\frac{Re \cdot Pr \cdot d_h}{L} \right)^{(1/3)} \left(\frac{\mu}{\mu_s} \right)^{0.14} \tag{A.2.1}$$

$$h_f = \frac{Nu \cdot k_{cond}}{d_h} \tag{A.2.2}$$

A.2.2 Mass transfer coefficient

In this study, the external film resistance is a limiting rate for water vapor adsorption on adsorbent-coated honeycomb rotor as approved in appendix C. Therefore, the mass transfer coefficient (k_f) is predicted using Lewis Relation (Perry, 1958) as follows:

$$k_f = \frac{h_f}{CH} \tag{A.2.3}$$

where $\qquad CH = (1.005+1.802*H) \tag{A.2.4}$

A.3 Calculation of vapor pressure of water

The correlation of vapor pressure of water (Perry, 1958) is

$$P_{sat} = \exp\left(68.756 - \left(\frac{7258.2}{T}\right) - (7.3037 \times \ln T) + (4.1653 \times 10^{-6})(T^2)\right) \quad \text{(A.3.1)}$$

The vapor pressure is in mmHg, and temperature is in Kelvins. This correlation accurately predicts in range of 273.16 to 647.13 K.

A.4 Calculation of relative humidity of air

In the atmosphere, air contains some water vapor or moisture and is referred to as *atmospheric air*. By contrast, air that contains no water vapor is called *dry air*. In dehumidification operations, it is often convenient to treat air as a mixture of water vapor and dry air since the composition of dry air remains relatively constant but the amount of water vapor changes as a result of condensation and evaporation from oceans, rivers, showers, and even the human body. Consequently, the usual basis for engineering calculations is a unit mass of vapor-free gas or dry air. Also, it is assumed that mixtures of gas and vapor follow the ideal-gas laws.

The amount of water vapor in the air can be specified in various ways. Probably the most logical way is to specify directly the mass of water vapor present in a unit mass of dry air. This is called absolute or specific humidity (also called humidity ratio) and is denoted by H. So defined, humidity depends only on the partial pressure of the vapor in the mixture when the total pressure is fixed. If the partial pressure of water vapor is P_w mmHg, the humidity ratio is

$$H = \frac{(MW)_w P_w}{(MW)_{da} P_{da}} \quad \text{(A.4.1)}$$

If $(MW)_w$ and $(MW)_{da}$ in equation (A.4.1) is replaced by 18.015 and 28.97 kg/kmol, respectively, humidity ratio can be easily calculated by the following equation (Mccabe, 1993).

$$H = \frac{(0.622)(P_w)}{(760 - P_w)} \tag{A.4.2}$$

By contrast, P_w can be calculated by rearranging the above equation as follows:

$$P_w = \frac{(H)(760)}{(0.622 + H)} \tag{A.4.3}$$

Alternatively, the amount of water vapor in the air can be specified by based on saturated air. It is called *relative humidity*, RH, which is defined as the ratio of the partial pressure of the vapor to the vapor pressure of the liquid at the gas temperature. It is usually expressed on a percentage basis, so 100% humidity means saturated gas and 0% humidity means vapor-free gas. By definition

$$RH = \frac{P_w}{P_{sat}} \times 100 \tag{A.4.4}$$

A.5 Calculation of specific volume of humid air

Specific volume of humid air, V_H, is the total volume of a unit mass of dry air plus whatever vapor it may contain at 1 atm and the gas temperature. From the gas laws, V_H in SI unit is related to humidity and temperature by the following equation (McCabe, 1993)

$$V_H = \frac{(22.4)(T)}{273}\left(\frac{1}{(MW)_{da}} + \frac{H}{(MW)_w}\right) \tag{A.5.1}$$

Replace $(MW)_{da}$ and $(MW)_w$ in the above equation by 28.97 and 18.015 kg/kmol, respectively to obtain

$$V_H = \frac{(22.4)(T)}{273}\left(\frac{18.015 + 28.97H}{(18.015 \times 28.97)}\right) \tag{A.5.2}$$

where V_H is in m^3/kg and T is in Kelvins.

A.6 Calculation of properties of air

A.6.1 Viscosity of air

The correlation for viscosity of air, which is a function of temperature, is determined by the following equation.

$$\mu = \mu_0 \left(\frac{T}{273} \right)^{0.65} \tag{A.6.1}$$

Here $\mu_0 = 0.0000172$ N/m·s

A.6.2 Conductivity of air

Conductivity of air is predicted using the following correlation.

$$k_{cond} = \left(\frac{1}{860.4115} \right) \left(\frac{8.2784}{(T+125)} \right) \left(\frac{T}{273} \right)^{1.5} \tag{A.6.2}$$

APPENDIX B

FORTH ORDER RUNGE-KUTTA METHOD

In this study, the mathematical model consists of the set of the ordinary differential equations (ODEs). To solve the simultaneous equations, the 4th order Runge-Kutta method is generally used as expressed in the following equation. Since the investigation focuses on four variables, i.e., W, Ts, H and Ta that are represented by X_1, X_2, X_3 and X_4, respectively, only four equations are necessarily presented.

$$
\begin{aligned}
X_{1,n+1} &= X_{1,n} + \frac{\Delta t}{6}\left(K_{1,X_1} + 2K_{2,X_1} + 2K_{3,X_1} + K_{4,X_1}\right) \\
X_{2,n+1} &= X_{2,n} + \frac{\Delta t}{6}\left(K_{1,X_2} + 2K_{2,X_2} + 2K_{3,X_2} + K_{4,X_2}\right) \\
X_{3,n+1} &= X_{3,n} + \frac{\Delta t}{6}\left(K_{1,X_3} + 2K_{2,X_3} + 2K_{3,X_3} + K_{4,X_3}\right) \\
X_{4,n+1} &= X_{4,n} + \frac{\Delta t}{6}\left(K_{1,X_4} + 2K_{2,X_4} + 2K_{3,X_4} + K_{4,X_4}\right)
\end{aligned}
\tag{B.1}
$$

Here, K denotes the Runge-Kutta constant and can be estimated as follows:

$$
\begin{aligned}
K_{1,X_1} &= \frac{dF_1\left(t_n, X_1, .X_2, X_3, X_4\right)}{dt} \\
K_{1,X_2} &= \frac{dF_2\left(t_n, X_1, .X_2, X_3, X_4\right)}{dt} \\
K_{1,X_3} &= \frac{dF_3\left(t_n, X_1, .X_2, X_3, X_4\right)}{dt} \\
K_{1,X_4} &= \frac{dF_4\left(t_n, X_1, .X_2, X_3, X_4\right)}{dt}
\end{aligned}
$$

$$K_{2,X_1} = \dfrac{dF_1\left(t_n + \dfrac{\Delta t}{2}, X_{1,n} + \dfrac{\Delta t \cdot K_{1,X_1}}{2}, X_{2,n} + \dfrac{\Delta t \cdot K_{1,X_2}}{2}, X_{3,n} + \dfrac{\Delta t \cdot K_{1,X_3}}{2}, X_{4,n} + \dfrac{\Delta t \cdot K_{1,X_4}}{2}\right)}{dt}$$

$$K_{2,X_2} = \dfrac{dF_2\left(t_n + \dfrac{\Delta t}{2}, X_{1,n} + \dfrac{\Delta t \cdot K_{1,X_1}}{2}, X_{2,n} + \dfrac{\Delta t \cdot K_{1,X_2}}{2}, X_{3,n} + \dfrac{\Delta t \cdot K_{1,X_3}}{2}, X_{4,n} + \dfrac{\Delta t \cdot K_{1,X_4}}{2}\right)}{dt}$$

$$K_{2,X_3} = \cdot \dfrac{dF_3\left(t_n + \dfrac{\Delta t}{2}, X_{1,n} + \dfrac{\Delta t \cdot K_{1,X_1}}{2}, X_{2,n} + \dfrac{\Delta t \cdot K_{1,X_2}}{2}, X_{3,n} + \dfrac{\Delta t \cdot K_{1,X_3}}{2}, X_{4,n} + \dfrac{\Delta t \cdot K_{1,X_4}}{2}\right)}{dt}$$

$$K_{2,X_4} = \cdot \dfrac{dF_4\left(t_n + \dfrac{\Delta t}{2}, X_{1,n} + \dfrac{\Delta t \cdot K_{1,X_1}}{2}, X_{2,n} + \dfrac{\Delta t \cdot K_{1,X_2}}{2}, X_{3,n} + \dfrac{\Delta t \cdot K_{1,X_3}}{2}, X_{4,n} + \dfrac{\Delta t \cdot K_{1,X_4}}{2}\right)}{dt}$$

$$K_{3,X_1} = \dfrac{dF_1\left(t_n + \dfrac{\Delta t}{2}, X_{1,n} + \dfrac{\Delta t \cdot K_{2,X_1}}{2}, X_{2,n} + \dfrac{\Delta t \cdot K_{2,X_2}}{2}, X_{3,n} + \dfrac{\Delta t \cdot K_{2,X_3}}{2}, X_{4,n} + \dfrac{\Delta t \cdot K_{2,X_4}}{2}\right)}{dt}$$

$$K_{3,X_2} = \dfrac{dF_2\left(t_n + \dfrac{\Delta t}{2}, X_{1,n} + \dfrac{\Delta t \cdot K_{2,X_1}}{2}, X_{2,n} + \dfrac{\Delta t \cdot K_{2,X_2}}{2}, X_{3,n} + \dfrac{\Delta t \cdot K_{2,X_3}}{2}, X_{4,n} + \dfrac{\Delta t \cdot K_{2,X_4}}{2}\right)}{dt}$$

$$K_{3,X_3} = \dfrac{dF_3\left(t_n + \dfrac{\Delta t}{2}, X_{1,n} + \dfrac{\Delta t \cdot K_{2,X_1}}{2}, X_{2,n} + \dfrac{\Delta t \cdot K_{2,X_2}}{2}, X_{3,n} + \dfrac{\Delta t \cdot K_{2,X_3}}{2}, X_{4,n} + \dfrac{\Delta t \cdot K_{2,X_4}}{2}\right)}{dt}$$

$$K_{3,X_4} = \dfrac{dF_4\left(t_n + \dfrac{\Delta t}{2}, X_{1,n} + \dfrac{\Delta t \cdot K_{2,X_1}}{2}, X_{2,n} + \dfrac{\Delta t \cdot K_{2,X_2}}{2}, X_{3,n} + \dfrac{\Delta t \cdot K_{2,X_3}}{2}, X_{4,n} + \dfrac{\Delta t \cdot K_{2,X_4}}{2}\right)}{dt}$$

$$K_{4,X_1} = \dfrac{dF_1\left(t_n + \Delta t, X_1 + \Delta t \cdot K_{3,X_1}, X_2 + \Delta t \cdot K_{3,X_2}, X_3 + \Delta t \cdot K_{3,X_3}, X_4 + \Delta t \cdot K_{3,X_4}\right)}{dt}$$

$$K_{4,X_2} = \dfrac{dF_2\left(t_n + \Delta t, X_1 + \Delta t \cdot K_{3,X_1}, X_2 + \Delta t \cdot K_{3,X_2}, X_3 + \Delta t \cdot K_{3,X_3}, X_4 + \Delta t \cdot K_{3,X_4}\right)}{dt}$$

$$K_{4,X_3} = \dfrac{dF_3\left(t_n + \Delta t, X_1 + \Delta t \cdot K_{3,X_1}, X_2 + \Delta t \cdot K_{3,X_2}, X_3 + \Delta t \cdot K_{3,X_3}, X_4 + \Delta t \cdot K_{3,X_4}\right)}{dt}$$

$$K_{4,X_4} = \dfrac{dF_4\left(t_n + \Delta t, X_1 + \Delta t \cdot K_{3,X_1}, X_2 + \Delta t \cdot K_{3,X_2}, X_3 + \Delta t \cdot K_{3,X_3}, X_4 + \Delta t \cdot K_{3,X_4}\right)}{dt}$$

APPENDIX C

THE DETERMINATION OF LIMITING RATE OF ADSORPTION

As mentioned in chapter 2, the overall mass transfer coefficient, k_0, presented in eqaution 2.22 consists of external film and intraparticle mass transfer resistance

$$\frac{1}{k_0^{'}a} = \frac{1}{k_f a} + \frac{R_p^2}{15\varepsilon_p D_p} \tag{2.22}$$

In fact, the overall terms can be estimated using only one of external film and intraparticle mass transfer coefficient or combined term as express in the above equation. It depends on the difference of the order of magnitude between those terms. So, this section is dedicated to verify the significant term for the calculation of mass transfer coefficient in honeycomb rotary dehumidifier.

The typical adsorbent, zeolite-13X, coated honeycomb rotor has been examined in this section. The investigated zeolite-13X powder coated honeycomb has a particle size in range of 1-10 μm (Macriss, 1977), that is, mean particle size is about 5 μm and the porosity of 0.334 (Takeuchi, 1976). Pore diffusion of zeolite-13X is determined by Knudsen diffusion empirical (Suzuki, 1990) as mentioned in section 2.5.2.

$$D_p = 9700 * r_p \sqrt{(T/MW_g)} \tag{2.18}$$

Where $\quad \varepsilon_p \quad$ is porosity of adsorbent particle (-)

$\quad D_p \quad$ is pore diffusivity (cm^2/s)

$\quad r_p \quad$ is pore radius (cm)

The external film mass transfer coefficient for passing air through the slot is given by using Lewis Relation (Perry, 1958) as discussed in appendix A.2.2. When the term of external and intraparticle mass transfer coefficient are substituted in equation 2.22, the overall term will be obtained as shown in Table C.1.

Table C.1 The calculated results of the overall, external and intraparticle mass transfer coefficient for various diameters of adsorbent particle at 298.15 K

$2r_p\,(\text{Å})$	$k_f a$	$\dfrac{15\varepsilon_p D_p}{R_P^2}$	$k_0' a$	Ref.
10.0	72.46	3.95×10^4	72.33	Yang, 1987
41.7	72.46	16.48×10^4	72.43	Hines and Ghosh, 1993

In conclusion, the external film resistance is a limiting control rate of mass transfer in a zeolites-coated honeycomb rotary dehumidifier. Similarly, it is satisfy to silica gel coated honeycomb rotor since powder form is used for coating honeycomb.

APPENDIX D

PRINCIPLE OF EXPERIMENTAL DESIGN

Factorial designs are widely used in experiments involving several factors where it is necessary to study the joint effect of these factors on a response. A general factorial design is that of k factors, each at only two levels. These levels may be quantitative, such as two values of temperature, pressure, or time; or they may be qualitative, such as two machines, two operators, the "high" and "low" levels of a factor, or perhaps the presence and absence of a factors. A complete replicate of such a design requires $2x2x\cdots\cdots x2 = 2^k$ observations and is called a 2^k factorial design.

D.1 The principle of the 2^k factorial design

The 2^k design is particularly useful in the early stages of experimental work, when they are likely to be many factors investigated. It provides the smallest number of treatment combinations with which k factors can be studied in a complete factorial arrangement. Because there are only two levels for each factor, we must assume that the response is approximately linear over the range of the factor levels chosen.

D.1.1 The two-factor of the 2^k factorial design

The first design in 2^k series is one with only two factors, say A and B, each run at two levels. This design is called a 2^2 factorial design. The levels of the factors may be arbitrarily called "low" and "high". As an example, consider an investigation into the effect of concentration of reactant and the presence of catalyst on the reaction time of a chemical process. Let concentration be factor A, and let the two levels of interest be 15%

and 25%. Catalyst is factor B, with the high level denoting the presence of the catalyst and the low level denoting its absence. Assuming three replicates, the data from this experiment are displayed below.

Table D.1 Example of the data experiment of 3 replicates

Treatment combination	Replicate			Total
	I	II	III	
A low, B low	28	25	27	80
A high, B low	36	32	32	100
A low, B high	18	19	23	60
A high, B high	31	30	29	90

By convention, we denote the effect of a factor by a capital Latin letter. Thus, "A" refers to the effect of factor A, "B" refers to the effect of factor B, and "AB" refers to the AB interaction. The treatment combinations in this design are usually represented by lowercase letters, as shown in Figure D.1. We see from the figure that the high level of any factor in the treatment combination is denoted by the corresponding lowercase letter, and the low level of a factor in the treatment combination is denoted by the absence of the corresponding letter. Thus, a represents the treatment combination of A at the high level and B at the low level, b represents A at the low level and B at the high level, ab represents both factors at the high level and (1) is used to denote both factors at the low level. This notation is used throughout the 2^k series.
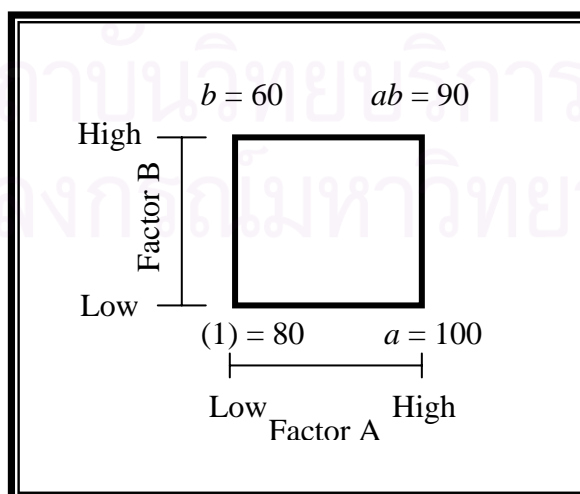
Figure D.1 Construction of treatment combinations of the 2^2 design

Define the average effect of a factor as the change in response produced by a change in the level of that factor, averaged over the levels of the other factor. Also, the lowercase letters (1), *a*, *b* and *ab* now represent the total of all *n* replicates taken at the treatment combination, as illustrated in Figure D.1. Now the effect of A at the low level of B is [*a*-(1)]/*n* and the effect of A at the high level of B is [*ab-b*]/*n*. Averaging these two quantities yields

$$A = \frac{1}{2n}[ab + a - b - (1)] \qquad (D.1)$$

The average B effect is found from the effect of B at the low level of A (i.e., [*b*-(1)]/*n*) and at the high level of A (i.e., [*b*-(1)]/*n*) as

$$B = \frac{1}{2n}[ab - a + b - (1)] \qquad (D.2)$$

Define the interaction effect AB as the average difference between the effect of A at the high level of B and the effect of A at the low level of B. Thus,

$$AB = \frac{1}{2n}[ab - a - b + (1)] \qquad (D.3)$$

Alternatively, we may define AB as the average difference between the effect of B at the high level of A and the effect of B at the low level of A. This will also lead to equation D.3.

These formulas for the effects of A, B and AB may be derived by another method. Note that the effect of A, equation D.1, is found by comparing the two treatment combinations on the right-hand side of the square in Figure D.1 with the two treatment combinations on the left-hand side. Also, the effect of B, equation D.2, is found by comparing the two observations on top of the square with the two observations on the bottom. Finally, the interaction effect AB is the sum of the right-to-left diagonal treatment combinations in the square [*ab* and (1)] minus the sum of the left-to-right diagonal treatment combination (*b* and *a*).

Kempthorne (1952) and Anderson and McLean (1974) call the total effect of A as
"*Contrast$_A$*". From equation D.1, a contrast of A is

$$\text{Contrast}_A \quad = \quad ab + a - b - (1) \qquad\qquad (D.4)$$

Similarly, Contrast$_B$ and Contrast$_{AB}$ can be defined, respectively, as

$$\text{Contrast}_B \quad = \quad ab - a + b - (1) \qquad\qquad (D.5)$$

$$\text{Contrast}_{AB} = \quad ab - a - b + (1) \qquad\qquad (D.6)$$

Conveniently, it can write down the treatment combinations in the order (1), *a*, *b*, *ab*.
This is referred to as *standard order*. Using this standard order, we see that the contrast
coefficients used in estimating the effects are

Table D.2 Algebraic signs for calculating effects in the 2^2 design

Treatment combination	Factorial effect			
	I	**A**	**B**	**AB**
(1)	+	-	-	+
a	+	+	-	-
b	+	-	+	-
ab	+	+	+	+

The contrast coefficients for estimating the interaction effect are just the product of
the corresponding coefficients for the two main effects. The contrast coefficient is always
either +1 or –1, and a table of plus and minus signs such as in Table D.2 can be used to
determine the proper sign for each treatment combination. The column headings in table
D.2 are the main effects, say A and B, the AB interaction, and I, which represents the total
or average of the entire experiment. Notice that the column corresponding to I has only
plus signs. The row designators are the treatment combinations. To find the contrast for
estimating any effect, simply multiply the signs in the appropriate column of the table by
the corresponding treatment combination and add. For example, to estimate A, the contrast
is $-(1) + a - b + ab$, which agrees with equation D.1.

D.1.2 The three-factor of the 2^k factorial design

Suppose that three factors, A, B and C, each at two levels, are under study. The design is called a 2^3 factorial, and the eight treatment combinations can now be displayed graphically as a cube, as shown in Figure D.2. We can write the treatment combinations in standard order as (1), *a*, *b*, *ab*, *c*, *ac*, *bc and abc*. Note that these lowercase letters also represent the total of all *n* observations taken at that particular treatment combination
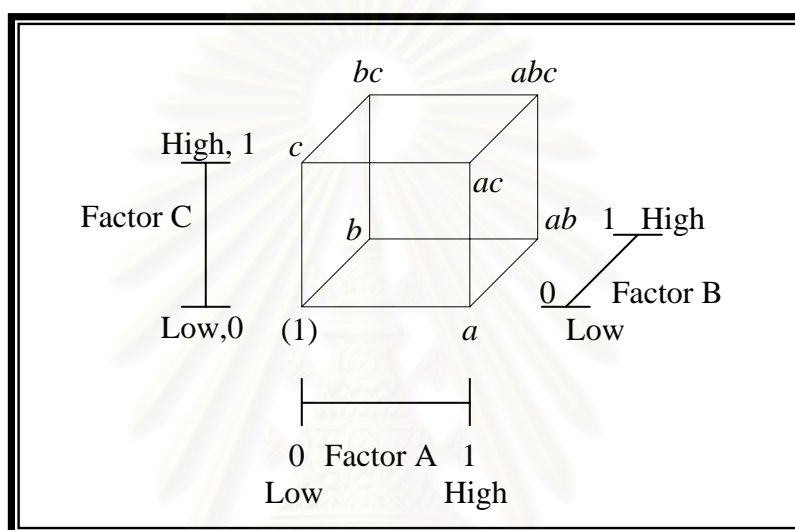
Figure D.2 Construction of treatment combination of the 2^3 design

The seven degrees of freedom between the eight treatment combinations are associated with the main effects of A, B, and C; the two-factor interactions AB, AC, and BC; and the three-factor interaction ABC. Consider estimating the main effect A. the effect of A when B and C are at the low level is [*a*-(1)]/*n*. Similarly, the effect of A when B is at the high level and C is at the low level is [*ab*-*b*]/*n*. The effect of A when C is at the high level and B is at the low level is [*ac*-*c*]/*n*. Finally, the effect of A when both B and C are at the high level is [*abc*-*bc*]/*n*. Thus, the average effect of A is just the average of these four, or

$$A = \frac{1}{4n}[a - (1) + ab - b + ac - c + abc - bc]$$

$$= \frac{1}{4n}[a + ab + ac + abc - (1) - b - c - bc] \qquad (D.7)$$

From the above equation, it is shown that the effect of A is a contrast between the four treatment combinations in the right face of the cube (where A is at the high level) and the four in the left face (where A is at the low level).

In similar manner, the effect of B is a contrast between the four treatment combinations in the front face of the cube and the four in the back. This yields

$$B = \frac{1}{4n} [b + ab + bc + abc - (1) - a - c - ac] \qquad (D.8)$$

The effect of C is a contrast between the four treatment combinations in the top face of the cube and the four in the bottom, that is,

$$C = \frac{1}{4n} [c + ac + bc + abc - (1) - a - b - ab] \qquad (D.9)$$

When C is at the low level, the effect of the AB interaction is the average difference in the A effect at the two levels of B, that is, $\{[ab - b] - [a - (1)]\}/(2n)$. When C is at the high level, the AB interaction is $[(abc - bc) - (ac - c)]/(2n)$. The average AB effect is just the average of these two, or

$$AB = \frac{1}{4n} [ab - b - a + (1) + abc - bc - ab + c] \qquad (D.10)$$

Similarly, we find the average effects of AC and BC as

$$AC = \frac{1}{4n} [(1) - a + b - ab - c + ac - bc + abc] \qquad (D.11)$$

and

$$BC = \frac{1}{4n} [(1) + a - b - ab - c - ac + bc + abc] \qquad (D.12)$$

The ABC effect is defined as the average difference between the AB interaction for the two different levels of C. Thus,

$$ABC = \frac{1}{4n} [abc - bc - ac + c - ab + b + a - (1)] \qquad (D.13)$$

In equation D.7 through D.13, the quantities in brackets are contrasts in the treatment combinations. A table of plus and minus signs can be developed from the contrast constants and is shown in Table D.3. Signs for the main effects are determined by associating a plus with the high level and a minus with the low level. Once the signs for the main effects have been established, the signs for the remaining columns can be obtained by multiplying the appropriate preceding columns, row by row. For example, the signs in the AB column are the product of the A and B column signs in each row. The contrast for any effect can be obtained easily from this table.

Table D.3 Algebraic signs for calculating effects in the 2^3 design

Treatment combination	Factorial effect							
	I	A	B	AB	C	AC	BC	ABC
(1)	+	-	-	+	-	+	+	-
a	+	+	-	-	-	-	+	+
b	+	-	+	-	-	+	-	+
ab	+	+	+	+	-	-	-	-
c	+	-	-	+	+	-	-	+
ac	+	+	-	-	+	+	-	-
bc	+	-	+	-	+	-	+	-
abc	+	+	+	+	+	+	+	+

Table D.3 has several interesting properties as follows:

- Except for column I, every column has an equal number of plus and minus signs.
- The sum of products of signs in any two columns is zero.
- Column I multiplied times any column leaves that column unchanged. That is, I is an identity element.
- The product of any two columns yields a column in the table. For example, A×B = AB, and AB × B = AB^2 = A

We see that the exponents in the products are formed by using modulus 2 arithmetic (the exponent can only be zero or one; if it is greater than one, it is reduced by multiples of two until it is either zero or one). All of these properties are implied by the orthogonality of the contrasts used to estimate the effects.

D.1.3 The general k-factor of the 2^k factorial design

The methods of analysis may be generalized to the case of a 2^k factorial design, that is, a design with k factors each at two levels. The statistical model for a 2^k design would include k main effects, $\dfrac{k!}{(k-2)!\,2!}$ two-factor interactions, $\dfrac{k!}{(k-3)!\,3!}$ two-factor interactions, …, one k-factor interaction. That is, for a 2^k design the complete model would contain 2k-1 effects. The notation introduced earlier for treatment combinations is also used here. For example, in a 2^5 design *abd* denotes the treatment combination with factors A, B, and D at the high level and factors C and E at the low level. The treatment combinations may be written in standard order by introducing the factors one at a time; each new factor being successively combined with those above it. For example, the standard order for a 2^4 design is (1), *a*, *b*, *ab*, *c*, *ac*, *bc*, *abc*, *d*, *ad*, *bd*, *abd*, *cd*, *acd*, *bcd*, and *abcd.*

To estimate an effect, we must first determine the contrast associated with that effect. This can always be done by using a table of plus and minus signs, such as table G.3. However, for large values of k this is awkward, and we prefer an alternate method. In general, we determine the contrast for effect AB…K by expanding the right-hand side of

$$\text{Contrast}_{AB\ldots K} = (a \pm 1)(b \pm 1)\ldots..(k \pm 1) \qquad (D.14)$$

In expanding equation D.14, ordinary algebra is used with "1" being replaced by (1) in the final expression. The sign in each set of parentheses is negative if the factor is included in the effect, and positive if the factor is not included. For example, the contrast for AB of the 2^3 factorial design is

$$\text{Contrast}_{AB} = (a - 1)(b - 1)(c + 1)$$
$$= [abc + ab + c + (1) - ac - bc - a - b]$$

Once the contrasts for the effects have been computed, we may estimate the effects according to

$$AB\ldots K = \frac{2}{n2^k} (\text{Contrast}_{AB\ldots K}) \qquad (D.15)$$

where n denotes the number of replicates.

D.2 Method of analysis of the factorial design

D.2.1 The analysis of variance

D.2.1.1 The two-factor of the 2^k factorial design

The simplest types of factorial design involve only two factors or sets of treatments. There are 2 levels of factor A and 2 levels of factor B, and these are arranged in a factorial design; that is, each replicate of the experiment contains all 4 treatment combinations. Assume there are *n* replicates of the experiment, and let y_{ijm} represent the observation taken under the ith level of factor A and the jth level of factor B in the mth replicate. The data will appear as in Table D.4. The order in which the 4*n* observations are taken is selected at random, so that this design is a completely randomized design.

Table D.4 Data arrangement for a 2^2 factorial design

Factor A	Factor B	
	Low (1)	High (2)
Low (1)	$(y_{11})_1,(y_{11})_2,\ldots(y_{11})_n$	$(y_{12})_1,(y_{12})_2,\ldots(y_{12})_n$
High (2)	$(y_{21})_1,(y_{21})_2,\ldots(y_{21})_n$	$(y_{22})_1,(y_{22})_2,\ldots(y_{22})_n$

In the statistical approach, the observations may be described by the linear statistical model

$$y_{ijm} = \mu + \tau_i + \beta_j + (\tau\beta)_{ij} + \varepsilon_{ijm} \qquad (G.16)$$

where $i = 1,2$; $j = 1,2$; and $m = 1,2,\ldots,n$

μ is   the overall mean

τ_i is   the effect of the ith level of factor A

β_j is   the effect of the jth level of factor B

$(\tau\beta)_{ij}$ is   the effect of the interaction between τ_i and β_j

ε_{ijm} is   a random error component

The objective of this method is to test appropriate hypothesis about the treatment effects and to estimate them. For hypothesis testing, the model errors are assumed to be normally and independently distributed random variables with mean zero and variance σ^2 that is assumed constant for all levels of the factor. The treatment effects are defined as deviations from the overall mean, so $\sum_{i=1}^{a} \tau_i = o$ and $\sum_{j=1}^{b} \beta_j = o$. Similarly, the interaction effects are fixed and defined so that $\sum_{i=1}^{a} (\tau\beta)_{ij} = \sum_{i=1}^{b} (\tau\beta)_{ij} = o$. Since there are n replicates of the experiment, there are $4n$ total observations.

In the two-factor factorial, both factors (or treatments), A and B, are of equal interest. Specifically, we are interested in testing hypotheses about the equality of the treatment effects of factor A, say

$$H_0: \quad \tau_1 = \tau_2 = 0$$

$$H_1: \quad \text{at least one } \tau_i \neq 0$$

(D.17a)

and the equality of the treatment effects of factor B, say

$$H_0: \quad \beta_1 = \beta_2 = 0$$

$$H_1: \quad \text{at least one } \beta_i \neq 0$$

(D.17b)

We are also interested in determining whether A and B treatments interact. Thus, we also wish to test

$$H_0: \quad (\tau\beta)_{ij} = 0 \qquad \text{for all i, j}$$

$$H_1: \quad \text{at least one } (\tau\beta)_{ij} \neq 0$$

(D.17c)

These hypotheses are tested using a two-factor analysis of variance, say F-tests. Consequently, it is necessary to compute the statistical values, that is, sum of squares and mean squares.

Let $y_{i..}$ denote the total of all observations under the ith level of factor A, $y_{.j.}$ denote the total of all observations under the jth level of factor B, y_{ij} denote the total of all observations in the ij^{th} cell, and $y..$ denote the grand total of all the observations. Define $\bar{y}_{i..}$, $\bar{y}_{.j.}$, $\bar{y}_{ij.}$, and $\bar{y}_{...}$ as the corresponding row, column, cell, and grand averages. Expressed mathematically

$$y_{i..} = \sum_{j=1}^{2}\sum_{m=1}^{n} y_{ijm} \qquad \bar{y}_{i..} = \frac{y_{i..}}{2n} \qquad i = 1,2 \qquad (D.18)$$

$$y_{.j.} = \sum_{i=1}^{2}\sum_{m=1}^{n} y_{ijm} \qquad \bar{y}_{.j.} = \frac{y_{.j.}}{2n} \qquad j = 1,2 \qquad (D.19)$$

$$y_{ij.} = \sum_{m=1}^{n} y_{ijm} \qquad \bar{y}_{ij.} = \frac{y_{ij.}}{n} \qquad i = 1,2 \text{ and } j = 1,2 \qquad (D.20)$$

$$y_{...} = \sum_{i=1}^{2}\sum_{j=1}^{2}\sum_{m=1}^{n} y_{ijm} \qquad \bar{y}_{...} = \frac{y_{...}}{4n} \qquad (D.21)$$

The total corrected sum of squares may be written as

$$\sum_{i=1}^{2}\sum_{j=1}^{2}\sum_{m=1}^{n}(y_{ijm} - \bar{y}_{...})^2 = \sum_{i=1}^{2}\sum_{j=1}^{2}\sum_{m=1}^{n}[(\bar{y}_{i..} - \bar{y}_{...}) + (\bar{y}_{.j.} - \bar{y}_{...})$$

$$+ (\bar{y}_{ij.} - \bar{y}_{i..} - \bar{y}_{.j.} - \bar{y}_{...}) + (y_{ijm} - \bar{y}_{ij.})]^2$$

$$= 2n\sum_{i=1}^{2}(\bar{y}_{i..} - \bar{y}_{...})^2 + 2n\sum_{j=1}^{2}(\bar{y}_{.j.} - \bar{y}_{...})^2 \qquad (D.22)$$

$$+ n\sum_{i=1}^{2}\sum_{j=1}^{2}(\bar{y}_{ij.} - \bar{y}_{i..} - \bar{y}_{.j.} + \bar{y}_{...})^2$$

$$+ \sum_{i=1}^{2}\sum_{j=1}^{2}\sum_{m=1}^{n}(y_{ijm} - \bar{y}_{ij.})^2$$

The total sum of squares has been partitioned into a sum of squares due to factor A (SS_A), a sum of squares due to factor B (SS_B), and a sum of squares due to error (SS_E). From the last component on the right-hand side of equation D.22, we see that there must be at least two replicates ($n \geq 2$) to obtain an error sum of squares. We may write equation D.22 symbolically as

$$SS_T = SS_A + SS_B + SS_{AB} + SS_E \tag{D.23}$$

The number of degrees of freedom associated with each sum of squares is shown in Table D.5

Table D.5 The number of degrees of freedom of the 2^2 factorial design

Effect	Degrees of freedom (d.f)
A	1
B	1
AB interaction	1
Error	4(n-1)
Total	4n-1

Each sum of squares divided by its degrees of freedom is a "***mean squares***". The expected values of the mean squares are

$$E(MS_A) = E\left(\frac{SS_A}{(d.f.)_A}\right) = \sigma^2 + 2n\sum_{i=1}^{2}\tau_i^2 \tag{D.24}$$

$$E(MS_B) = E\left(\frac{SS_B}{(d.f.)_B}\right) = \sigma^2 + 2n\sum_{j=1}^{2}\beta_j^2 \tag{D.25}$$

$$E(MS_{AB}) = E\left(\frac{SS_{AB}}{(d.f.)_{AB}}\right) = \sigma^2 + n\sum_{i=1}^{2}\sum_{j=1}^{2}(\tau\beta)_{ij}^2 \tag{D.26}$$

$$E(MS_E) = E\left(\frac{SS_E}{(d.f.)_E}\right) = \sigma^2 \tag{D.27}$$

Notice that, if the null hypotheses of no treatment effects of factor A, B and AB interaction are true, then MS_A, MS_B, MS_{AB}, and MS_E all estimate σ^2. However, if there are differences between treatment effects of factor A, then MS_A will be larger than MS_E. Similarly, if there are treatment effects of interaction present, then the corresponding mean squares will be larger than MS_E. Therefore, to test the significance of both main effects and their interaction, simply divide the corresponding mean square by the error mean square. Large values of this ratio imply that the data do not support the null hypothesis. That means the treatment effects that have large ratio are significant.

If we assume that the model is adequate and that the error term ε_{ijm} are normally and independently distributed with constant variance σ^2, then each of the ratios of mean squares MS_A/MS_E, MS_B/MS_E, and MS_{AB}/MS_E are distributed as F with $(d.f.)_A$, $(d.f.)_B$, and $(d.f.)_{AB}$ numerator degrees of freedom, respectively, and $(d.f.)_E$ denominator degrees of freedom, and the critical region would be the upper tail of the F distribution. The test procedure is usually summarized in an analysis of variance table, as shown in Table D.6.

Table D.6 The analysis of variance table for the 2^2 factorial design

Source of variation	Sum of squares	Degrees of freedom	Mean square	F_0
A	SS_A	1	$MS_A = SS_A$	MS_A/MS_E
B	SS_B	1	$MS_B = SS_B$	MS_B/MS_E
AB	SS_{AB}	1	$MS_{AB} = SS_{AB}$	MS_{AB}/MS_E
Error	SS_E	4(n-1)	$MS_E = SS_E / 4(n-1)$	
Total	SS_T	4n-1		

Computational formulas for the sums of squares in equation D.27 may be obtained easily. The total sum of squares is computed as usual by

$$SS_T = \sum_{i=1}^{2} \sum_{j=1}^{2} \frac{y_{ij.}^2}{n} - \frac{y_{...}^2}{4n} \qquad (D.28)$$

The sums of squares for main effects are

$$SS_A = \sum_{i=1}^{2} \frac{y_{i..}^2}{2n} - \frac{y_{...}^2}{4n} \qquad (D.29)$$

$$SS_B = \sum_{j=1}^{2} \frac{y_{.j.}^2}{2n} - \frac{y_{...}^2}{4n} \qquad (D.30)$$

In form of factorial design nomenclature, say (1), a, b and ab, it is easily to obtain SS_A and SS_B as follows:

$$SS_A = \frac{(Contrast_A)^2}{4n} \qquad (D.31)$$

$$SS_B = \frac{(Contrast_B)^2}{4n} \qquad (D.32)$$

Similarly, we can compute SS_{AB} as follows:

$$SS_{AB} = \frac{(Contrast_{AB})^2}{4n} \qquad (D.33)$$

We may compute SS_E by subtraction as

$$SS_E = SS_T - SS_{AB} - SS_A - SS_B \qquad (D.34)$$

D.2.1.2 The three-factor of 2^k factorial design

Consider the three-factor analysis of variance model

$$y_{ijml} = \mu + \tau_i + \beta_j + \gamma_m + (\tau\beta)_{ij} + (\tau\gamma)_{ik} + (\beta\gamma)_{jm} + (\tau\beta\gamma)_{ijm} + \varepsilon_{ijml} \qquad (D.35)$$

where $\quad i = 1,2 ; \quad j = 1,2 ; \quad m = 1,2 \text{ and } l = 1,2,\ldots,n$

Assuming that A, B, and C are fixed, the analysis of variance table is shown in table D.7. The F-tests on main effects and interactions follow directly from the expected mean squares.

Table D.7 The analysis of variance table for the 2^3 factorial design

Source of variation	Sum of squares	Degrees of freedom	Mean square	F_0
A	SS_A	1	$MS_A = SS_A$	MS_A/MS_E
B	SS_B	1	$MS_B = SS_B$	MS_B/MS_E
C	SS_C	1	$MS_C = SS_C$	MS_C/MS_E
AB	SS_{AB}	1	$MS_{AB} = SS_{AB}$	MS_{AB}/MS_E
AC	SS_{AC}	1	$MS_{AC} = SS_{AC}$	MS_{AC}/MS_E
BC	SS_{BC}	1	$MS_{BC} = SS_{BC}$	MS_{BC}/MS_E
ABC	SS_{ABC}	1	$MS_{ABC} = SS_{ABC}$	MS_{ABC}/MS_E
Error	SS_E	8(n-1)	$MS_E = SS_E / 8(n-1)$	
Total	SS_T	8n-1		

We will give the computing formulas for the sums of squares in Table D.7. The total sum of squares is found in the usual way as

$$SS_T = \sum_{i=1}^{2} \sum_{j=1}^{2} \sum_{m=1}^{2} \sum_{l=1}^{n} y_{ijml}^2 - \frac{y_{...}^2}{8n} \qquad (D.36)$$

The sums of squares for main effects are found from the totals for factors $A(y_{i...})$, $B(y_{.j..})$, and $C(y_{..m.})$ as follows :

$$SS_A = \frac{(Contrast_A)^2}{8n} \qquad (D.37)$$

$$SS_B = \frac{(Contrast_B)^2}{8n} \qquad (D.38)$$

$$SS_C = \frac{(Contrast_C)^2}{8n} \qquad (D.39)$$

Similarly, the two- and three-factor interaction sum of squares of the 2^3 factorial analysis are found from

$$SS_{AB} = \frac{(Contrast_{AB})^2}{8n} \qquad (D.40)$$

$$SS_{AC} = \frac{(Contrast_{AC})^2}{8n} \qquad (D.41)$$

$$SS_{BC} = \frac{(Contrast_{BC})^2}{8n} \qquad (D.42)$$

and

$$SS_{ABC} = \frac{(Contrast_{ABC})^2}{8n} \qquad (D.43)$$

The error sum of squares may be found by subtracting the sum of squares for each main effect and interaction from the total sum of squares as follows:

$$SS_E = SS_T - SS_{AB} - SS_{AC} - SS_{BC} - SS_{ABC} \qquad (D.44)$$

D.2.1.3 The general k-factor of the 2^k factorial design

The results for the two- and three-factor factorial design may be extended to the general case where there are a levels of factor A, b levels of factor B, c levels of factor C and so on, arranged in a factorial experiment. In general, there will be abc...n total observations, if there are n replicates of the complete experiment. Once again, note that we must have at least two replicates ($n \geq 2$) in order to determine a sum of squares due to error if all possible interactions are included in the model.

If all factors in the experiment are fixed, we may easily formulate and test hypotheses about the main effects and interactions. The test statistics for each main effect and interactions may be constructed by dividing the corresponding mean square for the effect or interaction by mean square error. All of these F-tests will be upper-tail, one-tail tests. The number of degrees of freedom for any main effect is the number of levels of the factor minus one, and the number of degrees of freedom for an interaction is the product of the number of degrees of freedom associated with the individual components of the in interaction.

We may compute the sums of squares of the 2^k factorial according to

$$SS_{AB...K} = \frac{(Contrast_{AB...K})^2}{n2^k} \tag{D.45}$$

The analysis of variance for the 2^k is summarized in Table D.8.

D.2.1.4 The single replicate of the 2^k factorial design

For even a moderate number of factors the total number of treatment combinations in a 2^k factorial design is large. For example, a 2^5 has 32 treatment combinations, a 2^6 has 64 treatment combinations, and so on. Since resources are usually limited, the number of replicates that the experimenter can employ may be restricted. Frequently, available resources only allow a single replicate of the design to be run, unless the experimenter is willing to omit some of the original factors.

Table D.8 The analysis of variance table for the 2^k factorial design

Type of treatment effect	Source of variation	Sum of squares	Degrees of freedom	Mean square	F_0
k main effect					
	A	SS_A	1	$MS_A = SS_A$	MS_A/MS_E
	B	SS_B	1	$MS_B = SS_B$	MS_B/MS_E
	M	M	M	M	M
	K	SS_K	1	$MS_K = SS_K$	MS_K/MS_E
$\binom{k}{2}$ Two-factor					
	AB	SS_{AB}	1	$MS_{AB} = SS_{AB}$	MS_{AB}/MS_E
interactions	AC	SS_{AC}	1	$MS_{AC} = SS_{AC}$	MS_{AC}/MS_E
	M	M	M	M	M
	JK	SS_{JK}	1	$MS_{JK} = SS_{JK}$	MS_{JK}/MS_E
$\binom{k}{3}$ Three-factor					
	ABC	SS_{ABC}	1	$MS_{ABC} = SS_{ABC}$	MS_{ABC}/MS_E
interactions	ABD	SS_{ABD}	1	$MS_{ABD} = SS_{ABD}$	MS_{ABD}/MS_E
	M	M	M	M	M
	IJK	SS_{IJK}	1	$MS_{IJK} = SS_{IJK}$	MS_{IJK}/MS_E
M	M	M	M	M	M
$\binom{k}{k}$ k-factor					
interactions	ABC..K	$SS_{ABC..K}$	1	$MS_{ABC..K} = SS_{ABC..K}$	$MS_{ABC..K}/MS_E$
	Error	SS_E	$2^k(n-1)$	$MS_E = SS_E/[2^k(n-1)]$	
	Total	SS_T	$n2^k-1$		

With only a single replicate of the 2^k, it is impossible to compute an estimate of experimental error, that is, a mean square for error. Thus, it seems that hypotheses concerning main effects and interactions cannot be tested. However, to estimate the experimental error, the usual approach to the analysis of a single replicate of the 2^k is to assume that certain high-order interactions are negligible, and combined them as the errors. We should select the interactions that will make up the error mean square before the data are analyzed, since testing high-order interactions and taking those that appear small as error can lead to substantial underestimation of the true experimental error. Usually, the smallest design for which this procedure is recommended is the 2^4. The practice of combining higher-order interaction mean squares to estimate the error is subject to criticism on statistical grounds. If some of these interactions are significant, then the estimate of error will be inflated. As a result, other significant effects may not be detected and the significant interactions taken as error will be discovered. As a general rule, it is

probably unwise to assume two-factor interactions to be zero without prior information. If most two-factor interactions are small, then it seems likely that all higher-order interactions will be insignificant also. Experimenters must use both their knowledge of the phenomena under study and common sense in the analysis of such a design. For example, if in the analysis of a 2^5 the main effects of A, B, and C as well as AB and AC are very large, then it is likely that ABC may be large. Thus, ABC should not be included in the interactions used as error. Such a decision is best made before ABC is examined.

D.2.2 Estimation of the treatment effects on normal probability paper

When analyzing data from unreplicated factorial designs, occasionally real high-order interactions occur. The use of an error mean square obtained by pooling high-order interactions is inappropriate in these cases. A method of analysis attributed to Daniel (1959) provides a simple way to overcome this problem. Daniel suggests plotting the estimates of the effects on normal probability paper. The effects that are negligible are normally distributed, with mean zero and variance σ^2, and will tend to fall along a straight line on this plot, while significant effects will have nonzero means and will not lie along the straight line.

For this method, all of the estimation of treatment effects is ordered from the smallest to the largest effects as shown in Table D.9. To plot on normal probability paper, the probability of each of effects must be calculated from equation D.46.

$$P_q = (q - 0.5)/N_Q \tag{D.46}$$

Table D.9 The order of treatment effect for analysis on normal probability paper

Order (q)	Treatment effect	Estimate of treatment effect	P_q
1	$(ABC...K)_{smallest}$	The smallest values	$0.5/N_Q$
M	M	M	M
N_Q	$(ABC...K)_{largest}$	The largest values	$(N_Q-0.5)/N_Q$

D.4 Fractional factorial designs

As the number of factors in a 2^k factorial design increases, the number of runs required for a complete replicate of the design rapidly outgrows the resources of most experimenters. A complete replicate of the 2^6 design requires 64 runs. In this design only 6 of 63 degrees of freedom correspond to main effects, and only 15 degrees of freedom correspond to two-factor interactions. The remaining 42 degrees of freedom are associated with three-factor and higher interactions.

If the experimenter can reasonably assume that certain high-order interactions are negligible, then information on main effects and low-order interactions may be obtained by running only a fraction of the complete factorial experiment. These fractional factorial designs are widely used in industrial research. A major use of fractional factorials is in screening experiments. These are experiments in which many factors are considered with the purpose of identifying those factors (if any) which have large effects. Screening experiments are usually performed in the early stages of a project when it is likely that many of the factors initially considered have little or no effect on the response. The factors that are identified as important are then investigated more thoroughly in subsequent experiments.

D.4.1 The principle of the one-half fraction of the 2^k design

A one-half fraction of the 2^k design contains 2^{k-1} runs and is often called *a 2^{k-1} fractional factorial design*. For example, suppose that we were investigating k = 4 factors (16 runs). In one-half fractional factorial design, it can only be run a half of 2^4, that is 8 runs. Then, the results will be analyzed, and then decide on the best set of runs to perform next stage of experimentation, which might involve adding or removing factors, changing responses, or varying some factors over new ranges. If necessary to resolve ambiguities, we can always run the complimentary fraction and complete the 2^4 design. Consequently, the fractional factorial designs often leads to great economy and efficiency in experimentation, particularly if the runs can be made sequentially.

For the simplicity, consider a situation in which three factors, each at two levels, are of interest, but the experimenters cannot afford to run all $2^3 = 8$ treatment combinations. They can, however, afford four runs, so this suggests a one-half fraction of a 2^3 one-half fraction of the 2^3 design is often called a 2^{3-1} design. The table of plus and minus signs for the 2^3 design is shown in Table D.10. Suppose we select the four treatment combinations a, b, c and abc as our one-half fraction. These treatment combinations are shown in the top half of Table D.10. We use both the conventional notation (*a, b, c,…*) and the plus and minus notation for the treatment combinations.

Table D.10 Plus and minus signs for the 2^3 factorial design

Treatment combination	Factorial effect							
	I	**A**	**B**	**C**	**AB**	**AC**	**BC**	**ABC**
a	+	+	-	-	-	-	+	+
b	+	-	+	-	-	+	-	+
c	+	-	-	+	+	-	-	+
abc	+	+	+	+	+	+	+	+
ab	+	+	+	-	+	-	-	-
ac	+	+	-	+	-	+	-	-
bc	+	-	+	+	-	-	+	-
(1)	+	-	-	-	+	+	+	-

Notice that the 2^{3-1} design is formed by selecting only those treatment combinations that yield a plus on the ABC effect. Thus, ABC is called *the generator of this particular fraction*. Furthermore, the identity element I is also always plus, so *the defining relation* for our design is

$$I = ABC \qquad (D.47)$$

The treatment combinations in the 2^{3-1} design yield three degrees of freedom that we may use to estimate the main effects. Referring to table we note that the linear combinations of the observations used to estimate the main effects of A, B, and C are

$$l_A = \frac{1}{2}(a - b - c + abc) \qquad (D.48)$$

$$l_B = \frac{1}{2}(-a + b - c + abc) \qquad (D.49)$$

$$l_C = \frac{1}{2}(-a - b + c + abc) \qquad (D.50)$$

It is also easy to verify that the linear combinations of the observations used to estimate the two-factor interactions are

$$l_{BC} = \frac{1}{2}(a-b-c+abc) \tag{D.51}$$

$$l_{AC} = \frac{1}{2}(-a+b-c+abc) \tag{D.52}$$

$$l_{AB} = \frac{1}{2}(-a-b+c+abc) \tag{D.53}$$

Thus, $l_A = l_{BC}$, $l_B = l_{AC}$, and $l_C = l_{AB}$, and consequently it is impossible to differentiate between A and BC, B and AC, and C and AB. In fact, we can show that when we estimate A, B, and C we are really estimating A+BC, B+AC, and C+AB. Two or more effects that have this property are called aliases. Thus, A and BC are aliases, B and AC are aliases, and C and AB are aliases. We indicate this by the notation

$$l_A \rightarrow A + BC$$
$$l_B \rightarrow B + AC$$
$$l_C \rightarrow C + AB$$

The alias structure for this design may be easily determined by using the defining relation $I = ABC$. Multiplying any effect by the defining relation modulus 2 yields the aliases for that effect. This yields as the alias of A

$$A \cdot I = A \cdot ABC$$
$$A = A^2 BC = BC$$

Since any effect times the identity I is just the original effect.. Similarly, we find the aliases of B and C as

$$B \cdot I = B \cdot ABC$$
$$B = AB^2 C = AC$$

and

$$C \cdot I = C \cdot ABC$$
$$C = ABC^2 = AB$$

Now suppose that we had chosen the other one-half fraction. The defining relation for this design is

$$I = -ABC \qquad\qquad (D.54)$$

The linear combination of the observations, say l'_A, l'_B, and l'_C from the alternate fraction give us

$$l'_A \to A - BC$$
$$l'_B \to B - AC$$
$$l'_C \to C - AB$$

Thus, when we estimate A, B, and C with this particular fraction, we are really estimating A-BC, B-AC, and C-AB

In practice, it does not matter which fraction is actually used. The fraction associated with $I = +ABC$ is usually called *"**the principal fraction**"*. Both fractions belong to the same family; that is, the two one-half fractions form a complete 2^3 design.

Suppose that after running one of the one-half fractions of the 2^3 design, the other one was also run. Thus, all 8 runs associated with the full 2^3 are now available. We may now obtain de-aliased estimates of all effects by analyzing the 8 runs as a full 2^3 design in two blocks of 4 runs each. This could also be done by adding and subtracting the linear combination of effects from the two individual fractions. All three pairs of linear combinations are shown in Table D.10.

Table D.10 Three pairs of linear combinations of the 2^3 design

i	$\frac{1}{2}(l_i + l'_i)$	$\frac{1}{2}(l_i - l'_i)$
A	$\frac{1}{2}(A + BC + A - BC) = A$	$\frac{1}{2}(A + BC - A + BC) = BC$
B	$\frac{1}{2}(B + AC + B - AC) = B$	$\frac{1}{2}(B + AC - B + AC) = AC$
C	$\frac{1}{2}(C + AB + C - AB) = C$	$\frac{1}{2}(C + AB - C + AB) = AB$

D.4.2 Constructing one-half fraction of the 2^k design

A one-half fraction of the 2^k design may be constructed by writing down the treatment combinations for a full 2^{k-1} factorial and then adding the kth factor by identifying its plus and minus levels with the plus and minus signs of the highest-order interaction ABC…(K-1). Therefore, the 2^{3-1} fractional factorial is obtained by writing down the full 2^2 factorial and then equating factor C to the AB interaction. The alternate fraction would be obtained by equating factor C to the –AB interaction. This approach is illustrated in Table D.11

Note that any interaction effect could be used to generate the column for the kth factor. However, using any effect other than ABC…(K-1) will not produce a design of highest possible resolution.

Table D.11 The two one-half fractions of the 2^3 design

Full 2^2 factorial		2^{3-1}, I = ABC			2^{3-1}, I = -ABC		
A	B	A	B	C = AB	A	B	C = -AB
-	-	-	-	+	-	-	-
+	-	+	-	-	+	-	+
-	+	-	+	-	-	+	+
+	+	+	+	+	+	+	-

APPENDIX E

THE ESTIMATION OF EFFECTS USING YATES' METHOD

Instead of using the table of plus and minus signs to obtain the contrasts for the effect estimates and the sums of squares, a simple tabular algorithm devised by Yates can be employed. To use Yates' method, construct a table with the treatment combinations and the corresponding treatment totals recorded in standard order, which means that each factor is introduced one at a time by combining it with all factor levels above it. Thus for a 2^2, the standard order is (1), a, b, ab, while for a 2^3 it is (1), a, b, ab, c, ac, bc, abc. Then follow this four-step procedure (Hines and Montgomery, 1990):

1. Label the adjacent column (1). Compute the entries in the top half of this column by adding the observations in adjacent pairs. Compute the entries in the bottom half of this column by changing the sign of the first entry in each pair of the original observations and adding the adjacent pairs.

2. Label the adjacent column (2). Construct column (2) using the entries in column (1). Follow the same procedure employed to generate column (1). Continue this process until k columns have been constructed. Column (k) contains the contrasts designated in the rows.

3. Calculate the sums of squares for the effects by squaring the entries in column k and dividing by 2^k for single replication.

4. Calculate the effect estimates by dividing the entries in column k by 2^{k-1} for single replication.

Accordingly, the estimated effect investigated in chapter 6 can be found easily as shown in Table E.1 and E.2.

Table E.1 The estimated effect of the 2^5 factorial design using Yates' method

Treatment combination	Efficiency (%)	(1)	(2)	(3)	(4)	(5)	Treatment effect	Estimated effect	Sum of squares
(1)	70.53	133.98	280.53	485.64	990.63	1994.14	I	-	-
a	63.44	146.56	205.11	504.99	1003.50	-148.83	A	-9.30	692.17
b	70.76	95.20	289.18	496.70	124.66	93.90	B	5.87	275.55
ab	75.80	109.91	215.81	506.80	-273.48	71.05	AB	4.44	157.77
c	35.97	138.53	258.15	58.76	55.37	-182.98	C	-11.44	1046.33
ac	59.23	150.64	238.56	65.90	38.54	318.07	AC	19.88	3161.54
bc	36.19	99.92	260.70	-134.21	53.48	26.05	BC	1.63	21.21
abc	73.72	115.89	246.10	-139.27	17.58	32.77	ABC	2.05	33.56
d	72.51	126.47	-2.04	27.29	-148.79	29.44	D	1.84	27.09
ad	66.02	131.67	60.80	28.08	-34.19	2.09	AD	0.13	0.14
bd	72.76	111.98	-1.36	19.80	131.46	-0.28	BD	-0.02	0.00
abd	77.89	126.58	67.26	18.74	186.62	1.85	ABD	0.12	0.11
cd	37.01	128.33	-113.39	26.40	5.99	7.04	CD	0.44	1.55
acd	62.91	132.37	-20.82	27.08	20.06	7.24	ACD	0.45	1.64
bcd	37.27	115.70	-116.66	8.20	5.97	2.99	BCD	0.19	0.28
abcd	78.62	130.40	-22.61	9.38	26.80	2.50	ABCD	0.16	0.20

Table E.1 (cont.) The estimated effect of the 2^5 factorial design using Yates' method

Treatment combination	Efficiency (%)	(1)	(2)	(3)	(4)	(5)	Treatment effect	Estimated effect	Sum of squares
e	90.98	-7.09	12.58	-75.42	19.34	12.87	E	0.80	5.18
ae	35.49	5.04	14.71	-73.37	10.10	-398.14	AE	-24.88	4953.55
be	94.78	23.27	12.11	-19.59	7.14	-16.83	BE	-1.05	8.85
abe	36.89	37.53	15.97	-14.60	-5.06	-35.90	ABE	-2.24	40.28
ce	63.84	-6.49	5.20	62.84	0.79	114.60	CE	7.16	410.38
ace	48.13	5.13	14.60	68.61	-1.06	55.16	ACE	3.45	95.08
bce	65.84	25.90	4.04	92.57	0.68	14.08	BCE	0.88	6.19
abce	60.73	41.36	14.70	94.05	1.18	20.84	ABCE	1.30	13.57
de	92.78	-55.50	12.13	2.13	2.06	-9.24	DE	-0.58	2.67
ade	35.56	-57.90	14.27	3.86	4.99	-12.20	ADE	-0.76	4.65
bde	95.90	-15.71	11.62	9.40	5.77	-1.85	BDE	-0.12	0.11
abde	36.47	-5.11	15.46	10.66	1.48	0.50	ABDE	0.03	0.01
cde	66.40	-57.22	-2.40	2.13	1.72	2.93	CDE	0.18	0.27
acde	49.30	-59.44	10.60	3.83	1.26	-4.29	ACDE	-0.27	0.57
bcde	67.96	-17.10	-2.21	13.00	1.70	-0.46	BCDE	-0.03	0.01
abcde	62.44	-5.51	11.59	13.80	0.80	-0.90	ABCDE	-0.06	0.03

Table E.2 The estimated effects of the 2^4 factorial design using Yate's method

Treatment combination	Efficiency (%)	(1)	(2)	(3)	(4)	Treatment effect	Effect	Sum of squares
(1)	70.53	133.98	280.53	485.64	982.35	-	-	-
a	63.44	146.56	205.11	496.70	-75.46	A+BCE	-9.43	355.87
b	70.76	95.20	258.15	58.76	47.09	B+ACE	5.89	132.59
ab	75.80	109.91	238.56	-134.21	34.60	AB+CE	4.33	74.82
c	35.97	126.47	-2.04	27.29	-95.01	C+ABE	-11.88	564.22
ac	59.23	131.67	60.80	19.80	155.41	AC+BE	19.43	1509.58
bc	36.19	111.98	-113.39	26.40	11.53	BC+AE	1.44	8.31
abc	73.72	126.58	-20.82	8.20	15.13	ABC+E	1.89	14.31
e	90.98	-7.09	12.58	-75.42	11.06	E+ABC	1.38	7.64
ae	35.49	5.04	14.71	-19.59	-192.97	AE+BC	-24.12	2327.31
be	94.78	23.27	5.20	62.84	-7.49	BE+AC	-0.94	3.51
abe	36.89	37.53	14.60	92.57	-18.20	ABE+C	-2.28	20.70
ce	63.84	-55.50	12.13	2.13	55.83	CE+AB	6.98	194.82
ace	48.13	-57.90	14.27	9.40	29.72	ACE+B	3.72	55.22
bce	65.84	-15.71	-2.40	2.13	7.27	BCE+D	0.91	3.30
abce	60.73	-5.11	10.60	13.00	10.87	ABCE	1.36	7.38

APPENDIX F

THE ANALYSIS OF VARIANCE (ANOVA)

As mentioned in chapter 6, mass velocity of hot air that is denoted by D for factorial design is, of course, an insignificant effect. So, this method considers merely four-factors, say, A, B, C and E.

Assumption of analysis of variance (ANOVA):
- Negligible high-order interaction (3-, 4- and 5-factor interaction)

For ANOVA method principally mentioned in appendix D, sum of squares, degree of freedom mean squares and F_0 are necessary in order to analyze with F distribution (Montgomery, 1984). Using Table D.8, their estimations can be obtained as shown in Table F.1.

Table F.1 Analysis of variance of the 2^4 factorial design for the dehumidification on a silica gel coated honeycomb rotary dehumidifier

Effect	Sum of squares	Degree of freedom	Mean squares	Fo
A	355.87	1	355.87	17.63*
B	138.39	1	132.59	6.57
C	564.22	1	564.22	27.95*
E	7.64	1	7.64	0.38
AB	74.82	1	74.82	3.71
AC	1509.58	1	1509.58	74.79*
AE	2327.31	1	2327.31	115.30*
BC	8.31	1	8.31	0.41
BE	3.51	1	3.51	0.17
CE	194.82	1	194.82	9.65
Error	100.92	5	20.18	
Total	5285.59	15		

Since the varied significance of the system, α, will change the significant effects, we focused on the situation with the differently significance, say, at $\alpha = 0.01$ and 0.05, as follows:

For $F_{0.01,1,5} = 16.26$, the significant effects are A, C, AC and AE interaction, say rotational speed, mass velocity of humid air, interaction between rotational speed and mass velocity of humid air and interaction between rotational speed and length of rotor.

For $F_{0.05,1,5} = 6.61$, the significant effects are A, C, AC, AE and CE interaction, say rotational speed, mass velocity of humid air, interaction between rotational speed and mass velocity of humid air, interaction between rotational speed and length of rotor and interaction between mass velocity of humid air and length of rotor.

APPENDIX G

THE RESULTS OF INSIGNIFICANT EFFECTS
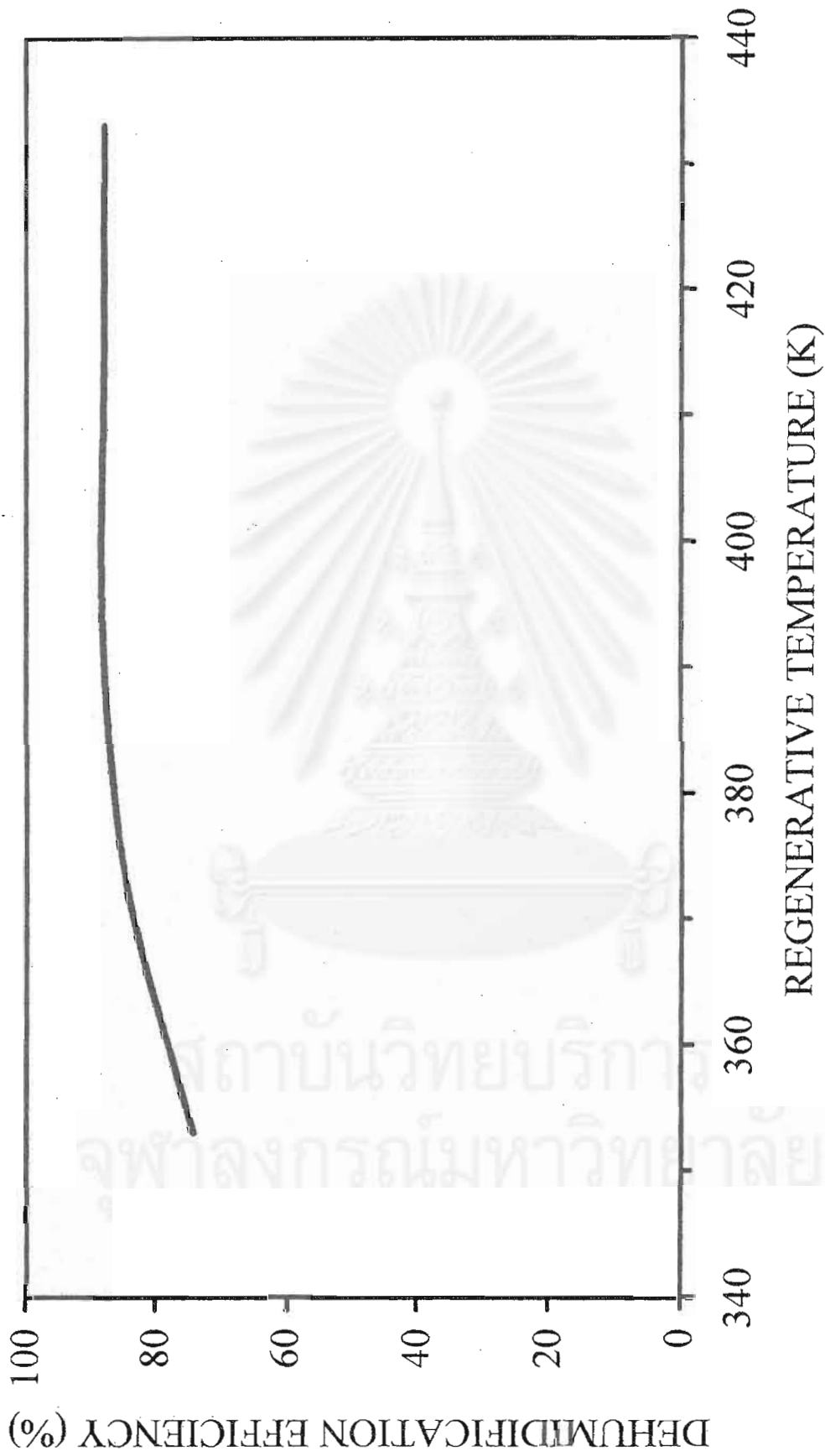
Figure G.1 Effect of the regenerative temperature on the dehumidification efficiency of the silica gel coated honeycomb rotary dehumidifier (Treg-SG-Effect Condition)
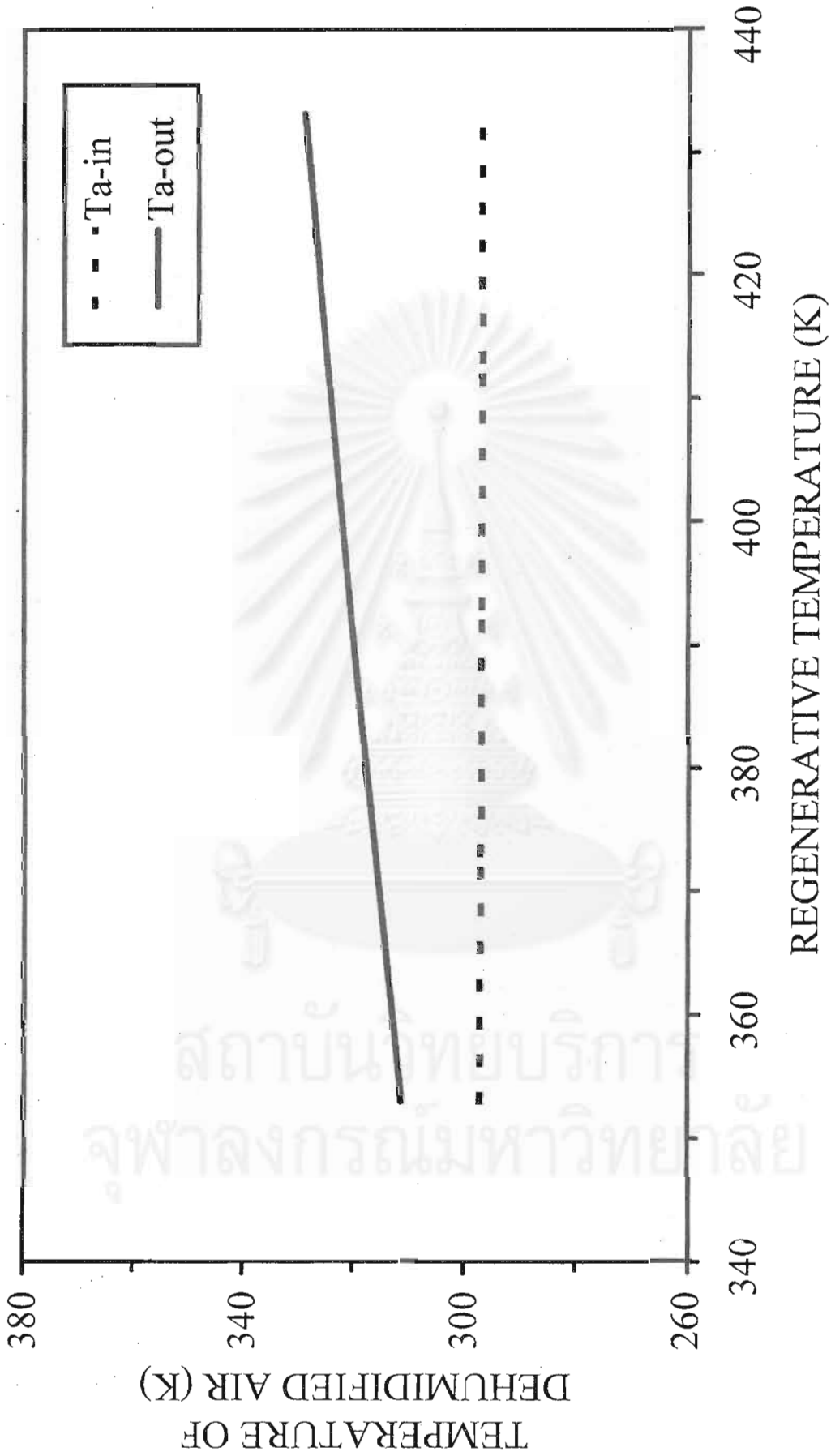
Figure G.2 Effect of the regenerative temperature on the dehumidified air temperature of the silica gel coated honeycomb rotary dehumidifier (Treg-SG-Effect Condition)

Figure G.3 Effect of the mass velocity of hot air on the dehumidification efficiency of the silica gel coated honeycomb rotary dehumidifier (Greg-SG-Effect Condition)
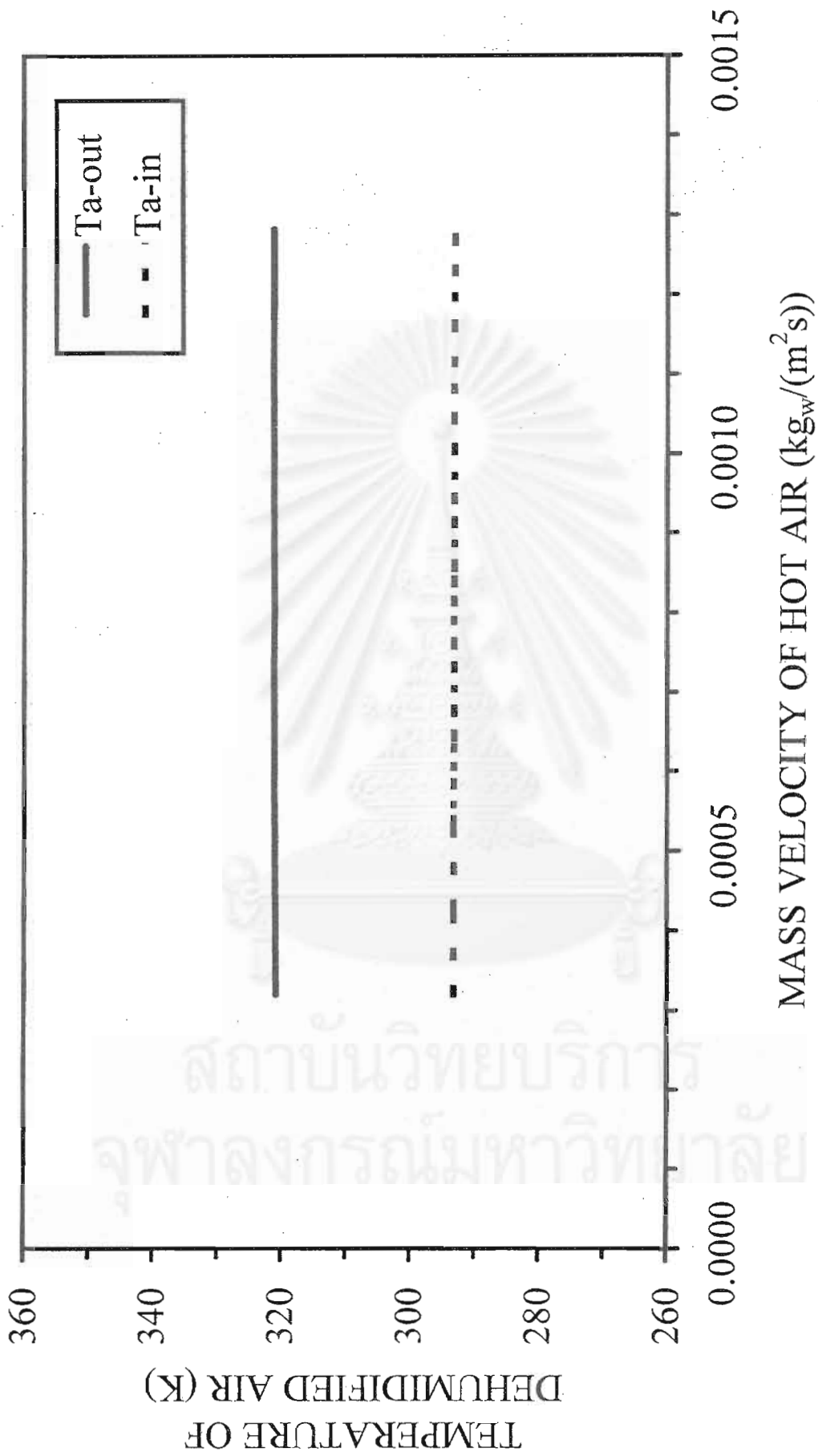
Figure G.4 Effect of the mass velocity of hot air on the dehumidified air temperature of the silica gel coated honeycomb rotary dehumidifier (Greg-SG-Effect Condition)

APPENDIX H

EXPERIMENTAL AND PREDICTED DATA FOR
MODELING VALIDATION

Table H.1 Experimental and predicted data of dehumidified air humidity and the efficiency of a silica gel coated rotary dehumidifier at various rotational speeds (H_{in} = 0.0045 kg_w/kg_{da} and T_{reg} =413 K)

Rotational speed of the rotor (rph)	Dehumidified air humidity (kg_w/kg_{da})		Dehumidification efficiency (%)	
	Experimental data	Predicted data	Experimental data	Predicted data
3.3	1.17E-03	1.34E-03	74.00	70.22
6.6	3.95E-04	4.35E-04	91.22	90.30
13.2	8.66E-04	6.78E-04	80.76	84.93

Table H.2 Experimental and predicted data of air temperature of the silica gel coated rotary dehumidifier at 3.3 rph (H_{in} = 0.0045 kg$_w$/kg$_{da}$ and T_{reg} = 413 K)

Angle of rotor	Air temperature (K)											
	Experimental data						Predicted data					
	Z = 0.0	Z = 0.2	Z = 0.4	Z = 0.6	Z = 0.8	Z = 1.0	Z = 0.0	Z = 0.2	Z = 0.4	Z = 0.6	Z = 0.8	Z = 1.0
10-15	320.00	400.00	402.00	403.00	404.00	405.00	297.30	305.87	311.67	323.58	344.15	367.71
30	297.30	308.00	311.00	312.00	317.00	320.10	297.30	303.16	306.91	308.58	309.80	312.38
60	297.30	303.10	308.50	311.80	312.20	312.00	297.30	300.37	303.87	306.42	307.93	308.65
90	297.30	301.00	305.20	308.50	310.00	310.50	297.30	298.99	301.72	304.26	306.25	307.61
120	297.30	300.50	303.40	305.00	309.00	310.20	297.30	298.25	300.28	302.52	304.53	306.18
150	297.30	300.20	301.00	303.00	308.20	309.00	297.30	297.84	299.32	301.19	303.08	304.77
180	297.30	300.00	300.60	301.50	305.00	307.20	297.30	297.61	298.66	300.19	301.87	303.48
210	297.30	299.40	300.50	300.50	303.00	305.00	297.30	297.48	298.21	299.43	300.89	302.39
240	297.30	299.00	300.20	300.00	302.00	304.00	297.30	297.41	297.91	298.87	300.11	301.46
270	297.30	298.10	300.00	300.00	301.00	302.00	297.30	297.38	297.71	298.44	299.49	300.69
300	325.00	325.00	329.50	370.00	405.50	413.00	330.92	339.52	387.90	412.48	413.12	413.14
330	360.00	405.00	409.20	410.50	412.00	413.00	413.03	413.05	413.07	413.10	413.12	413.14
360	408.00	408.50	409.00	410.00	412.00	413.00	413.04	413.05	413.07	413.10	413.12	413.14

Table H.3 Experimental and predicted data of air temperature of the silica gel coated rotary dehumidifier at 6.6 rph (H_{in} = 0.0045 kg$_w$/kg$_{da}$ and T_{reg} = 413 K)

Angle of rotor	Air temperature (K)											
	Experimental data						Predicted data					
	Z = 0.0	Z = 0.2	Z = 0.4	Z = 0.6	Z = 0.8	Z = 1.0	Z = 0.0	Z = 0.2	Z = 0.4	Z = 0.6	Z = 0.8	Z = 1.0
10-15	304.00	350.00	410.00	411.50	412.50	413.00	297.30	322.12	361.09	391.13	405.39	410.67
30	297.30	308.00	314.00	324.00	360.00	385.00	297.30	307.30	320.59	344.83	371.98	392.23
60	297.30	305.00	311.00	312.00	312.20	313.00	297.30	303.44	307.57	310.81	317.06	329.18
90	297.30	303.00	308.50	311.00	312.00	312.00	297.30	301.69	305.65	308.02	309.38	311.04
120	297.30	301.50	307.00	310.00	311.50	311.50	297.30	300.51	304.13	306.77	308.36	309.18
150	297.30	300.20	305.20	308.20	311.50	311.50	297.30	299.68	302.90	305.59	307.49	308.61
180	297.30	298.00	304.00	307.00	311.00	311.00	297.30	299.07	301.89	304.50	306.54	307.96
210	297.30	297.80	302.50	305.00	311.00	311.00	297.30	298.65	301.09	303.57	305.66	307.24
240	297.30	297.80	302.00	304.00	309.00	311.50	297.30	298.30	300.40	302.69	304.76	306.46
270	297.30	297.80	299.50	303.00	308.50	310.00	297.30	298.07	299.86	301.98	303.99	305.73
300	325.50	327.50	335.00	359.00	400.50	413.00	321.91	324.52	334.21	360.31	402.31	412.71
330	328.00	342.00	388.20	408.50	412.50	413.00	337.40	351.85	397.72	411.19	413.00	413.13
360	335.00	390.00	408.00	411.50	412.50	413.00	400.62	409.06	412.67	413.07	413.10	413.13

Table H.4 Experimental and predicted data of air temperature of the silica gel coated rotary dehumidifier at 13.2 rph (H_{in} = 0.0045 kg$_w$/kg$_{da}$ and T_{reg} =413 K)

Angle of rotor	Air temperature (K)											
	Experimental data						Predicted data					
	Z = 0.0	Z = 0.2	Z = 0.4	Z = 0.6	Z = 0.8	Z = 1.0	Z = 0.0	Z = 0.2	Z = 0.4	Z = 0.6	Z = 0.8	Z = 1.0
10-15	315.00	322.00	338.00	391.00	408.00	412.00	297.30	307.24	332.62	369.54	395.88	407.73
30	297.30	299.50	308.50	336.00	356.00	402.00	297.30	302.39	317.10	344.31	374.50	395.65
60	297.30	297.50	300.00	307.00	316.00	330.00	297.30	300.67	306.84	316.86	334.86	358.70
90	297.30	297.50	298.00	305.00	309.00	312.00	297.30	300.16	304.78	309.22	316.00	328.73
120	297.30	297.50	298.00	304.00	308.50	311.50	297.30	299.77	303.87	307.28	310.17	315.06
150	297.30	297.50	298.00	303.00	308.00	310.00	297.30	299.43	303.15	306.41	308.54	310.53
180	297.30	297.50	298.00	302.00	307.00	309.20	297.30	299.15	302.53	305.71	307.85	309.18
210	297.30	297.50	297.50	301.00	306.00	309.00	297.30	298.90	302.00	305.05	307.30	308.64
240	297.30	297.50	297.50	299.50	305.00	308.00	297.30	298.70	301.53	304.47	306.77	308.25
270	297.30	297.50	297.50	299.00	304.00	307.00	297.30	298.51	301.12	303.93	306.25	307.85
300	305.00	310.00	318.50	332.50	358.00	413.00	307.21	311.78	324.10	339.91	368.87	407.36
330	322.50	323.00	328.50	356.50	403.00	413.00	322.77	326.88	341.70	375.38	405.59	412.80
360	323.00	325.00	338.00	390.00	408.00	412.00	330.08	339.10	375.59	405.47	412.21	413.13

Table H.5 Experimental and predicted data of the dehumidified air temperature of the silica gel coated rotary dehumidifier at various rotational speeds (H_{in} = 0.0045 kg_w/kg_{da} and T_{reg} =413 K)

Angle of rotor	Dehumidified air temperature (K)									
	Experimental data					Predicted data				
	3.5 rph	4.4 rph	6.2 rph	12.5 rph	28.0 rph	3.5 rph	4.4 rph	6.2 rph	12.5 rph	28.0 rph
10-15	391.00	391.00	400.00	411.00	406.00	396.80	405.31	410.28	408.42	393.43
30	329.00	334.00	377.00	406.00	400.00	332.45	357.56	388.03	396.31	382.00
60	317.00	318.00	317.00	369.00	372.00	305.15	306.90	320.81	356.31	359.72
90	315.00	315.00	314.00	326.00	352.00	304.46	304.84	306.03	324.00	340.96
120	313.00	312.00	308.00	314.00	334.00	303.60	304.34	304.91	310.22	326.92
150	312.00	311.00	309.00	311.00	322.00	302.53	303.62	304.57	306.07	317.33
180	312.00	310.00	309.00	311.00	314.00	301.40	302.79	304.17	305.00	311.25
210	308.00	309.00	308.00	310.00	310.00	300.36	301.87	303.64	304.64	307.62
240	307.00	308.00	307.00	310.00	309.00	299.42	301.00	303.06	304.39	305.55
270	305.00	307.00	306.00	310.00	309.00	298.55	300.21	302.42	304.16	304.38

Table H.6 Experimental and predicted data of the dehumidified air humidity of the silica gel coated rotary dehumidifier at various rotational speeds (H_{in} = 0.0045 kg_w/kg_{da} and T_{reg} =413 K)

| Angle of rotor | Dehumidified air humidity (kg_w/kg_{da}) | | | | | | | | | |
| | Experimental data | | | | | Predicted data | | | | |
	3.5 rph	4.4 rph	6.2 rph	12.5 rph	28.0 rph	3.5 rph	4.4 rph	6.2 rph	12.5 rph	28.0 rph
10-15	2.79E-03	2.84E-03	2.97E-03	5.04E-03	7.65E-03	1.63E-04	2.95E-04	5.62E-04	3.02E-03	6.95E-03
30	2.16E-04	3.38E-04	6.75E-04	2.05E-03	4.05E-03	1.73E-05	3.52E-05	1.07E-04	8.38E-04	4.66E-03
60	2.21E-04	3.11E-04	2.25E-04	4.14E-04	1.71E-03	5.67E-05	2.65E-05	1.48E-05	1.39E-04	2.12E-03
90	2.34E-04	3.11E-04	2.34E-04	2.34E-04	5.63E-04	2.32E-04	1.06E-04	3.29E-05	5.42E-05	1.13E-03
120	2.70E-04	3.60E-04	2.70E-04	2.70E-04	2.79E-04	5.52E-04	2.81E-04	8.89E-05	5.61E-05	7.37E-04
150	3.38E-04	3.60E-04	2.25E-04	2.25E-04	2.48E-04	9.56E-04	5.44E-04	1.92E-04	8.32E-05	5.90E-04
180	7.65E-04	4.05E-04	2.48E-04	2.12E-04	2.12E-04	1.37E-03	8.61E-04	3.45E-04	1.28E-04	5.49E-04
210	1.22E-03	4.50E-04	2.48E-04	2.12E-04	2.48E-04	1.77E-03	1.19E-03	5.39E-04	1.89E-04	5.60E-04
240	1.58E-03	6.30E-04	2.52E-04	2.12E-04	2.48E-04	2.13E-03	1.52E-03	7.61E-04	2.65E-04	6.00E-04
270	2.03E-03	8.10E-04	2.57E-04	2.12E-04	2.70E-04	2.45E-03	1.83E-03	9.94E-04	3.55E-04	6.27E-04

Table H.7 Experimental and predicted data of the dehumidified air temperature of the silica gel coated rotary dehumidifier at various inlet humidity ($\varphi = 6.2$ rph and $T_{reg} = 413$ K)

Angle of rotor	Dehumidified air temperature (K)							
	Experimental data				Predicted data			
	$H_{in} = 3.0\times10^{-3}$ kg_w/kg_{da}	$H_{in} = 4.3\times10^{-3}$ kg_w/kg_{da}	$H_{in} = 7.3\times10^{-3}$ kg_w/kg_{da}	$H_{in} = 14.2\times10^{-3}$ kg_w/kg_{da}	$H_{in} = 3.0\times10^{-3}$ kg_w/kg_{da}	$H_{in} = 4.3\times10^{-3}$ kg_w/kg_{da}	$H_{in} = 7.3\times10^{-3}$ kg_w/kg_{da}	$H_{in} = 14.2\times10^{-3}$ kg_w/kg_{da}
10-15	395.00	388.00	388.00	394.00	410.25	410.22	409.22	404.35
30	371.00	360.00	360.00	369.00	386.39	387.26	384.54	373.68
60	307.00	322.00	322.00	350.00	316.34	321.96	327.03	335.06
90	306.80	316.00	316.00	342.00	302.68	309.02	316.41	326.42
120	306.20	314.00	314.00	330.00	301.85	307.98	314.41	322.12
150	305.50	313.50	313.50	323.00	301.69	307.43	312.74	319.11
180	305.00	312.00	312.00	316.00	301.52	306.78	311.18	316.75
210	304.50	313.00	313.00	310.00	301.27	306.02	309.80	314.83
240	304.00	310.00	310.00	308.00	300.96	305.28	308.54	313.20
270	303.00	309.00	309.00	306.00	300.60	304.53	307.43	311.78

Table H.8 Experimental and predicted data of the dehumidified air humidity of the silica gel coated rotary dehumidifier at various inlet humidity

(φ = 6.2 rph and T_{reg} = 413 K)

Angle of rotor	Dehumidified air humidity (kg_w/kg_{da})							
	Experimental data				Predicted data			
	H_{in} = 3.0x10^{-3} kg_w/kg_{da}	H_{in} = 4.3x10^{-3} kg_w/kg_{da}	H_{in} = 7.3x10^{-3} kg_w/kg_{da}	H_{in} = 14.2x10^{-3} kg_w/kg_{da}	H_{in} = 3.0x10^{-3} kg_w/kg_{da}	H_{in} = 4.3x10^{-3} kg_w/kg_{da}	H_{in} = 7.3x10^{-3} kg_w/kg_{da}	H_{in} = 14.2x10^{-3} kg_w/kg_{da}
10-15	2.10E-03	3.87E-03	4.53E-03	9.94E-03	3.32E-04	6.02E-04	1.09E-03	3.44E-03
30	3.00E-04	4.13E-04	5.33E-04	1.96E-03	4.88E-05	1.29E-04	3.68E-04	2.12E-03
60	1.53E-04	1.29E-04	2.92E-04	1.70E-03	5.21E-06	2.46E-05	1.65E-04	2.55E-03
90	1.56E-04	2.06E-04	3.43E-04	2.84E-03	1.23E-05	6.21E-05	4.24E-04	4.02E-03
120	1.59E-04	2.58E-04	7.08E-04	5.25E-03	3.31E-05	1.70E-04	9.10E-04	5.22E-03
150	1.65E-04	3.44E-04	1.17E-03	7.10E-03	7.39E-05	3.51E-04	1.45E-03	6.17E-03
180	1.80E-04	3.87E-04	1.90E-03	7.81E-03	1.41E-04	5.91E-04	1.97E-03	6.95E-03
210	1.86E-04	4.73E-04	2.70E-03	8.52E-03	2.37E-04	8.62E-04	2.45E-03	7.62E-03
240	1.89E-04	6.02E-04	3.29E-03	8.95E-03	3.60E-04	1.15E-03	2.89E-03	8.20E-03
270	1.95E-04	7.74E-04	3.65E-03	9.09E-03	5.04E-04	1.42E-03	3.28E-03	8.70E-03

CURRICULUM VITAE

Miss Ornjira Rungarunsangchai was born on October 28, 1976 in Bangkok, Thailand. She finished high school from Suankularb Wittayalai Nonthaburi at Nonthaburi, Thailand in 1994 and received the Bachelor degree of Engineering in Chemical Engineering from Faculty of Engineering, Srinakharinwirot University, Bangkok, Thailand in 1998. She continued the Master of Engineering in Chemical Engineering Program at Chulalongkorn University in 1998 and graduated in 2001.